Investigating the nature of the secondary binding site of the human β_1-adrenoceptor using fluorescent ligands and confocal microscopy

Karolina Gherbi, BSc

Thesis submitted to the University of Nottingham
for the degree of Doctor of Philosophy

JULY 2013

Abstract

CGP 12177 is a high affinity β-blocker that antagonises agonist responses mediated through the catecholamine binding site of the human β_1-adrenoceptor (β_1AR). However, CGP 12177 also exerts agonist activity through a secondary, low affinity "CGP 12177" binding site/conformational state of the β_1AR. In this thesis, we aimed to further our understanding of the nature of the secondary "CGP 12177" site by investigating ligand-receptor interactions at this site at the single cell level, using fluorescent derivatives of CGP 12177 (BODIPY-TMR-CGP, BY-CGP) and propranolol (BODIPY630/650-S-PEG8-propranolol, BY-PROP) in confocal microscopy studies. Initial studies demonstrated that both fluorescent β-adrenoceptor ligands displayed similar pharmacology at the human β_1AR to their respective parent compounds, and that both ligands allowed visualisation of β_1AR expressed in CHO cells. Using BY-CGP in a live cell fluorescence-based automated screening assay revealed two-phase antagonist displacement binding curves. In subsequent kinetic binding studies performed on a confocal perfusion system, we used infinite dilution conditions to determine dissociation rates of BY-CGP in the absence and presence of unlabelled ligands at the single cell level. BY-CGP dissociation rates were enhanced in the presence of unlabelled ligands, thus highlighting an allosteric mechanism of action of CGP 12177 at the human β_1AR. Preliminary data using bimolecular fluorescence complementation suggested that these co-operative interactions between the two β_1-adrenoceptor binding sites were mediated across a β_1-adrenoceptor homodimer interface.

Acknowledgements

I would like to thank my supervisors Professor Steve Hill and Dr Steve Briddon for all their help throughout the past 3.5 years: from making this PhD position available to me, encouraging an independent nature in the lab, helpful discussions that guided me through a challenging project, to supporting the attendance of national and international conferences to present my data, and the reading of this thesis in record time! I am enormously grateful to them both!

I would also like to thank the Medical Research Council for providing me with funding for my PhD, without which I would not have been able to do any research at all.

Having been part of the Institute of Cell Signalling group for the past 3.5 years has meant making new friends and having many great times at work (and outside of work). I cannot thank everyone in ICS enough for making it an incredibly enjoyable place to work in (and I am not just saying that because of the frequent supply of sweets and cakes by everyone), and for helping me with any questions I might have had. In particular, I would like to thank Dr Leigh Stoddart for teaching and helping me with close to everything I could ever want to know or need, Dr Lauren May for teaching me how to use the confocal perfusion system, Tim Self for always being there to answer any microscopy related questions (and cries of help when the microscope did not do what it was supposed to do) and Dr Ross Corriden and Dr Rachel Thomas for many very helpful and interesting discussions of my (and their) data.

I also thank Anne Webber and Marleen Groenen for keeping the main lab and tissue culture lab perfectly organised and stocked that it was a joy to work in, and June McCulloch for always managing to autoclave everything in time when I had made some late decisions on doing Molecular Biology work.

Finally, I would like to thank my family and friends, who quietly in the background have always supported and encouraged me throughout my studies, and to my husband Ray, who was particularly patient with me during the time it took me to write this thesis.

Abbreviations

β_1AR	β_1-adrenoceptor
AC	adenylyl cyclase
BY-CGP	BODIPY-TMR-CGP 12177 (bordifluoropyrromethane-tetramethylrhodamine-(±)CGP 12177)
BY-PROP	BODIPY630/650-S-PEG8-propranolol
cAMP	adenosine-3',5'-cyclic monophosphate
CGP 12177	4-[3-[(1,1-dimethylethyl)amino]2-hydroxypropoxy]-1,3-dihydro-2H-benzimidazol-2-one
CGP 20712A	[2-(3-carbamoyl-4-hydroxyphenoxy)-ethyl-amino]-3-[4-(1-methyl-4-trifluoromethyl-2-imidazolyl)-phenoxy]-2-propanolmethanesulfonate
CHO	Chinese hamster ovary
CRE	cAMP response element
DMEM/F12	Dulbecco's modified Eagle's medium/nutrient mixture F12
dpm	disintegrations per minute
DMSO	dimethyl-sulphoxide
EC_{50}	concentration at which half the system maximal response occurs
E_{MAX}	maximal system response
FCS	fetal calf serum
G proteins	guanine nucleotide-binding regulatory proteins
GPCR	G protein-coupled receptor
HBSS	HEPES buffered saline solution
IBMX	3-isobutyl-1-methylxanthine
IC_{50}	concentration at which half maximum inhibition occurs
ICI 188,551	(±)-1-[2,3-(dihydro-7-methyl-1*H*-inden-4-yl)oxy]-3-[(1-methylethyl)-amino]-2-butanol

K_D	concentration at which half the receptors are occupied
k_{off}	dissociation (off) rate constant
k_{on}	association (on) rate constant
k_{onobs}	observed association rate
PBS	phosphate buffered saline
PKA	protein kinase A
propranolol	(RS)-1-(isopropylamino)-3-(1-naphthyloxy)propan-2-ol
SPAP	secreted placental alkaline phosphatase
TM	transmembrane
YFP	yellow fluorescent protein
YFP_N	N-terminal YFP fragment
YFP_C	C-terminal YFP fragment

Table of contents

Chapter 1

Introduction

1.1 The GPCR superfamily

G protein-coupled receptors (GPCRs) are important signalling receptors that are activated by external stimuli to transmit signals into cellular responses by coupling to G proteins and activating intracellular effector proteins (Pierce *et al.*, 2002). GPCRs recognise a great variety of signals, such as light photons, ions, organic odorants, nucleotides, biogenic amines, lipids, small peptides and proteins and in turn are responsible for a diverse range of cellular and physiological responses (Bockaert *et al.*, 1999; Pierce *et al.*, 2002). 1-2 % of the human genome contains genes that encode at least 1,000 GPCRs (Fredriksson *et al.*, 2005; Tuteja, 2009). In addition, this receptor class has also been found in a variety of other species, including vertebrate (Strotmann *et al.*, 2011) and invertebrate animals (Styer *et al.*, 2008; Yoshiura *et al.*, 2012), plants (Misra *et al.*, 2007; Tuteja, 2009) and fungi (Xue *et al.*, 2008).

GPCRs are large proteins of circa 300-800 amino acids (Gentles *et al.*, 1999) that fold into seven α helices that span the entire depth of the plasma membrane (i.e. transmembrane, TM; Figure 1.1) of a cell, and thus have lipophilic properties in the transmembrane region and hydrophilic properties on either sides of the membrane in the extra- and intracellular space. Great differences in sequence length are seen mainly in a stretch of amino acids at the beginning and end of a GPCR protein sequence, referred to as the extracellular N- and intracellular C-terminus, respectively (Tuteja, 2009). Three intracellular (IL1-3) and three extracellular (EL1-3) loops connect the seven transmembrane regions (TM1-7), which are arranged in a rough circular

conformation. Whilst this basic structure is observed for all GPCRs, some receptors share little or no sequence similarity at all, which resulted in the classification of GPCRs into 6 different classes (A-F) based on sequence similarity (Kolakowski, 1994).

Class A (rhodopsin receptor family) constitutes the biggest class of GPCRs, which bind small-molecule ligands. This class is further subdivided into three groups based on where the endogenous ligands bind their receptors. Group 1 contains GPCRs such as rhodopsin and the β-adrenoceptors, whose ligand binding pocket is in the transmembrane region (Rasmussen *et al.*, 2007). Group 2 contains receptors (e.g. neuropeptide Y receptors and chemokine receptors) whose peptide ligands bind the N-terminus, the extracellular loops and the extracellular parts of the TM regions. Ligands that bind to receptors of group 3 (e.g. glycoprotein hormone receptors FSHR and TSHR) bind to a larger N-terminus region and the extracellular loops (Tuteja, 2009). Class B GPCRs (secretin receptor family) are activated upon binding of their peptide ligands (e.g. calcitonin peptides) to a large extracellular N-terminus domain and the extracellular loops (Barwell *et al.*, 2012). Class C GPCRs include metabotropic glutamate receptors, $GABA_B$ and Ca^{2+} sensing receptors, which have a very large N-terminal domain in a very characteristic bi-lobial clam-shell-like conformation to which the ligands bind (Brauner-Osborne *et al.*, 2007). The other classes are made up of the fungus pheromone receptor family (class D; reviewed in Xue *et al.*, 2008), cAMP receptor family (class E; Tuteja, 2009) and class F frizzled/smoothened receptor family (Malbon, 2004).

Other classifications of GPCRs have been proposed, such as the family 1-5 system (Bockaert *et al.*, 1999) and the GRAFS system that identified the five main families glutamate, rhodopsin, adhesion, frizzled/taste2 and secretin based on phylogenic analysis of human GPCRs (Fredriksson *et al.*, 2003).

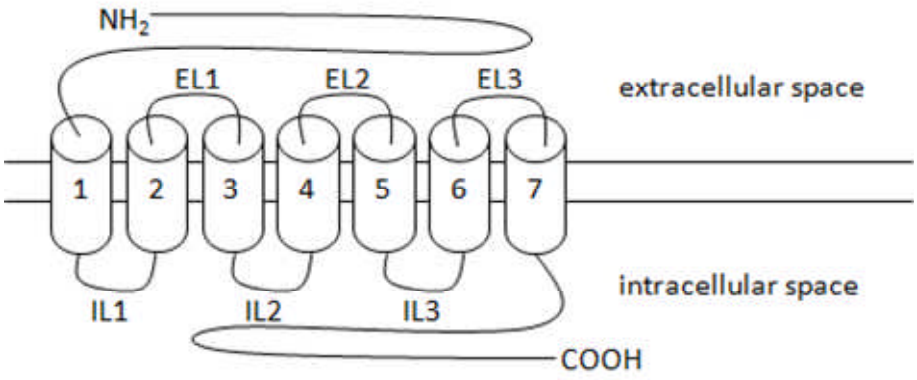

Figure 1.1 Schematic diagram of the characteristic GPCR structure. Seven transmembrane regions (1-7) are connected by three intracellular loops (IL1-3) and three extracellular loops (EL1-3) and have an extracellular N-terminal and an intracellular C-terminal domain.

1.2 The β-adrenoceptor family

The β-adrenoceptor family belongs to the Class A (rhodopsin receptor family) of the G protein-coupled receptor superfamily. Three subtypes of the β-adrenoceptor family have been identified: the β_1-, β_2- and β_3-adrenoceptors (Emorine *et al.*, 1992; Frielle *et al.*, 1987; Frielle *et al.*, 1988), which are predominantly (but not exclusively) expressed in the heart (Brodde *et al.*, 2006), lung and adipose tissues (Mutlu *et al.*, 2008), respectively. In addition, β-adrenoceptors are also expressed in vascular smooth muscle cells and throughout the central nervous system (Guimaraes *et al.*, 2001; Mantyh *et al.*, 1995). The β-adrenoceptors' endogenous ligands are the catecholamines adrenaline and noradrenaline, which are synthesised from the amino acid tyrosine in chromaffin cells of the adrenal medulla in the adrenal gland, and are then released into the blood stream (Perlman *et al.*, 1977). Noradrenaline is also synthesised in postganglionic neurons of the sympathetic nervous system. Binding of the endogenous ligands to β-adrenoceptors stimulates the sympathetic nervous system which tightly regulates various body systems during activity (Iriki *et al.*, 2012) as seen, for example, in the fight-or-flight response, where stimulated β_1- and β_2-adrenoceptors cause cardiac muscle contraction leading to an increase in the heart rate, and smooth muscle relaxation resulting in dilation of the airways, respectively (Mutlu *et al.*, 2008). In contrast, the β_3-adrenoceptor mediates lipolysis and thermogenesis in adipose tissues upon receptor activation (Collins *et al.*, 2004; Sawa *et al.*, 2006).

In the clinic, β_1-adrenoceptor antagonists (β-blockers) are widely used to decrease cardiac output in a variety of cardiovascular diseases, including angina pectoris, ischaemic heart disease and myocardial infarction (Baker *et al.*, 2011b; Poirier *et al.*, 2012; Sanz-Rosa *et al.*, 2012). By binding to the β_1-adrenoceptor they prevent the binding of the endogenous ligands to the receptor and thus, its activation, which reduces the rate and the force of cardiac contraction, thereby reducing cardiac output and blood pressure (Poirier *et al.*, 2012). In ischemic heart disease, the heart muscle becomes ischemic (oxygen-starved) when the blood flow in the coronary arteries (that deliver blood to the heart) is not sufficient (e.g. due to obstruction by an atherosclerotic plaque) to meet the demands of the heart muscle (e.g. during exercise where the heart muscle increases the cardiac output) which can cause severe chest pains (angina pectoris). The use of β-blockers reduces the workload of the heart, which in turn reduces the oxygen demand of the heart muscle. In myocardial infarction (heart attack), a ruptured atherosclerotic plaque causes severe obstruction of a coronary artery, which leads to severe ischemia and oxygen deprivation, resulting in death of the myocardial tissue supplied by that artery (Sanz-Rosa *et al.*, 2012). It has been shown that the long-term use of β-blockers reduces mortality of myocardial infarction (Freemantle *et al.*, 1999) and that β-blocker treatment during early myocardial infarction reduces the infarct size (Galcera-Tomas *et al.*, 2001).

In contrast to β-blockers, β-adrenoceptor agonists are used to stimulate the β_2-adrenoceptor in the management of pulmonary diseases including asthma

(Cazzola *et al.*, 2012). In asthma, the inflammation of the airways leads to increased contractility of the airway smooth muscles, which causes the airways to narrow, thus making breathing difficult (Hogg, 1984). The activation of the β_2-adrenoceptor expressed in smooth muscle cells in the lung causes the dilation of the airways (Cazzola *et al.*, 2012). The β_3-adrenoceptor is subject of investigations as a potential therapeutic target in the treatment of a variety of diseases including obesity, as the β_3-adrenoceptor has been implicated in the mobilisation of stored fatty acids in white adipose tissue (Bachman *et al.*, 2002; Collins *et al.*, 2004; Sawa *et al.*, 2006). In addition, the β_3-adrenoceptor agonist mirabegron has been approved as a treatment of overactive bladder within the last two years (Chapple *et al.*, 2013; Svalo *et al.*, 2013).

1.3 The human β_1-adrenoceptor

1.3.1 Structure

The ADRB1 gene on chromosome 10q25.3 (Ensembl genome database) codes for the human β_1-adrenoceptor, whose cDNA was isolated and cloned in 1987 to reveal a DNA sequence of 1431 base pairs and a protein sequence of 477 amino acids (Frielle *et al.*, 1987). Interestingly, the β_1- and β_2-adrenoceptor only share a 54 % sequence identity, with the main differences observed in the intra- and extracellular regions (Frielle *et al.*, 1987). The amino acid sequence of the β_1-adrenoceptor was proposed to fold into a secondary structure of seven α helical transmembrane domains and connecting extra-

and intracellular loops based on a hydropathy analysis (Frielle *et al.*, 1987). The three-dimensional model of bacteriorhodopsin was solved using electron microscopy in 1975 (Henderson *et al.*, 1975) and provided an insight into how the transmembrane regions of the β_1-adrenoceptor and other GPCRs would be arranged in the plasma membrane. In 2000, the crystal structure of rhodopsin was obtained (Palczewski *et al.*, 2000), which was then used in homology modelling approaches to not only predict the 3D structure of a variety of GPCRs but also to better understand ligand binding and receptor activation process (Ballesteros *et al.*, 2001; Vaidehi *et al.*, 2002). Finally, in 2008, the first crystal structure of the turkey β_1-adrenoceptor was solved (Warne *et al.*, 2008).

The N-terminus of the β_1-adrenoceptor has been described to contain an N-linked glycan on the asparagines residues at position 15 (Frielle *et al.*, 1987; Hakalahti *et al.*, 2010b), which was reported to play a role in trafficking of the receptor to the cell surface (He *et al.*, 2002). The second extracellular loop (EL2) has been demonstrated to play a role in ligand binding to the receptor as it forms the entrance of the ligand into the transmembrane binding pocket (Warne *et al.*, 2008). In the transmembrane region, the β_1-adrenoceptor shares 74 % sequence identity with the β_2-adrenoceptor (Frielle *et al.*, 1987), and the transmembrane binding site of the two receptors has been shown to be near identical in recent comparisons of the two crystal structures (Warne *et al.*, 2008). Subtype selectivity is proposed to be achieved by EL2 where the electrostatic environment is different in the two receptor subtypes (Warne *et*

al., 2008). The three residues aspartic acid (D), arginine (R) and tyrosine (Y) in the transmembrane domain of GPCRs make up the highly conserved DRY motif, which is associated with receptor activation, and was also present in the structure of the turkey β-adrenoceptor (Warne *et al.*, 2008). On the intracellular side of the plasma membrane, the second intracellular loop is in fact a short alpha helix (helix 8) that lies parallel to the membrane surface and binds to the G protein which ultimately relays the signal from the receptor into the cell by interacting with a variety of effector proteins (Shan *et al.*, 2010; Warne *et al.*, 2008; Wong *et al.*, 1990). The third intracellular loop (IL3) is the largest intracellular loop (Frielle *et al.*, 1987) and contains phosphorylation sites that are targeted by protein kinase A (PKA) and G protein regulated kinases (GRK) mediating receptor desensitisation (Freedman *et al.*, 1995) and recruitment of β-arrestin (Noor *et al.*, 2011), a scaffolding protein that mediates internalisation and interactions with other signalling proteins (Hall, 2004; Tilley *et al.*, 2009). IL3 also has a proline-rich region (Green *et al.*, 1994), which allows interaction with proteins containing the SH3 domain, such as proteins in the Src-tyrosine kinase family (Sun *et al.*, 2007). Another example is the SH3 domain-containing proteins endophilin1-3, which increases agonist-induced internalisation of β_1-adrenoceptors, highlighting a role of C-terminal interacting proteins in the regulation of β_1AR signalling (Tang *et al.*, 1999). The amino acid sequence ESKV in the C-terminus of the β_1-adrenoceptor facilitates the interaction with proteins containing a PSD-95/Discs-large/ZO-1-homology (PDZ) domain, such as PSD-95 (Hu *et al.*, 2000), that have a wide range of roles in receptor signalling and trafficking

(Hall, 2004; Marchese *et al.*, 2008). For example, the PDZ domain-containing proteins CNRasGEF (a guanine nucleotide exchange protein) and GIPC (GAIP-interacting protein C) are expressed in the heart, and coimmunoprecipitation and yeast two-hybrid screen experiments revealed their association with the β_1-adrenoceptor (Hu *et al.*, 2003b; Pak *et al.*, 2002). The β_1-adrenoceptor activates Ras via CNRasGEF when stimulated with an agonist, and this agonist-induced activation of Ras was abolished by β_1AR mutants that could no longer bind CNRasGEF (Pak *et al.*, 2002). The overexpression of GIPC was observed to cause a decrease in β_1-adrenoceptor-mediated ERK1/2 activation, thus contributing to the regulation of β_1-adrenoceptor signalling (Hu *et al.*, 2003b).

Two polymorphisms of the human β_1-adrenoceptor have been described; Ser49Gly and Arg389Gly in the N- and C-terminal region of the receptor, respectively (Borjesson *et al.*, 2000; Maqbool *et al.*, 1999; Mason *et al.*, 1999). The polymorphism at position 49 affects the extent of agonist-induced receptor downregulation (Levin *et al.*, 2002; Rathz *et al.*, 2002). The C-terminal polymorphism at position 389 causes an increased response to agonists (Mason *et al.*, 1999) and, in the clinic, is associated with higher risk of left ventricular hypertrophy (i.e. increased cardiac mass) in hypertensive patients (Fu *et al.*, 2008) and following acute myocardial infarction (Hakalahti *et al.*, 2010a). Crucially however, neither polymorphism has been linked to causing diseases (Brodde, 2008).

1.3.2 Ligand binding and receptor activation

The first crystal structure of the turkey β_1-adrenoceptor was resolved with antagonist cyanopindolol bound to the receptor, and 15 residues from TM3, 5, 6, 7 and EL2 were identified to make direct contact with the ligand in the ligand binding pocket (Warne *et al.*, 2008). Since then, the crystal structure of the receptor bound to full agonists isoprenaline and carmoterol, partial agonists salbutamol and dobutamine, and biased agonists bucindolol and carvedilol have been resolved, and a total of 23 residues have been listed to facilitate ligand binding (Warne *et al.*, 2012; Warne *et al.*, 2011; Warne *et al.*, 2008). A 1 Å (=0.1 nm) contraction of the ligand binding site was observed in the presence of agonists, but not the antagonist, which may lead to the conformational change necessary to activate the receptor (Warne *et al.*, 2011). The binding of the two full agonists to the receptor was described to involve hydrogen bonding with two conserved serine residues in TM5, whereas the two partial agonists only displayed hydrogen bonding to one of those two serine residues (Warne *et al.*, 2011), which may be a structural feature contributing to the reduced efficacy partial agonists exhibit compared to full agonists. Interestingly, the extracellular loop 2 has been identified to play an important role in ligand binding affinity and, potentially, subtype selectivity, firstly through its α-helical structure that acts to stabilise the entrance to the binding site and secondly, through its electrostatic environment, that is very different to that in the β_2-adrenoceptor (Rasmussen *et al.*, 2007; Warne *et al.*, 2008). The ligand binding interactions facilitated by

residues in EL2 may also be important for the effects of biased ligands (Warne *et al.*, 2012).

Below the ligand binding site, at the cytoplasmic end of TM3, is the location of the DRY motif. This is a highly conserved motif in GPCRs consisting of the three consecutive amino acids aspartic acid (D), arginine (R) and tyrosine (Y) in TM3, and is important in receptor activation (Audet *et al.*, 2012; Deupi *et al.*, 2007). A salt bridge that forms between the positively charged amino acid arginine of the DRY motif, and a negatively charged glutamic acid residue in TM6 has been described as the "ionic lock" (Angel *et al.*, 2009; Deupi *et al.*, 2007). In the inactive conformation of the receptor, the TM domains are arranged such that non-covalent interactions between the two residues "lock" the receptor into a closed state, and that, upon ligand binding and receptor activation, the TM domains rearrange to an open (i.e. active) state, i.e. the distance between the two residues is too great for any interactions to occur (Angel *et al.*, 2009; Audet *et al.*, 2012; Deupi *et al.*, 2007). In an activated receptor, this conformational change is linked to the binding of the G proteins to the receptor. However, this amino acid interaction was not found in the structure of the turkey β_1-adrenoceptor, even though the receptor structure was complexed with an antagonist when it was resolved, thus representing an inactive conformation. This, at least, questions the structural role of the ionic lock in the structure of the inactive conformation of the receptor (Audet *et al.*, 2012; Warne *et al.*, 2008). Another residue that has been implicated to play a role in receptor activation is a tryptophan in TM6 (W303 in human β_1AR),

which is reported to re-organise upon ligand binding, together with other residues including a highly conserved proline to cause TM6 to bend in a rotamer toggle switch, thus allowing G protein binding (Deupi *et al.*, 2007).

1.3.3 β_1-adrenoceptor-induced intracellular signalling

G proteins

GPCRs transmit the signal they receive from the bound ligand inside the cell by coupling to heterotrimeric G proteins (guanine nucleotide-binding proteins), that consist of one of each α, β and γ subunits. The intracellular loop 2 is reported to provide a docking site for the α subunit of the G protein (Tesmer, 2010) to act as a switch upon receptor activation, by directly interacting with the DRY motif within TM3 of GPCRs, facilitating G protein binding and activation (Burstein *et al.*, 1998; Warne *et al.*, 2008). The C-terminal domain is also implicated in facilitating G protein coupling (Palm *et al.*, 1989), especially via helix 8 (a stretch of 10 residues a few residues following TM7) that may aid G protein binding (Delos Santos *et al.*, 2006).

The inactive G protein has GDP bound to its α subunit. G protein binding to an activated receptor causes a conformational change in the α subunit of the G protein that results in GDP release, which is followed by the binding of GTP to the α subunit and the subsequent dissociation of the heterotrimeric protein into two subunits: the G_α subunit and the $G_{\beta\gamma}$ subunits (Hamm, 1998; Simonds, 1999). Both subunits are signalling units in their own right, activating downstream signalling pathways. This signalling, however, is terminated

when the intrinsic GTPase activity of the α subunit causes hydrolysis of GTP to GDP, as this stops further activation of effector proteins and allows re-association with the βγ subunit. This activation/inactivation cycle of G proteins is regulated by two main enzymes; guanine nucleotide exchange factors (GEFs) facilitate the GDP release and exchange with GTP to activate the G protein, whereas GTPase activating proteins (GAPs) increase the hydrolysis of GTP to GDP, thus inactivating the α subunit (Tesmer, 2010).

There are 20 different α subunits, 6 different β subunits and 12 different γ subunits, which are collectively subdivided into four main groups based on the α subunit: G_s, G_i, $G_{q/11}$ and $G_{12/13}$ (Hamm, 1998). Following ligand binding, GPCRs couple to one or more G protein families. The $G_{s\alpha}$ subunit activates the transmembrane effector enzyme adenylyl cyclase (AC), which generates the second messenger cAMP (see below). The $G_{\alpha i}$ subunit inhibits adenylyl cyclase activity, thus reducing cAMP levels in the cell. $G_{\alpha q/11}$ activates the effector protein phospholipase Cβ (PLCβ), which cleaves phosphotidylinositol 4,5-biphosphate (PIP_2) in the plasma membrane to release two second messenger molecules: diacylglycerol (DAG) and inositol phosphate (Gutkind *et al.*, 2009). $G_{\alpha 12/13}$ subunits activate Rho-GEFs, which then go on to activate the small G protein RhoA (Shi *et al.*, 2000). Furthermore, all Gα subunits also activate the mitogen activating protein (MAP) kinase pathway by interaction with the tyrosine kinase Src (Ma *et al.*, 2000; New *et al.*, 2007). βγ subunits have been reported to activate adenylyl cyclases, PLC and GRKs (Simonds, 1999; Zhong

et al., 1999), as well as ion channels and several kinases (Hamm, 1998). All three β-adrenoceptors predominantly couple to G_s.

Adenylyl cyclase and intracellular cAMP

Nine different types of the adenylyl cyclase protein family (AC1-9) have thus far been identified with varying expression patterns and regulatory properties (Simonds, 1999; Sunahara *et al.*, 2002). Adenylyl cyclases are large transmembrane proteins that consist of an intracellular N-terminal domain, two segments of 6 membrane spanning α helices, two homologous large intracellular loops (one following each transmembrane domain), and an intracellular C-terminal tail (Simonds, 1999). For activation of the enzyme, the two cytoplasmic domains dimerise to form a catalytic pocket within their domain interface, in which adenosine triphosphate (ATP) is converted to 3'-5'-cyclic adenosine monophosphate (cAMP) and pyrophosphate (Simonds, 1999; Tesmer *et al.*, 1999). The $G_{s\alpha}$ subunit binds to the N-terminal domain and both of the cytoplasmic domains to stabilise the active conformation of the enzyme, thus increasing its catalytic activity (Hanoune *et al.*, 2001; Tesmer *et al.*, 1997). The lipophilic diterpene molecule forskolin (a *Coleus forskohlii* plant product) also increases activity of all types of adenylyl cyclases, but does so through direct stabilising interactions with a hydrophobic pocket between the two cytoplasmic domains (Zhang *et al.*, 1997), thus bypassing the G protein-mediated adenylyl cyclase activation pathway. The $G_{i\alpha}$ subunit confers an inhibitory effect on adenylyl cyclase and thus, acts to decrease cAMP levels in the cell (Simonds, 1999; Sunahara *et al.*, 2002). AC1, AC3 and AC8 isoforms of

adenylyl cyclases are also activated by calcium/calmodulin, whereas AC5, AC6 and AC9 are inhibited by calcium (Hanoune *et al.*, 2001; Ostrom *et al.*, 2003; Sunahara *et al.*, 2002). Other AC regulators include protein kinase A (PKA) and protein kinase C (PKC) and the $G_{\beta\gamma}$ subunit (Hanoune *et al.*, 2001; Sunahara *et al.*, 2002). These various regulatory mechanisms, in conjunction with tissue specific expression of the different AC isoforms, tightly control the level of cAMP in the cell and thus generate highly diverse and specific signalling outcomes (Ostrom *et al.*, 2012). In cardiac myocytes, cAMP levels are raised by activation of AC isoforms 5 and 6 (Ostrom *et al.*, 2001; Pierre *et al.*, 2009). Furthermore, Ostrom *et al.* (2001) have localised the β_1-adrenoceptor together with AC6 in caveolae membrane microdomains, and have also demonstrated that the proximity of the receptor to its effector enzyme determines the efficiency by which the enzyme is activated (Ostrom *et al.*, 2001). This compartmentalisation extends from the plasma membrane (receptor and effector protein) through into the cell, where cAMP levels are regulated by degradation to AMP by localised phosphodiesterases (PDEs) and downstream signalling proteins such as PKA, which bind cAMP molecules, and together "mop" up the cAMP molecules, thus confining them to a specific subcellular location (Stangherlin *et al.*, 2011; Xiang, 2011). There are 11 PDE families, and all PDEs contain a catalytic site that binds to cyclic nucleotides and an N-terminal domain that allows regulation of PDE activity (Stangherlin *et al.*, 2012). In human atrium tissue, it has been shown that, following activation of the β_1-adrenoceptor, cAMP levels were reduced in the presence

of PDE3 (Kaumann *et al.*, 2007) and were increased in the presence of PDE inhibitors (Sarsero *et al.*, 2003).

Protein kinase A and downstream events

The PKA protein consists of two catalytic and two regulatory subunits in the inactive state. When the cAMP levels in the cell rise, two molecules of cAMP bind to each of the two PKA regulatory subunits. This causes the release of the two catalytic subunits, which then go on to phosphorylate target proteins in the cell (Taylor *et al.*, 2012). In cardiac myocytes, the cAMP-dependent PKA targets the protein phospholamban, which, once phosphorylated, activates the SERCA2a, i.e. sarco-endoplasmic Ca^{2+}-ATPase (Cerra *et al.*, 2012). SERCA2a facilitates Ca^{2+} entry into the sarcoplasmic reticulum, thereby increasing the Ca^{2+} stores. PKA also phosphorylates the voltage-gated L-type calcium channel dihydropyridine receptor (DHPR) in the cell membrane to increase Ca^{2+} uptake into the cell (Endoh, 2008; Haase *et al.*, 1993; Yan *et al.*, 2011). Cardiac muscle cells are excitable cells, where a membrane potential is established based on the concentration gradients of ions across the cell membrane with the voltage (charge separation) being negative inside the cell compared to the extracellular space. Upon membrane depolarisation, Ca^{2+} enters the cells through DHPRs (Endoh, 2008; Polakova *et al.*, 2008). Increased Ca^{2+} levels in the cell then results in the release of Ca^{2+} from the sarcoplasmic reticulum via the calcium-induced calcium release (CICR) mechanism, where Ca^{2+} itself activates ryanodine receptors (RyR) expressed on the sarcoplasmic reticulum in cardiac myocytes (Endoh, 2008; Van Petegem, 2012). Released Ca^{2+} then

binds to troponin-C, a contractile regulatory subunit of troponin that forms part of the thin (actin) filaments in the contractile apparatus in cardiac muscles (Endoh, 2008) and thus controls the calcium-mediated interactions between actin and myosin in cardiac muscles. Following contraction, intracellular Ca^{2+} levels are reduced by Ca^{2+} uptake into the stores of the sarcoplasmic reticulum via SERCA2a as well as Na^{+}/Ca^{2+} exchange and Ca^{2+} pumps (Endoh, 2008; Yang *et al.*, 2009).

Since PKA activity is cAMP-dependent, decreasing cAMP levels directly results in reduced PKA activity. Interestingly, active PKA also phosphorylates and activates PDEs, which in turn breaks down cAMP, thus creating a negative feedback mechanism. PKAs (as well as ACs and PDEs) are confined to distinct subcellular locations such as mitochondria, nucleus and cell membrane, by A-kinase anchoring proteins (AKAPs), thus controlling their selectivity (Christian *et al.*, 2011; Stangherlin *et al.*, 2012; Tilley, 2011). AKAP79/150 and mAKAPβ have been associated with AC5 and/or 6 and thus may play a role in cardiac myocytes (Christian *et al.*, 2011). AKAPs also bind other signalling proteins, including PDEs, which contributes to the spatially controlled signalling of cAMP (Christian *et al.*, 2011), although in adult mice cardiac myocytes non-localised far-reaching cAMP signalling in response to β_1-adrenoceptor stimulation has been observed (Nikolaev *et al.*, 2006).

The above cellular response is directly mediated by the cAMP/PKA pathway. In the cell, components of this pathway may also interact with other pathways (Gerits *et al.*, 2008), such as the mitogen-activated protein kinase

(MAPK) pathway that leads to activation of ERK1/2, JNK, p38 and cellular responses of cell growth, proliferation and apoptosis (Gerits *et al.*, 2008; Liang *et al.*, 2003). Downstream effects such as gene expression may also be activated or inhibited via the pathway involving the transcription factor cAMP-response-element-binding (CREB). CREB is activated by PKA that translocated to the nucleus. Once phosphorylated, CREB then binds to the CRE DNA sequence, where it is then bound by, and thus co-activated by, a CREB-binding protein (CBP), which results in initiation or inhibition of gene transcription (Shaywitz *et al.*, 1999).

Receptor phosphorylation and internalisation

The C-terminal tail of the β_1-adrenoceptor is rich in serine and threonine residues, which are phosphorylation sites of PKAs and GRKs, G protein-coupled receptor kinases (Frielle *et al.*, 1987; Granier *et al.*, 2007; Nobles *et al.*, 2011). Receptor phosphorylation, following continuous receptor activation, results in receptor desensitisation and internalisation from the plasma membrane into the cell (Drake *et al.*, 2006; Liang *et al.*, 2004). GRK phosphorylated sites are bound by β-arrestin, which then mediates receptor internalisation via clathrin-coated pits (Drake *et al.*, 2006; Luttrell *et al.*, 2002; Wolfe *et al.*, 2007b). GPCRs are tethered to clathrin-coated pit proteins, such as clathrin and the adaptor protein AP2, via the scaffolding protein β-arrestin. Dynamin proteins then facilitate the pinching off of the clathrin-coated pit into endosomal compartments within the cell (Jean-Alphonse *et al.*, 2011). The receptors then follow either the recycling pathway from early endosomes,

where the receptors are dephosphorylated and resensitised, back to the cell surface, or the degradation pathway from early to late endosomes and lysosomes, where the receptors become ubiquitinated and thus degraded (Drake *et al.*, 2006; Jean-Alphonse *et al.*, 2011; Marchese *et al.*, 2013). The β_1AR has been reported to be resistant to ubiquitination (Liang *et al.*, 2004). Zhang *et al.* (1997) demonstrated the role of β-arrestin and the clathrin-coated pit-mediated endocytosis pathway in the regulation of β_2AR signalling by overexpressing a dominant negative mutant of β-arrestin and dynamin, both of which decreased receptor dephosphorylation and resensitisation (Zhang *et al.*, 1997). Many GPCRs are internalised via this mechanism of endocytosis, including the β_2-adrenoceptor, AT1 angiotensin receptor and PAR1 (Gaborik *et al.*, 2004; Wolfe *et al.*, 2007a; Zhang *et al.*, 1997). The β_2-adrenoceptor readily desensitises and internalises following stimulation by the agonist isoprenaline (McLean *et al.*, 2000). The β_1AR is more resistant to receptor desensitisation, internalisation and degradation than the β_2-adrenoceptor (Liang *et al.*, 2004), but displays increased internalisation when co-expressed and heterodimerised with β_2ARs (Mercier *et al.*, 2002).

Interestingly, PKA receptor phosphorylation also induces receptor internalisation, but via caveolae-mediated endocytosis (Rapacciuolo *et al.*, 2003). Caveolae are formed by caveolin proteins and cholesterol embedded in the plasma membrane, and are pinched off the membrane by the dynamin protein to facilitate endocytosis (Kiss *et al.*, 2009; Veyrat-Durebex *et al.*, 2005). Receptor internalisation is generally associated with a termination of G

protein-dependent signalling, as β-arrestin binding to desensitised phosphorylated receptors uncouples the receptors from the G proteins (Luttrell *et al.*, 2002). However continued signalling following internalisation has been shown for TSH receptors, PTH receptors and $S1P_1$ receptors (Calebiro *et al.*, 2009; Estrada *et al.*, 2009; Ferrandon *et al.*, 2009). Whether this is also true for the β-adrenoceptors has not yet been investigated.

G protein-independent signalling

A ligand that binds to a receptor may utilise different residues within the receptor binding site, and these different noncovalent ionic interactions may cause different conformational changes within the receptor that transmit to the C-terminus (Warne *et al.*, 2012). The C-terminus has been described as the site of β-arrestin binding, which has also been linked to different downstream signalling effects than those associated with G protein coupling, i.e. G protein-independent signalling events (DeWire *et al.*, 2007; Tilley, 2011). These different pathways have led to the discovery of biased ligands, which preferentially activate one signalling pathway to a greater extent than another (Rajagopal *et al.*, 2011). Two β-arrestin proteins (β-arrestin 1 and 2) are known and have been implicated in a variety of cellular responses such as cardiomyocyte contractility and cytoskeletal organisation, as a downstream result of β-arrestins interacting with small GTPases RhoA, actin and myosin (Tilley, 2011). Furthermore, β-arrestin signalling has been linked to the MAP kinase ERK1/2, Jnk and p38 pathways (DeWire *et al.*, 2007). Interestingly, G protein-dependent signalling leads to increased nuclear ERK1/2 signalling,

whereas ERK1/2 signalling mediated by β-arrestin has been localised to the cytosol, where it plays a role in cardiomyocyte survival (Tilley, 2011). ERK1/2 signalling is typically mediated by activation of receptor tyrosine kinases (RTK), such as EGFR, the epidermal growth factor receptor (Patel *et al.*, 2008). However, the β_1-adrenoceptor can also activate EGFR via β-arrestin, thus resulting in ERK1/2 signalling and cross-talk of GPCR and RTK signalling, which has been linked to cardioprotection (Noma *et al.*, 2007; Patel *et al.*, 2008).

1.4 GPCR dimerisation

The association of a GCPR to another GPCR, of either the same or a different subtype, to form homo- or heterodimers, respectively, was first suggested based on data obtained in biochemical assays, including photoaffinity labelling and coimmunoprecipitation experiments (Bouvier, 2001; Franco *et al.*, 2007). Dimerisation of Class C GPCRs, such as mGluR5 and $GABA_B$ receptors, was shown in coimmunoprecipitation experiments (Kaupmann *et al.*, 1998; Romano *et al.*, 1996). Dimerisation of Class A GPCRs was also observed in biochemical assays, and dimers and higher order oligomers were reported for the β_2-adrenoceptor, muscarinic receptors and opioid receptors (Avissar *et al.*, 1983; Cvejic *et al.*, 1997; Hebert *et al.*, 1996). However, these studies have several limitations, such as specificity and sensitivity (e.g. antibodies used in Western blotting experiments), and whether dimerisation is induced by solubilisation of membranes. Fluorescent and bioluminescence resonance energy transfer (FRET and BRET, respectively) assays use fluorescent and bioluminescent proteins that are fused to the two proteins of

interest to detect and localise GPCR dimers in real time (Marullo *et al.*, 2007). A RET signal is detected when the fluorophores are within 10 nm of each other, and receptor-receptor interactions have been reported for β_2-adrenoceptor, adenosine A_{2A} and muscarinic M_2 homodimers, and $GABA_B$ heterodimer (Canals *et al.*, 2004; Fung *et al.*, 2009; Maurel *et al.*, 2008; Pisterzi *et al.*, 2010). However, the orientation and distance of the fluorophores are the deciding factor in the efficiency of the RET signal and whether RET is detected or not (Iqbal *et al.*, 2008; Marullo *et al.*, 2007; Vogel *et al.*, 2006). Furthermore, the majority of experiments that were performed to detect interaction of two GPCRs used recombinant cell systems where the GPCRs of interest were overexpressed. This could lead to random collision of receptors as they diffuse through the membrane, although negative controls are performed using non-interacting receptor and the expression levels are optimised (Marullo *et al.*, 2007). In addition, the above listed techniques suggest close proximity of receptors, but do not necessarily imply receptor-receptor interactions. However, using total internal reflection fluorescence microscopy (TIRF-M), the association of fluorescently labelled receptors into dimers and higher oligomeric structures at the single molecule level is monitored directly in real time, thus highlighting the dynamics of receptor-receptor interactions (Calebiro *et al.*, 2013; Hern *et al.*, 2010; Kasai *et al.*, 2011). Interestingly, β_2-adrenoceptors were observed to formed stable dimers, whereas β_1-adrenoceptor dimers appeared transient with 70 % of the receptor population being monomeric in low density expressing cells (Calebiro *et al.*, 2013; Dorsch *et al.*, 2009). Whilst these single molecule

studies are performed using low receptor expression levels, recombinant cell lines do not represent the physiologically relevant native membrane environment, which can influence receptor organisation and diffusion in the cell membrane (Pucadyil *et al.*, 2007).

For the class C GPCR $GABAB_B$ receptor, heterodimerisation of $GABA_{B1}$ and $GABA_{B2}$ receptor is vital for the activity of the receptor dimer as one protomer facilitates ligand binding and the other protomer transmits the signal (Jones *et al.*, 1998; White *et al.*, 1998). Apart from orphan receptors, all class C GPCRs constitutively homo- or heterodimerise (Kniazeff *et al.*, 2011). As mentioned above, class A GPCRs have been shown to be able to form dimers, however, their role and functional relevance is still subject to investigations, although several roles have been reported, such as receptor synthesis and maturation, and receptor trafficking following internalisation (Bulenger *et al.*, 2005; Cao *et al.*, 2005; Jordan *et al.*, 1999). However, in the plasma membrane, the monomeric GPCR has been described as the minimal functional unit (Chabre *et al.*, 2005). Furthermore, the activation of only one leukotriene B4 receptor in a dimer conformation was shown to be enough to cause G protein coupling (Damian *et al.*, 2006). This is termed asymmetric activation and has also been reported for rhodopsin and the β_2-adrenoceptor (Bayburt *et al.*, 2007; Whorton *et al.*, 2007; Whorton *et al.*, 2008). In contrast, both protomers are activated in symmetric activation, which was shown to lead to more efficient activation for serotonin type 4 receptor dimers (Pellissier *et al.*, 2011). In dopamine D1 and D2 heterodimers, agonist binding

to both protomer is also required, and interestingly, results in coupling to the $G_{q/11}$ protein that the monomeric D1 and D2 receptors do not couple to (Rashid *et al.*, 2007). Allosteric modulation describes the simultaneous binding of the endogenous receptor-activating ligand and an allosteric ligand to two different binding sites on a receptor complex. Whilst the second (allosteric) binding site may be within a monomeric receptor (Gregory *et al.*, 2010), allosteric interactions across dimers have been described for a variety of GPCR dimers including muscarinic, adenosine A_3 and dopamine receptors, resulting in modulated ligand affinities and/or efficacies (Birdsall *et al.*, 2005; Han *et al.*, 2009; May *et al.*, 2011; Milligan *et al.*, 2007). Other functional outputs, such as recruitment and signalling of β-arrestin as well as internalisation of GPCR dimers still need to be investigated (Gurevich *et al.*, 2008). However, it is clear that GPCR dimerisation adds to their signalling diversity (Nakata *et al.*, 2010), which may be exploited for therapeutic purposes (Congreve *et al.*, 2010; Dalrymple *et al.*, 2008; Panetta *et al.*, 2008).

1.5 GPCR pharmacology principles

1.5.1 Agonists, antagonists and inverse agonists

As described above, in order to induce a cellular response a ligand has to firstly bind to its receptor, and secondly activate it to transmit the external stimulus into the cell. The affinity of a ligand for its receptor describes how well that ligand binds its receptor (Kenakin, 1990). The ability of the ligand to stimulate the receptor to cause a response, however, is described as efficacy

(Kenakin, 2008). The β-adrenoceptor endogenous ligands adrenaline and noradrenaline bind to and activate the β_1-adrenoceptor and thus are agonists at that receptor. Agonists that display high efficacy are known as full agonists, whereas partial agonists have low efficacy. Low efficacy agonists exert a submaximal cellular response compared to full agonists that exert a maximal cellular response. In addition, a partial agonist occupies all available receptors to induce a cellular response, whereas an efficacious full agonist is able to cause a response by occupying only a fraction of available receptors. Thus, the observed level of cellular response also depends on the number of available receptors, as a low efficacy agonist may appear to be a full agonist if receptor numbers are high enough. Highly efficacious agonists at the β_1-adrenoceptor include isoprenaline and cimaterol, and salbutamol and dobutamine are examples of low efficacy (partial) agonists. The effects of an agonist at a receptor can be inhibited by blocking the binding of that agonist to the receptor. This can be done by using a ligand that also has affinity for that same receptor. If this ligand does not cause a cellular response, i.e. it exerts no efficacy because it does not activate the receptor, then it is classed as an antagonist. Antagonists that inhibit β-adrenergic signalling are called β-blockers and include propranolol and atenolol (Baker, 2005). Alternatively, the ligand may be a different agonist that causes a smaller response (i.e. partial agonist) or a different response, such as biased ligand bucindolol and carvedilol (Galandrin *et al.*, 2008; Wisler *et al.*, 2007). Yet another ligand may reduce the basal activity of the receptor (i.e. in the absence of any agonists) and thus be an inverse agonist.

An antagonist may bind the receptor in a reversible or irreversible manner. Irreversibility of a ligand may be achieved by covalently linking to a residue on the receptor. Alternatively, ligands that bind to the receptor via strong non-covalent bonds (i.e. not strictly irreversible), may display very slow dissociation rates and thus appear irreversible. This effectively "removes" receptors as the agonist has less available receptors to bind to. Under these conditions, less efficacious agonists may be revealed as they utilise a greater number of receptors than a highly efficacious agonist to yield the same level of response (Kenakin, 1997; Leff, 1995a). Reversible antagonists are further divided into competitive and non-competitive antagonists. Competitive antagonists bind to the same site as the agonist they are competing against, to block a cellular response. Thus, with higher agonist concentrations the inhibitory effect of the antagonist used can be overcome. Non-competitive antagonists do not compete with the agonist for the same endogenous (orthosteric) binding site, but instead bind to a topographically distinct (allosteric) binding site of the receptor and influence the agonist effects via allosteric interactions (see below).

According to the two-state model of agonist action, two receptor conformations (active, R*, and inactive, R) coexist in equilibrium (Leff, 1995b). An agonist preferentially binds to and stabilises the active receptor conformation, thus directing the equilibrium towards R*. An inverse agonist binds to and stabilises the inactive receptor state, thus directing equilibrium towards R. Neutral antagonists, however, do not affect the equilibrium of the

two receptor states as they bind to both conformations with the same affinity (Leff, 1995b). This model was extended to the three-state model to include an additional active conformation of the receptor (R* and R**) to take into account multiple receptor-effector coupling events, i.e. the active receptor conformation may couple to different G proteins (Leff *et al.*, 1997). Further extensions lead to the cubic ternary complex (CTC) model, where both the active and inactive receptor may be bound to a ligand and/or G protein or not. In this model, the transition of an agonist bound receptor (AR*) to an agonist bound receptor that couples to a G protein (AR*G) represents the efficacy parameter (Weiss *et al.*, 1996). Other receptor models have been derived from the CTC to include, for example, a second ligand binding within the same receptor or receptor dimerisation (Christopoulos *et al.*, 2002; Franco *et al.*, 2006).

1.5.2 Allosteric modulators

An endogenous ligand binds to the endogenous (orthosteric) binding site of its receptor. A ligand that binds to a topographically distinct (allosteric) binding site on the same receptor is an allosteric ligand. Thus, both the orthosteric and allosteric ligand can be bound to the same receptor at the same time. The binding of an allosteric ligand to a receptor causes a conformational change in the receptor that negatively or positively alters the interactions the endogenous ligand makes with the orthosteric binding site, i.e. it affects its binding affinity (Christopoulos *et al.*, 2002). Crucially, allosteric interactions (also termed co-operativity) between two ligands

binding to their binding sites are reciprocal. The binding of multiple ligands to a receptor at the same time and the allosteric interactions between multiple binding sites were incorporated into the extended ternary complex (ETC) model (Christopoulos *et al.*, 2002). The simplified scheme in Figure 1.2 shows the binding of ligands A and B to the receptor R, which is described by their respective affinities K_a and K_b. However, the binding of A to the receptor already bound by B is described by its affinity to the receptor and the co-operativity factor α, i.e. αK_a. The same co-operativity factor affects the binding of ligand B to the receptor already bound by A, highlighting the reciprocal nature of the co-operativity between two binding sites (Christopoulos *et al.*, 2002). Allosteric modulation has been reported for a variety of GPCRs, including muscarinic, free fatty acids, chemokine and metabolic glutamate receptors (Birdsall *et al.*, 2005; Knoflach *et al.*, 2001; Milligan, 2009; Watts *et al.*, 2012). Allosteric ligands have also been shown to affect the efficacy of an agonist at a given receptor. Thus, the concentration-response curve of an agonist is left-shifted by a positive allosteric modulator (PAM) and right-shifted by a negative allosteric modulator (NAM). Crucially, allosteric effects are saturable, which eventually leads to a bunching up of the agonist concentration-response curve, which clearly distinguishes allosteric from competitive interactions (Christopoulos *et al.*, 2002; Smith *et al.*, 2010). Furthermore, some allosteric ligands have been found to display efficacy themselves, i.e. cause a functional response, and have been termed allosteric agonists or ago-allosteric ligands (Langmead *et al.*, 2006; Smith *et al.*, 2010).

Ago-allosteric ligands have been described at the muscarinic M2 receptor (May *et al.*, 2007) and the free fatty acid 2 receptor (Milligan, 2009).

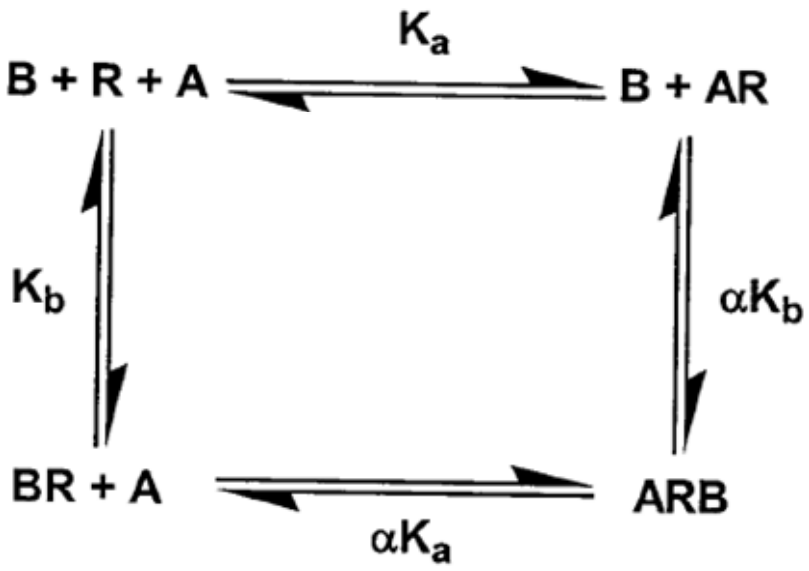

Figure 1.2 Model describing the binding of two ligands A and B to the receptor R, which is governed by their affinity towards the unbound receptor (K_a and K_b, respectively) and the co-operativity factor α. Taken from Christopoulos *et al.* (2002).

1.6 CGP 12177 at the β_1-adrenoceptor

CGP 12177 was synthesized by Staehelin *et al.* (1983) as a hydrophilic β-blocker and radioligand to facilitate ligand binding studies in whole cell assays (Staehelin *et al.*, 1983). CGP 12177 was shown to antagonise catecholamine responses at the β_1-adrenoceptor with high affinity, but was also shown to exhibit agonist effects at much higher (circa 100-fold) concentrations (Kaumann *et al.*, 1997; Staehelin *et al.*, 1983). These agonist effects were not as pronounced as those stimulated by the full agonist isoprenaline, i.e. they were partial. Since a partial agonist occupies all available receptors to produce the maximum effect possible, the EC_{50} of a partial agonist is expected to be similar to its affinity. Because of this discrepancy of the EC_{50} and affinity values CGP 12177 was termed a non-conventional partial agonist (Kaumann, 1989). The antagonist and partial agonist effects of CGP 12177 were not only observed in human but also in a variety of other mammalian cardiac tissues (Lowe *et al.*, 1999; Sarsero *et al.*, 1998). Other non-conventional partial agonists have also been described (Figure 1.3), including pindolol (Baker *et al.*, 2003a; Joseph *et al.*, 2003; Kaumann *et al.*, 1980). Interestingly, studies using selective β_1- and β_2-adrenoceptor antagonists (CGP 20712A and ICI 118,551 respectively) to attribute these partial agonist effects to a β-adrenoceptor subtype revealed that these stimulatory effects appeared resistant to β-blocker treatment at the concentrations used to inhibit isoprenaline-induced effects at the two receptor subtypes. Thus, the partial agonist effects seen at high concentrations of CGP 12177 are inhibited by antagonists with low

affinity. This led to the proposal that these partial agonist effects are mediated through an additional fourth β-adrenoceptor (Kaumann, 1997). However, studies performed on human and rat β_1-adrenoceptors expressed in a recombinant cell line suggested that the β_1-adrenoceptor alone was sufficient to observe the complex pharmacology of CGP 12177, and the putative β_4-adrenoceptor was described as a low affinity site or state of the β_1-adrenoceptor (Pak *et al.*, 1996). This notion was also suggested following desensitisation experiments in a rat model of cardiac failure that revealed exactly comparable desensitisation responses for the β_1- and putative β_4-adrenoceptor (Kompa *et al.*, 1999). Finally, studies on cardiac tissues isolated from β_2AR and β_1/β_2AR knockout mice definitively demonstrated that the β_1-adrenoceptor was responsible for the partial agonist effects of CGP 12177 (Kaumann *et al.*, 2001). Several other studies confirmed these findings, describing CGP 12177 antagonist effects at the high affinity β_1-adrenoceptor site (β_{1H}; site 1) and partial agonist effects at the low affinity β_1-adrenoceptor site (β_{1L}; site 2) that are resistant to β-blockers at the concentrations used to inhibit isoprenaline-induced agonist effects at the high affinity site (Baker *et al.*, 2003a; Joseph *et al.*, 2004; Konkar *et al.*, 2000; Pak *et al.*, 1996). The difference in CGP 12177 affinities at the two sites is at least 1.5 orders of magnitude (Kaumann *et al.*, 2008). The availability of a radiolabelled version of CGP 12177 made it an ideal ligand in studies to further understand the two β_1-adrenoceptor sites or conformations. For example, in addition to establishing two-site binding of [^{3}H]-CGP 12177 to the β_1-adrenoceptor in equilibrium binding experiments, Joseph *et al.* (2004) reported a circa 20-fold

slower dissociation rate of [^{3}H]-CGP 12177 off the high than off the low affinity β_1-adrenocptor binding site (Joseph *et al.*, 2004). However, the nature of this secondary β_1-adrenoceptor site is still not understood. An effort was made by Baker *et al.* (2008) to identify key residues involved in the binding of ligands to the high and low affinity β_1-adrenoceptor sites using a site-directed mutagenesis approach. However, introduced mutations that affected ligand binding to one site also affected ligand binding to the other site (Baker *et al.*, 2008). This could be due to structural implications that affect both sites which may be reflected in co-operativity between the two binding sites. This could, for example, be the case if the receptor transitioned from one to another conformation. Perhaps binding of ligand to one site is necessary to facilitate the binding of ligand to the second site. Alternatively, β_1-adrenoceptor homodimerisation may facilitate the two-site binding β_1AR pharmacology.

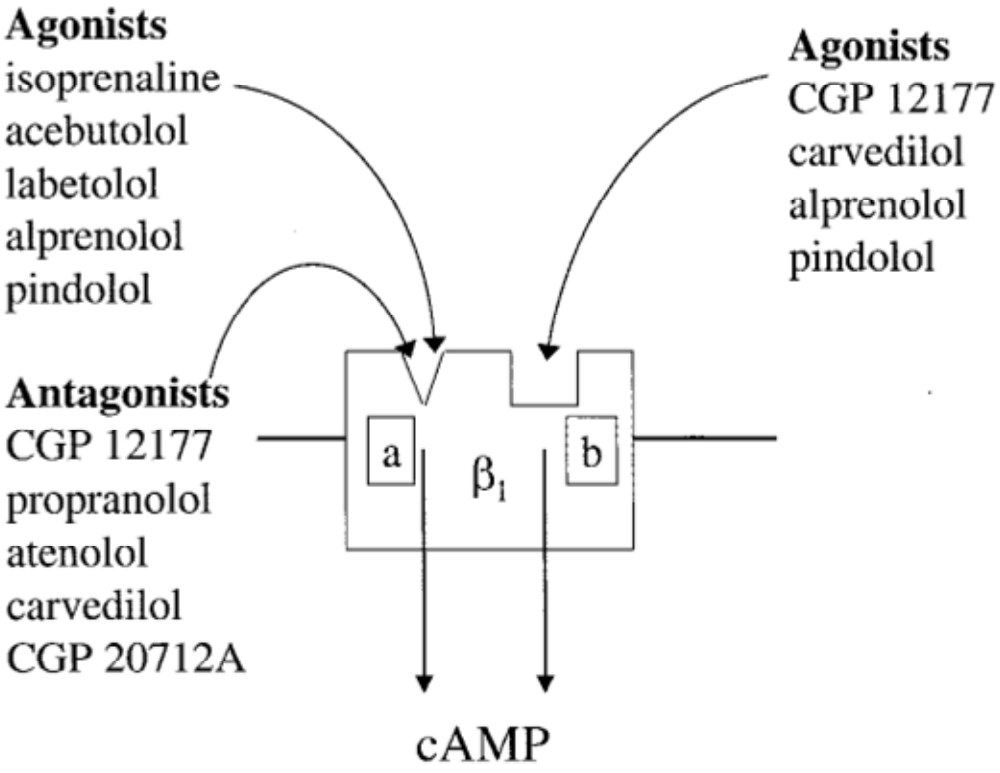

Figure 1.3 Schematic representation of the two-site binding site model for the β_1-adrenoceptor. Site a represents the high affinity binding site, whereas site b represents the low affinity binding site. The nature of the secondary binding site has not yet been described, and may be a second binding site on the β_1-adrenoceptor, an additional active conformational state of the receptor or possibly an additional β_1-adrenceptor in a homodimeric complex. Taken from Baker *et al.* (2003).

1.7 Studying receptor-ligand interactions

1.7.1 Functional assays

The ability of an agonist to activate the receptor and cause a response is measured in functional assays. Thus, the potency of an agonist in a functional assay is determined by both its affinity and efficacy. Furthermore, the affinity of a competitive antagonist can be derived in functional assays from the shift of the agonist concentration-response curve caused by the presence of a fixed concentration of antagonist. Functional assay may measure the extent of G protein activation (GTPγS assay), a change in levels of second messenger molecules (e.g. cAMP) or the levels of a reporter gene that is transcribed in response to receptor activation. One of the main considerations for choosing a given functional readout is the signal:noise ratio, where the minimum (basal) and maximum response and the difference between those two is defined. Thus, basal levels of a second messenger in unstimulated cells as well as breakdown of that molecule need to be taken into account. For example, the [^{3}H]cAMP accumulation assay uses PDE inhibitors, which prevent the breakdown of [^{3}H]cAMP, thereby increasing the signal over basal (noise) ratio.

A reporter gene assay is downstream of second messenger production and takes several hours to allow transcription of the reporter gene (McDonnell *et al.*, 1998). The reporter gene codes for a protein that has unique properties (e.g. thermostability, unique substrate for an enzyme, fluorescent or luminescent properties) which make it easily distinguishable from

endogenous proteins and easily detectable (Hill *et al.*, 2001). The secreted placental alkaline protein (SPAP), for example, is thermostable at 65 °C, whereas endogenous alkaline proteins are not. Therefore, the subsequent hydrolysis of the substrate *p*-nitrophenylphosphate (PNPP) to *p*-nitrophenol (PNP) is entirely due to SPAP present in the sample, as a result of receptor activation. The colour change associated with PNPP hydrolysis is then quantified by measuring the optical density of each sample. The transcription of a reporter gene is initiated by a transcription factor binding to its designated promoter region. A CRE promoter is used for SPAP transcription and is activated as a downstream effect of the cAMP/PKA pathway (Baker *et al.*, 2004).

However, because gene reporter assay are downstream effects of a signalling cascade, it is possible that other cellular pathways may interact with the pathway whose outcomes are being monitored. The presence of serum in cell culture medium activates the MAP kinase pathway, stimulating cell growth and proliferation (Hill *et al.*, 2001). This is kept to a minimum by keeping the cells in serum-free medium for a day before experimentation (McDonnell *et al.*, 1998). In addition, ligands may interfere with downstream components and receptors may be desensitised and/or internalised as a result of prolonged receptor stimulation. This could lead to false potency values, which is why additional functional assays should be carried out to confirm activity of a given ligand at the receptor. Whilst there are potential caveats and interferences with functional assays that monitor downstream responses, it

does allow pharmacological analysis of a longer term response and may be more physiologically relevant (Baker *et al.*, 2003c). Physiological responses may also be measured in end-organ response assays and include organ bath studies that, for example, measure the rate and force of cardiac contraction in isolated tissues.

1.7.2 Conventional radioligand binding techniques

Radiolabelled ligands have been widely used in experimental studies to examine the binding of ligands to a given receptor. Equilibrium saturation binding experiments are used to determine the affinity of the labelled ligand for a receptor. Increasing concentrations of the labelled ligand are used in these experiments to establish the maximum binding capacity of the ligand to the receptor which is dependent on the numbers of receptors, thus this particular technique is also used to gain information on receptor expression in the system used (Bylund *et al.*, 1993). In classic equilibrium competition experiments, the unlabelled and labeled ligand compete for the same binding site on unoccupied receptors. Providing the ligand binding properties of the labelled ligand are known, the affinities of unlabelled ligands can be derived in equilibrium binding assays (Cheng, 2001). Time course assays allow the determination of kinetic parameters of the labelled ligand, and unlabelled competitor ligands in the presence of the labelled ligand (Motulsky *et al.*, 1984). Thus, affinity values as well as kinetic parameters of unlabelled ligands can be obtained using one well-characterised radiolabelled ligand, and this

has been one of the main approaches to identify new ligands in drug discovery programs (Noel *et al.*, 2001).

Radioactive isotopes used to label small molecule ligands include the very small radioisotope ^{3}H, which is not expected to alter the pharmacology of the ligand of interest. However, bigger isotopes (^{125}I) may be used to label the ligand of interest, and these may potentially adversely affect the pharmacology and physicochemical properties of the ligand under investigation. In either case, full characterisation of the pharmacological properties of the radiolabelled ligand is required prior to investigations of the binding properties of unlabelled ligands. Importantly, the use of radioactive isotopes is associated with strict Health and Safety regulations, as these substances are harmful to the user and the environment, if not stored, handled and disposed off appropriately. In light of this, alternative ways of labelling receptors and ligands have been developed and used, which include the use of fluorophores.

1.7.3 Fluorescent receptors

Fluorescent proteins (FPs) are circa 27 kDa proteins that absorb light of a given wavelength (and energy) and emit light at longer wavelength (lower energy), and, when fused to the protein of interest, have been used to visualise the distribution of a protein of interest in cells (Deckert *et al.*, 2006) and tissues (Scherrer *et al.*, 2006). The green fluorescent protein (GFP) was isolated from the jellyfish *Aequorea victoria* (avGFP) in 1962 (Shimomura *et*

al., 1962) and cloned in 1992 (Prasher *et al.*, 1992). The wild-type avGFP had two excitation spectra; a major and minor excitation peak at 395 nm and 475 nm, respectively (Day *et al.*, 2009; Heim *et al.*, 1995). The introduction of one mutation (S65T) resulted in a shift of the major excitation peak to 490 nm and increased brightness (Heim *et al.*, 1995). An additional mutation (F64L) improved the folding efficiency of GFP at 37 °C, resulting in the enhanced GFP (eGFP) version (Day *et al.*, 2009). The crystal structure of GFP was solved in 1996 (Ormo *et al.*, 1996; Yang *et al.*, 1996), which revealed an eleven-stranded β-barrel structure that, in its centre, holds the chromophore 4-(p-hydroxybenzylidene)imidazolidin-5-one (HBI), which is only fluorescent if surrounded by a properly folded protein structure (Day *et al.*, 2009). Mutations that changed residues around the chromophore were found to shift the fluorescent spectrum of the chromophore, thus resulting in spectral variants of the enhanced GFP version, including blue FP (eBFP; 383-445nm), cyan FP (eCFP; 439-476 nm) and yellow FP (eYFP; 514-527 nm) variants (Day *et al.*, 2009). Additional mutagenesis and engineering studies further improved brightness, photostability and pH sensitivity of fluorescent proteins (Day *et al.*, 2009; Sample *et al.*, 2009). In addition, FPs showed tendencies to form dimers or higher oligomeric complexes, which led to the engineering of monomeric FPs to avoid artificial aggregation of proteins to which the FPs were fused (Sample *et al.*, 2009). The palette of fluorescence proteins was increased when a fluorescent protein was isolated from the sea anemone *D. striata*, DsRed, which was excited at 558 nm and emitted at 583 nm. Using a longer wavelength (i.e. lower energy) laser is better tolerated when working

with live cells and reduces autofluorescence interference. Extensive mutagenesis efforts on the DsRed protein led to a series of monomeric red FPs that emit in the orange (551-575 nm), red (576-610 nm) and far-red (611-660) spectrum (Sample *et al.*, 2009). Spectral variants of fluorescent proteins allow the simultaneous labelling of two or more proteins of interest to monitor their distribution and interaction (Falk *et al.*, 2001; Herrick-Davis *et al.*, 2006; Overton *et al.*, 2002). The fusion of a 27 kDa protein to a GPCR protein results in a large fusion protein that is desired to behave in a similar manner to its untagged counterpart. Indeed, comparable ligand binding affinities were established at the GFP-tagged β_1- and β_2-adrenoceptors and β_1- and β_2-adrenoceptors that were not tagged with GFP (McLean *et al.*, 2000). However, internalisation and degradation of the GFP-tagged β-adrenoceptors has been observed to be slower than untagged receptors (McLean *et al.*, 2000). This may not be unexpected, as the C-terminus of a GPCR plays an important role in initiating internalisation and degradation processes.

An alternative strategy to fluorescently label a receptor uses the SNAP-tag that is fused to the N-terminal end of a protein of interest. The SNAP-tag technology is based on the human DNA repair protein O^6-alkylguanine-transferase (hAGT) which removes an alkyl group from a guanine base of DNA and transfers it onto a reactive cysteine residue within itself (Figure 1.4) in a covalent thioether bond (Pegg, 2011). Human AGT (207 amino acids) can also react with O^6-benzylguanine (BG) substrates (Pegg, 2011). Keppler *et al.* (2003) first described the use of BG derivatives, such as BG-Fluorescein, for the

labelling of hAGT fusion proteins *in vivo* (Keppler *et al.*, 2003). Subsequent protein engineering led to the smaller 20kDa (180 amino acids) SNAP-tag and increased enzyme activity compared to wild-type hAGT (Juillerat *et al.*, 2003; Juillerat *et al.*, 2005; Keppler *et al.*, 2003), thus enhancing specificity of protein labelling. The observation that the nature of the label does not influence the reaction rate of hAGT with its substrate led to the synthesis of a great variety of SNAP-tag fluorescent labels (excitation range from 360-782 nm commercially available), which makes this technology particularly flexible and adaptable to experimental needs. Another main advantage is the use of cell impermeable substrates to label SNAP-tagged membrane proteins. The SNAP-tag is chemically inert to other biomolecules such as double-stranded DNA and, it is not restricted to a certain subcellular location (Juillerat *et al.*, 2005). The irreversible and specific labelling of target proteins, which are preferentially N-terminally fused to the SNAP-tag (Tirat *et al.*, 2006), has been successfully used, for example, to create an EGFR-specific imaging probe by fusing the SNAP-tag to a single-chain antibody fragment (Kampmeier *et al.*, 2010). The applications of the SNAP-tag have been broadened with the engineering of the CLIP-tag, which is another hAGT mutant. Gautier *et al.* (2008) introduced eight mutations to redesign the active site of the SNAP-tag, resulting in specificity for benzylcytosine (BC) derivatives (Gautier *et al.*, 2008). Using the CLIP-tag in conjunction with the SNAP-tag allows the simultaneous labelling of target proteins with two different fluorophores for co-localisation purposes as well as protein-protein interaction studies.

Alternative peptide- and protein-tags include His-tag (6 amino acids, oligo-histidine sequence that binds to nickel or cobalt and uses nickel-nitrilotriacetic acid fluorophores such as NTA-FITC-Ni^{2+}) and HaloTag™ (297 amino acids, mutated haloalkane dehalogenase that covalently binds fluorescent haloalkane ligands) to label proteins of interest (Bohme *et al.*, 2009; Los *et al.*, 2008). Fluorescently labelled antibodies may also be used that either directly or indirectly (i.e. one or two antibody method) recognise a specific epitope which may be a part of the receptor of interest or an engineered tag such as HA-tag, FLAG-tag or c-myc-tag at the N-terminus of the receptor (Bohme *et al.*, 2009). Most fluorescent tags require the fusion of the tag to the protein of interest, which involves generation of a DNA construct and its transfection into a host cell line, thus this method does not have the potential of labelling native receptor in native cells, but is invaluable in establishing an understanding of fundamental properties of cellular and membrane-bound proteins.

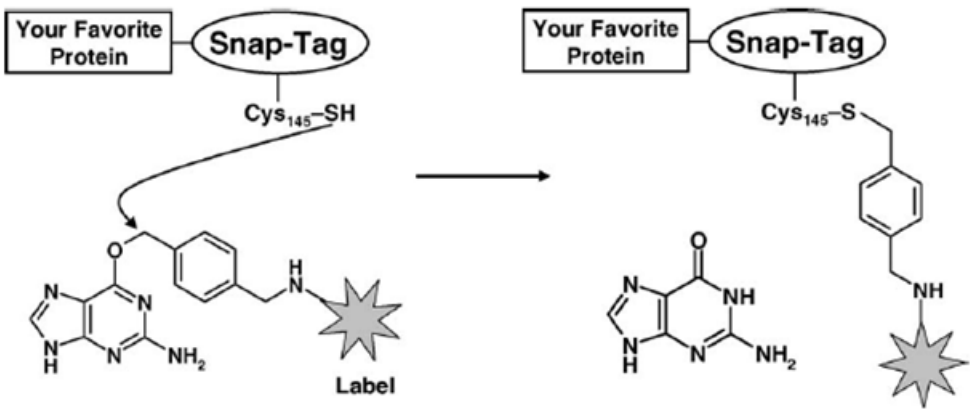

Figure 1.4 Schematic representation of the SNAP-tag labelling reaction. The benzylguanine (BG) SNAP-tag substrate is linked to a fluorophore. In a suicide reaction by the SNAP-tag, the fluorophore is covalently linked to the SNAP-tag, thus labelling the receptor. The reaction releases a free guanine molecule. Taken from Tirat *et al.* (2006).

1.7.4 Fluorescent ligands

Fluorescently labelled ligands are being used increasingly (Baker *et al.*, 2003d; Daly *et al.*, 2010; May *et al.*, 2010a; Stoddart *et al.*, 2012) as they are not only a safer alternative to radiolabelled ligands, but also allow visualisation of ligand binding to the receptor in living cells and can be used to label native receptors in primary cells. In addition, it may not always be possible to label a ligand of choice with a radioactive isotope, or a radioligand for a given receptor may not be commercially available. A fluorescent ligand is synthesized by chemically coupling the ligand of interest to a fluorophore. The fluorophore itself is a similar size to a small molecular weight ligand, thus its addition to the pharmacophore structure can dramatically alter the ligands pharmacological profile at a given receptor (Middleton *et al.*, 2005). A linker may be used to space apart the pharmacophore and the fluorophore in an attempt to avoid interference with the ligand binding to and activating the receptor (Baker *et al.*, 2010; Middleton *et al.*, 2005). Interestingly, the affinity of a ligand may not only be reduced, but may be improved when labelled with a fluorophore (Vernall *et al.*, 2012). However, there are no definitive guidelines of point of fluorophore attachment, linker length and composition that will guarantee a fluorescent ligand of low nanomolar affinity, making the synthesis of a functional fluorescent ligand a potentially lengthy process. However, there are many advantages to using a fluorescent ligand over a (not necessarily easier to synthesise) radioligand that include (1) visualisation of total and non-specific levels of ligand binding, (2) localisation of receptor distribution, (3) use in single cell and single molecule studies and (4) labelling

of endogenous receptors in primary cells. The investigation of ligand-receptor interactions in a physiologically relevant environment is perhaps the most important feature, as there is a growing appreciation of the effect of other receptors, cellular signalling and scaffolding proteins on the signalling pathway that is initiated (Kenakin *et al.*, 2010; Williams *et al.*, 2009). In contrast, most radioligand binding assays were done in membrane preparations, where the membrane structure was disrupted and most intracellular components were lost. Fluorescent ligands have been used in binding experiments in low and medium throughput formats (Baker *et al.*, 2003d; Loison *et al.*, 2012; Stoddart *et al.*, 2012) and in kinetic binding experiments at the single cell level (May *et al.*, 2010a; May *et al.*, 2011). As with radioligands, not just antagonist, but also agonists may be fluorescently labelled. This allows the specific labelling of different receptor conformations (active and inactive) by using low concentrations of the agonist or antagonist, as has been done in studies on the A_3 adenosine receptor (Cordeaux *et al.*, 2008). To date, fluorescently labelled noradrenaline, CGP 12177 and propranolol have been used in the literature to label β-adrenoceptors (Baker *et al.*, 2011a; Baker *et al.*, 2003d; Prenner *et al.*, 2007). Baker *et al.* (2003) described the pharmacology and binding properties of the fluorescent analogue of CGP 12177, BODIPY-TMR-CGP, at the human β_2-adrenoceptor expressed in Chinese hamster ovary cells, whereas Briones *et al.* (2005) used this fluorescent ligand to investigate the β-adrenoceptor distribution in the vascular wall of mesenteric rat artery tissues (Briones *et al.*, 2005). However,

the pharmacological properties of BODIPY-TMR-CGP have not yet been characterised at the β_1- and β_3-adrenoceptors.

1.7.5 Fluorescent imaging techniques

Fluorescently labelled proteins and ligands can be used in a variety of microscopy assays to investigate ligand binding, receptor internalisation and trafficking and protein-protein interactions in real time in living cells.

Binding assays

In principle, the same binding assays that use radiolabelled ligands can be performed using fluorescently labelled ligands in conjunction with confocal fluorescence microscopy, and saturation, competition and kinetic binding assays have been carried out on recombinant cells (Baker *et al.*, 2003d; May *et al.*, 2010a; May *et al.*, 2011; Stoddart *et al.*, 2012). Fluorescence based screening assays have the potential to be used in medium- and high-throughput ligand screening formats (Nomura *et al.*, 2008; Stoddart *et al.*, 2012). As with radioligands, the total and non-specific binding properties of a fluorescent ligand will have to be well defined before it is used in competition binding assays to determine affinity values of competitor ligands. To further ensure ligand binding specificity, the fluorescent ligand may be used in binding experiments on cells expressing a fluorescently tagged receptor (May *et al.*, 2011). In this set-up, the main considerations are to use two fluorescent labels that are spectrally separated as far as possible. This will avoid fluorescence bleed-through, which describes the fluorescence spectrum

of one fluorophore artificially being registered in the fluorescence readout of the second fluorophore (e.g. the emission fluorescence of the tagged receptor "bleeds" through the optical filter used to capture emission for the fluorescent ligand, thus recording a false level of ligand binding). If possible, the optical filters used can also be adjusted accordingly to help avoid fluorescence bleed-through. Fluorescently labelled ligands may be used alone or in conjunction with fluorescently tagged receptors in single molecule ligand binding studies using fluorescence correlation spectroscopy (FCS) and fluorescence cross correlation spectroscopy (FCCS), respectively (Briddon *et al.*, 2007). FCS records the fluctuations in fluorescence intensities that are caused by fluorescently labelled species (free ligand, ligand-bound receptor) moving through a small defined confocal volume (~0.3 fL) that can be placed anywhere in the cell (e.g. spanning the cell membrane). Free ligand and ligand-bound receptor species are then separated based on their different dwell times, i.e. a small free ligand moves faster through the detection volume than a much larger ligand-bound receptor that is embedded in the cell membrane. Since free and bound ligand can be clearly quantified, binding properties of ligands to receptors in distinct membrane environments can be determined (Briddon *et al.*, 2007).

Functional assays

Fluorescence confocal microscopy is also used to investigate functional responses to agonists in living cells in real time. As such, the recruitment of β-arrestin to the receptor or the internalisation of a fluorescently labelled

receptor may be monitored in single cells or in cell populations (Kilpatrick *et al.*, 2010; Stoddart *et al.*, 2012). The trafficking of multiple proteins labelled with wavelength-separated fluorophores may be observed in response to different ligands (Serge *et al.*, 2011; Teichmann *et al.*, 2012; Wagener *et al.*, 2009). Some studies have also used fluorescent second messengers (e.g. Ca^{2+} binding to the green fluorescent Fluo-4 dye enhances its fluorescence) in conjunction with fluorescent ligands in a combined binding and functional assay, thus investigating the dynamics of ligand-induced responses (Cordeaux *et al.*, 2008).

Protein-protein interactions

When two fluorescently labelled species (e.g. a ligand and a receptor) are detected using two different ligands, overlapping (or merging) of the two captured images reveals areas (pixels) in which both fluorescent species were detected and are thus colocalised in that area. This infers that the two species are in close proximity to one another. Colocalisation coefficients are routinely used in cell biology studies to also indicate a biological interaction based on a statistically significant relationship between the fluorophores detected per pixel (Zinchuk *et al.*, 2007).

Förster and bioluminescence resonance energy transfer techniques (FRET and BRET, respectively) are often used to determine potential interactions between two proteins. In FRET, two proteins thought to be interacting with one another are fused to a donor (e.g. CFP) and acceptor (e.g. YFP)

fluorescent protein that have a partial emission/excitation spectral overlap. Only the donor fluorophore is excited using a laser, as the photons emitted by the donor fluorophore then excite the acceptor fluorophore. This transfer of energy from one to the other fluorophore is only possible if the two fluorophores are in close proximity to one another (within 10 nm). Thus, if the two proteins interact with one another and are in close proximity to each other, YFP fluorescence increases, whereas CFP fluorescence decreases, and vice versa (Fernandez-Duenas *et al.*, 2012). The same principle is applied in BRET assays, where a bioluminescent *Renilla reniformis* luciferase (Rluc) enzyme is used as a donor and GFP is used as the acceptor protein (Salahpour *et al.*, 2012). Rluc produces the initial photon emission upon degradation of its substrate coelenterazine (Salahpour *et al.*, 2012). FRET and BRET assays have been used to detect ligand-receptor, receptor-receptor and receptor-protein interactions (Audet *et al.*, 2010; Canals *et al.*, 2004; Gales *et al.*, 2005; Loison *et al.*, 2012; Milligan, 2004). Another approach to detecting protein-protein interactions is bimolecular fluorescence complementation (BiFC), where the N-terminal and C-terminal non-fluorescent half of a fluorescent protein (e.g. YFP_N and YFP_C) are fused to two interacting proteins. Upon interaction of the two proteins (e.g. receptor dimerisation), the two YFP halves reconstitute to a full length YFP that is fluorescent (Figure 1.5). Thus, detection of YFP fluorescence indicates protein-protein interactions (Ciruela *et al.*, 2010). For example, oligomerisation of adenosine A_{2A} receptors and β_2-adrenoceptors have been shown using BiFC (Kilpatrick *et al.*, 2012; Vidi *et al.*, 2010). The process of reconstitution of the full length fluorescent protein is

irreversible, and as such does not allow the investigation of the dynamics of receptor-receptor interactions. N-terminal fluorescence tags, such as SNAP and CLIP-tags, can also be used in any of the above fluorescence microscopy experiments (Fernandez-Duenas *et al.*, 2012). For example, the SNAP-tag technology has been used in combination with FRET to establish receptor-receptor and ligand-receptor interactions (Leyris *et al.*, 2011; Maurel *et al.*, 2008). In addition, SNAP and CLIP-tag specific cross-linking has been proposed by Gautier *et al.* (2009), where two different SNAP and CLIP-tagged proteins can be covalently linked by a specific cross-linking BG-BC substrate when the two tags are in close proximity to one another (Gautier *et al.*, 2009; Reymond *et al.*, 2011). Furthermore, a split SNAP-tag protein complementation method has been reported that can be used in a BiFC approach (Mie *et al.*, 2012). When designing any of the above experiments, the expression levels of the two potentially interacting proteins introduced into a cell system has to be optimized to avoid random aggregation of these proteins leading to false RET or BiFC signals. Similarly, fluorescence bleed-through in FRET has to be avoided and FRET of known non-interacting proteins should serve as a negative control (Fernandez-Duenas *et al.*, 2012).

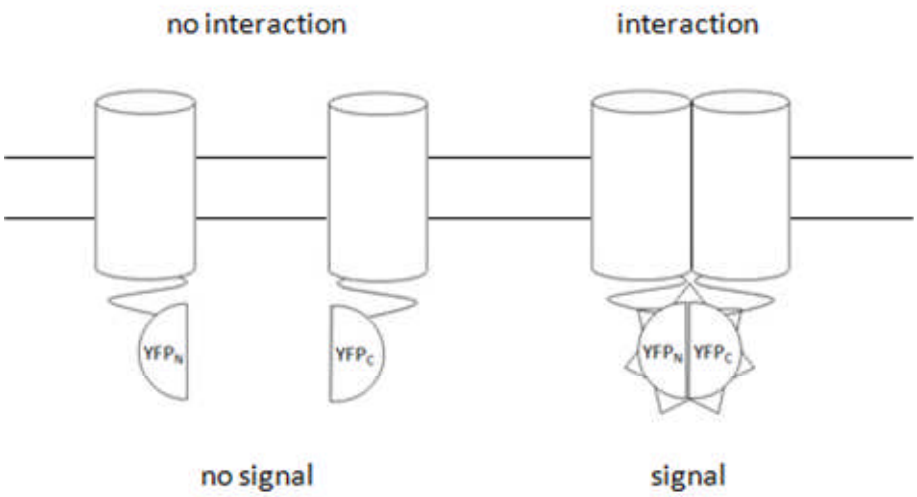

Figure 1.5 Schematic diagram of the principle of bimolecular fluorescence complementation (BiFC). Two non-fluorescent N- and C-terminal halves (YFP_N and YFP_C) of the yellow fluorescent protein tagged to two proteins of interest reconstitute upon interaction of these two proteins. The reconstituted YFP is fully functional and its fluorescence can be detected in fluorescence microscopy applications.

1.8 Aims

The aim of this thesis was to investigate the nature of the secondary binding site of the human β_1-adrenoceptor using a confocal microscopy approach. As described above, the complex pharmacology of CGP 12177 at the β_1-adrenoceptor is well documented in the literature and has now been firmly attributed to the β_1-adrenoceptor rather than a fourth β-adrenoceptor. It is proposed that the β_1-adrenoceptor has two binding sites through which the different effects of CGP 12177 are exerted, and affinity values of multiple ligands have been established at both sites. However, the nature of the secondary site is not yet understood as a mutagenesis study aiming to identify key residues of either binding site was inconclusive. In this thesis we aimed to use the fluorescently labelled CGP 12177 analogue BODIPY-TMR-CGP in conjunction with confocal microscopy approaches to further investigate the ligand-receptor interactions at the β_1-adrenoceptor with the view to gain insight into the nature of the secondary β_1-adrenoceptor site.

Chapter 2

Materials and Methods

2.1 Materials

CHO-K1, CHO-CRE SPAP cells, CHO-β_1-SPAP and CHO-β_2-SPAP cells were a kind gift from Dr Jillian G Baker. All cell culture hardware was purchased from Fisher Scientific (Loughborough, UK) and all medium reagents, including phosphate-buffered saline (PBS), were from Sigma Aldrich (Gillingham, UK) except for foetal calf serum (FCS), which was obtained from PAA laboratories (Pasching, Austria). The chemicals diethanolamine (DEA), NaCl, $MgCl_2.6H_2O$, HCl, KCl, $MgSO_4$, HEPES, sodium pyruvate, $NaHCO_3$, $CaCl_2$, NaOH, Tris-Base, Boric acid, EDTA, PNPP and DMSO were obtained from Sigma Chemicals (Poole, UK). The SNAP-tag vector and the SNAP-Surface™ Alexa Fluor® 488 were obtained from New England Biolabs (Ipswich, MA, USA). All oligonucleotide primers used in this study were synthesized by Eurogentec (Seraing, Belgium). PolyMate Additive was purchased from Bioline (London, UK). The GenElute™ miniprep, maxiprep, gel extraction and PCR purification kits were purchased from Sigma Aldrich (Gillingham, UK). The QuikChange™ site-directed mutagenesis kit was purchased from Stratagene (Amsterdam, Netherlands). Lipofectamine, competent Top10 F' *E. coli* cells, SOC media and the pcDNA3.1(Neo+) and pcDNA3.1(Zeo+) vectors were from Invitrogen (Paisley,UK). All restriction enzymes, *Pfu* Ultra DNA polymerase and the 1 kb DNA ladder were purchased from Promega (Madison, WI). All other molecular biology reagents were from Sigma (Gillingham, UK). All DNA sequencing was done by the DNA Sequencing Laboratory, School of Biomedical Sciences at the University of Nottingham. The compounds forskolin, isoproterenol

hydrochloride (isoprenaline), cimaterol, (S)-(-)-propranolol hydrochloride, CGP 20712A dihydrochloride and ICI-118,551 were from Tocris Cookson (Avonmouth, Bristol, UK). The fluorescent CGP 12177 analogue BODIPY-TMR-CGP was obtained from Dr Jill Baker who had originally purchased this compound from Molecular Probes (Eugene, OR). The fluorescent propranolol derivative BODIPY630/650-S-PEG8-propranolol was purchased from CellAura (Nottingham, UK). The [^{3}H]-adenosine was from Amersham Biosciences UK, Ltd. (Buckinghamshire, UK), the poly-prep columns were from Bio-Rad (Hercules, CA), and the scintillation fluid was from PerkinElmer (Groningen, Netherlands). All other chemicals were obtained from Sigma Aldrich (Gillingham, UK).

2.2 Cell culture

The Chinese hamster ovary (CHO) CHO-K1 cell line, a proline-deficient subclone from the original CHO line (which was first isolated by Puck *et al.* (1958)), was used in experiments throughout this thesis. The CHO-K1 cell line exhibits epithelial morphology and grows in an adherent monolayer. They were maintained in Dulbecco's modified Eagle's medium nutrient mixture F12 (DMEM/F12) medium supplemented with 10 % foetal calf serum (FCS) and 2 mM L-glutamine (=growth medium) in cell culture incubators maintaining a humidified atmosphere of 5 % CO_2/ 95 % air. All cell culture techniques were carried out in class II laminar flow cell culture hoods. All cell culture medium and solutions used were pre-warmed in a 37 °C water bath before use to avoid any harsh temperature changes and stress to the cells. Following

passaging of cells into cell culture flasks and seeding of cells into plates for experimentation, the cells were returned to the cell culture incubator (37 °C, 5 % CO_2/95 % air atmosphere) to allow cells to adhere and grow until used for further passaging or experimentation.

Passaging of cells

The cells used in this study were generally maintained in 75 cm^2 tissue culture treated flasks (T75s) and grown to confluence. For passaging, the growth medium was removed from the flask and cells were washed with 5-10 mL phosphate buffered saline (PBS) to remove any remaining serum off the cells and the flask. Cells were lifted off the bottom of the flask by incubation in 1 mL 1x trypsin-EDTA at 37 °C in a cell culture incubator. Trypsin is a serine protease and is used here to hydrolyse proteins that facilitate the adherence of the cells to the cell culture dish. After 2-3 minutes the cells were loosened and easily dislodged by the addition of 5 mL growth medium, which also prohibited any further action of trypsin on the cells. The cells were then centrifuged at 1000 rpm for 5 minutes and the supernatant discarded. The cell pellet was then resuspended in 10 mL growth medium and the appropriate amount was transferred into a new T75 flask. Cells were routinely passaged at a 1:10-1:20 dilution once a week. Multiple flasks were gained from one T75 to keep the passage number low and flasks were used for experiments the next week.

Seeding cells into plates

96-well plates

Cells were seeded into 96-well plates for CRE-mediated SPAP transcription, ImageXpress (IX) Ultra confocal plate reader and PHERAstar *FS* plate reader experiments. The cells from one T75 flask were detached from the bottom of the flask as described above (see above *Passaging of cells*). The cell pellet was then resuspended in 10 mL growth medium and 2 mL of this was then transferred to a further 8 mL of growth medium (to make up 10 mL in total, i.e. a 1:5 dilution). Of that, 100 µL were transferred into each well of a 96-well plate (0.3 cm^2 surface area per well). The same dilution (1:5) was used for CRE-mediated SPAP transcription, IX Ultra confocal and PHERAstar *FS* plate reader experiments, however, cells for SPAP gene reporter experiments were plated out 48 hours prior to experimentation and cells for IX Ultra confocal and PHERAstar *FS* plate reader experiments were seeded 24 hours prior to experimentation. This was done to allow cells for SPAP gene reporter experiments to be serum starved 24 hours prior to experimentation.

24-well plates

The cells were prepared into a 10 mL cell resuspension as described above for 96-well plates. The same dilution (1:5) was prepared and 500 µL of a 10 mL cell suspension was added to each well of a 24-well cell culture plate (2cm^2 surface area per well) for [^{3}H]cAMP accumulation experiments. Cells seeded into these plates were used for experimentation the following day.

6-well plates

6-well cell culture plates were used to seed cells to be used in confocal perfusion experiments. A circular (3.2 cm in diameter) glass coverslip was placed into each well of a 6-well plate. Cells of one T75 flask were lifted off the bottom of the flask as described above (see above *Passaging of cells*). The cell pellet was then resuspended in 6 mL of growth medium, of which 2 mL (for a 1:3 dilution) were transferred to a further 10 mL of growth medium (for a total of 12 mL). 2 mL of this cell suspension were then transferred onto the glass coverslips in each well of a 6-well plate (9.6 cm^2 surface area per well). The seeded cells were used in experiments the following day.

8-well glass chambers

Cells were prepared into a 10 mL resuspension as described above for 96-well plates and seeded into 8-well Labtek borosilicate chambered-coverglass plates (Nalgene Nunc International, Fisher Scientific, Loughborough, UK) for confocal microscopy experiments. From the 10 mL cell suspension, 1 mL was transferred into a further 19 mL of growth medium (1:20 dilution). From this cell suspension, 400 µL were added to each well of an 8-well plate. The cells were used in confocal imaging experiments two days after seeding.

Long term storage and thawing of cells

Foetal calf serum was supplemented with 10 % (v/v) DMSO (to constitute the "freezing medium") in the cell culture hood and subsequently sterilised by filtration using a 10 mL syringe and a 0.2 µm sterile filter. The cryoprotective agent DMSO prevents damage to cell walls by ice crystals that form during the

freezing process, thus improving cell viability and recovery after thawing. Cells to be frozen were detached from the bottom of a T75 flask and spun as described above (see *Passaging cells*). The cell pellet was then resuspended in 2 mL of freezing medium by careful trituration before aliquoting 1 mL of the cell suspension into a 2 mL labelled cryogenic tube. Thus, one T75 flask of confluent cells generated two aliquots of cells in freezing medium. The tightly capped cryogenic tubes were then put into an isopropanol-filled cryogenic freezing container that allows controlled and gradual freezing of the cells at a rate of 1 °C per minute in the -80 °C freezer. After 24 hours, the cryogenic tubes were then placed into liquid nitrogen (-176 °C) for long term storage.

Cells in cryogenic tubes were taken out of liquid nitrogen storage and the tubes were thawed in a 37 °C water bath (for circa 2 minutes). The cells were then immediately placed into a T75 flask containing 20 mL pre-warmed growth media. Working as quickly as possible reduces the risk of prolonged stress for the cells and aids the survival and recovery of a larger proportion of cells. The cells in the T75 flask were placed into the cell culture incubator at 37 °C and in a 5 % CO_2/95 % air atmosphere. The following day, the growth medium was replaced by fresh growth medium to remove any cell debris from cells that had died during the thawing process. Cells were grown to confluence and passaged once before being used for experimentation.

2.2 Generation of new cell lines

Cells used for transfection were either CHO-K1 cells or a clonal cell line of CHO cells already expressing the CRE-SPAP (CS) reporter gene construct (CHO-CS cells). These cells were cultured in T25 flasks to be able to use a lower amount of DNA and the transfection agent lipofectamine.

Transfection of cells to generate a stable mixed population cell line

The DNA used in transfections was a circular eukaryotic expression plasmid (pcDNA3.1) consisting of the desired receptor (e.g. human β_1-adrenoceptor) and an antibody resistance gene (e.g. neomycin). The DNA was in solution (in double-distilled H_2O) and the concentration determined using a UV spectrophotometer (see *Molecular biology: Maxi-prep*). The transfection agent used was lipofectamine, a lipophilic agent that coats the DNA, making it more membrane permeable to facilitate the uptake of the DNA. Two solutions were prepared:

Solution A = 3 µg DNA + OPTIMEM (to make up a total of 300 µL)

Solution B = 30 µL lipofectamine + 270 µL OPTIMEM

The two solutions were combined (= transfection mix; total volume 600 µL) and left at room temperature for 1.5 hours.

After 1 hour, the growth medium on cells that were grown to 60-70 % confluence in a T25 flask, was replaced with 3 mL OPTIMEM medium and the cells were incubated for 30 minutes at 37 °C in a 5 % CO_2/95 % air atmosphere. Following this, the transfection mix was added to the cells and the cells were

incubated at 37 °C in a 5 % CO_2/95 % air atmosphere for 24 h to allow the uptake of DNA by the cells. The next day the OPTIMEM media containing the transfection mix was removed and the cells were washed by the addition and removal of 10 mL DPBS to remove any cells that died during the transfection process, and replaced with 10 mL of fresh growth media to allow the cells that survived to recover. Cells that recovered from the transfection process would start to express the new proteins and thus, the selection process was started the next day.

Selection for the transfected cells was started 24-48 hours after transfection by replacing the growth medium with growth medium supplemented with the relevant antibiotic (e.g. 1 mg/mL geneticin (G418) or 500 µg/mL zeocin; =selection medium). Successfully transfected cells will express the desired receptor and the antibiotic resistance gene. Antibiotic resistance allows the cell to survive the cytotoxic effects of a given antibiotic. This treatment caused death of cells not expressing the transfected construct. In addition, cells that have not incorporated the transfected construct into the nuclear DNA of the cell, but only transiently (e.g. in the cytoplasm) expressed the antibiotic resistance protein, would also not survive the antibiotic treatment past a few division cycles. Thus, only cells that have incorporated the transfected construct into their nuclear DNA have the means for survival. However, the insertion of the external DNA is a random process and may disrupt DNA sequences essential to the survival and growth of the cell, in which case this cell will also not survive. The same would be the case for cells

in which the transfected construct was inserted into an inactive region of the DNA, thus resulting in very low (or no) transcription of the introduced sequences. Every couple of days, the selection medium was replaced with fresh selection medium to remove cells that had died during the selection process. After 1-2 weeks, the cells were passaged and placed into a new T25 flask. When the rate of cell death declined and the cell population grew confluent, the cells were moved to a T75 flask and grown to confluence. This cell population was a mixed population stable cell line where every cell expressed the new proteins at a different level.

Dilution cloning and generation of a stable clonal cell line

When it was desired to generate a stable clonal cell line, the mixed population cell line was grown to confluence and the cells were detached from the bottom of the flask and centrifuged as described above (see *Passaging cells*). The cell pellet was resuspended in 20 mL growth media, and 20 µL were transferred into another 20 mL of growth medium. From that cell suspension, 100 µL and 120 µL were added to 20 mL of selection media, generating final 200,000- and 167,000-fold dilutions. 200 µL of each dilution was transferred into 96 wells of a 96-well plate (i.e. one plate per dilution) with the aim to place only one cell into each well, thus isolating a single cell that can be grown into a clonal cell line. Both dilutions used here resulted in 0-3 cells per well.

After 48 hours, both 96-well plates were examined and the number of cells counted in each well. Only wells containing one cell were marked and re-

examined 48 hours later. Most of the single cells had grown into small colonies (= a clone) which were left to grow to about 40-50 % confluence in the well. At this stage, the cells tend to grow on top of each other rather than in a defined monolayer which means that 100 % confluence is unlikely to be achieved. The selection medium was then removed from the wells containing single colonies and the cells were washed by addition and removal of 100 µL DPBS. Then, 100 µL trypsin was added to each marked well. After 2-3 minutes, the trypsin was pipetted up and down to loosen the cells off the bottom of the well. The trypsin and the cells were then added to 1 mL selection media in a well of a 24-well plate (1:7 dilution by surface area difference). This was done for all wells that were marked to contain a single cell colony. Once confluent in the 24-well plate, the cells were moved to 6-well plates (1:5 dilution) and then to T25 flasks (1:3 dilution) and finally to T75 flasks (1:3 dilution). From there each clone was tested for the presence and functionality of the transfected gene of interest.

Transient transfection of cells

CHO-K1 cells were seeded into assay plates/flasks and grown to 60-70 % confluence. Transient transfections were then carried out in the same manner as described for transfections to generate stable cell lines (see above), but the volumes of the reagents were adjusted as outlined in Table 2.1. Following transfection and incubation of cells in a cell culture incubator at 37 °C overnight, the cells were not exposed a selection medium, resulting in a cell population where not all cells have taken up the DNA construct. Cells that

have taken up the DNA construct will only express the proteins encoded in the DNA construct transiently (and each cell will do so at a different level), i.e. do not incorporate the DNA into their nuclear DNA. This is mainly due to time limitations as cells that are transiently transfected, are used for experimentation within the next couple of days.

Table 2.1 Volumes of reagents used to transiently transfect CHO-K1 cells seeded into 8-well plates, 6-well plates and T75 flasks. The amount of DNA used is total amount for the entire 8-well and 6-well plate assuming transfection of cells in all 8 and 6 wells, respectively. The total volume is the combined volume of solution A and B.

	8-well plate	6-well plate	T75 flask
Solution A			
Total DNA	1.2 µg	4.5 µg	10 µg
OPTIMEM medium	200 µL	300 µL	300 µL
Solution B			
Lipofectamine	20 µL	50 µL	100 µL
OPTIMEM medium	260 µL	850 µL	600 µL
Total volume	480 µL	1.2 mL	1 mL
Addition per well/flask	60 µL	0.2 mL	1 mL
Final volume per well/flask	300 µL	2 mL	10 mL

2.3 Molecular Biology

Generation of a SNAP-tagged receptor fusion protein

For experiments carried out for this thesis, the SNAP-tag was fused to the N-terminus of the human β_1-adrenoceptor (accession number: NM_000684) to generate a SNAP-tagged β_1-adrenoceptor fusion protein. To achieve this, the steps outlined below were followed to incorporate the β_1AR sequence (=insert) into a pcDNA3.1(Neo) plasmid (=vector) that already contained the SNAP-tag sequence (pcDNA3.1(Neo)-SNAP; kindly provided by Dr Holliday; SNAP-tag sequence between *Kpn*I and *Bam*HI restriction enzyme sites).

Polymerase chain reaction

First, the polymerase chain reaction (PCR) was used to amplify the β_1AR receptor DNA sequence. Two short oligonucleotides (primers) were used to hybridize to the sequences at the start (forward primer) and end (reverse primer) of the β_1AR DNA sequence, thus defining the DNA region that was amplified. The sequence of these primers is complementary to the start and end of the sequence to be amplified. In addition, the primers were designed to introduce *Bam*HI (GGATCC) and *Eco*RI (GAATTC) restriction enzyme sites (short DNA sequence that are recognized by restriction enzymes which cut the DNA at precisely that site) immediately before and after the β_1AR sequence, respectively. This allowed the insertion of the β_1AR sequence exactly downstream of the SNAP-tag sequence in the plasmid vector (see vector map in Figure 2.1), thus fusing the SNAP-tag to the β_1-adrenoceptor.

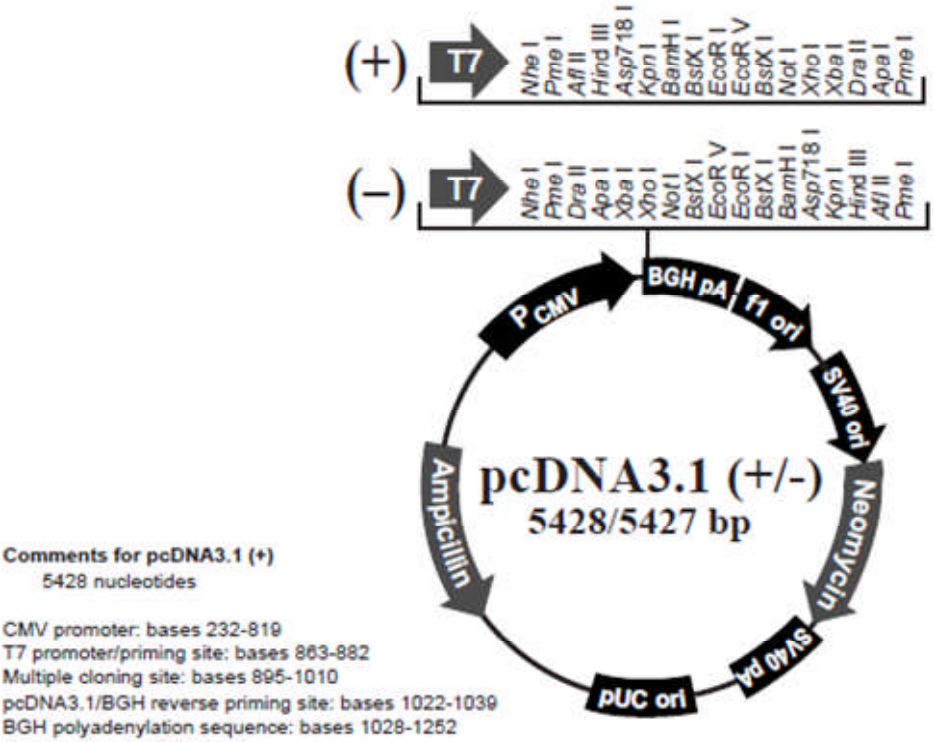

Comments for pcDNA3.1 (+)
5428 nucleotides

CMV promoter: bases 232-819
T7 promoter/priming site: bases 863-882
Multiple cloning site: bases 895-1010
pcDNA3.1/BGH reverse priming site: bases 1022-1039
BGH polyadenylation sequence: bases 1028-1252
f1 origin: bases 1298-1726
SV40 early promoter and origin: bases 1731-2074
Neomycin resistance gene (ORF): bases 2136-2930
SV40 early polyadenylation signal: bases 3104-3234
pUC origin: bases 3617-4287 (complementary strand)
Ampicillin resistance gene (*bla*): bases 4432-5428 (complementary strand)
ORF: bases 4432-5292 (complementary strand)
Ribosome binding site: bases 5300-5304 (complementary strand)
bla promoter (P3): bases 5327-5333 (complementary strand)

Figure 2.1 Map of the pcDNA3.1(Neo+/-) plasmid vector. The SNAP-tag sequence was inserted between the *Kpn*I and *Bam*HI restriction enzyme site in the pcDNA3.1(Neo)-SNAP vector used here. Consequently, the β_1AR sequence was inserted between the *Bam*HI and *Eco*RI restriction sites to generate a continuous SNAP-β_1AR sequence. This schematic (including the vector composition details) was taken from the invitrogen™ life technologies website (www.invitrogen.com).

Other considerations when designing the PCR primers included (1) an overhang sequence (increases restriction enzyme activity on the target sequence fragment), (2) a mismatch to mutate the receptor start codon (to allow continuous transcription of the fusion protein DNA sequence) and (3) length of the primer sequence that directly compliments the target DNA (i.e. served as a primer; circa 17 bases). The designed β_1AR forward and reverse primers used for this PCR process were 5' – CCGCC/GGATCC/CTG GGC GCG GGG GTG CTC G – 3' (18 complementary bases, 66 °C) and 5' – GGCGG/GAATTC/CTA CAC CTT GGA TTC CGA GG – 3' (20 complementary bases, 62 °C), respectively. The melting temperature (T_m) of primers that form correctly base-paired hybrids was calculated using the following equation:

$$\mathbf{T_m} = \left(\mathbf{4x[G+C]} + (\mathbf{2x[A+T]})\right)\mathbf{°C} \qquad \text{(eq. 1)}$$

For the PCR mixture, 50 ng of template DNA (kindly provided by Dr Baker) was used. To this, 125 ng of each primer, 10 mM dNTP (final concentration; containing the four deoxyribonucleotide triphosphates dATP, dTTP, dCTP, dGTP), 1 unit of proof-reading *Pfu* DNA polymerase and 10x *Pfu* DNA polymerase compatible buffer (1x final concentration) were added to a 200 µL clear thin-walled flat-capped PCR tube. 2x PolyMate Additive (1x final concentration) was also added to the PCR mixture to reduce the formation of secondary structures of the GC rich β_1AR template DNA. Finally, ddH_2O was added to make up a total volume of 50 µL. A control PCR mixture containing exactly the same components but without the template DNA (the volume of the ddH_2O was adjusted accordingly), was also prepared to highlight potential

contamination of the PCR sample. The PCR mixture was then placed in an Eppendorf Mastercylcer® Gradient thermal cycler that controls the temperature and time of each step of a PCR cycle. A PCR cycle (Figure 2.2) starts with the denaturation step (95 °C, 1 minute), where the two strands of the double stranded template DNA was separated into single strands. The temperature was then cooled to 61 °C for 1 minute to allow the primers to attach to the appropriate positions on the β_1AR DNA sequence (i.e. hybridization step). The annealing temperature is ideally 1-2 °C lower than the lowest melting temperature of the primers used, to favour specific primer-template hybrid to form (this temperature should be too high for mismatched hybrids). Lastly, the primer extension step in the PCR cycle is performed at the optimal temperature of the thermostable *Pfu* DNA polymerase (72 °C, 3 minutes), which synthesises complementary strands along each single template strand as an extension of the primers in 5'→ 3' direction. This PCR cycle was repeated 29 times generating 2^{30} linear copies of the β_1AR sequence from each double-stranded template DNA molecule.

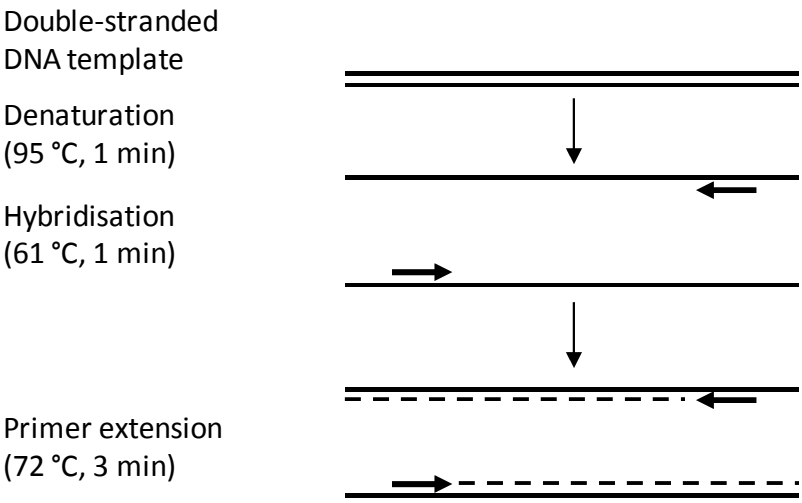

Figure 2.2 Schematic representation of the steps involved in the PCR cycle. Double-stranded template DNA was denatured into single strands to which the single-stranded PCR primers hybridise. *Pfu* DNA polymerase then synthesised new strands complementary to the template DNA sequence, thus generating two double-stranded DNA sequences. In the next PCR cycle, both of these two DNA sequences were denatured again with each single strand acting as a template, which resulted in the exponential amplification of the target sequence.

Double-digest of insert and vector DNA sequences

To confirm that the PCR was successful, 5 µL of the PCR sample was used to confirm the presence and approximate size of the amplified target sequence in a gel electrophoresis analysis (as described below). Following this, 20 µL of the remaining PCR sample was transferred to a 500 µL sterile Eppendorf tube and treated with 1 µL of each of the restriction enzymes *Bam*HI and *Eco*RI in a 'double-digest' reaction. *Bam*HI and *Eco*RI cut their restriction enzyme site DNA sequences in a staggered fashion leaving a 4 nucleotide overhang ("sticky ends") on each strand, which helps to ensure that the target DNA sequence is inserted in the right orientation. Then, 5 µL of the restriction enzyme buffer E (Promega, Madison, USA; the composition of this buffer was compatible with both restriction enzymes used, such that it did not hinder their activity) and 23 µL of ddH_2O were added. The contents of the double-digest mixture were mixed thoroughly, and then placed onto a heating block for 2 hours at 37 °C.

To allow successful insertion of the β_1AR sequence into the pcDNA3.1(Neo)-SNAP plasmid vector (kindly provided by Dr Holliday), the vector DNA was treated with the same two restriction enzymes in a double-digest reaction as described above for the PCR sample containing the insert DNA fragment. 2 µL of the plasmid vector maxi-prep DNA was transferred to a sterile 500 µL Eppendorf tube. To this, 1 µL of each restriction enzyme, 5 µL of compatible buffer E and 41 µL of ddH_2O were added to make up a total of 50 µL. The

sample was mixed and then incubated on the heating block for 2 hours at 37 °C.

Analysis and isolation of the insert DNA fragment using gel electrophoresis

Following this, the digested PCR sample was analysed by agarose gel electrophoresis which allows the separation of DNA molecules according to their size (smaller negatively charged DNA molecules migrate quicker than larger DNA molecules through the pores of the gel towards the positive pole in an electric field). A 1 % (w/v) agarose gel was prepared by dissolving 0.3 g agarose in 30 mL TBE buffer (90 mM Tris-Base, 90 mM Boric acid, 2 mM EDTA), before heating the solution for 2 minutes. The solution was then cooled down to touch and 3 µL Ethidium Bromide was added. This allowed the amplified fragment to be visible as a discrete band under ultraviolet (UV) light exposure. The still liquid gel was poured into a gel cast. Once the gel was set and placed into a gel tank together with TBE buffer, 40 µL of the dyed PCR sample (50 µL PCR sample was mixed with 10 µL of a loading dye) run on the gel (80 V, 45 minutes) alongside 6 µL of a 1 kb DNA ladder (5 µL DNA ladder + 1 µL loading dye), which would allow a rough estimation of the size of the resulting bands. The visible loading dye contained 0.4 % orange G, 0.03 % bromophenol blue and 0.03 % xylene cyanol, which run at 50 bp, 300 bp and 4 kpb, respectively and thus allow the tracking of DNA migration during gel electrophoresis.

Following this, the DNA fragment of the correct size was cut out of the gel in a UV light box using a razor blade. This was done as quickly as possible to

minimise damaging effects on the base-pairing in the DNA fragment. The gel slice containing the DNA fragment was then purified using a GenElute™ gel extraction kit (Sigma Aldrich, Gillingham, UK) according to the manufacturer's instruction. Briefly, the gel was solubilised using a chaotropic agent at 60 °C and isopropanol added to precipitate the DNA. The solution was then transferred to a spin column catching the DNA in the column. A 70 % ethanol wash solution was then used to remove salts and other impurities from the column, before the purified DNA fragment was eluted in 50 µL elution buffer. The purified plasmid vector DNA sample was then stored in a -20 °C freezer and used in the ligation step the next day.

SAP treatment and purification of the vector DNA sequence

Following the double-digest reaction, two restriction enzymes in the reaction mix were inactivated by incubating the reaction mix at 65 °C for 20 minutes. Then, 40 µL of the double-digest sample were transferred into a new sterile 500 µL Eppendorf tube, to which 2 µL of the shrimp alkaline phosphatase (SAP) enzyme and 5 µL of SAP buffer and 3 µL ddH_2O were added (total volume of 50 µL). This SAP reaction mix was incubated for 1.5 hour at 37 °C, before the SAP enzyme was inactivated in a 20 minutes incubation at 65 °C. The SAP enzyme removes phosphates from exposed nucleotides (i.e. where a DNA break occurred, such as the one caused by restriction enzymes). This prevents self-ligation of the exposed ends of the vector DNA sequence. Following the SAP treatment, the vector DNA sequence was purified using a GenElute™ PCR purification kit (Sigma Aldrich, Gillingham, UK) according to the

manufacturer's instruction. Briefly, a spin column method was used to remove protein, nucleic acid and other contaminants within the SAP treated sample and to precipitate and elute the purified DNA sample, which was then stored in a -20 °C freezer and used in the ligation step the next day.

Ligation of the insert DNA fragment into the plasmid vector

The ligation of the insert DNA fragment into the plasmid vector generates a recombinant DNA molecule containing the desired DNA sequence (i.e. SNAP-tagged β_1-adrenoceptor). To 500 µL sterile Eppendorf tubes, 7 µL of purified insert DNA and 1 µL of purified vector DNA were added (i.e. 7:1 insert:vector ratio). To attempt optimisation of the ligation step, ligation reaction with an insert:vector ratio of 6:2 were also set up. To each Eppendorf tube, 1 µL of ligase buffer and 1 µL of the ligase enzyme were added (10 µL total volume). The ligase enzyme forms new phosphodiester bonds between adjacent nucleotides in each DNA strand, thus joining two DNA molecules together. A control reaction was also set up, containing double-distilled water instead of insert DNA, but the same amount of vector DNA (i.e. 1 or 2 µL), ligase buffer and ligase enzyme. The "sticky" overhanging ends of the vector DNA sequence (created in the double-digest procedure) are different on either end of its sequence, which reduces the chance of vector re-ligation without an insert. This effect of vector re-ligation was tested in the control ligation reaction. The "sticky" ends of the vector, however, are compatible with the "sticky" ends created in the insert fragment DNA sequence, and form base-pairs through hydrogen bonding, which makes the ligation process more

efficient. The ligation mixtures were incubated for 5 hours at room temperature (circa 21 °C) and were subsequently used to transform competent *E. coli* cells.

Site-directed mutagenesis

The introduction of the D138A point mutation (changing a single base-pair in the DNA sequence, i.e. GAC to GCC) into the β_1AR DNA sequence of the pcDNA3.1(Neo)-SNAP-β_1AR vector was achieved using the QuickChange site-directed mutagenesis kit (Stratagene, Amsterdam, Netherlands), a PCR-based site-directed mutagenesis procedure, according to the manufacturer's instruction. Two exactly complementary mutagenic primers were designed, so that they both annealed to the same sequence on opposite DNA strands, containing the mismatched base (that introduces the desired mutation) in the centre of each primer sequence. Another consideration in primer design was the GC content (≥40 %), length (25-45 bases) and the melting temperature (T_m), which is ideally above 78 °C and was calculated using the below equation:

$$\mathbf{T_m = 81.5 + 0.41\ (\%\ GC) - \frac{675}{N} -\ \%\ mismatch} \qquad \text{(eq. 2)}$$

where N is the overall primer length in bases and the % GC and % mismatch content is simply obtained by dividing the number of GC bases or number of mismatched bases over N. A melting temperature of 78.4 °C was calculated for the designed β_{1D138A}AR primers (forward primer 5' GGACCTCAGTGGC CGTGCTGTGCGT 3'; reverse primer 5' ACGCACAGCACGGCCACTGAGGTCC 3').

For the mutagenesis PCR mixture 50 ng of the template DNA (pcDNA3.1(Neo)-SNAP-β_1AR), 125 ng of each of the mutagenic primers, 10 mM of dNTPs (final concentration), 2x PolyMate additive (1x final concentration), 10x *Pfu* DNA polymerase compatible buffer (1x final concentration) and 1 µL of proof-reading *Pfu* DNA polymerase were added to 200 µL PCR tubes, and made up to a total volume of 50 µL using ddH_2O.

The mutagenesis PCR cycle (Figure 2.3) follows a similar pattern as described above, starting with the denaturation step (double stranded template DNA denatures to single DNA strands; 95 °C, 30 seconds), followed by the hybridisation step (primers attach to the target DNA sequence; 58 °C, 2 minutes) and completed by the primer extension step (synthesis of complementary strands along the template DNA by *Pfu* DNA polymerase; 68 °C, 10 minutes). The hybridisation temperature is much lower than the T_m of the primers, which allows specific hybridisation of primers that contain a mismatched base to the target template DNA sequence. In addition, the elongation step is much longer in this PCR, because the entire plasmid DNA (containing the target DNA sequence) is amplified as an extension of the primers. This PCR cycle was repeated 17 times. The final PCR sample contains both the original (non-mutated) DNA template and the newly synthesised (mutated) DNA sequences.

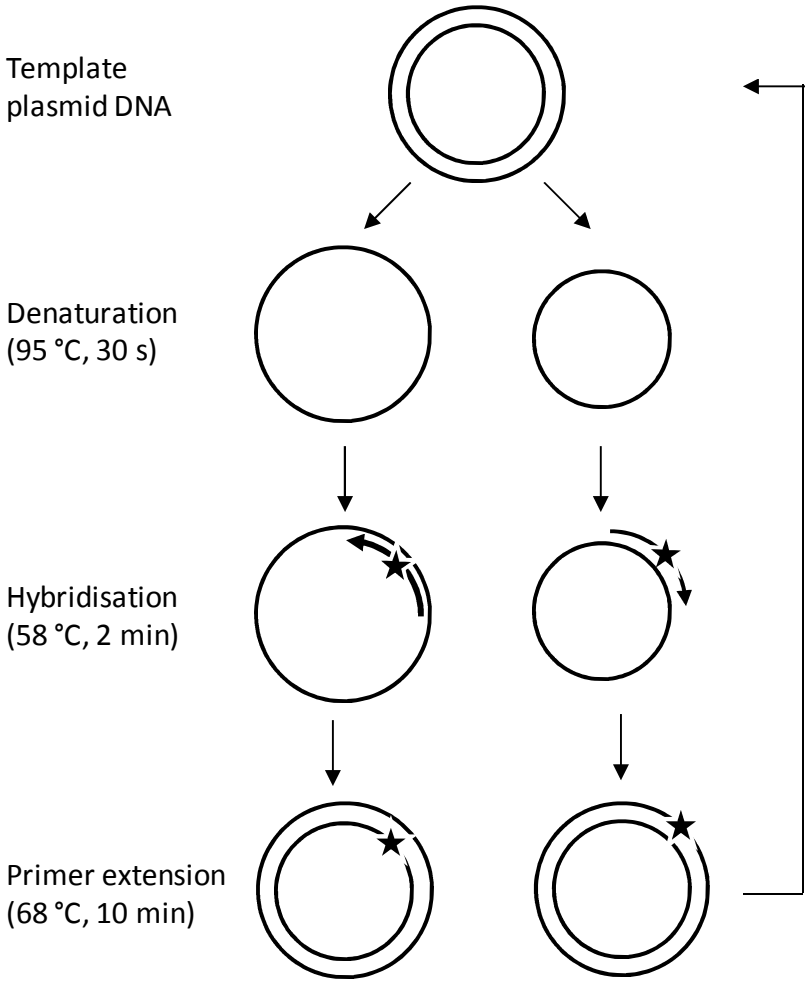

Figure 2.3 Schematic representation of the steps involved in the site-directed mutagenesis PCR cycle. Using a template plasmid DNA molecule that contains the target gene sequence to be mutated and mutagenic primers that hybridise to a specified region of the target sequence, a mutation is introduced into newly synthesised DNA sequences.

Following the PCR process, 1 µL of the *Dpn*I restriction enzyme was added to the final PCR mixture and thoroughly mixed into the sample. The PCR sample was then placed on a heating block for 1 hour at 37 °C. The *Dpn*I restriction enzyme digests methylated DNA (i.e. only the original (non-mutated) template DNA). The original template DNA was methylated as a result of DNA replication by E. coli cells (Casadesus *et al.*, 2006). 2 µL of the *Dpn*I-digested PCR sample were then immediately used to transform competent *E. coli* cells as described below.

DNA amplification and purification

Transformation of competent *E. coli* cells

First, the commercial chemically competent Top 10 F' *E. coli* cells were thawed gently on ice for 15-30 minutes. 25 µL of *E. coli* cells were then transferred into sterile pre-cooled 1.5mL Eppendorf tubes per transformation reaction. To these cells 1 µL of each ligation mix (including the vector-only control) were added and incubated on ice for a further 30 minutes. This allowed the DNA to associate with the cell exterior of the competent cells. Next, the Eppendorf tubes were held into a 42 °C water bath for 30 seconds to heat-shock the cells, which causes the DNA uptake by the cells into the cytoplasm. After that, the tubes were placed back on ice for 2 minutes, before 250 µL of room temperature SOC medium (nutrient-rich bacterial growth medium) was added to each Eppendorf tube (this was done near a Bunsen burner to maintain sterile conditions). The cells were incubated at 37 °C for 1 hour with gentle agitation (225 rpm) to allow time for plasmid replication and

expression. 200 µL of each Eppendorf tube were then plated out (near a Bunsen burner) onto pre-warmed agar selection plates containing 50 µg/mL of the antibiotic ampicillin and incubated at 37 °C overnight (o/n; circa 16 hours). Only cells that had successfully taken up the recombinant DNA molecule were able to express the ampicillin-resistance protein needed to survive in these conditions and thus, grow colonies. The pcDNA3.1 plasmid vector is able to independently replicate within the bacterial cell (high copy number) and is passed on to daughter cell with each cell division. The next day, the agar plates were placed in the fridge (to stop bacterial cell growth) for storage or single colonies were picked immediately to continue the amplification of plasmid vector DNA.

Mini-prep

At least two single *E. coli* colonies per positive agar plate (i.e. a ligation mix that contained vector and insert DNA was used to transform the *E. coli* cells) were picked using a sterile pipette tip near a Bunsen burner. The picked colonies were inoculated in 5 mL broth containing ampicillin at 37 °C o/n (circa 16 hours). This allowed the small bacterial colonies to continue to grow, and hence continued the amplification of the plasmid vector. The next day, 1.5 mL of each bacterial culture was used to isolate the plasmid DNA using a GenElute™ mini-prep kit (Sigma Aldrich, Gillingham, UK) according to the manufacturer's instructions. Briefly, a spin column method was used to lyse the bacterial cells, followed by removal of cell debris, protein and nucleic acid contamination, before the DNA sample was eluted. The mini-prep DNA

samples were then stored in a -20 °C freezer until used to generate maxi-prep DNA stocks.

A small sample of the purified plasmid DNA was then digested (using the two restriction enzymes used to facilitate the insertion of the target DNA sequence into the vector) and subsequently analysed using gel electrophoresis to confirm the presence and correct size of the insert. If the insert was of the expected size, a small DNA sample was sent to be sequenced to check the correct sequence of the DNA. If a site-directed mutagenesis PCR reaction was performed, the sequence containing the desired mutation was inserted to a native plasmid vector that does not contain potential mutations that may have been introduced during the PCR amplification reaction.

Maxi-prep

If the sequencing confirmed that the correct insert was present with the correct sequence, the mini-prep DNA (concentrations of circa 50 ng/µL) was then used to transform *E. coli* cells exactly as outlined above. Following transformation and o/n ampicillin agar plate incubation, two colonies were picked and inoculated in 5 mL broth for circa 8 hours at 37 °C. Following this, each 5 mL bacterial culture was transferred into 150 mL agar broth (containing 50 µg/mL ampicillin) and inoculated o/n (circa 16 hours) to grow to a larger colony, further amplifying the plasmid DNA copies. The next day, the plasmid DNA was isolated from each 150 mL bacterial culture using the GenElute™ maxi-prep kit (Sigma Aldrich, Gillingham, UK) according to the

manufacturer's instructions. In essence, it followed the same principles as outlined for the mini-prep procedure, but at a larger scale. The concentration of the isolated plasmid DNA was then determined using a UV spectrophotometer (Eppendorf BioPhotometer) that reads absorbance at 260 nm (a wavelength at which DNA absorbs light) and computes the DNA concentration form that value. The DNA samples (concentrations of circa 500 ng/μL) were then stored in a -20 °C freezer until used to transfect cells for experimentation.

DNA sequencing

To check the sequence of the inserted DNA sequence was correct and not altered at any point during the process of generating the receptor fusion protein, a small DNA sample (generally a mini-prep DNA sample) was sent to the DNA sequencing lab at the University of Nottingham. Primers used in the sequencing reactions included T7 forward primer (5'-TAATACGACTCATATA GGG-3'), BGH reverse primer (5'-TAGAAGGCACAGTCGAGG-3') and the β_1-adrenoceptor reverse primer (5'-GGCGGGAATTCCTACACCTTGGATTCCGAGG-3').

2.4 [^{3}H]cAMP accumulation assay

The accumulation of [^{3}H]cAMP is used as a measure of adenylyl cyclase activity in response to receptor activation, as intracellular pools of adenine nucleotides, such as ATP, are labelled with [^{3}H]adenine and the adenylyl cyclase enzyme facilitates the conversion of [^{3}H]ATP to [^{3}H]cAMP.

Column preparation

Dowex

Distilled water was added to Dowex AC '50' 50W-4X resin (hydrogen form) mesh 200-400 (1:1 (v/v)) and constantly stirred. Whilst this mix was being stirred, 2.4 mL were transferred into Bio-Rad "poly-prep" columns. Before each experiment the columns were regenerated with 10 mL 1 M HCl followed by 2 washes of 10 mL distilled water each. After each experiment the columns were cleaned using 10 mL 1 M NaCl followed by 2 washes of 10 mL distilled water to dissolve and remove any cell debris left following the experiment. Following this the rack holding the columns was placed in a tray containing enough water to come at least halfway up each column. This ensured that the columns did not dry out before the next experiment.

Alumina

To each Bio-Rad "poly-prep" column 0.6 g of Neutral alumina WN-3 was added. Before each experiment the columns were prepared with 2 washes of 10 mL 100 mM imidazole. This was repeated after each experiment to clean the columns.

Assay

This was based on the assay developed by Donaldson *et al.* (1988). Cells were seeded into 24-well plates as described above (see *Cell culture*). Where cells transiently transfected with bimolecular fluorescence complementation (BiFC) DNA constructs were used, cells from a T75 flask were first transiently

transfected and then seeded into 24-well plates (see *Cell culture*) and then prepared as described below (*Confocal microscopy*). On the day of the experiment, 100 µL of growth medium containing 1 µL [^{3}H]adenine per well (i.e. 25 µL [^{3}H]adenine in 2.5 mL growth medium) was added to each well. The assay plate was then incubated for 2 hours at 37 °C in a cell culture incubator to allow [^{3}H]adenine to label intracellular pools of adenine nucleotides. Following this, the cells were washed once by the addition and removal of 400 µL of growth medium to remove extracellular [^{3}H]adenine. Then, 450 µL of growth medium containing 1 mM IBMX (3-isobutyl-1-methylxanthine, a phosphodiesterase inhibitor) was added to each well. An additional 50 µL of growth medium containing 1 mM IBMX was added to negative control wells (unstimulated cells, i.e. basal readings). The growth medium containing 1 mM IBMX was used to make up the desired concentrations of ligands used in the experiment. 50 µL of increasing agonist concentrations were added to designated wells and 50 µL of a chosen agonist concentration were added to positive control wells. If an antagonist was used, 50 µL of antagonist and 50 µL of agonist were added simultaneously to 400 µL of growth medium containing 1 mM IBMX per well. The total volume per well was 500 µL. The assay plate was incubated for 5 hours at 37 °C in a cell culture incubator. Finally, the reaction was stopped by the addition of 50 µL 1 M HCl to all wells, followed by the addition of 100 µL of [^{14}C]cAMP solution (0.25 µL [^{14}C]cAMP in 2.5 mL ddH_2O per plate) to all wells, before freezing and storing of the assay plates and the remaining [^{14}C]cAMP solution in a radioactivity-

designated -20 °C freezer until transferring samples to the columns for [^{3}H]cAMP and [^{14}C]cAMP recovery.

[^{3}H]cAMP and [^{14}C]cAMP recovery

The method of sequential Dowex and alumina chromatography was based on that described by Salomon *et al.* (1974), and was used to resolve [^{3}H]cAMP from [^{3}H]ATP. The assay plates were thawed at room temperature and the whole well contents (650 µL) were transferred to the corresponding Dowex columns. The negatively charged nucleotides (cAMP, AMP, ADP and ATP molecules) are adsorbed into the resin of the columns, even though the columns are themselves negatively charged. Following the addition of 3 mL of distilled water, the most negatively charged nucleotides (ATP and ADP) are pushed through the columns first as the repulsion of the negative charges between these nucleotides and the column is the greatest. The columns were then placed directly above the alumina columns and the remaining nucleotides ([^{3}H]cAMP, [^{14}C]cAMP, unlabelled cAMP and AMP) were eluted into the alumina columns using 6 mL distilled water. The alumina columns were then placed directly over 20 mL scintillation vials and 5 mL 0.1 M imidazole was added to each column to elute the cAMP molecules. 100 µL of [^{14}C]cAMP was also directly added (i.e. did not pass through columns) to three additional scintillation vials representing 100 % (maximum possible) [^{14}C]cAMP detection control samples (which can be compared to actual detection of [^{14}C]cAMP recovered through columns). To all scintillation vials, 8 mL of scintillation fluid was added. The vials were capped and then counted

on a β-counter capable of dual counting both [^{3}H]cAMP and [^{14}]cAMP simultaneously in 4 minutes per vial.

β-particle counting and dual counting

The [^{14}C] and [^{3}H] radioisotopes decay by emitting β-particles, which transfer energy to scintillators, which in turn re-emit the absorbed energy in the form of light. These emitted photons were then counted using a scintillation counter to give counts per minute (cpm). A control radioactive sample was brought alongside each vial and the efficiency of the scintillation fluid/elute mix was tested. From this efficiency, the counts per minutes were then corrected to disintegrations per minute (dpm) to give a more accurate indication of the total radioactive decay occurring in each vial. Dual counting relies on the two different isotopes decaying with sufficiently different energies. The β-particles emitted from [^{14}C] have more energy than those from [^{3}H] and so the shower of light produced by these β-particles is recognised by the counter as a different species from that of the [^{3}H] β-particles.

The [^{3}H]cAMP accumulation data shown in this thesis is expressed in dpm units where raw (actual) data is shown. Where necessary for comparison across different assay plates, data was normalised using the negative (unstimulated cells, i.e. basal read = 0 %) and positive (chosen agonist concentration, i.e. stimulated cells = 100 %) control data. The [^{14}C]cAMP 100% [^{14}C]cAMP detection control samples allowed calculation of the efficiency of

the columns to recover [^{14}C]cAMP by comparing dpm values obtained from experimental samples to those obtained in the control vials. This helped identify outliers in the [^{3}H]cAMP data set that were due to column inefficiency. Fresh Dowex and alumina columns were prepared as described above, when necessary.

2.5 CRE-mediated SPAP transcription assay

CHO cells expressing the CRE-SPAP reporter gene construct were used in this assay. In these cells, the gene for SPAP (secreted placental alkaline phosphatase) was under the control of a cAMP response element (CRE), thus facilitating SPAP transcription in the presence of cAMP. This assay was used as a downstream measurement of cAMP production in response to receptor activation, and was based on the method developed by McDonnell *et al.* (1998) and further optimised for the investigating of the pharmacology of β-adrenoceptor ligands at β-adrenoceptors by Baker *et al.* (2004). Cells were seeded into 96-well plates two days prior to experimentation (as described in *Cell culture*). The following day, the cells were serum starved, which minimised further production of cAMP by the cells that are normally stimulated by the growth medium to survive, grow and divide. This reduces cAMP interference in the SPAP gene reporter assay. The growth medium was removed using a sterile pipette tip attached to the vacuum pump in the cell culture incubator. A volume of 100 µL serum free medium (DMEM/F12 supplemented with 2 mM L-glutamine only) was added to each well and the plate was then returned to the cell culture incubator until the following day.

On the day of the experiment, the cells were used in either agonist or antagonist mode experiments.

Agonist mode

On the day of experimentation, the serum-free medium was removed and replaced with 90 µL fresh serum-free medium. Then, 10 µL of increasing concentrations of agonist (10x final concentrations) were added to the serum-free media in the designated wells of the 96-well plate (at least triplicate determinations of each condition). 10 µL serum-free medium was added to 6 negative control wells (i.e. unstimulated cells) and 10 µL of 100 µM cimaterol (i.e. 10 µM final concentration) was added to 6 positive control wells (i.e. maximally stimulated cells). The 96-well plate was then incubated for 5 hours at 37 °C in a humidified atmosphere of 5 % CO_2/95 % air. After the 5 hour incubation, the medium and drugs were removed and replaced with 40 µL of fresh serum-free media and incubated for a further hour to collect the (heat resistant) secreted placental alkaline phosphatase. Then, the assay plate was heated to 65 °C in an air oven for 30 minutes to destroy any endogenous alkaline phosphatases. Following this, the plate was cooled to 21 ˚C before the addition of 100 µL of 5 mM *p*-nitrophenylphosphate (PNPP) in diethanolamine (DEA) buffer (100 mM DEA, 280 mM NaCl, 0.5 mM $MgCl_2.6H_2O$, pH 9.85) to each well. The assay plate was then incubated at 37 °C in air for 20 minutes, in which the SPAP enzyme hydrolyses its substrate PNPP to the yellow *p*-nitrophenol (PNP) under alkaline conditions (created by the basic DEA buffer). Thus, the CRE-dependent SPAP reporter activity could be

monitored by following the colour change from pink to yellow in cell culture serum-free medium.

Antagonist mode

To establish affinity values of antagonists, agonist concentration-response curves in the absence and presence of one or more fixed antagonist concentrations were performed. On the day of experimentation, the serum-free medium was removed and replaced with 80 µL fresh serum-free medium. Then, cells were incubated with 10 µL of serum-free medium (control agonist concentration-response curve in the absence of antagonist) and the desired fixed concentrations of antagonist (10x final concentration) for 1 h at 37 °C in a 5 % CO_2/95 % air atmosphere. After 1 hour, 10 µL of increasing concentrations of the agonist (10x final concentration) was added to the designated wells. 10 µL of serum-free medium was added to negative control wells (i.e. unstimulated cells) and antagonist control wells (i.e. wells that contained the fixed concentration of the antagonist, but no agonist to establish effects of the antagonist on its own). 10 µL of 100 µM cimaterol was added to positive control wells (i.e. maximally stimulated cells). All determinations were triplicates. Following these additions, the assay plate was incubated for a further 5 hours at 37 °C in a 5% CO_2/95 % air atmosphere. After this 5 hour agonist incubation step, the assay follows the same protocol to collect and detect the CRE-mediated SPAP levels as described above in *Agonist mode*.

Data collection

Once the hydrolysis of PNPP to the yellow PNP had taken place and the associated colour change had occurred following a 20 minute incubation time (unless otherwise specified), absorbance was read at 405 nm using an MRX plate reader (Dynatech Labs, Chantilly, VA) to quantify the CRE-dependent SPAP reporter activity. Optical density (OD) readings were obtained with higher readings corresponding to higher levels of yellow PNP and thus, higher amounts of SPAP present in that particular well as a result of higher cAMP levels. The OD readings can be converted to SPAP concentrations in mU per mL (McDonnell *et al.*, 1998) using the following equation:

$$[\mathbf{SPAP}](\mathbf{mU/mL}) = \mathbf{A/18.5tV} \qquad \text{(eq. 3)}$$

where A = optical density, t = time of incubation and V = volume of the sample (40 µL in all experiments). Since the optical density readings vary with the time of incubation, the incubation times of every assay plate were recorded.

In addition, any fluctuations in temperature during the experiment also had marked effects on the transcription/translation and secretion of SPAP. Potential deviations from the optimal 37 °C temperature of the assay plate and assay solutions (e.g. serum-free medium and ligand solutions) thus contribute to variations in final optical density readings. This is why data shown in this thesis are either actual raw data (i.e. unmodified optical density readings) or data that was normalised to control data obtained on the same

assay plate (generally expressed in percentages with unstimulated cells representing 0 % and the 10 μM cimaterol response representing 100 %).

2.6 Confocal microscopy

HEPES-buffered saline solution (HBSS; 147 mM NaCl, 24 mM KCl, 1.3 mM $CaCl_2$, 1 mM $MgSO_4$, 10 mM HEPES, 2 mM sodium pyruvate, 1.43 mM $NaHCO_3$, pH 7.45) containing 4.5 mM D-glucose was used as the imaging buffer in all experiments outlined below and was pre-warmed before use to the stated temperature in which the experiments were carried out. Imaging buffer was used to dilute both BODIPY-TMR-CGP and BODIPY630/650-S-PEG(8)-propranolol fluorescent ligands from a 1 mM DMSO stock to achieve the desired concentrations and to dilute the DMSO content to concentration ≤ 0.01 % (v/v; final concentrations), reducing potential harmful effects of this solvent on the cells (Brayton, 1986). Incubation of cells in a cell culture incubator refers to a 5 % CO_2/95 % air atmosphere.

SNAP-tag labelling

Cells expressing SNAP-tagged wild-type or D138A mutant β_1-adrenoceptors were grown to confluence in 8-well plates as described above (see *Cell culture*). Prior to experimentation, the growth medium was removed off the cells and replaced with fresh medium containing 1 μM of the cell impermeable SNAP-tag substrate SNAP-Surface® 488 (BG-488; New England Biolabs, Ipswich, MA). The cells were then incubated at 37 °C in a cell culture incubator for 30 minutes in the dark (unless otherwise stated). Following this,

the medium containing the SNAP-tag substrate was removed and the cells were washed twice in imaging buffer (pre-warmed to 37 °C), before incubating the cells in 200 µL imaging buffer in a cell culture incubator (37 °C) for a further 30 minutes in the dark. Finally, the imaging buffer was replaced with 400 µL fresh imaging buffer and the cells used immediately for imaging.

Saturation binding experiments

The protocol used here was based on that described by Baker *et al.* (2003d) for the BODIPY-TMR-CGP ligand on CHO cells expressing the β_2-adrenoceptor. BODIPY-TMR-CGP and BODIPY630/650-S-PEG8-propranolol saturation binding experiments were performed at room temperature (circa 21 °C) using CHO-β_1-CS and CHO-β_2-CS cells seeded into 8-well plates (as described in *Cell culture*). Immediately prior to experimentation, the growth medium was removed and the cells were then washed once with imaging buffer, before the addition of 360 µL imaging buffer to each well. The 8-well plate was placed onto the microscope stage and 40 µL (i.e. 10x dilution to final concentration) of a range of concentrations from 3-100 nM (final concentrations) of either BODIPY-TMR-CGP or BODIPY630/650-S-PEG8-propranolol were added to designated wells. The cells were exposed to the fluorescent ligand for 10 minutes before imaging. To ensure strict exposure time for all cells and to allow circa 5 minutes to image each well, the addition of fluorescent ligands to designated wells was staggered.

Competition binding experiments

This method was also based on that described by Baker *et al.* (2003d) for the BODIPY-TMR-CGP ligand on CHO cells expressing β_2-adrenoceptors. BODIPY-TMR-CGP and BODIPY630/650-S-PEG(8)-propranolol inhibition binding experiments were performed at room temperature (circa 21 °C) using CHO-β_1-CS and CHO-β_2-CS cells seeded into 8-well plates (as described in *Cell culture*). CHO-CS cells were used as a negative control. On the day of experimentation, the growth medium was removed and the cells washed once with pre-warmed imaging buffer, before 360 µL of imaging buffer was added to the positive control well, measuring total binding, and the negative control well (containing CHO-CS cells), measuring non-specific binding levels. 360 µL of imaging buffer containing increasing concentrations of the competitor (0.01-1000 nM) was added to the designated wells. The cells were then incubated for 30 minutes at 37 °C in a cell culture incubator. Following this, the plate was mounted on the microscope stage and the experiment started by the addition of 40 µL of the desired concentration of the fluorescent ligand to the first well, which was imaged after a further 10 minutes. To ensure the same exposure time of cells to the fluorescent ligand in all wells and to allow a 5 minute imaging time for each well, the addition of the fluorescent ligand and imaging of the wells was staggered and carefully timed. Where cells expressing SNAP-tagged receptors were used, the SNAP-tag labelling was performed first (as described above) and the 30 minute incubation step following the washout of the SNAP-tag substrate was substituted for the 30 minute incubation of the competitor ligand.

Internalisation experiments

For internalisation experiments, SNAP-tagged β_1-adrenoceptor cells were seeded into 8-well plates as described in *Cell culture* and the SNAP-tagged receptors were labelled as described above, but using 360 µL imaging buffer in the final incubation step. Next, the 8-well plate was mounted onto the microscope stage. The unlabelled ligands to be used were diluted in imaging buffer to the desired concentrations (10x final concentration). Before addition of any ligands, the first well was imaged to allow optimisation of microscope settings (laser power, gain and offset), which were then kept constant for all other wells throughout the experiment. Following this, 40 µL of the ligand was added to the first well and imaged immediately (at a different site than that used to determine the microscope settings; time point 0 minutes). After 60 minutes incubation of the ligand, the well was imaged again (time point 60 minutes).

Bimolecular fluorescence complementation (BiFC) experiments

Using the bimolecular fluorescence complementation (BiFC) approach, two non-fluorescent N- and C-terminal halves of a fluorescence protein (e.g. yellow fluorescence protein, YFP) are attached to two potentially interacting proteins (e.g. dimerising receptors). Upon receptor dimerisation, the two non-fluorescent YFP halves then come together and reconstitute the full length fluorescent YFP, thus the detection of YFP fluorescence indicates an interaction of the two proteins studied and was used in this thesis to detect β_1-adrenoceptor homodimers in living cells. For this, CHO-K1 cells were

seeded into wells of an 8-well plate (day 1) and transiently transfected with YFP_N-tagged and YFP_C-tagged β_1-adrenoceptor recombinant DNA the following day (day 2) as described in *Generation of new cell lines*. The next day (day 3), the transfection medium was removed off the cells and replaced with fresh growth medium, before the cells were placed back into the cell culture incubator (37 °C, 5 % CO_2/95 % air atmosphere). After circa 6 hours, the cells were then moved into a 30 °C incubator (5 % CO_2/95 % air atmosphere) to allow the maturation of the fluorophore following correct protein folding. On day 4, the cells were used for experimentation.

Confocal imaging

All confocal imaging experiments were performed on the Zeiss LSM710 confocal microscope (unless otherwise stated) with a Zeiss 40x1.3NA oil immersion lens (Zeiss, Jena, Germany). The laser that emits light at a wavelength closest to the wavelength needed to cause maximum excitation of the chosen fluorophore was used. Upon excitation, the fluorophore then emits light itself at a longer wavelength, which is captured using the appropriate wavelength filter. The fluorophores, lasers and microscope settings used throughout this thesis are summarized in Table 2.2. The pinhole diameter used in all confocal experiments was 1 airy unit (AU), which represents a near optimal setting that reduces out-of-focus emission contributions without the loss of intensity of the measured fluorophore. The pinhole setting and the laser wavelength used determine the optical slice thickness (z section; with 1 AU pinhole settings, the shorter the wavelength,

the thinner the optical slice). The first well of an 8-well plate was used for calibration in each experiment. The cells were imaged and the range indicator was set to determine brightness (detector gain) of the bound ligand and the contrast (amplitude offset) such that pixels were either over-saturated or below the detection limit. The maximal image brightness was then set to a value greater than that achieved with the control well so that brighter binding could be detected. The confocal settings (laser power, digital values for image brightness, background and contrast) were then kept constant for the rest of the experimental day. This allowed direct comparisons between wells to be made. This area of the first well used to determine the settings was subjected to laser exposure much more than any other area and hence had potential for more photobleaching. A second area of the well was therefore selected for the first image of the control well of that plate.

Table 2.2 Excitation and emission wavelengths of the fluorescent molecules used in studies within this thesis are listed together with the lasers and microscope settings used to image cells treated with these fluorescent molecules.

	fluorophore excitation/emission	laser type	laser wavelength	Microscope settings used			
				emission filter	gain	offset	optical slice
BG-488	506/526	Argon	488 nm	505 nm long-pass	600-1100	0-1	0.37 µm
BODIPY-TMR-CGP	545/570	Helium-Neon	543 nm	550 nm long-pass	600-1100	0-1	0.40 µm
BODIPY-TMR-CGP	545/570	Helium-Neon	561 nm	565 nm long-pass	600-1100	0-1	0.41 µm
BODIPY630/650-S-PEG(8)-propranolol	630/650	Helium-Neon	633 nm	650 nm long-pass	600-1100	0-1	0.46 µm
yellow fluorescent protein	514/527	Argon	488 nm	505 nm long-pass	600-1100	0-1	0.37 µm

Where two lasers were used at the same time (e.g. 488 nm and 561 nm lasers to image BODIPY-TMR-CGP binding to SNAP-tagged β_1-adrenoceptors), the multitracking facility in the Zeiss imaging software was used. This allowed the sample to be illuminated with one laser at a time in order to avoid any bleed through of the laser used (e.g. 488 nm) causing excitation of the fluorophore used (e.g. BODIPY-TMR-CGP). For the same reason, the emission filter of the higher energy fluorophore was also adjusted (e.g. 505-550 nm band-pass filter was used to capture BG-488 fluorescence). Furthermore, the pinhole (thus the optical slice thickness) was set for the highest wavelength laser used (i.e. 561 nm laser, if both 488 and 561 nm laser where used) and the optical slice thickness was then matched for the second laser. Using two lasers also increased the total well laser exposure time. To correct for that, fewer frames were taken (4-8 frame scans, 1024x1024 pixels), thus limiting each image to approximately one minute laser exposure.

Data collection

Using 8-well plates limits the number of experimental conditions that can be tested in a given experiment. In the experiments described above, every well represented a different experimental condition (e.g. different concentration of fluorescent ligand or inhibitor ligand or internalising ligand). However, 2-4 different areas were imaged within a given well and each image was analysed as described below, thus providing duplicate to quadruplicate measures per condition within a single experiment. The *n* numbers stated throughout this

thesis for these experiments, however, refer to number of separate experiments set up and carried out (i.e. different experimental days).

Total image intensity analysis

All images taken on the Zeiss LSM710 microscope were captured using an 8bit greyscale, which allows for 256 different intensity levels of a given pixel (from 0-255; where 0 represents the weakest and 255 the strongest fluorescence intensity). All data analysis was carried out using Zeiss Zen2010 software (Carl Zeiss, Jena, Germany). This provides the frequency of pixels recorded at each of the 256 greyscale intensities for each image taken. The total image intensity (arbitrary units) is calculated as the sum of the product of frequency x greyscale intensity for each of the 256 grey scale intensity values. This value was then divided by the total number of pixels per image (1024x1024 for the total image) to give the average pixel intensity.

Region of interest (ROI) analysis

Where stated, regions of interest were drawn around the membrane of a given number of cells (stated for each experiment) in each image taken. The Zeiss software provides the frequency of pixels recorded at the 256 greyscale intensities and the number of pixels in the combined area of the drawn regions of interest of one image, and thus allows quantitative analysis as described above using average pixel intensities that refer to the regions of interest only.

Co-localisation analysis

Where two different wavelengths were used to image two different fluorescently labelled molecules (e.g. SNAP-tagged β_1-adrenoceptor using 488 nm and BODIPY-TMR-CGP binding using 561 nm excitation wavelengths), the individual images obtained for each wavelength were merged. These images are shown in colour, where yellow pixels clearly identify regions of spatial overlap of the two fluorescently labelled molecules. The fluorescence intensities of each individual channel, however, are shown in monochrome to allow better visualisation of the greyscale intensities of the pixels in each channel (from 0, i.e. black, to 255, i.e. white pixels).

Where used, a co-localisation plot was obtained and a crosshair placed on this plot to highlight the region of co-localised pixels (region 3). To do this, a region of interest was drawn on the background of the image away from the cells and the average intensity and its standard deviation (SD) of this region were collected in each of the two channels. The crosshair was then placed to the intensity levels calculated from adding the average background pixel intensity to 2x its standard deviation. This represents the background fluorescent intensity. Pixels with intensity values greater than those calculated in both channels will be located in region 3 and represent co-localised pixels (i.e. yellow pixels in the merged image).

2.7 ImageXpress Ultra confocal plate reader

Assay

The protocol of this assay was based on that described by Stoddart *et al.* (2012). CHO-β_1-CS or CHO-β_2-CS cells were seeded into 60 wells of a thin clear-bottomed black wall 96 well plate (Greiner Bio-One Ltd, Stonehouse, UK) 18-24 hours prior to experimentation (see *Cell culture*). The outermost wells of the 96-well plate were excluded to avoid edge effects of confocal analysis of the wells, leaving 60 wells for experimentation. On the day of the experiment, the growth medium was removed and the cells were washed once by the addition and removal of 100 µL pre-warmed imaging buffer (HBSS containing 4.5 mM D-glucose), before 80 µL of imaging buffer was pipetted into each of the 60 wells. All ligands used in these experiments were diluted in imaging buffer to the desired concentrations and 10 µL of increasing concentrations of competitor ligand (i.e. at 10x final concentration) were added to the designated wells on the assay plate. 10 µL of imaging buffer were also added to positive control (measuring total binding of fluorescent ligand to CHO-β_1-CS or CHO-β_2-CS cells). The assay plate was then incubated for 30 minutes (unless otherwise stated) at 37 °C in a 0 % CO_2/100 % air atmosphere cell culture incubator. Following this, 10 µL of the desired fixed concentration of BODIPY-TMR-CGP was added to all 60 wells and the plate was then incubated for 1 hour at room temperature (circa 21 °C) in the dark (unless otherwise stated). After 1 hour, the imaging buffer containing all ligands was removed, the cells were washed once by addition and removal of

100 µL imaging buffer, before 100 µL imaging buffer was added to each well. Following this, the assay plate was immediately read on the ImageXpress (IX) Ultra confocal plate reader. A 561 nm (40 % laser power) was used to excite BODIPY-TMR-CGP and emission was captured through a 565-605 nm band-pass filter. BODIPY630/650-S-PEG8-propranolol was excited using a 635 nm laser (20 % laser power) with emission collected through a 640-685 nm band-pass filter. The focus (z position of the bottom of the first well) and laser gain settings used were adjusted and optimized for each plate. The raw data of different assay plates can therefore not be directly compared. In order to do that and to be able to group data from different experiments, the data was normalized as a percentage of total (100 %) and non-specific binding values (0 %; fluorescent ligand binding to CHO-β_1-CS or CHO-β_2-CS cells in the presence of the highest concentration of inhibitor compound, e.g. 100 µM) determined on each plate.

Automated image analysis

The IX Ultra confocal plate reader is equipped with a Plan Fluor 40x NA0.6 extra-long working distance objective and automatically captured confocal images in 16bit greyscale at four different central sites in each well, taking circa 20 minute to read an entire plate (60 wells). Total image intensities of each image were then obtained using a multiwavelength cell scoring algorithm within the MetaXpress 2.0 software (Molecular Devices, Sunnyvale, USA). This analysis provided integrated intensity values for each imaged site per well and experimental conditions were tested in duplicates (i.e. 8

separate images were analysed for a given experimental condition in a single experiment).

2.8 PHERAstar *FS* plate reader

This assay was performed using the above protocol for measuring fluorescent ligand binding to living cells on the ImageXpress Ultra confocal plate reader. The same materials, ligands and solutions were used. This was done to allow direct comparison of fluorescent ligand binding data obtained on two different plate readers. Following the assay, the assay plate was first read on the PHERAstar *FS* plate reader (BMG Labtech GmbH, Ortenberg, Germany). The optimal focal height (z positioning of the plate), gain setting and exposure time were determined automatically for every plate. A high energy Xenon flash lamp (spectral range of 230-750 nm) and a 545 nm filter were used to excite BODIPY-TMR-CGP with BODIPY-TMR-CGP emission being detected by photomultiplier tubes. The fluorescence intensity in each well was assessed in 81 reads per well in a read time of circa 3 minutes per plate (60 wells). The PHERAstar *FS* data output is in numerical (arbitrary range of 0-260,000) and visual form (e.g. rainbow colouring with the red and blue colours representing high and low levels of binding of the fluorescent ligand, respectively).

2.9 Confocal perfusion system

The association and dissociation of a fluorescent ligand was visualised and quantified at the single-cell level using a perfusion system as described by May *et al.* (2010a) in conjunction with either the Zeiss LSM510 or the Zeiss

LSM710 confocal microscope. A pressure pump was connected to a closed perfusion system, which allowed the constant perfusion of fluid from six reservoirs through an imaging chamber and into a runoff (Figure 2.4). Cells were grown to near confluence on 32 mm glass coverslips placed into wells of 6-well plates (see *Cell culture*) one day prior to experimentation. Where transient transfection of cells with BiFC DNA constructs was required, the cells were plated out three days prior to experimentation and then prepared as described above (*see Confocal microscopy*). On the day of the experiment, the growth medium was removed from one 6-well plate and the wells were washed once in pre-warmed (37 °C) imaging buffer (HBSS containing 4.5 mM D-glucose) and subsequently kept in 2 mL imaging buffer at 37 °C until used for experimentation (the cells were kept in these conditions for no longer than 2 hours). To start experimentation, the coverslip was placed into a specially designed imaging chamber, which was tightly closed and then placed onto a heated (37 °C) microscope stage where it was connected to tubes on either side that facilitated the flow of fluid through the imaging chamber. Following this, the reservoir supplying the imaging buffer was switched on to perfuse over the cells in a laminar flow imaging chamber that holds a total volume of 400 µL, thus allowing ≥ 12 fluid exchanges per min at a flow rate of ≥ 5 mL/min (May *et al.*, 2010a). Following this, an area of cells was selected using the eyepiece of the microscope and the required laser, emission filters and time series mode were set up. BODIPY-TMR-CGP was excited using a 543 nm Helium-Neon laser on the Zeiss LSM510 microscope and a 561 nm Helium-Neon laser at the Zeiss LSM710 microscope with emission collected through a

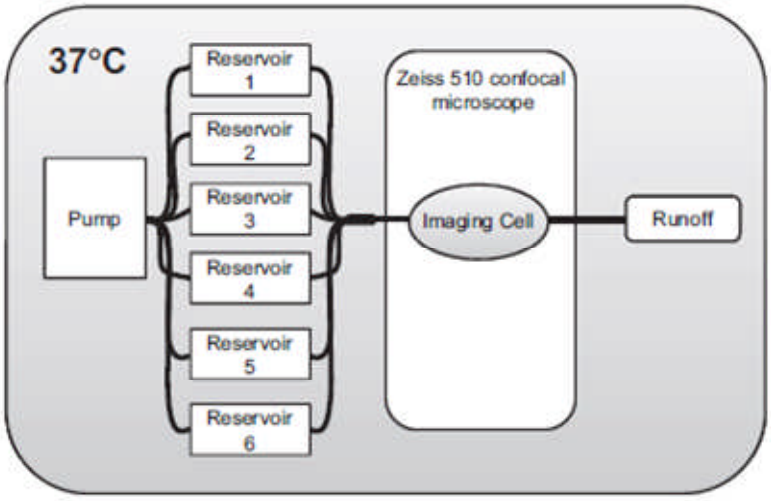

Figure 2.4 The set-up of the closed perfusion system in conjunction with the Zeiss LSM510 confocal microscope. The pump allows the flow of fluid at constant pressure from a reservoir through the imaging chamber (imaging cell) and into a runoff. The entire system is temperature-controlled and kept at 37 °C. Figure taken from May *et al.* (2010b).

560 and 565 nm long-pass filter, respectively; BODIPY630/650-S-PEG8-propranolol was excited using a 633 nm argon laser and a 650 nm long-pass filter at both confocal microscopes. Where cells transiently transfected with BiFC DNA constructs were used, YFP and BODIPY-TMR-CGP were excited using a 488 nm argon laser and 561 nm Helium-Neon laser, respectively with emission being captured through a 505-550 nm narrow band-pass and a 565 nm long band-pass filter, respectively (these experiments were carried out using the Zeiss LSM710 confocal microscope).

Association and dissociation kinetic binding experiments

The association and dissociation kinetics of increasing concentrations (3-100 nM) of BODIPY-TMR-CGP and BODIPY630/650-S-PEG8-propranolol were investigated. Both fluorescent ligands used in perfusion experiments were diluted in ddH_2O to working concentrations (100x desired final concentrations) and subsequently kept on ice. When used, 400 µL of the ligand (at working concentration) was added to 40 mL imaging buffer in a designated reservoir. First, a 20-30 second baseline fluorescence read was taken in the presence of only imaging buffer. To initiate association of the fluorescent ligand, the flow of fluid from the reservoir containing imaging buffer (reservoir 1) was stopped and the reservoir containing the fluorescent ligand (reservoir 2) was switched on for a given length of time (e.g. 5 minutes). After that, flow of fluid from reservoir 2 was stopped and reservoir 1 was again switched on to begin dissociation of the fluorescent ligand (generally performed for the same amount of time as the association). Thus, this system uses infinite dilution to

remove the labelled ligand, which is possible due a sharp change in concentration caused by the selected pressure and flow rate for these experiments (May *et al.*, 2010a). Throughout the experiment (from baseline to dissociation read) transmitted light and fluorescence images were captured every 2-3 seconds (512x512 pixels, 2 averages per images). The first glass coverslip (slide) was used to establish the optimal microscope settings (laser power, gain and offset) as described above in *Confocal microscopy*. These settings were then kept constant within each experiment and between experiments performed on different days using both CHO-β_1-CS (used to measure total binding) and CHO-CS cells (used to measure non-specific binding levels) to allow for direct comparison of total and non-specific fluorescent ligand binding levels at the different concentrations tested.

Dissociation kinetic binding experiments in the presence of unlabelled ligands

All unlabelled ligands were diluted in ddH_2O to working concentrations (10,000x desired final concentration) and 4 µL of the ligand at working concentration was added to 40 mL imaging buffer in designated reservoir (reservoir 3). The association of the fluorescent ligand was achieved as outlined above. Following association, the flow of fluid from reservoir 2 (imaging buffer containing the fluorescent ligand; as defined above) was stopped and reservoir 3 was switched on, thus initiating the dissociation of the fluorescent ligand in the presence of an unlabelled ligand (for a given amount of time, e.g. 5 minutes). Control dissociation reads in the absence of

any unlabelled ligand were performed on each experimental day. Transmitted light and fluorescence images were captured every 2-3 seconds and the microscope settings were set using the first slide (as described above) and then kept constant within each experiment, but adjusted, if necessary, between experiments on different days. Dissociation kinetic data was therefore expressed in % fluorescent intensity, allowing experimental data from different days to be grouped.

Data collection

During each experiment, 8bit images recording the fluorescence intensity of the fluorescent ligand binding to cells in the perfusion imaging chamber were captured. To analyse and quantify the association and dissociation kinetics of the fluorescent ligands, regions of interest (ROIs) were drawn around the membranes of ten single cells of each imaged slide. Cells containing oversaturated pixels were identified using the range palette and were excluded from the analysis. For cells with low fluorescent intensity, the transmitted light image was used to aid cell selection. The Zeiss software then provided average pixel intensity values for each ROI (10 ROIs per slide), which were plotted against time. The changes in fluorescent intensity over time were then analysed to obtain association and dissociation rates (see *Data analysis*) for either each single cell or per slide (i.e. grouped data from 10 single cells). For kinetic data shown in this thesis, an *n* number of 1 refers to data obtained from one slide. Within each experiment, each condition (e.g. concentration of unlabelled ligand) was investigated on at least two slides.

Throughout this thesis, the number of different experimental days, in which the *n* numbers were acquired, is also stated.

2.10 Data analysis

All data were fitted using the GraphPad Prism 5.0 software (San Diego, USA) using non-linear regression analysis (unless otherwise stated).

Functional experiments

Agonist concentration responses

Sigmoidal agonist concentration-response curves were fitted to the following equation:

$$\mathbf{Response} = (\mathbf{E_{MAX}} \cdot [\mathbf{agonist}])/([\mathbf{agonist}] + \mathbf{EC_{50}}) \quad \text{(eq. 4)}$$

Where E_{MAX} is the maximal system response, [agonist] is the concentration of the agonist, and EC_{50} is the concentration that produces 50 % of the maximal system response.

CGP 12177 two site functional response curves

CGP 12177 concentration-response curves obtained in the presence of a fixed concentration of agonist were fitted using a two-site analysis equation:

$$\mathbf{Response} = \mathbf{Basal} + (\mathbf{A_R} - \mathbf{Basal})\left[\mathbf{1} - \frac{[\mathbf{C}]}{([\mathbf{C}]+\mathbf{IC_{50}})}\right] + \mathbf{C_{MAX}}\left[\frac{[\mathbf{C}]}{([\mathbf{C}]+\mathbf{EC_{50}})}\right] \quad \text{(eq. 5)}$$

where Basal is the response produced in the absence of any agonist, A_R is the measured response to the fixed concentration of agonist, [C] is the concentration of competitor (CGP 12177), IC_{50} is the concentration of competitor required to inhibit the agonist-stimulation by 50 %, C_{MAX} is the maximal stimulation produced by the competitor and EC_{50} is the concentration of the competitor (CGP 12177) required to produce 50 % of the maximal stimulation of that competitor.

Antagonist K_D value calculations

Agonist concentration-response curves in the absence and presence of a fixed concentration of antagonist were fitted to eq. 4. Antagonist equilibrium dissociation constants (K_D values) were then determined by observing the shift in the concentration-response curve by a fixed antagonist concentration (assuming competitive antagonism and equilibrium assay conditions) using the equation below:

$$\mathbf{DR = 1 + [B]/K_D} \qquad \text{(eq. 6)}$$

where K_D is as defined above, and DR (dose-ratio) is the ratio of the concentrations of agonist required to produce the same response in the absence and presence of a fixed concentration of antagonist [B] (Figure 2.5; Arunlakshana *et al.* (1959)).

Where three increasing concentrations of antagonist were used in the same experiment, Schild plots were determined using the equation:

$$\mathbf{Log\ (DR-1) = log[B] - log\ [K_D]} \qquad \text{(eq. 7)}$$

where DR, [B] and [K_D] are as defined previously. The log (DR-1) was then plotted on the Y-axis and the log [B] was plotted on the X-axis to yield a straight line. The slope of this line was determined using linear regression analysis:

$$\mathbf{Y = (slope \cdot X) + intercept} \qquad \text{(eq. 8)}$$

where Y and X are as defined above. A slope of 1 is indicative of competitive antagonism and the intercept of the straight line with the Y-axis (i.e. Y=0) yields the log K_D of the antagonist.

Where partial agonists were used to shift concentration-response curves of full(er) agonists, K_D values of the competing partial agonist were determined according to the method of Stephenson (1956) using the following equation:

$$\mathbf{K_D = \frac{Y \cdot [P]}{1-Y}} \qquad \text{(eq. 9)} \qquad \text{where} \qquad \mathbf{Y = \frac{[A_2]-[A_1]}{[A_3]}} \qquad \text{(eq. 10)}$$

where [P] is the partial agonist concentration, [A_1] is the concentration of the full agonist at which the concentration-response curve of the full agonist in the absence and presence of the partial agonist cross (i.e. cause the same response), [A_2] is the concentration of the full agonist causing a given response (that is greater than that of the partial agonist) and [A_3] is the concentration of the full agonist in the presence of the partial agonist causing the same response as [A_2] (Figure 2.6).

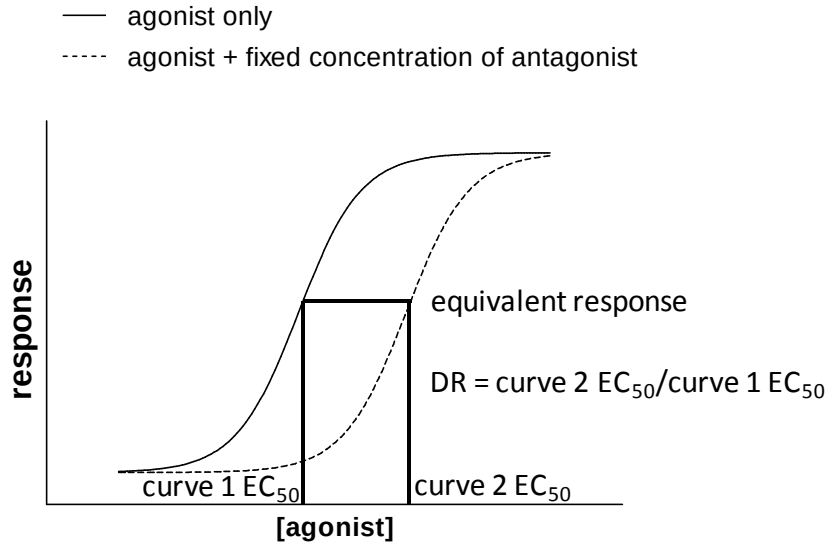

Figure 2.5 Schematic representation of the calculation of the dose-ration (DR) of curve 1 (agonist concentration-response curve) and curve 2 (agonist concentration-response curve in the presence of a fixed concentration of antagonist). The dose-ration is then used to calculate the K_D value of the antagonist.

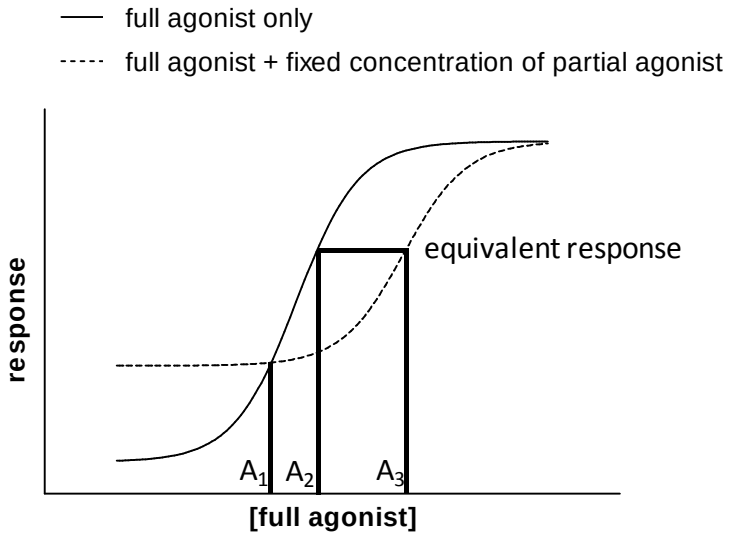

Figure 2.6 Schematic representation of A_1, A_2 and A_3 full agonist concentrations in the absence and presence of a fixed concentration of partial agonist. These parameters are used in the method of Stephenson (1956) to determine the K_D value of the partial agonist.

Partial agonist K_D value calculations

The affinity (K_D) of partial agonists was estimated according to the operational model of partial agonism (Leff *et al.*, 1985), where concentration-responses of partial agonists were obtained in the absence of a full(er) agonist (as described above). However, a concentration-response curve of a full agonist was obtained in the same experiment to define the system maximal response.

$$\mathbf{E} = \frac{\mathbf{E_{MAX}} \cdot \boldsymbol{\tau} \cdot [\mathbf{A}]}{\mathbf{K_A} + [\mathbf{A}] + \boldsymbol{\tau} \cdot [\mathbf{A}]} \qquad \text{(eq. 11)}$$

where E is a biological effect (operational maximum) and E_{MAX} is the maximal system response that was determined by obtaining a concentration-response curve of the full agonist cimaterol at the same time as the concentration-response curve of the partial agonist. The parameter τ and K_A are the (operational) efficacy and dissociation constant of the partial agonist and [A] is the concentration of the partial agonist.

Equilibrium fluorescent ligand binding experiment

Saturation binding experiments

When measuring the binding of fluorescent ligands to living cells using confocal microscopy, the average pixel intensity values obtained at each concentration of fluorescent ligand (i.e. total binding values) were fitted using the following equation:

$$\mathbf{Fluorescence\ intensity} = \frac{\mathbf{B_{MAX}} \cdot [\mathbf{B}]}{[\mathbf{B}] + \mathbf{K_D}} + (\mathbf{M} \times \mathbf{B}) + \mathbf{C} \qquad \text{(eq. 12)}$$

where B_{MAX} is the maximal fluorescence intensity, [B] is the concentration of the fluorescent ligand, M is the slope of the non-specific binding component and C is the intercept with the Y-axis (i.e. background image intensity).

Inhibition binding experiments

Total and non-specific binding of a fixed concentration of fluorescent ligand was determined on each assay plate in each experiment, which allowed the displacement of binding for all unlabelled ligands to be expressed as percentage of uninhibited binding. Curves of the inhibition of the binding of a fixed concentration of fluorescent ligand were fitted to a one-site inhibition equation:

$$\% \ \mathbf{uninhibited\ binding} = \frac{(\mathbf{Totals - NSB})}{([\mathbf{D}]/\mathbf{IC_{50}} + \mathbf{1})} + \mathbf{NSB} \qquad \text{(eq. 13)}$$

where Totals is the level of total binding of the fluorescent ligand, NSB is the level of non-specific binding of the fluorescent ligand, [D] is the concentration of the unlabelled inhibitor ligand and IC_{50} is the concentration of this inhibitor ligand to achieve a 50 % inhibition of the total binding of the fluorescent ligand. The CGP 20712A curve of the inhibition of the binding of 2 nM BODIPY-TMR-CGP displayed a shallower slope of binding inhibition (Figure 4.17 and 4.18) and was fitted to the following equation:

$$\% \ \mathbf{uninhibited\ binding} = \frac{(\mathbf{Totals - NSB})}{([\mathbf{D}]|\mathbf{IC_{50}} + \mathbf{1})^{\mathbf{n}}} + \mathbf{NSB} \qquad \text{(eq. 14)}$$

where the Totals, NSB, D and IC_{50} parameters are the same as outlined for equation 13, and n is the Hill slope coefficient. If the inhibition of the binding of the fluorescent ligand followed two phases (e.g. in CHO-β_1-CS cells), a two-site inhibition equation was used:

$$\%\ \mathbf{uninhibited\ binding} = \frac{\mathbf{Span \cdot Fraction_{high}}}{(\mathbf{[D]/IC_{50high}+1})} + \frac{\mathbf{Span \cdot Fraction_{low}}}{(\mathbf{[D]/IC_{50low}+1})} + \mathbf{NSB} \quad \text{(eq. 15)}$$

where [D] and NSB are as defined above, Span is the difference between the level of total and non-specific binding of the fluorescent ligand and $Fraction_{high}$ and $Fraction_{low}$ represent the proportion of fluorescent ligand binding that is inhibited by lower inhibitor concentrations (yielding IC_{50high}) and higher inhibitor concentrations (yielding IC_{50low}). Where applicable, antagonist affinity values (K_D) were calculated using the Cheng-Prusoff equation:

$$\mathbf{K_D} = \frac{\mathbf{IC_{50}}}{\mathbf{1+([BODIPY-TMR-CGP]/K_D BODIPY-TMR-CGP)}} \quad \text{(eq. 16)}$$

where the previously determined IC_{50} value of the unlabelled ligand and the known concentration and affinity of the labeled ligand BODIPY-TMR-CGP are used.

Kinetic fluorescent ligand binding experiments

Association and dissociation rate constants

Association kinetics data were fitted using the following monoexponential association equation:

$$\mathbf{Y} = \mathbf{Y_0} + (\mathbf{Plateau} - \mathbf{Y_0})(\mathbf{1} - \mathbf{e}^{-\mathbf{k_{onobs} \cdot t}}) \quad \text{(eq. 17)}$$

where Y_0 is the level of binding of the fluorescent ligand at time (t) 0 (i.e. baseline fluorescence read), Plateau is the level of binding of the fluorescent ligand at infinite time, e is a mathematical constant (Euler's number, approximate value of 2.718), and k_{onobs} is the rate of observed association. If a low level of non-specific binding (less than 10 % of total binding) was observed for a given concentration of a fluorescent ligand, the dissociation kinetic data was then analysed using the following monoexponential (one-phase) decay equation:

$$\mathbf{Y} = (\mathbf{Y_0} - \mathbf{Plateau}) \cdot \mathbf{e}^{-\mathbf{koff \cdot t}} + \mathbf{Plateau} \quad \text{(eq. 18)}$$

where Y_0, Plateau and t are the same as defined above, with Y_0 representing total binding levels of fluorescent ligand at the start of the dissociation (i.e. t=0). The k_{off} is the dissociation rate of the fluorescent ligand. Where a greater level of non-specific binding was observed (greater than 10 % of total binding), the dissociation kinetic data were fitted to a two-phase exponential decay function:

$$\mathbf{Y} = \mathbf{Plateau} + \mathbf{Span_{fast}} \cdot \mathbf{e}^{-\mathbf{k_{off(fast)} \cdot t}} + \mathbf{Span_{slow}} \cdot \mathbf{e}^{-\mathbf{k_{off(slow)} \cdot t}} \quad \text{(eq. 19)}$$

where Plateau and t are as defined above, and $Span_{fast}$ and $Span_{slow}$ represent the proportion of Y_0-Plateau accounted for by the fast ($k_{off(fast)}$) and slow ($k_{off(slow)}$) dissociation rate, respectively. Within this analysis, $k_{off(fast)}$ and Plateau was constrained to the average rate of dissociation and the average

Plateau (in %) reached by the fluorescent ligand in control CHO-CS cells (i.e. cell not expressing the receptor of interest). The association rate constants were then calculated using the following equation:

$$\mathbf{k_{on}} = \frac{\mathbf{k_{onobs} - k_{off(slow)}}}{[\mathbf{fluorescent\ ligand}]} \quad \text{(eq. 20)}$$

where the kinetic parameters k_{onobs} and $k_{off(slow)}$ were previously determined.

Kinetically-derived equilibrium K_D value calculations

The negative logarithms of the equilibrium dissociation constant (pK_D) were determined from kinetic parameters using the following equation:

$$\mathbf{pK_D} = -\mathbf{log}\left(\frac{\mathbf{k_{off(slow)}}}{\mathbf{kon}}\right) \quad \text{(eq. 21)}$$

where the kinetic parameters $k_{off(slow)}$ and k_{on} were previously determined.

Statistical analysis

All statistical analyses were performed using GraphPad Prism 5.0 software (San Diego, USA). Statistical analysis involved a one-sample t test to compare the mean of a set of values obtained in several different experiments to a hypothetical value (e.g. Schild slopes were compared to a hypothetical Schild slope of 1.0). Unpaired t-tests were used, where two sets of values determined in several different experiments were compared. One-way (analysis of variance) ANOVA was used to compare three or more sets of values determined in several different experiments. To follow the one-way

ANOVA, the Tukey's post hoc multiple comparison test was used to compare two or more sets of values to a set of control values, or the Bonferroni's post hoc multiple comparison test was used to compare each set of values to all of the other sets of values. In all cases, statistical significance was reflected in $P < 0.05$ (represents a less than 5 % chance that the interactions compared happen by chance, thus indicating significance). If applicable, a preferred fit was determined with statistical significance of $P < 0.05$ (partial F test and analysis of residuals performed during fitting of data).

Chapter 3

The pharmacology of CGP 12177 at the native and SNAP-tagged human β_1-adrenoceptor.

3.1 Introduction

The cardiostimulatory effects mediated by the β_1-adrenoceptor upon activation by the endogenous ligands adrenaline and noradrenaline are inhibited by β-blockers, such as propranolol, in a variety of cardiac diseases, such as angina pectoris (Brodde *et al.*, 1999). At the β_1-adrenoceptor CGP 12177 has been described as a potent antagonist (Haddad *et al.*, 1987; Staehelin *et al.*, 1983), but was also shown to exhibit agonist activity at higher concentrations, which is resistant to β-blocker actions at the concentrations used to inhibit catecholamine-mediated β_1-adrenoceptor stimulation (Kaumann *et al.*, 2001; Konkar *et al.*, 2000; Pak *et al.*, 1996). This led to the two-site hypothesis of the β_1-adrenoceptor which describes a high affinity site 1 (catecholamine site) and a low affinity site 2 ("CGP 12177" site; Pak *et al.* (1996)). This pharmacology was observed in recombinant (Baker *et al.*, 2003a; Joseph *et al.*, 2004; Konkar *et al.*, 2000) and human (Kaumann *et al.*, 2007) and animal tissue preparations (Lowe *et al.*, 1999; Sillence *et al.*, 2005). However, the nature of the second "CGP 12177" site, and how CGP 12177 is able to display antagonist and agonist effects at the same receptor is not yet known. A mutagenesis study carried out by Baker *et al.* (2008) aimed to locate and distinguish the two proposed binding sites of the β_1-adrenoceptor by identifying key amino acid residues involved in the ligand binding to the two sites. Eight single point mutations were introduced and all were found to have similar effects on both the high and low affinity β_1-adrenoceptor binding site (Baker *et al.*, 2008).

Using fluorescently labelled G protein-coupled receptors and fluorescent ligands in conjunction with confocal microscopy has allowed the investigation of receptor-ligand interactions in live cells and provided insight into ligand-induced receptor trafficking, receptor dimerisation and receptor co-operativity (Briddon *et al.*, 2008; Calebiro *et al.*, 2013; May *et al.*, 2011). - Fluorescently tagging a G protein-coupled receptor (GPCR) has traditionally been achieved using fluorescent proteins (FPs) such as green FP (GFP) or yellow FP (YFP). An alternative fluorescent tag is the SNAP-tag, which is an engineered truncated version of the DNA repair protein O^6-alkylguanine alkyltransferase, and is fused to the N-terminus of the receptor of interest (Keppler *et al.*, 2003). In a suicide reaction, the 20 kDa SNAP-tag removes the benzyl group, which is linked to a fluorophore (e.g. Alexa Fluor 488 dye), from its benzylguanine (BG) substrate and transfers it onto a cysteine residue within its active site, thereby covalently and irreversibly linking a fluorophore to the SNAP-tagged receptor (Keppler *et al.*, 2003; Tirat *et al.*, 2006). The SNAP-tag has been used in a variety of studies, including protein visualisation and localisation studies in living cells (Campos *et al.*, 2011; Gong *et al.*, 2012), GPCR oligomerisation studies using fluorescence resonance energy transfer (FRET) (Alvarez-Curto *et al.*, 2010; Maurel *et al.*, 2008) and protein-protein interactions studies using a split SNAP-tag protein complementation assay (Mie *et al.*, 2012). The main advantages of the SNAP-tag are its low non-specific labelling and the fact that its BG substrate can be linked to a range of fluorophores, thereby allowing a choice of wavelength in which to image the tagged receptor. This allows greater flexibility and ease as the same construct

or cell line can be used in multiple experiments, especially when used in conjunction with other labelled receptors or potentially interacting proteins and fluorescent ligands. Using the SNAP-tag technology in an imaging approach to investigate the β_1AR pharmacology may provide new insights into the nature of the second site of this receptor. Single cell and single molecule techniques such as confocal microscopy and fluorescence correlation spectroscopy (FCS) detect fluorescently labelled species that can be tracked over time, allowing changes (e.g. internalisation, membrane diffusion, receptor oligomerisation) in response to various ligands (agonists and antagonists) to be measured (Briddon *et al.*, 2007; Calebiro *et al.*, 2013; May *et al.*, 2011).

In this chapter we aimed (1) to generate and stably express the SNAP-tagged human β_1-adrenoceptor fusion protein in CHO-CS cells, and (2) to characterise the pharmacology of CGP 12177 at both the native (untagged) and SNAP-tagged human β_1-adrenoceptor expressed in CHO-CS cells using the CRE-mediated SPAP transcription assay, with the long term aim to use both cell lines and the CRE-SPAP reporter gene assay throughout this thesis to investigate the nature of the second site of the β_1-adrenoceptor in both functional and imaging studies.

3.2 Methods

Molecular Biology

All steps outlined in *Materials and Methods: Generation of a SNAP-tagged receptor fusion protein* were carried out. For this, the plasmid vector pcDNA3.1(+) containing the neomycin antibiotic resistance gene was used. The SNAP-tag DNA was obtained from Dr Holliday. The β_1-adrenoceptor (accession number: NM_000684) template DNA was from a β_1-adrenoceptor construct previously made by Dr Baker. The following PCR primers were designed and used for β_1AR amplification: 5' primer (5' – CCGCC/GGATCC/CTG GGC GCG GGG GTG CTC G – 3') containing both a *BamH*I cleavage site and a mismatch to mutate the receptor start codon (ATG–CTG), 3' primer (5' – GGCGG/GAATTC/CTA CAC CTT GGA TTC CGA GG – 3') containing an *EcoR*I site.

Generation of a CHO cell line expressing SNAP-tagged human β_1-adrenoceptors

This was carried out as described in *Materials and Methods: Generation of new cell lines*. Here, the SNAP-tagged human β_1-adrenoceptor fusion protein construct was transfected into CHO-K1 cells stably expressing the CRE-SPAP reporter gene (CHO-CS cells; McDonnell *et al.* (1998)).

Cell culture

The CHO-β_1-CS cell line and the generated CHO-CS cell lines expressing the SNAP-tagged β_1-adrenoceptor were used in this chapter. The cell lines were maintained in growth media (see *Materials and Methods: Cell culture* for

details) which was supplemented with 1 mg/mL of geneticin (G418) for maintenance of cell lines transfected with the SNAP-tagged β_1-adrenoceptor construct.

SNAP-tag labelling and confocal microscopy

This was performed as described in *Materials and Methods: Confocal microscopy* using 8-well borosilicate chambered-coverglass plates imaged on a Zeiss LSM710 laser scanning microscope with a 40x1.3NA oil immersion lens. Labelling of cell surface SNAP-tagged β_1-adrenoceptors was achieved using 1 µM impermeable SNAP-tag substrate SNAP-Surface® 488 BG-488 (final concentration; 10 min, in the dark, 21 °C). The confocal settings used to image SNAP-tag labelling were as follows: 488 nm excitation using an argon laser with emission captured through a 505-634 nm filter (1024x1024 pixels, averaging at 4 frames). A pinhole diameter of 1 Airy unit was used.

IX Ultra confocal plate reader

CHO-CS cell lines stably expressing SNAP-tagged β_1AR were imaged on the IX Ultra confocal plate reader using a Plan Fluor 40x NA0.6 objective as described in *Materials and Methods: ImageXpress Ultra confocal plate reader*.

CRE-mediated SPAP transcription

The CRE-dependent transcription of secreted placental alkaline phosphatase (SPAP) was determined in agonist and antagonist mode as described in *Materials and Methods: CRE-mediated SPAP transcription assay*.

3.3 Results

Generation of the SNAP-tagged human β_1AR construct

The SNAP-tag sequence used in this study contains an 84 base long signal sequence (sig; s) upstream of the SNAP-tag sequence (SNAP; s). Throughout this thesis the SNAP-tag refers to the sequence including both the signal and the SNAP-tag sequence, which is denoted by a prefix of 'sig.SNAP' or 'ss' in DNA constructs and cell lines.

The signal sequence is, once transcribed, required for the correct membrane insertion and targeting of the SNAP-β_1AR fusion protein in the cell. Indeed, the first 25 (75 bases) amino acids of the signal sequence are identical to the first 25 amino acids (including the ATG start codon) of the (house mouse) 5-hydroxytryptamine (serotonin) 3A (5-HT3A) receptor sequence (accession number AY605711; see Appendix I S1 for alignment of the two sequences), a ligand-gated ion channel membrane protein (Hargreaves *et al.*, 1994). The downstream SNAP-tag sequence is 549 bases in length and starts with a Leucine residue as the Methionine start codon was mutated to allow the continuous transcription downstream of the signal sequence. In total, the complete SNAP-tag (including the signal sequence) is 633 bases long and was inserted into the plasmid vector pcDNA3.1(Neo+) (see *Methods* for detailed vector map) between the restriction enzyme sites of *Kpn*I and *BamH*I (633 bp, Figure3.1, lane 2).

The β_1AR sequence was amplified in a PCR reaction using forward and reverse primers which were designed to introduce *BamH*I (upstream of the start of the β_1AR sequence) and *EcoR*I (downstream of the end of the β_1AR sequence) restriction enzyme sites and a mutated start codon (Methionine to Leucine) to allow for continued transcription downstream of the SNAP-tag sequence. The β_1AR sequence was then inserted into the pcDNA3.1(Neo+) plasmid vector already containing the SNAP-tag sequence between the restriction enzyme site *BamH*I and *EcoR*I (1434 bp, Figure 3.1, lane 3), thus fusing the SNAP-tag to the N-terminal of the β_1-adrenoceptor between restriction enzyme site *Kpn*I and *EcoR*I (2067 bp, Figure 3.1, lane 4). The entire sig.SNAP-β_1AR sequence in the pcDNA3.1(Neo+) plasmid vector has been confirmed by DNA sequencing (see Appendix I S2 for DNA and protein sequence of entire fusion protein).

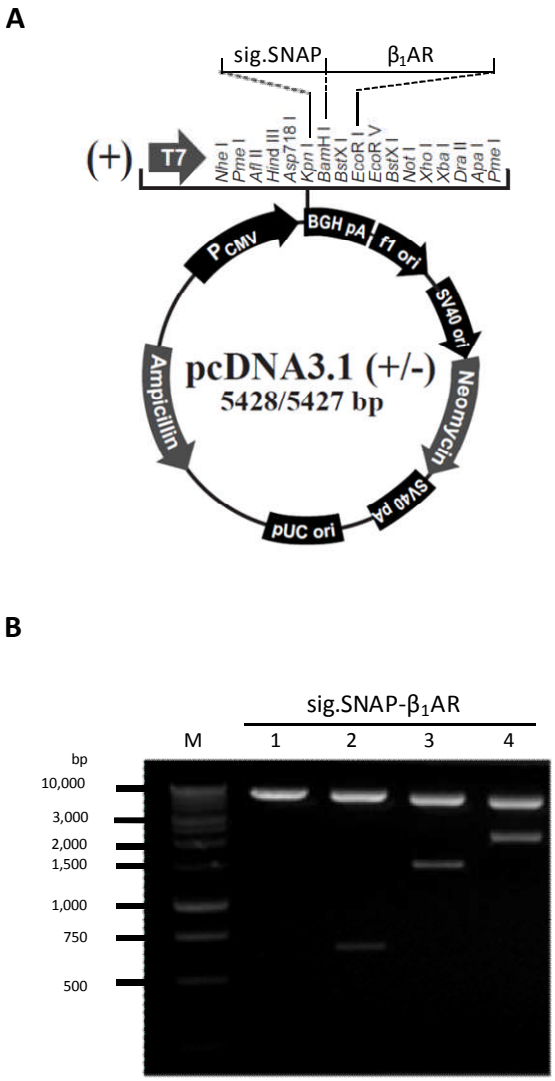

Figure 3.1 **A**, schematic diagram of the pcDNA3.1(Neo+) vector, the restriction enzyme sites within its multiple cloning site and the restriction enzymes used to insert the sig.SNAP-β_1AR construct. **B**, restriction enzyme digests of the sig.SNAP-β_1AR construct were run on a 1% agarose gel. Lane 1, following a *Kpn*I digest the gel shows the linearised vector containing the entire sig.SNAP-β_1AR construct in one band (7501 bp). Lane 2, following a *Kpn*I/*BamH*I double digest the gel shows the sig.SNAP-tag insert (lower band, 633 bp) and the linearised vector containing the β_1AR sequence (upper band, 6862 bp). Lane 3, following a *BamH*I/*EcoR*I double digest the gel shows the β_1AR insert (lower band, 1434 bp) and the linearised vector containing the sig.SNAP sequence (upper band, 6061 bp). Lane 4, following a *Kpn*I/*EcoR*I double digest the gel shows the sig.SNAP-β_1AR insert (*Kpn*I/*EcoR*I digest, lower band, 2073 bp) and the linearised empty vector (upper band, 5428 bp). Lane M represents the 1 kb DNA marker lane that yields bands of increasing known sizes which are listed in base pairs (bp) to the left of the image of the gel.

Generation of a CHO cell line stably expressing the SNAP-tagged human β_1AR

The sigSNAP-β_1AR construct was transfected into CHO-CS cells. Following dilution cloning, 15 clones were generated and each clonal cell line was screened for (1) cell surface receptor expression and (2) receptor functionality. The expression of SNAP-tagged β_1-adrenoceptors on the cell surface was examined using confocal microscopy following the labelling of the SNAP-tag using a cell membrane impermeable benzyl-guanine (BG) substrate linked to a 488 nm excited fluorophore (BG-488). All 15 clonal cell lines were imaged (Appendix I S3 and S4); 5 showed SNAP-tagged β_1AR expression on the cell membrane (such as clone F6; Figure 3.2B), whereas the remaining 10 clonal cell lines showed no BG-488 labelling (e.g. clone A9; Figure 3.2C). CHO-CS cells expressing the native (untagged) β_1AR cells were also exposed to BG-488 and imaged, and no non-specific labelling effect of the BG-488 substrate could be observed (Figure 3.2A). Receptor functionality was investigated using the CRE SPAP reporter assay, as all clonal cell lines contained the CRE-SPAP promoter-reporter gene construct. The CRE-mediated SPAP secretion of unstimulated cells (basal) and of cells stimulated by 100 µM forskolin (as a positive control) and by 10 µM isoprenaline and 10 µM cimaterol were determined to give an indication of the functionality of the SNAP-tagged β_1-adrenoceptor and to determine the assay window of each cell line (using 'value over baseline' calculations; Figure 3.2). All 10 cell lines that were found not to express the SNAP-tagged β_1AR also showed no response to the β-adrenoceptor agonists isoprenaline and cimaterol, but only to forskolin, suggesting a lack of the

receptor as the CRE-mediated SPAP transcription was not impaired (Figure 3.2C, clone A9). All 5 cell lines that were found to express the SNAP-tagged β_1-adrenoceptor also responded to both β-adrenoceptor ligands (Figure 3.2B, clone F6). CHO-ssβ_1-CS clone F6 showed a good level of expression of SNAP-tagged β_1-adrenoceptors albeit heterogeneous. A clonal cell line originates from one single cell and therefore consists of cells of identical genomic DNA. Thus, cells of a clonal cell line have the potential to express proteins encoded in the genomic DNA at the same level. The observed heterogeneous expression level of the CHO-ssβ_1-CS F6 cell line may have been due to it originating from more than one single cell. In order to try to generate a homogeneous clonal cell line, clone F6 was dilution cloned and its sub-clones were screened using the same strategy as outlined above. Cell surface expression of SNAP-tagged β_1-adrenoceptors in CHO-ssβ_1F6-CS clones was examined using the IX Ultra confocal plate reader to allow for imaging of all clones at the same time under the same conditions. The fluorescence intensities of the fluorophore linked to SNAP-tagged β_1-adrenoceptors can be seen for all clones in the montage image of the imaged plate (Figure 3.3B) and vary from low (clone F6.45) to high (clone F6.1 and F6.13). As all 48 F6 sub-clones showed expression of the SNAP-tagged β_1-adrenoceptor, they were all tested for receptor functionality. All clones showed good functional responses, the responses of five F6 sub-clones are shown in Figure 3.3C (in comparison to the response seen in the parental CHO-ssβ_1-CS F6 clone). Subsequent confocal imaging of the sub-clones revealed a heterogeneous expression level of SNAP-tagged β_1-adrenoceptors (e.g. CHO-ssβ_1-CS clone F6.1, Figure 3.3D)

as seen in the parent F6 cell line. This suggests that this heterogeneity is an inherent feature of the expression of this receptor construct in CHO-CS cells following lipofectamine transfection. Nevertheless, the CHO-ssβ_1-CS clone F6.1 cell line was chosen and used for all subsequent experiment in this thesis and is referred to as the CHO-ssβ_1-CS cell line.

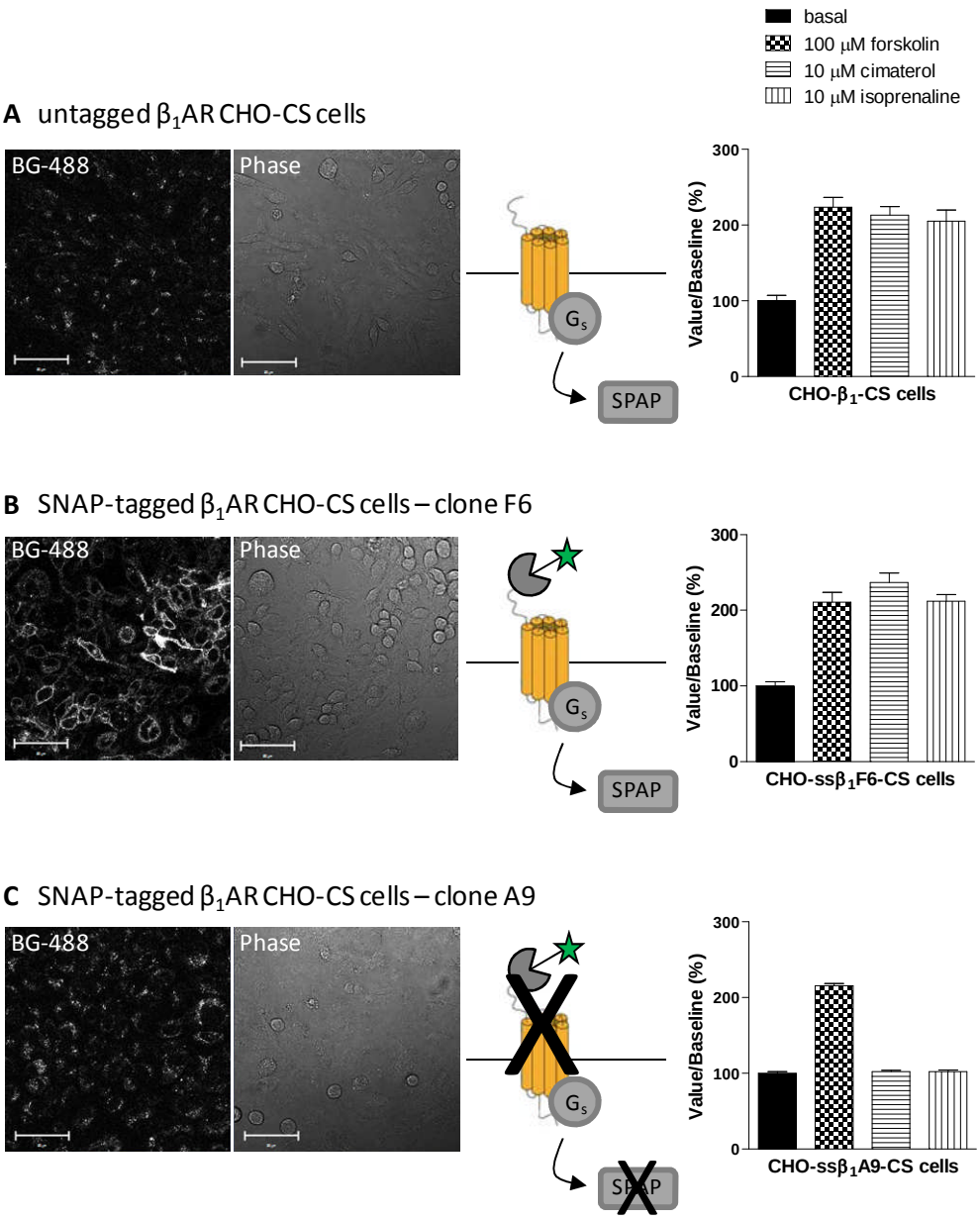

Figure 3.2 Screening CHO-ssβ_1-CS clones for cell surface receptor expression and functionality. **A**, CHO-CS cells expressing the untagged β_1AR were included in the screen as a negative SNAP-tag labelling control and a positive control in the SPAP assay. Data are shown for **B**, CHO-ssβ_1-CS clone F6 and **C**, clone A9. The left hand panel shows confocal images following incubation with 1 µM BG-488 (30 min, 37 °C). The right hand panel shows the response measured in the SPAP assay under unstimulated conditions (basal) and when stimulated with forskolin, isoprenaline and cimaterol. Data shown are mean ± s.e.m. of triplicate determinations from one experiment. The middle panel schematically describes the concept behind the screening strategy used here which links receptor function to expression. Scale bars = 50 µm.

A plate map

F6	F6.1	F6.2	F6.3	F6.4	F6.5	F6.6	F6.7	F6.8	F6.9
F6.10	F6.11	F6.12	F6.13	F6.14	F6.15	F6.16	F6.17	F6.18	F6.19
F6.20	F6.21	F6.22	F6.23	F6.24	F6.25	F6.26	F6.27	F6.28	F6.29
F6.30	F6.31	F6.32	F6.33	F6.34	F6.35	F6.36	F6.37	F6.38	F6.39
F6.40	F6.41	F6.42	F6.43	F6.44	F6.45	F6.46	F6.47	F6.48	

B SNAP-tag labelling with BG-488

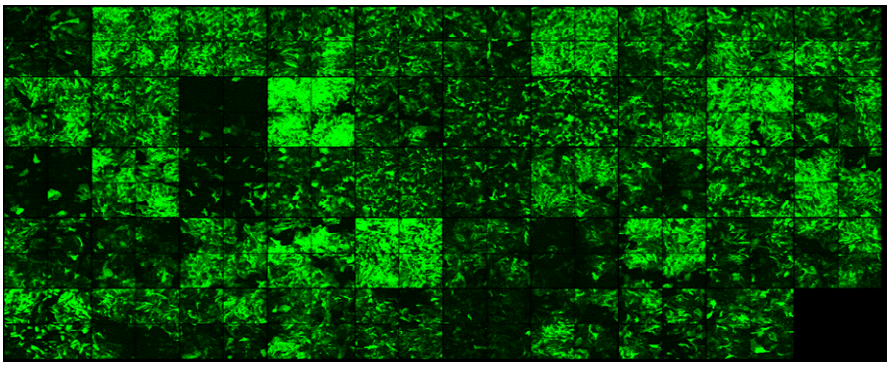

C

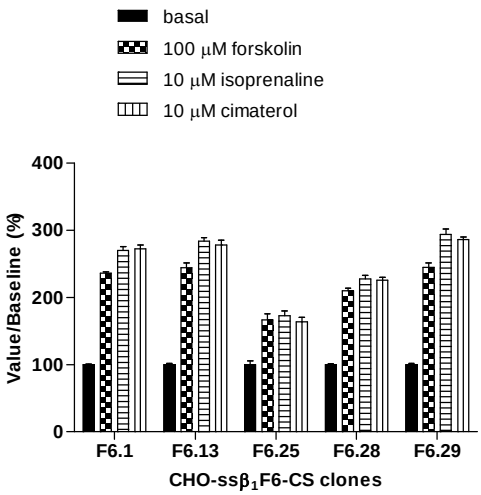

D

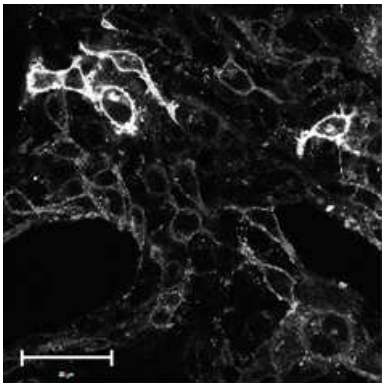

Figure 3.3 CHO-ssβ_1F6-CS clonal cell lines were screened for cell surface receptor expression following SNAP-tag labelling using BG-488 in a 96-well plate format. **A**, plate map identifying the clonal cell lines in the 49 wells used. **B**, montage image of CHO-ssβ_1F6-CS clones (four images per well, i.e. clone) following BG-488 labelling. **C**, CRE-mediated SPAP transcription of CHO-ssβ_1F6-CS parental clone and five selected sub-clones in unstimulated cells (basal) and in response to 100 µM forskolin, 10 µM isoprenaline and 10 µM cimaterol. **D**, confocal image of sub-clone F6.1 following BG-488 labelling. Scale bar = 50 µm.

Loss of expression over time of the SNAP-tagged human β_1AR in CHO-CS cells

The cimaterol concentration-response curve obtained at a late passage (passage 18) compared to that of a very early passage (passage 6) was right-shifted (Figure 3.4A) and the pEC_{50} derived from that curve (7.27; Table 3.1) was reduced compared to that from the earlier passage (8.20; Table 3.1). This was not observed for the partial agonist CGP 12177 as its pEC_{50} remained unchanged from cells at passage 6 (7.68; Figure 3.4B; Table 3.1) to cells at passage 18 (7.51; Table 3.1). However, the maximal response of CGP 12177 reduced from 73.8 % (of 10 µM cimaterol, passage 6) to 37.8 % (of 10 µM cimaterol, passage 18). This observed trend of reduced efficacy (reduced pEC_{50} of full agonist, smaller maximal response of partial agonist) may indicate a reduced receptor reserve (through a lower level of receptor expression) in the system. Interestingly, a similar trend was observed using CHO-CS cells expressing the native (untagged) β_1-adrenoceptor (Figure 3.4C, D), suggesting that this is not a SNAP-tag specific observation. Furthermore, these data highlight that the CGP 12177 and cimaterol responses are dependent on the level of β_1-adrenoceptor expression, indicating that the actions of these two ligands at the β_1-adrenoceptor are specific.

To further confirm a reduction of the expression level of SNAP-tagged β_1-adrenoceptors over time, confocal images of CHO-ssβ_1-CS cells were taken at various passages, following BG-488 labelling to visualise the SNAP-tagged β_1-adrenoceptors expressed on the cell surface (Figure 3.5). Indeed, a similar

trend was observed as the number of cells labelled by BG-488 in any given field of view decreased with increasing passages.

As such, both the CHO-β_1-CS and the CHO-ssβ_1-CS clonal cell lines were used only for up to 5 passages for all subsequent experiments in this thesis.

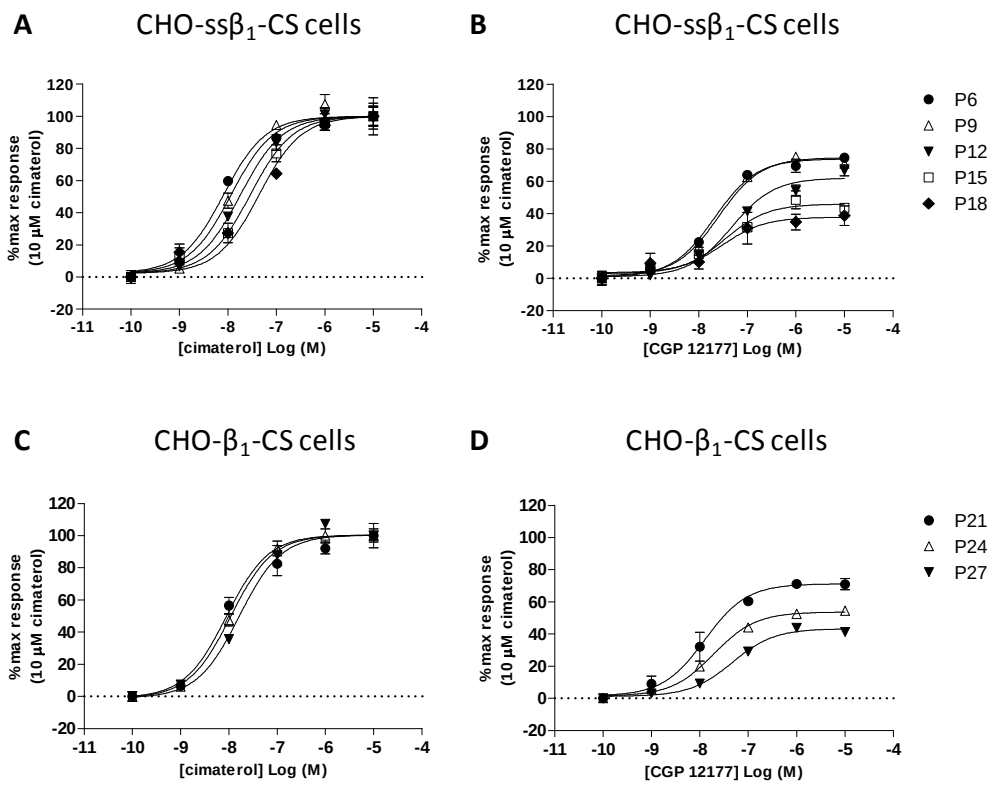

Figure 3.4 Loss of expression of the SNAP-tagged and native β_1-adrenoceptor in CHO-CS cells over time. CRE-mediated SPAP transcription of cimaterol and CGP 12177 at various passage numbers of the CHO-ssβ_1-CS cell line (panel **A** and **B**, respectively) and CHO-β_1-CS cell line (panel **C** and **D**, respectively). Data were normalised to maximum SPAP production levels determined by 10 µM cimaterol for each passage number. Data are mean ± s.e.m of triplicate determinations from a single experiment.

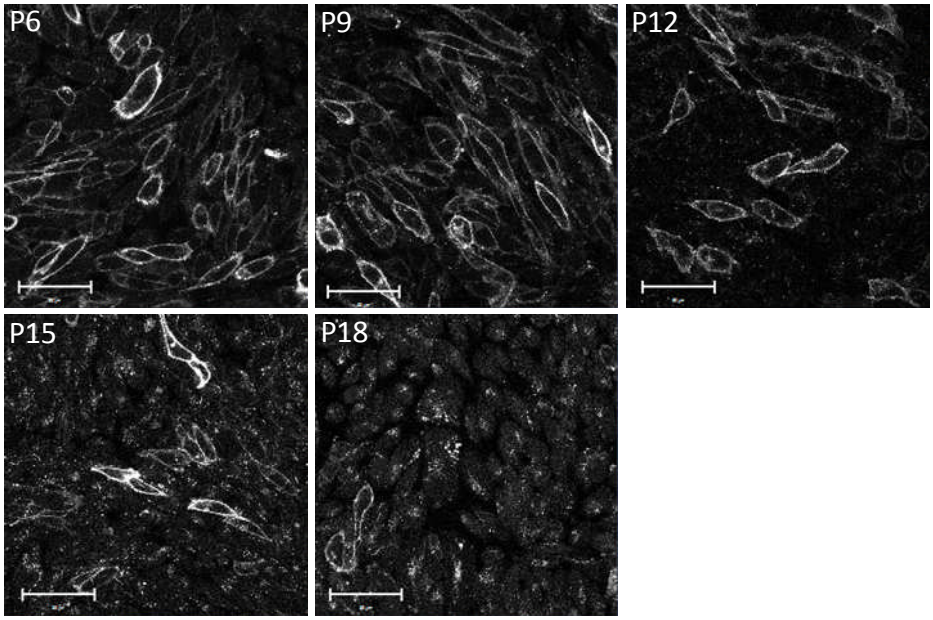

Figure 3.5 Confocal images of CHO-ssβ_1-CS cell line at various passages following incubation with the SNAP-tag substrate BG-488 (1 µM, 37 °C, 30 min). Cells were imaged at room temperature and the same microscope settings were used for all passage numbers shown. Scale bar = 50 µm.

Table 3.1 Potency parameters of cimaterol and CGP 12177 at various passage numbers of the CHO-ssβ_1-CS and CHO-β_1-CS cell line. Data are from one single experiment per passage number.

	cimaterol	CGP 12177	
	pEC_{50}	*pEC_{50}*	*E_{MAX} (% cimaterol)*
CHO-ssβ_1-CS cells			
P6	8.20	7.68	73.8
P9	7.94	7.60	74.6
P12	7.76	7.33	62.0
P15	7.51	7.45	46.0
P18	7.27	7.51	37.8
CHO-β_1-CS cells			
P21	8.05	7.90	71.2
P24	7.97	7.72	53.6
P27	7.79	7.33	43.3

Two-site pharmacology at the native and SNAP-tagged human β_1AR expressed in CHO-CS cells

Firstly, the potencies of β-adrenoceptor ligands in CHO-β_1-CS and CHO-ssβ_1-CS cells were investigated, and determined to be similar in both cell lines (P > 0.05, unpaired t-test, Figure 3.6; Table 3.2). Forskolin was used as a positive control of CRE-mediated SPAP transcription as it raises cAMP levels by activating adenylyl cyclase directly (Zhang *et al.*, 1997). Forskolin stimulated CRE-mediated gene transcription to give concentration-dependent increases in SPAP secretion in CHO-β_1-CS cells (pEC_{50} 5.48 ± 0.14, E_{MAX} 123.1 ± 6.0 % of 10 μM cimaterol, 1.67 ± 0.10 fold over basal, n=9) and CHO-ssβ_1-CS (pEC_{50} 5.52 ± 0.41, E_{MAX} 109.7 ± 11.4 % of 10 μM cimaterol, 1.78 ± 0.08 fold over basal, n=3). The β-adrenoceptor agonists isoprenaline and cimaterol-induced CRE-mediated SPAP transcription with pEC_{50} values of 7.16 ± 0.21 (E_{MAX} 109.0 ± 3.5 % of 10 μM cimaterol, n=8) and 7.93 ± 0.06 (E_{MAX} set to 100 %, n=25), respectively in CHO-β_1-CS cells and 7.00 ± 0.16 (E_{MAX} 117.7 ± 3.0 % of 10 μM cimaterol, n=4) and 7.90 ± 0.06 (E_{MAX} set to 100 %, n=20), respectively, in CHO-ssβ_1-CS cells. CGP 12177 also elicited a concentration-dependent increase in CRE-mediated SPAP secretion albeit with a smaller maximal response compared to full agonist cimaterol, in both CHO-β_1-CS and CHO-ssβ_1-CS cells. The pEC_{50} values derived from the concentration-response curve were 7.73 ± 0.11 (E_{MAX} 45.2 ± 3.5 % of 10 μM cimaterol, n=13) and 7.88 ± 0.12 (E_{MAX} 57.5 ± 4.9 % of 10 μM cimaterol, n=16) in CHO-β_1-CS cells and CHO-ssβ_1-CS, respectively. This partial agonist effect of CGP 12177 is reported in the literature to occur through the low affinity secondary binding site of the β_1-

adrenoceptor, whereas isoprenaline and cimaterol effects are mediated through the high affinity catecholamine site (Joseph *et al.*, 2004; Konkar *et al.*, 2000; Pak *et al.*, 1996).

The potency of an agonist is dictated by two parameters: efficacy and affinity. For a partial agonist (an agonist that has low efficacy), its EC_{50} would be expected to be similar to its K_D. The pK_D for CGP 12177 derived from the CGP 12177 partial agonist concentration-response curve using the operational model of partial agonism (Leff *et al.*, 1993) was determined to be 7.58 ± 0.13 (n=13; Table 3.2) and 7.49 ± 0.13 (n=16; Table 3.2) in CHO-β_1-CS and CHO-ssβ_1-CS cells, respectively.

The β-adrenoceptor antagonists CGP 20712A and propranolol were also tested in this assay format, but neither ligand induced an increase in SPAP secretion (Figure 3.7; Table 3.2) and as such confirmed that they have no efficacy in this assay in both CHO-β_1-CS and CHO-ssβ_1-CS cell lines.

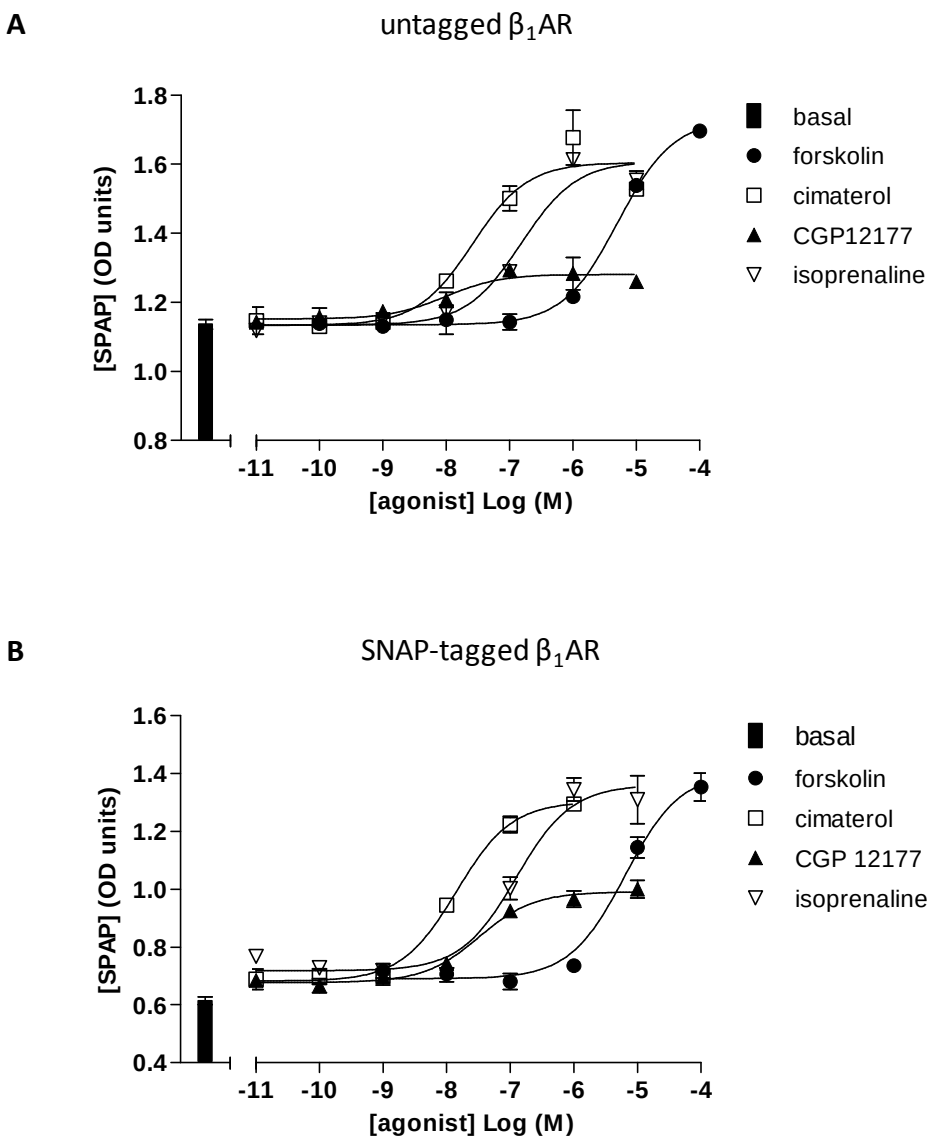

Figure 3.6 CRE-mediated SPAP transcription in response to forskolin, cimaterol, CGP 12177 and isoprenaline in **A**, CHO-β_1-CS and **B**, CHO-ssβ_1-CS cells. Bar graphs show basal SPAP secretion from unstimulated cells. Data are mean ± s.e.m. of triplicate determinations from a single experiment. The single experiment data shown is representative of at least A, eight and B, three separate experiments for each ligand in the respective cell lines.

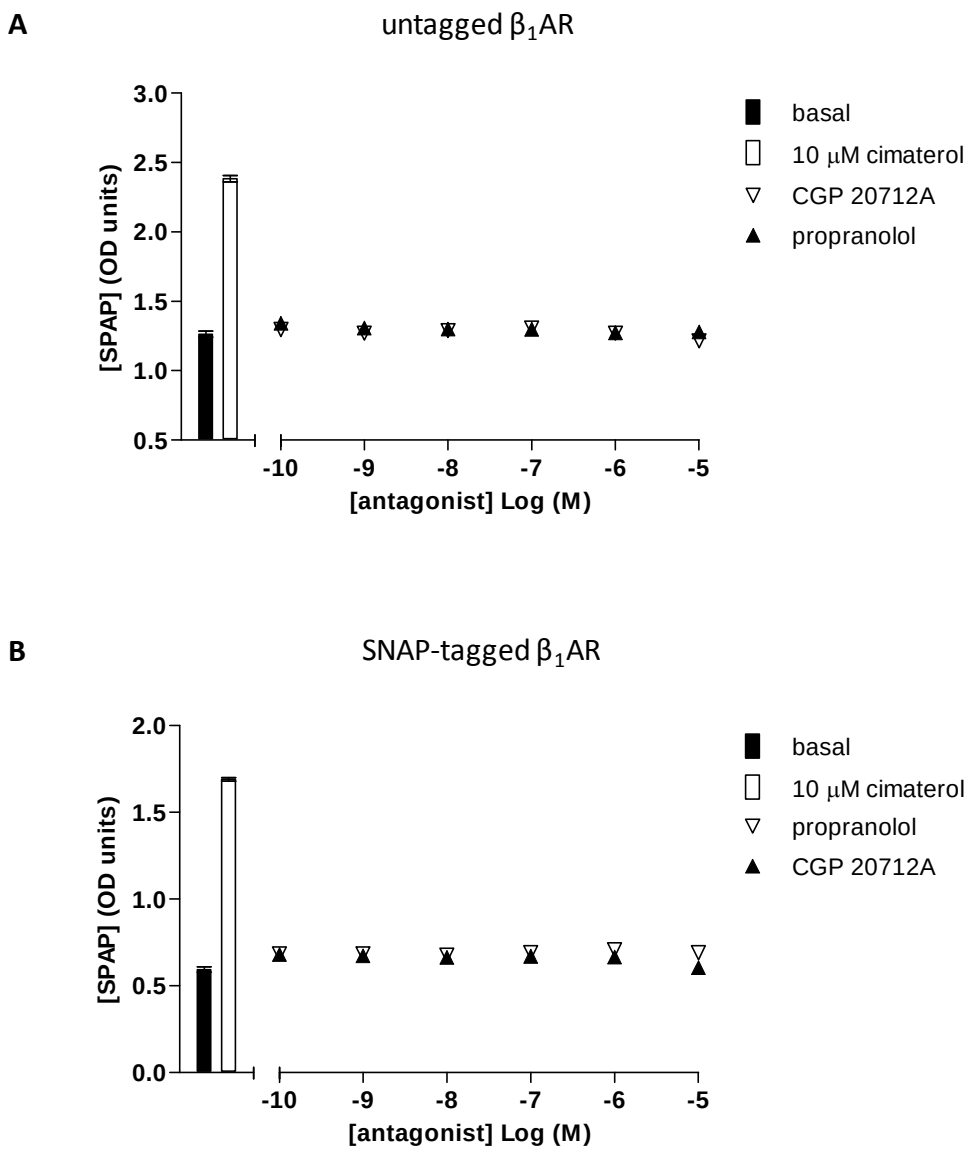

Figure 3.7 CRE-mediated SPAP transcription in response to β-adrenoceptor antagonists propranolol and CGP 20712A in **A**, CHO-β_1-CS and **B**, CHO-ssβ_1-CS cells. Bar graphs show basal SPAP secretion and that in response to 10 μM cimaterol. Data are mean ± s.e.m. of triplicate determinations from a single experiment. The single experiment data shown is representative of at least A, six and B, five separate experiments for each ligand in the respective cell lines.

Table 3.2 Potency parameters of β-adrenoceptor ligands at CHO-β_1-CS and CHO-ssβ_1-CS cells obtained in the CRE-mediated gene (SPAP) reporter assay. Data are mean ± s.e.m. of a given (n) number of separate experiments. No statistical significance of data obtained in CHO-β_1-CS and CHO-ssβ_1F6.1-CS cells was determined using unpaired t-test (statistical significance defined as $P < 0.05$).

	CHO-β_1-CS cells			CHO-ssβ_1F6.1-CS cells		
	pEC_{50}	E_{MAX} (% 10 µM cimaterol)	n	pEC_{50}	E_{MAX} (% 10 µM cimaterol)	n
forskolin	5.48 ± 0.14	123.1 ± 6.0	9	5.52 ± 0.41	109.7 ± 11.4	3
isoprenaline	7.16 ± 0.21	109.0 ± 3.5	8	7.00 ± 0.16	117.7 ± 3.0	4
cimaterol	7.93 ± 0.06	100	25	7.90 ± 0.06	100	20
CGP 12177	7.73 ± 0.11	45.2 ± 3.5	13	7.88 ± 0.12	57.5 ± 4.9	16
propranolol	no detectable response up to 10 µM		8	no detectable response up to 10 µM		8
CGP 20712A	no detectable response up to 10 µM		6	no detectable response up to 10 µM		5

Following this, the affinities of β-adrenoceptor antagonists CGP 20712A and propranolol for the high affinity catecholamine β_1-adrenoceptor site were examined at the native and SNAP-tagged β_1-adrenoceptor expressed in CHO-CS cells (Table 3.3). Both antagonists caused parallel rightward shifts of the cimaterol concentration-response curve in CHO-β_1-CS and CHO-ssβ_1-CS cells. The affinity of CGP 20712A was not significantly different in the two cell lines ($P > 0.05$, unpaired t-test), with pA_2 values of 8.84 ± 0.11 (Schild slope 1.17 ± 0.07, n=5) and 8.82 ± 0.16 (Schild slope 1.21 ± 0.09, n=7) in CHO-β_1-CS (Figure 3.8) and CHO-ssβ_1-CS cells (Figure 3.9), respectively. The affinity value determined for propranolol against cimaterol at the native β_1AR (pA_2 8.65 ± 0.07, Schild slope 1.00 ± 0.04, n=23; Figure 3.10) also compared well to that obtained at the SNAP-tagged β_1AR (pA_2 8.45 ± 0.07, Schild slope 1.16 ± 0.05, n=15; Figure 3.11; $P > 0.05$, unpaired t-test). The Schild slopes obtained for both antagonists against cimaterol at both the native and the SNAP-tagged β_1-adrenoceptor were not significantly different to unity ($P > 0.05$, one-sample t-test comparison to hypothetical value of 1.0), suggesting that the interactions between the antagonists and cimaterol at the high affinity catecholamine site are competitive, and were not affected by the N-terminal SNAP-tag.

CGP 12177, when used as an antagonist, was able to inhibit the cimaterol-stimulated response in a manner consistent with its partial agonist actions in both CHO-β_1-CS and CHO-ssβ_1-CS cells (Figure 3.12). The cimaterol concentration-response curves were right-shifted in the presence of

increasing CGP 12177 concentrations. However, at the concentrations of CGP 12177 used, the basal levels of the cimaterol concentration-response curves were raised, which is in line with the CGP 12177 agonist effect described above. Using the partial agonist method of Stephenson (1956), a log pK_B value of 9.61 ± 0.06 (n=10) and 9.52 ± 0.10 (n=6) for CGP 12177 at the high affinity catecholamine site was obtained in CHO-β_1-CS and CHO-ssβ_1-CS cells, respectively.

For any ligand, its affinity to a given receptor would be expected to be constant. However, the calculated K_D value for CGP 12177 when used to antagonise cimaterol was two orders of magnitude lower than the K_D value derived from the CGP 12177 partial agonist response curve obtained in the same assay on CHO-β_1-CS ($P < 0.01$, unpaired t-test) and CHO-ssβ_1-CS ($P < 0.01$, unpaired t-test) cells. This CGP 12177 pharmacology at the β_1-adrenoceptor is in line with previously reported data that led to the two-site binding site hypothesis for the β_1-adrenoceptor that describes a 'high affinity site 1' catecholamine site (where CGP 12177 potently inhibits β-adrenoceptor agonists such as cimaterol) and a 'low affinity site 2' CGP 12177 site (where CGP 12177 exhibits partial agonist effects; Pak *et al.* (1996)).

A untagged β_1AR

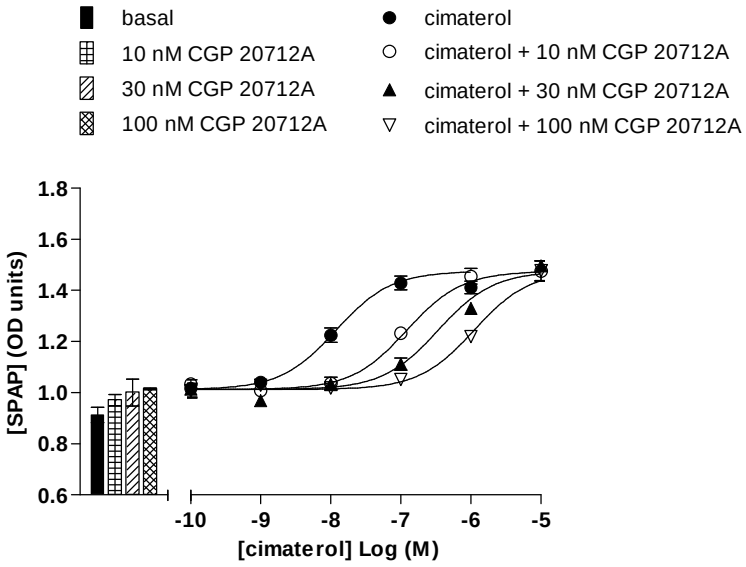

B

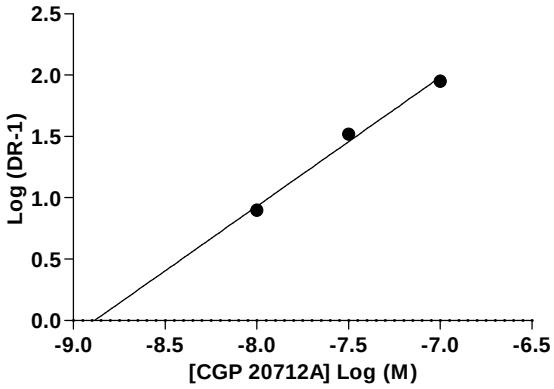

Figure 3.8 A, CRE-mediated SPAP transcription to cimaterol in the absence and presence of 10, 30 and 100 nM CGP 20712A in CHO-β_1-CS cells. Bar graphs show basal SPAP secretion from unstimulated cells and that in response to 10, 30 and 100 nM CGP 20712A alone. Data are mean ± s.e.m. of triplicate determinations from a single experiment which is representative of five separate experiments. **B**, Schild plot of data shown in A (slope 1.05, R^2 0.99).

A SNAP-tagged β_1AR

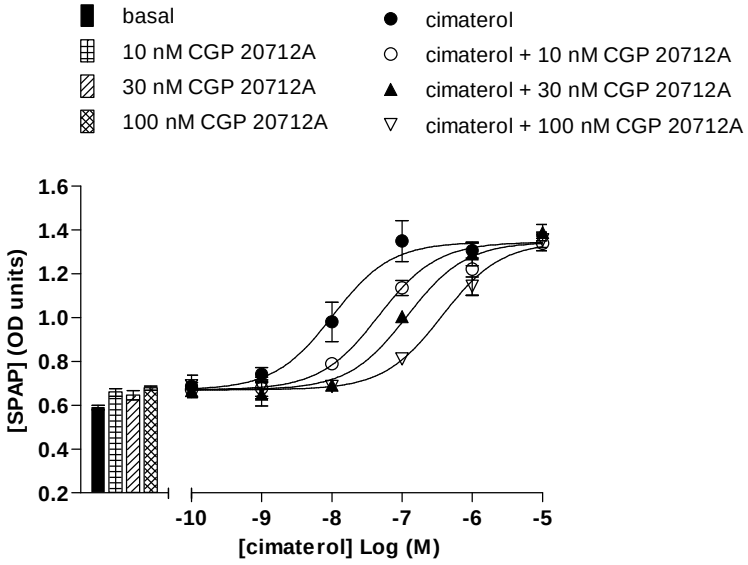

B

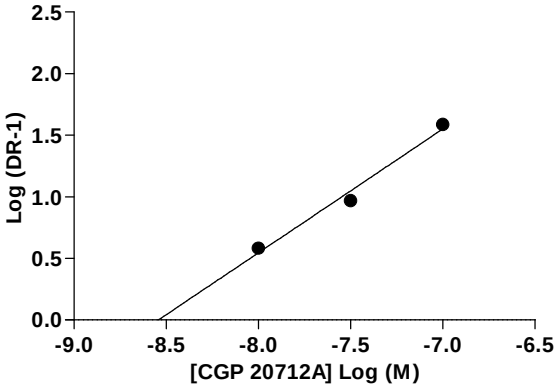

Figure 3.9 A, CRE-mediated SPAP transcription to cimaterol in the absence and presence of 10, 30 and 100 nM CGP 20712A in CHO-ssβ_1-CS cells. Bar graphs show basal SPAP secretion from unstimulated cells and that in response to 10, 30 and 100 nM CGP 20712A alone. Data are mean ± s.e.m. of triplicate determinations from a single experiment which is representative of seven separate experiments. **B**, Schild plot of data shown in B (slope 1.00, R^2 0.98).

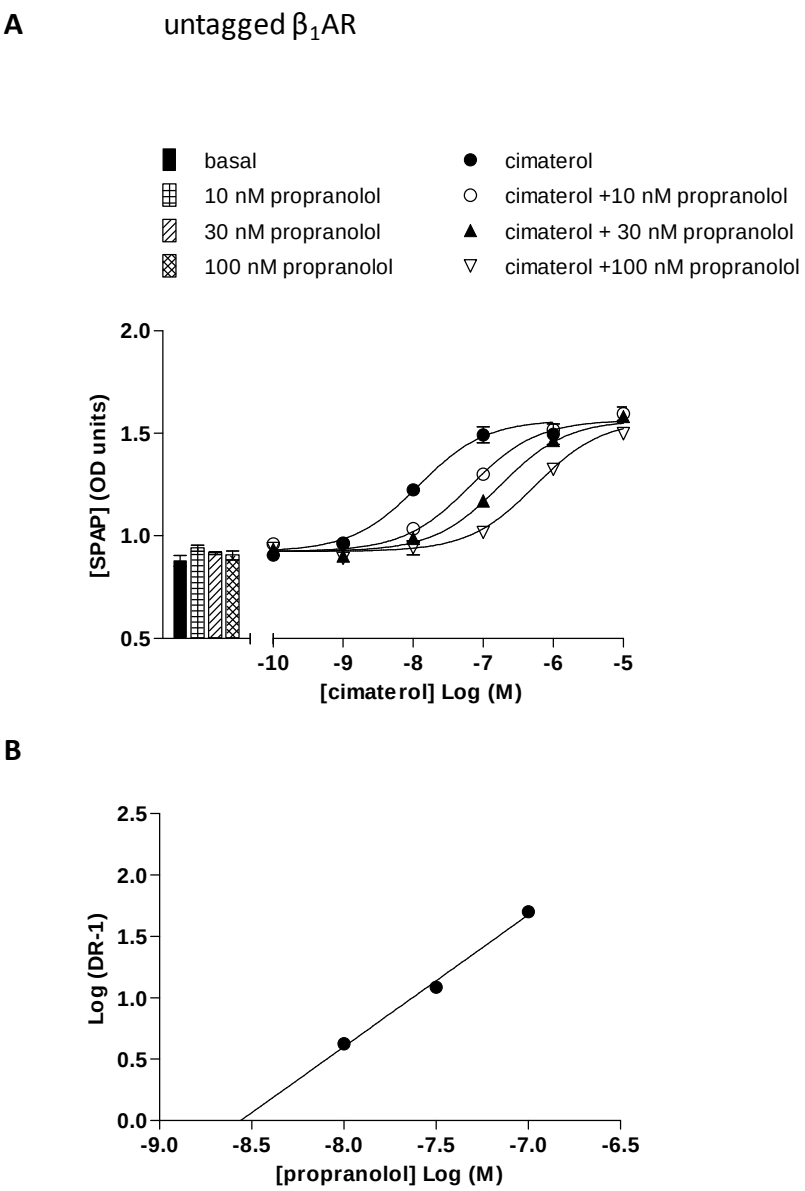

Figure 3.10 A, CRE-mediated SPAP transcription of cimaterol in the absence and presence of 10, 30 and 100 nM propranolol in CHO-β_1-CS cells. Bar graphs show basal SPAP secretion levels of unstimulated cells and that of cells treated with 10, 30 and 100 nM propranolol only. Data are mean ± s.e.m. from a single experiment which is representative of 23 separate experiments. **B**, Schild plot of data shown in A (slope 1.08, R^2 1.00).

A SNAP-tagged β_1AR

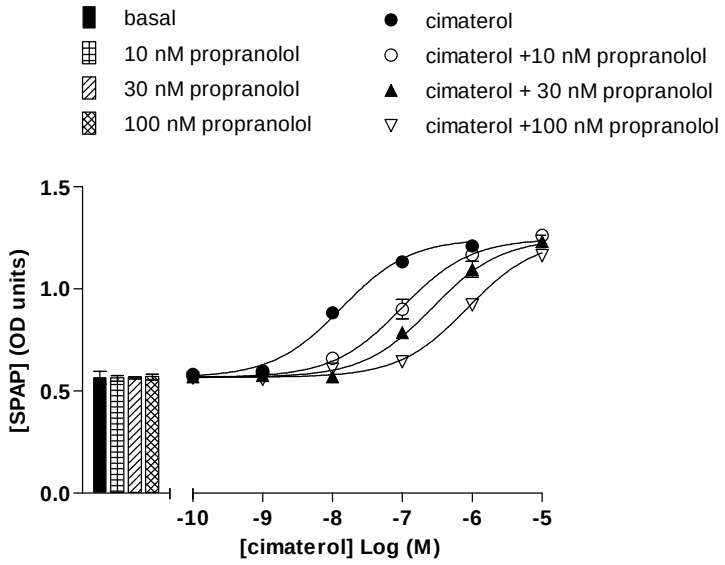

B

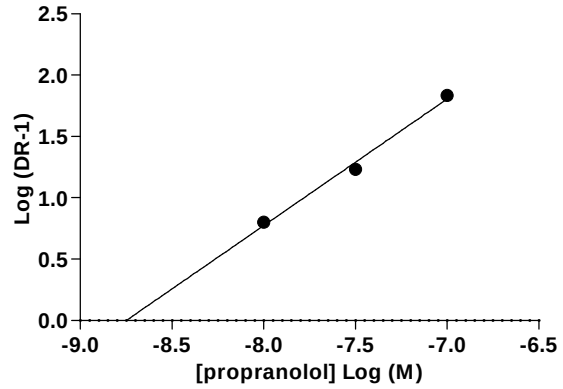

Figure 3.11 A, CRE-mediated SPAP transcription of cimaterol in the absence and presence of 10, 30 and 100 nM propranolol in CHO-ssβ_1-CS cells. Bar graphs show basal SPAP secretion levels of unstimulated cells and that of cells treated with 10, 30 and 100 nM propranolol only. Data are mean ± s.e.m. from a single experiment which is representative of 15 separate experiments. **B**, Schild plot of data shown in B (slope 1.03, R^2 0.98).

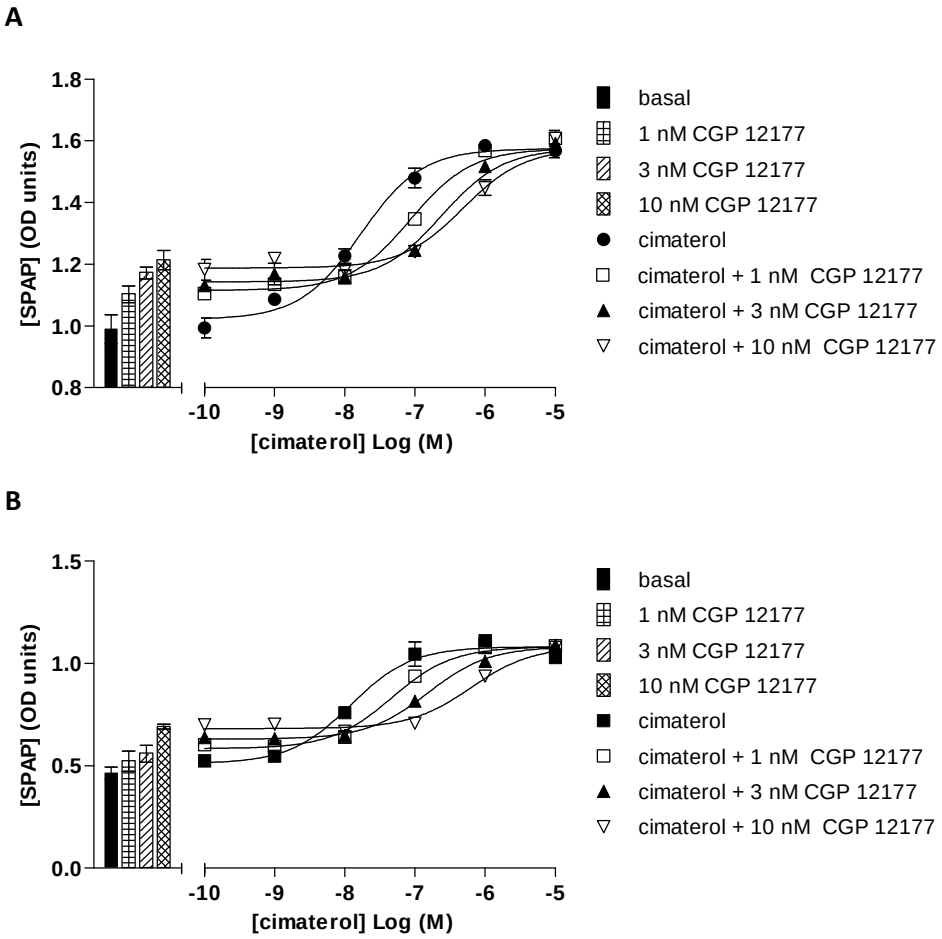

Figure 3.12 CRE-mediated SPAP transcription of cimaterol in the absence and presence of 1, 3 and 10 nM CGP 12177 in **A**, CHO-β_1-CS and **B**, CHO-ssβ_1-CS cells. Bars show basal SPAP secretion of unstimulated cells and that in response to 1, 3 and 10 nM CGP 12177 alone. Data are mean ± s.e.m. of triplicate determinations from a single experiment which is representative of A, 10 and B, 6 separate experiments.

The agonist effect of CGP 12177 is reported to be resistant to β-blocker action at the concentrations used to inhibit agonist-mediated stimulation of β_1AR through the catecholamine site (Baker *et al.*, 2003a; Konkar *et al.*, 2000). To confirm that we observe similar pharmacology in the CHO-CS cells expressing the native and also the SNAP-tagged β_1AR, we determined the affinity values of CGP 20712A and propranolol using CGP 12177 as the agonist in both CHO-β_1-CS and CHO-ssβ_1-CS cells.

CGP 20712A caused parallel rightward shifts of the CGP 12177 concentration-response curve in both cell lines, yielding similar pA_2 values in the two cell lines ($P > 0.05$, unpaired t-test) of 6.73 ± 0.22 (Schild slope 1.22 ± 0.21, n=7) and 6.79 ± 0.23 (Schild slope 1.18 ± 0.16, n=9) in CHO-β_1-CS (Figure 3.13) and CHO-ssβ_1-CS cells (Figure 3.14), respectively (Table 3.3). Increasing propranolol concentrations also caused right-ward shifts of the CGP 12177 concentration-response curves to give a pA_2 value of 6.04 ± 0.18 (Schild slope 0.85 ± 0.09, n=5) and 6.32 ± 0.13 (Schild slope 1.00 ± 0.12, n=8) in CHO-β_1-CS (Figure 3.15) and CHO-ssβ_1-CS cells (Figure 3.16), respectively. The Schild slopes obtained for CGP 20712A and propranolol against CGP 12177 at both the native and SNAP-tagged β_1-adrenoceptor were not significantly different from unity ($P > 0.05$, one-sample t-test performed for each ligand in comparison to a hypothetical value of 1.0), indicating a competitive interaction between the antagonist and CGP 12177 at the secondary β_1-adrenoceptor site.

According to classical receptor theory, the affinity of an antagonist for a given receptor should be independent of the agonist used. However, the affinity values calculated for CGP 20712A and propranolol against β-adrenoceptor agonist cimaterol is two orders of magnitude higher than affinity values calculated for the two antagonists when CGP 12177 was used as an agonist, in both CHO-β_1-CS ($P < 0.01$, unpaired t-test performed for both antagonists) and CHO-ssβ_1-CS cells ($P < 0.01$, unpaired t-test performed for both antagonists). This is in line with the two-site binding hypothesis for the β_1-adrenoceptor and describes the 'resistance' of the CGP 12177 partial agonist effect to β-blocker actions (Baker *et al.*, 2003a; Joseph *et al.*, 2004).

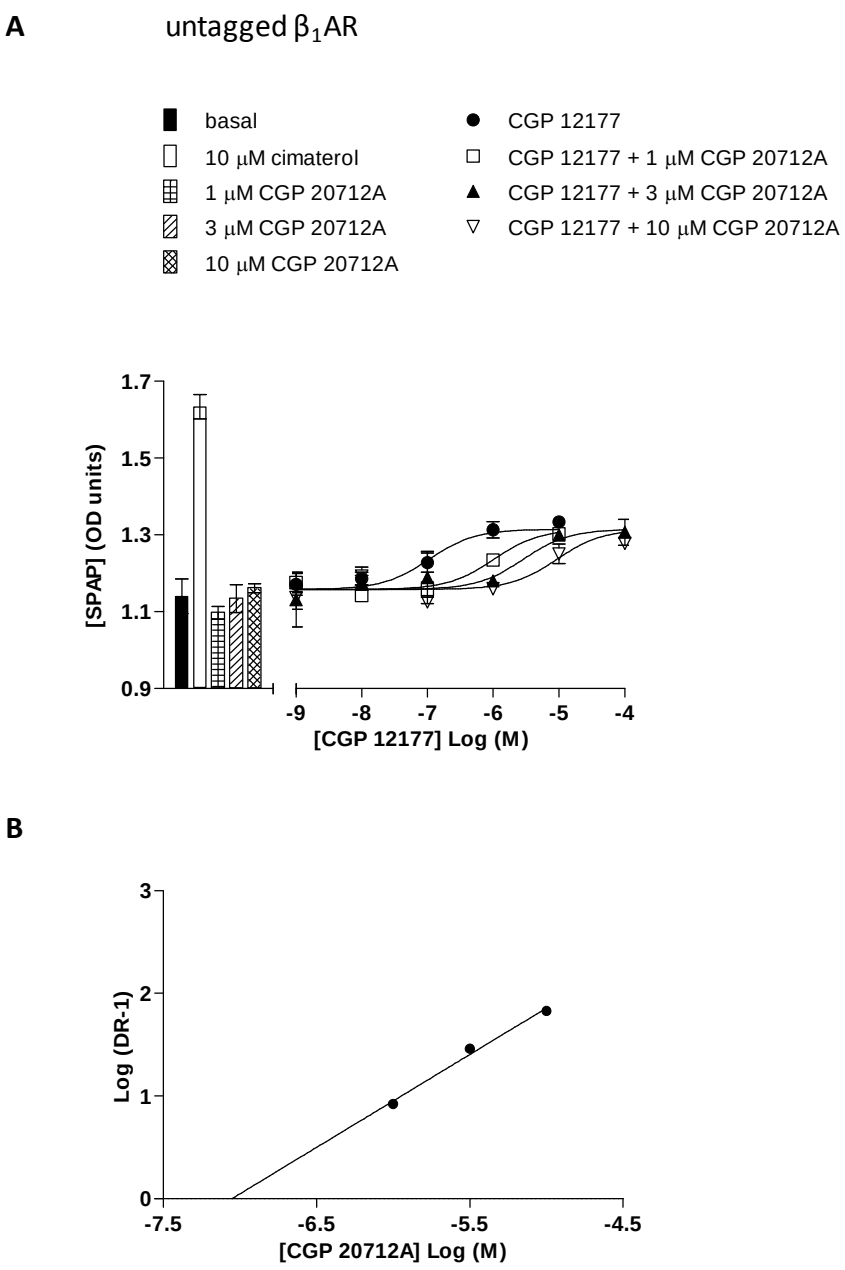

Figure 3.13 A, CRE-mediated SPAP transcription of CGP 12177 in the absence and presence of 1, 3 and 10 μM CGP 20712A in CHO-β_1-CS cells. Bar graphs show basal SPAP secretion of unstimulated cells and that in response to 10 μM cimaterol and 1, 3 and 10 μM CGP 20712A alone. Data are mean ± s.e.m. of triplicate determinations from a single experiment which is representative of seven separate experiments. **B**, Schild plot of data shown in A (slope 0.90, R^2 0.99).

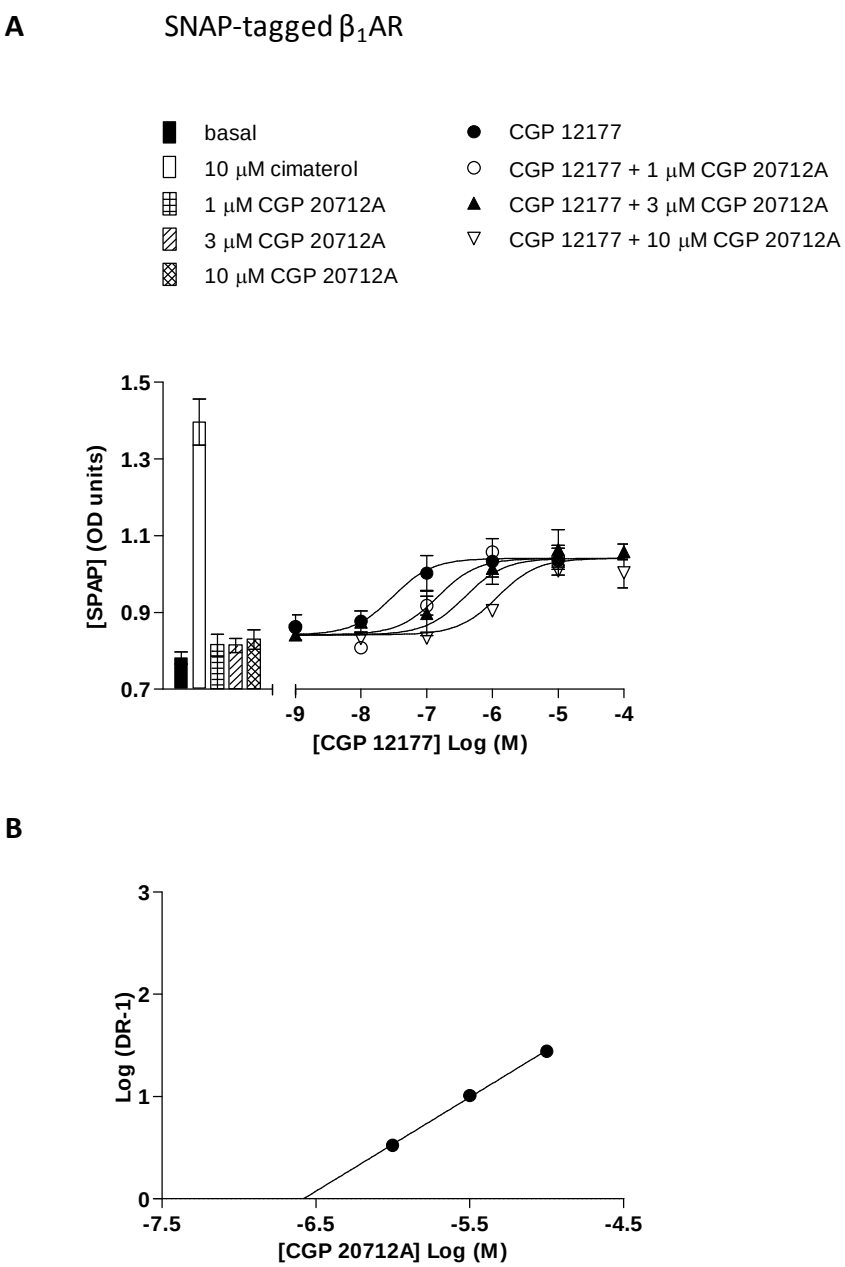

Figure 3.14 A, CRE-mediated SPAP transcription of CGP 12177 in the absence and presence of 1, 3 and 10 μM CGP 20712A in CHO-ssβ$_1$-CS cells. Bar graphs show basal SPAP secretion of unstimulated cells and that in response to 10 μM cimaterol and 1, 3 and 10 μM CGP 20712A alone. Data are mean ± s.e.m. of triplicate determinations from a single experiment which is representative of nine separate experiments. **B**, Schild plot of data shown in B (slope 1.09, R^2 1.00).

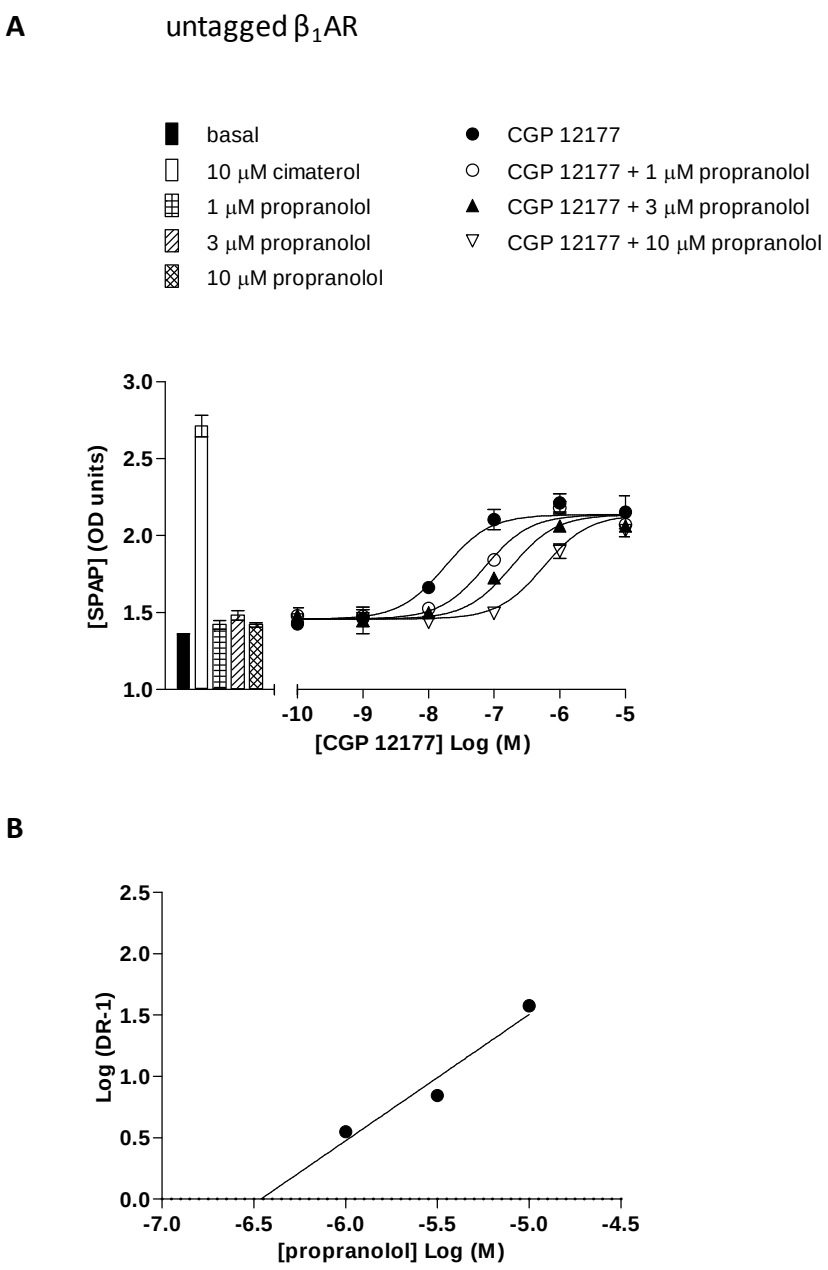

Figure 3.15 A, CRE-mediated SPAP transcription of CGP 12177 in the absence and presence of 1, 3 and 10 μM propranolol in CHO-β_1-CS cells. Bar graphs show basal SPAP production in unstimulated cells and that in response to 10 μM cimaterol and 1, 3 and 10 μM propranolol alone. Data are mean ± s.e.m. of triplicate determinations from a single experiment which is representative of five separate experiments. **B**, Schild plot of data shown in A (slope 1.03, R^2 0.94).

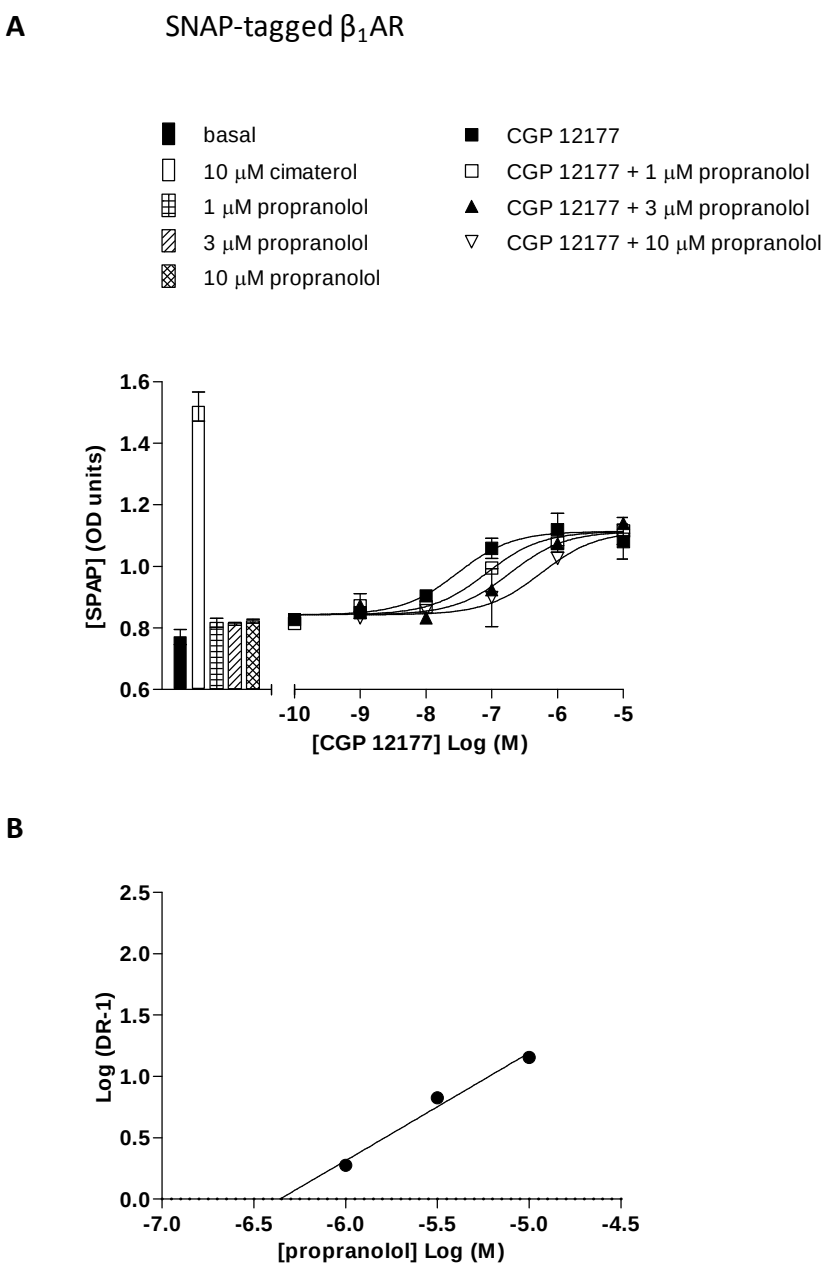

Figure 3.16 A, CRE-mediated SPAP transcription of CGP 12177 in the absence and presence of 1, 3 and 10 μM propranolol in CHO-ssβ$_1$-CS cells. Bar graphs show basal SPAP production in unstimulated cells and that in response to 10 μM cimaterol and 1, 3 and 10 μM propranolol alone. Data are mean ± s.e.m. of triplicate determinations from a single experiment which is representative of eight separate experiments. **B**, Schild plot of data shown in B (slope 0.88, R^2 0.98).

Table 3.3 Affinity values of β-adrenoceptor ligands at the SNAP-tagged and native β_1-adrenoceptor expressed in CHO-CS cells. Data are mean ± s.e.m. of a given (n) number of separate experiments. * denotes statistical significance ($p < 0.01$, unpaired t-test); for given antagonist compared K_D value obtained with CGP 12177 as an agonist to K_D value obtained with cimaterol as an agonist; for CGP 12177 compared K_D value obtained from partial agonist response curve using the operational model of partial agonism to K_D value obtained against cimaterol using the partial agonism method of Stephenson (1956). Affinity values of each ligand for β_1-adrenoceptor site 1 and site 2 determined at the native receptor were compared to those obtained at the SNAP-tagged receptor using unpaired t-tests, and no statistically significant difference in affinity values was determined ($P > 0.05$).

	CHO-β_1-CS cells			CHO-ssβ_1-CS cells		
agonist cimaterol (site 1)	pA_2	Schild slope	n	pA_2	Schild slope	n
CGP 20712A	8.84 ± 0.11	1.27 ± 0.12	5	8.82 ± 0.16	1.21 ± 0.09	7
propranolol	8.65 ± 0.07	1.00 ± 0.04	23	8.45 ± 0.07	1.16 ± 0.05	15
CGP 12177	9.61 ± 0.06	n/a	10	9.52 ± 0.10	n/a	6
agonist CGP 12177 (site 2)						
CGP 20712A	6.73 ± 0.22*	1.22 ± 0.21	7	6.79 ± 0.23*	1.18 ± 0.16	9
propranolol	6.04 ± 0.18*	0.85 ± 0.09	5	6.32 ± 0.13*	1.00 ± 0.12	8
CGP 12177 (partial agonism pK_A)	7.58 ± 0.13*	n/a	13	7.49 ± 0.13*	n/a	16

3.4 Discussion

The SNAP-tag technology provides an alternative strategy for the fluorescent labelling of target proteins, its main advantages being that the SNAP-tag can be linked to a variety of different fluorophores to fit experimental needs, and that cell impermeable labels are available to allow selective labelling of cell surface over intracellular proteins. In this chapter, the SNAP-tag was fused to the N-terminus of the β_1-adrenoceptor and expressed in Chinese hamster ovary (CHO) cells already containing a cAMP response element (CRE) promoter and a secreted placental alkaline phosphatase (SPAP) reporter gene. Stable clonal CHO-sigSNAP-β_1 cell lines (CHO-ssβ_1-CS) were generated and screened for cell surface receptor expression (using fluorescent confocal microscopy) and receptor functionality (in the CRE-SPAP gene transcription assay), with the view to be able to use the same clonal cell line for both imaging and functional studies.

The SNAP-tag is labelled in a suicide enzymatic reaction by means of a benzylguanine (BG) substrate linked to a fluorophore (e.g. AF-488), resulting in the fluorophore being covalently and irreversibly linked to the SNAP-tag. Here, the membrane impermeable substrate BG-488 was used to label SNAP-tagged β_1AR expressed on the cell surface of CHO-CS cells. This labelling strategy revealed a number of clonal cell lines that showed expression of the target fusion protein on the cell membrane. The SNAP-tag was engineered to be highly specific for its substrates, a result of truncations and multiple mutations in the active site of the human DNA repair protein O^6-

methylguanine methyltransferase (MGMT) (see Appendix I S5 for comparison of human MGMT protein sequence with engineered SNAP-tag protein sequence). This enzyme removes the methyl group from its DNA target O^6-methylguanine base to prevention of mutations, cytotoxicity and tumor development (Pegg, 2011). For prevention of the labelling process by an endogenous O^6-alkylguanine alkyltransferase, a cell impermeable SNAP-tag substrate was used in this study, but in addition CHO cell lines are deficient in this DNA repair protein (Gautier *et al.*, 2008). Equally, the engineered SNAP-tag is reported to display low intrinsic activity towards other proteins and biomolecules, such as double-stranded DNA, in cells (Juillerat *et al.*, 2005). In line with this, no non-specific labelling effects of BG-488 on cells expressing untagged β_1-adrenoceptors were observed.

No SNAP-tagged β_1AR expression was observed in ten clonal cell lines. However, they still expressed the antibiotic resistance gene product to allow these cell lines to survive in a geneticin enriched environment. Why is the resistance gene product, but not the β_1AR receptor expressed? The BG-488 concentration used here was not optimized, but a high concentration (1 µM) was used to ensure the presence of excess levels of substrate during the incubation process, and this amount was clearly sufficient to label receptors in five CHO-ssβ_1-CS cell lines. Incomplete integration of the plasmid may have occurred, with the result that (1) only a part of the plasmid vector (that included the antibiotic resistance gene but not the SNAP-tagged β_1-adrenoceptor gene) was successfully incorporated into the genomic DNA of

the cell; or (2) that the SNAP-tagged β_1-adrenoceptor sequence was integrated in a heavily methylated region of the genomic DNA and as such is not transcribed at all or at levels too low to detect. Although expression of SNAP-tagged β_1-adrenoceptors was observed for five clonal cell lines, the level of expression was clearly heterogeneous, with cell surface expression levels ranging from undetectable to high for cells within the same cell line. Since these are stable clonal cell lines that have shown some receptor expression, we can presume that both the antibiotic resistance and the SNAP-tagged β_1-adrenoceptor sequence were incorporated into the genomic DNA of the cell. This integration, however, may still be unstable, leading to the cell removing the receptor DNA. Alternatively, differences in the transcription and translation machinery of individual cells (within one clonal cell line) in terms of their rate or activation / inactivation at different steps, may be a contributing factor. Having used a cell membrane impermeable SNAP-tag substrate in this study, an estimation of expression efficiency of the SNAP-tagged β_1-adrenoceptors and thus a potential effect of fusing the N-terminal SNAP-tag to the β_1-adrenoceptor could not be determined. The use of a membrane permeable SNAP-tag substrate may have been useful here as a large numbers of SNAP-tagged β_1-adrenoceptors inside the cell may have highlighted issues with the transport of the fusion protein to the membrane. Western blotting experiments could have been used to further confirm those findings. It is also noteworthy that the N-terminus of the β_1-adrenoceptor has been reported to be subject to cleavage by proteases (Hakalahti *et al.*, 2010b), which would provide a mechanism that removes the N-terminal SNAP-tag,

thus resulting in a homogeneous cell line (comparable receptor expression in cells of clonal cell line) that appears heterogeneous when labelling with a SNAP-tag substrate. A fluorescent ligand binding approach could be used to test whether the same heterogenty is observed when labelling the receptor directly instead of the N-terminal SNAP-tag.

A CHO cell line was used in this study because it does not express the β_1-adrenoceptor endogenously. If unstable integration of the plasmid vector into the genomic DNA was the cause of the varied receptor expression level, we envisioned being able to correct that by dilution cloning one clone (CHO-ssβ_1-CS clone F6) again with the aim to select a sub-clone that has stably integrated the receptor construct into its genomic DNA and is capable of expressing the fusion protein on the cell membrane long term. The number of clones obtained in this screen was unsurprisingly greater (48) as the source was a clonal cell line rather than a transfected cell population. However, it appeared that heterogeneity within each sub-clone was still evident, even though less pronounced. Interestingly, with increasing passages of a clonal cell line generated from one sub-clone (CHO-ssβ_1-CS clone F6.1), the level of receptor expression also decreased and appeared increasingly heterogeneous, although these observations were not further tested in a radioligand binding assay that would have allowed better quantification of receptor expression levels in this cell line over time. This may be caused by two scenarios where (1) the receptor DNA is still present within the genomic DNA but the cell finds it increasingly difficult to transport the receptors to the surface (as only cell

surface receptors were labelled), or (2) the receptor DNA but not the resistance gene sequence was removed or silenced by the host cell (Palmer *et al.*, 1991). It may be a combination of the two scenarios where initially the cells express the fusion protein at good levels, but cannot sustain the expression of the fusion protein, whose transcription is driven by the immediate-early cytomegalovirus (CMV) promoter. Whilst the strong enhancement of gene transcription is desired for good expression levels of the receptor, the constitutive expression of the protein places increased stress on host cells to facilitate transcription, translation, post-translational modification, transport to the membrane and degradation. Over time (passage), cells that cannot cope with the continuous expression of the fusion protein die, leaving only cells behind which can cope because they either express the protein at a very low level (if at all), or have removed the receptor gene entirely. This results in a cell line which gradually expresses the target protein less and less. Different transfection vectors and systems have been used to try to address some of the issues mentioned above. Viral vectors such as the Adenovirus and Semliki Forest virus (SFV) achieve much higher expression levels in mammalian cells (Drazner *et al.*, 1997; Sen *et al.*, 2003) although viral vectors are mainly used in structural biology investigations (Lundstrom *et al.*, 2006). Inducible systems, however, allow expression of the target protein only when needed for experiments thereby reducing stress for cells. A cold-inducible expression system, for example, results in low expression levels at 37 °C and high expression levels at 33 °C temperatures (Boorsma *et al.*, 2000). However, this is not suitable for studies using

physiological conditions. A tetracycline-inducible system in which transcription of the target gene is turned on in the presence of tetracycline and has been used in *in vitro* (Chelikani *et al.*, 2006; Lee *et al.*, 2010) and *in vivo* studies (Fan *et al.*, 2012; Stieger *et al.*, 2009). If time had allowed, this would have been a valid strategy here to try to improve expression of SNAP-tagged β_1-adrenoceptors.

The second screening criterion was receptor functionality. Testing both receptor expression and functionality decreases the chance of selecting false positives: if only receptor expression is tested, we may assume functionality of expressed receptors, however, receptor function may be impaired due to incorrect folding events. Similarly, if only receptor function is tested, we may assume good receptor expression, however, very few receptors are needed for efficacious agonists to cause a maximal system response, which may not be enough receptors to allow detection in imaging studies. In addition, integration of the SNAP-tagged β_1AR construct (or a different part of the plasmid vector) in one (or more) of the six CRE promoter elements in the CHO-CS cells could have inactivated those resulting in different levels of transcription rates of the reporter gene (i.e. functional response readout). To investigate receptor function, the responses to forskolin, isoprenaline and cimaterol were determined. Forskolin activates adenylyl cyclase directly via a GPCR independent route, resulting in a rise in intracellular cAMP which can go on to activate the CRE SPAP reporter gene, and thus provides a read-out of the presence and functionality of the CRE-SPAP reporter gene complex. The β-

AR agonists isoprenaline and cimaterol however, can cause a rise of cAMP levels in the cell only by stimulating the SNAP-tagged β_1-AR. As such, for observation of a response to only forskolin but not to the agonists an impaired CRE-SPAP promoter gene could be ruled out and would have to be due to the absence of the SNAP-tagged β_1-adrenoceptor or possible interference of the SNAP-tag. However, for all clones, receptor expression (or lack of it) could be directly linked to receptor functionality (or lack of it), providing first clues that the SNAP-tag did not interfere with β-AR agonists isoprenaline and cimaterol binding to and activating the β_1-adrenoceptor.

The SNAP-tag has been fused to a variety of Class A and C GPCRs for reasons such as receptor visualisation and to investigate protein-protein interactions (Alvarez-Curto *et al.*, 2010; Maurel *et al.*, 2008), with no reports of the SNAP-tag causing hindrance or interference. Interference of the SNAP-tag with the receptor of interest is not expected (Gautier *et al.*, 2008; Keppler *et al.*, 2003), although no study has yet used a SNAP-tagged β_1-adrenoceptor fusion protein. Isoprenaline and cimaterol behaved as full agonists in cell lines expressing the native (untagged) and SNAP-tagged β_1-adrenoceptor, which demonstrates that the SNAP-tagged β_1-adrenoceptor was functional. CGP 12177 also exhibited agonist effects although it was less efficacious, producing a smaller maximal response than cimaterol in the same assay. Partial agonist responses of CGP 12177 have also been observed in human (Joseph *et al.*, 2003) and ferret myocardial preparations (Lowe *et al.*, 1999) and in recombinant systems using various assays (Joseph *et al.*, 2004; Konkar *et al.*, 2000). Whilst

the EC_{50} values for the agonists compared well between the native and the SNAP-tagged β_1-adrenoceptor, it did not provide a clear insight into possible effects of the fusion of the SNAP-tag to the N-terminus of the β_1-adrenoceptor on the binding properties of ligands to the receptor as any effects on affinity may have been masked by receptor expression differences between the two cell lines. As such, we investigated the affinity values of β-AR antagonists and CGP 12177 at the native and SNAP-tagged β_1-adrenoceptor. For a partial agonist, its affinity can be derived from its concentration-response curve using the operational model of partial agonism (Leff *et al.*, 1993) and is expected to be similar to its EC_{50} value as a partial agonist occupies all available receptors (i.e. no receptor reserve) in order to elicit its cellular response. This was indeed the case for CGP 12177 with affinity values in the region of circa 29 nM for both the untagged and SNAP-tagged β_1-adrenoceptor. However, when used as an antagonist to inhibit cimaterol-induced β_1-adrencoeptor responses, CGP 12177 displayed sub-nanomolar affinity (circa 0.3 nM) at both receptors. The affinity value of a ligand for its receptor is a constant, and according to classical receptor theory, should be similar regardless of the assay format used (e.g. partial agonism and inhibition of full agonist) to determine this value (Kenakin, 2005). Here, the two affinity values calculated for CGP 12177 are 100-fold different. This is in line with the literature that reports a two-site binding site hypothesis for the β_1-adrenoceptor describing a 'high affinity' catecholamine site 1 of the β_1-adrenoceptor where CGP 12177 inhibits β-AR agonist actions and a second 'low affinity' site 2 of the β_1-adrenoceptor where CGP 12177 exhibits agonist

activity (Baker *et al.*, 2003a; Joseph *et al.*, 2004; Konkar *et al.*, 2000). Here we confirmed that we were able to detect the previously described β_1-adrenoceptor pharmacology at the human β_1-adrenoceptor expressed in CHO cells using the SPAP gene reporter assay.

The data shown in this chapter indicates that the N-terminal SNAP-tag did not affect the ligand binding properties at the β_1AR, as similar affinities of β-AR ligands were observed at the native and tagged receptor at both site 1 and site 2 of the β_1-adrenoceptor. The affinities obtained for antagonists propranolol and CGP 20712A at the two β_1-adrenoceptor sites displayed similar differences as those determined for CGP 12177. Affinity values derived when inhibiting cimaterol concentration-response curves were at least 1.5 orders of magnitude higher than affinity values obtained when CGP 12177 was used as an agonist. According to classical receptor theory, the use of a different agonist to establish affinity values should not affect the affinity of an antagonist for a given receptor (Kenakin, 2008). Consistent discrepancies in affinity values as seen here have traditionally been attributed to ligands binding to a different receptor (Arunlakshana *et al.*, 1959; Black *et al.*, 1972) or a different binding site of a receptor (Konkar *et al.*, 2000). However, Baker *et al.* (2003c) showed that affinities of antagonists for the β_2-adrenoceptor were reduced when using a highly efficacious agonist that induces receptor phosphorylation which results in a different receptor conformation. Partial agonists were not found to have the same effect (Baker *et al.*, 2003c). However, studies using β_1AR knockout mice (Kaumann *et al.*, 2001) and

recombinant β_1AR (Konkar *et al.*, 2000; Pak *et al.*, 1996) have clearly demonstrated that the β_1-adrenoceptor alone was responsible for the observed two-site pharmacology. Here, the highly efficacious agonist cimaterol was used to determined affinity values for site 1. If the determined affinities of the βAR antagonists used here were affected by the use of a highly efficacious agonist as described by Baker *et al.* (2003c), it would have resulted in underestimated affinity values of the antagonists at the high affinity binding site, thus potentially pointing to even higher antagonist affinity values at the catecholamine site, which would further increase the differences in affinities of antagonist for the two different sites. The low affinities of propranolol and CGP 20712A at site 2 also show that the CGP 12177 agonist effect is antagonised at much higher β-blocker concentrations, which is consistent with the findings of Konkar *et al.* (2000) and Baker *et al.* (2003a) and the proposed two-site model of the β_1-adrenoceptor. Furthermore, the interactions between the antagonists and either cimaterol (site 1) or CGP 12177 (site 2) appear competitive as Schild slopes similar to 1.0 were obtained. In this study, we have not investigated the β_1-adrenoceptor two-site pharmacology in a different functional or binding assay to rule out artefacts associated with receptor over-expression, the cell line or the assay, as data presented here is in excellent agreement with values reported in the literature where a variety of expression levels and functional and binding assays on membrane, whole cell and tissue preparations were used (Baker *et al.*, 2003a; Joseph *et al.*, 2004; Kaumann *et al.*, 2008; Konkar *et al.*, 2000).

3.5 Conclusion

In this chapter, the SNAP-tag was successfully fused to the N-terminus of the β_1-adrenoceptor and the fusion protein expressed in CHO-CS cells. Clear visualisation of SNAP-tagged β_1AR was observed at the cell surface without any detectable non-specific labelling effect effects. The SNAP-tag technology was successfully used to screen for clonal cell lines expressing the fusion protein. However, expression of the fusion protein appeared to decline with increasing passages. Furthermore, the two-site pharmacology has been observed at the native human β_1-adrenoceptor expressed in CHO-CS cells using the CRE-SPAP gene reporter assay. This pharmacology was unaltered by the fusion of the SNAP-tag to the N-terminus of the β_1-adrenoceptor. As such, the CHO-β_1-CS and CHO-ssβ_1-CS cell lines can be used to further investigate the two-site hypothesis in subsequent studies.

Chapter 4

The pharmacology and imaging of BODIPY-TMR-CGP and BODIPY630/650-S-PEG8-propranolol at the human β_1-adrenoceptor

4.1 Introduction

Fluorescent ligands provide an alternative to radiolabelled ligands in studies determining the affinity values of unlabelled competitor ligands for GPCRs (McGrath *et al.*, 1996; Stoddart *et al.*, 2012). The use of fluorescent ligands allows direct visualisation of the receptor of interest in its native environment (Becker *et al.*, 2001; Schneider *et al.*, 2007). Functional and binding studies have been carried out on cell populations (Baker *et al.*, 2003d; Stoddart *et al.*, 2012) and single living cells (Briddon *et al.*, 2007; Hara *et al.*, 2009; May *et al.*, 2010b) using fluorescent ligands alone or in conjunction with fluorescently labelled receptors (May *et al.*, 2011).

A large variety of fluorophores are commercially available, and BODIPY derivatives in particular have been widely used in biological disciplines to achieve the labelling of protein targets (Hara *et al.*, 2009; Rayo *et al.*, 2011; Ying *et al.*, 2011). Fluorescent ligands are generated by chemically coupling a fluorophore to the ligand of interest via a linker (Middleton *et al.*, 2005). However, the fluorophore itself is comparable in size to a small molecular weight ligand and thus can markedly influence the pharmacology of that ligand (Baker *et al.*, 2010). The affinity of a ligand can be reduced but also increased (Vernall *et al.*, 2012).

CGP 12177 antagonises β-adrenoceptor agonists at the endogenous high affinity catecholamine site (site 1) of the β_1-adrenoceptor, but has also been shown to exert agonist actions through a second low affinity “CGP 12177” site

(site 2) of the β_1-adrenoceptor (Baker *et al.*, 2003a; Konkar *et al.*, 2000; Pak *et al.*, 1996). As a hydrophilic ligand it has been labelled with radioisotopes (Dubois *et al.*, 1996; Staehelin *et al.*, 1983) and used extensively to determine affinity values of unlabelled antagonists (Baker, 2005; Joseph *et al.*, 2004).

BODIPY-TMR-CGP is a tetramethylrhodamine (TMR) derivative of the β-adrenoceptor ligand CGP 12177 (BY-CGP; Figure 4.1A) and its binding and functional properties have been characterised at the human β_2-adrenoceptors in CHO cells (Baker *et al.*, 2003d) and it has been used for visualisation of adrenoceptors in mouse vascular tissue (Daly *et al.*, 2010). To date, no fluorescent ligand has been fully evaluated at the human β_1-adrenoceptor, but the high affinity of the CGP 12177 with which it antagonises β-adrenoceptor agonists at the endogenous catecholamine site of the β_1-adrenoceptor may suggest a potential use of the fluorescent CGP 12177 derivative to visualise the native β_1-adrenoceptor. Furthermore, a fluorescent ligand that displays a similar pharmacology to CGP 12177 at the β_1-adrenoceptor would allow the investigation of receptor-ligand interactions to further our understanding of the nature of the second "CGP 12177" site 2 of the receptor.

In this chapter, we investigated the binding of two fluorescent β-adrenoceptor ligands: BODIPY-TMR-CGP and BODIPY630/650-S-PEG8-propranolol (a derivative of the β-adrenoceptor antagonist propranolol; BY-PROP; Figure 4.1B). We aimed to evaluate the pharmacology of both fluorescent ligands at the human β_1-adrenoceptor expressed in CHO-CS cells,

using the same functional assay that was used to investigate the pharmacology of their unlabelled counterparts (Chapter 3). Secondly, we aimed to use confocal microscopy to determine the binding properties of both fluorescent ligands and to visualise the β_1-adrenoceptor in CHO-β_1-CS cells with the view to use these fluorescent ligands in subsequent fluorescence microscopy experiments that allow the investigation of ligand-receptor interactions at the single cell level in real time.

A

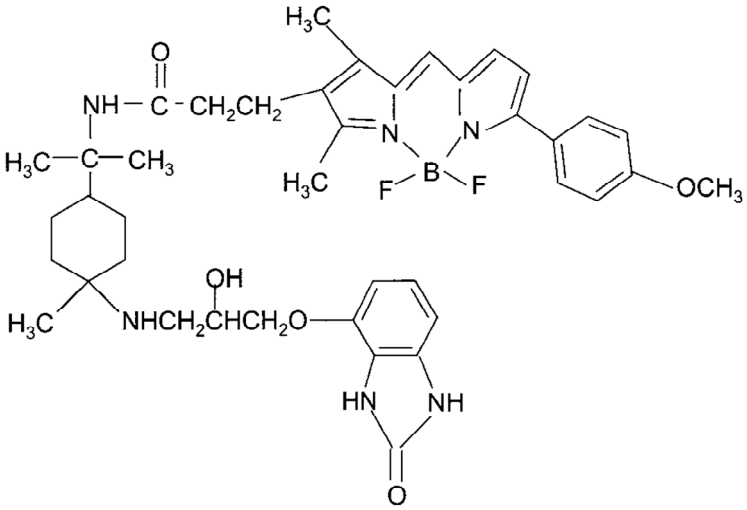

B

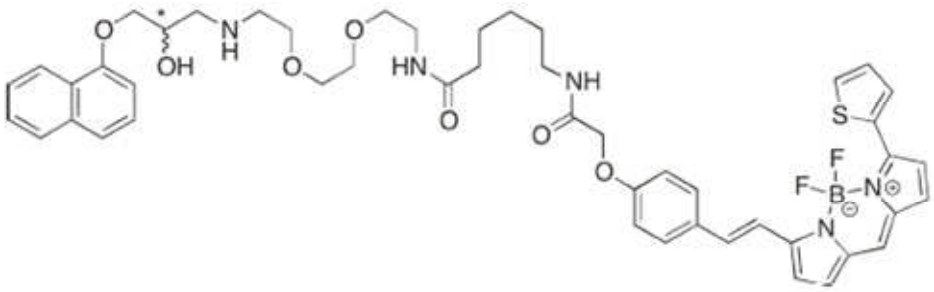

Figure 4.1 Structure of **A**, BODIPY-TMR-CGP (taken from Baker *et al.* (2003d)) and **B**, BODIPY630/650-S-PEG8-propranolol (taken from Baker *et al.* (2011a)).

4.2 Methods

Cell culture

The CHO-β_1-CS and CHO-CS cell lines were maintained as described in *Methods: Cell culture*. CHO-ssβ_1-CS cells were maintained in growth media supplemented with 1 mg/mL geneticin (G418).

CRE-mediated SPAP transcription

The CRE-dependent transcription of secreted placental alkaline phosphatase (SPAP) was determined in agonist and antagonist mode as described in *Methods: CRE-mediated SPAP transcription assay*.

Confocal microscopy

This was performed as described in *Methods: Confocal microscopy* using 8-well borosilicate chambered-coverglass plates imaged on a Zeiss LSM710 laser scanning microscope with a 40x1.3NA oil immersion lens. In this chapter, BODIPY-TMR-CGP (BY-CGP) and BODIPY630/650-S-PEG8-propranolol (BY-PROP) binding to the β_1-adrenoceptor was investigated in co-localisation studies with the SNAP-tagged β_1-adrenoceptor expressed in CHO-CS cells, and saturation and displacement binding studies in CHO-β_1-CS cells as outlined in *Methods: Confocal microscopy*. Cell surface SNAP-tagged β_1-adrenoceptors were labelled using 1 µM BG-488 (final concentration; 30 min, in the dark, 37 °C). A 543 nm and 633 nm HeNe and 488 nm argon lasers were used to excite BY-CGP, BY-PROP and BG-488, respectively. A variable spectral

detection system was used to capture emission at 545-580 nm, 645-680 nm and 480-530 nm, respectively. All images were taken at 1024x1024 pixels, averaging at 4 frames. A pinhole diameter of 1 Airy unit was used. The laser power, gain and offset settings were kept constant throughout each experiment to allow direct comparison of binding levels for each fluorescent ligand.

Internalisation

This was performed as described in *Methods: Confocal microscopy* using the CHO-ssβ_1-CS cell line. Cell surface SNAP-tagged β_1-adrenoceptors were labelled using 1 µM BG-488 (final concentration; 10 min, in the dark, 21 °C) and imaged using 488 nm argon laser excitation with emission captured through a 480-530 nm filter (1024x1024 pixels, averaging at 4 frames). A pinhole diameter of 1 Airy unit was used.

4.3 Results

CRE-mediated SPAP transcription

Initial experiments focussed on characterising the pharmacology of the fluorescent CGP 12177 ligand, BODIPY-TMR-CGP (BY-CGP), and confirming that it had similar pharmacological properties to the parent compound and could thus be a useful tool in the investigation of the secondary β_1-adrenoceptor site. In the CRE-mediated SPAP transcription assay, BY-CGP caused a concentration-dependent secretion of SPAP that was 25.6 ± 3.2 % of the maximum cimaterol response with a pEC_{50} of 7.12 ± 0.13 (n=8, Figure 4.2, Table 4.1), and thus, like the parent compound (Chapter 3, Figure 3.6), appeared as a partial agonist in this system. Using cimaterol as a full agonist to determine the system maximum response, the pK_D for BY-CGP was extracted from its concentration-response curve using the operational model of partial agonism (Leff *et al.*, 1993) and was determined to be 7.06 ± 0.13 (n=8). Fixed concentrations of BY-CGP shifted the cimaterol concentration-response curve in a manner consistent with its partial agonist actions, giving a pK_D value of 9.23 ± 0.06 (n=10, Figure 4.3A). This was two orders of magnitude different to the affinity value derived from its partial agonist response curve, which was consistent with the two-site binding hypothesis for the β_1-adrenoceptor described in previous studies (Baker *et al.*, 2003a; Konkar *et al.*, 2000; Pak *et al.*, 1996). To further confirm the lower affinity of BY-CGP at the second site, CGP 12177 concentration-response curves were obtained in the absence and presence of two fixed concentrations of BY-CGP, giving a

pK_D of 7.28 ± 0.22 (n=3, Figure 4.3B), which was in good agreement with the value derived from the partial agonist response curve.

To demonstrate that the BY-CGP agonist response, like the CGP 12177 agonist response (Chapter 3, Figure 3.13 and 3.15), required much higher β-blocker concentrations to be inhibited compared to the cimaterol agonist response, BY-CGP-stimulated SPAP secretion was measured in the absence and presence of 1 μM propranolol, giving an apparent pK_D value for propranolol of 6.46 ± 0.26 (n=3, Figure 4.4). Due to cost implications of using very high concentrations of the fluorescent ligand, the inhibitory effects of only one unlabelled antagonist at only one concentration could be tested.

BODIPY630/650-S-PEG8-propranolol (BY-PROP) showed no efficacy in the SPAP gene reporter assay as the SPAP secretion levels were unchanged for all BY-PROP concentrations used and compared to the levels observed in unstimulated (basal) conditions (Figure 4.5) and thus, like its parent compound (Chapter 3, Figure 3.7), appeared as an antagonist in this system. Fixed concentrations of BY-PROP caused parallel rightward shifts of cimaterol concentration response curves, yielding a pK_D value of 7.55 ± 0.05 (n=8, Figure 4.6). From the shifts of the cimaterol concentration-response curves, using the Schild plot analysis, a Schild slope of 1.16 ± 0.07 (n=8) was determined, which was not significantly different from unity ($P > 0.05$, one-sample t-test in comparison to a hypothetical value of 1.0) and thus indicating a competitive interaction between the two ligands at the catecholamine β_1-adrenoceptor site. To determine the affinity of BY-PROP for the secondary β_1-adrenoceptor

site, CGP 12177 concentration-response curves in the absence and presence of 1 µM BY-PROP were obtained. Due to the expense of using high concentrations of the fluorescent ligand, only one fixed concentration was used to shift the CGP 12177 concentration-response curve. From this a pK_D value of 6.57 ± 0.20 (n=4, Figure 4.7) was estimated.

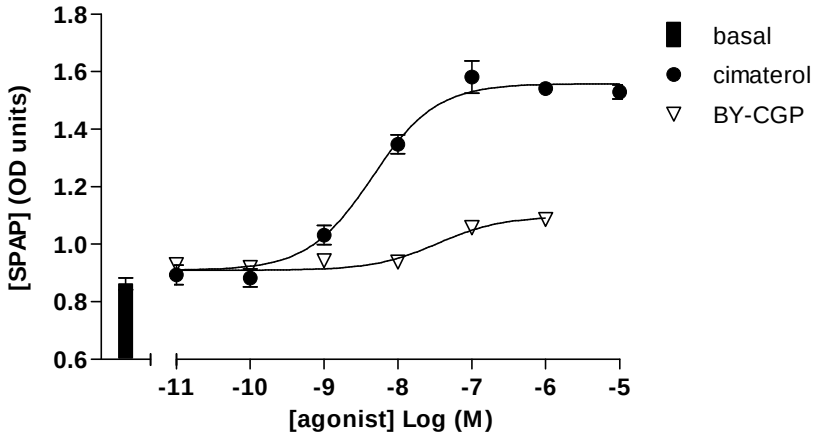

Figure 4.2 CRE-mediated SPAP secretion in response to cimaterol and BODIPY-TMR-CGP (BY-CGP) in CHO-β_1-CS cells. Bar represents SPAP secretion from unstimulated cells. Data points are mean ± s.e.m. of triplicate determinations from a single experiment which is representative of at least eight separate experiments.

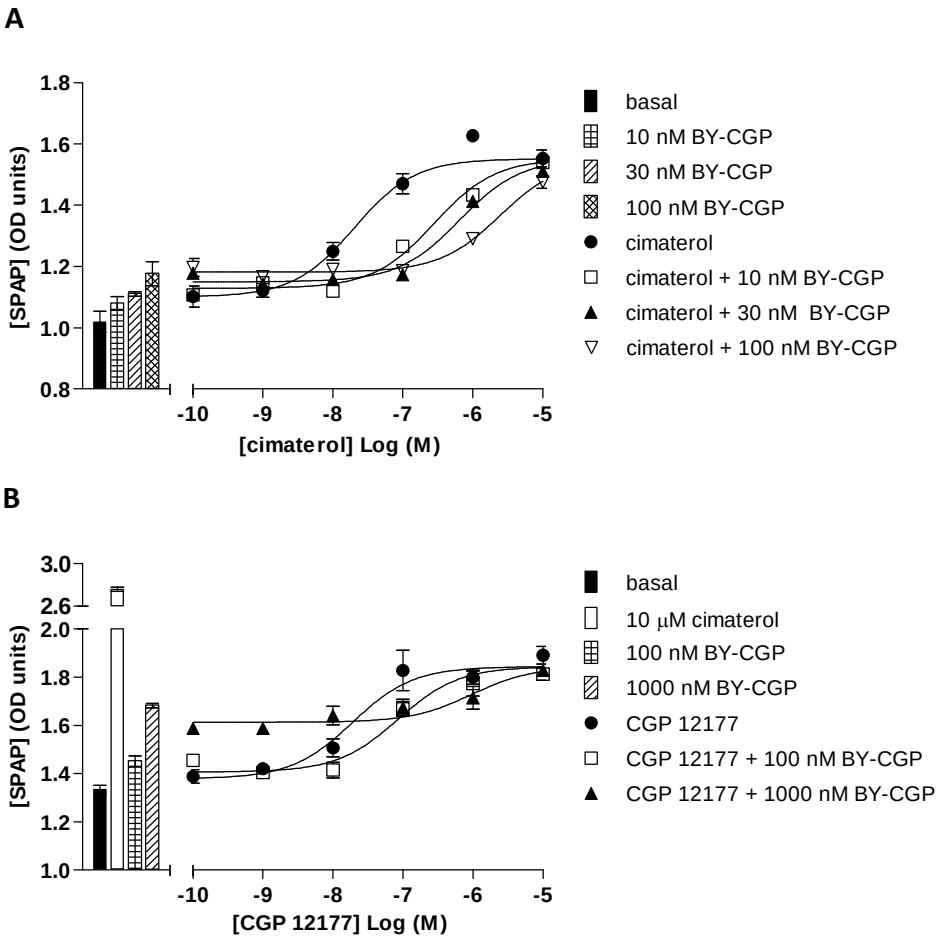

Figure 4.3 SPAP secretion in response to **A**, cimaterol and **B**, CGP 12177 in the absence and presence of BODIPY-TMR-CGP (BY-CGP). The bars represent basal SPAP secretion and that in response to the fixed BODIPY-TMR-CGP concentrations used. SPAP secretion in response to 10 μM cimaterol was also determined in panel B. Data points are mean ± s.e.m. of triplicate determinations from a single experiment and are representative at least three separate experiments.

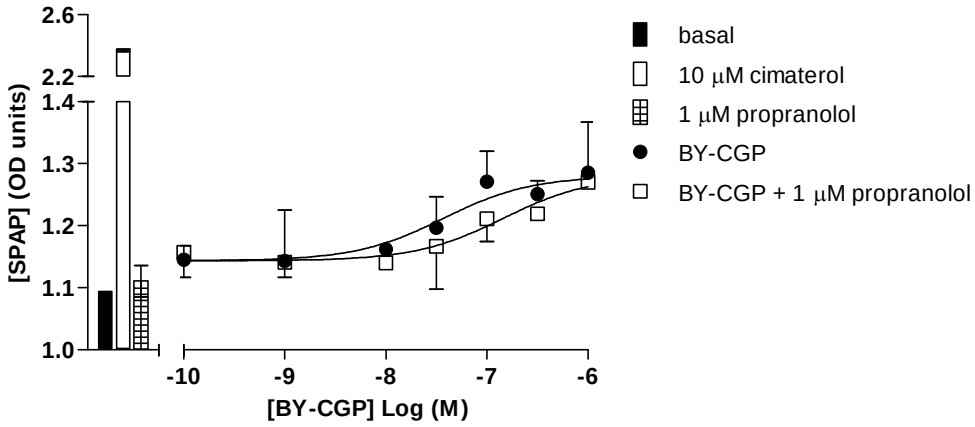

Figure 4.4 SPAP secretion induced by BODIPY-TMR-CGP (BY-CGP) in the absence and presence of 1 μM propranolol. Bars represent basal SPAP secretion from unstimulated cells, SPAP secretion in response to 10 μM cimaterol and 1 μM propranolol alone. Data points are mean ± s.e.m. of triplicate determinations of a single experiment which is representative of 3 separate experiments.

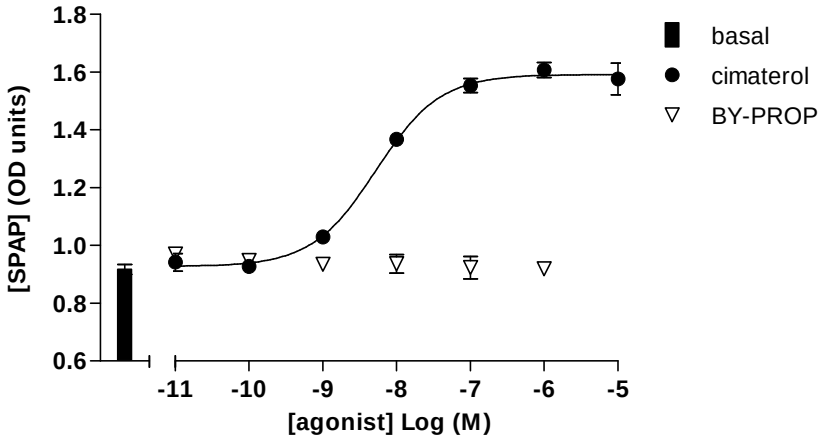

Figure 4.5 CRE-mediated SPAP secretion in response to cimaterol and BODIPY630/650-S-PEG8-propranolol (BY-PROP) in CHO-β_1-CS cells. Bar represents SPAP secretion from unstimulated cells. Data points are mean ± s.e.m. of triplicate determinations from a single experiment which is representative of at least four separate experiments.

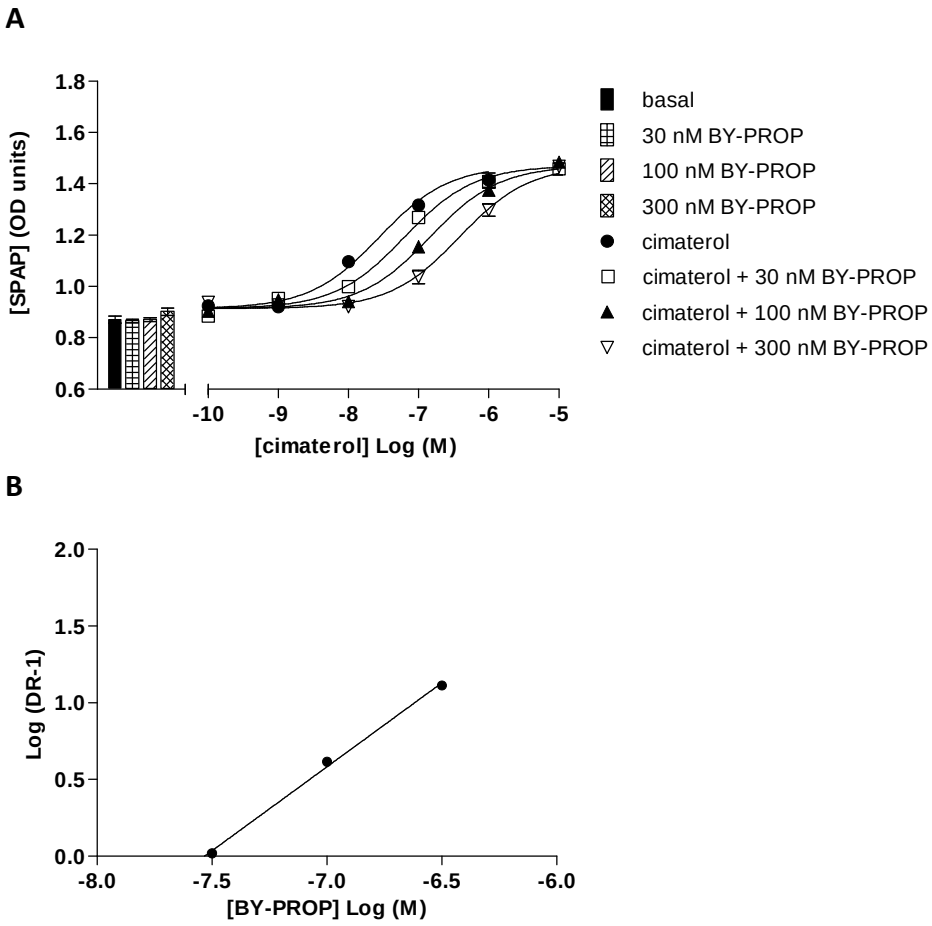

Figure 4.6 A, SPAP secretion of cimaterol in the absence and presence of increasing concentrations of BODIPY630/650-S-PEG8-propranolol (BY-PROP). Bars show basal SPAP secretion from unstimulated cells and that in response to 30, 100 and 300 nM BY-PROP. Data points are mean ± s.e.m. of triplicate determinations from a single experiment and are representative of a total of eight separate experiments. **B**, Schild plot of data shown in A (slope 1.09, R^2 1.00).

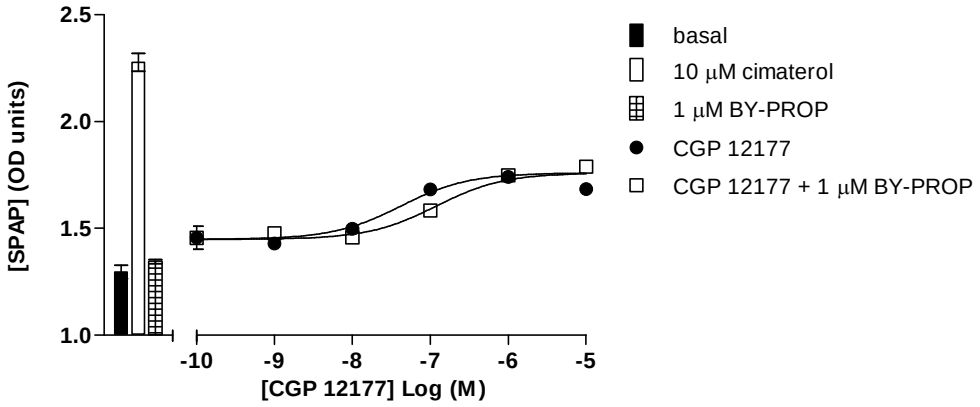

Figure 4.7 SPAP secretion of CGP 12177 in the absence and presence of 1 μM BODIPY630/650-S-PEG8-propranolol (BY-PROP). Bars show basal SPAP secretion from unstimulated cells and that in response to 10 μM cimaterol and 1 μM BY-PROP alone. Data points are mean ± s.e.m. of triplicate determinations from a single experiment and are representative of a total of three separate experiments.

Table 4.1 Potency and affinity parameters of BODIPY-TMR-CGP 12177 (BY-CGP) and BODIPY630/650-S-PEG8-propranolol (BY-PROP) compared to their respective parent ligands. Data are mean ± s.e.m of (n) numbers of separate experiments. Data shown for unlabelled CGP 12177 and propranolol were obtained in Chapter 3.

	CGP 12177	n	BY-CGP	n	propranolol	n	BY-PROP	n
pEC_{50}	7.73 ± 0.11	14	7.12 ± 0.13	8	no response	8	no response	4
E_{MAX} (% cimaterol)	47.8 ± 3.6	14	25.6 ± 3.2	8	no response	8	no response	4
pK_A (partial agonism)	7.62 ± 0.13	14	7.06 ± 0.13	8	n/a		n/a	
pA_2 (agonist CGP 12177)	n/a		7.28 ± 0.22	3	6.04 ± 0.18	5	6.57 ± 0.20	4
pA_2 (agonist cimaterol)	9.61 ± 0.06	10	9.23 ± 0.06	10	8.65 ± 0.07	23	7.55 ± 0.05	8
pA_2 (agonist BY-CGP)					6.46 ± 0.26	3		

Responses of β-AR ligands are specific to CHO cells expressing the β_1-adrenoceptor

To show that the CRE-mediated SPAP transcription in response to β-adrenoceptor ligands was specific to the β_1-adrenoceptor expressed in CHO cells, all βAR ligands used throughout this thesis were tested in CHO-CS cells (i.e. cells containing the CRE-SPAP reporter, but not the β_1-adrenoceptor gene) and untransfected CHO-K1 cells (i.e. cells not transfected with either the CRE-SPAP reporter or the β_1-adrenoceptor). No SPAP secretion was detected in untransfected CHO-K1 cells following treatment with any of the ligands used (Figure 4.8). However, forskolin stimulated a CRE-SPAP response in control CHO-CS cells (pEC_{50} 5.14 ± 0.04, n=3; Figure 4.8A) similar to that seen in CHO-β_1-CS cells (pEC_{50} 5.48; chapter 3, Figure 3.1). There was no stimulation of SPAP secretion in response to any of the β-agonists and antagonists used in control CHO-CS cells (n=3; Figure 4.8B). These data confirm that the SPAP responses to β-agonists described throughout this thesis were dependent on the presence of the transfected β_1-adrenoceptor.

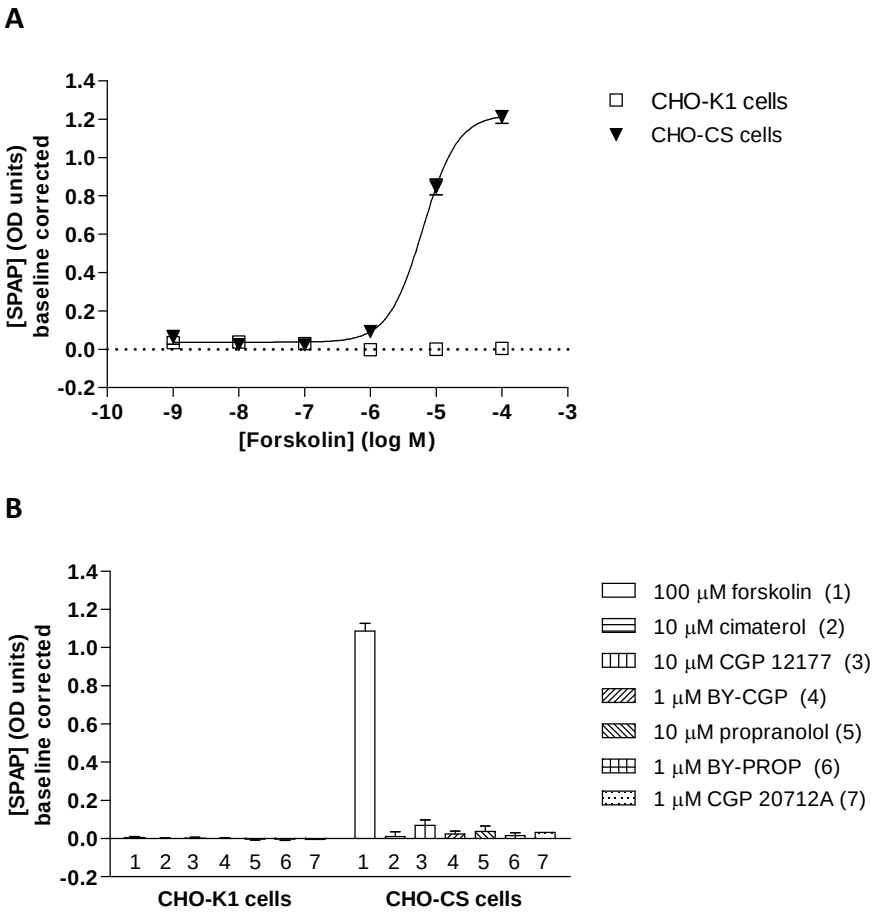

Figure 4.8 A, CRE-mediated SPAP transcription of forskolin in CHO-K1 and CHO-CS cells. **B**, SPAP secretion in response to 10 µM cimaterol, 10 µM CGP 12177, 1µM BODIPY-TMR-CGP 12177 (BY-CGP), 10 µM propranolol, 1 µM BODIPY630/650-S-PEG8-propranolol (BY-PROP) and 1 µM CGP 20712A in CHO-K1 and CHO-CS cells. Response to 100 µM forskolin was also measured as a control.

BY-CGP and BY-PROP binding to the SNAP-tagged human β_1AR

In order to confirm that BODIPY-TMR-CGP and BODIPY630/650-S-PEG8-propanolol were able to specifically label the β_1-adrenoceptor, their binding to the SNAP-tagged β_1-adrenoceptor in CHO-ssβ_1-CS cells was examined. The cell impermeable SNAP-tag substrate BG-488 was used to label cell surface SNAP-tagged β_1-adrenoceptors and clear membrane labelling can be seen in CHO-ssβ_1-CS cells when imaged using the 488 nm (green) channel. As previously described (Chapter 3), the expression of the SNAP-tagged β_1-adrenoceptor is not homogenous and different expression levels of the SNAP-tagged β_1-adrenoceptor can be seen in Figure 4.9 and 4.10. However, only a very small percentage of cells showed no or very low expression of the receptor such that it was not detected at the settings used. 2 nM BODIPY-TMR-CGP (circa 3x K_D concentration at site 1; Figure 4.9) and 20 nM BY-PROP (circa 1x K_D concentration at site 1; Figure 4.10) were able to bind to CHO-ssβ_1-CS cells and clear membrane labelling was observed in the 543 nm and 633 nm (both red) channels, respectively. It can also be seen that cells with greater SNAP-β_1 expression were able to bind more of the fluorescent ligand used. When superimposed (yellow pixels), the binding of both fluorescent ligands was clearly seen to localise well with the cell membrane SNAP-tagged β_1AR fluorescence. The co-localisation plots show that most pixels are in quadrant 3 representing co-localisation of SNAP-β_1 (Ch1) and fluorescent ligand (Ch2). Furthermore, BY-CGP and BY-PROP binding levels were reduced in the presence of 100 nM CGP 20712A (60 x K_D concentration at the catecholamine site to achieve complete inhibition; pre-incubation for 30

minutes at 37 °C), whilst good SNAP-tagged β_1-adrenoceptor labelling with BG-488 was seen. The co-localisation plot now shows most pixels in quadrant 1, representing SNAP-tagged β_1-adrenoceptors labelled with BG-488 but not with the fluorescent ligand. This indicates that both fluorescent ligands specifically bind to the SNAP-tagged receptor.

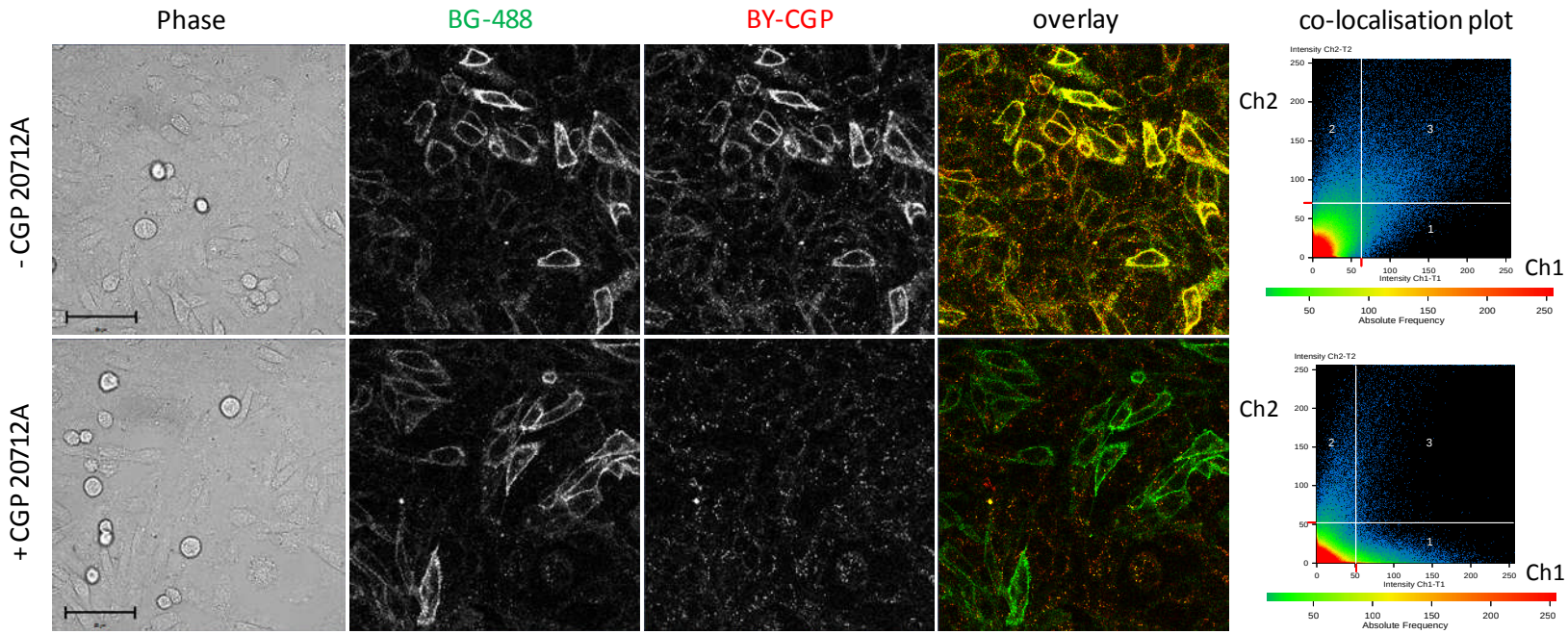

Figure 4.9 Binding of 2 nM BY-CGP to CHO-ssβ_1-CS cells in the absence and presence of 100 nM CGP 20712A. The panels from left to right show the phase contrast image of the field of view imaged, the fluorescence monitored in the green (488 nm) channel (BG-488 labelled SNAP-tagged β_1-adrenoceptors), the fluorescence monitored in the red 543 nm channel (2 nM BY-CGP), an overlay of the images collected in the 488 nm (Ch1) and 561 nm (Ch2) channel with co-localisation of red and green fluorescence shown by the yellow pixels, and a co-localisation plot with co-localised pixels in compartment 3. Co-localisation analysis was done as described in *Methods* (Chapter 2). Prior to imaging, the CHO-ssβ_1-CS cells were incubated with 1 µM BG-488 (30 mins, 37 °C) to label the SNAP-tagged β_1-adrenoceptor. The cells were then washed and pre-incubated with 100 nM CGP 20712A (30 mins, 37 °C) before the cells were exposed to 2 nM BY-CGP (10 min, 21 °C). Both CGP 20712A and BY-CGP were not washed out before imaging. Scale bars = 50 µm.

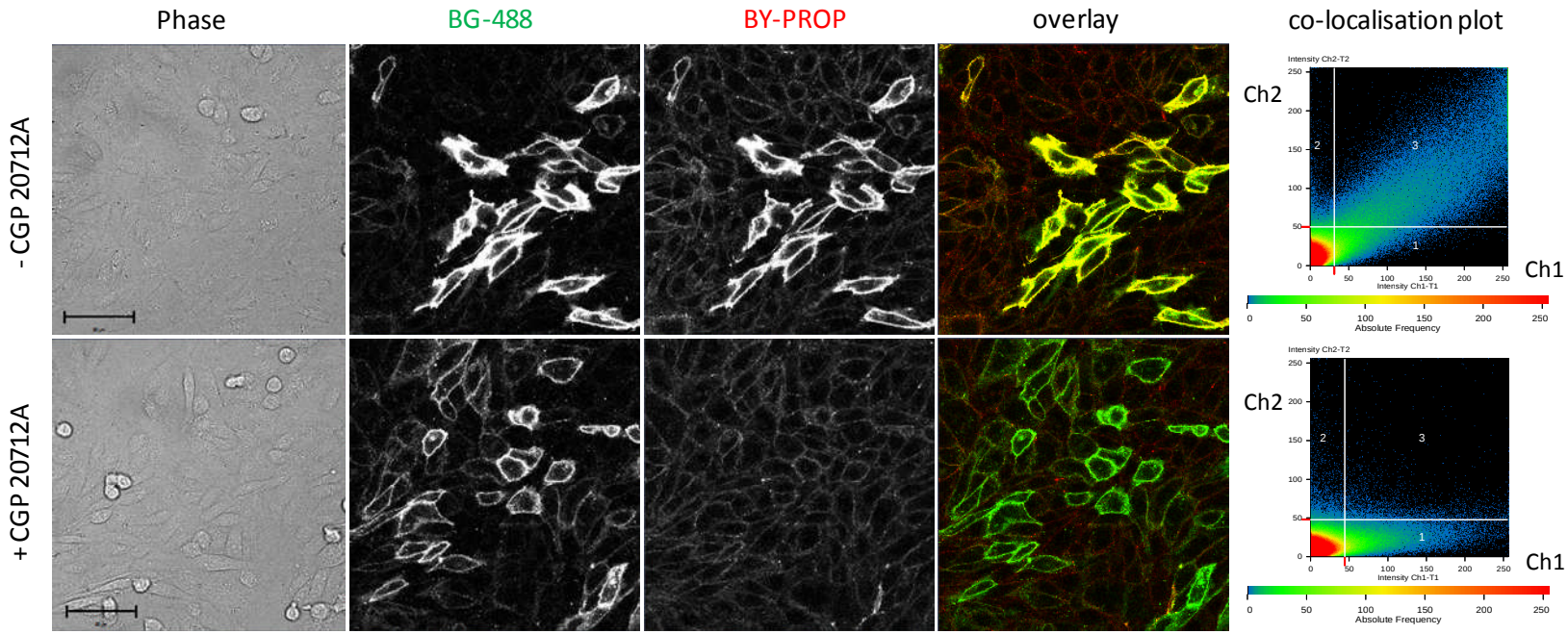

Figure 4.10 Binding of 20 nM BY-PROP to CHO-ssβ_1-CS cells in the absence and presence of 100 nM CGP 20712A. The panels from left to right show the phase contrast image of the field of view imaged, the fluorescence monitored in the green (488 nm) channel (BG-488 labelled SNAP-tagged β_1-adrenoceptors), the fluorescence monitored in the red (633 nm) channel (20 nM BY-PROP), an overlay of the images collected in the 488 nm (Ch1) and 633 nm (Ch2) channel with co-localisation of red and green fluorescence shown by the yellow pixels, and a co-localisation plot with co-localised pixels in compartment 3. Co-localisation analysis was done as described in *Methods* (Chapter 2). Prior to imaging, the CHO-ssβ_1-CS cells were incubated with 1 µM BG-488 (30 mins, 37 °C) to label the SNAP-tagged β_1-adrenoceptor. The cells were then washed and pre-incubated with 100 nM CGP 20712A (30 mins, 37 °C) before exposure of cells to 2 nM BY-PROP (10 min, 21 °C). Both CGP 20712A and BY-PROP were not washed out before imaging. Scale bars = 50 µm.

BY-CGP and BY-PROP binding to the native human β_1AR

Before undertaking the first studies to visualise the β_1-adrenoceptor using fluorescently labelled CGP 12177 and propranolol, we confirmed that we could visualise the β_2-adrenoceptor using the fluorescently labelled CGP 12177, as has been previously reported (Baker *et al.*, 2003d). Here, we examined the binding of BODIPY-TMR-CGP (BY-CGP) and BODIPY630/650-S-PEG8-propranolol (BY-PROP) to CHO-β_2-CS cells. Figure 4.11 shows clear membrane labelling of 20 nM BY-CGP in CHO-β_2-CS cells, which could be inhibited by pre-incubation with 1 μM of the β_2-adrenoceptor selective antagonist ICI 118,551. No detectable BY-CGP binding was observed to CHO-CS cells, indicating that the binding of BY-CGP to the β_2AR was specific. Clear labelling of CHO-β_2-CS cell membranes was also seen following exposure of these cells to 3 nM BY-PROP (Figure 4.12), which was inhibited in a concentration-dependent manner by ICI 118,551. The β_1-selective antagonist CGP 20712A was also able to inhibit BY-PROP binding albeit at 1000 fold higher concentrations, which is in line with the lower affinity CGP 20712A has for the β_2-adrenoceptor compared to ICI 118,551 (Baker, 2005).

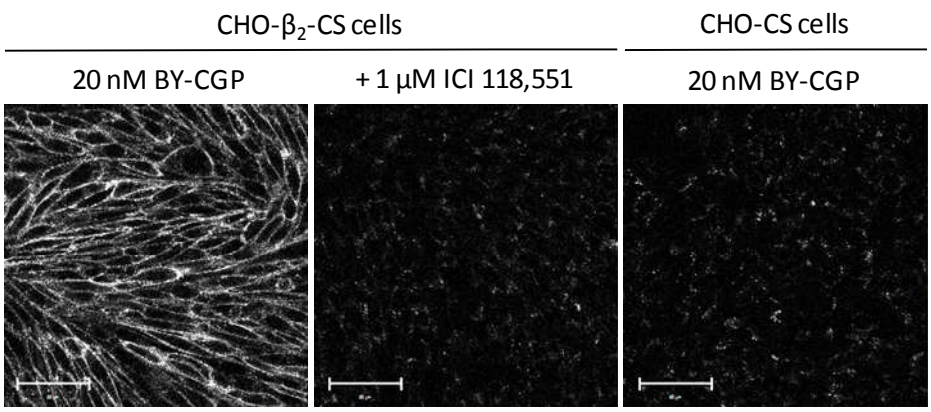

Figure 4.11 Binding of 20 nM BODIPY-TMR-CGP 12177 (BY-CGP) to CHO-β_2-CS and CHO-CS cells. BY-CGP binding (10 min, 21 °C) to CHO-β_2-CS cells was inhibited to non-specific binding levels in the presence of 1 µM ICI 118,551 (pre-incubation for 30 minutes at 37 °C). Images are representatives of a total of two images taken per well on one experimental day. Scale bar = 50 µm.

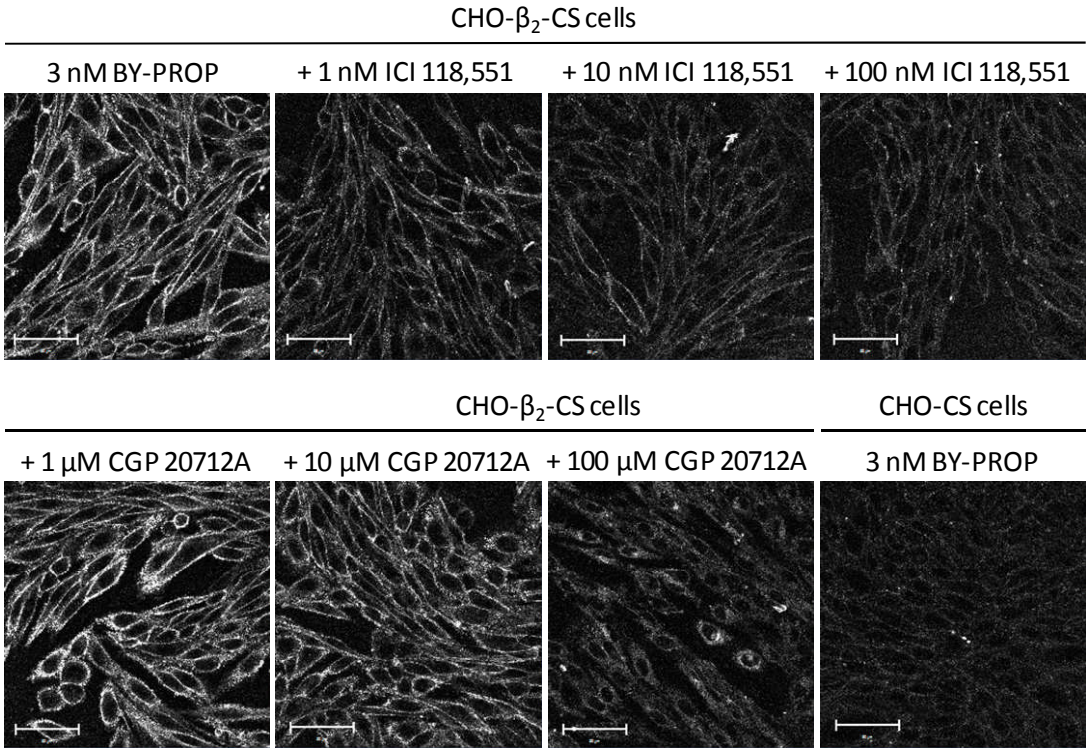

Figure 4.12 Binding of 3 nM BODIPY-S-PEG8-propranolol (BY-PROP; 10 min, 21 °C) to CHO-β_2-CS and CHO-CS cells in the absence and presence of 1, 10 and 100 nM ICI 118,551 and 1, 10 and 100 µM CGP 20712A (antagonist pre-incubation for 30 minutes at 37 °C). Non-specific binding of 3 nM BY-PROP was determined in CHO-CS cells. Images are representatives of a total of three images taken of different fields of view within each well on four separate experimental days. Scale bar = 50 µm.

Next, we examined the binding of both fluorescent ligands to the native β_1-adrenoceptor in CHO-β_1-CS cells. Both, 2 nM BODIPY-TMR-CGP (BY-CGP) and 20 nM BODIPY630/650-S-PEG8-propranolol (BY-PROP) were able to label the plasma membrane of CHO-β_1-CS cells following 10 minutes exposure at 21 °C (Figure 4.13). CHO-CS cells (cells not expressing the β_1-adrenoceptor) did not show clear membrane labelling with the two fluorescent ligands under the same conditions (Figure 4.13). The binding of BY-CGP and BY-PROP to CHO-β_1-CS cells could be displaced by 100 nM CGP 20712A (pre-incubation for 30 minutes at 37 °C) to levels comparable to those detected at CHO-CS cells (i.e. non-specific). Pre-incubation of CHO-CS cells with CGP 20712A did not reduce the level of BY-CGP and BY-PROP binding any further.

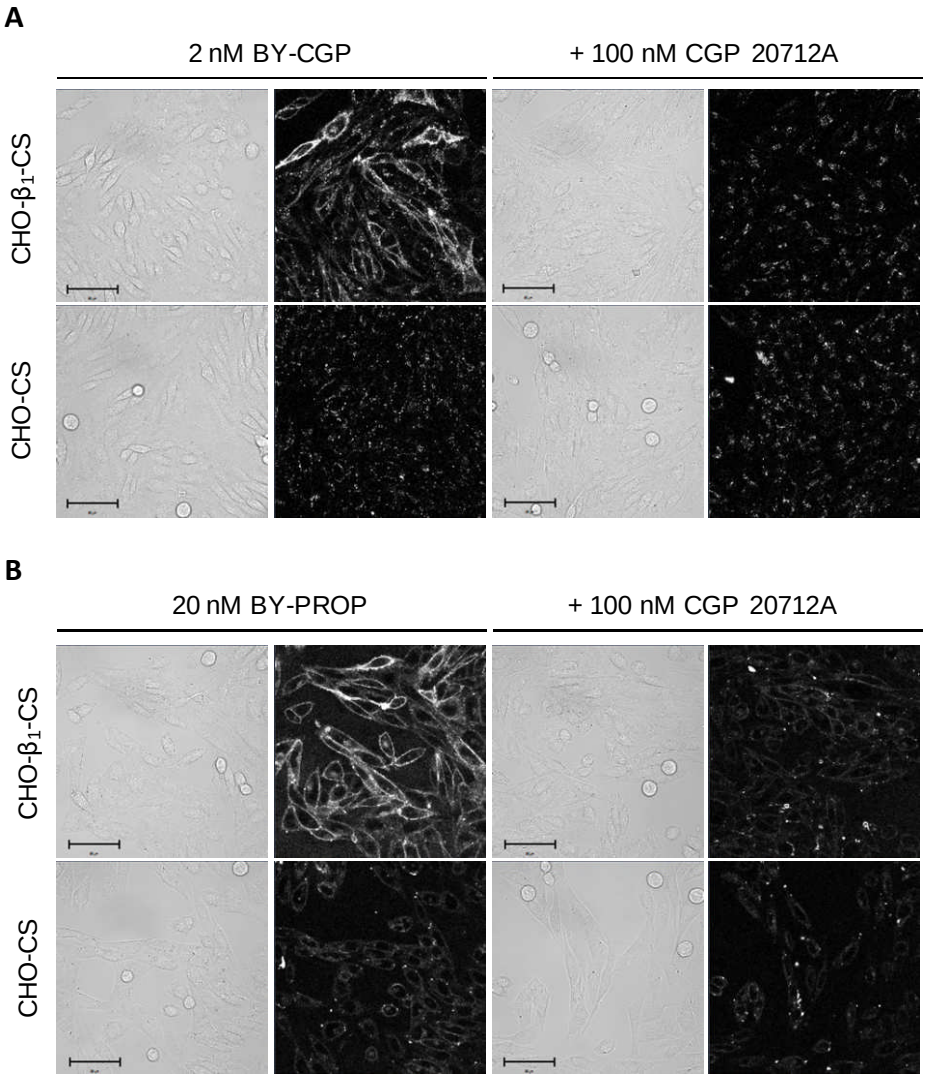

Figure 4.13 Binding of **A**, 2nM BY-CGP and **B**, 20 nM BY-PROP to CHO-β_1-CS and CHO-CS cells. Confocal images were taken following pre-incubation with HBSS in the absence and presence of 100 nM CGP 20712A (30 min, 37 °C) and 10 minute exposure (at 21 °C) of A, 2 nM BY-CGP and B, 20 nM BY-PROP. For each fluorescent ligand the microscope settings were kept constant for all wells. Images are representative of at least two different fields of view per well per experimental day. This experiment was repeated on at least three separate days. Scale bar = 50 µm.

Following this, we aimed to confirm the affinity values determined for both fluorescent ligands in functional studies by examining the binding affinity of both fluorescent ligands to the native β_1-adrenoceptor in saturation binding experiments. Thus, the binding of a range of concentrations (3-100 nM) of BY-CGP (Figure 4.14) and BY-PROP (Figure 4.15) to CHO-β_1-CS cells was assessed. For BY-CGP, clear concentration-dependent membrane labelling was seen up to 50 nM in CHO-β_1-CS cells. At BY-CGP concentrations higher than 50 nM (i.e. 100 nM in Figure 4.14A), intracellular BY-CGP could be seen in addition to membrane labelling. A similar observation of high BY-CGP concentrations resulting in intracellular fluorescence was reported for this ligand in CHO cells expressing the β_2-adrenoceptor (Baker *et al.*, 2003d). In order to obtain affinity values, the image fluorescence (i.e. level of BY-CGP binding) was quantified and analysed. Quantification of image fluorescence was achieved using two different methods: (1) total image intensities which included non-specific background and intracellular fluorescence, and (2) cell membrane analysis by drawing regions of interest (ROIs) around membranes of six cells per field of view (which were then averaged per given field of view). Non-specific binding was not derived separately in the presence of a high concentration of unlabelled antagonist. Instead, the quantified fluorescence intensity values per concentration of fluorescent ligand were analysed using non-linear total binding curve fits (for equation used see *Methods: Data analysis* section). This analysis determined the level and slope of background non-specific binding (shown in dotted lines, Figure 4.14B and C) from the total binding curve fits. As expected, a higher non-specific binding component was

present using the total image intensity analysis (55.9 ± 11.1 % of total binding, n=4; Figure 4.14B) compared to data obtained from membrane regions that excluded the intracellular fluorescence (41.8 ± 5.6 % of total binding, n=4; Figure 4.14C). However, the pK_D values taken from the total binding curves using the total image intensity and cell membrane intensity were 7.77 ± 0.13 (n=4) and 8.10 ± 0.09 (n=4), respectively, and were not statistically different from one another ($P > 0.05$, unpaired t-test; specific binding curves compared in Figure 4.14D).

The fluorescent propranolol derivative BY-PROP also showed clear membrane labelling up to 30 nM (Figure 4.15A). At higher concentrations, intracellular fluorescence was observed, although it was less pronounced than the clear membrane labelling. The images were analysed for BY-PROP fluorescence intensity and quantified using total image intensity (Figure 4.15B) and cell membrane analysis (Figure 4.15C) as described above for BY-CGP. The non-specific binding component (dotted lines in Figure 4.15B and C) was derived from the total binding curve fits which was higher using total image intensity analysis (55.6 ± 18.5 % of total binding, n=3; Figure 4.15B) than cell membrane analysis (15.2 ± 0.9 % of total binding, n=3; Figure 4.15C). The obtained pK_D values of 7.23 ± 0.07 (n=3) and 7.19 ± 0.12 (n=3) using total image and cell membrane analysis, respectively, were not statistically different ($P > 0.05$, unpaired t-test; Figure 4.15D).

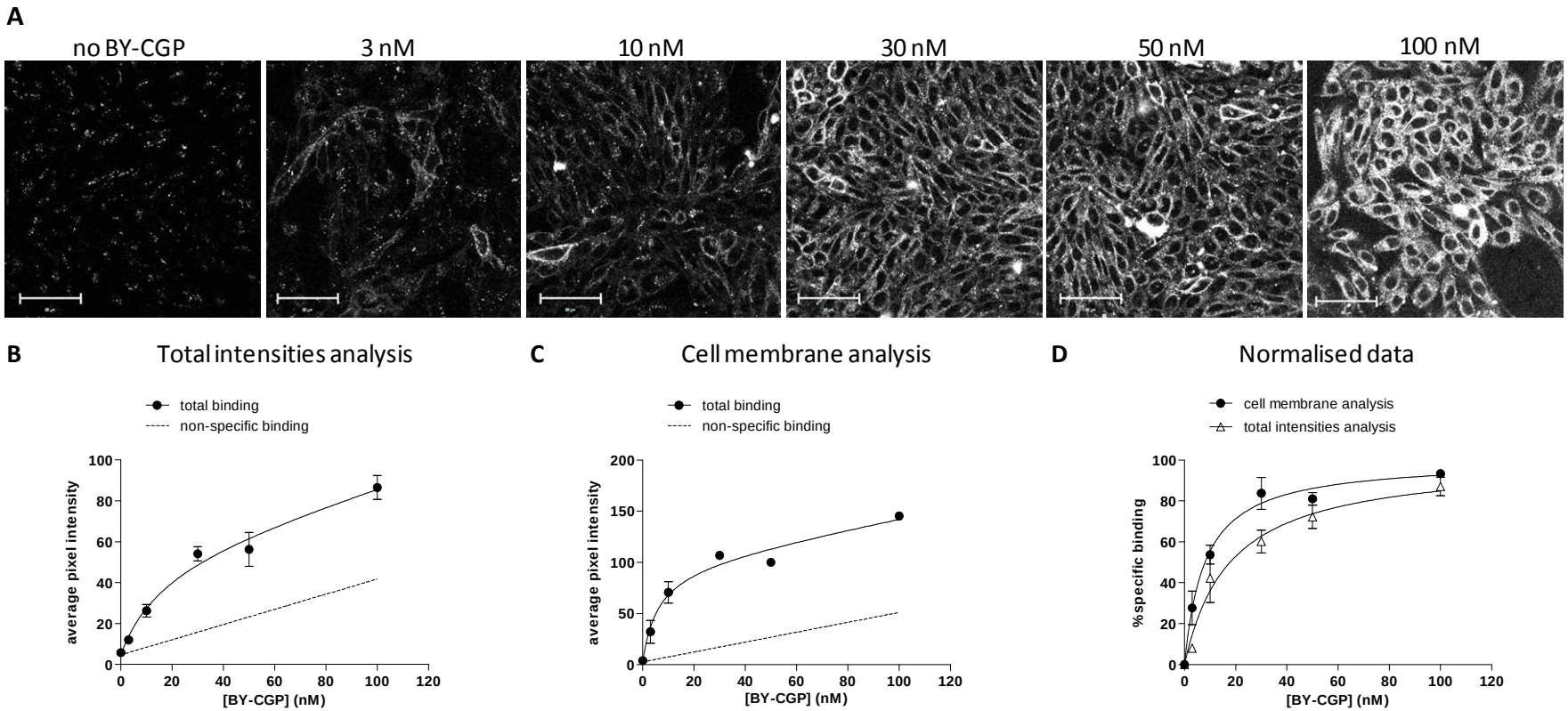

Figure 4.14 A, Binding of increasing concentrations of BY-CGP to CHO-β_1-CS cells. Scale bar = 50 µm. Images were analysed using **B**, total intensity analysis and **C**, cell membrane analysis (fluorescence intensity data obtained from drawing regions of interest around the membrane of six cells per field of view) to give total and non-specific and **D**, specific binding (normalised) data. Images are from one experiment and are representative of at least two additional images taken on the same day and of two additional experiments. Quantitative data obtained from images shown in A.

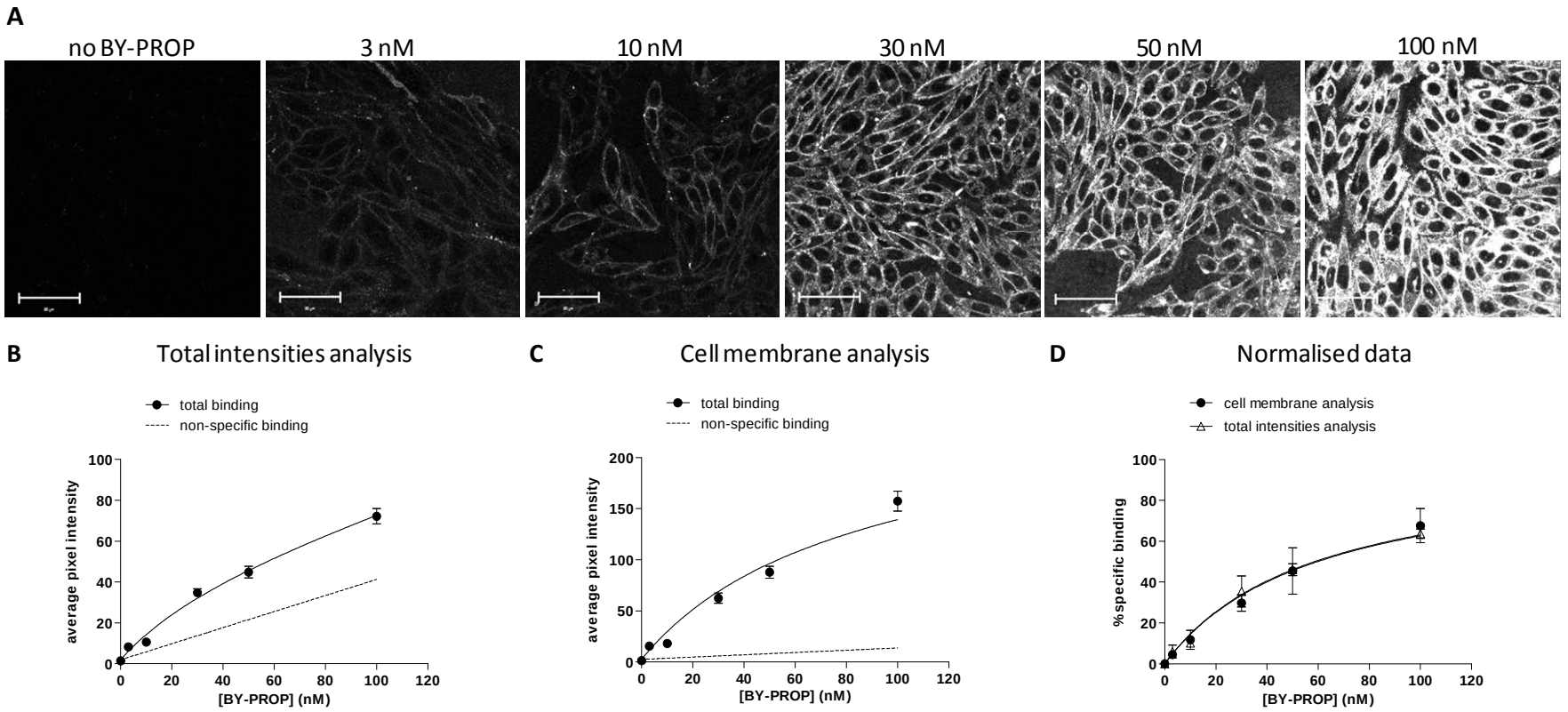

Figure 4.15 Binding of increasing concentrations of BY-PROP to CHO-β_1-CS cells. Scale bar = 50 µm. Images were analysed using **B**, total intensity analysis and **C**, cell membrane analysis (fluorescence intensity data obtained from drawing regions of interest around the membrane of six cells per field of view) to give total and non-specific and **D**, specific binding (normalised) data. Images are from one experiment and are representative of at least two additional images taken on the same day and of two additional experiments. Quantitative data obtained from images shown in A.

Pre-incubation with increasing concentrations of CGP 20712A inhibited the binding of 2 and 20 nM BODIPY-TMR in CHO-β_1-CS cells (Figure 4.16 and Figure 4.17, respectively). The pIC_{50} values obtained for the inhibition of 2 nM and 20 nM BODIPY-TMR-CGP binding by CGP 20712A were 9.03 ± 0.08 (n=4) and 8.76 ± 0.18 (n=3), respectively. This right-ward shift of the CGP 20712A inhibition curve is expected when competing against a higher concentration of the labelled ligand. Total binding levels of 2 and 20 nM BY-CGP to CHO-β_1-CS cells were obtained in the absence of CGP 20712A, whilst non-specific binding and background fluorescence was determined in CHO-CS cells (i.e. cells not expressing the β_1-adrenoceptor). Both displacement binding curves were normalised to total (100 %) and non-specific (0 %) binding levels to give specific binding curves which could be directly compared (Figure 4.18). Interestingly, the slope of the CGP 20712A inhibition curves is shallower (although not statistically significant; $P > 0.05$, unpaired t-test) when displacing 20 nM BY-CGP (-0.72 ± 0.06, n=3), than it is when antagonising 2 nM BY-CGP (-1.06 ± 0.14, n=4). However, the displacement slope of CGP 20712A inhibiting 20 nM BY-CGP binding was significantly shallower than a slope of unity ($P < 0.05$, one-sample t-test comparison to hypothetical value of 1.0).

Pre-incubation with CGP 20712A was also able to displace the binding of 20 nM BY-PROP in CHO-β_1-CS cells and a pIC_{50} of 8.85 ± 0.12 (n=4) was determined (Figure 4.19). Total binding of 20 nM BY-PROP was measured in the absence of CGP 20712A in CHO-β_1-CS cells and non-specific binding was

assessed in CHO-CS cells. The inhibition slope of CGP 20712A displacing 20 nM BY-PROP was -1.06 ± 0.31 (n=3).

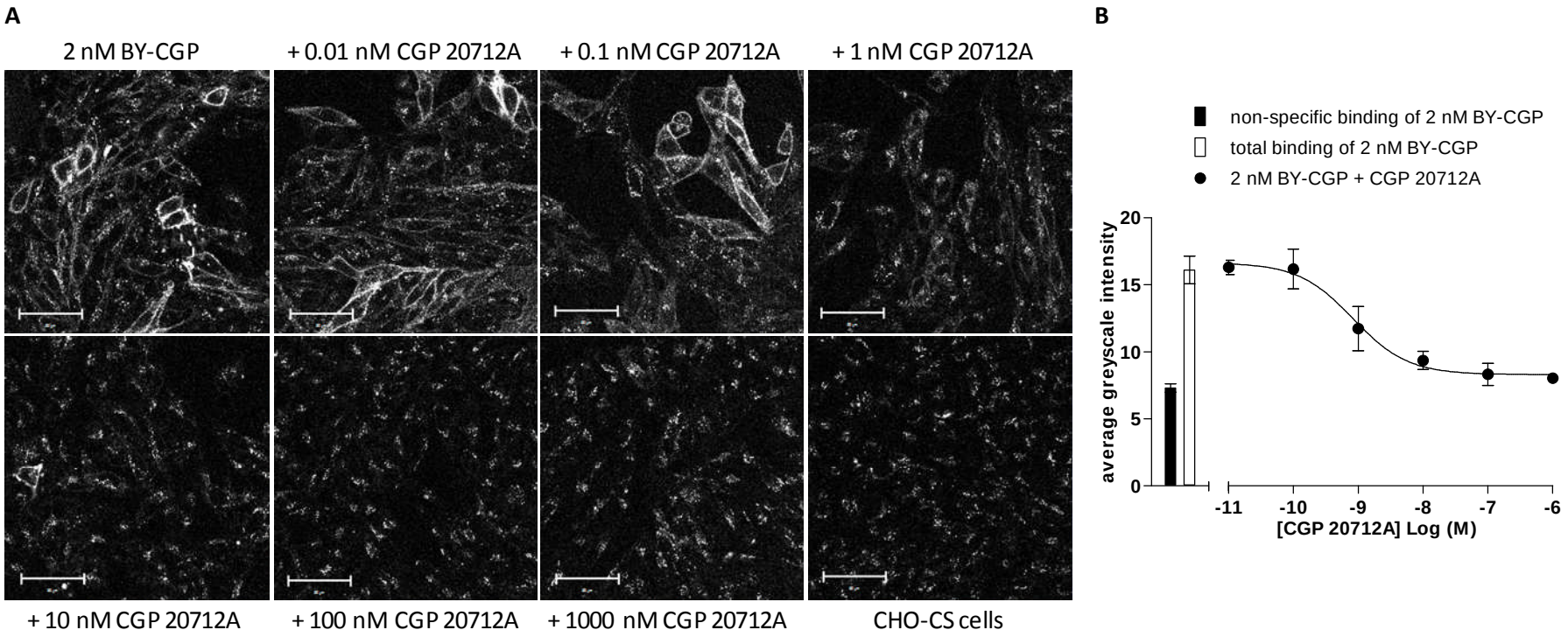

Figure 4.16 A, confocal images of 2 nM BY-CGP binding to CHO-β_1-CS cells in the absence and presence of increasing concentrations of CGP 20712A. **B**, quantitative data of images shown in A. Bar graphs show 2 nM BY-CGP binding levels determined in CHO-CS cells (non-specific binding) and CHO-β_1-CS cells (total binding). The images shown are representative of two additional images taken of different field of views within the same well, and are representatives of images taken on a total of four separate experimental days. Scale bar = 50 µm.

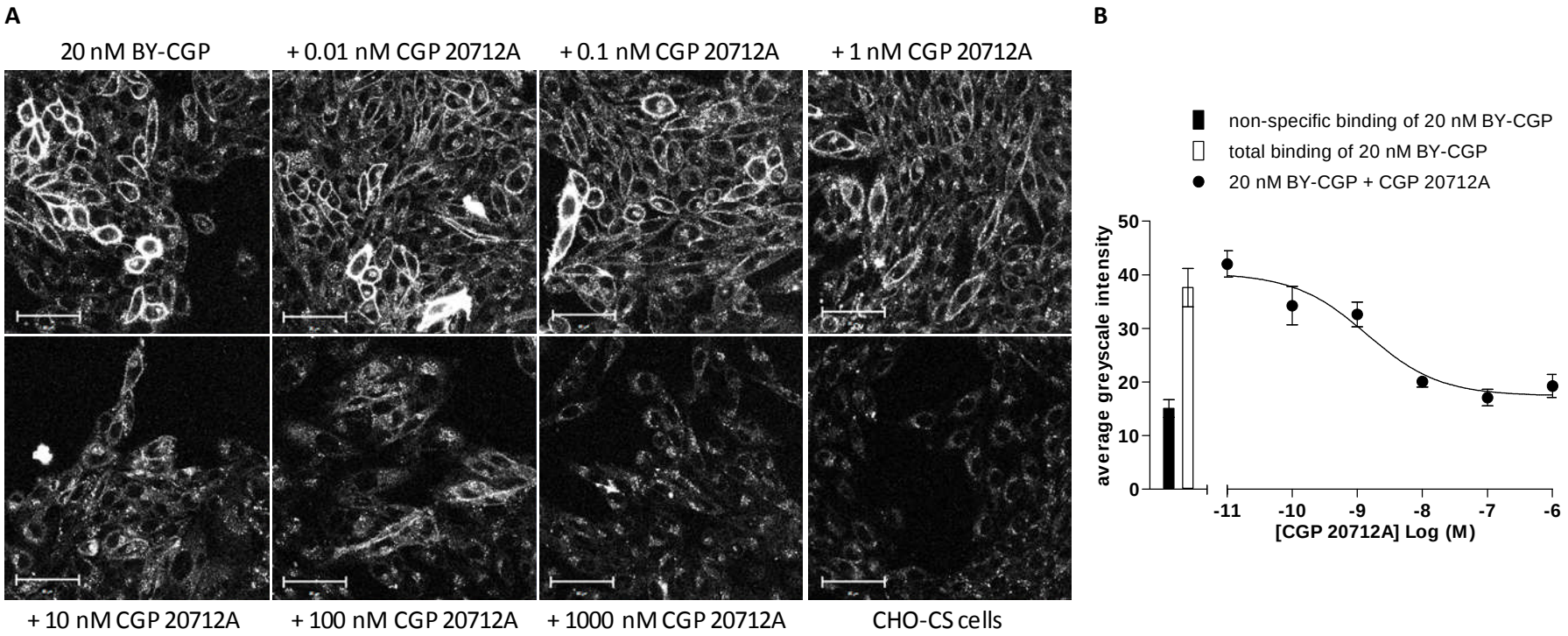

Figure 4.17 A, confocal images of 20 nM BY-CGP binding to CHO-β_1-CS cells in the absence and presence of increasing concentrations of CGP 20712A. **B**, quantitative data of images shown in A. Bar graphs show 20 nM BY-CGP binding levels determined in CHO-CS cells (non-specific binding) and CHO-β_1-CS cells (total binding). The images shown are representative of two additional images taken of different field of views within the same well, and are representatives of images taken on a total of three separate experimental days. Scale bar = 50 µm.

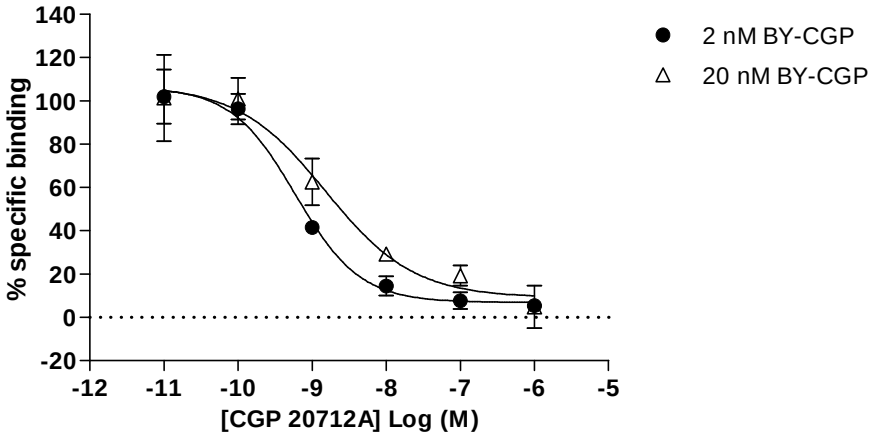

Figure 4.18 CGP 20712A inhibition of 2 and 20 nM BY-CGP binding to CHO-β_1-CS cells. Both binding curves were normalised to their respective total (100%) and non-specific (0%) binding levels to give normalised specific binding data. Data shown are pooled data from at least three separate experiments.

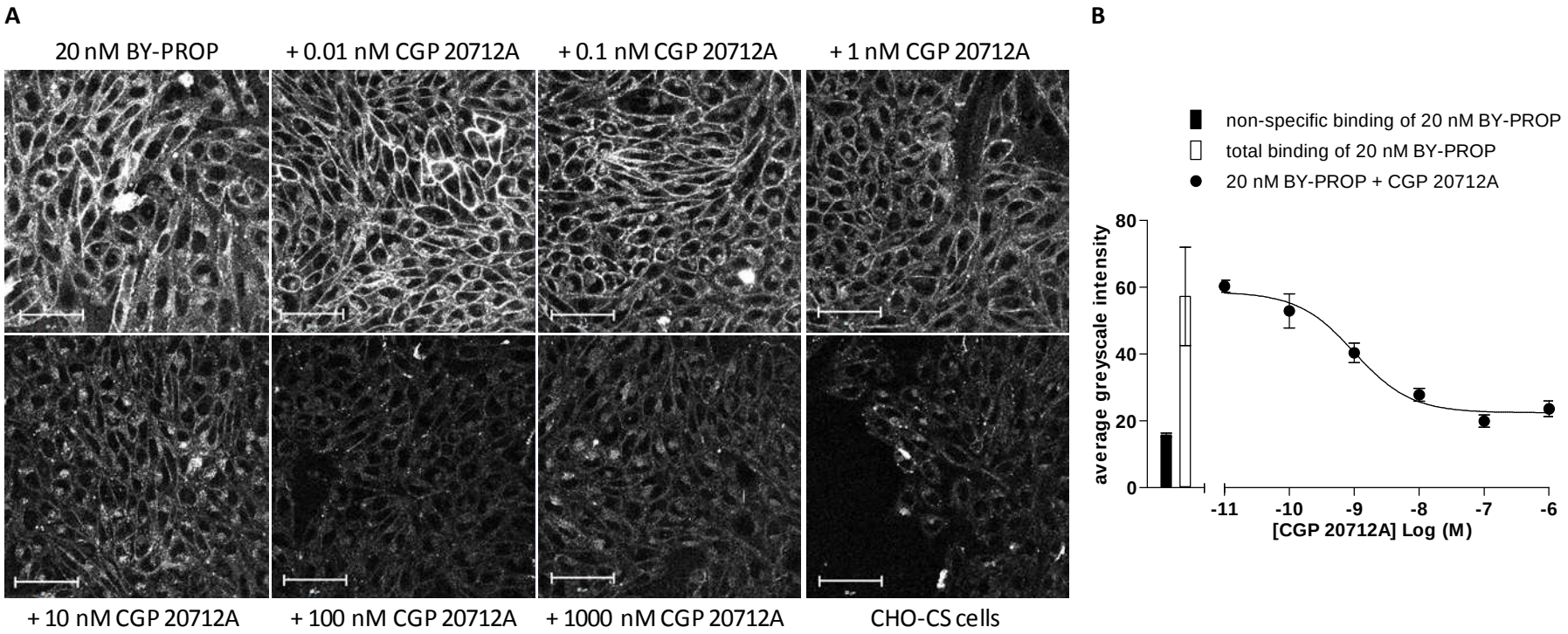

Figure 4.19 A, confocal images of 20 nM BY-PROP binding to CHO-β_1-CS cells in the absence and presence of increasing concentrations of CGP 20712A. **B**, The fluorescence intensities of the images shown in A were quantified using total image intensity analysis. Bar graphs show 20 nM BY-PROP binding levels determined in CHO-CS cells (non-specific binding) and CHO-β_1-CS cells (total binding). Images are representatives of two additional images taken of different fields of view within the same well and are representative of a total of four separate experimental days. Scale bar = 50 µm.

Internalisation of the β_1-adrenoceptor by BY-CGP

Receptor internalisation removes receptors from the cell surface to regulate receptor-mediated cellular responses (Jean-Alphonse *et al.*, 2011). Thus, using a fluorescently labelled agonist in binding experiments may result in fewer receptors being available at the cell surface following a given incubation time. As a result, reduced levels of binding of the fluorescent ligand may be observed that are due to receptors having being internalised instead of binding being displaced by the competing ligand. To ensure that this was not case using the low efficacy fluorescent agonist BODIPY-TMR-CGP, we investigated whether BODIPY-TMR-CGP caused internalisation of the SNAP-tagged β_1-adrenoceptor. When treated with HEPES-buffered saline solution (HBSS) buffer alone (negative control), no internalisation of SNAP-tagged β_1-adrenoceptors was observed (Figure 4.20). However, treatment of CHO-ssβ_1-CS cells with 10 µM isoprenaline (positive control) resulted in visible internalisation of the SNAP-tagged β_1-adrenoceptor. The fluorescence intensity of the cell membrane appeared reduced after treatment with 10 µM isoprenaline, and aggregated SNAP-tagged β_1-adrenoceptors were seen in the intracellular space (see white arrows in Figure 4.20). In contrast, treatment with 10 µM CGP 12177 and 1 µM BY-CGP did not result in intracellular aggregates of SNAP-tagged β_1-adrenoceptors, suggesting that neither ligand caused internalisation of the SNAP-tagged β_1-adrenoceptor after 60 minutes (Figure 4.20). It can, however, be seen that the shape of cells exposed to 10 µM CGP 12177 and 1 µM BY-CGP was changed after 60 minutes (white arrows in Figure 4.20). This was not observed in the negative control (HBSS treatment)

and indicates that CGP 12177 and BY-CGP treatment elicited cellular responses that did not involve the internalisation of the receptor in an incubation time of 60 minutes.

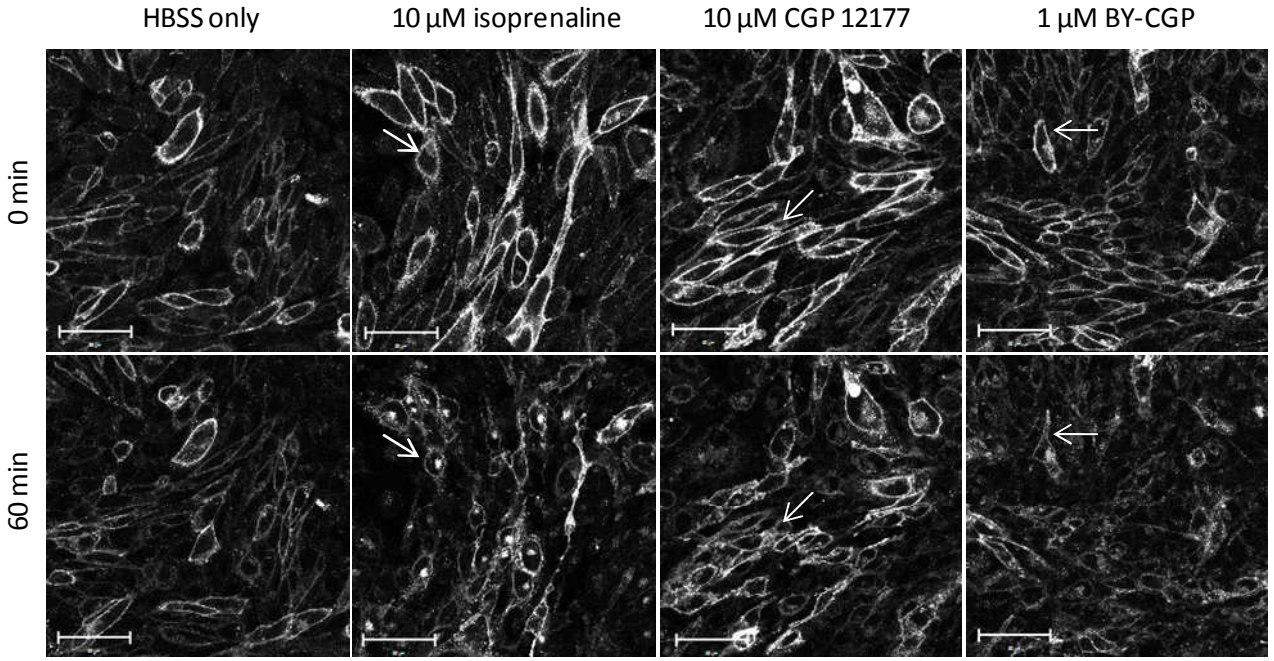

Figure 4.20 Confocal images of CHO-ssβ_1-CS cells that were incubated with 1 µM BG-488 (30 mins, 37 °C) in order to label the SNAP-tagged β_1-adrenoceptor. SNAP-tagged β_1-adrenoceptors were imaged before (0 min) and after (60 min) treatment with HBSS buffer, 10 µM isoprenaline, 10 µM CGP 12177 and 1 µM BY-CGP. The arrows point out internalisation of SNAP-tagged β_1-adrenoceptors following 60 minute exposure to 10 µM isoprenaline and change of cell shape without detectable SNAP-tagged β_1AR internalisation following 60 minute incubation with 10 µM CGP 12177 and 1 µM BY-CGP. Images are representative of a further two images taken on the same day of experimentation and images obtained in two additional separate experiments. Scale bar = 50 µm.

4.4 Discussion

Fluorescent ligands allow the visualisation and therefore the localisation of the native receptor in living cells using confocal microscopy. However, the coupling of a large fluorophore to a small molecular weight ligand can markedly affect its pharmacological profile (Baker *et al.*, 2010; Middleton *et al.*, 2005). In this chapter, we described the pharmacology of two fluorescent ligands at the human β_1-adrenoceptor: BODIPY-TMR-CGP, a CGP 12177 derivative (BY-CGP) and BODIPY630/650-S-PEG8-propranolol, a fluorescent analogue of propranolol (BY-PROP).

Firstly, we investigated the efficacy and affinity of both fluorescent ligands at the human β_1-adrenoceptor expressed in CHO-CS cells. BY-PROP exerted no efficacy of its own and antagonised cimaterol at the catecholamine site of the β_1-adrenoceptor with a 13-fold lower affinity compared to its parent compound. Interestingly however, BY-PROP displayed a higher affinity at the secondary site of the β_1-adrenoceptor compared to is unlabelled counterpart, albeit only 3-fold. Affinity values of an antagonist would be expected to be similar regardless of the agonist used, but the affinity value determined for BY-PROP against cimaterol was one order of magnitude higher than that obtained against CGP 12177 which is in line with the two sites hypothesis of the β_1-adrenoceptor and is similar to the pharmacology described for its parent ligand propranolol in Chapter 3.

BY-CGP displayed a similar pharmacology to its parent compound CGP 12177, albeit with a reduced affinity at both the high and low affinity site of the human β_1-adrenoceptor. Like CGP 12177, BY-CGP caused parallel right-ward shifts of the cimaterol concentration response curve. This suggests that the two ligands are competing for the same site, i.e. the catecholamine site (site 1) of the β_1-adrenoceptor. The raised basal levels of the cimaterol curves caused in the presence of increasing BY-CGP concentrations are reminiscent of the raised basal levels caused by CGP 12177 in the same assay format, suggesting that BY-CGP also exerts agonist activity. Indeed, BY-CGP retained agonist activity through the second low affinity site of the β_1-adrenoceptor, albeit with lower efficacy (25.6 % of that determined using the full agonist cimaterol) compared to CGP 12177 (47.8 % of the cimaterol response; Chapter 3). BY-CGP showed no response in CHO-CS and CHO-K1 cells, indicating that the responses seen are mediated through the β_1-adrenoceptor. The affinity value of BY-CGP derived from its partial agonist response curve was similar to that determined when used to antagonise the agonist actions of CGP 12177. BY-CGP caused parallel right-ward shifts of the CGP 12177 concentration-response curves, whilst also raising the basal levels of the CGP 12177 response curves in a manner consistent with the partial agonist actions of BY-CGP. Against CGP 12177, both the antagonist and agonist effects of BY-CGP, are mediated through the secondary β_1-adrenoceptor site. According to classical receptor theory the affinity values of a ligand for a given receptor (or receptor site) would be expected to be similar even though two different methods were used to derive the affinity value (Kenakin *et al.*, 1984). This

holds true for the BY-CGP data at the secondary site of the β_1-adrenoceptor (partial agonism K_D circa 87 nM; pA_2 (agonist CGP 12177) circa 52 nM). However, the affinity value determined for BY-CGP against cimaterol was 1.5 orders of magnitude higher than the affinity value derived from its partial agonist response (or against CGP 12177) which is consistent with the two-site hypothesis of the β_1-adrenoceptor.

Furthermore, in order to shift the BY-CGP concentration-response curve to a similar extent as the cimaterol concentration-response curve (see Chapter 3), a 100-fold higher concentration of propranolol had to be used. Interestingly, the affinity value of propranolol derived from the shifted BY-CGP concentration-response curve was comparable to that obtained when inhibiting CGP 12177 (Table 4.1). Thus, it appears that the affinity values are independent of the agonist used at the secondary β_1-adrenoceptor site. Unfortunately we could not confirm this for a different antagonist such as CGP 20712A due to the costs implicated in using high concentration of the fluorescent ligand (which is needed for a full concentration-response curve). This agonist independence is also true for the catecholamine site 1 of the β_1-adrenoceptor, as the affinity values established for propranolol and CGP 20712A using cimaterol as the agonist (Chapter 3) all compare well to affinity values that were reported against β-adrenoceptor agonist isoprenaline (Baker *et al.*, 2003a). This provides strong evidence that the changes in affinity seen against cimaterol and CGP 12177 are due to the two ligands eliciting their response through two different receptor sites or conformations.

As mentioned above the BY-CGP affinities were reduced at both sites of the β_1-adrenoceptor compared to CGP 12177. It is noteworthy that the affinity of BY-CGP was reduced 2-fold at the high affinity and 4-fold at the low affinity site of the β_1-adrenoceptor. Thus, the addition of a fluorophore to CGP 12177 resulted in a fluorescent ligand whose binding affinity is reduced by equal measures at both sites of the β_1-adrenoceptor. This is intriguing as one would expect that a chemical change of a ligand (especially one that results in a molecule twice the size of the parent compound) will have different effects at different binding sites, i.e. binding sites of different electrostatic composition and environment as they can or cannot provide more hydrogen bond, ionic or van der Waals interactions (Klebe *et al.*, 1997). Whilst similar affinity changes may be caused by different ligand-receptor interactions in different binding pockets, it is also consistent with two binding pockets that are in fact the same but have become 'two' binding sites in a β_1-adrenoceptor homodimer. The low affinities associated with the 'second' site may be due to conformational changes as a result of dimer formation (Breitwieser, 2004). This theory would be in line with a mutagenesis study carried out by Baker *et al.* (2008) to identify amino acid residues that play key roles in the binding of various ligands to site 1 and site 2 of the β_1-adrenoceptor. Every residue identified to cause a loss of affinity of ligand for site 1 (therefore being a crucial residue of this binding site) was also found to cause a loss of affinity of the same ligand at the second site of the β_1-adrenoceptor (Baker *et al.*, 2008). Not one residue could be isolated to only affect one but not the other binding site. This β_1-adrenoceptor homodimer hypothesis is examined in Chapter 7.

CGP 12177 has also been described as partial agonist with high affinity at the β_2-adrenoceptor (Baker *et al.*, 2002). Interestingly, BY-CGP retained its efficacy, but displayed a 100-fold lower affinity (21 nM) at the β_2-adrenoceptor compared to CGP 12177 at that receptor (Baker *et al.*, 2003d). Whilst the affinity of CGP 12177 for the β_2AR (0.22 nM, Baker *et al.* (2002)) is very similar to that of the catecholamine site 1 of the β_1AR (0.25 nM), the fluorescent CGP 12177 derivative is 35-fold selective for the high affinity site of the β_1-adrenoceptor over the β_2-adrenoceptor. This further highlights the effects that the addition of fluorophore to a ligand can have at different binding sites.

The binding properties of BODIPY-TMR-CGP and BY-PROP were investigated in living cells using confocal microscopy. We were able to confirm the previously reported binding of BODIPY-TMR-CGP 12177 to the human β_2-adrenoceptor (Baker *et al.*, 2003d). BODIPY-TMR-CGP 12177 binding to CHO-β_2-CS cells was displaced by the β_2-adrenoceptor selective antagonist ICI 118,551 and the β_1-adrenoceptor selective antagonist CGP 20712A in line with their reported affinities for the receptor (Baker, 2005).

The binding specificity of both fluorescent ligands was clearly demonstrated at both the SNAP-tagged and native β_1-adrenoceptor expressed in CHO-CS cells (for functional data of both fluorescent ligands at the SNAP-tagged β_1-adrenoceptor see Appendix I S6 and S7). Localised membrane labelling of 2 and 20 nM BY-CGP and 20 nM BY-PROP was seen in CHO-β_1-CS cells and could be displaced using β_1-adrenoceptor selective antagonist CGP 20712A. The

concentrations of BY-CGP and BY-PROP used to achieve clear membrane labelling were in line with affinity values determined for the two ligands in functional studies. No detectable binding of BY-CGP could be seen to CHO-CS cells (i.e. cells that do not express the β_1-adrenoceptor), indicating its selectivity to the β_1-adrenoceptor. Very low, but more apparent membrane labelling of CHO-CS cells was seen by 20 nM BY-PROP, which is consistent with the reported lipophilicity of propranolol (Neil-Dwyer *et al.*, 1981) and the BODIPY fluorophore (Sueyoshi *et al.*, 2011). However, the selectivity of BY-PROP to the β_1-adrenoceptor resulted in total binding that was markedly greater than non-specific binding.

The membrane labelling of BY-CGP and BY-PROP of CHO-β_1-CS cells was concentration-dependent and saturable. However, at concentrations of 30 nM and above, low levels of diffuse intracellular fluorescence were observed for both ligands. CGP 12177 and its fluorescent counterpart have been described as hydrophilic ligands (Baker *et al.*, 2003a; Staehelin *et al.*, 1983). The hydrophobicity of BY-PROP would suggest that BY-PROP crosses the cell membrane more readily than BY-CGP thus resulting in higher intracellular fluorescence. However, the non-specific binding levels determined for BY-PROP (55.6 % of total binding) were similar to those for BY-CGP (55.9 % of total binding) using the total image average fluorescence intensity analysis method. The non-specific binding component was theoretically determined from a one-site total binding fit for both fluorescent ligands and, in the case of BY-CGP may be artificially increased due to 100 nM BY-CGP labeling circa

50 % of the secondary low affinity β_1-adrenoceptor sites. Whilst the same principle applies to BY-PROP, its affinity for the secondary β_1-adrenoceptor site is lower (K_{Dsite2} ~270 nM) and would therefore contribute less to an overestimation of non-specific binding determined from a one-site total binding fit. In addition, intracellular fluorescence may be due to the internalisation of fluorescent ligands via the receptor (Baker *et al.*, 2003d; Daly *et al.*, 2003; Rose *et al.*, 2012). Rapid ligand-receptor dissociation inside the cell would lead to accumulation of intracellular fluorescence, whilst the receptor recycles back to the surface, leading to no (or little) observed receptor endocytosis. Here, no marked internalization of SNAP-tagged β_1-adrenoceptors was observed. Receptor-mediated internalization of fluorescent ligands may be prevented by preincubation with an unlabelled antagonist, but no distinguishable level or localisation of BY-CGP and BY-PROP fluorescence was observed in untransfected (CHO-CS) cells compared CHO-β_1-CS cells treated with 100 µM CGP 20712A in the conditions used, suggesting a β_1-adrenoceptor independent route for intracellular fluorescence. Using the total image intensity analysis method, the fluorescence intensity of the entire image was measured, including the fluorescence intensities of the cytoplasm and of cells with very low (or no) receptor expression and of parts of the image that did not contain any cells were included in the analysis. This firstly resulted in lower average fluorescence intensities per any given image, and secondly, increased the non-specific binding fraction. However, potential interference of non-membrane related fluorescence can be avoided by drawing regions of interests (ROIs) around the cell membranes of a number of

cells within one image. Using this analysis method, the non-specific binding levels were reduced for BY-CGP (41.8 % of total binding) and BY-PROP (15.2 % of total binding) compared to the total image analysis. This suggests that the majority of the BY-CGP non-specific binding is membrane related whereas the majority of the non-specific binding of BY-PROP was related to intracellular fluorescence as the non-specific binding fraction was reduced markedly using the ROI intensity analysis. Interestingly, the K_D values that were derived from the total binding curves using the two different analysis method compared well for both fluorescent ligands, suggesting that either method can be used for the analysis of the binding properties of fluorescent ligands.

The K_D values for BY-CGP and BY-PROP derived from the saturation binding curves did not compare to the affinity values determined in the CRE-mediated SPAP transcription assay (Table 4.2). The saturation binding analysis for the determination of an affinity value assumes that equilibrium has been reached. However, images were taken after 10 min exposure to the fluorescent ligand, after which it is unlikely that equilibrium was reached. The kinetics of BY-PROP and BY-CGP at the β_1-adrenoceptor are not known, but slow dissociation rates were reported for a radiolabelled CGP 12177 derivative at the β_1-adrenoceptor (Joseph *et al.*, 2004). Slow kinetics have also been attributed to BY-CGP, albeit at the human β_2-adrenoceptor (Baker *et al.*, 2003d). The affinity values are likely to be underestimated, if the fluorescent ligand has slow kinetics as it would not have had enough time to label all available receptors. It could be assumed that an increased incubation time

would result in a higher affinity value, possibly one that compares to the affinity value for the β_1-adrenoceptor site 1 obtained in functional experiments. Furthermore, if equilibrium was reached, a two-phase specific binding curve of BY-CGP might be expected, as full receptor occupancy will have been achieved by 100 nM (the highest concentration used in the saturation binding assay) BY-CGP at the high affinity site of the β_1-adrenoceptor and greater than 50 % of receptor occupancy at the site 2. However, even when a defined secondary binding phase is not detected (as shown here), we know from earlier functional studies that both fluorescent ligands bind to the secondary site, which will be reflected in the apparent K_D value calculated. As the fluorescent ligand concentrations are increased more secondary site binding will be recruited, which will have the effect of masking early saturation of the curve. Without detailed information of the kinetic parameters of the fluorescent ligands it is difficult to be sure that equilibrium conditions were achieved. In addition, the kinetic parameters of the same ligand will be different at the two sites of the β_1-adrenoceptor (Joseph *et al.*, 2004). The kinetics of BY-CGP and BY-PROP are examined in more detail in Chapter 6.

Both BY-PROP and BY-CGP binding could be displaced in a concentration-dependent manner by CGP 20712A. The CGP 20712A IC_{50} value was greater when inhibiting 20 nM (30 x K_{Dsite1}) than 2 nM (3 x K_{Dsite1}) BY-CGP as would be expected for two ligands competing for the same binding site, however the inhibition slope of CGP 20712A was shallower (-0.7) when inhibiting 20 nM

BY-CGP than when inhibiting 2 nM (-1.0). This suggests there was some competition binding resistance to increasing CGP 20712A concentrations which could be due a proportion of the second low affinity β_1-adrenoceptor site, as 20 nM is also 0.3 x K_{Dsite2} and thus labels approximately 16 % of site 2 (2 nM of BY-CGP is 0.03 x K_{Dsite2} and labels only 2 % of site 2). As described for the saturation binding assay, equilibrium is unlikely to have been reached after 10 minutes of incubation with the fluorescent ligand, thus the shallower slope could be an artefact of hemi-equilibrium. Alternatively, it may point to receptor-ligand interactions at both the high and low affinity binding site of the β_1-adrenoceptor. This is further explored in Chapter 5.

4.5 Conclusion

The fluorescent derivatives of propranolol (BY-PROP) and CGP 12177 (BY-CGP) displayed similar pharmacological profiles compared to their respective parent compounds in the CRE-mediated SPAP transcription assay. Crucially, BY-CGP retained agonist activity through the secondary low affinity site of the β_1-adrenoceptor. Confocal microscopy studies demonstrated clear membrane labelling by both fluorescent ligands in a β_1-adrenoceptor selective manner. Interestingly, displacement binding studies revealed a shallower CGP 20712A inhibition slope against 20 nM BY-CGP than 2 nM BY-CGP, possibly indicating the receptor-ligand interactions at the second β_1-adrenoceptor sites. Higher throughput automated confocal microscopy approaches could be used to investigate whether the shallower displacement slope is dependent on BY-CGP binding to the secondary β_1-adrenoceptor site, as it would allow investigation of binding of a range of BY-CGP concentrations in the presence of a range of β-adrenoceptor ligands.

Chapter 5

Live cell high-content fluorescent ligand binding assay using BODIPY-TMR-CGP and BODIPY630/650-S-PEG8-propranolol

5.1 Introduction

Cell-based ligand binding studies are traditionally carried out using radiolabelled ligands (Hulme *et al.*, 2010). Fluorescently labelled ligands, which have become more readily available in recent years (Daly *et al.*, 2010; Middleton *et al.*, 2005; Vernall *et al.*, 2012), circumvent the safety risks associated with the use of radioisotopes and allow visualisation of ligand binding to living cells. Other advantages of fluorescent ligands include their application in ligand binding studies in single cell as well as cell population assays, primary as well as recombinant cells, real time as well as end-point binding assays. However, more importantly, there is no need to separate free from bound ligand in fluorescent ligand binding assays as is traditionally done in radioligand binding assays. This is because some fluorophores are quenched in aqueous solution, resulting in detection of fluorescent ligand bound to receptors in the lipid environment of the cell membrane. Thus, high throughput assays using fluorescent ligands alone or in conjunction with a fluorescently labelled receptor have the potential to replace radiolabelled ligands for the purpose of determining affinity parameters of unlabelled ligands and have most recently been described for the arginine-vasopressin V_2 and adenosine A_3 and A_1 receptor (Loison *et al.*, 2012; Stoddart *et al.*, 2012).

The pharmacology of the fluorescent ligand BODIPY-TMR-CGP (a CGP 12177 analogue) has been described at the human β_2-adrenoceptor (Baker *et al.*, 2003d). In the previous chapter, we described BODIPY-TMR-CGP as a high affinity fluorescent ligand at the human β_1-adrenoceptor that allows specific

labelling of the receptor in living cells (Chapter 4). We also showed that BODIPY-TMR-CGP binds to both the high affinity catecholamine site 1 and the low affinity "CGP 12177" site 2 of the β_1-adrenoceptor whilst, like its parent compound, retaining agonist efficacy through the second low affinity site.

In this chapter, we aimed to set up a live cell high-content screening fluorescent ligand binding assay using the fluorescent ligands BODIPY-TMR-CGP and BY-PROP (a derivative of the β-adrenoceptor antagonist propranolol) and the IX Ultra confocal plate reader. This higher throughput method will allow further investigation of the ligand-receptor interactions at the second low affinity site of the human β_1-adrenoceptor. In addition, we aimed to compare the high-content IX Ultra confocal plate reader to the high-throughput plate reader PHERAstar *FS* for the determination of antagonists affinity values in a live cell ligand binding assay format.

5.2 Methods

Cell culture

This was performed as described in *Methods: Cell culture*. The cell lines used in this chapter were CHO-β_1-CS and CHO-β_2-CS. CHO-CS cells were used as controls were appropriate.

IX Ultra confocal plate reader

This was performed as outline in *Methods: ImageXpress Ultra confocal plate reader*. When reproducing the data obtained on the Zeiss LSM710 confocal microscope, the following incubation times were used: 30 min pre-incubation of CGP 20712A (37 °C), then 10 min exposure to the fluorescent ligand (21 °C). Unless otherwise stated, for all other experiments the antagonists were incubated for 1 hour at 37 °C, before addition of the fluorescent ligand for another hour and incubation at 21 °C.

PHERAstar *FS* plate reader

This was performed as outlined in *Methods: PHERAstar FS plate reader*. For direct comparison of data obtained from the same assay plate, each plate was read on the PHERAstar *FS* plate reader first and immediately afterwards read on the IX Ultra confocal plate reader.

Data analysis

The data analysis of displacement binding data was carried out as described in *Methods: Data analysis*. GraphPad Prism 5.0 was used to determine whether

a one-site or a two-site inhibition fit was preferred on every displacement binding curve. Using GrpahPad Prism 5.0, a preferred fit was determined with statistical significance of $P < 0.05$ (partial F test and analysis of residuals performed during fitting of data). The preferred fit was then used to derive IC_{50} and K_I values of the antagonists.

5.3 Results

Comparison of manual versus automated determination of BY-CGP and BY-PROP binding to CHO-β_1-CS cells

Firstly, we aimed to reproduce the binding data obtained manually in 8-well plates using the Zeiss710 LSM confocal microscope (Chapter 4), in a high-content screen automated format using 96-well plates and the IX Ultra confocal plate reader. The latter approach allows the introduction of more competing ligand concentrations, thus allowing better definition of concentration-displacement curves and simultaneous screening of multiple compounds. The same incubation times and temperatures for both antagonist and fluorescent ligand incubations were used as in binding experiments described in Chapter 4. A CGP 20712A inhibition curve against 20 nM BODIPY-TMR-CGP (BY-CGP) with duplicate determinations of 12 data points was obtained (Figure 5.1A). The total (T) and non-specific (B, basal) binding levels of 20 nM BY-CGP were determined in CHO-β_1-CS and CHO-CS cells, respectively. The montage image gives a good indication of the level of BY-CGP binding across the plate (Figure 5.1B). The IX Ultra confocal plate reader captures 4 different sites per well and reads an entire assay plate in vertical serpentine fashion (i.e. along columns starting with column B) in circa 20 minutes. No systematic change in the clear membrane labelling by 20 nM BY-CGP in the absence (totals) of CGP 20712A was observed across the plate. Furthermore, the duplicate wells of each BY-CGP binding condition tested (i.e. absence and presence of varying antagonist concentrations) showed

comparable levels of BY-CGP binding and fluorescence intensity (Figure 5.1B), indicating this fluorescence-based binding assay as a robust assay format for the investigation of the displacement of BY-CGP binding to CHO-β_1-CS cells.

The binding levels of 20 nM BY-CGP to CHO-CS cells were similar to those obtained in CHO-β_1-CS cells in the presence of 100 µM CGP 20712A suggesting that the non-specific binding levels can be determined using either strategy (Figure 5.1C). The data were analysed using the MetaXpress software and integrated fluorescence intensity (average fluorescence intensity per pixel) of the whole image was plotted against the CGP 20712A concentrations used (Figure 5.1D). The pIC_{50} of CGP 20712A against 20 nM BY-CGP was 8.56 ± 0.07 (n=3) with a slope of -0.78 ± 0.13 (n=3) when analysed using a 4 parameter equation. The inhibition curves obtained using manual and automated confocal microscopy approach were very similar with overlaying data points (Figure 5.2A). However, the secondary shoulder, which is seen at higher CGP 20712A concentrations and causes this shallower slope, is better defined in the 12-point inhibition curve and could be analysed separately using a two-site equation to yield pIC_{50} values for site 1 and site 2 of 8.49 ± 0.04 and -4.89 ± 0.24 (n=3), respectively, with a relative fraction of the high affinity to the low affinity site of 91.6 ± 2.4 % (n=3; Figure 5.2B).

A

T	-11	-10	-9	-8.5	-11	-10	-9	-8.5	T
B	-8	-7.5	-7	-6.5	-8	-7.5	-7	-6.5	B
T	-6	-5.5	-5	-4.5	-6	-5.5	-5	-4.5	T

B

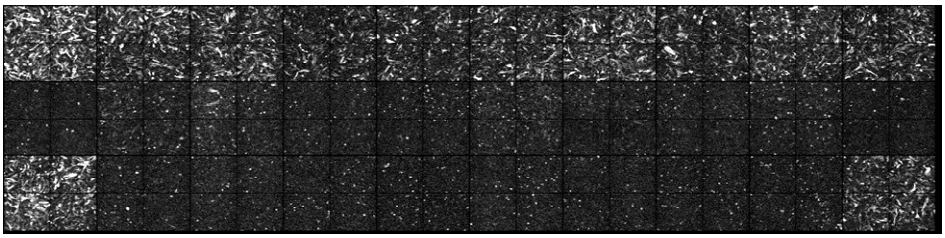

C

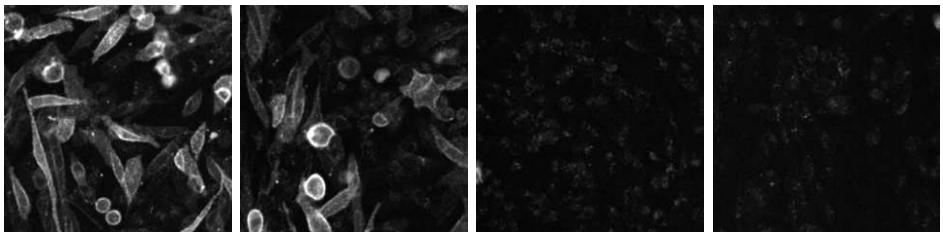

D

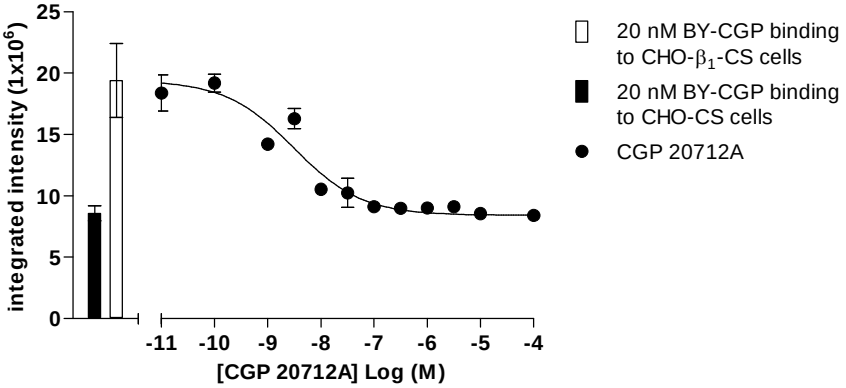

Figure 5.1 Inhibition of 20 nM BY-CGP binding to the human β_1-adrenoceptor. **A**, plate map of 30 wells highlighting the designated wells for total (T) and non-specific binding (B, basal) binding of 20 nM BY-CGP and chosen log concentrations of CGP 20712A. **B**, montage image of 20 nM BY-CGP binding levels in all 30 wells (4 images per well) used in this experiment. **C**, confocal image of 20 nM BY-CGP non-specific (basals) binding to CHO-CS cells and binding to CHO-β_1-CS cells in the absence (totals) and presence of 10^{-11} M and 10^{-4} M CGP 20712A. Each image is representative of 4 images taken per well. **D**, quantification of all images shown in A. The data shown here are from a single experiment with the error bars indicating range of error for duplicate determinations for all CGP 20712A concentration and the bar graph describing non-specific BY-CGP binding levels. Quadruplicate determinations of total BY-CGP binding are shown as mean ± s.e.m. in the designated bar graph. This experiment is representative of three separate experiments.

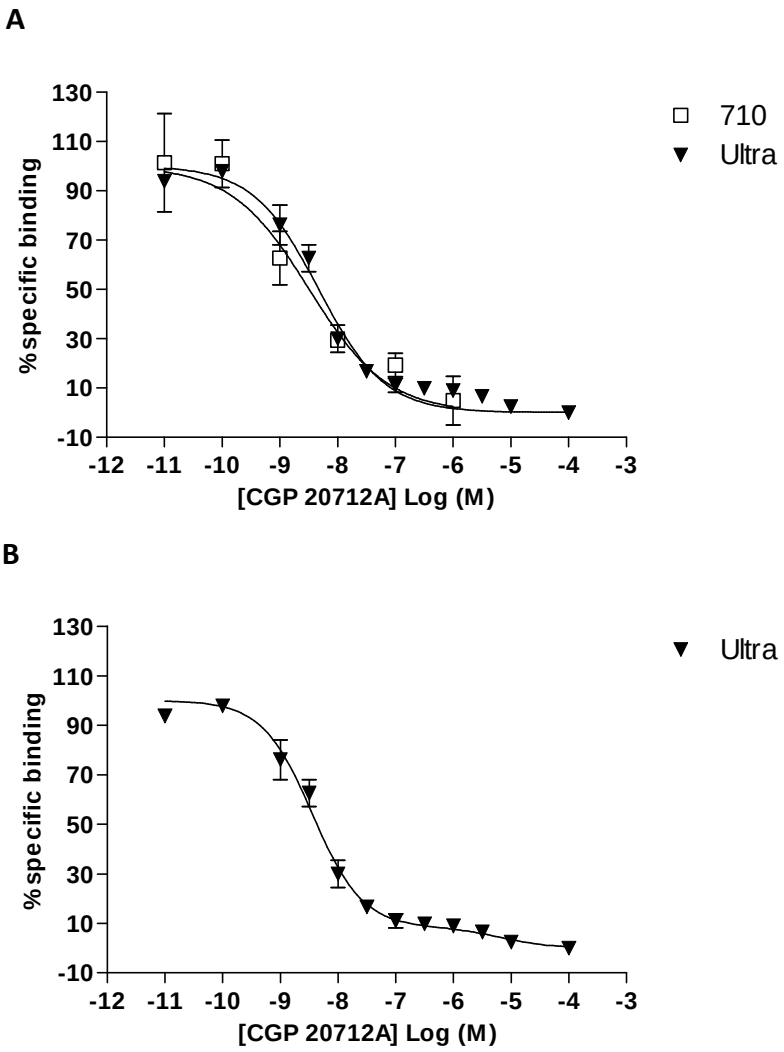

Figure 5.2 20 nM BY-CGP binding to CHO-β_1-CS cells in the presence of increasing concentrations of CGP 20712A. **A**, comparison of CGP 20712A displacement binding curves determined manually on the Zeiss710 confocal microscope and using the automated approach on the IX Ultra confocal plate reader. Both inhibition curves were analysed using a 4 parameter equation. **B**, CGP 20712A displacing binding curve determined using the IX Ultra confocal plate reader analysed using the two-site displacement binding fit.

Next, we assessed the binding of 20 nM BY-PROP to CHO-β_1-CS cells using the automated confocal plate reader system. Again, the same antagonist and fluorescent ligand incubation times and temperatures were used as in experiments using the Zeiss LSM710 confocal microscope (Chapter 4) to validate the use of the automated confocal microscopy approach for this fluorescent ligand. As can be seen in Figure 5.3B the binding of BY-PROP to CHO-β_1-CS is highly variable for duplicate readings across the assay plate, which is reflected in the large range of error associated with the mean for every data point of the CGP 20712A displacement binding curve (Figure 5.3D). This variability of BY-PROP binding did not appear to be associated with specific CGP 20712A concentrations (e.g. the duplicates of 10^{-8} M CGP 20712A concentrations on the assay plate show marked differences in measured fluorescent intensity, Figure 5.3B). The individual images shown in Figure 5.3C also highlight bright, non-specific fluorescent particles, which may be dead cells that have taken up high amounts of the fluorescent ligand or aggregates of the fluorescent ligand. In the total image intensity analysis used to quantify BY-PROP binding to CHO-β_1-CS cells, these bright particles will have contributed to an overall smaller assay window of BY-PROP binding as specific BY-PROP binding fluorescence was lower than that of the bright particles. However, it is unlikely that those contributed to the high fluorescence variability observed for duplicate determinations as they were present in all wells to similar degrees. High levels of intracellular BY-PROP fluorescence could be seen in CHO-CS cells (cells not expressing the β_1-adrenoceptor), which further limits the detection of a defined robust assay window. However,

the binding levels of BY-PROP to CHO-CS cells were comparable to those seen at CHO-β_1-CS cells in the presence of 100 μM CGP 20712A (Figure 5.3C), suggesting that the BY-PROP intracellular fluorescence is not caused by a β_1-adrenoceptor mediated process.

A

T	-11	-10	-9	-8.5	-11	-10	-9	-8.5	T
B	-8	-7.5	-7	-6.5	-8	-7.5	-7	-6.5	B
T	-6	-5.5	-5	-4.5	-6	-5.5	-5	-4.5	T

B

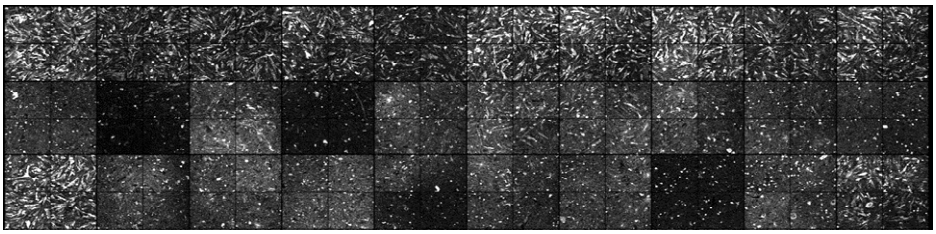

C

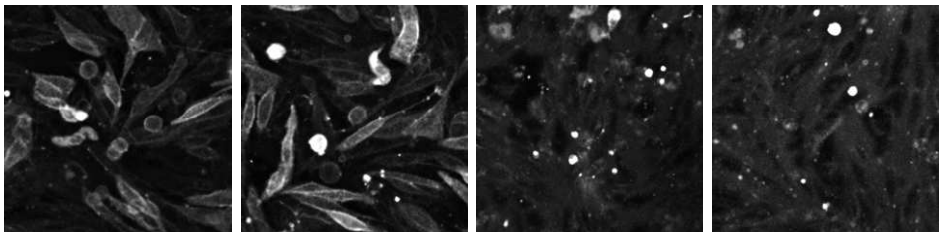

Totals 10^{-11} M 10^{-4} M Basals

D

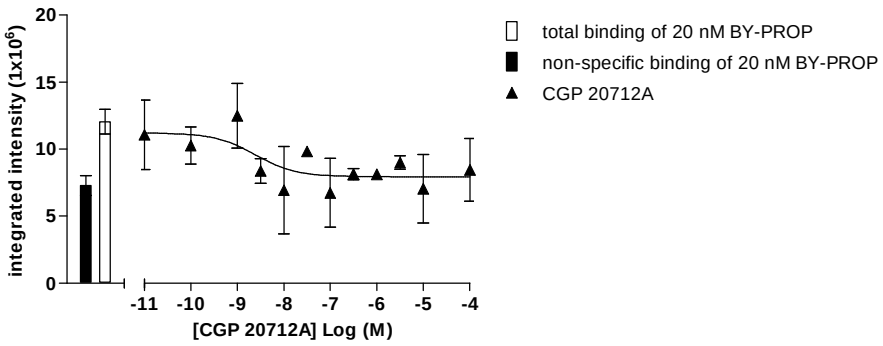

Figure 5.3 Inhibition of 20 nM BY-PROP binding to the human β_1-adrenoceptor. **A**, plate map of 30 wells highlighting the designated wells for total (T) and non-specific binding (B, basal) binding of 20 nM BY-PROP and chosen concentrations of CGP 20712A. **B**, montage image of 20 nM BY-PROP binding levels in all 30 wells (4 images per well) used in this experiment. **C**, confocal images of 20 nM BY-PROP non-specific (basals) binding to CHO-CS cells and binding to CHO-β_1-CS cells in the absence (totals) and presence of 10^{-11} M and 10^{-4} M CGP 20712A. Each image is representative of 4 images taken per well. **D**, quantification of all images shown in A. The data shown here is from a single experiment with the error bars indicating range of error for duplicate determinations. This experiment is representative of three separate experiments.

Optimising conditions for a high-content live cell equilibrium binding assay

Initial experiments were designed to match previous experimental conditions used on the LSM710. However, to achieve equilibrium conditions, the antagonist pre-incubation was increased to 1 hour (37 °C) and the effects of varying fluorescent ligand incubation temperature and time was assessed. Following CGP 20712A pre-incubation, BY-CGP and BY-PROP were incubated for 30 minutes at room temperature (21 °C) and at 37 °C. This increase in incubation temperature enhances the kinetics of ligand binding to the receptor, thereby speeding up the time it takes to reach equilibrium conditions. The absolute fluorescence intensity value of 20 nM BY-CGP binding to CHO-β_1-CS cells was increased at 37 °C compared to 21 °C suggesting equilibrium conditions were not reached at 21 °C. In addition, the CGP 20712A displacement binding curve was shifted at 37 °C compared to 21 °C incubation conditions, resulting in increased IC_{50} values at site 1 (pIC_{50} 8.53 and 8.83 at 37 °C and 21 °C, n=1, respectively) and decreased IC_{50} values at site 2 (pIC_{50} 5.26 and 4.61 at 37 °C and 21 °C, n=1, respectively; Figure 5.4). The confocal images taken by the IX Ultra plate reader show less defined membrane labelling of BY-CGP at 37 °C in CHO-β_1-CS cells, and the intracellular fluorescence appears to be increased at higher incubation temperatures.

A similar observation of less defined membrane labelling at 37 °C was made for BY-PROP binding to CHO-β_1-CS cells (Figure 5.5). Interestingly, the

absolute fluorescence intensity values obtained for the CGP 20712A displacement binding curves were similar at the two BY-PROP incubation temperatures used. No IC_{50} values could be derived from the CGP 20712A inhibition curves obtained following BY-PROP incubation at 21 °C and 37 °C, as intra-experimental variability was too great and was not improved in comparison to the initial incubation conditions used above (when replicating the manual confocal microscopy data).

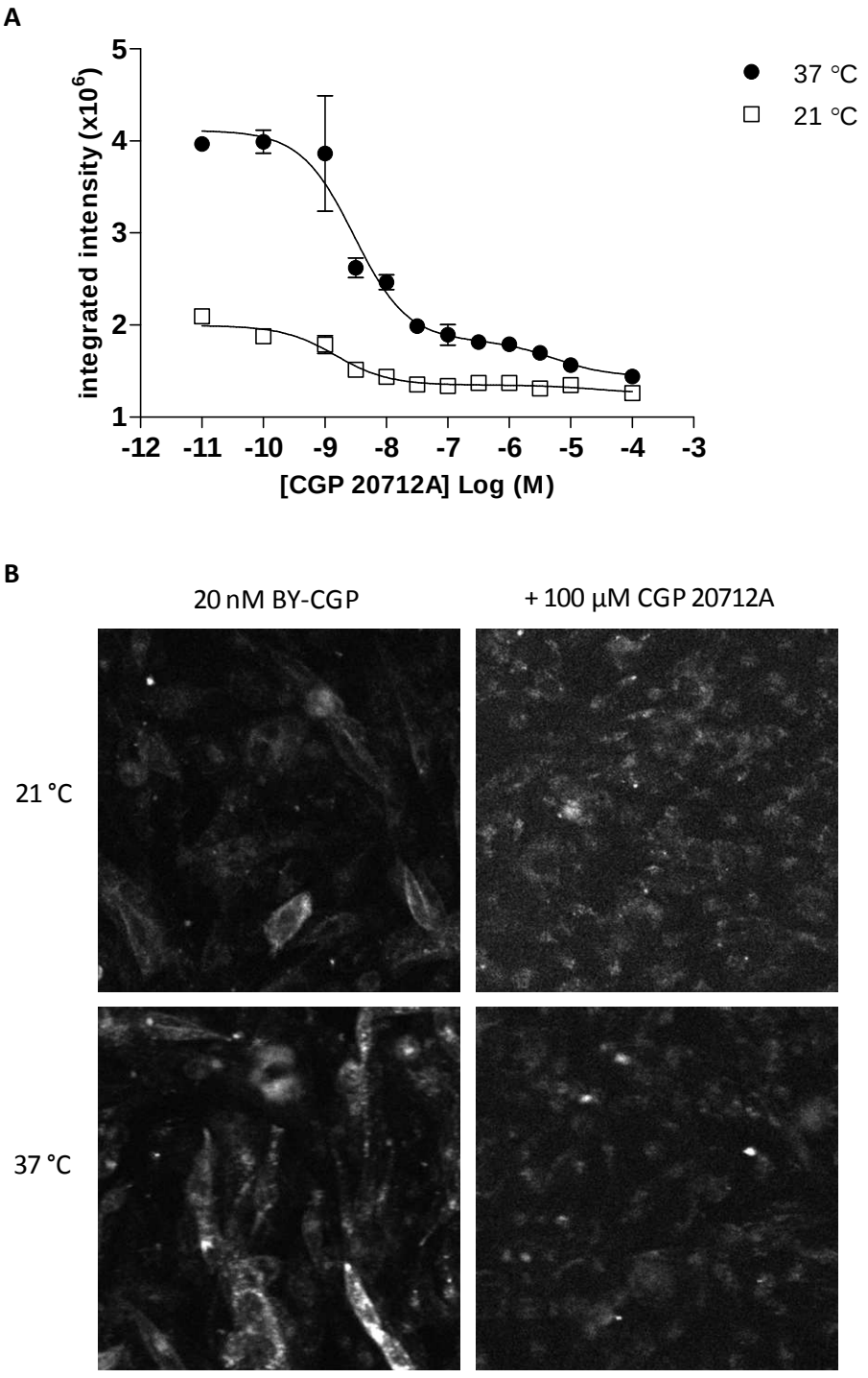

Figure 5.4 A, CGP 20712A displacement of 20 nM BY-CGP binding to CHO-β_1-CS cells following a 30 minute incubation of BY-CGP at 21 °C and 37 °C. Data are mean ± range of error of duplicate determinations from one single experiment. **B**, confocal images of 20 nM BY-CGP binding to CHO-β_1-CS cells in the absence (left panel) and presence (right panel) of 100 µM CGP 20712A following incubation at 21 °C (top panel) and 37 °C (bottom panel).

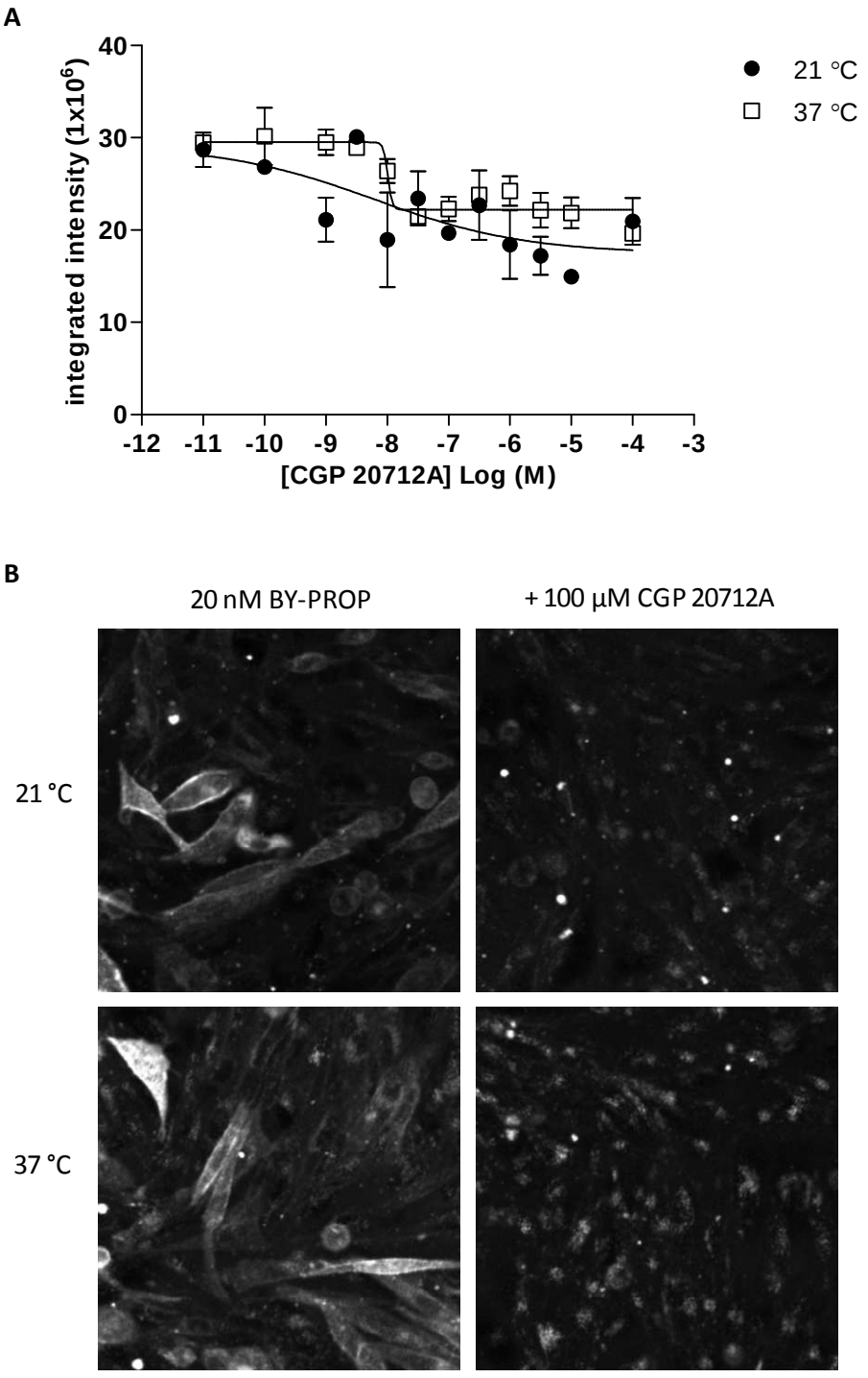

Figure 5.5 A, CGP 20712A displacement of 20 nM BY-PROP binding to CHO-β_1-CS cells following a 30 minute incubation of BY-PROP at 21 °C and 37 °C. Data are mean ± range of error of duplicate determinations from one single experiment. **B**, confocal images of 20 nM BY-PROP binding to CHO-β_1-CS cells in the absence (left panel) and presence (right panel) of 100 µM CGP 20712A following incubation at 21 °C (top panel) and 37 °C (bottom panel).

Next, CGP 20712A displacement binding curves were obtained following BY-CGP and BY-PROP incubation times of 30 and 60 minutes at 21 °C. The IC_{50} values of CGP 20712A against 20 nM BY-CGP at site 1 were 8.37 (n=1) and 8.30 (n=1) following a 30 and 60 minute incubation, respectively. At site 2 the pIC_{50} values were also very similar with values of 5.37 (n=1) and 5.22 (n=1) determined for 30 and 60 minutes incubation time, respectively (Figure 5.6). The fluorescence intensity values determined following a 60 minutes incubation time of BY-CGP were higher for both total (20 nM BY-CGP binding in the absence of CGP 20712A) and non-specific (20 nM BY-CGP binding in the presence of 100 μM CGP 20712A) binding than those determined after 30 minutes incubation of the fluorescent ligand. We have already shown that a much higher concentration (1 μM) of the low efficacy agonist BY-CGP caused no detectable internalisation of the SNAP-tagged β_1-adrenoceptor following a 60 minutes incubation time at 21 °C (Chapter 4, Figure 4.20), which was consistent with the clear membrane labelling of 20 nM BY-CGP observed here following 30 and 60 minutes incubation times. BY-PROP also showed good membrane labelling of CHO-β_1-CS cells (Figure 5.7), albeit with greater intracellular fluorescence than observed for BY-CGP. The binding levels of BY-PROP were similar between the two different incubation conditions used and the quantified data was still too variable to determine confident and reproducible displacement binding parameters.

Whilst we could not be certain that equilibrium conditions were achieved, all subsequent experiments on the IX Ultra confocal plate reader used BY-CGP

only, with 60 minute incubation at 21 °C, to limit non-specific binding and internalisation effects.

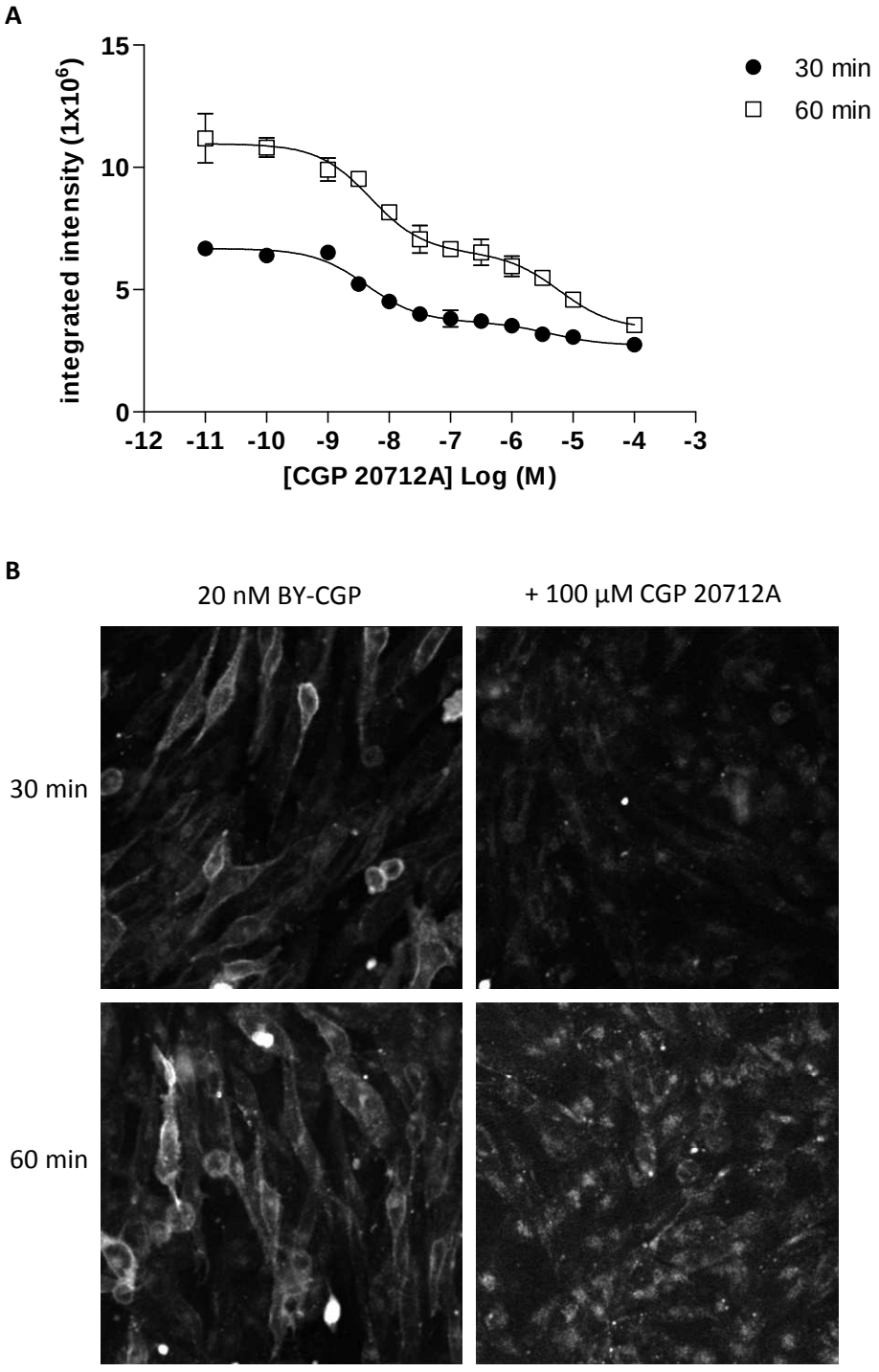

Figure 5.6 A, CGP 20712A displacement of 20 nM BY-CGP binding to CHO-β_1-CS cells following a 30 and 60 minute incubation of BY-CGP at 21 °C. Data are mean ± range of error of duplicate determinations from one single experiment. **B**, confocal images of 20 nM BY-CGP binding to CHO-β_1-CS cells in the absence (left panel) and presence (right panel) of 100 µM CGP 20712A following a 30 (top panel) and 60 (bottom panel) minute incubation.

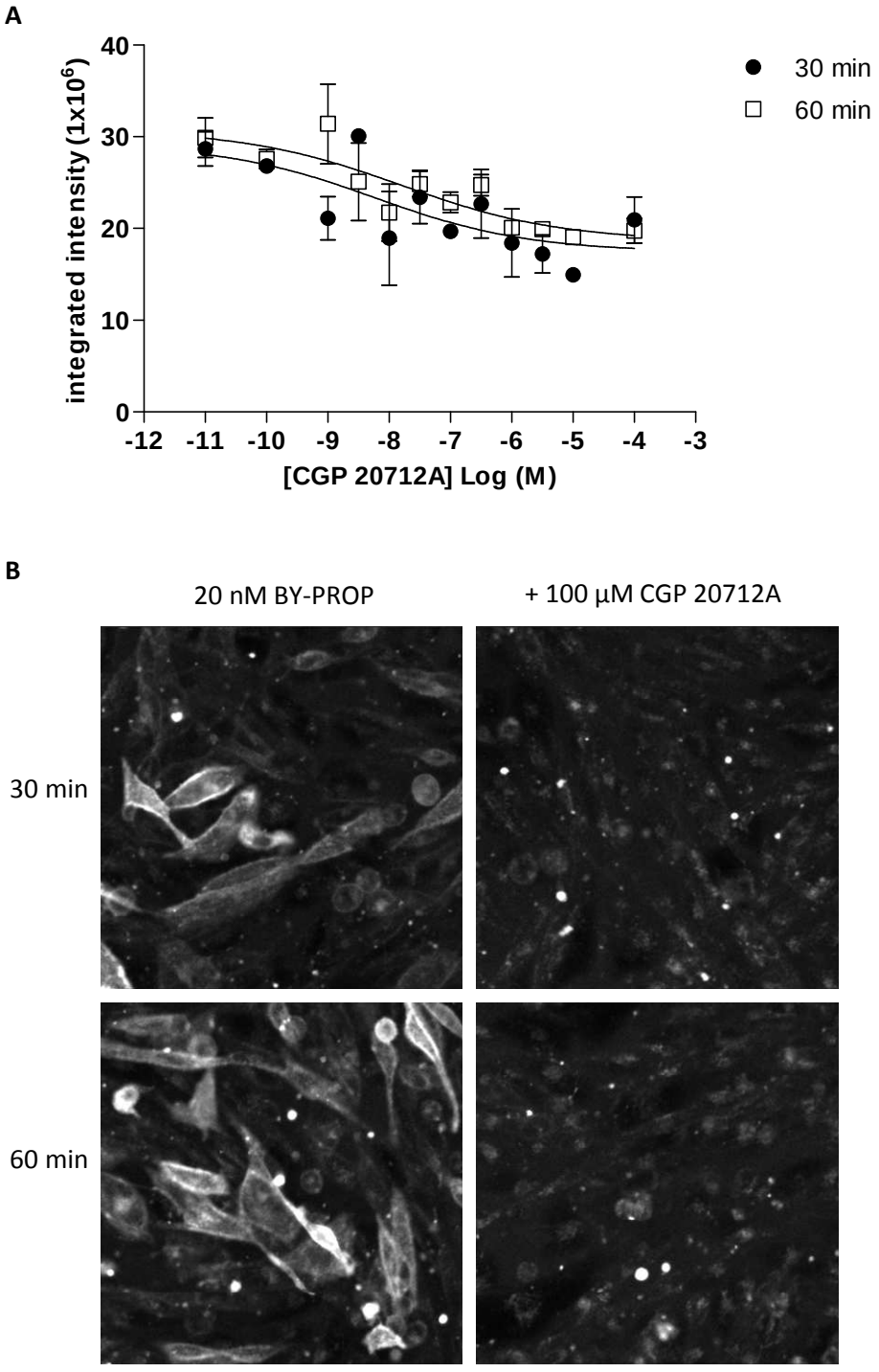

Figure 5.7 A, CGP 20712A displacement of 20 nM BY-PROP binding to CHO-β_1-CS cells following a 30 and 60 minute incubation of BY-PROP at 21 °C. Data are mean ± range of error of duplicate determinations from one single experiment. **B**, confocal images of 20 nM BY-PROP binding to CHO-β_1-CS cells in the absence (left panel) and presence (right panel) of 100 µM CGP 20712A following a 30 (top panel) and 60 (bottom panel) minute incubation.

Determination of BY-CGP binding parameters to the human β_1- and β_2-adrenoceptor using the high-content IX Ultra confocal plate reader

Since it was not possible to use a BY-CGP concentration as low as 2 nM to predominantly label the high affinity catecholamine site of the β_1-adrenoceptor, we aimed instead to use higher concentrations of BY-CGP with the hypothesis that increasing concentrations of BY-CGP will increase the occupancy of the second low affinity β_1-adrenoceptor site. First, we assessed the binding of 10, 20 and 100 nM BY-CGP in the presence of increasing concentrations of CGP 20712A. Indeed, the second phase of the two-phase binding curve appeared to become more pronounced with increasing BY-CGP concentrations, which was observed in the decrease of the percentage of the BY-CGP bound high affinity site to the overall BY-CGP bound sites (89.1 ± 1.2 %, 85.8 ± 1.2 % and 58.3 ± 4.0 % for 10, 20 and 100 nM BY-CGP, respectively; Figure 5.8A). Furthermore, the CGP 20712A competition curve shifted rightward with increasing BY-CGP concentrations. This rightward shift could be seen for both the high affinity and the low affinity site. The pIC_{50} values derived from the displacement binding curves for 10, 20 and 100 nM were 8.76 ± 0.04 (n=4), 8.68 ± 0.03 (n=4) and 8.21 ± 0.11 (n=6), respectively, at the high affinity site. The pIC_{50} values determined for site 2 for 10, 20, 100 nM were 5.54 ± 0.03 (n=4), 5.16 ± 0.12 (n=4) and 5.07 ± 0.09 (n=6), respectively (Table 5.1). The IC_{50} values of CGP 20712A was significantly lower when inhibiting 100 nM BY-CGP compared to 10 nM BY-CGP at both site 1 and site 2 ($P < 0.05$, two-way ANOVA followed by Bonferroni's post hoc test).

From equilibrium competition binding antagonist IC_{50} values, the affinity values of antagonists that are competing for the same binding site with a labelled ligand can be determined using the Cheng-Prusoff equation. Taking into account the BY-CGP concentration used, and the affinity of BY-CGP for site 1 and site 2 of the β_1-adrenoceptor (as determined in the CRE-mediated SPAP transcription assay; Chapter 4), CGP 20712A affinity values were calculated for each BY-CGP concentration and are summarised in Table 5.1.

Similar rightward shifts of antagonist displacement binding curves were seen for increasing BY-CGP concentration when displaced by propranolol and CGP 12177 (Figure 5.8B and C, respectively). Increasing IC_{50} values were determined for both propranolol and CGP 12177 when displacing increasing concentrations of BY-CGP (Table 5.1). Furthermore, the secondary phase of the two-phase displacement binding curves was also increasingly pronounced with increasing BY-CGP concentrations when displaced by propranolol (percentage of BY-CGP bound to site 1 in ratio to overall BY-CGP-bound β_1AR sites: 89.3 ± 0.4 %, 87.0 ± 0.6 % and 72.1 ± 3.7 % for 10, 20 and 100 nM BY-CGP, respectively) and CGP 12177 (92.6 ± 1.3 %, 88.8 ± 0.6 % and 72.2 ± 2.1% for 10, 20 and 100 nM BY-CGP, respectively).

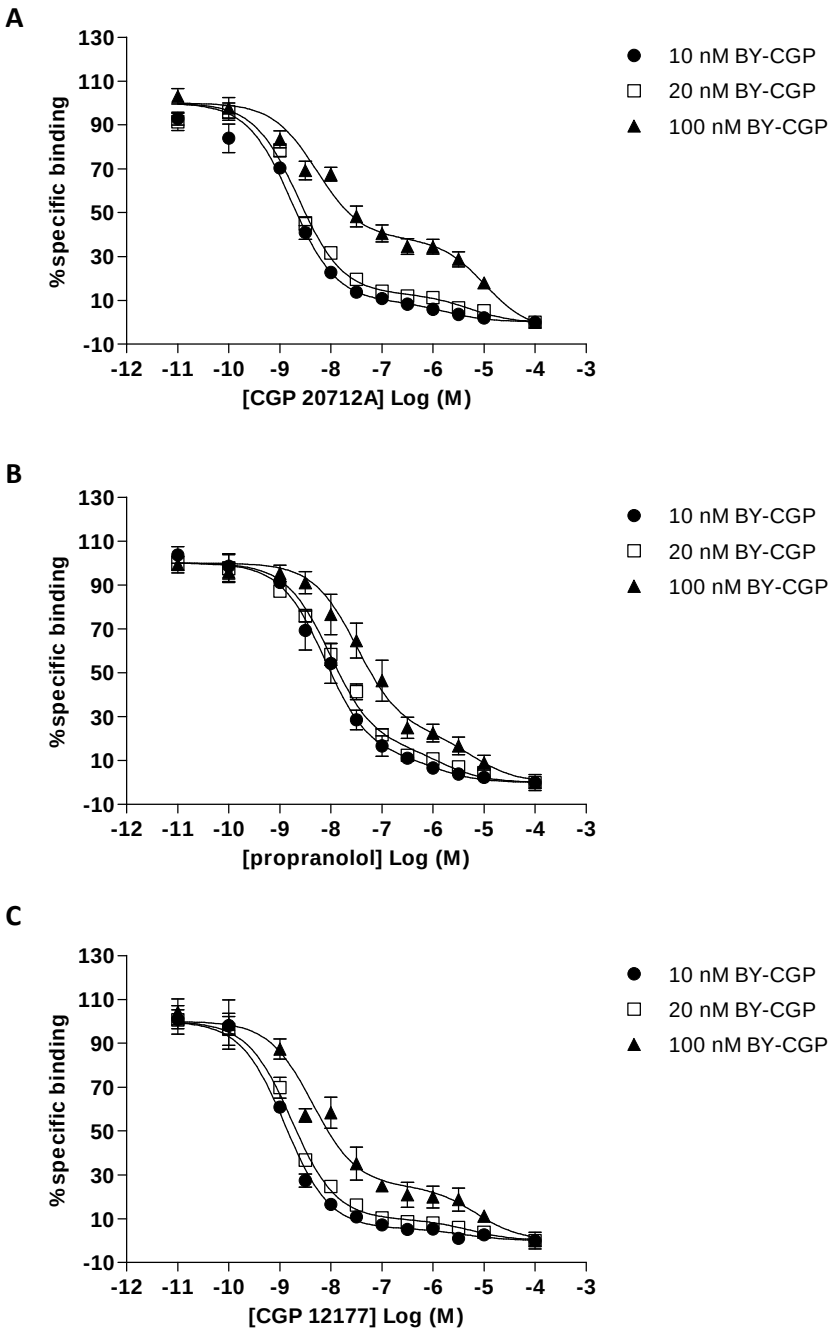

Figure 5.8 Displacement of 10, 20, 100 nM BY-CGP binding to CHO-β_1-CS cells by **A**, CGP 20712A, **B**, propranolol and **C**, CGP 12177. The data was normalised to total binding (BY-CGP binding to CHO-β_1-CS cells; 100 %) and non-specific binding (BY-CGP binding to CHO-β_1-CS cells in the presence of 100 μM antagonist; 0 %) for each BY-CGP concentration used. The data shown are normalised data representing the mean ± s.e.m. of combined data from 4-6 separate experiments per BY-CGP concentration.

Table 5.1 Summary of pIC_{50} and pK_I values of CGP 20712A, propranolol and CGP 12177 against 10, 20 and 100 nM BY-CGP binding to CHO-β_1-CS cells. The pK_I values were determined using the Cheng-Prusoff equation and BY-CGP affinity values for the β_1-adrenoceptor site 1 and site 2 determined in the CRE-mediated SPAP transcription assay (Chapter 4). Data are mean ± s.e.m of *n* separate experiments. both pIC_{50} and pK_I values determined at site 1 were significantly different ($P < 0.05$) from those determined for site 2, and * denotes statistical significance ($P < 0.05$) from pIC_{50} or pK_I value determined for [a]10 nM BY-CGP and [b]20 nM BY-CGP as determined by two-way ANOVA followed by Bonferroni's multiple comparison test

	CGP 20712A			propranolol			CGP 12177		
	site 1	*site 2*	*n*	*site 1*	*site 2*	*n*	*site 1*	*site 2*	*n*
pIC_{50}									
10 nM BY-CGP	8.76 ± 0.04	5.54 ± 0.03	4	7.94 ± 0.18	5.33 ± 0.12	3	8.93 ± 0.04	5.57 ± 0.20	3
20 nM BY-CGP	8.68 ± 0.03	5.16 ± 0.12	4	7.76 ± 0.13	5.19 ± 0.09	3	8.77 ± 0.07	5.36 ± 0.15	3
100 nM BY-CGP	8.21 ± 0.11*[a,b]	5.07 ± 0.09*[a]	6	7.12 ± 0.02*[a,b]	5.01 ± 0.06	3	8.19 ± 0.13*[a]	5.27 ± 0.16	3
pK_I									
10 nM BY-CGP	10.01 ± 0.04	5.59 ± 0.03	4	9.19 ± 0.18	5.37 ± 0.12	3	10.18 ± 0.04	5.62 ± 0.20	3
20 nM BY-CGP	10.21 ± 0.03	5.25 ± 0.12	4	9.29 ± 0.13	5.33 ± 0.08	3	10.31 ± 0.07	5.45 ± 0.15	3
100 nM BY-CGP	10.44 ± 0.11*[a]	5.41 ± 0.09	6	9.34 ± 0.02	5.34 ± 0.06	3	10.42 ± 0.13	5.60 ± 0.16	3

BY-CGP has already been characterised at the β_2-adrenoceptor in functional and fluorescence imaging binding studies (Baker *et al.*, 2003d). Unlike the β_1-adrenoceptor, only one binding site has been described at the β_2-adrenoceptor, to which BY-CGP binds with low nanomolar affinity (Baker *et al.*, 2003d). We have already shown clear membrane labelling of CHO-β_2-CS cells by BY-CGP using the manual confocal microscopy approach (Chapter 4). Here, we examined the binding of BY-CGP to the human β_2-adrenoceptor in CHO-β_2-CS cells using the IX Ultra confocal plate reader, in order to confirm that the second site displacement binding curves seen at the β_1-adrenoceptor were not an artefact of the experiment conditions used.

Using 20 nM BY-CGP, we saw clear membrane labelling of CHO-β_2-CS cells (Figure 5.9B). Non-specific binding levels detected in CHO-CS cells were very low and comparable to levels measured in CHO-β_2-CS cells in the presence of 100 μM propranolol (Figure 5.9C). In addition, the binding of 20 nM BY-CGP was displaced by propranolol in a concentration-dependent manner, suggesting that BY-CGP binding was specific to the β_2-adrenoceptor expressed in CHO-β_2-CS cells. BY-CGP has been described as a long acting partial agonist at the human β_2-adrenoceptor (Baker *et al.*, 2003d), but no BY-CGP-mediated internalisation was apparent following a 60 minutes exposure to the fluorescent ligand at 21 °C (Figure 5.9B), suggesting that any reduced BY-CGP binding to CHO-β_2-CS was due to antagonist displacement.

10, 20 and 100 nM BY-CGP binding was inhibited by β_2-selective antagonist ICI 118,551 and non-selective β-adrenoceptor antagonists propranolol and CGP

12177. The antagonist displacement binding curves were right-shifted in the presence of increasing BY-CGP concentrations (Figure 5.10). As a result, increasing IC_{50} values were determined with increasing BY-CGP concentrations for ICI 118,551, propranolol and CGP 12177 (Table 5.2). From these IC_{50} values and the BY-CGP affinity value reported in the literature for the β_2-adrenoceptor (25 nM; Baker *et al.* (2003d)), the antagonist affinity values were determined using the Cheng-Prusoff equation (Table 5.2). All inhibition curves obtained in CHO-β_2-CS cells preferred a one-phase binding fit, suggesting that the two-phase binding fit is specific of the ligand interactions with the β_1-adrenoceptor.

A

T	-11	-10	-9	-8.5	-11	-10	-9	-8.5	B
B	-8	-7.5	-7	-6.5	-8	-7.5	-7	-6.5	T
T	-6	-5.5	-5	-4.5	-6	-5.5	-5	-4.5	B

B

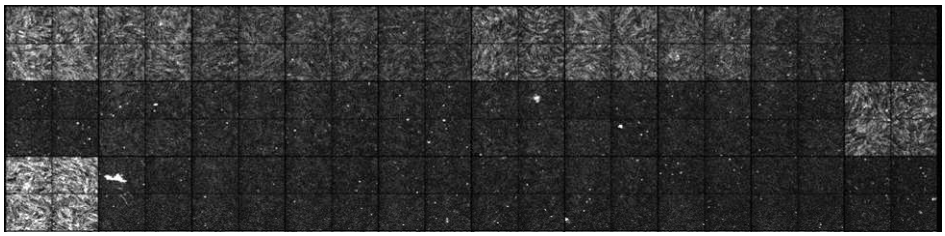

C

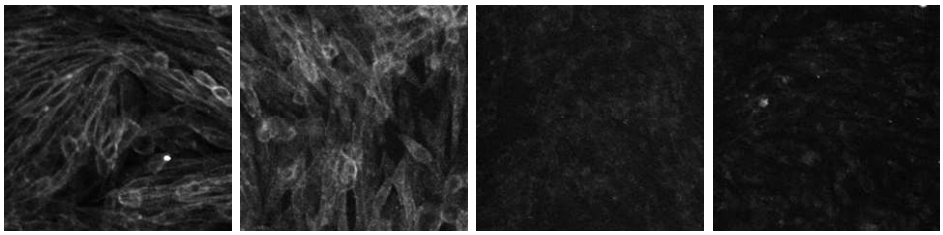

Totals 10^{-11} M 10^{-4} M Basals

D

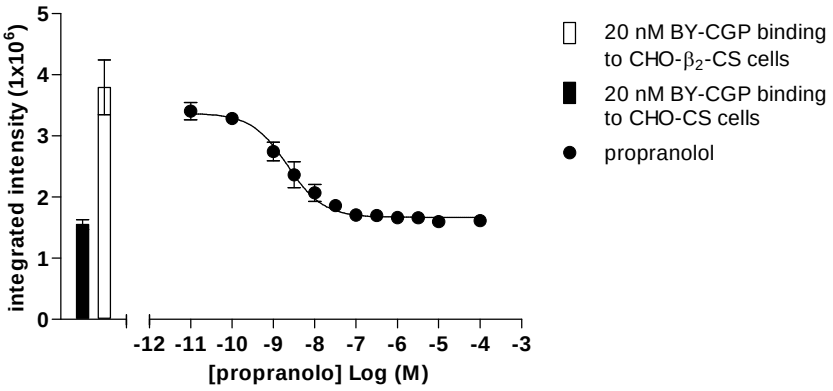

Figure 5.9 Inhibition of 20 nM BY-CGP binding to the human β_2-adrenoceptor. **A**, plate map of 30 wells highlighting the designated wells for total (T) and non-specific binding (B, basal) binding of 20 nM BY-CGP and chosen concentrations (in M) of propranolol. **B**, montage image of 20 nM BY-CGP binding levels in all 30 wells (4 images per well) used in this experiment. **C**, confocal image of 20 nM BY-CGP non-specific (basals) binding to CHO-CS cells and binding to CHO-β_2-CS cells in the absence (totals) and presence of 0.01 nM (-11) and 100 µM (-4) CGP 20712A. Each image is representative of 4 images taken per well. **D**, quantification of all images shown in A. The data shown here are from a single experiment with the error bars indicating range of error for duplicate determinations. This experiment is representative of three separate experiments.

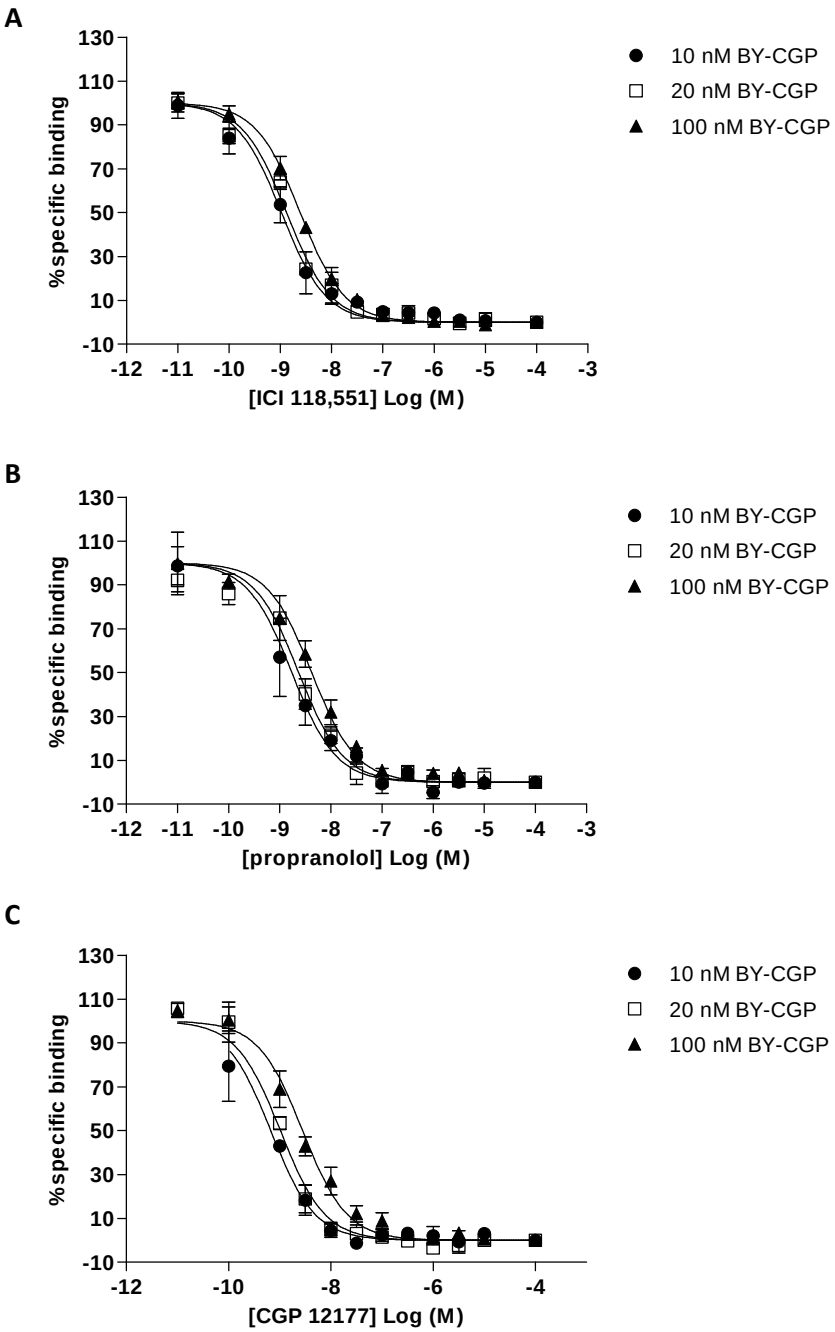

Figure 5.10 Displacement of 10, 20, 100 nM BY-CGP binding to CHO-β_2-CS cells by **A**, ICI 118,551 and **B**, propranolol and **C**, CGP 12177. The data were normalised to total binding (BY-CGP binding to CHO-β_2-CS cells; 100 %) and non-specific binding (BY-CGP binding to CHO-CS cells; 0 %) for each BY-CGP concentration used. The normalised data is the mean of at least two separate experiments pooled together with error bars representing range of error (where only two separate experiments were performed) and standard error of the mean (where three separate experiments were performed).

Table 5.2 Summary of IC_{50} values of ICI 118,551, propranolol and CGP 12177 at CHO-β_2-CS cells. The pK_I values were determined using the Cheng-Prusoff equation and the BY-CGP affinity value for the β_2-adrenoceptor reported by Baker *et al.* (2003d). Data shown are mean ± s.e.m of *n* separate experiments. For each antagonist, the IC_{50} values obtained for 10, 20 and 100 nM BY-CGP were not statistically different ($P > 0.05$, one-way ANOVA followed by Bonferroni's multiple comparison test). The same analysis was performed for K_I values of each antagonist, and no statistical difference ($P > 0.05$) was determined.

	ICI 118,551	n	propranolol	n	CGP 12177	n
pIC_{50}						
10 nM BY-CGP	9.00 ± 0.25	3	9.02; 8.46	2	9.11; 9.17	2
20 nM BY-CGP	8.95 ± 0.12	3	8.65 ± 0.18	3	8.70; 8.99	2
100 nM BY-CGP	8.61 ± 0.02	3	8.43 ± 0.17	3	8.51 ± 0.13	3
pK_I						
10 nM BY-CGP	9.14 ± 0.25	3	9.16; 8.61	2	9.25; 9.32	2
20 nM BY-CGP	9.20 ± 0.12	3	8.91 ± 0.18	3	8.96; 9.24	2
100 nM BY-CGP	9.31 ± 0.02	3	9.13 ± 0.17	3	9.20 ± 0.13	3

The rightward shifts of the two-phase antagonist displacement curves describing the inhibition of the binding of increasing BY-CGP concentrations at the β_1-adrenoceptor may be indicative of competitive interactions between the labelled and unlabelled (competitor) ligands at both β_1-adrenoceptor sites. However, similar shifts may also be caused by allosteric modulators that negatively affect the binding of BY-CGP to the β_1-adrenoceptor (Christopoulos *et al.*, 2002; Hulme *et al.*, 2010). A competitive interaction between ligands competing for the same binding site should result in log IC_{50} values that can be fitted to a slope of unity using linear regression analysis when plotted against the concentrations of the labelled ligand used to obtain the antagonist IC_{50} values. Using this analysis, the slopes describing the interactions of CGP 20712A, propranolol and CGP 12177 at the high affinity β_1-adrenoceptor site 1 were 0.57 ± 0.11(n=4), 0.84 ± 0.17 (n=3) and 0.76 ± 0.12 (n=3), respectively (Figure 5.11A). When plotting the IC_{50} values obtained from the secondary inhibition phase, slope of 0.39 ± 0.13 (n=4), 0.31 ± 0.12 (n=3) and 0.27 ± 0.22 (n=3) were determined for CGP 20712A, propranolol and CGP 12177, respectively (Figure 5.11B). Whilst the slope describing ligand binding interactions of CGP 20712A at site 1, and the slopes for all three antagonists at site 2 were significantly different to unity ($P < 0.05$, one-sample t-test comparison to hypothetical value of 1.0), it is important to note that we could not be certain whether equilibrium conditions were achieved in the fluorescence-based binding assay used to derive the antagonist IC_{50} values. Slopes significantly different to unity were also obtained for ICI 118,551 (0.40 ± 0.21, n=3), propranolol (0.32 ± 0.25, n=3) and CGP 12177 (0.60 ± 0.16, n=3)

at the β_2-adrenoceptor, respectively ($P < 0.05$, one-sample t-test comparison to hypothetical value of 1.0; Figure 5.11C). Only one binding site has been described for the human β_2-adrenoceptor, to which the fluorescent analogue of CGP 12177 binds (Baker *et al.*, 2003d). However, the interactions of this fluorescent ligand at the β_2-adrenoceptor are long lasting (Baker *et al.*, 2003d), such that it is unlikely that equilibrium conditions were achieved in the binding assay used here. This highlights the effects of non-equilibrium conditions on the log IC_{50} ratio plot used here, and demonstrates that this analysis cannot be used under these conditions to gain insight into the mechanisms of interaction between ligands at the human β_1-adrenoceptor.

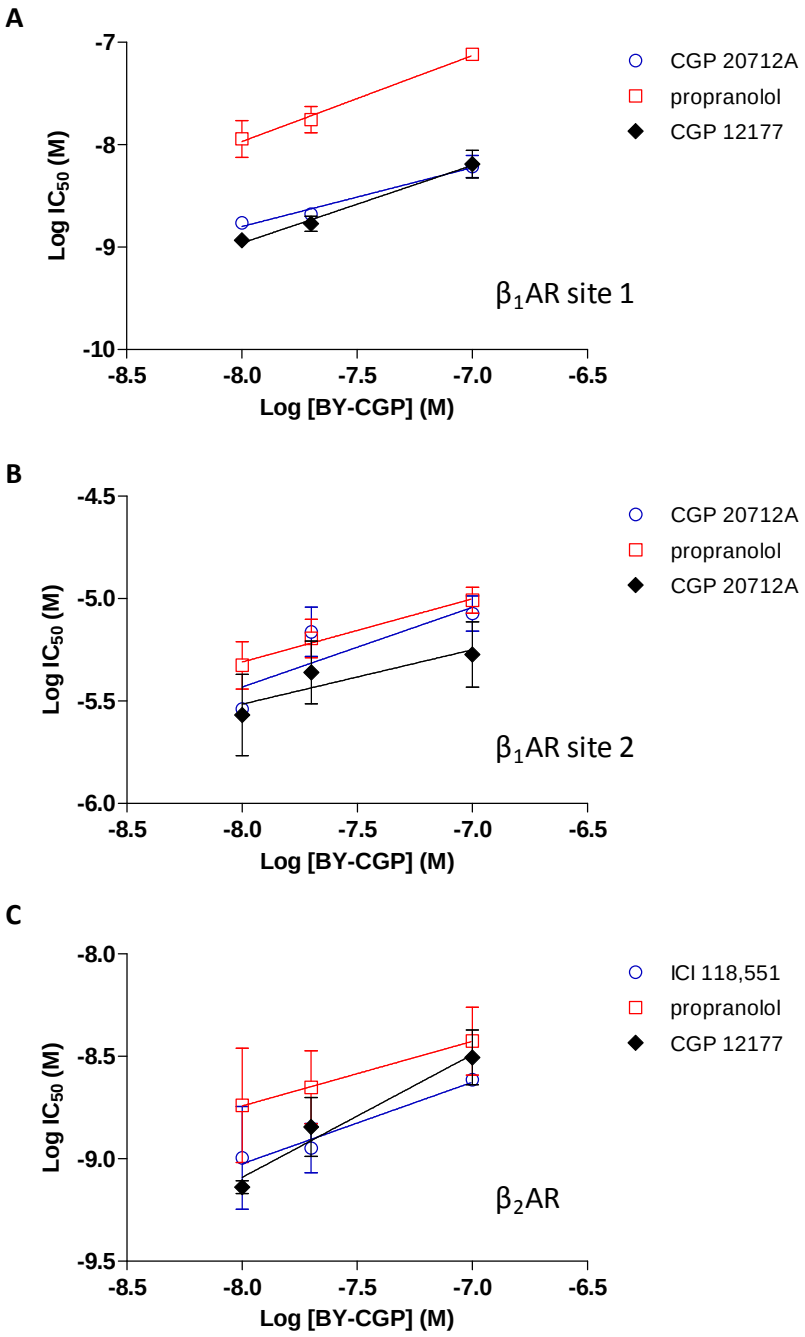

Figure 5.11 The log IC_{50} values obtained for CGP 20712A, propranolol and CGP 12177 at the **A**, β_1-adrenoceptor site 1 and **B**, site 2 (in Figure 5.8 and Table 5.1) were plotted against the log of the BY-CGP concentration used to determine these IC_{50} values (Table 5.2). **C**, the same analysis was performed using log IC_{50} values of ICI 118,551, propranolol and CGP 12177 obtained at the β_2-adrenoceptor (in Figure 5.10 and Table 5.2). Data are mean ± s.e.m. of 3-4 separate experiments.

Different gain settings were used for measuring the different BY-CGP concentrations on the IX Ultra confocal plate reader to maximise the signal-to-noise ratio for each concentration. To confirm that higher BY-CGP concentration yield higher fluorescence intensity readings as a result of BY-CGP binding to the β_1- and β_2-adrenoceptor in CHO cells, saturation binding experiments were carried out. The binding of increasing BY-CGP concentrations in the absence (total binding) and presence (non-specific binding) of 100 nM CGP 20712A (CHO-β_1-CS cells; Figure 5.12) and 100 nM ICI 118,551 (CHO-β_2-CS cells; Figure 5.13) was determined. The specific binding of BY-CGP was saturable at the β_1- and the β_2-adrenoceptor, and both binding curves were preferably fit to a one-site saturation binding curve. The pK_D value derived from the saturation binding curves of BY-CGP at the β_1-adrenoceptor was 6.69 ± 0.17 (n=3). Two separate saturation binding experiments were performed using CHO-β_2-CS cells yielding pK_D values 7.13 and 7.43.

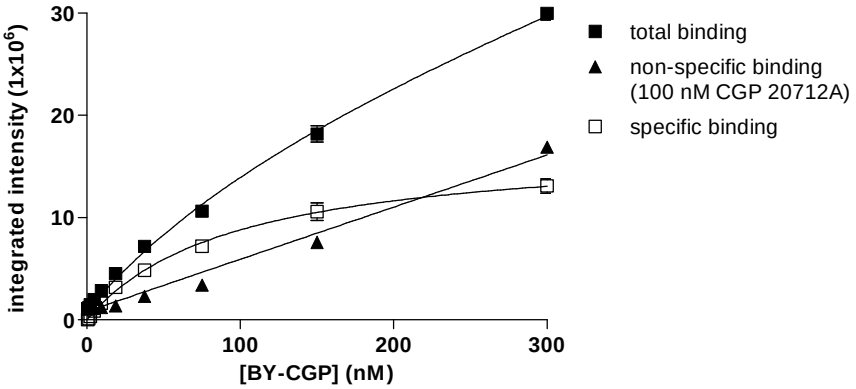

Figure 5.12 The binding of increasing concentrations of BY-CGP to CHO-β_1-CS cells was determined in the absence (total binding) and presence (non-specific binding) of 100 nM CGP 20712A. The non-specific binding levels were deducted from total binding to give specific binding data of BY-CGP to CHO-β_1-CS cells. The data shown are from a single experiment with error bars showing range of error of duplicate determinations. These data are representative of three separate experiments.

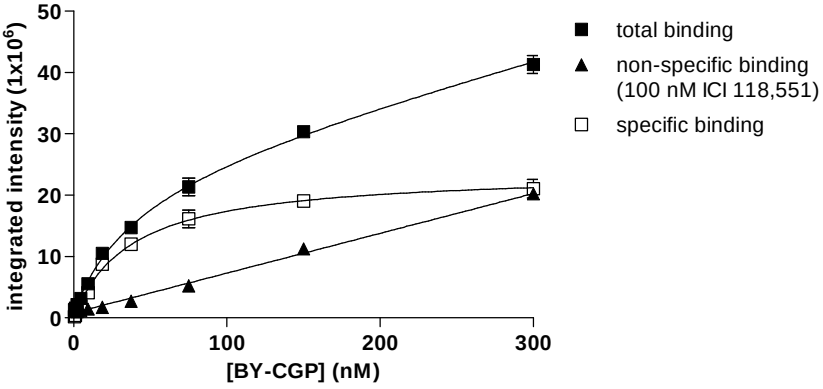

Figure 5.13 The binding of increasing concentrations of BY-CGP to CHO-β_2-CS cells was determined in the absence (total binding) and presence (non-specific binding) of 100 nM ICI 118,551. The non-specific binding levels were deducted from total binding to give specific binding data of BY-CGP to CHO-β_2-CS cells. The data shown are from a single experiment with error bars showing range of error of duplicate determinations. These data are representative of two separate experiments.

Determination of BY-CGP binding parameters to the human β_1- and β_2-adrenoceptor using the high-throughput PHERAstar *FS* plate reader

Whilst the IX Ultra confocal plate reader delivers confocal images of each well to allow visualisation of the binding of a fluorescent ligand to living cells, it takes circa 20 minutes to read one 96-well plate. A faster, high-throughput plate reader is the PHERAstar *FS*, which measures the fluorescence intensity in each well without taking confocal images, thus it takes circa 3 minutes to read one 96-well plate. Here, we compare the BY-CGP binding data obtained using both plate readers. Each plate was read first on the PHERAstar *FS* and immediately afterwards on the IX Ultra confocal plate reader to allow for direct comparison of data from the same assay plate. We examined the inhibition of 10 nM BY-CGP binding to CHO-β_1-CS and CHO-β_2-CS cells by the non-selective β-adrenoceptor antagonist propranolol, the β_1-selective antagonist CGP 20712A and the β_2-selective antagonist ICI 118,551. As can be seen in Figure 5.14 and 5.15, the IX Ultra and PHERAstar *FS* montage images of the assay plates compare well at both receptors, respectively.

At the β_1-adrenoceptor (Figure 5.14), a two-site fit was the preferred fit for the CGP 20712A inhibition curve and similar IC_{50} values of CGP 20712A at site 1 and site 2, and percentages of BY-CGP-bound site 1 of overall BY-CGP-bound receptor sites were determined using the PHERAstar *FS* (pIC_{50} site 1: 8.71 ± 0.08, site 2: 4.81 ± 0.48, percentage site 1: 85.1 ± 4.9 %, n=4) and the IX Ultra (site 1: 8.44 ± 0.05, site 2: 4.75 ± 0.50, percentage site 1: 90.7 ± 3.4 %, n=4; $P >$ 0.05, unpaired t-test performed for each parameter). The definition of the

propranolol inhibition curve was not great enough to detect a second displacement binding phase, although it can be seen that the data points were very similar to those for CGP 20712A. Propranolol pIC_{50} values obtained using the PHERAstar *FS* were 9.11 ± 0.26 (n=4) and compared well to those determined from data obtained using the IX Ultra confocal plate reader (pIC_{50} 8.95 ± 0.11, n=4; $P > 0.05$, unpaired t-test). The ICI 118,551 displacement curve was right-shifted compared to the CGP 20712A and propranolol inhibition curves, and similar IC_{50} values were determined from the PHERAstar *FS* (pIC_{50} of 7.56 ± 0.16, n=4) and the IX Ultra data (pIC_{50} 7.45 ± 0.05, n=4; $P >$ 0.05, unpaired t-test).

At the β_2-adrenoceptor (Figure 5.15) all inhibition binding curves were fitted to a one-site binding equation. ICI 118,551 displayed similar pIC_{50} values of 8.73 ± 0.06 (n=4) and 8.67 ± 0.01 (n=4) determined from PHERAstar *FS* and IX Ultra data, respectively ($P > 0.05$, unpaired t-test). Propranolol also displaced 10 nM BY-CGP binding with comparable pIC_{50} values of 9.00 ± 0.08 (n=4, PHERAstar *FS*) and 8.98 ± 0.09 (n=4, IX Ultra; $P > 0.05$, unpaired t-test). The CGP 20712A displacement curve was right-shifted at the β_2-adrenoceptor with pIC_{50} values of 5.68 ± 0.06 (n=3, PHERAstar *FS*) and 5.57 ± 0.03 (n=3, IX Ultra; $P > 0.05$, unpaired t-test).

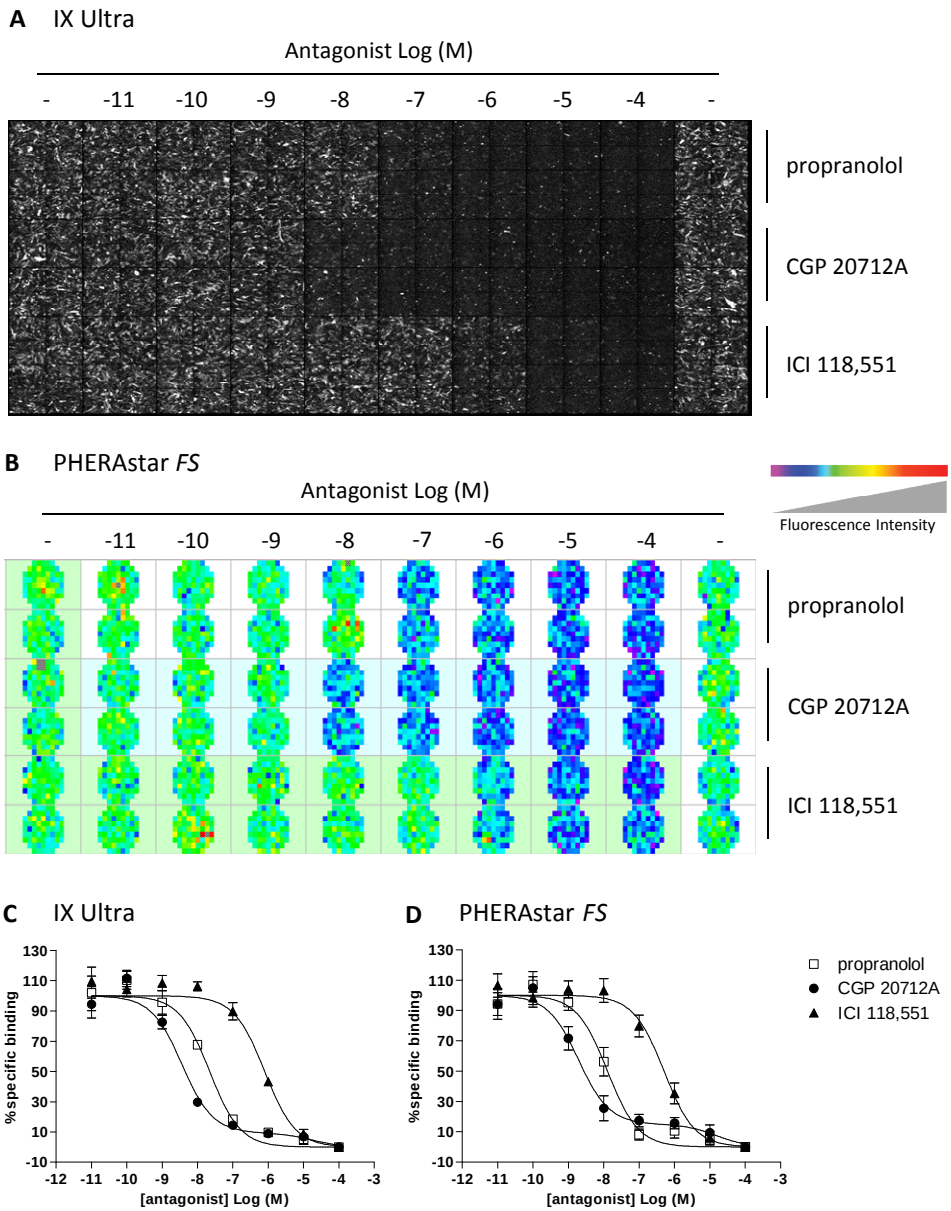

Figure 5.14 Binding of 10 nM BY-CGP to CHO-β_1-CS cells in the absence and presence of unlabelled competitor ligands. **A**, montage image showing the fluorescent intensity of BY-CGP binding determined on the IX Ultra confocal plate reader and **B**, the PHERAstar *FS* plate reader. **C**, inhibition curves of propranolol, CGP 20712A and ICI 118,551 obtained from the IX Ultra confocal plate reader data shown in A and **D**, the PHERAstar *FS* data shown in B. The data shown are mean ± s.e.m. from a single experiment and are representative of three separate experiments.

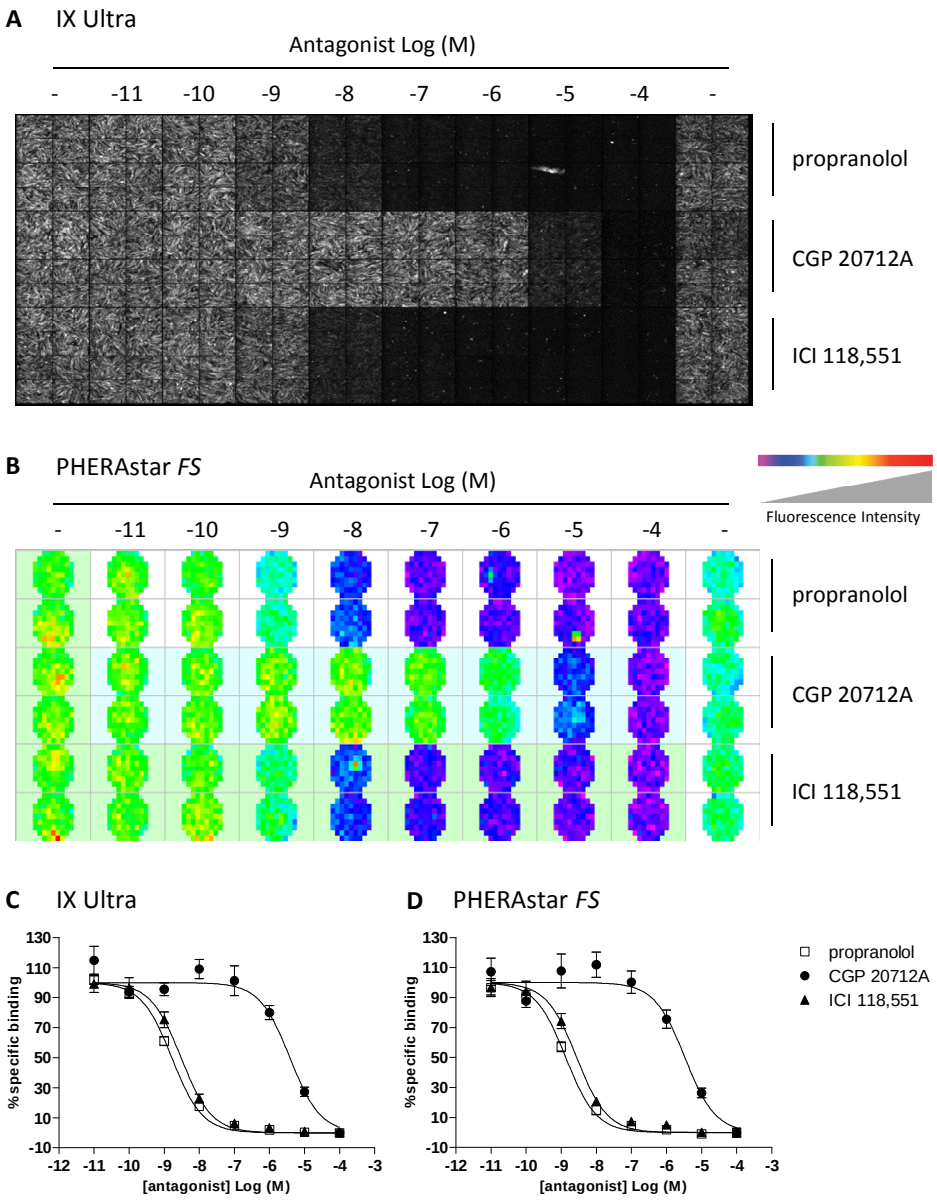

Figure 5.15 Binding of 10 nM BY-CGP to CHO-β_2-CS cells in the absence and presence of unlabelled competitor ligands. **A**, montage image showing the fluorescent intensity of BY-CGP binding determined on the IX Ultra confocal plate reader and **B**, the PHERAstar *FS* plate reader. **C**, inhibition curves of propranolol, CGP 20712A and ICI 118,551 obtained from the IX Ultra confocal plate reader data shown in A and **D**, the PHERAstar *FS* data shown in B. The data shown are mean ± s.e.m. from a single experiment and are representative of three separate experiments.

5.4 Discussion

Fluorescent ligands allow the visualisation of native receptors in living cells and thus facilitate investigations of receptor-ligand interactions without any of the safety hazards or disposal costs associated with using radioisotopes for similar studies. Here, we examined the use of the fluorescently labelled β-adrenoceptor ligands CGP 12177 and propranolol in a live cell automated high-content screening format with the aim to further assess the ligand binding characteristics of the secondary low affinity binding site of the β_1-adrenoceptor.

The IX Ultra confocal plate reader automatically captured and analysed confocal images from four separate sites in each well used on a 96-well assay plate. Using the same experimental conditions (incubation times and temperatures) in both manual and automated confocal microscopy approaches, the data obtained for CGP 20712A inhibiting the binding of 20 nM BY-CGP compared very well. Additional data points clearly defined a secondary binding inhibition phase which was best fitted to a two-site displacement binding curve. However, the use of BY-PROP proved unsuccessful in this assay due to great intra-experimental variability. This may have been due to a lower affinity of BY-PROP for the β_1-adrenoceptor. A higher, sub-nanomolar affinity of BY-PROP was determined for the β_2-adrenoceptor by Baker *et al.* (2011a), which is consistent with the clear membrane labelling observed of 3 nM BY-PROP in CHO-β_2-CS cells (Chapter 4, Figure 4.12; Baker *et al.* (2011a)). The 20 nM BY-PROP concentration used in

CHO-β_1-CS cells was similar to the affinity value of BY-PROP for the catecholamine site 1 of the β_1-adrenoceptor (circa 28 nM) compared to a circa 30-fold K_D concentration of BY-CGP (K_D circa 0.6 nM) used in experiments in the same cells. It takes longer for ligands to reach equilibrium at low concentrations than at higher concentrations, which is one of the reasons why it is desirable to have a high affinity labelled ligand for competition binding experiments. In addition, the lipophilic properties of BY-PROP as well as a short incubation time may have been contributing factors in the variability of data points observed. The diffusion time for a "sticky" ligand may have been limited in the assay conditions used, although increasing incubation times and temperatures did not seem to resolve this problem. Furthermore, using total image intensity analysis the intracellular fluorescence intensities were included in the analysis of the confocal images and ultimately contributed to a reduced assay window in which the displacement of BY-PROP binding to CHO-β_1-CS cells could be measured.

Using a 96-well format allowed the investigation of the secondary low affinity binding site of the β_1-adrenoceptor in more detail by examining receptor-ligand interactions of multiple BY-CGP concentrations and competitor ligands. Increasing BY-CGP concentrations resulted in rightward shifted displacement binding curves of CGP 20712A, propranolol and CGP 12177. The IC_{50} values for both site 1 and site 2 increased with increasing BY-CGP concentrations which is indicative of competitive antagonism at both sites. The derived affinity values, however, did not compare well with the affinity values obtained for

the three antagonists in the CRE-mediated SPAP transcription assay in Chapter 3 (Table 5.3). An incubation time of 5 hours with both the antagonist and the agonist present is necessary in the CRE-SPAP assay to allow for transcription of the reporter gene. This was a considerably longer incubation time than was used in the competition binding experiments used in this chapter and thus allowed more time for antagonist and agonist to reach equilibrium or at least a closer-to-equilibrium state in the gene reporter assay. Equilibrium is achieved when the concentrations of free and bound ligand/receptor do not change any more and the same number of ligand molecules associate with the receptor as dissociate. The Cheng-Prusoff equation was used to derive the affinity values of the antagonists from their IC_{50} values against different BY-CGP concentrations. This equation assumes equilibrium conditions in the competition binding assay and mutually exclusive binding sites (i.e. no allosteric interactions between multiple binding sites). To check whether equilibrium has been reached displacement binding curves can be obtained using different incubation times. The binding curves will shift until equilibrium is reached. Alternatively, Motulsky *et al.* (1984) have estimated that four times the dissociation half time (of the slowest dissociating ligand) is needed to reach equilibrium. BODIPY-TMR-CGP was described as a long-acting partial agonist at the β_2-adrenoceptor (Baker *et al.*, 2003d). A slow dissociation off rate from the β_1-adrenoceptor can also be assumed, because the fluorescence intensity reading of a given BY-CGP concentration was unchanged across the assay plate following the washout of all ligands and a 20 minute read time on the IX Ultra confocal plate reader. A

Table 5.3 Comparison of affinity values of CGP 20712A, propranolol and CGP 12177 at the human β_1-adrenoceptor obtained in the CRE-mediated SPAP transcription assay and the BODIPY-TMR-CGP live cell high-content screening binding assay. Data are mean ± s.e.m. of (n) separate experiments. [1]The CRE-SPAP data shown here was obtained in experiments described in Chapter 3. *statistical significance ($P < 0.05$) of difference in affinity values determined in the BY-CGP binding assay compared to affinities obtained in the CRE-SPAP assay, according to unpaired t-test analysis

	BY-CGP binding assay		CRE-SPAP assay[1]	
	pK_I	n	pK_B	n
CGP 20712A				
site 1	10.29 ± 0.06*	6	8.84 ± 0.11	5
site 2	5.40 ± 0.09*	6	6.73 ± 0.22	7
propranolol				
site 1	9.28 ± 0.10*	3	8.65 ± 0.07	23
site 2	5.35 ± 0.06*	3	6.04 ± 0.18	5
CGP 12177				
site 1	10.30 ± 0.07*	3	9.61 ± 0.06	10
site 2	5.56 ± 0.17*	3	7.58 ± 0.13	13

fast dissociating ligand would have resulted in lower fluorescence intensity readings following washout of the ligand. But without knowing the exact kinetic parameters of the ligands involved it is difficult to predict when equilibrium might be reached. However, reading of the assay plate on the IX Ultra confocal plate reader in the presence (rather than the absence) of both unlabelled and labelled ligands may have improved the competition binding data, particularly for BY-CGP binding to the lower affinity secondary β_1-adrenoceptor site and also when using the fluorescent propranolol ligand. Equilibrium is achieved when the rate of ligand-receptor formation is equal to the rate of ligand-receptor dissociation, thus including free ligand, free receptors and ligand-bound receptor complexes. The wash step used in the experiments described in this chapter removed the free ligands, thereby facilitating the opportunity of ligand-receptor complexes to dissociate and to attempt to reach a new equilibrium in "washed" conditions. This may have resulted in an underestimation of the amount of bound fluorescent ligand and contributed to lower BY-CGP site 2 and BY-PROP binding levels, although the competition binding data obtained from the IX Ultra confocal plate reader (20 minute read per plate) and the PHERAstar *FS* plate reader (3 minute read per plate) did not show a noticeable difference in the fluorescent ligand binding data for the antagonists tested. The binding kinetics of BY-CGP and BY-PROP to CHO-β_1-CS are investigated in more detail in Chapter 6. In addition, increased incubation times and temperatures of BY-CGP appeared to increase the non-specific cytoplasmic fluorescence intensity measured, thus making long incubation times difficult.

Interestingly, the affinity values determined for site 1 are overestimated in the binding assay whereas the affinity values for the second site are underestimated for all three antagonists tested, in comparison to the affinity values obtained in the SPAP assay (Chapter 3). This suggests that the kinetics of BY-CGP are very different at the two sites potentially with faster kinetics at site 2 and slower kinetics at site 1. If BY-CGP displays slow kinetics at site 1 it could mean that less receptor sites will have been occupied in a shorter incubation time than if equilibrium was reached, thus allowing the unlabelled antagonist to compete against less ligand than is presumed, resulting in the antagonists to appear more potent at that site. However, overestimation of antagonist affinities may also be due to slow antagonist dissociation rates, especially following the antagonist pre-incubation used in these experiments. By contrast, faster BY-CGP kinetics at site 2 could mean that "too much" ligand initially associates with the receptor site, thus giving the antagonists "too much" to compete against, making them appear less potent at that site. This is consistent with the shifts of IC_{50} values observed at site 1 and site 2 when BY-CGP incubation was carried out at 37 °C compared to 21 °C. A comparable shift of the IC_{50} values, however, was not seen when increasing the incubation time from 30 to 60 minutes at 21 °C. Whilst not observing a shift of the displacement binding curve can be indicative of having reached equilibrium it may also mask very slow kinetics of the fluorescent ligand. In fact, Joseph *et al.* (2004) reported a circa 20-fold faster dissociation rate of the radioligand [^{3}H]-CGP 12177 off the low affinity site than off the high affinity site (Joseph *et al.*, 2004). However, the addition of a large fluorophore

to the small molecule CGP 12177 cannot be compared to the addition of a comparably small radioisotope and the kinetic parameters of BY-CGP at the β_1-adrenoceptor are examined in Chapter 6.

The lower affinity values determined for the high affinity β_1-adrenoceptor site 1 in the CRE-SPAP assay compared to the BY-CGP binding may also have been due to receptor desensitisation caused by using the full agonist cimaterol in the CRE-SPAP assay. Lower affinities were measured for β-adrenoceptor ligands in the CRE-SPAP assay when using a full agonist compared to using a partial agonist (Baker *et al.*, 2003c). In addition, a potential impact of an allosteric mechanism of action being responsible for the secondary site may also be considered, as allosteric modulators that cause negative co-operativity between two binding sites may display similar pharmacology to competitive antagonists, and may not easily identified using an equilibrium binding approach (Christopoulos *et al.*, 2002). Such a mechanism that links the two β_1-adrenoceptor binding sites also invalidates the use of the Cheng-Prusoff equation to derive antagonist affinity values from the IC_{50} values in the competition binding assay.

Confocal images of the CHO-β_2-CS cell line revealed a homogenous cell line with good levels of BY-CGP binding to all cells. Displacement binding curves of three β-adrenoceptor antagonists obtained using CHO-β_2-CS cells were best fitted using a one-site displacement binding curve, indicating that the two-site binding fit preferred at the β_1-adrenoceptor is specific to the receptor and not due to artefacts of the assay format. The affinity values that were calculated

for the antagonists at the β_2-adrenoceptor were in good agreement with values reported in the literature (Baker (2005); Table 5.4). Considering the proposed slow kinetics of BY-CGP at the β_2-adrenoceptor (Baker *et al.*, 2003d), this was unexpected.

Interestingly, the proportion of the second site also increased with increasing BY-CGP concentrations. This is consistent with increased labelling of the second site by higher concentrations due to higher occupancy at the second site of the β_1-adrenoceptor (Figure 5.16, Table 5.5). From the percent occupancy of 10, 20 and 100 nM BY-CGP at site 1 and site 2, the percentage of BY-CGP bound to the high affinity site over the low affinity site was calculated (i.e. theoretical percentage site 1; Table 5.5) for each BY-CGP concentration used, and those values compared well to the values obtained from experimental data. The calculated values were based on the assumption that both sites were present in equal proportions (i.e. 1:1), which would mean for each site 1 there is also a site 2, which would be the case if the β_1-adrenoceptor did in fact have two separate binding sites or if the receptor was present in stable homodimers thus also providing two binding sites. Experimental data, however, suggests that β_1-adrenoceptors exist in transient homodimer formations (Dorsch *et al.*, 2009; Calebiro *et al.*, 2013). Furthermore, these calculations were based on the assumption that equilibrium had been reached in the assay which, as discussed above, is unlikely.

Table 5.4 Comparison of affinity values of ICI 118,551, propranolol and CGP 12177 at the human β_2-adrenoceptor obtained in the BODIPY-TMR-CGP live cell high-content screening binding assay with values determined in a [^{3}H]-CGP 12177 competition binding assay (Baker *et al.*, 2005). Data are mean ± s.e.m. of (n) separate experiments.

	BODIPY-TMR-CGP binding assay		[^{3}H]-CGP 12177 binding assay
	pK_I	n	pK_B
ICI 118,551	9.22 ± 0.13	3	9.26
propranolol	9.00 ± 0.15	4	9.08
CGP 12177	9.20 ± 0.08	3	9.39

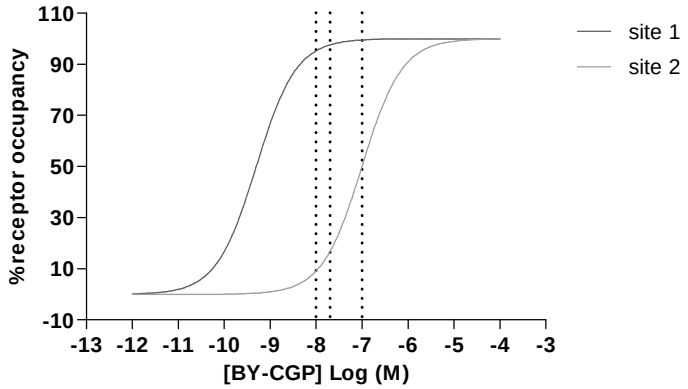

Figure 5.16 BY-CGP occupancy curves at the high affinity catecholamine site 1 and low affinity "CGP 12177" site 2 of the β_1-adrenoceptor. The occupancy curves were determined using the affinity constants of BY-CGP at the high and low affinity site of the β_1-adrenoceptor derived in the CRE-mediated SPAP transcription assay in Chapter 4. The dotted lines highlight the % occupancy at the β_1-adrenoceptor site 1 and site 2 for 10, 20 and 100 nM BY-CGP.

Table 5.5 Summary of percentage of 10, 20 and 100 nM BY-CGP bound to site 1 and site 2 of the β_1-adrenoceptor (taken from the BY-CGP occupancy curves shown in Figure 5.16) and the calculated (theoretical) and experimentally obtained percentages of 10, 20 and 100 nM BY-CGP binding to site 1 over site 2 of the β_1-adrenoceptor.

	% bound		% site 1	% site 1				
	site 1	site 2	theoretical	experimental				
				CGP 20712A	n	propranolol	n	CGP 12177	n
10 nM BY-CGP	95.0	8.7	91.2	89.1 ± 1.2	4	89.3 ± 0.4	3	92.6 ± 1.3	3
20 nM BY-CGP	97.6	16.7	85.4	85.8 ± 1.2	3	87.0 ± 0.6	3	88.8 ± 0.6	3
100 nM BY-CGP	99.5	49.1	66.9	58.3 ± 4.0	6	72.1 ± 3.7	3	72.2 ± 2.1	3

The saturation binding data best fitted to a one-site specific binding curve and the K_D value obtained for BY-CGP at the β_1-adrenoceptor (circa 202 nM) was similar to the affinity value of BY-CGP determined for the second low affinity β_1-adrenoceptor site (circa 87 nM) in the CRE-SPAP assay (Chapter 4). This may be because the circa 100-fold difference in affinity (K_{Dsite1} circa 0.6 nM) is difficult to capture in one saturation binding curve which spans ten BY-CGP concentrations from 0.6 – 300 nM. The affinity value of BY-CGP at the first β_1-adrenoceptor site is circa 0.6 nM (Chapter 4) and was the lowest concentration and first data point of the saturation binding curve. Furthermore, additional data points facilitating an even broader range of BY-CGP concentrations would not necessarily have enabled the detection of both sites due to the limits in the dynamic range the IX Ultra plate reader can detect at any given gain setting. The gain settings used in the experiments for this study were always optimised to the highest BY-CGP concentration used (i.e. the concentration which resulted in the highest reading of fluorescence intensity) and thus "better" at detecting higher than lower fluorescence intensities.

As mentioned earlier, the IX Ultra confocal plate reader has a read time of 20 minutes per assay plate. The PHERAstar *FS* plate reader has a much quicker read time of circa 3 minutes in which it records the fluorescence intensity of 81 sites per well of a 96-well plate. Whilst it does not capture confocal images of the wells and thus collects only numerical data, this plate reader provides an opportunity for higher throughput screening campaigns. The IC_{50} values of

ICI 118,551, propranolol and CGP 20712A against 10 nM BY-CGP at the β_1- and β_2-adrenoceptor were determined using the IX Ultra confocal plate reader and the PHERAstar *FS* plate reader and were in excellent agreement and all three antagonists inhibited the binding of 10 nM BY-CGP according to their attributed β-adrenoceptor selectivities. This highlights the potential use of the PHERAstar *FS* plate reader for high-throughput screening programs but also demonstrates the versatile use of the BODIPY-TMR-CGP ligand in multiple assays using different methods of detecting ligand binding parameters.

5.5 Conclusion

We have successfully used the fluorescent ligand BODIPY-TMR-CGP in a live cell fluorescence-based ligand binding assay to examine ligand binding parameters at the β_1- and the β_2-adrenoceptor expressed in CHO cells. The fluorescent propranolol derivative BY-PROP however could not be used in this assay format due to high non-specific binding levels. The high-content IX Ultra confocal plate reader allowed the automatic capture and analysis of confocal images of every well of the assay plate and revealed two-phase displacement binding curves of antagonists against BY-CGP. In addition, we examined the high-throughput PHERAstar *FS* plate reader as an alternative high-throughput screening platform and data obtained on this plate reader compared well to data determined on the IX Ultra. Both plate readers provide the opportunity for screening programs to determine affinity values of unlabelled ligands at the native β_1- and β_2-receptors in their native membrane environment.

Chapter 6

Investigating kinetic parameters of BODIPY-TMR-CGP and BODIPY630/650-S-PEG8-propranolol binding at the human β_1-adrenoceptor at the single cell level

6.1 Introduction

The determination of the dissociation rate of a radiolabelled ligand at a G protein-coupled receptor (GPCR) is traditionally achieved by preventing the re-association of the radioligand with its receptor through the addition of a saturating concentration of the unlabelled counterpart at various time points (Dowling *et al.*, 2006; May *et al.*, 2007). The dissociation rate of a labelled ligand is not affected in the presence of a competitive ligand if both ligands target the same binding site of a monomeric receptor. However, secondary binding sites and receptor dimerisation provide allosteric sites to which unlabelled ligands can potentially bind and thus affect the dissociation rate of the labelled ligand (Christopoulos *et al.*, 2002). In a confocal perfusion system, assay buffer is perfused over live cells in an imaging cell perfusion chamber at a constant flow rate of at least 12 complete fluid exchanges within the perfusion chamber, to allow the determination of kinetic parameters of a fluorescently labelled ligand under infinite dilution conditions (May *et al.*, 2010a). Using this method, the dissociated labelled ligand is physically removed from the receptor without the need for high concentrations of unlabelled ligands. Using a confocal microscopy approach to address the kinetics of receptor-ligand interactions allows visualisation of ligand binding to single living cells under physiological conditions (37 °C) and the investigation of the dynamics of receptor-ligand interactions in real time and is particularly useful when the presence, number or nature of potential allosteric binding sites of a GPCR is not yet fully known.

The β_1-adrenoceptor has been reported to have two binding sites or conformations. Endogenous ligands adrenaline and nor-adrenaline exhibit their stimulatory effects through the orthosteric catecholamine site which are effectively inhibited by β-blockers such as CGP 12177. However, CGP 12177 was also found to exert agonist effects at approximately 100-fold higher concentrations through a lower affinity "CGP 12177" β_1-adrenoceptor site (Baker *et al.*, 2003a; Konkar *et al.*, 2000; Pak *et al.*, 1996).

In chapter 4 of this thesis we described the binding of two fluorescent β-adrenoceptor ligands BODIPY-TMR-CGP (a CGP 12177 derivative) and BODIPY630/650-S-PEG8-propranolol (an analogue of propranolol) to both, the orthosteric high affinity and the secondary "CGP 12177" low affinity binding site of the β_1-adrenoceptor. In this chapter, we aimed to characterise the kinetic parameters of these two fluorescent ligands at the human β_1-adrenoceptor and secondly, to examine the effects of unlabelled ligands on the dissociation rate of the fluorescent ligands under infinite dilution conditions in single living cells to further our understanding of the dynamics of the ligand binding to the β_1-adrenoceptor and a potential role of the secondary β_1-adrenoceptor binding site.

6.2 Methods

Cell culture

This was performed as described in *Methods: Cell culture*. CHO-β_1-CS and CHO-CS cell lines were used in this chapter.

Confocal perfusion system

The perfusion experiments were carried out at 37 °C as described in *Methods: Confocal perfusion system*. The confocal perfusion systems of both, the Zeiss LSM510 and LSM710 microscope, were used. Confocal and transmitted light images of live cells were taken every 2-3 seconds. BY-CGP fluorescence intensity was measured using a 543 nm and 561 nm excitation wavelength on the LSM510 and LSM710 confocal microscope, respectively. The fluorescence intensity of BY-PROP was measured using a 633 nm wavelength on both microscopes. The use of both confocal perfusion systems was validated by comparing kinetic data of the fluorescent adenosine derivative ABA-X-BY630 (for structure see Middleton *et al.* (2007)) at the adenosine A_3 receptor obtained using the above two microscopes to published data (Appendix I S8).

Data analysis

The equations describing the curve fits used in this chapter are listed and described in *Methods: Data analysis*. GraphPad Prism 5.0 was used to fit all kinetic data. Association traces of fluorescent ligands were fit using a monophasic exponential fit. The association plateau predicted by GraphPad

Prism 5.0 was used to define 100 % of ligand binding to allow data to be normalised and grouped. For the analysis of dissociation rates, a monophasic exponential fit was compared to a two-phase decay equation to find the best fit, which was then used to derive the dissociation rate. This was done for every concentration of fluorescent ligand used.

6.3 Results

Characterising the kinetic parameters of BODIPY-TMR-CGP at the human β_1-adrenoceptor

The Zeiss LSM510 confocal microscope was used in conjunction with a closed perfusion system that allowed the constant perfusion of ligands or buffer from switch-operated fluid reservoirs, thus allowing the determination of kinetic parameters of the fluorescent ligand under infinite dilution conditions. Using a pump, constant pressure generated a fluid flow rate that was constant, which ensured that the imaged cells were kept in focus during the captured time series. The fluid flow was maintained at a rate fast enough to generate the necessary number of fluid exchanges per minute (≥ 12 exchanges per minute, i.e. 5 mL per minute) within the perfusion imaging chamber that allowed sharp changes in concentration upon reservoir switching (May *et al.*, 2010a). Confocal and phase images were taken every 3 seconds before perfusion of the fluorescent ligand (to obtain a 30 seconds recording of the baseline fluorescence for a given coverslip of cells), during its perfusion (to obtain a trace of association) and after its perfusion (i.e. perfusion of buffer to obtain a trace of dissociation; Figure 6.1B). Drawing regions of interests (ROIs) around the membranes of individual cells allowed the analysis of kinetic parameters at the single cell level (Figure 6.1A). Actual (raw) fluorescence intensity data varied from cell to cell, but the normalised data was similar for the cells examined (Figure 6.1C).

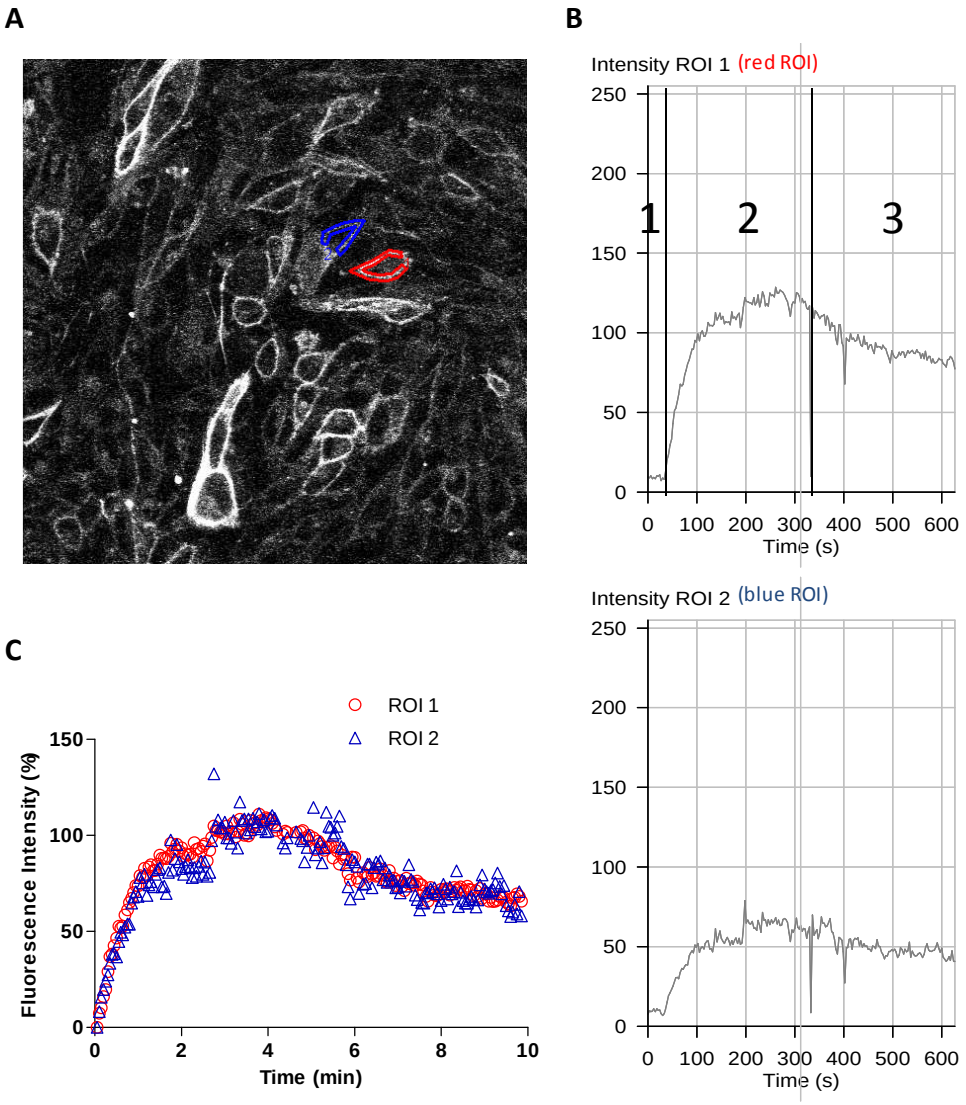

Figure 6.1 Analysis of BY-CGP fluorescence intensities in CHO-β_1-CS cells at the single cell level. **A**, regions of interest (ROIs) were drawn around the membrane of individual cells to obtain fluorescence intensity readings over time. **B**, BY-CGP fluorescence intensities were measured from 0-30 seconds to obtain a baseline fluorescence read by perfusing HBSS buffer only (1), from 30-330 seconds to determine BY-CGP association by perfusing BY-CGP (2) and from 330-630 seconds to determine BY-CGP dissociation by perfusing HBSS buffer only (3). The actual (raw) BY-CGP fluorescence intensity traces are shown for two individual cells (red and blue ROI). **C**, baseline-corrected normalised association and dissociation data of cell 1 (ROI 1, red) and cell 2 (ROI 2, blue).

The association and dissociation of 10, 30 and 100 nM BY-CGP at the human β_1-adrenoceptor were examined. The same microscope settings were used for all BY-CGP concentrations used on both CHO-β_1-CS and CHO-CS cells, to allow the direct comparison of fluorescence intensities between the three BY-CGP concentrations and the two cell lines. The CHO-CS cell line was used to define the non-specific binding component of BY-CGP binding. The fluorescence intensity increased with increasing BY-CGP concentrations and increasing exposure time to BY-CGP in both CHO-β_1-CS (Figure 6.2) and CHO-CS (Figure 6.3) cells. The same trend could be seen for low levels of diffuse intracellular fluorescence in both cell lines, suggesting that the cytoplasmic non-specific fluorescence intensity is not β_1-adrenoceptor-mediated. Clear membrane labelling of BY-CGP was only evident in CHO-β_1-CS cells and not in CHO-CS cells, thus the phase image was used to define the plasma membrane of cells to draw ROIs (Figure 6.4). As expected, the non-specific cell membrane-associated fluorescence intensity in CHO-CS cells was markedly lower than the total binding cell membrane-associated fluorescence intensity measured in CHO-β_1-CS cells (Figure 6.4 and 6.5).

The association and dissociation traces obtained in CHO-CS could only be accurately analysed for 30 and 100 nM BY-CGP. Monoexponential association and dissociation equations were used and revealed rapid observed association (k_{onobs}; 1.40 ± 0.26 min^{-1}, n=6 and 1.56 ± 0.11 min^{-1}, n=4 for 30 and 100 nM BY-CGP, respectively) and dissociation rates (k_{off}; 2.46 ± 0.48 min^{-1}, n=6 and 2.46 ± 0.09 min^{-1}, n=4 for 30 and 100 nM BY-CGP, respectively; Figure

6.5; Table 6.1), which is characteristic of non-specific binding components (May *et al.*, 2010b).

The association traces obtained in CHO-β_1-CS cells revealed that the fluorescence intensity increase from 30 to 100 nM BY-CGP was smaller than that from 10 to 30 nM, suggesting saturability of BY-CGP binding to CHO-β_1-CS cells (Figure 6.5C). This was not the case with the non-specific binding component determined in CHO-CS cells which was best described as a linear relationship for the three concentrations tested (Figure 6.5D), and is characteristic of non-specific binding components. The association of 10, 30 and 100 nM BY-CGP was monoexponential in CHO-β_1-CS cells and a plateau of BY-CGP binding was reached following five minutes exposure of CHO-β_1-CS cells to 30 and 100 nM, but not 10 nM BY-CGP. The observed association rates (k_{onobs}) derived were concentration-dependent with 0.59 ± 0.08 min^{-1} (n=6), 1.64 ± 0.08 min^{-1} (n=6) and 3.07 ± 0.15 min^{-1} (n=3) for 10, 30 and 100 nM BY-CGP, respectively. The dissociation of 10 nM BY-CGP was also monoexponential, however two components, a fast ($k_{off(fast)}$) and a slow ($k_{off(slow)}$) component, were detected in the dissociation of 30 and 100 nM BY-CGP. The rate of the fast dissociation component was comparable to the dissociation rate determined in CHO-CS cells and, as expected for a non-specific binding component, its proportion was increased at higher BY-CGP concentrations. The fast component of BY-CGP dissociation curves obtained in CHO-β_1-CS cells was constrained to the average dissociation rate obtained in CHO-CS cells (2.46 min^{-1}). The slow dissociation component determined for 10,

30 and 100 nM BY-CGP were 0.08 ± 0.01 min^{-1} (n=6), 0.09 ± 0.01 min^{-1} (n=6) and 0.14 ± 0.02 min^{-1} (n=3), respectively, and were significantly slower than the fast component described in CHO-CS cells ($P < 0.05$, two-way ANOVA followed by Bonferroni's post hoc test). Interestingly, the dissociation rate determined for 100 nM BY-CGP was markedly faster than that determined for 10 nM BY-CGP ($P < 0.05$, one-way ANOVA followed by Tukey's post hoc test). This may be due to allosteric effects caused by 100 nM BY-CGP binding to the secondary β_1-adrenoceptor site that were not evident for 10 nM BY-CGP due to its lower occupancy at the secondary β_1-adrenoceptor site compared to 100 nM BY-CGP. The concentration-independence of the dissociation rates of 10 and 30 nM BY-CGP, and the concentration-dependence of the observed association rates of 10, 30 and 100 nM BY-CGP at the β_1-adrenoceptor was clearly seen for normalised grouped data as well as single cell data (Figure 6.6). The k_{onobs} and the $k_{off(slow)}$ of each BY-CGP concentration were used to determine the association rate constants (k_{on}). The k_{on} and the $k_{off(slow)}$ were then used to calculate the equilibrium dissociation constant (K_D) for each BY-CGP concentration and are summarised in Table 6.1.

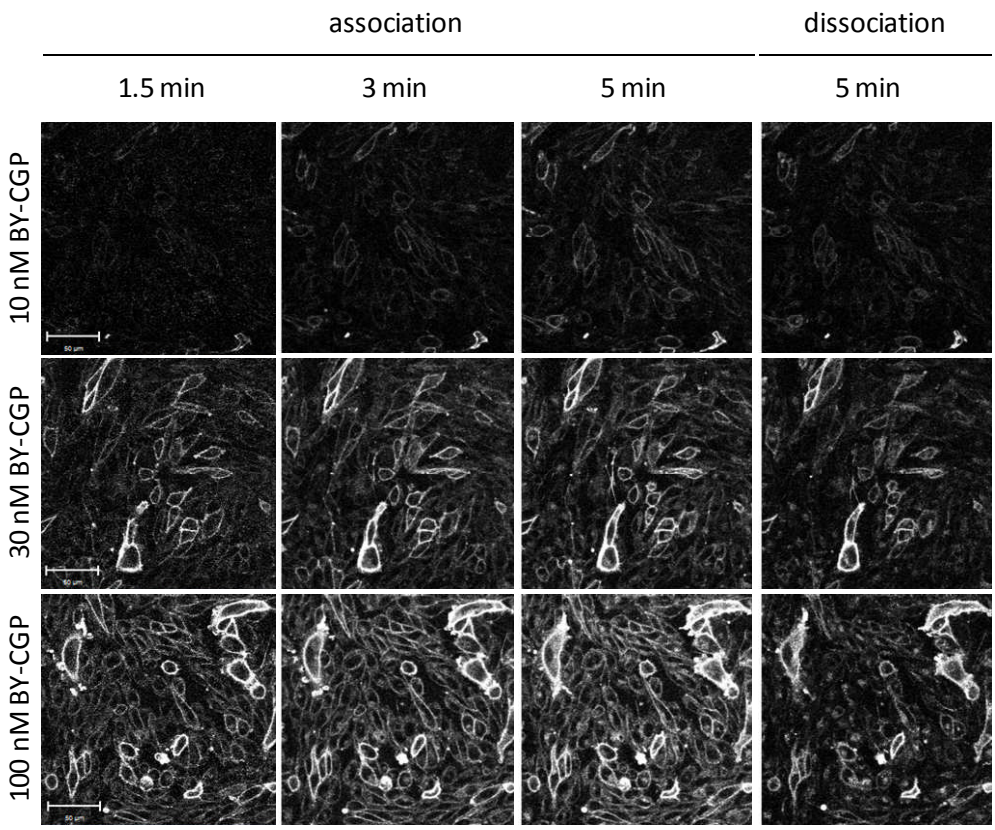

Figure 6.2 Confocal images of 10, 30 and 100 nM BY-CGP binding to CHO-β_1-CS cells after 1.5, 3 and 5 minutes association and 5 minutes dissociation under infinite dilution conditions. The microscope settings were kept constant for the recordings of fluorescence intensities of all three BY-CGP concentrations used to allow for direct comparison of the level of BY-CGP binding. Images are representatives of a total of 4-6 confocal perfusion slides per BY-CGP concentration, obtained on three separate experimental days. Scale bars = 50 µm.

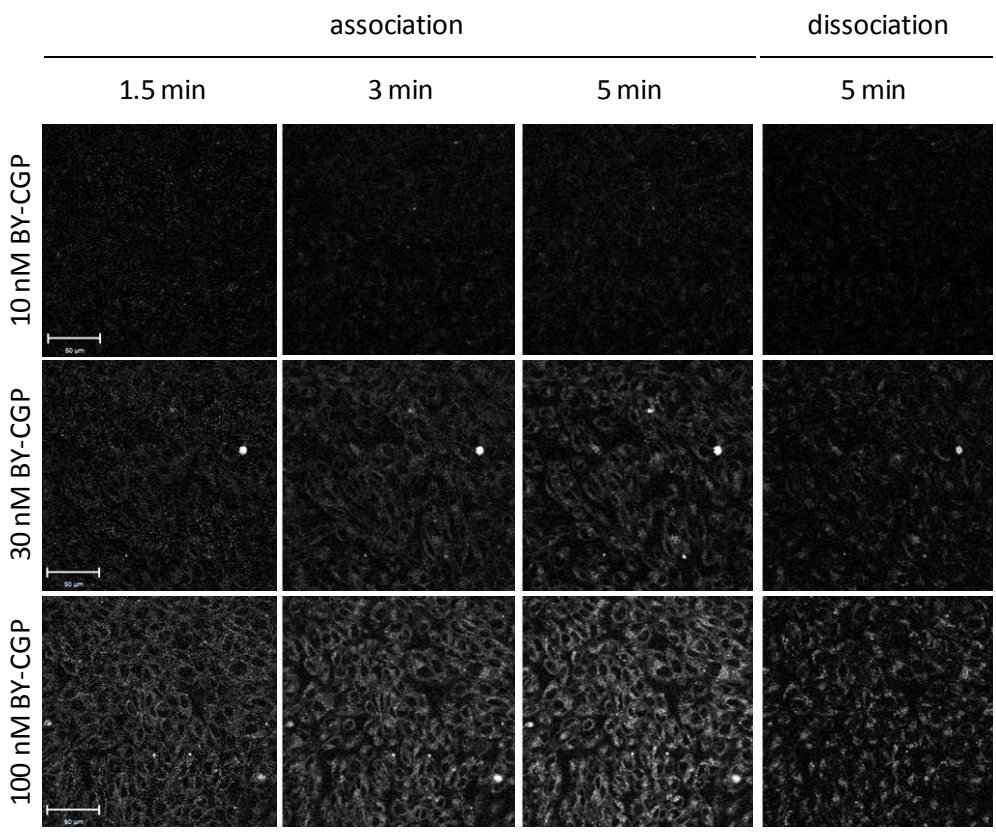

Figure 6.3 Confocal images of 10, 30 and 100 nM BY-CGP binding to CHO-CS cells after 1.5, 3 and 5 minutes association and 5 minutes dissociation under infinite dilution conditions. The microscope settings were kept constant for the recordings of fluorescence intensities of all three BY-CGP concentrations and are also the same settings that were used to image BY-CGP binding to CHO-β_1-CS cells (Figure 6.6) used to allow for direct comparison of the level of BY-CGP binding. Images are representatives of a total of 3-6 confocal perfusion slides per BY-CGP concentration, obtained on three separate experimental days. Scale bars = 50 µm.

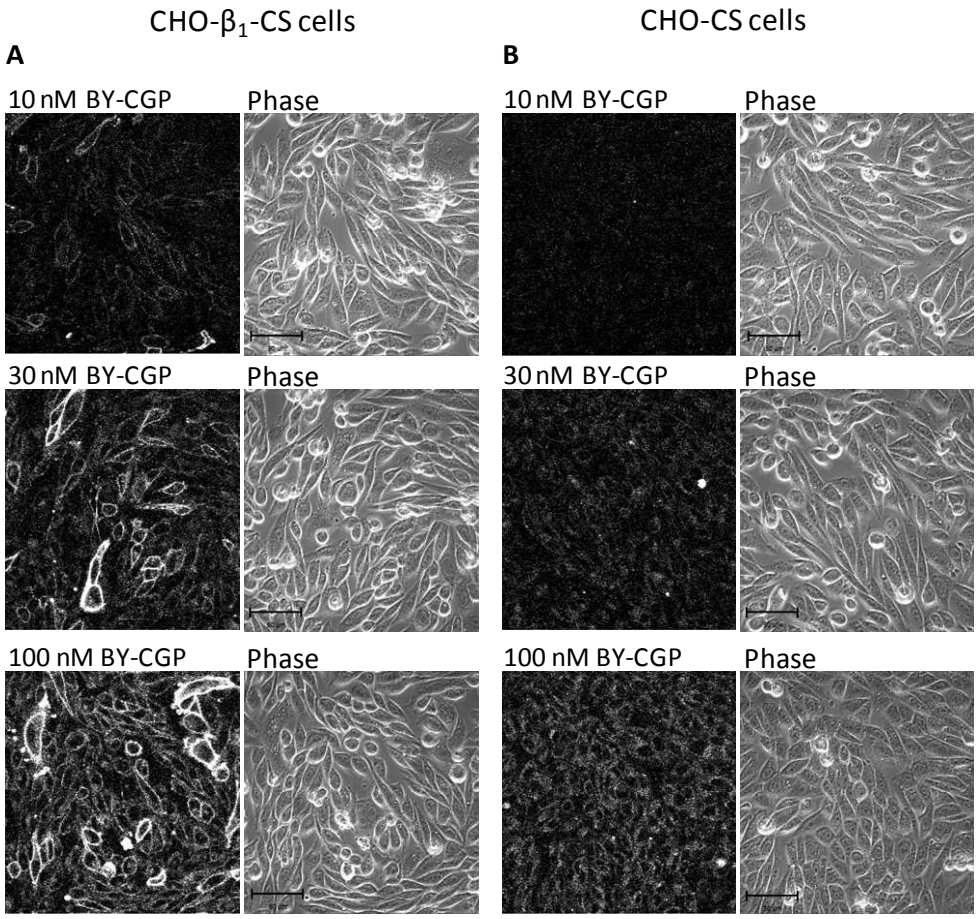

Figure 6.4 Confocal images of 10, 30 and 100 nM BY-CGP binding to **A**, CHO-β_1-CS and **B**, CHO-CS cells following 5 minutes association and 5 minutes dissociation under infinite dilution conditions. The microscope settings were kept constant for the recordings of fluorescence intensities of all three BY-CGP concentrations in both CHO-β_1-CS and CHO-CS cells to allow for direct comparison of the level of BY-CGP binding. Images are representatives of a total of 3-6 confocal perfusion slides per BY-CGP concentration, obtained on three separate experimental days. Scale bars = 50 µm.

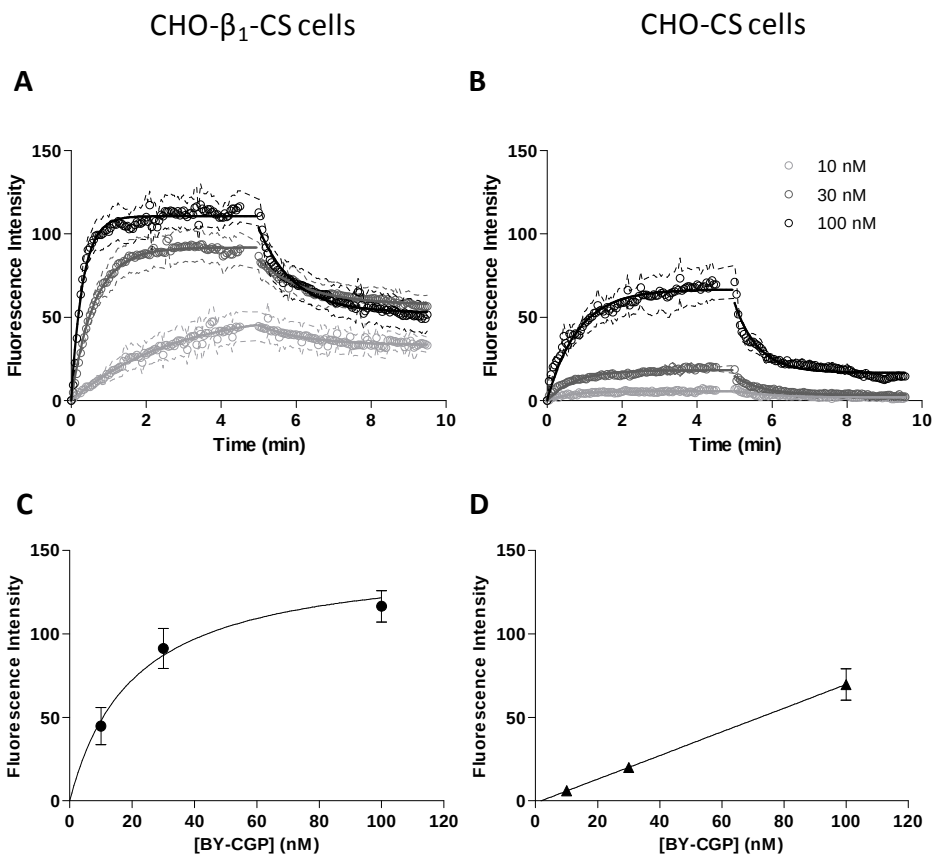

Figure 6.5 Association and dissociation of 10, 30 and 100 nM BY-CGP at CHO-β_1-CS and CHO-CS cells. Confocal images shown in Figure 6.4 were analysed by drawing regions of interests (ROIs) around the membrane of 10 cells per field of view, and the measured fluorescence intensity was then plotted against time for **A**, CHO-β_1-CS and **B**, CHO-CS cells. The fluorescence intensity values measured in **C**, CHO-β_1-CS and **D**, CHO-CS cells following 5 min association of 10, 30 and 100 nM BY-CGP were plotted against the corresponding BY-CGP concentration, and highlight the saturable binding of BY-CGP to CHO-β_1-CS, but not CHO-CS cells at the concentrations used. The quantitative data show the mean of grouped data ± s.e.m. of 3-6 separate confocal perfusion slides obtained on three separate experimental days.

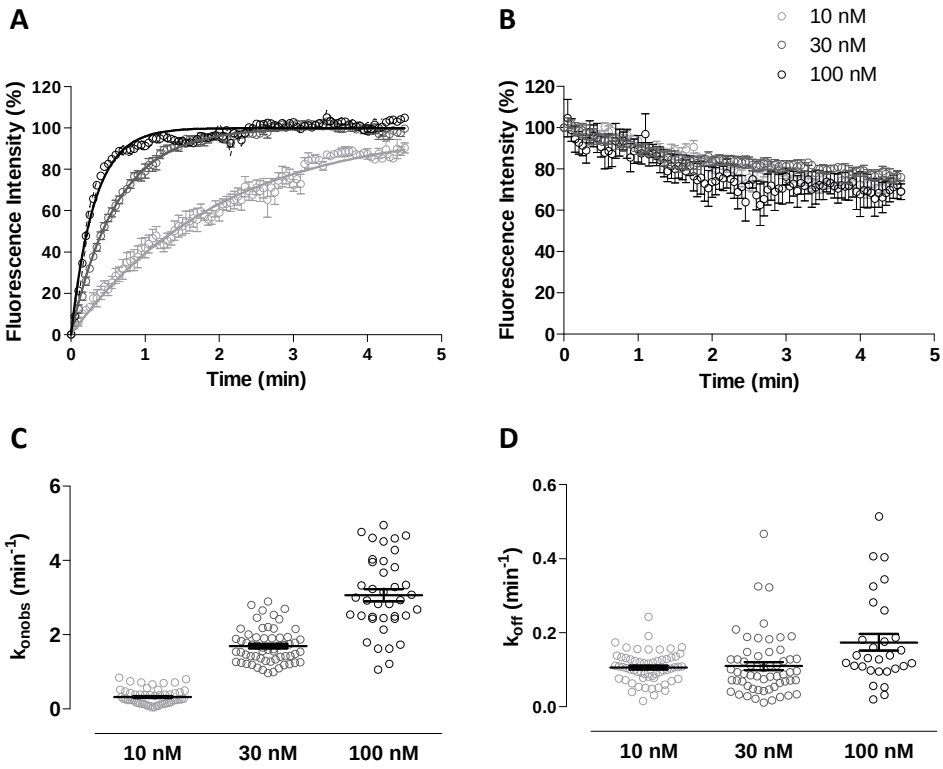

Figure 6.6 Association and dissociation kinetics of 10, 30 and 100 nM BY-CGP at CHO-β_1-CS cells. Normalised **A**, association and **B**, dissociation data of BY-CGP. Data shown are mean ± s.e.m of at least three separate experiments. **C**, observed association rate and **D**, dissociation rate constant for 10, 30 and 100 nM BY-CGP with each replicate representing the kinetic parameter of one single cell. The data shown are mean ± s.e.m of 30-60 replicates obtained from 3-6 confocal perfusion slides on three separate experimental days.

Table 6.1 Kinetic parameters of 10, 30 and 100 nM BY-CGP at CHO-β_1-CS and CHO-CS cells. Data are mean ± s.e.m with *n* representing the number of separate experiments carried out. In each experiment, regions of interest were drawn around the membrane of 10 cells. *denotes statistically significant difference ($P < 0.05$) from the value determined for [a]10 nM and [b]30 nM BY-CGP within the same cell line, and † denotes statistically significant difference ($P < 0.05$) from the value determined for the same concentration in a different cell line (two-way ANOVA followed by Bonferroni's multiple comparison test)

BODIPY-TMR-CGP	k_{onobs}	$k_{off(fast)}$	$k_{off(slow)}$	k_{on}	pK_D	n
	min^{-1}	min^{-1}	min^{-1}	$x\ 10^6\ M^{-1}\ min^{-1}$		
CHO-CS						
10 nM	N/A	N/A				6
30 nM	1.40 ± 0.26	2.46 ± 0.48				6
100 nM	1.56 ± 0.11	2.46 ± 0.09				4
CHO-β_1-CS						
10 nM	0.59 ± 0.08	N/A	0.08 ± 0.01†	4.81 ± 0.82	8.64 ± 0.11	6
30 nM	1.64 ± 0.08*[a]	2.46	0.09 ± 0.01†	5.17 ± 0.28	8.77 ± 0.08	6
100 nM	3.07 ± 0.15*[a,b] †	2.46	0.14 ± 0.02*[a] †	2.93 ± 0.17	8.33 ± 0.09*[b]	3

Characterising the kinetic parameters of BY-PROP at the human β_1-adrenoceptor

Confocal and phase images were taken every 3 seconds on the Zeiss LSM510 confocal microscope using the same settings for all BY-PROP concentrations on both CHO-β_1-CS and CHO-CS cells to allow the direct comparison of fluorescence intensities between total (CHO-β_1-CS cells) and non-specific (CHO-CS cells) binding of the three BY-PROP concentrations used. Clear membrane labelling of 10, 30 and 100 nM BY-PROP could be seen following 1.5 minutes association of BY-PROP in CHO-β_1-CS (Figure 6.7) and CHO-CS (Figure 6.8) cells. As expected, the fluorescence intensity increased with increasing BY-PROP concentrations. However, the non-specific intracellular fluorescence also increased with increasing BY-PROP concentrations and prolonged BY-PROP association in both cell lines and made it difficult to clearly define the plasma membrane of cells. Even the perfusion of buffer for 10 minutes did not appear to cause the dissociation of BY-PROP in CHO-β_1-CS cells. In CHO-CS cells, the dissociation of BY-PROP was also difficult to visualise which was mainly due to the very high levels of intracellular fluorescence intensity. Thus, the very early time points were used to draw the regions of interests in both cell lines. The association and dissociation traces obtained from these ROIs revealed that the actual (raw) fluorescence intensities measured in CHO-β_1-CS and CHO-CS cells were very similar for each BY-PROP concentration used (Figure 6.9 and 6.10). The observed association rates (k_{onobs}) obtained in CHO-CS cells significantly increased with increasing BY-PROP concentrations (Table 6.2). The dissociation rates of 10,

30 and 100 nM BY-PROP in CHO-CS cells were determined using monophasic exponential curve fits, and were expectedly similar for all three BY-PROP concentrations tested (Table 6.2), but were substantially slower than those determined for BY-CGP in CHO-CS cells ($P < 0.05$, two-way ANOVA followed by Bonferroni's multiple comparison test). This suggests that the BY-PROP non-specific binding is of a different nature, where the much slower dissociation rates may, for example, be due to increased association of BY-PROP with the cell membrane. The non-specific component of BY-PROP binding does not follow a linear regression (Figure 6.10D), but fits to a saturation hyperbola for the concentrations tested, as does the total binding component of BY-PROP binding determined at CHO-β_1-CS cells (Figure 6.10C). The saturability of BY-PROP binding to both CHO-β_1-CS and CHO-CS cells at the concentrations used suggests similar affinities of BY-PROP to non-specific and receptor specific binding sites.

The observed association rates in CHO-β_1-CS cells were enhanced with increasing BY-PROP concentrations (0.14 ± 0.02 min^{-1}, n=6, 0.17 ± 0.01 min^{-1}, n=7 and 0.26 ± 0.04 min^{-1}, n=6 for 10, 30 and 100 nM BY-PROP, respectively; Figure 6.11; Table 6.2). Interestingly, only for 100 nM BY-PROP was the observed association rate significantly different from the observed association rate obtained in CHO-CS cells ($P < 0.05$, two-way ANOVA followed by Bonferroni's multiple comparison test; Table 6.2). The dissociation traces obtained in CHO-β_1-CS cells were best fitted using a monophasic exponential decay curve fit as the non-specific component defined in CHO-CS cells could

not be detected, even though the non-specific (CHO-CS cells) dissociation rates were significantly faster than those derived in CHO-β_1-CS cells ($P < 0.05$, two-way ANOVA followed by Bonferroni's multiple comparison test). This suggests that the binding of BY-PROP to the β_1-adrenoceptor affects the non-specific off rate ($k_{off(fast)}$). The dissociation rates of 100 nM BY-PROP in CHO-β_1-CS cells was significantly faster than those obtained for 10 and 30 nM BY-PROP, which may be due to an increased inclusion of 'false positives', i.e. cells that were analysed by drawing membrane ROIs as they showed clear membrane labelling following BY-PROP association, but did not express the β_1-adrenoceptor, thus resulting in increased non-specific off rates. This can be seen in Figure 6.11D where dissociation rates of individual analysed cells are shown and the dotted line highlights the mean dissociation rate (0.27 min^{-1}) of BY-PROP in CHO-CS cells (i.e. non-specific dissociation). The observed association rate and dissociation rate determined for each BY-PROP concentration was used to determine the association rate (k_{on}) and the equilibrium dissociation constant (K_D) and are summarised in Table 6.2.

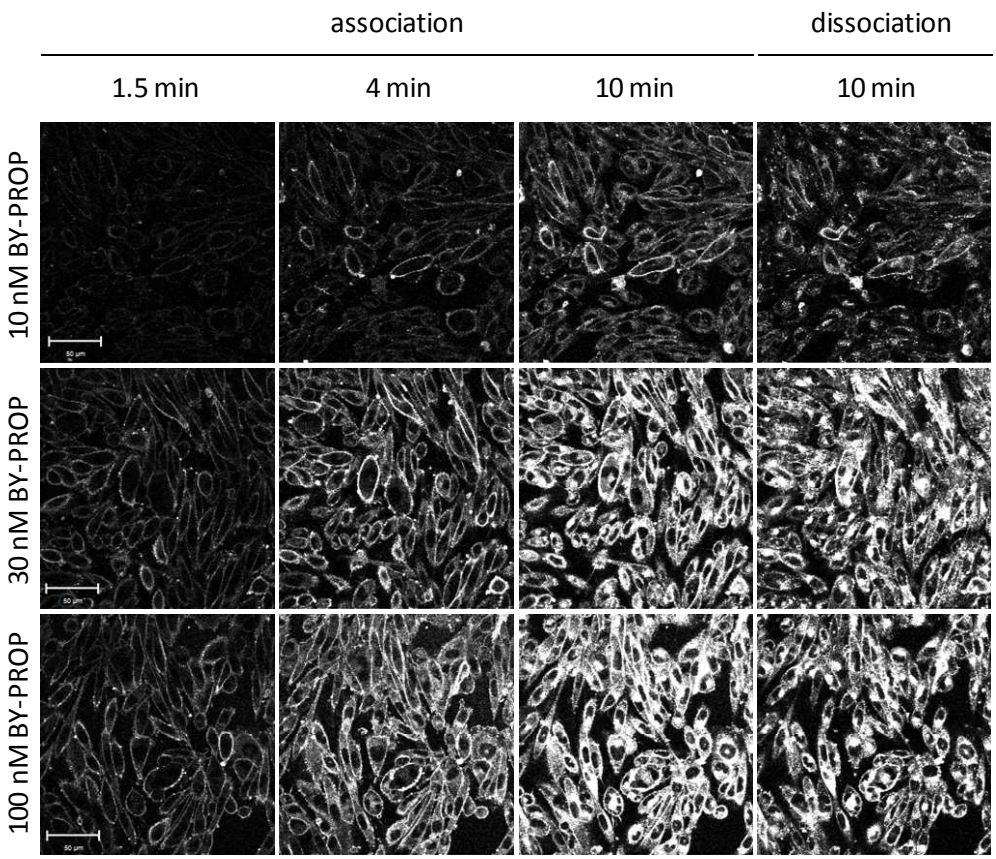

Figure 6.7 Confocal images of 10, 30 and 100 nM BY-PROP binding to CHO-β_1-CS cells after 1.5, 4 and 10 minutes association and 10 minutes dissociation under infinite dilution conditions. The microscope settings were kept constant for the recordings of fluorescence intensities of all three BY-PROP concentrations used to allow for direct comparison of the level of BY-PROP binding. Images are representatives of a total of 6-7 confocal perfusion slides per BY-CGP concentration, obtained on four separate experimental days. Scale bars = 50 µm.

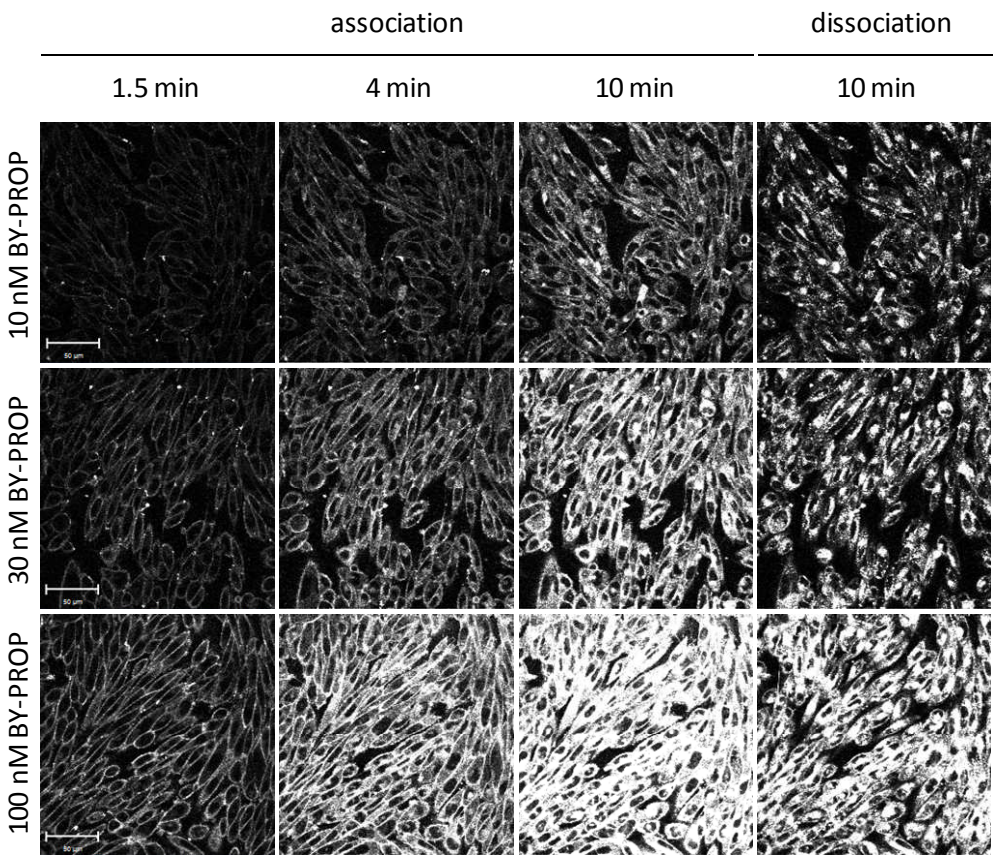

Figure 6.8 Confocal images of 10, 30 and 100 nM BY-PROP binding to CHO-CS cells after 1.5, 4 and 10 minutes association and 10 minutes dissociation under infinite dilution conditions. The microscope settings were kept constant for the recordings of fluorescence intensities of all three BY-PROP concentrations and are also the same settings that were used to image BY-PROP binding to CHO-β_1-CS cells (Figure 6.6) used to allow for direct comparison of the level of BY-PROP binding. Images are representatives of a total of 3-5 confocal perfusion slides per BY-CGP concentration, obtained on three separate experimental days. Scale bars = 50 µm.

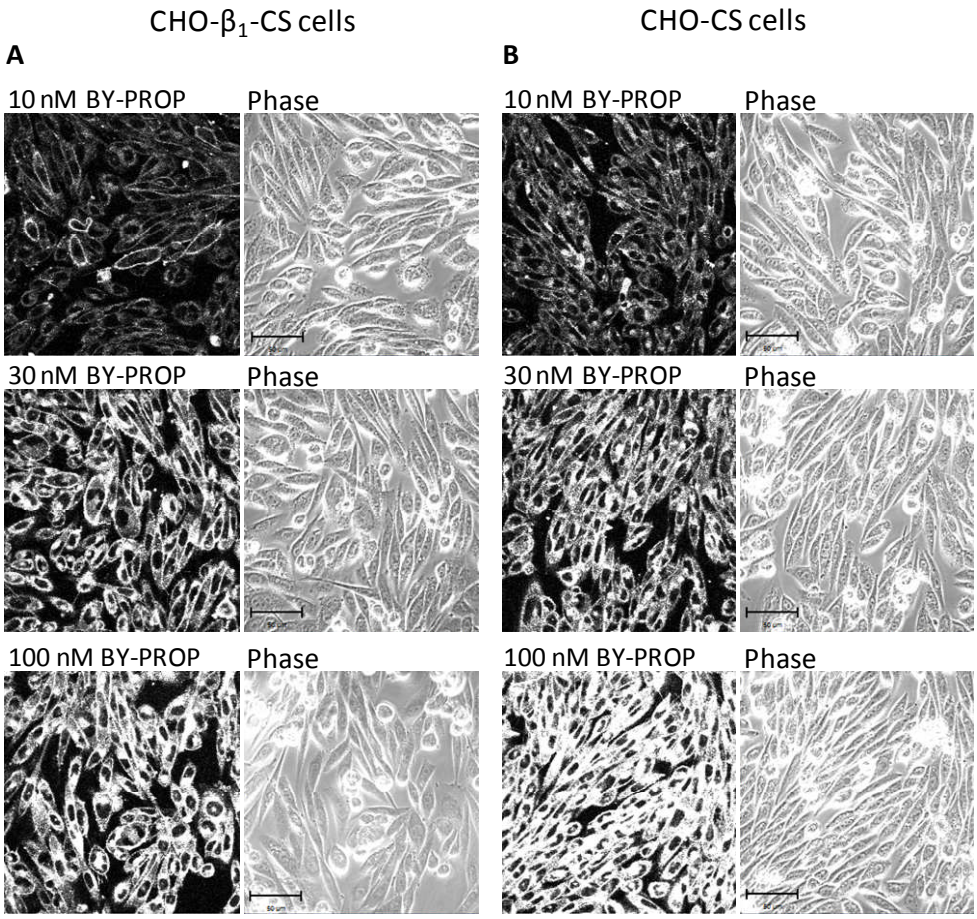

Figure 6.9 Confocal images of 10, 30 and 100 nM BY-PROP binding to **A**, CHO-β_1-CS and **B**, CHO-CS cells following 10 minutes association and 10 minutes dissociation under infinite dilution conditions. The microscope settings were kept constant for the recordings of fluorescence intensities of all three BY-PROP concentrations in both CHO-β_1-CS and CHO-CS cells to allow for direct comparison of the level of BY-PROP binding. Images are representatives of a total of 3-7 confocal perfusion slides per BY-PROP concentration, obtained on 3-4 separate experimental days. Scale bars = 50 µm.

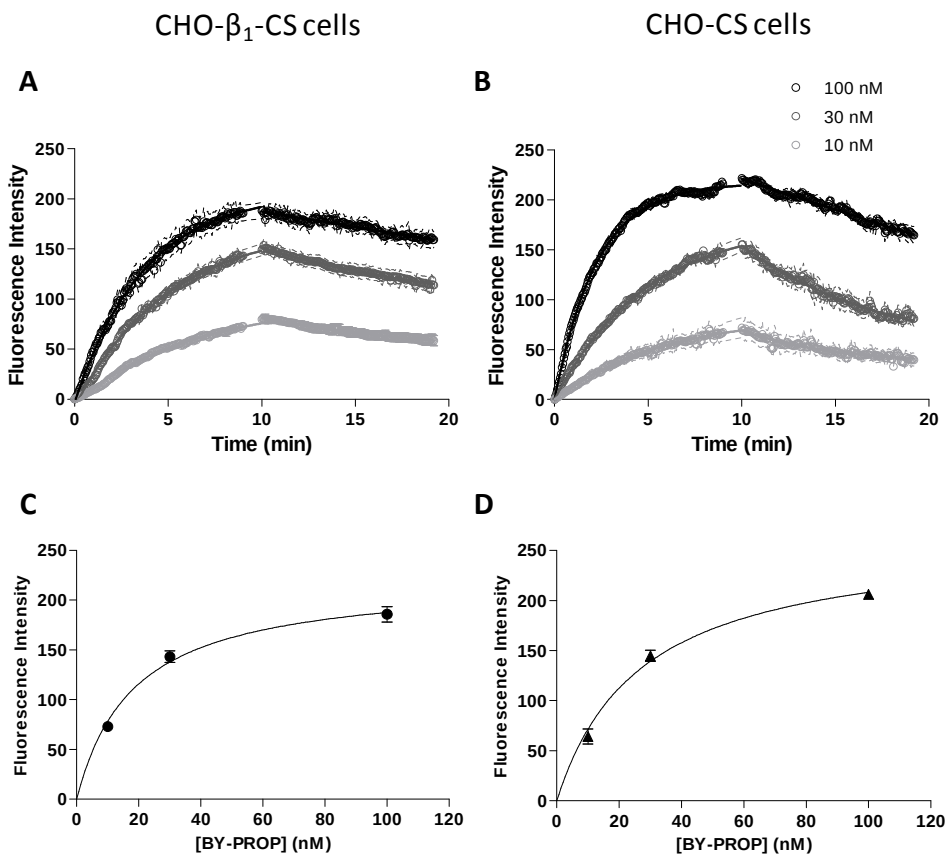

Figure 6.10 Association and dissociation of 10, 30 and 100 nM BY-PROP at CHO-β_1-CS and CHO-CS cells. Confocal images shown in Figure 6.9 were analysed by drawing regions of interests (ROIs) around the membrane of 10 cells per field of view, and the measured fluorescence intensity was then plotted against time for **A**, CHO-β_1-CS and **B**, CHO-CS cells. The fluorescence intensity values measured in **C**, CHO-β_1-CS and **D**, CHO-CS cells following 5 min association of 10, 30 and 100 nM BY-PROP were plotted against the corresponding BY-PROP concentration, and highlight that the binding of BY-PROP to both CHO-β_1-CS and CHO-CS cells is saturable at the concentrations used. The quantitative data show the mean of grouped data ± s.e.m. of 3-7 separate confocal perfusion slides obtained on 3-4 separate experimental days.

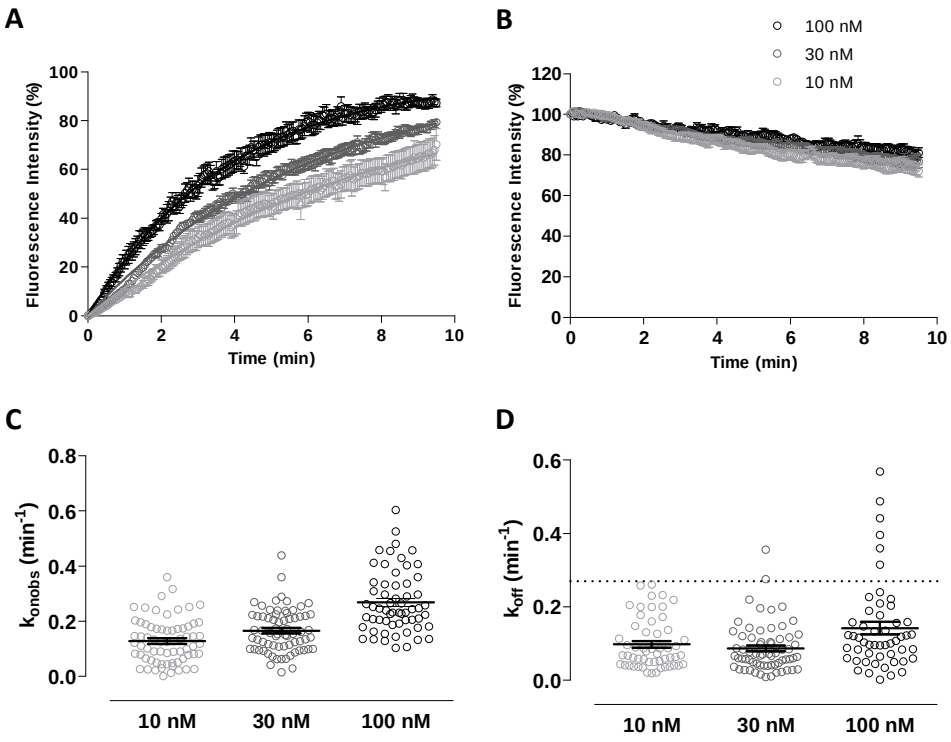

Figure 6.11 Association and dissociation kinetics of 10, 30 and 100 nM BY-PROP at CHO-β_1-CS cells. Normalised **A**, association and **B**, dissociation data of BY-PROP. Data shown is mean ± s.e.m of at least six separate experiments. **C**, observed association rate and **D**, dissociation rate constant for 10, 30 and 100 nM BY-CGP with each replicate representing the kinetic parameter of one single cell. The mean ± s.e.m of at least sixty replicates is shown. The dotted line represents the mean dissociation rate of BY-PROP determined in CHO-CS cells.

Table 6.2 Kinetic parameters of 10, 30 and 100 nM BY-PROP binding to CHO-β_1-CS and CHO-CS cells. Data are mean ± s.e.m with n representing the number of separate perfusion preparations used. *denotes statistically significant difference ($P < 0.05$) from the value determined for [a]10 nM and [b]30 nM BY-PROP within the same cell line, and † denotes statistically significant difference ($P < 0.05$) from the value determined for the same concentration in a different cell line (two-way ANOVA followed by Bonferroni's multiple comparison test)

BY-PROP	k_{onobs}	$k_{off(fast)}$	$k_{off(slow)}$	k_{on}	pK_D	n
	min^{-1}	*min^{-1}*	*min^{-1}*	*x 10^6 M^{-1} min^{-1}*		
CHO-CS						
10 nM	0.14 ± 0.02	0.28 ± 0.07				3
30 nM	0.21 ± 0.02*[a]	0.26 ± 0.03				6
100 nM	0.45 ± 0.04*[a,b]	0.26 ± 0.08				4
CHO-β_1-CS						
10 nM	0.14 ± 0.02	n.d.	0.07 ± 0.01[†]	6.20 ± 1.86	7.72 ± 0.32	6
30 nM	0.17 ± 0.01	n.d.	0.07 ± 0.01[†]	3.21 ± 0.47	7.67 ± 0.13	7
100 nM	0.26 ± 0.04*[a,b †]	n.d.	0.12 ± 0.01*[a,b †]	1.41 ± 0.46*[a]	6.95 ± 0.17	6

The high intensity levels of non-specific binding fluorescence and the slow dissociation of BY-PROP observed in CHO-CS cells may be due to the lipophilicity of BY-PROP. Previous binding experiments using BY-PROP (Chapter 4) were performed at 21 °C, whereas perfusion experiments were carried out at 37 °C. Increased temperature has been associated with increased membrane fluidity (Vigh *et al.*, 2007), which may increase the inclusion of lipophilic ligands such as BY-PROP in the cell membrane. To test that hypothesis the binding of BY-PROP and BY-CGP in the absence (total binding) and presence (non-specific binding) of 1 µM CGP 20712A in CHO-β_1-CS and CHO-CS cells in 8-well plates under static (no perfusion) conditions was tested. The assay window of BY-PROP binding at 21 °C was small but clearly defined, in line with previous BY-PROP data obtained in experiments carried out at 21 °C (Chapter 4). However, this assay window was lost at 37 °C due to increased non-specific intracellular fluorescence intensities (Figure 6.12). In contrast, the assay window of BY-CGP was not compromised at higher temperatures (Figure 6.13). As a result, we used BY-CGP in subsequent kinetic experiments on the confocal perfusion system.

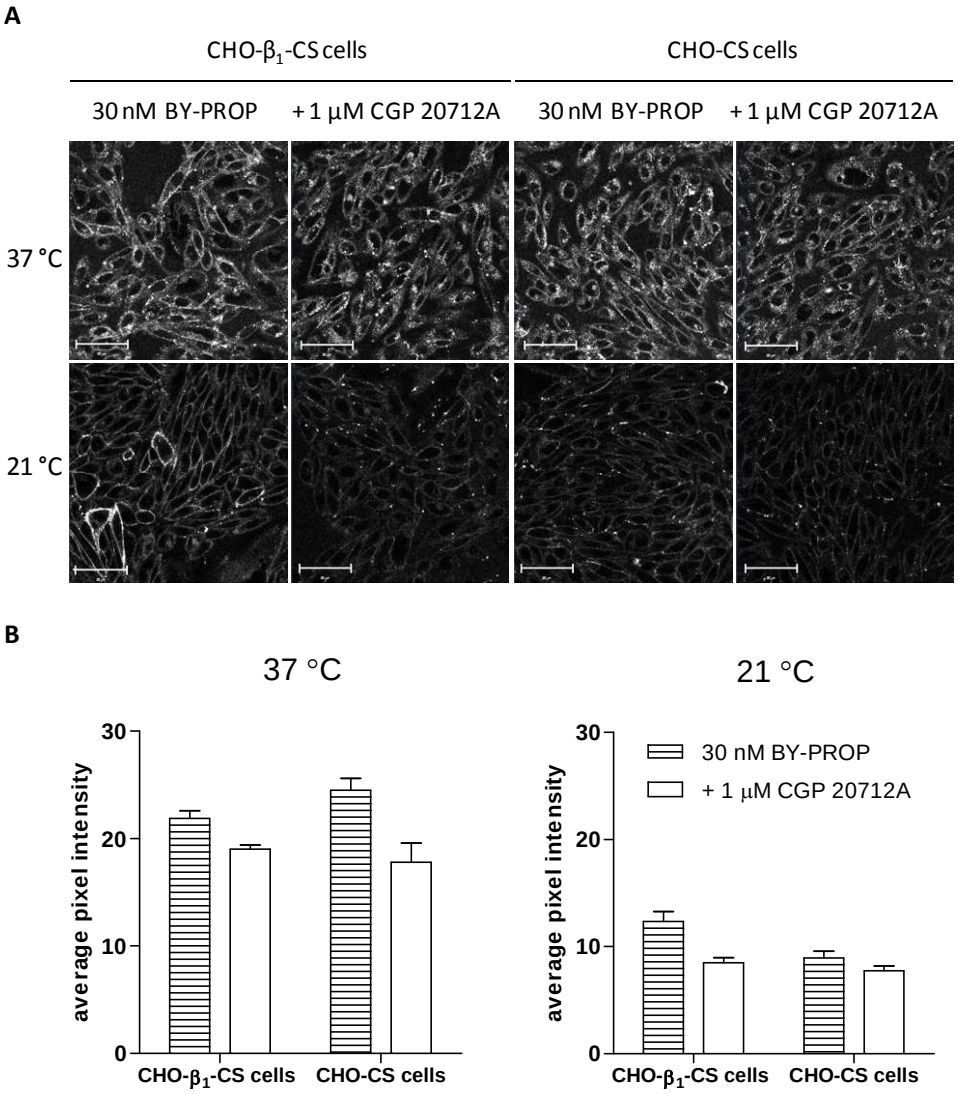

Figure 6.12 A, confocal images of 30 nM BY-PROP binding to CHO-β_1-CS and CHO-CS cells after 10 minutes exposure to BY-PROP at 37 °C (top panel) and 21 °C (bottom panel) in the absence and presence of 1 μM CGP 20712A (30 min pre-incubation with antagonist at 37 °C). **B**, the confocal images shown in A were analysed using total image intensity analysis and the data shown is representative of three separate experiments. Scale bars = 50 μm.

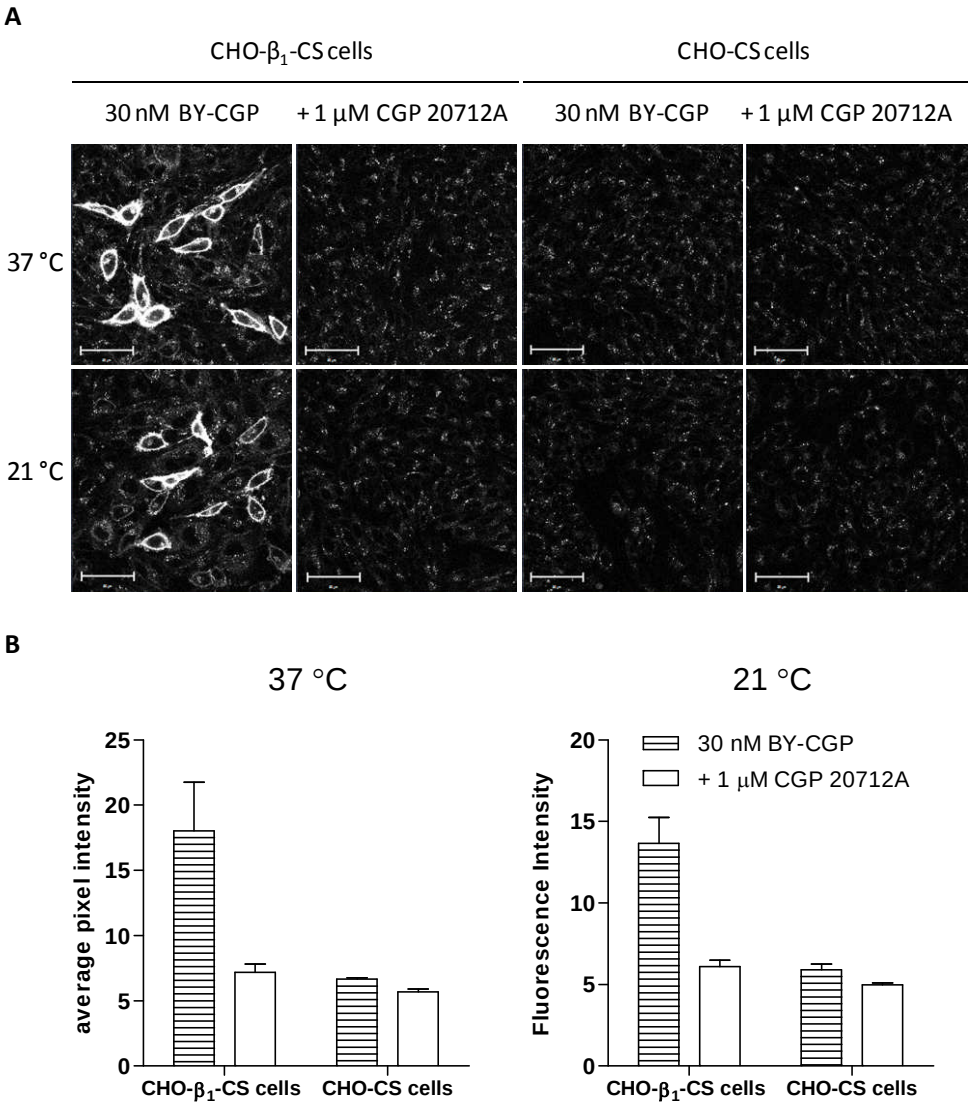

Figure 6.13 A, confocal images of 30 nM BY-CGP binding to CHO-β_1-CS and CHO-CS cells after 10 minutes exposure to BY-CGP at 37 °C (top panel) and 21 °C (bottom panel) in the absence and presence of 1 μM CGP 20712A. **B**, the confocal images shown in A were analysed using total image intensity analysis and the data shown is representative of three separate experiments. Scale bars = 50 μm.

Effects of unlabelled ligands on the dissociation of 30 nM BY-CGP at the human β_1-adrenoceptor

The dissociation rate of a ligand should not be altered in the presence of a second ligand if it competes for the same binding site. However, if the second ligand binds to a second binding site, resulting conformational changes could lead to co-operative (allosteric) effects, i.e. the dissociation rate of the first ligand (usually the labelled ligand) may be decreased or enhanced (Christopoulos *et al.*, 2002; May *et al.*, 2007). Using the perfusion system, the infinite dilution prevents the re-association of dissociated ligand (May *et al.*, 2010a; May *et al.*, 2010b). This allows dissociation rates of the labelled ligand to be determined in the absence of unlabelled competitor ligands and can then be compared to the dissociation rate of the labelled ligand in the presence of unlabelled competitor ligands. This is a very powerful tool in the detection of potential allosteric interactions between two ligands binding to a receptor (Christopoulos *et al.*, 2002).

Here, we examined the effect of increasing CGP 12177 and propranolol concentrations on the dissociation of 30 nM BY-CGP. Both the Zeiss LSM510 and LSM710 microscopes were used for these studies. The microscope settings used were optimised at the start of each experiment and then kept constant within each experiment. The data was normalised and fitted using a two-phase decay equation constraining the fast dissociation component to the non-specific binding dissociation rate determined in CHO-CS cells above. The slow component of the dissociation rate of 30 nM determined using the

Zeiss LSM510 microscope was 0.14 ± 0.02 min^{-1} (n=7) and compared well to the dissociation rate determined using the Zeiss LSM710 microscope (0.12 ± 0.02 min^{-1}, n=7; unpaired t-test) in the absence of unlabelled ligand. The dissociation rate of BY-CGP was significantly enhanced in the presence of 10 µM CGP 12177 (0.26 ± 0.01 min^{-1}, n=5), but not in the presence of 1 µM CGP 12177 (0.18 ± 0.01 min^{-1}, n=5 and 0.19 ± 0.02 min^{-1}, n=3 using the LSM510 and LSM710 microscope, respectively; Figure 6.14; Table 6.3; $P < 0.05$, one-way ANOVA followed by Dunnett's post hoc test). The dissociation rate of 30 nM BY-CGP was also significantly enhanced in the presence of 10 µM propranolol (0.33 ± 0.04 min^{-1}, n=5; Figure 6.15), but not in the presence of 1 µM propranolol (0.18 ± 0.04 min^{-1}, n=5, LSM510; 0.20 ± 0.03 min^{-1}, n=3, LSM710; $P < 0.05$, one-way ANOVA followed by Dunnett's post hoc test). Concentrations lower than 1 µM CGP 12177 and propranolol also did not significantly affect the dissociation of 30 nM BY-CGP, whereas concentrations higher than 10 µM did (Table 6.3). The effects of 1 and 10 µM CGP 12177 and propranolol on the dissociation rate of 30 nM BY-CGP at the single cell level can be seen in Figure 6.14 and 6.15.

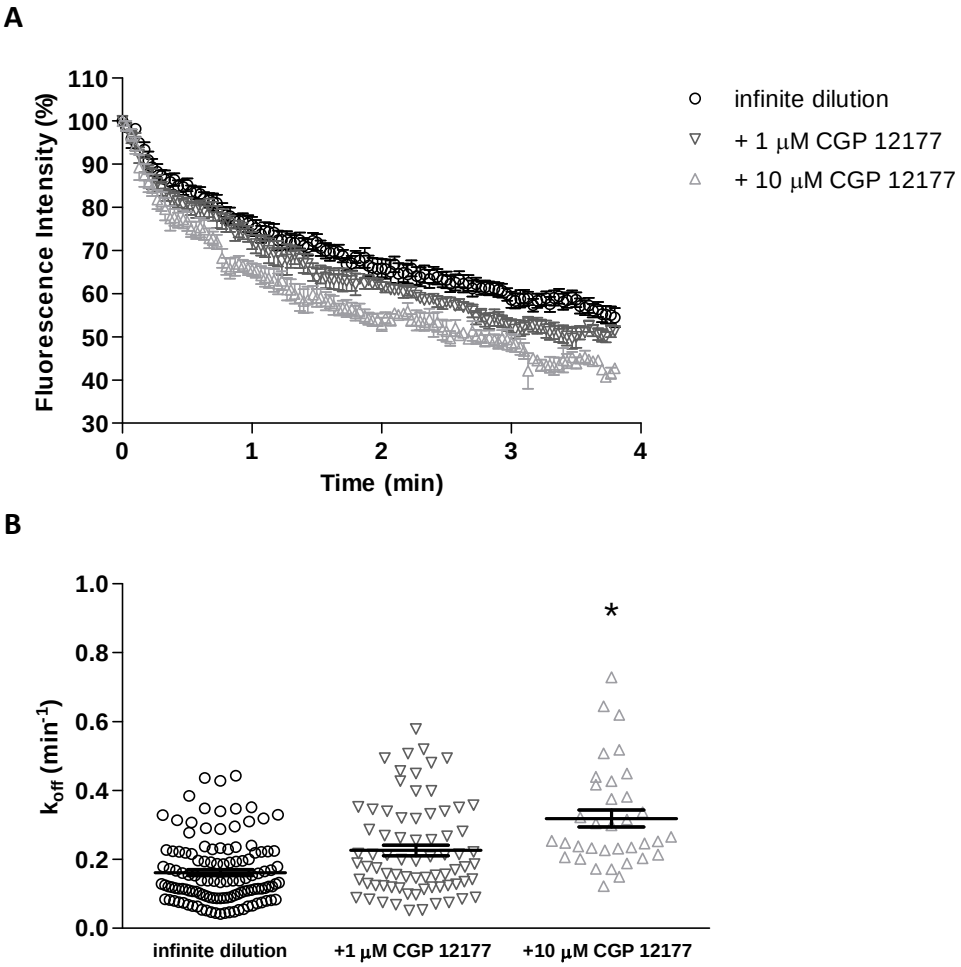

Figure 6.14 A, grouped data showing the dissociation of 30 nM BY-CGP under infinite dilution conditions in the absence and presence of 1 and 10 μM CGP 12177. Data are mean ± s.e.m of 3-7 separate experiments in each of which ROIs were drawn around membranes of ten cells. **B**, dissociation rate constants of 30 nM BY-CGP in the absence and presence of 1 and 10 μM CGP 12177 with each replicate representing one single cell. The mean ± s.e.m shown is of 30-70 replicates. *denotes statistical significance (P < 0.05) as determined by one-way ANOVA analysis followed by Dunnett's multiple comparison test.

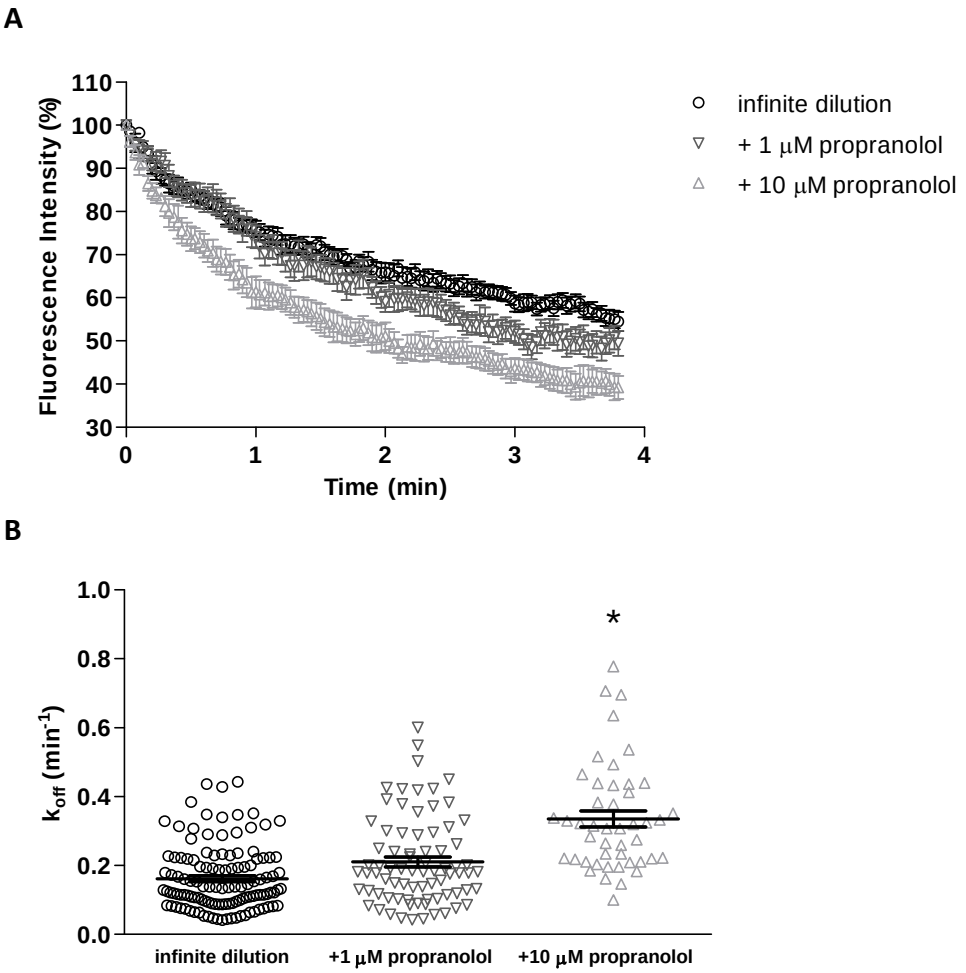

Figure 6.15 A, grouped data showing the dissociation of 30 nM BY-CGP under infinite dilution conditions in the absence and presence of 1 and 10 μM propranolol. Data are mean ± s.e.m of 3-7 separate experiments in each of which ROIs were drawn around membranes of ten cells. **B**, dissociation rate constants of 30 nM BY-CGP in the absence and presence of 1 and 10 μM propranolol with each replicate representing one single cell. The mean ± s.e.m shown is of 30-70 replicates. * denotes statistical significance ($P < 0.05$) as determined by one-way ANOVA analysis followed by Dunnett's multiple comparison test.

Table 6.3 Dissociation rate constants of 30 nM BY-CGP in the absence and presence of CGP 12177 and propranolol. Data was collected using either the LSM510 or LSM710 confocal perfusion system. Data are mean ± s.e.m and n represents the number of separate perfusion preparations used. * statistically significant ($p < 0.05$) to control conditions (infinite dilution) as determined by one-way ANOVA analysis followed by Dunnett's post hoc test

	CGP 12177				propranolol			
	LSM510		LSM710		LSM510		LSM710	
30 nM BY-CGP	k_{off} (min^{-1})	*n*	k_{off} (min^{-1})	*n*	k_{off} (min^{-1})	*n*	k_{off} (min^{-1})	*n*
infinite dilution	0.14 ± 0.02	7	0.12 ± 0.02	7	0.14 ± 0.02	7	0.12 ± 0.02	7
+ 0.1 nM	0.18 ± 0.04	5			0.14 ± 0.02	4		
+ 1 nM	0.15 ± 0.01	4			0.13 ± 0.02	5		
+ 10 nM	0.17 ± 0.01	5			0.18 ± 0.04	5		
+ 100 nM	0.20 ± 0.01	3			0.19 ± 0.02	5		
+ 1 µM	0.18 ± 0.01	5	0.19 ± 0.02	3	0.18 ± 0.04	5	0.20 ± 0.03	3
+ 10 µM			0.26 ± 0.01*	5			0.33 ± 0.04*	5
+ 100 µM			0.32; 0.21*	2			0.34 ± 0.06*	4

Effects of unlabelled ligands on the dissociation of 3 nM BY-CGP at the human β_1-adrenoceptor

From the BY-CGP affinities for the first and second site of the β_1-adrenoceptor and the occupancy curves (Chapter 4) we know that the occupancy of 30 nM BY-CGP at site 1 and site 2 is 98 and 23 %, respectively. In contrast, 3 nM BY-CGP labels 86 and 3 % of the β_1-adrenoceptor site 1 and site 2, respectively. Using a BY-CGP concentration as low as 3 nM, limits the competition of labelled and unlabelled ligand at the second β_1-adrenoceptor site (Figure 6.16), which may result in increased effects of unlabelled ligands on the dissociation rate of BY-CGP at the high affinity catecholamine site. However, imaging of lower concentrations of fluorescent ligands on the confocal microscope was difficult due to a reduced signal:noise ratio. In order to detect the binding of 3 nM BY-CGP to CHO-β_1-CS cells, the laser power and gain had to be increased. This is why this BY-CGP concentration was not included with the above data (10-100 nM BY-CGP data), as 3 nM BY-CGP binding was not detectable with the settings that were used to measure 10-100 nM BY-CGP binding kinetics.

First, we assessed the association and dissociation kinetics of 3 nM BY-CGP at CHO-β_1-CS and CHO-CS cells (Figure 6.17). The fluorescence intensities measured in CHO-CS cells were too low to accurately determine observed association and dissociation rates. However, the non-specific binding component was too low to be detected in the 3 nM BY-CGP dissociation trace obtained in CHO-β_1-CS cells, and therefore was analysed using a one-phase

dissociation equation. This gave a dissociation rate of 0.09 ± 0.01 min^{-1} (n=9) in the absence of unlabelled ligands, which was similar to the dissociation rate obtained for 10, 30 and 100 nM BY-CGP above (P > 0.05, one-way ANOVA followed by Tukey's post hoc test). Following a four minute exposure to 3 nM BY-CGP, the association trace did not reach a plateau and the association rate could not be accurately determined from this trace. However, when analysed in combination with the dissociation trace an association rate of 5.27 ± 0.53 x 10^7 M^{-1} min^{-1} (n=9), a dissociation rate of 0.08 ± 0.01 min^{-1} (n=9) and a pK_D of 8.83 ± 0.06 (n=9) was determined (Figure 6.17).

The dissociation rate of 3 nM BY-CGP was significantly enhanced in the presence of 100 nM (0.21 ± 0.02 min^{-1},n=5), 1 µM (0.20 ± 0.02 min^{-1}, n=7) and 10 µM (0.22 ± 0.03 min^{-1}, n=5) CGP 12177 (P < 0.05, one-way ANOVA followed by Dunnett's post hoc test; Figure 6.18; Table 6.4). The effect of the enhanced dissociation rate appeared to saturate, which is characteristic of allosteric interactions (Christopoulos *et al.*, 2002). The dissociation rate was enhanced to a similar extent in the presence of 1 µM (0.19 ± 0.01 min^{-1}, n=6) and 10 µM (0.22 ± 0.03 min^{-1}, n=5) propranolol (Figure 6.19; Table 6.4). The midpoint of the concentration-response curve fitted through dissociation rates plotted against concentrations of unlabelled ligand revealed the affinity of the unlabelled ligand to the allosteric (secondary β_1-adrenoceptor) site with a ligand bound to the orthosteric (catecholamine β_1-adrenoceptor) site (K_B upon α, with α being the co-operativity factor describing the co-operative interaction between two binding sites). The pK_B/α determined for CGP 12177

and propranolol against 3 nM BY-CGP were 7.79 ± 0.34 (n=5) and 6.65 ± 0.33 (n=3), respectively.

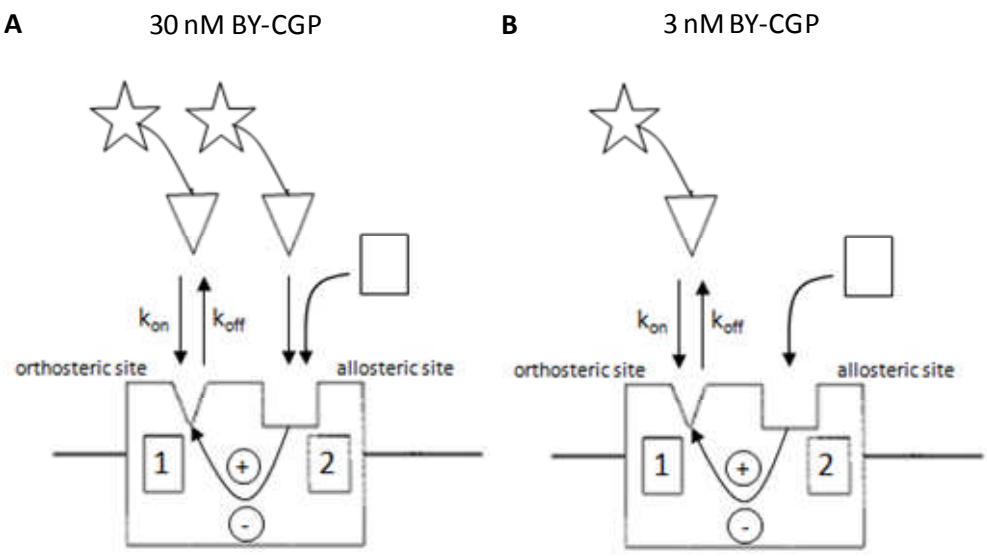

Figure 6.16 Schematic representation of **A**, 30 nM and **B**, 3 nM BY-CGP binding to the high (site 1) and low (site 2) affinity site of the β_1-adrenoceptor in the presence of an unlabelled ligand. 30 nM BY-CGP is 0.3 x K_D concentration at the secondary β_1-adrenoceptor site. Labelling of site 2 by 30 nM BY-CGP prevents the binding of unlabelled ligands to the same site and thus prevents the detection of potential positive or negative allosteric effects caused by the binding of unlabelled ligands on the ligand binding kinetics of the labelled ligand binding to the orthosteric site 1.

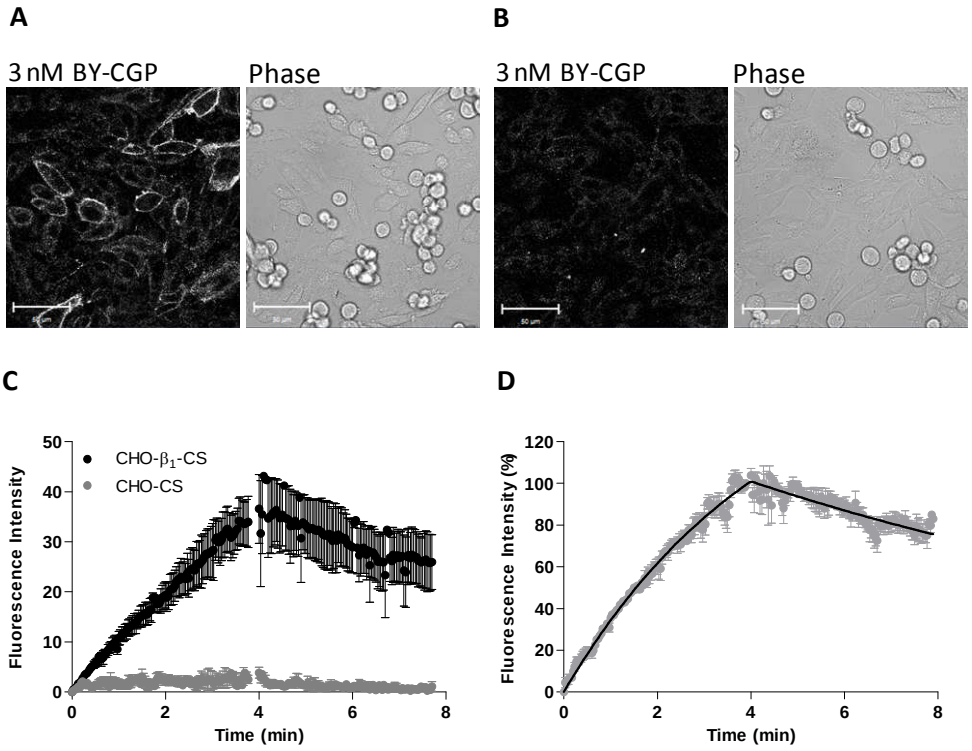

Figure 6.17 Association and dissociation of 3 nM BY-CGP measured in CHO-β_1-CS and CHO-CS cells. Confocal images show BY-CGP binding to **A**, CHO-β_1-CS and **B**, CHO-CS cells after 4 minutes BY-CGP association. Scale bar = 50 µm. **C**, The data was analysed by drawing regions of interests (ROIs) around the membrane of 10 cells per field of view and the measured fluorescence intensity was then plotted against time for CHO-β_1-CS and CHO-CS cells. The confocal images are representative of images taken during at least three separate experiments. **D**, Normalised data showing the mean of grouped data ± s.e.m. of nine separate experiments.

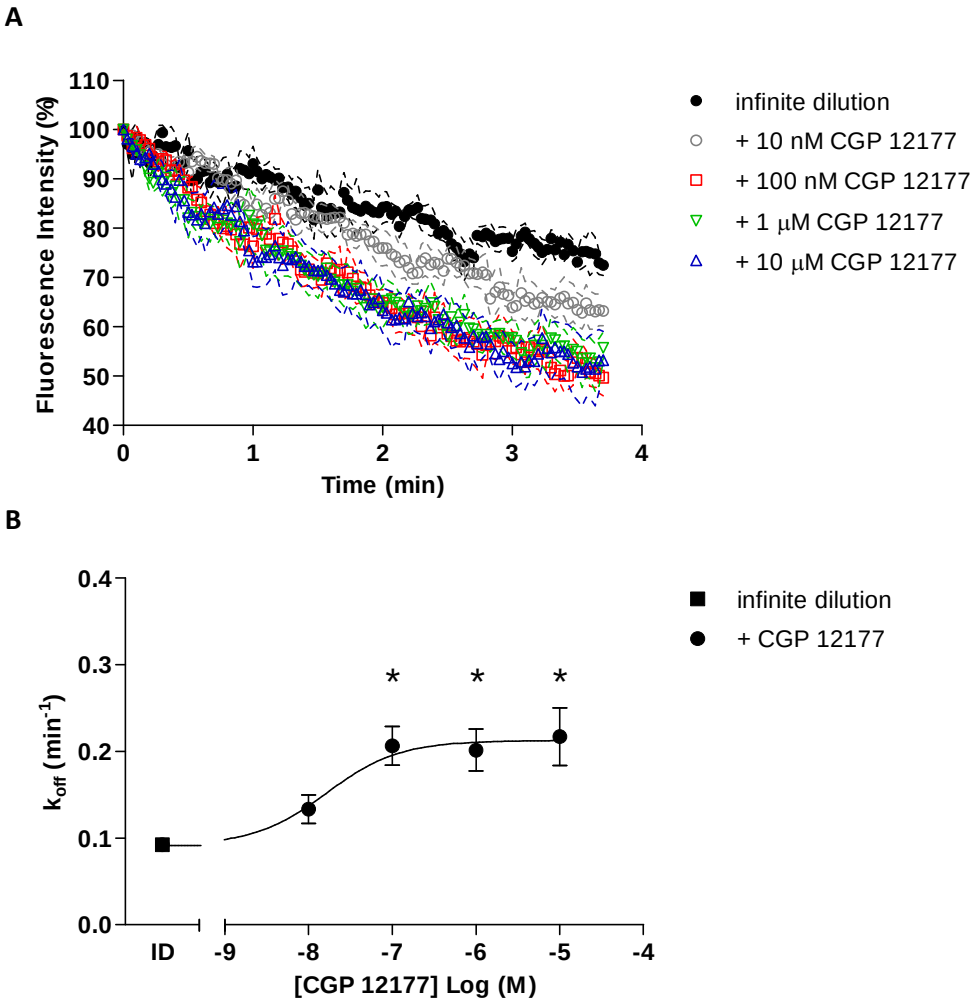

Figure 6.18 A, grouped data showing the dissociation of 3 nM BY-CGP under infinite dilution conditions in the absence and presence of 10 nM, 100 nM, 1 μM and 10 μM CGP 12177. Data are mean ± s.e.m of at least five separate experiments. **B**, dissociation rate constants of 3 nM BY-CGP in the absence and presence of increasing CGP 12177 concentrations. Data are mean ± s.e.m of at least five separate experiments. *denotes statistical significance ($P < 0.05$) as determined by one-way ANOVA analysis followed by Dunnett's multiple comparison test.

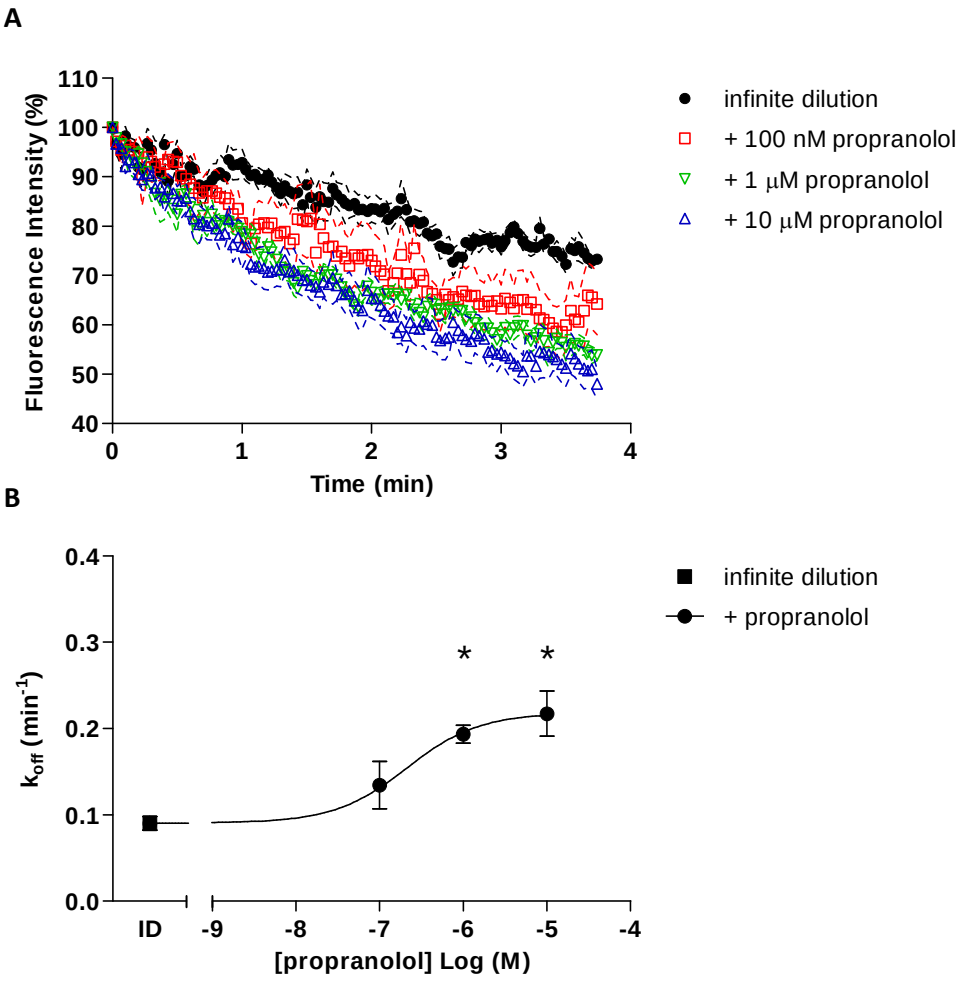

Figure 6.19 A, grouped data showing the dissociation of 3 nM BY-CGP under infinite dilution conditions in the absence and presence of 100 nM, 1 μM and 10 μM propranolol. Data are mean ± s.e.m of at least four separate experiments. **B**, dissociation rate constants of 3 nM BY-CGP in the absence and presence of increasing CGP 12177 concentrations. Data are mean ± s.e.m of at least four separate experiments. *denotes statistical significance ($P < 0.05$) as determined by one-way ANOVA analysis followed by Dunnett's multiple comparison test.

Table 6.4 Dissociation rate constants of 3nM BY-CGP in the absence and presence of CGP 12177 and propranolol. Data are mean ± s.e.m of (n) separate slide preparations. n.d. not determined; * statistically significant ($P < 0.05$) from control conditions (infinite dilution) as determined by one-way ANOVA analysis followed by Dunnett's post hoc test

	CGP 12177		propranolol	
3 nM BY-CGP	$k_{off}(min^{-1})$	*n*	$k_{off}(min^{-1})$	*n*
infinite dilution	0.09 ± 0.01	9	0.09 ± 0.01	9
+ 10 nM	0.13 ± 0.02	6	n.d.	
+ 100 nM	0.21 ± 0.02*	5	0.13 ± 0.03	3
+ 1 µM	0.20 ± 0.02*	7	0.19 ± 0.01*	6
+ 10 µM	0.22 ± 0.03*	5	0.22 ± 0.03*	5

6.4 Discussion

Here we examined the kinetic properties of BODIPY-TMR-CGP and BODIPY630/650-S-PEG8-propranolol in single living cells to establish whether co-operative interactions between the two proposed β_1-adrenoceptor binding sites play a role in the receptor-ligand interactions at the human β_1-adrenoceptor.

The difference of the BY-CGP dissociation rates in the absence and the presence of unlabelled ligands revealed co-operativity between the two proposed high and low affinity β_1-adrenoceptor sites. Using a closed perfusion system under constant controlled pressure allows a constant flow rate of labelled ligand from one reservoir followed by a sharp concentration gradient upon switching to the buffer reservoir that facilitates the removal of the labelled ligand and thus, the measurement of its dissociation (May *et al.*, 2010a). The determination of kinetic parameters under infinite dilution conditions is the main advantage over radioligand dissociation experiments that use unlabelled competitor ligands to prevent the re-association of the radioligand (Christopoulos *et al.*, 1997; May *et al.*, 2010a). It is widely appreciated that the presence of unlabelled ligands can profoundly affect the dissociation rate of a labelled ligand due to allosteric effects which may be caused through a second binding site (Gao *et al.*, 2001; Lazareno *et al.*, 2000; Lazareno *et al.*, 2002) or dimerisation (Christopoulos *et al.*, 2002; May *et al.*, 2011; Smith *et al.*, 2010). In addition, there is a growing appreciation that intracellular signalling proteins can also cause allosteric effects and generate

distinct subsets of receptor conformations that ultimately display unique receptor-ligand interactions resulting in, for example, ligand bias (Goupil *et al.*, 2010; Kenakin *et al.*, 2010; Luttrell *et al.*, 2011). To fully appreciate the complexity of receptor-ligand interactions it is vital to maintain the correct membrane and cellular environment at physiological conditions, creating a need for non-invasive pharmacological techniques. The perfusion system used in this chapter allows the visualisation of dynamic receptor-ligand interactions in real time in single cells using non-invasive fluorescent ligands and as such provides the opportunity to study the pharmacology of ligands on endogenous receptors in primary cells.

First, we examined the kinetic parameters of the fluorescent analogue of CGP 12177 (BODIPY-TMR-CGP; BY-CGP) binding to the human β_1-adrenoceptor and showed that the specific binding of BY-CGP to the β_1-adrenoceptor was well defined, with greater levels of BY-CGP binding observed in CHO-β_1-CS than in CHO-CS cells. In CHO-CS cells, the dissociation traces did not come down to the same level of fluorescence intensity as was measured at the start of each experiment. This was most likely due to the ROIs that were drawn around cell membranes that also included a small proportion of cytoplasm. Thus, residual intracellular fluorescence that does not dissociate, forms the plateau of dissociation traces in CHO-CS cells. In CHO-β_1-CS cells, the observed association rates were dependent on the BY-CGP concentrations used, whereas the dissociation rates were independent for 10 and 30 nM BY-CGP. A five minute perfusion of buffer was not enough to see complete dissociation

of BY-CGP. The β_1-adrenoceptor-specific dissociation component was monophasic unlike the two components detected in the dissociation of [^{3}H]-CGP 12177 (Joseph *et al.*, 2004). The BY-CGP dissociation rates determined here are likely that of the catecholamine site as, for example, the dissociation rates of 30 nM and 3 nM BY-CGP were not significantly different (compared data obtained on the Zeiss LSM710 microscope; unpaired t-test) and we know that 3 nM BY-CGP predominantly binds to the high affinity site 1 of the β_1-adrenoceptor. This is not altogether unsurprising considering that BY-CGP has a circa 150-fold higher affinity for the catecholamine site 1 than the secondary site 2 of the β_1-adrenoceptor. In addition, this data would also be consistent with a faster dissociation of BY-CGP off the secondary site compared to the catecholamine site, as a faster dissociation of a smaller proportion of BY-CGP off site 2 would be masked by the slower dissociation of a larger proportion of BY-CGP off site 1, at least at the BY-CGP concentrations used here. Much higher BY-CGP concentrations would have to be tested, possibly also at longer dissociation reads than five minutes, to examine this further. However, using very high BY-CGP concentrations is costly. Interestingly, the K_D derived from the kinetic parameters obtained for 3 nM BY-CGP (circa 2.6 nM) compares well to the affinity value of BY-CGP determined in functional studies (0.6 nM, Chapter 4) for the high affinity site of the β_1-adrenoceptor.

Next, we aimed to investigate potential allosteric effects between the two proposed β_1-adrenoceptor binding sites by monitoring the dissociation rate of

30 nM BY-CGP in the absence and presence of increasing concentrations of unlabelled ligands under infinite dilution conditions. The dissociation rate of 30 nM BY-CGP was enhanced only in the presence of very high concentrations of CGP 12177 and propranolol (10 and 100 μM). Both ligands have much higher affinity (at least 100-fold) for site 1 than site 2, but at the concentrations used will bind to both sites. The dissociation rate of a labelled ligand is not altered in the presence of a competitive ligand, as such any change in the dissociation rate will have been caused by the unlabelled ligand binding to a secondary site. However, we know from previous studies that 30 nM BY-CGP also binds to the secondary β_1-adrenoceptor site (Chapter 4). This poses two potential problems; firstly, it causes competition of the unlabelled ligand with BY-CGP at the second site and therefore reduces any potential allosteric effects that may be caused by the binding of the unlabelled ligands to this site and may explain why the dissociation rate of 30 nM BY-CGP was only enhanced in the presence of very high concentrations of CGP 12177 and propranolol. Secondly, BY-CGP binding to the secondary site may itself allosterically affect its own dissociation rate off site 1. However, considering that for CGP 12177 a concentration greater than its K_{Dsite2} was needed to see any effects on the dissociation rate, it is unlikely that a 0.3 x K_{Dsite2} concentration of BY-CGP caused a significant effect. Furthermore, the dissociation rate observed for 30 nM BY-CGP was similar to that for 3 nM BY-CGP (which predominantly binds to site 1), suggesting that no significant allosteric interactions were detectable for 30 nM. In contrast, the dissociation rate of 100 nM BY-CGP was enhanced compared to the dissociation rate

determined for 10 nM BY-CGP under infinite dilution condition. Considering the effect of unlabelled CGP 12177, it is likely that the fluorescent CGP 12177 analogue can also elicit allosteric interactions between the two β_1-adrenoceptor binding sites at higher concentrations.

To avoid these complications, we used 3 nM BY-CGP to investigate the effects of unlabelled ligands on the dissociation rate of BY-CGP. Using a lower BY-CGP concentration, the BY-CGP dissociation rate was enhanced by 100 nM CGP 12177 and propranolol (and concentrations above). The effects must occur through the secondary site as we know 3 nM predominantly binds site 1. This clearly demonstrates that two separate β_1-adrenoceptor binding sites can be occupied at the same time and the binding of a ligand to a secondary β_1-adrenoceptor site affects the ligand binding properties at the catecholamine site of the β_1-adrenoceptor. Furthermore, the affinities of CGP 12177 and propranolol determined from plotting the dissociation rates against the concentrations of unlabelled ligands (K_B/α circa 16 and 224 nM, respectively) compared well to the affinity values of CGP 12177 and propranolol for the secondary β_1-adrenoceptor site in functional studies (circa 19 and 912 nM, respectively; $P < 0.05$, unpaired t-test for each ligand comparing affinity values obtained in two different assays). This was expected as both reflect the affinity of the ligand to the secondary site with site 1 being ligand-bound. Thus, the site 2 affinity values determined in this thesis are products of the affinity of the ligands to the secondary site of a free receptor (i.e. no ligand bound to site 1) and the co-operativity factor α. However, all ligands used in

this thesis have a much higher affinity for site 1 than site 2, making it impossible to determine affinity values to site 2 without a ligand being bound to site 1 and therefore to establish a co-operativity factor describing the allosteric interaction between the two binding sites. However, the co-operativity between two sites is reciprocal (May *et al.*, 2011), thus the examination of the dissociation rates of the fluorescent propranolol derivative BODIPY630/650-S-PEG8-propranolol (BY-PROP) in the absence and presence of unlabelled CGP 12177 in the same assay format would be expected to confirm the findings obtained using BY-CGP and unlabelled propranolol.

When examining the association and dissociation kinetics of BY-PROP in CHO-β_1-CS (total binding) and CHO-CS (non-specific binding) cells, the non-specific fluorescence intensity levels of BY-PROP binding were as high as the total fluorescence intensity BY-PROP binding levels, suggesting no specific binding of BY-PROP to CHO-β_1-CS cells. Furthermore, the observed association rates for 10 and 30 BY-PROP concentrations were similar in CHO-CS cells and in CHO-β_1-CS cells. Only for 100 nM BY-PROP, a significant difference in the observed association rates in the two cell lines was determined, to suggest specific binding of BY-PROP to the receptor. From previous chapters in this thesis (Chapter 4), however, we know that BY-PROP does bind to the β_1-adrenoceptor expressed in CHO-CS cells at the concentrations used here. Indeed, close inspection of the BY-PROP dissociation rates derived from CHO-β_1-CS and CHO-CS cells also suggests specific BY-PROP binding to the β_1-adrenoceptor. The non-specific binding component could not be detected in

the dissociation rates determined in CHO-β_1-CS cells like we could for BY-CGP. This suggests that the presence of the β_1-adrenocepor in CHO-β_1-CS cells affected the dissociation of the non-specific binding component. This could potentially be explained by a mechanism in which BY-PROP association with the membrane in both CHO-CS and CHO-β_1-CS cells is faster than its association to the receptor alone, which results in the slow association to the receptor being masked by the faster association to the membrane environment. From a 'membrane sink', BY-PROP may then diffuse to the receptor, where once it is bound to the receptor its dissociation is significantly slowed (Figure 4.20), which strongly suggests that BY-PROP binds to the β_1-adrenoceptor in CHO-β_1-CS cells. It also indicates that the fluorescent ligand does not dissociate off the receptor back into the membrane environment, which is described as the mechanism of action for long-acting β_2-adrenoceptor agonists formoterol and salmeterol (Green *et al.*, 1996; Vauquelin *et al.*, 2009; Waldeck, 1996). If this was the case, the dissociation rate of BY-PROP off the β_1-adrenoceptor would be expected to be masked by the dissociation off the membrane and be similar to the dissociation rate seen in CHO-CS cells (as is the case for the association of BY-PROP).

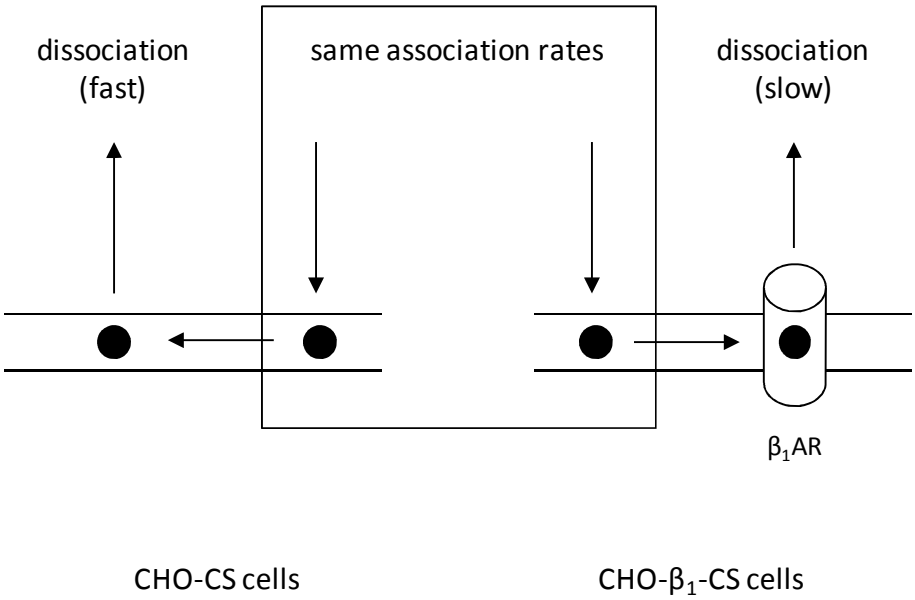

Figure 4.20 Schematic representation describing a potential mechanism of BY-PROP binding to CHO-CS cells and CHO-β_1-CS cells. BY-PROP association rates determined in CHO-CS and CHO-β_1-CS cells were similar, whilst BY-PROP dissociation was markedly slower in CHO-β_1-CS cells compared to CHO-CS cells. Thus, the first step of BY-PROP association with the β_1-adrenoceptor may be the association to the membrane, which is described by the same association rates in cells expressing the receptor and cells not expressing the receptor. This is followed by lateral membrane diffusion of BY-PROP to the receptor. Once BY-PROP is bound to the β_1-adrenoceptor, its dissociation is slowed. The markedly slower dissociation rate therefore reveals the specific interaction of BY-PROP with the β_1-adrenoceptor.

Even though the fluorescent derivative of propranolol is a lipophilic ligand, thus favouring the membrane environment and leading to membrane-associated non-specific binding levels, the non-specific binding levels of BY-PROP observed in previous imaging studies on the confocal microscope were not as high as seen here. One of the main differences of previous confocal studies and the perfusion experiments is the constant perfusion of buffer and ligand over the living cells at a rate of ≥ 12 complete fluid exchanges per minute (i.e. 5 mL/min) within the perfusion chamber (May *et al.*, 2010a). Under these conditions cells may experience fluid shear stress which has been reported to increase membrane fluidity (Haidekker *et al.*, 2000) and as such the uptake of a lipophilic ligand may also be increased. This did not appear to be an issue for BY-CGP. Another main difference was the temperature which was kept constant at 37 °C in all perfusion experiments to ensure optimal physiological conditions for the live cells used in the experiment. Even under static (no perfusion) conditions, the non-specific levels of BY-PROP binding at 37 °C (compared to 21 °C) were too high to clearly define a specific binding assay window. Increasing temperatures are also associated with increased fluidity of plasma membranes and, in the case of lipophilic ligand, higher non-specific binding levels. Thirdly, some of the high intracellular fluorescence intensity of BY-PROP will also have been measured in the region of interests (ROIs) drawn around the cell membranes and since the intracellular fluorescence cannot be “dissociated” or washed away it may make the BY-PROP dissociation seem slower than it actually is, especially in the CHO-CS cells which displayed very high levels of intracellular fluorescence intensity.

Nevertheless, the K_D derived from the association and dissociation rates for 10 and 30 nM BY-PROP (19 and 21 nM, respectively) compared very well to the affinity value determined at site 1 for BY-PROP in functional studies (28 nM; Chapter 4). Although not statistically significantly different, the kinetically derived affinity value for 100 nM BY-PROP was circa 5-fold lower (112 nM), which may be due to the unexpectedly faster dissociation rate of 100 nM BY-PROP. The faster dissociation rates of BY-PROP observed in CHO-CS cells could not be included in the analysis of the dissociation rate of BY-PROP measured in CHO-β_1-CS cells possibly because they were too similar to be accurately separated apart in the curve fit. Thus, the enhanced dissociation rate of 100 nM seen in CHO-β_1-CS cells may be an artefact of increased non-specific binding at 100 nM BY-PROP. In addition, it is noteworthy that even after 10 minutes association of 10 and 30 nM BY-PROP to the β_1-adrenoceptor expressed in CHO-CS cells a plateau could not be reached. The dissociation rates of 10, 30 and 100 nM BY-PROP were also very slow. Thus, it was difficult to accurately determine observed association and dissociation rates which are reflected in the affinity values calculated for each BY-PROP concentration. Unfortunately, it was beyond the scope of this thesis to test and characterise additional novel fluorescent propranolol ligands to potentially identify a ligand that displayed lower non-specific binding levels and faster association and dissociation rates, thus making it more suitable to kinetic binding experiments using the confocal perfusion system.

The data shown here points to the presence of two separate, topographically distinct binding sites which now poses the question as to what and where that binding site is. Using a mutagenesis approach, Baker *et al.* (2008) mutated eight amino acids of the human β_1-adrencoeptor and determined the binding and functional properties of β-adrenoceptor ligands at each receptor mutation. Interestingly, this study concluded that the two binding sites must be overlapping as residues that affected site 1 also affected site 2 (Baker *et al.*, 2008). An alternative explanation may be that the second β_1-adrenoceptor is in fact a second orthosteric catecholamine site that is provided by a second β_1-adrenoceptor in a homodimer formation which now represents an allosteric site to which β-adrenoceptor ligands have lower affinity.

6.5 Conclusion

The kinetic parameters of BODIPY-TMR-CGP (a CGP 12177 analogue) were successfully determined, and the kinetically derived K_D could be compared to the affinity value of BY-CGP for the high affinity catecholamine site of the β-adrenoceptor determined in previous functional studies (Chapter 4). The dissociation rates were independent of BODIPY-TMR-CGP concentrations used and revealed only one specific dissociation rate component, which was that of the primary high affinity catecholamine site. 3 nM BY-CGP was used to predominantly label the high affinity catecholamine site, and the dissociation rate of 3 nM BODIPY-TMR-CGP was enhanced in the presence of unlabelled CGP 12177 and propranolol demonstrating co-operative interactions between two distinct β_1-adrenoceptor binding sites. We could not investigate the reciprocal nature of the observed allosteric effect, as the fluorescent derivative of propranolol, BODIPY630/650-S-PEG8-propranolol, proved too lipophilic to detect well defined specific binding to the β_1-adrenoceptor in the confocal perfusion system at the concentrations used. However, affinity values derived from the change in BY-CGP dissociation rates with increasing CGP 12177 and propranolol concentrations compared well to those from previous functional studies (Chapter 4), which further supports an allosteric mode of action of CGP 12177 at the β_1-adrenoceptor.

Chapter 7

Investigating a role of dimerisation in co-operative interactions and functional responses of human β_1-adrenoceptors

7.1 Introduction

The examination of the dissociation rate of 3 nM BY-CGP in the absence and presence of unlabelled β-adrenoceptor ligands CGP 12177 and propranolol revealed negative co-operativity between the two proposed β_1-adrenoceptor binding sites (Chapter 6). An allosteric binding site is described to be topographically distinct from the orthosteric site, which could describe a second binding site within a monomeric receptor, but could also describe a second binding site provided by a second receptor in a homodimer formation (May *et al.*, 2011). A mutagenesis study carried out by Baker *et al.* (2008) concluded that the two proposed β_1-adrenoceptor binding sites must overlap. Here, we investigate whether the observed co-operative effects are mediated across a β_1AR homodimer interface and whether the secondary β_1-adrenoceptor site is a second β_1AR in a homodimer formation. A similar mode of action of co-operativity has recently been described for the A_3 adenosine receptor (May *et al.*, 2011). The formation of GPCR dimers can be detected using bimolecular fluorescence complementation (BiFC) where two non-fluorescent halves of a split fluorescence protein (FP) are fused to the C-terminus of the target GPCRs and reconstitute to a fully functional fluorescent protein upon receptor dimerisation (Rose *et al.*, 2010). The reconstitution of N- and C-terminal YFP fragments (YFP_N and YFP_C, respectively) to a full length YFP is an irreversible process, which results in receptors that have formed into dimers being trapped in that formation (Kerppola, 2008). Crucially, the YFP fragments fused to proteins of interest do not affect the efficiency of

dimerisation of the proteins under investigation as demonstrated by Hu *et al.* (2003a) for the heterodimerisation of the transcription factors Fos and Jun (Hu *et al.*, 2003a). Homodimerisation of the β_1AR has been reported to be transient (Calebiro *et al.*, 2013; Dorsch *et al.*, 2009). Thus, using BiFC, we aimed not only to detect but also to irreversibly lock transient β_1-adrenoceptors homodimers into stable homodimers, and to investigate the effect of trapping β_1AR homodimers on the dissociation rate of BODIPY-TMR-CGP. To further confirm the potential role of the secondary β_1-adrenoceptor site (i.e. one β_1-adrenoceptor protomer), we mutated the aspartic acid amino acid residue 138 of the β_1-adrenoceptor to alanine. This mutation has been shown to disrupt the binding of ligands to both the orthosteric (site 1) and allosteric site (site 2) of the β_1-adrenoceptor (Baker *et al.*, 2008) and we hypothesised that constrained β_1AR dimers containing a non-ligand binding protomer would reverse the effects on the BODIPY-TMR-CGP dissociation kinetics seen in constrained wild-type dimers and more closely match the pharmacology described in CHO-β_1-CS cells (Chapter 6). Finally, we also examined the functional response of CHO cells expressing β_1AR homodimers containing a wild-type or non-ligand binding second β_1AR protomer.

7.2 Methods

Molecular Biology

As described in *Methods: Molecular Biology*, the D138A (aspartic acid, GAC -> alanine, GCC) mutation was introduced into the β_1YFP_C construct, which was made in the Hill lab in 2007 and used as the DNA template in the mutagenesis reaction. The forward (5'-GGACCTCAGTGGCCGTGCTGTGCGT-3') and reverse (5'-ACGCACAGCACGGCCACTGAGGTCC–3') mutagenesis primers containing the desired point mutation were designed and used in the β_1AR mutagenesis reaction. The resultant $\beta_{1D138A}YFP_C$ and the original β_1YFP_C sequences were inserted into separate plasmid vector pcDNA3.1(+) containing the zeocin antibiotic resistance gene. The plasmid pcDNA3.1(+) vectors containing the neomycin antibiotic resistance and either the β_1YFP or the β_1YFP_N sequences were also made in the Hill lab in 2007 and used in studies presented in this chapter.

Cell culture

This was performed as described in *Methods: Cell culture*. CHO-K1 cells were used for stable and transient transfections. CHO-β_1-CS cells were used as a control where appropriate.

Transient transfections

Transient transfections were carried out as outline in *Methods: Generation of new cell lines*. The total amount of DNA used per well was 150 ng and 750 ng

in 8-well and 6-well plates, respectively. For transient transfections in T75 flasks, a total of 10 µg DNA was used. Cells were used for experimentation 48 hours following transfection.

Generation of stable cell lines

In this chapter, the clonal stable cell line CHO-β_1YFP_N was generated using 3 µg DNA to transfect CHO-K1 cells grown to 70 % confluence in a T25 flask. The transfection was performed as outlined in *Methods: Generation of new cell lines*, followed by selection of transfectants, dilution cloning and generation of a stable cell line. The initial selection of transfectants and the maintenance of the stable cell line were achieved through supplementation of the growth media with 100 µg/mL of geneticin (G418).

Subsequently CHO-β_1YFP_N cells were grown to 70 % confluence in a T25 flask and transfected with either 3 µg β_1YFP_C or $\beta_{1D138A}YFP_C$ DNA to generate stable mixed population CHO-β_1YFP_N-β_1YFP_C and CHO-β_1YFP_N-$\beta_{1D138A}YFP_C$ cell lines. Both cell lines were maintained using the growth media supplemented with 100 µg/mL geneticin and 50 µg/mL zeocin.

Confocal microscopy

This was performed as described in *Methods: Confocal microscopy* using 8-well borosilicate chambered-coverglass plates imaged on a Zeiss LSM710 laser scanning microscope with a 40x1.3NA oil immersion lens. YFP fluorescence was imaged using an argon laser and 488 nm excitation with emission

captured through a 505-634 nm filter and BODIPY-TMR-CGP fluorescence was imaged using a 561 nm DPSS laser with emission captured through a 565 nm long-pass filter (1024x1024 pixels, averaging at 4 frames). A pinhole diameter of 1 Airy unit was used. For bimolecular fluorescence complementation (BiFC) experiments, transiently transfected cells were incubated at 30 °C overnight (circa 16 hours) before imaging.

Confocal perfusion system

The perfusion system of the Zeiss LSM710 confocal microscope was used and experiments were carried out as described in *Methods: Confocal perfusion system*. Confocal and transmitted light images of live cells were taken every 2 seconds. BY-CGP fluorescence intensity was measured using a 561 nm excitation wavelength.

[^{3}H]cAMP accumulation assay

This was performed as described in *Methods: [^{3}H]cAMP accumulation assay*. The exact same experimental setup was used on cells stably and transiently expressing the desired β_1-adrenoceptor constructs.

7.3 Results

Detecting β_1-adrenoceptor homodimers using BiFC

In bimolecular fluorescence complementation (BiFC) approaches, two fragments of a fluorescent protein, which on their own are not fluorescent, come together when in close proximity to one another, to reconstitute the full length fluorescent protein which is fluorescent (Rose *et al.*, 2010). The N-terminal fragment (amino acids 1-155), the C-terminal fragment (amino acids 156-239) of the yellow fluorescent protein (YFP_N and YFP_C, respectively) and the full length YFP (amino acids 1-239) were each fused to the C-terminal end of the human β_1-adrenoceptor generating the β_1YFP_N and β_1YFP_C constructs (all constructs were made in the Hill lab in 2007; all constructs were sequenced before being used in this study and the DNA and protein sequence of each construct are listed in Appendix I S9-11).

First, we examined the fluorescence intensities of the individual β_1YFP (Figure 7.1), β_1YFP_N (Figure 7.2) and β_1YFP_C constructs (Figure 7.3) transiently transfected into CHO-K1 cells. The expression of the constructs was confirmed by measuring the binding of 20 nM BY-CGP to all transfected cells. Clear membrane labelling of all transfected cells was observed following 10 minute exposure to 20 nM BY-CGP, indicating good cell surface expression of all three constructs. Good YFP fluorescence could also be seen in membranes of cells transfected with β_1YFP, but not β_1YFP_N and β_1YFP_C. The β_1YFP_N and β_1YFP_C constructs were transiently co-transfected in CHO-K1 to investigate the

fluorescence of reconstituted YFP upon β_1-adrenoceptor homodimerisation (Figure 7.4). Clear membrane labelling of 20 nM BY-CGP demonstrated the cell surface expression of either β_1YFP_N or/and β_1YFP_C, whereas the YFP fluorescence indicated that β_1AR homodimerisation and reconstitution of the YFP had taken place. It is noteworthy that the fluorescence of the reconstituted YFP was dimmer than that of the full length YFP and a higher gain setting had to be used to detect it (1100 instead of 600). Using these higher gain settings on cells transfected with the YFP_N and YFP_C fragments only revealed higher background YFP fluorescence indicating the detected BiFC fluorescence was specific.

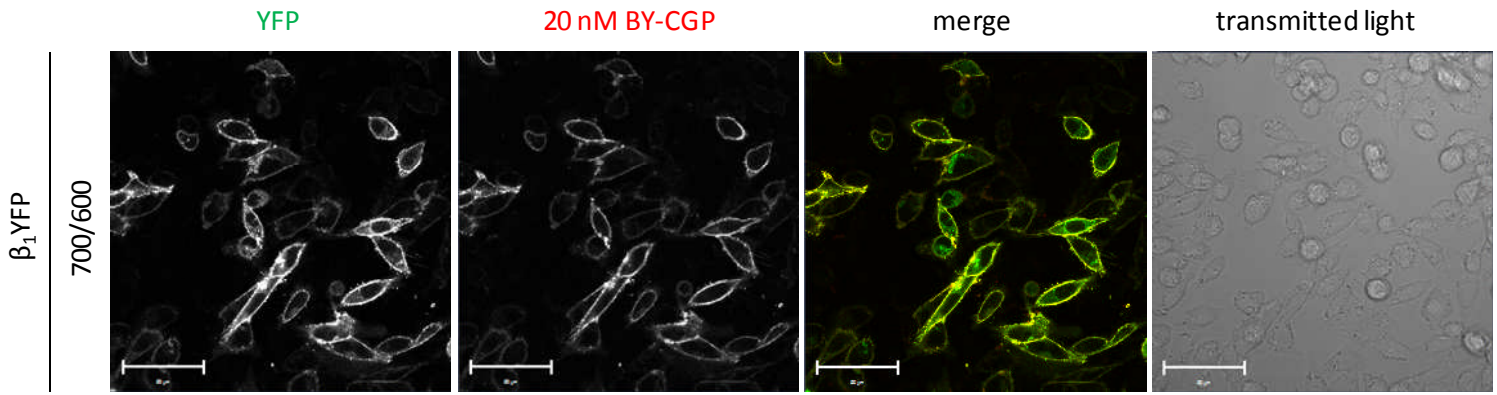

Figure 7.1 Confocal images of 20 nM BY-CGP binding to the YFP-tagged β_1-receptor construct transiently expressed in CHO-K1 cells. The fluorescence intensity of the full length YFP was measured in channel 488 using a gain setting of 700. The binding of 20 nM BY-CGP to the expressed YFP-tagged β_1-adrenoceptors was measured using the 543 channel (with a gain setting of 600). The merged images highlight co-localisation of cell surface YFP-tagged β_1-adrenoceptor (green) and BY-CGP binding (red) to these receptors in yellow pixels. The images are representative of two different fields of view imaged on one experimental day. Scale bar = 50 µm.

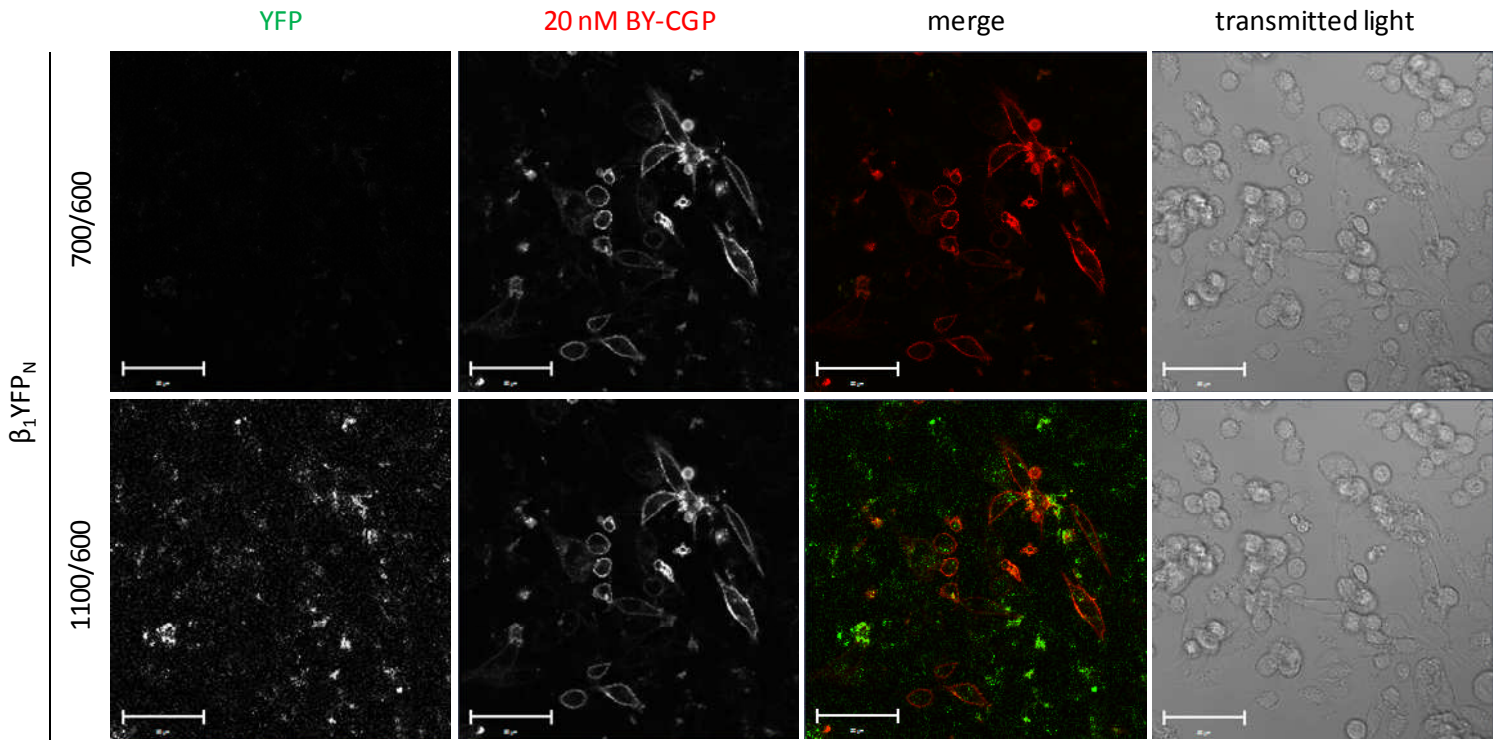

Figure 7.2 Confocal imaging of 20 nM BY-CGP binding to YFP_N-tagged β_1-receptor constructs transiently expressed in CHO-K1 cells. YFP fluorescence intensity was measured in channel 488 using two different gain settings: 700 and 1100. The binding of 20 nM BY-CGP to the expressed YFP_N-tagged β_1-adrenoceptors was measured using the 543 channel (gain setting 600 in all images). The merged images highlight co-localisation of cell surface YFP_N-tagged β_1-adrenoceptor (green) and BY-CGP binding (red) to these receptors in yellow pixels. The images are representative of two different fields of view imaged on one experimental day. Scale bar = 50 µm.

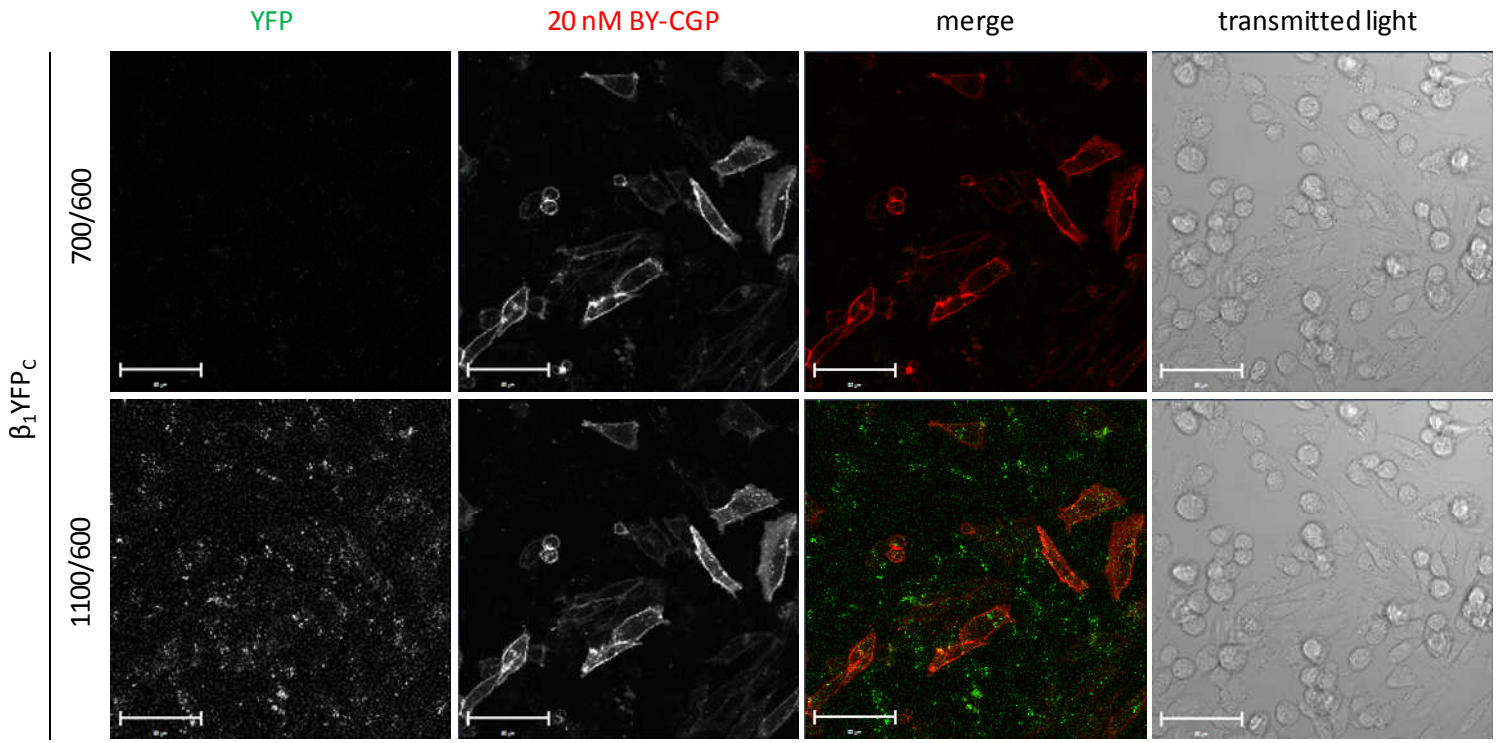

Figure 7.3 Confocal imaging of 20 nM BY-CGP binding to YFP_C-tagged β_1-receptor constructs transiently expressed in CHO-K1 cells. YFP fluorescence intensity was measured in channel 488 using two different gain settings: 700 and 1100. The binding of 20 nM BY-CGP to the expressed YFP_C-tagged β_1-adrenoceptors was measured using the 543 channel (gain setting 600 in all images). The merged images highlight co-localisation of cell surface YFP_C-tagged β_1-adrenoceptor (green) and BY-CGP binding (red) to these receptors in yellow pixels. The images are representative of two different fields of view imaged on one experimental day. Scale bar = 50 µm.

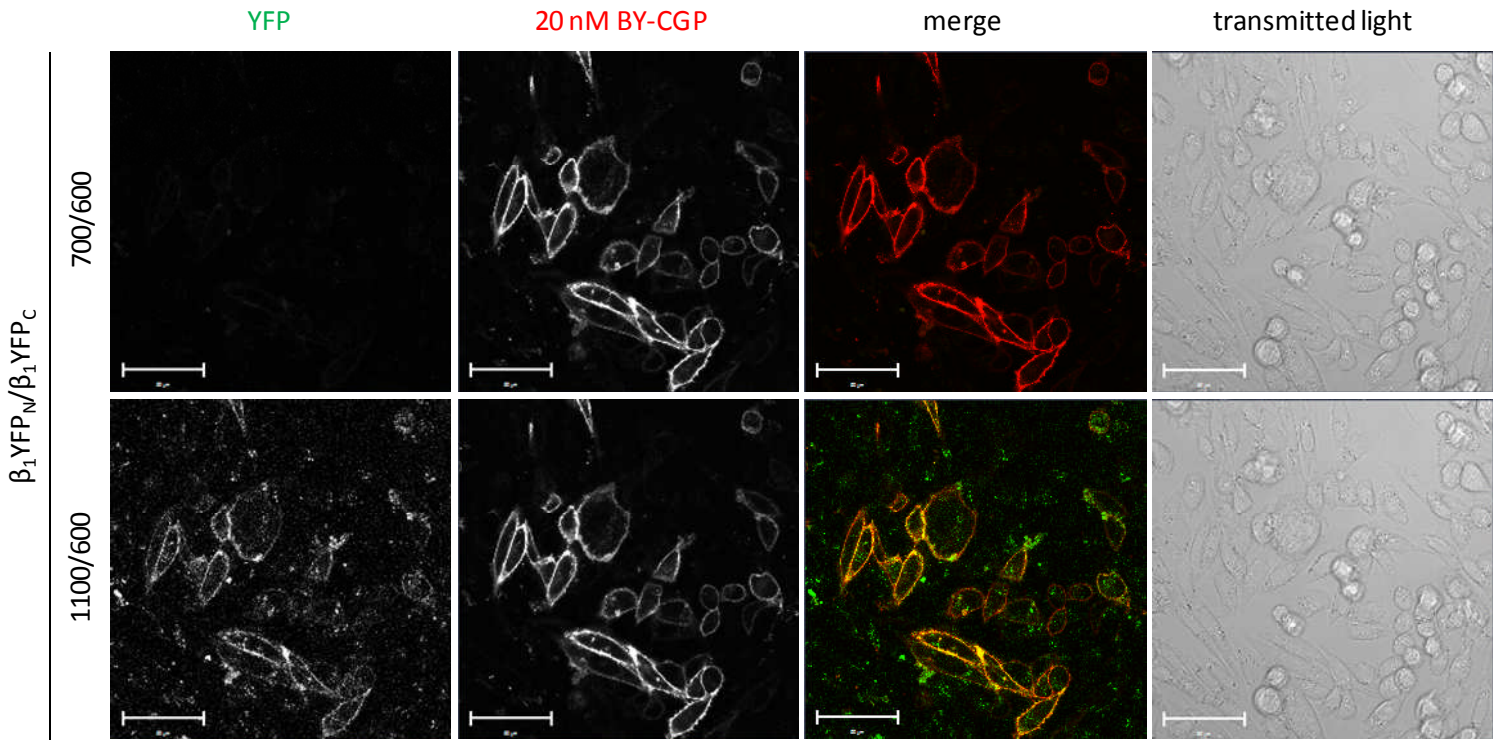

Figure 7.4 Confocal imaging of 20 nM BY-CGP binding to CHO-K1 cells transiently transfected with β_1YFP_N and β_1YFP_C constructs. The fluorescence intensity of the re-constituted YFP was measured in channel 488 using two different gain settings: 700 and 1100. The binding of 20 nM BY-CGP to expressed YFP_N- and YFP_C-tagged β_1-adrenoceptors was measured using the 543 channel (gain setting 600 in all images). The merged images highlight co-localisation of cell surface $YFP_{reconstituted}$-tagged β_1-adrenoceptor homodimers (green) and BY-CGP binding (red) to these receptor complexes in yellow pixels. The images are representative of two different fields of view imaged on one experimental day. Scale bar = 50 µm.

Investigating the dissociation rate of 3 nM BODIPY-TMR-CGP at wild-type β_1AR homodimers constrained and detected by BiFC

Homodimerisation of β_1-adrenoceptors has been reported to be transient (Calebiro *et al.*, 2013; Dorsch *et al.*, 2009). Using BiFC, the dimers that formed at any given time were trapped and stabilised, which allowed their detection and pharmacological investigation. Constraining dimers using BiFC will increase the percentage of β_1-adrenoceptors dimers as a result of BiFC-mediated prevention of dimer dissociation into receptor monomers. This would be expected to enhance any dimer-mediated pharmacological effects, although we could not determine what that increase in percentage of dimers was, and therefore could not know what increase (if any) of an effect to expect. To investigate the BODIPY-TMR-CGP binding kinetics at irreversibly constrained stable wild-type β_1AR homodimers, CHO-K1 cells were transiently transfected with the two non-fluorescent wild-type β_1-adrenoceptor constructs β_1YFP_N and β_1YFP_C, and stable β_1AR homodimers were detected by measuring YFP fluorescence. In these cells, the fluorescence intensity of YFP and BODIPY-TMR-CGP was measured every two seconds during a four minute association followed by a four minutes dissociation. In order to determine the BY-CGP binding kinetics to β_1AR homodimers, regions of interests (ROIs) were drawn around membranes of cells that were identified to express homodimers by YFP fluorescence. The obtained association traces of 3 nM BODIPY-TMR-CGP did not reach a plateau in 4 minutes (Figure 7.5), and association rates could not be accurately determined. However, the dissociation rate of 3 nM BODIPY-TMR-CGP was quantified using a

monophasic exponential decay equation and was determined to be 0.019 ± 0.006 min^{-1} (n=5), which was significantly slower than the dissociation rate determined in CHO-β_1-CS cells (i.e. unconstrained transient β_1AR homodimers, Chapter 6; $P < 0.05$, two-way ANOVA analysis followed by Bonferroni's multiple comparison test). This indicates that the formation of β_1AR into dimers affected the conformation of the catecholamine binding site such that the dissociation rate of 3 nM BY-CGP was slowed, suggesting distinct BY-CGP dissociation kinetics at β_1-adrenoceptor dimers compared to β_1-adrenoceptor monomers.

The binding levels of 3 nM BODIPY-TMR-CGP (BY-CGP) to CHO-K1 cells expressing $\beta_1YFP_N/\beta_1YFP_C$ homodimers were unchanged following a four minute dissociation in the absence of unlabelled ligands. However, reduced binding of 3 nM BY-CGP was observed following dissociation in the presence of 1 µM CGP 12177 and 1 µM propranolol (Figure 7.6). YFP fluorescence was measured at the same time as BY-CGP fluorescence to confirm the presence of β_1-adrenoceptor homodimers (Figure 7.6). The dissociation rates of 3 nM BY-CGP in the presence of 1 µM CGP 12177 and 1 µM propranolol were determined to be 0.186 ± 0.008 min^{-1} (n=6) and 0.189 ± 0.007 min^{-1} (n=6), respectively, and were significantly faster than the dissociation rate determined above in the absence of unlabelled ligands ($P < 0.05$, two-way ANOVA followed by Bonferroni's post hoc test; Figure 7.7). The change in the 3 nM BY-CGP dissociation rate in the absence and presence of unlabelled ligands was 2-fold in CHO-β_1-CS cells (Chapter 6, Table 6.4), but was 10-fold in

CHO-K1 cells expressing wild-type β_1YFP_N/ β_1YFP_C homodimers. This fold increase in the effects of unlabelled ligands on the BY-CGP dissociation rate in cells expressing a greater percentage of dimers (constrained β_1YFP_N/β_1YFP_C dimers unable to dissociate) than in cells expressing unconstrained transient β_1AR dimers (dimer dissociation unrestricted in CHO-β_1-CS cells), suggests that the effects of the unlabelled ligands are mediated through a secondary β_1-adrenoceptor site across a homodimer interface.

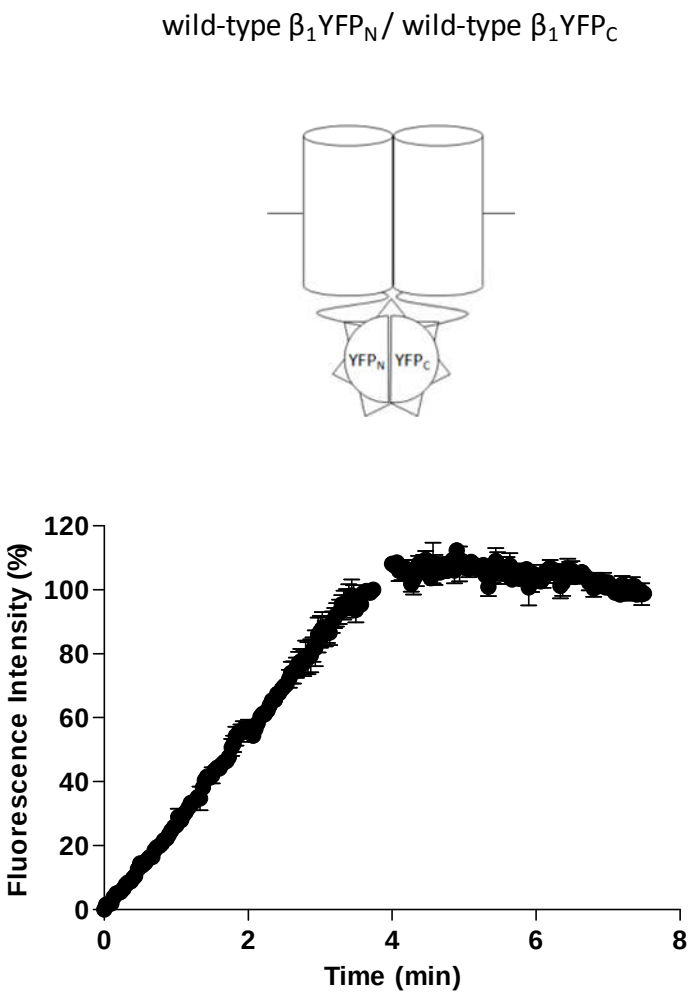

Figure 7.5 Normalised association and dissociation of 3 nM BY-CGP in CHO-K1 cells transiently expressing β_1YFP$_N$/β_1YFP$_C$ homodimers constrained by BiFC. Data shown are mean ± s.e.m. of data from five separate perfusion slides imaged on three separate experimental days. For each experiment regions of interest were drawn around the membranes of 10 individual cells.

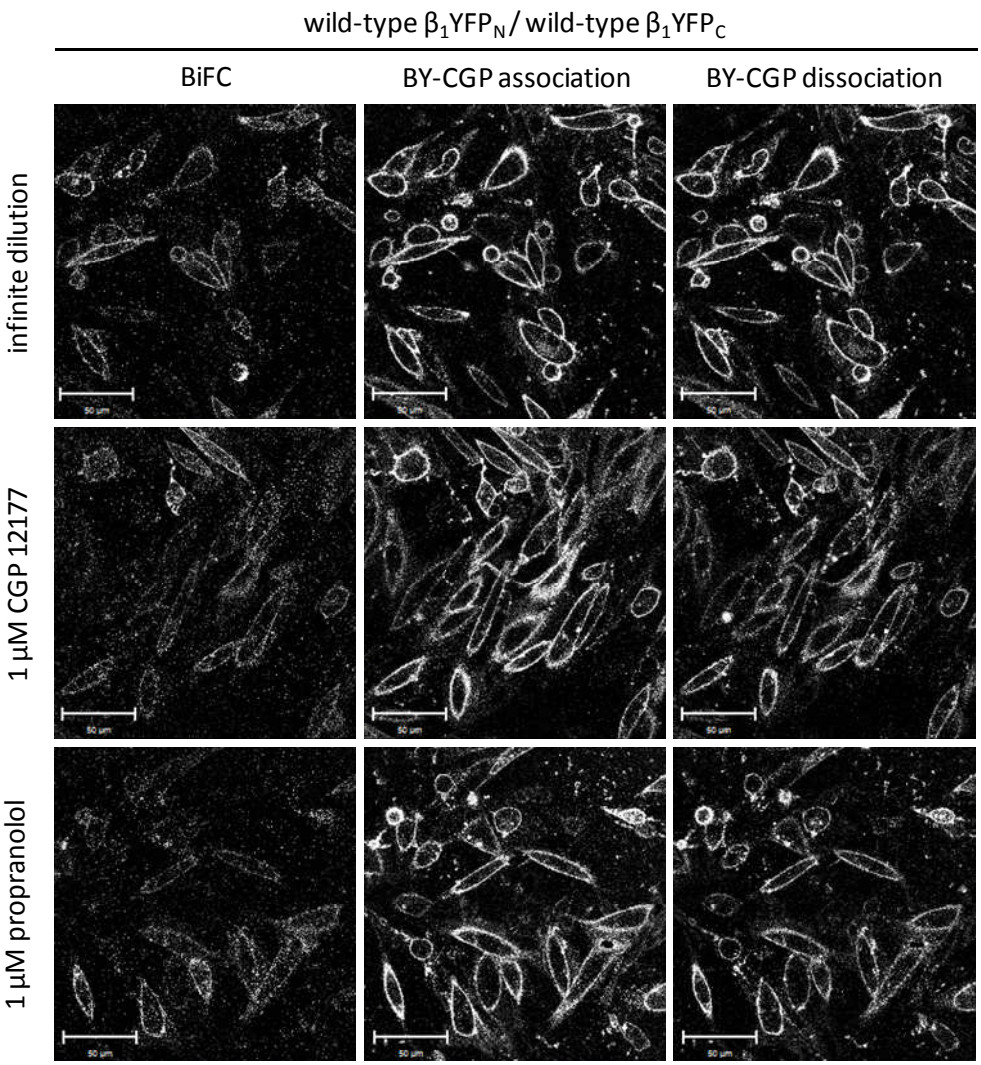

Figure 7.6 Binding of 3 nM BY-CGP to CHO-K1 cells transiently expressing $\beta_1YFP_N/\beta_1YFP_C$ constrained by BiFC. Confocal images following 4 min BODIPY-TMR-CGP association and a further 4 minutes of dissociation in the absence (infinite dilution) and presence of either 1 µM CGP 12177 or 1 µM propranolol. The fluorescence of YFP-tagged β_1-adrenoceptor homodimers was measured simultaneously. Images are representative of six separate perfusion slides imaged on three separate experimental days. Scale bar = 50 µm.

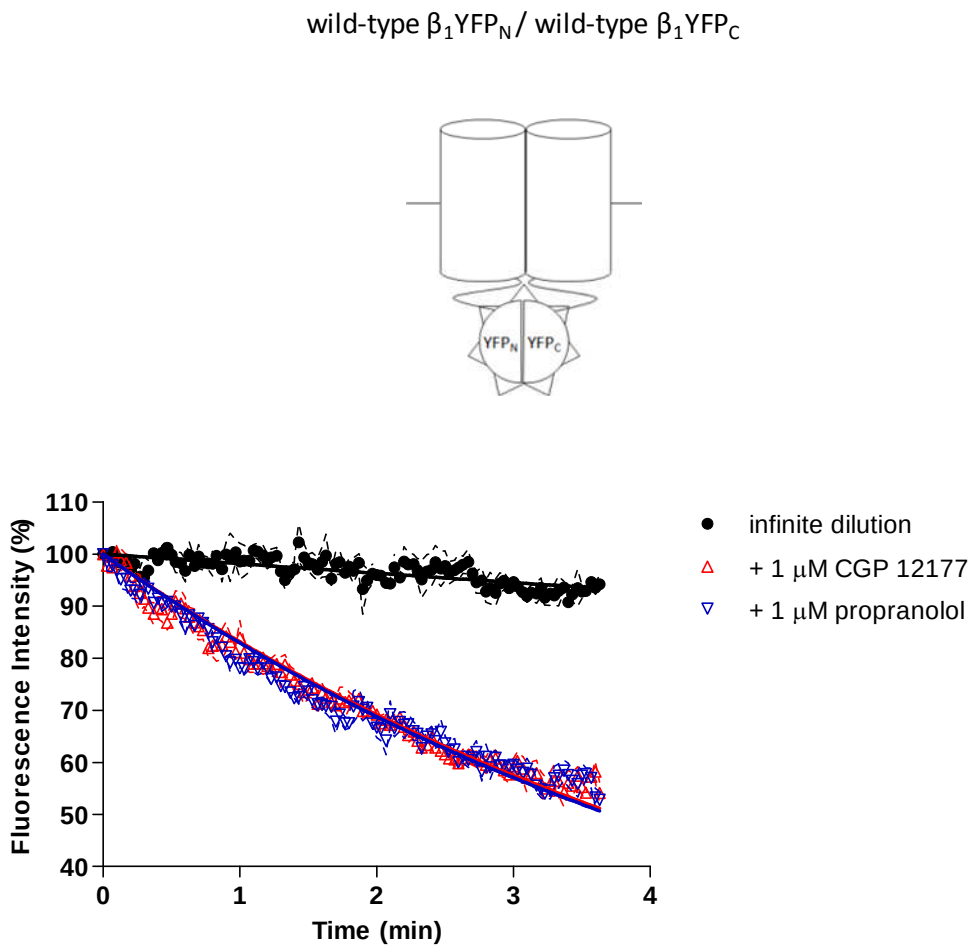

Figure 7.7 Dissociation of 3 nM BY-CGP from CHO-K1 cells transiently expressing β_1-YFP_N/β_1-YFP_C homodimers constrained by BiFC in the absence and presence of 1 μM CGP 12177 and 1 μM propranolol. Data are mean ± s.e.m. of data obtained from 5-6 separate perfusion slides imaged on three separate experimental days. For each perfusion slide, regions of interest were drawn around the membranes of 10 individual cells.

Effect of a non-ligand binding β_1AR protomer on the dissociation rate of 3 nM BODIPY-TMR-CGP at constrained β_1AR homodimers

Next, we aimed to confirm whether the enhanced difference between the BODIPY-TMR-CGP dissociation rate in the absence and presence of unlabelled ligands observed in constrained wild-type β_1AR homodimers compared to CHO-β_1-CS cells, is in fact due to the constrained presence of a second site in form of a second β_1AR protomer in a β_1AR homodimer complex. In order to achieve this, we introduced the D138A mutation into the human β_1-adrenoceptor sequence, which has been shown to abolish binding of β-adrenoceptor ligands to both β_1-adrenoceptor sites (Baker *et al.*, 2008). If the second site is facilitated by a second β_1-adrenoceptor protomer in a homodimer formation, then the introduction of the D138A mutation would "remove" the second site and with that the ability of unlabelled ligands to affect the BODIPY-TMR-CGP dissociation rate through allosteric interactions across the homodimer interface (Figure 7.8). This mutation, however, would not be expected to affect the BODIPY-TMR-CGP dissociation rate, if the second site was facilitated within one β_1AR protomer.

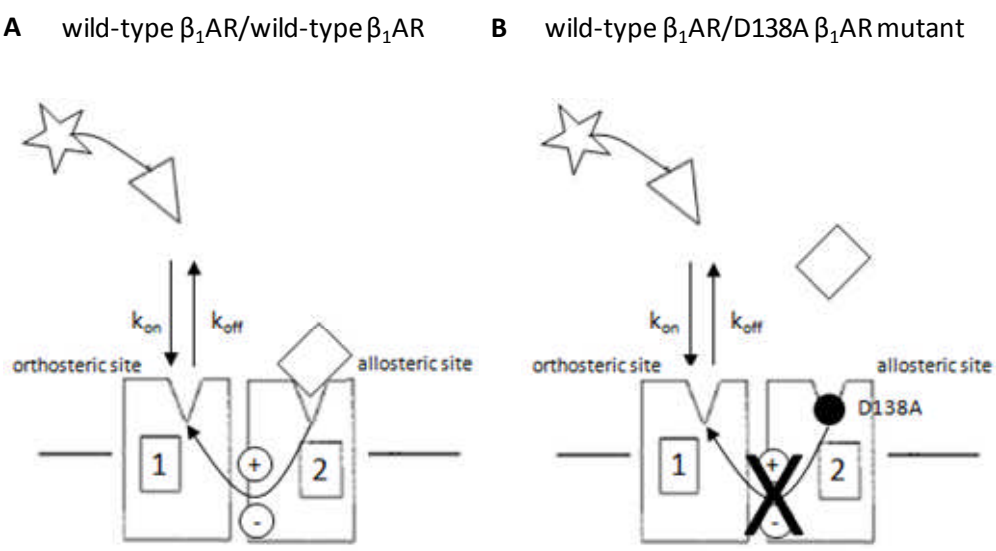

Figure 7.8 Schematic diagram detailing potential allosteric effects on the ligand-binding properties of a labelled ligand caused by an unlabelled ligand across a homodimer interface. **A**, the kinetic parameters of a labelled ligand at the orthosteric site (protomer 1, e.g. native β_1AR) may be positively or negatively affected by the binding of an unlabelled ligand to an allosteric site (protomer 2, e.g. native β_1AR). **B**, these allosteric effects are inhibited if the binding of the unlabelled ligand to the allosteric site is prevented, for example, by the introduction of a single amino acid change. For the β_1-adrenoceptor, the non-ligand binding mutation D138A (Baker *et al.*, 2008) was chosen.

First, we confirmed that the D138A mutation abolished ligand binding to the β_1-adrenoceptor. We generated a D138A β_1-adrenoceptor mutant fused to the SNAP-tag ($ss\beta_{1D138A}$; for DNA and protein sequence see Appendix I S12) in order to visualise the mutant receptor and confirm its expression on the cell surface following transient transfection. Indeed, no binding of 2 nM BODIPY-TMR-CGP could be seen in CHO-K1 cells transfected with the $ss\beta_{1D138A}$ construct, but clear membrane fluorescence following labelling of the SNAP-tag with 1 µM BG-488 confirmed the cell surface expression of the receptor construct (Figure 7.9). The SNAP-tagged native β_1AR was also transiently transfected as a positive control, and clear fluorescence of the BG-488 labelled SNAP-tag and 2 nM BY-CGP binding to the receptor could be seen (Figure 7.9), indicating that the lack of BY-CGP fluorescence seen for the $ss\beta_{1D138A}$ transfected cells was due to the mutation introduced into the β_1-adrenoceptor.

Following this, the same mutation was introduced into the β_1YFP_C construct to generate the $\beta_{1D138A}YFP_C$ construct (for DNA and protein sequence see Appendix I S13). No YFP fluorescence was detected in CHO-K1 cells transfected with the $\beta_{1D138A}YFP_C$ construct and no BODIPY-TMR-CGP fluorescence was observed following a 10 minute exposure to 3 nM BODIPY-TMR-CGP (Figure 7.10). However, when co-transfected with wild-type β_1YFP_N, YFP and BY-CGP fluorescence was detected, indicating that β_1-adrenoceptor homodimerisation and reconstitution of the YFP had taken place (Figure 7.10). The BODIPY-TMR-CGP fluorescence measured represents the binding of

BODIPY-TMR-CGP to the β_1YFP_N construct either as part of a $\beta_1YFP_N/\beta_{1D138A}YFP_C$ homodimer (yellow pixels in merged image), a $\beta_1YFP_N/\beta_1YFP_N$ homodimer or a monomer (latter two scenarios are both reflected in BODIPY-TMR-CGP fluorescence only, i.e. red pixels in merged image).

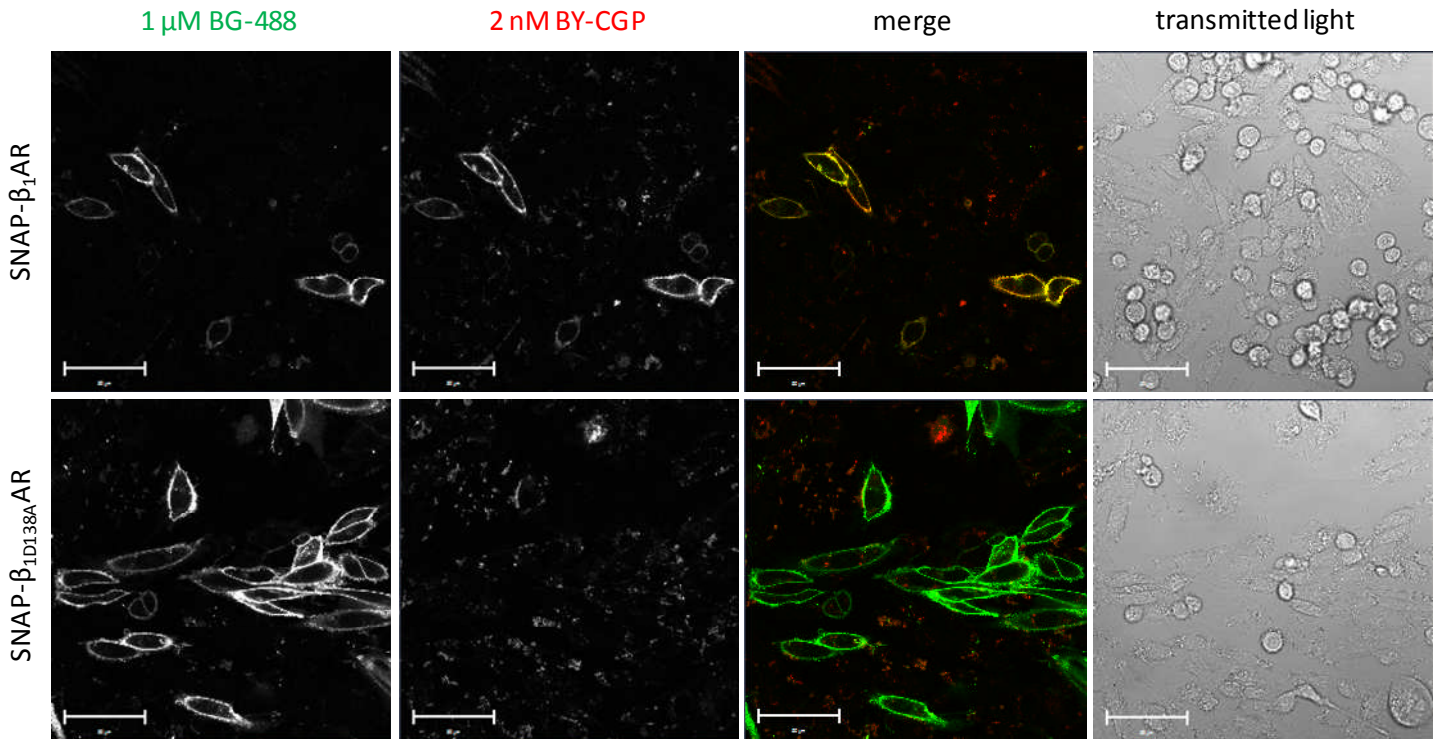

Figure 7.9 Confocal imaging of non-ligand binding β_{1D138A} receptor mutation. The presence of the wild-type (top panel) and mutant (bottom panel) β_1-adrenoceptor was visualised by labelling the SNAP-tag with 1 µM BG-488 (30 mins, 37 °C) prior to imaging its fluorescence using 488 nm excitation. The ligand binding properties of the wild-type and mutant receptor was examined by exposing the cells to 2 nM BY-CGP (10 mins, 37 °C). BY-CGP fluorescence was measured using 543 nm excitation. The merged images highlight co-localisation of cell surface SNAP-tagged β_1-adrenoceptors (green) and BY-CGP binding (red) to these receptors in yellow pixels. The images are representative of two different fields of view imaged on one experimental day. Scale bar = 50 µm.

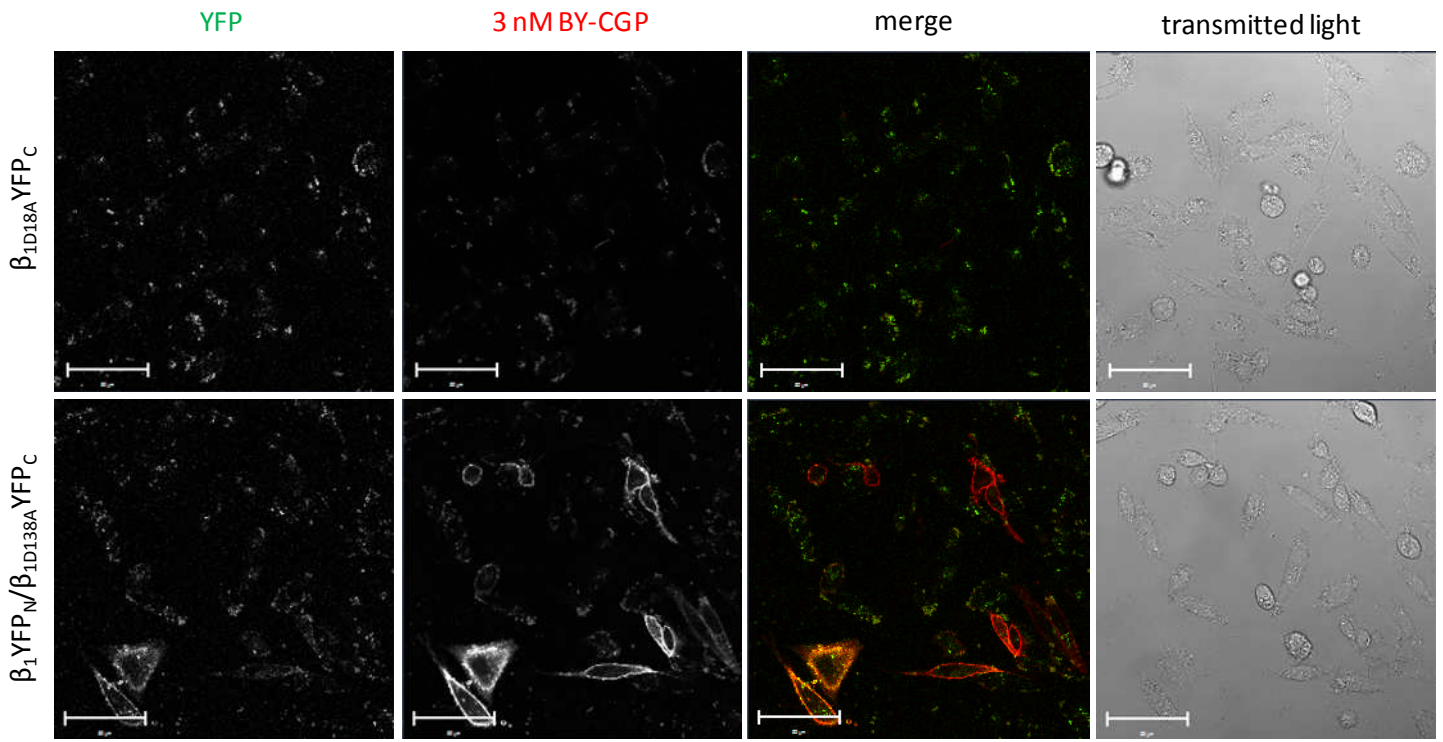

Figure 7.10 Confocal imaging of non-ligand binding β_{1D138A} receptor mutation using BiFC. The fluorescence intensities of the YFP-tag and 3 nM BY-CGP were measured in the 488 and 543 channel, respectively, for the mutant $\beta_{1D138}YFP_C$ construct alone (top panel) and when co-transfected with wild-type β_1YFP_N (bottom panel). The merged images highlight co-localisation of cell surface $YFP_{reconstituted}$-tagged β_1-adrenoceptor homodimers (green) and BY-CGP binding (red) to these receptor complexes in yellow pixels. The images are representative of two different fields of view imaged on one experimental day. Scale bar = 50 µm.

Following these imaging studies, we investigated the dissociation rate of 3 nM BODIPY-TMR-CGP in CHO-K1 cells transiently transfected with one wild-type and one non-ligand binding receptor mutant β_1-adrenoceptor construct ($\beta_1YFP_N/\beta_{1D138A}YFP_C$) using the confocal perfusion system. YFP and BY-CGP fluorescence was measured every two seconds during a four minute association followed by a four minutes dissociation. The association traces of 3 nM BODIPY-TMR-CGP in cells expressing $\beta_1YFP_N/\beta_{1D138A}YFP_C$ homodimers did not reach a plateau after four minutes (Figure 7.11), and association rates could not be accurately determined. However, when comparing the normalised association traces obtained for 3 nM BY-CGP at unconstrained (i.e. transient) β_1AR, constrained $\beta_1YFP_N/\beta_1YFP_C$ homodimers and $\beta_1YFP_N/\beta_{1D138A}YFP_C$ homodimers, it appeared that the association rates were very similar during the duration tested (4 minutes; Figure 7.12A). The dissociation rate of 3 nM BODIPY-TMR-CGP in cells expressing $\beta_1YFP_N/\beta_{1D138A}YFP_C$ homodimers was quantified using monophasic exponential decay equations and was determined to be 0.054 ± 0.011 min^{-1} (n=5), which was slower than the dissociation rate determined in CHO-β_1-CS cells (Chapter 6), but faster than the dissociation rate determined in constrained wild-type β_1AR homodimers, although the observed differences were not statistically significant (P > 0.05, two-way ANOVA followed by Bonferroni's multiple comparison test; Figure 7.12B). This difference, albeit small, may suggest that the introduced mutation influenced the dimer conformation, thereby affecting the BY-CGP dissociation kinetics. Alternatively, the dissociation rate intermediate between the transient dimers

and constrained wild-type dimers ($\beta_1YFP_N/\beta_1YFP_C$ as described above) may represent a different (smaller) percentage of constrained stable dimers of the overall population of receptors in the transiently transfected cells, resulting in a smaller observed effect in cells expressing $\beta_1YFP_N/\beta_{1D138A}YFP_C$ compared to cells expressing $\beta_1YFP_N/\beta_1YFP_C$ homodimers.

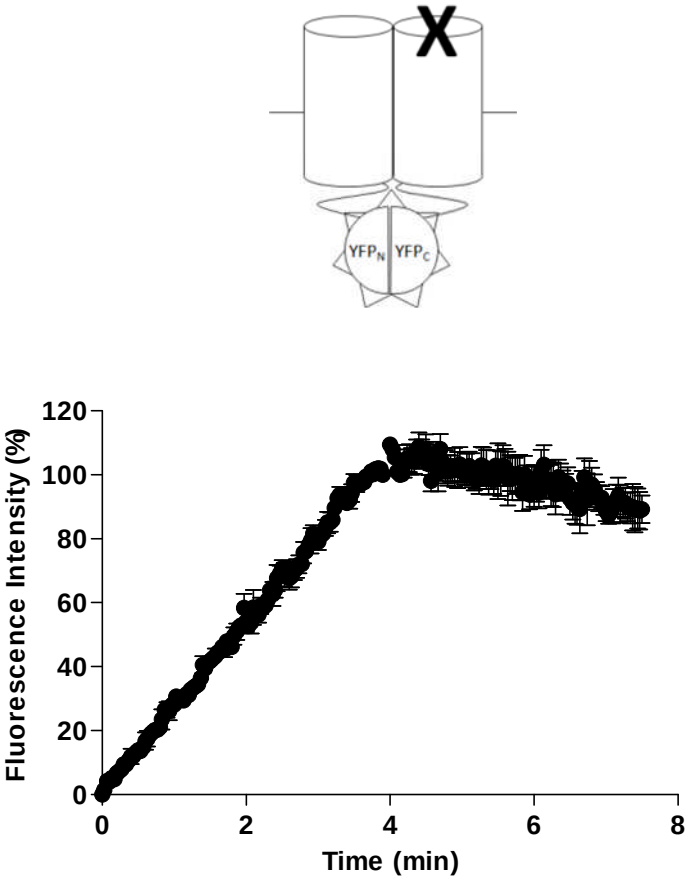

Figure 7.11 Normalised association and dissociation of 3 nM BY-CGP in CHO-K1 cells transiently expressing $\beta_1YFP_N/\beta_{1D138A}YFP_C$ homodimers constrained by BiFC. Data shown are mean ± s.e.m. of data from five separate perfusion slides imaged on three separate experimental days. For each experiment regions of interest were drawn around the membranes of 10 individual cells.

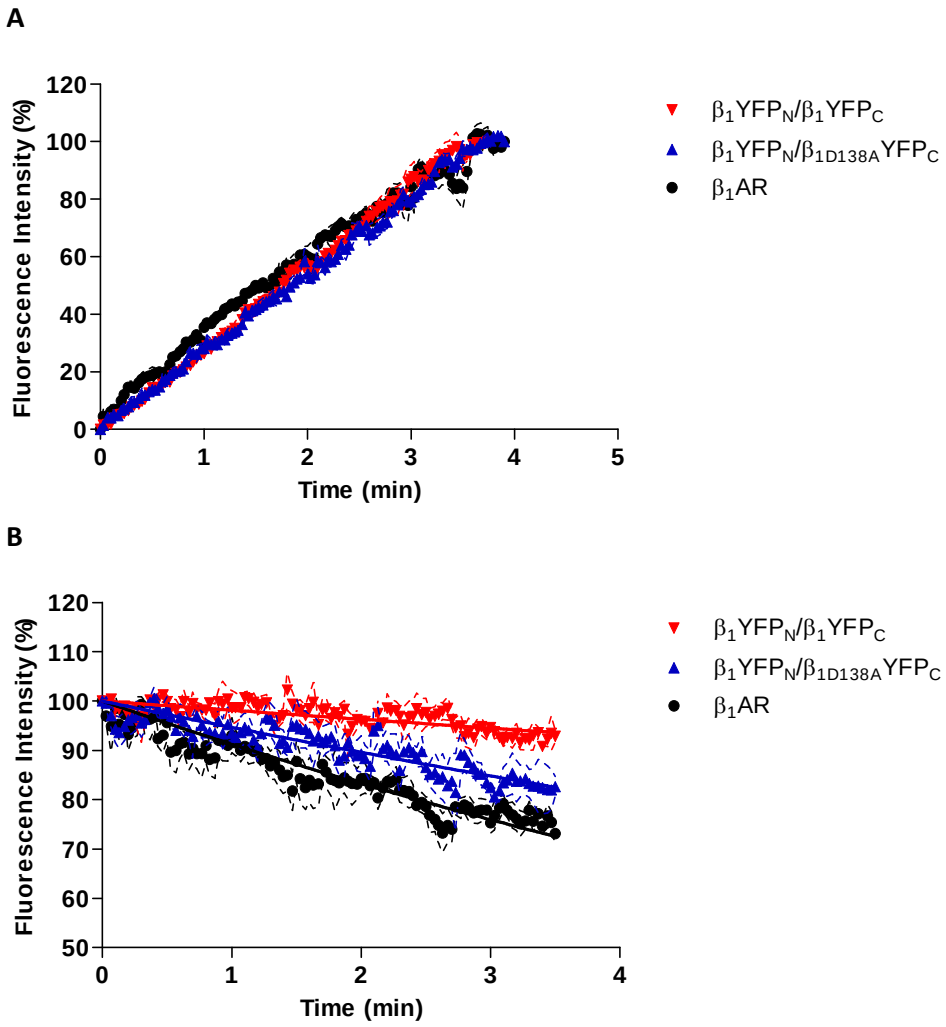

Figure 7.12 A, association and **B**, dissociation of 3 nM BODIPY-TMR-CGP 12177 (BY-CGP) to untagged native β_1AR (transient dimers in CHO-β_1-CS cells; data from Chapter 6) and CHO-K1 cells expressing $\beta_1YFP_N/\beta_1YFP_C$ (wild-type BiFC trapped dimers) and $\beta_1YFP_N/\beta_{1D138A}YFP_C$ (wild-type/non-ligand binding mutant BiFC trapped dimers). Data are mean ± s.e.m. of data obtained from 5-9 separate perfusion slides on 3-7 separate experimental days. For each perfusion slide, ROIs were drawn around the membranes of 10 individual cells.

Reduced binding of 3 nM BY-CGP to CHO-K1 cells expressing $\beta_1YFP_N/\beta_{1D138A}YFP_C$ homodimers can be seen following four minute dissociation in the presence of unlabelled ligands (Figure 7.13). YFP fluorescence was measured at the same time as BY-CGP fluorescence to confirm the formation of β_1-adrenoceptor homodimers (Figure 7.13). In cells expressing $\beta_1YFP_N/\beta_{1D138A}YFP_C$ homodimers, the dissociation rate of 3 nM BODIPY-TMR-CGP was increased in the presence of 1 µM CGP 12177 (k_{off} 0.169 ± 0.010 min^{-1}, n=6) and 1 µM propranolol (k_{off} 0.144 ± 0.009 min^{-1}, n=5, $P < 0.05$, two-way ANOVA followed by Bonferroni's post hoc test; Figure 7.14; Table 7.1). Although the BY-CGP dissociation rate in the presence of 1 µM propranolol appeared slower than that determined in CHO-β_1-CS cells and cells expressing wild-type $\beta_1YFP_N/\beta_1YFP_C$ homodimers (Table 7.1), the differences were not statistically significant ($P < 0.05$, two-way ANOVA followed by Bonferroni's post hoc test). Interestingly, the difference in the 3 nM BODIPY-TMR-CGP dissociation rate in the presence of unlabelled ligands compared to in the absence of unlabelled ligands was 3-fold in cells expressing constrained wild-type/mutant β_1AR homodimers ($\beta_1YFP_N/\beta_{1D138A}YFP_C$), which was comparable to the difference seen in CHO-β_1-CS cells (2-fold; Chapter 6, Table 6.4).

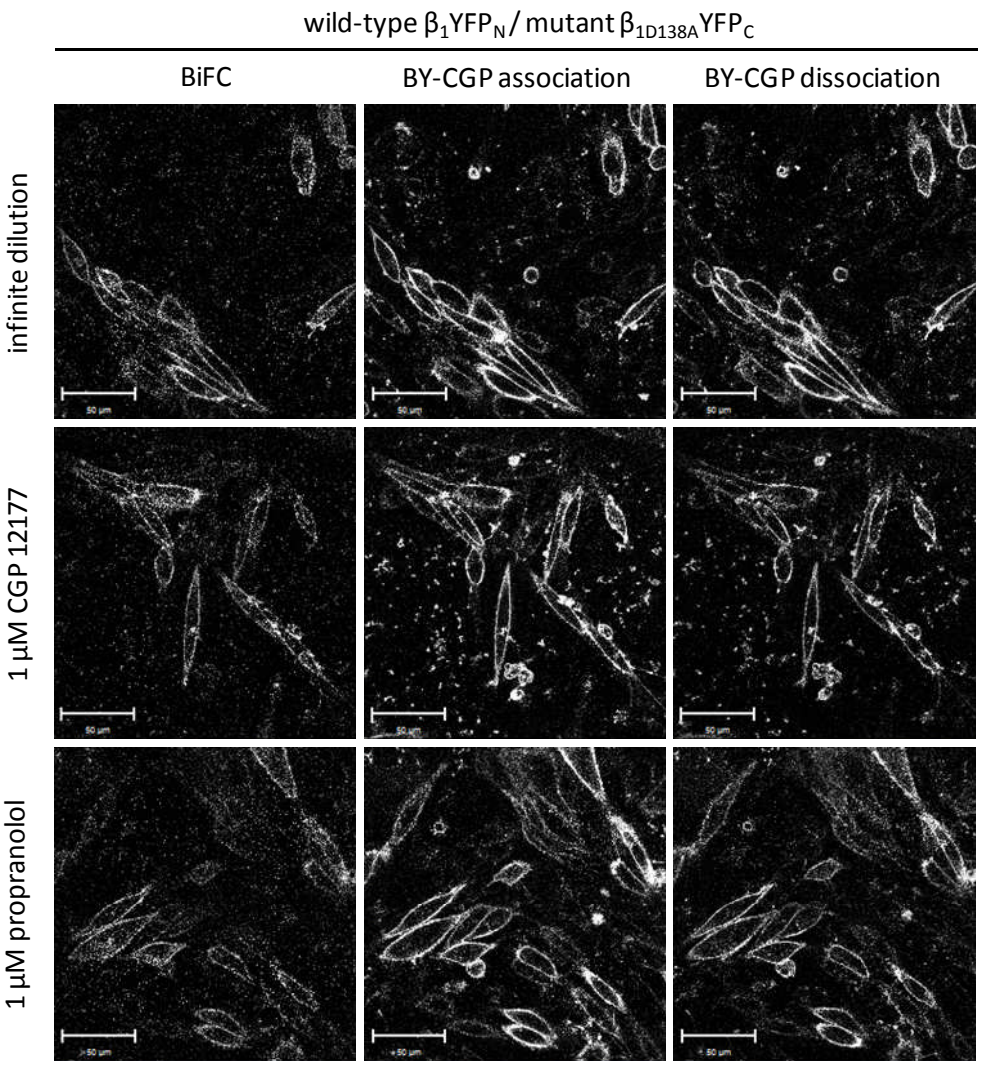

Figure 7.13 Binding of 3 nM BY-CGP to CHO-K1 cells transiently expressing β_1YFP$_N$/β_{1D138A}YFP$_C$ homodimers constrained by BiFC. Confocal images following 4 min BY-CGP association and a further 4 minutes of dissociation in the absence (infinite dilution) and presence of either 1 µM CGP 12177 or 1 µM propranolol. The fluorescence of YFP-tagged β_1-adrenoceptor homodimers was measured simultaneously. Images are representative of 5-6 separate perfusion slides imaged on three separate experimental days. Scale bar = 50 µm.

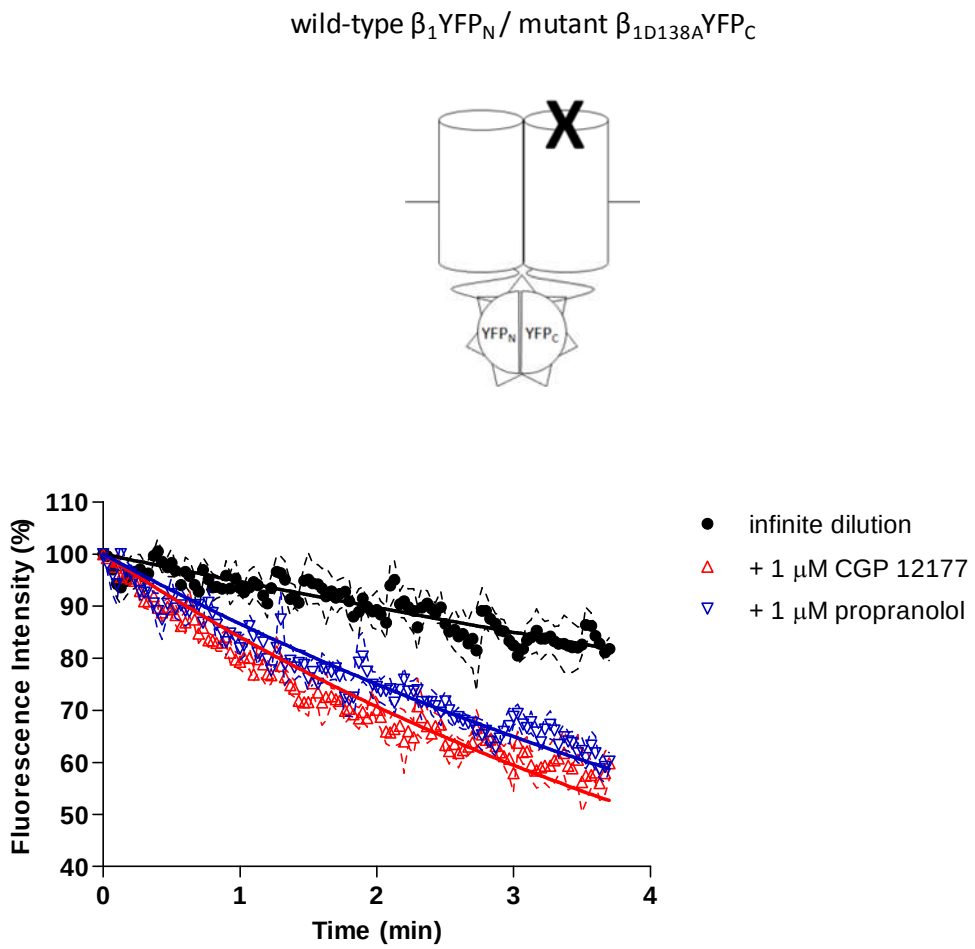

Figure 7.14 Dissociation of 3 nM BY-CGP from CHO-K1 cells transiently expressing **A**, β_1-YFP$_N$/β_1-YFP$_C$ and **B**, β_1-YFP$_N$/β_{1D138A}-YFP$_C$ in the absence and presence of 1 μM CGP 12177 and 1 μM propranolol. Data are mean ± s.e.m. of data obtained from 5-6 separate perfusion slides imaged on three separate experimental days. For each perfusion slide, regions of interest were drawn around the membranes of 10 individual cells.

Table 7.1 Summary of dissociation rates of 3 nM BY-CGP in the absence and presence of 1 µM CGP 12177 and 1 µM propranolol determined in CHO-CS cells stably expressing the native β_1-adrenoceptor and in CHO-K1 cells transiently co-transfected with the β_1–YFP_N and β_1-YFP_C constructs and the β_1-YFP_N and β_{1D138A}-YFP_C constructs. [1]CHO-β_1-CS data was determined in Chapter 6. Data are mean ± s.e.m. of (n) separate perfusion slide preparations. *statistical significance ($P < 0.05$) of values compared to the value determined [a]under control conditions (infinite dilution) and [b]in the presence of 1 µM propranolol within each set of β_1AR homodimers (transients in CHO-β1-CS cells, constrained wild-type $\beta_1YFP_N/\beta_1YFP_C$ and constrained wild-type/mutant $\beta_1YFP_N/\beta_{1D138A}YFP_C$ homodimers) as determined by two-way ANOVA analysis followed by Bonferroni's post hoc test; [†]statistical significance ($P < 0.05$) of values compared to the equivalent value determined in [c]CHO-β_1-CS cells and [d]$\beta_1YFP_N/\beta_1YFP_C$ co-transfected CHO-K1 cells according to two-way ANOVA analysis followed by Bonferroni's post hoc test.

	CHO-β_1-CS cells[1]		$\beta_1YFP_N/\beta_1YFP_C$		$\beta_1YFP_N/\beta_{1D138A}YFP_C$	
	k_{off} (min^{-1})	*n*	k_{off} (min^{-1})	*n*	k_{off} (min^{-1})	*n*
infinite dilution	0.092 ± 0.008	9	0.019 ± 0.006[†a]	4	0.054 ± 0.011	5
+ 1 µM CGP 12177	0.202 ± 0.024*[a]	7	0.186 ± 0.008*[a]	6	0.169 ± 0.010*[a]	6
+ 1 µM propranolol	0.194 ± 0.010*[a]	6	0.189 ± 0.007*[a]	6	0.144 ± 0.009*[a]	5

Functional response of constrained β_1AR homodimers to β-adrenoceptor agonists

Following the kinetic binding studies, we aimed to investigate whether dimerisation of β_1-adrenoceptors played a role in the functional responses mediated by the receptor. For this, a stable clonal CHO-β_1YFP_N cell line was generated and subsequently transfected with either the β_1YFP_C or the $\beta_{1D138A}YFP_C$ construct to generate two further stable cell lines: CHO-$\beta_1YFP_N/\beta_1YFP_C$ and CHO-$\beta_1YFP_N/\beta_{1D138A}YFP_C$. Studies investigating the oligomerisation state of receptors at the single molecule level demonstrated that β_1-adrenoceptors form transient homodimers (Calebiro *et al.*, 2013). In the CHO-$\beta_1YFP_N/\beta_1YFP_C$ and CHO-$\beta_1YFP_N/\beta_{1D138A}YFP_C$ cell lines, YFP_N- and YFP_C-tagged β_1-adrenoceptors that spontaneously formed dimers, were trapped in stable conformations as a result of the irreversibility of the reconstitution of the full length YFP from YFP_N and YFP_C fragments that were brought into close proximity through specific interactions between β_1-adrenoceptors. Whilst we could not directly determine the expression levels of β_1YFP_N, β_1YFP_C and $\beta_{1D138A}YFP_C$ in the CHO-$\beta_1YFP_N/\beta_1YFP_C$ and CHO-$\beta_1YFP_N/\beta_{1D138A}YFP_C$ cell lines, and the percentage of YFP fragment-tagged β_1-adrenoceptors that dimerised, we aimed to increase the percentage of β_1AR dimers in these two cell lines through BiFC. Using this approach, we detected changes in BY-CGP dissociation rates, and we hypothesised that it may also highlight altered β_1AR pharmacology in a functional assay.

CGP 12177 has been described to antagonise β-adrenoceptor agonist actions at the catecholamine site of the β_1-adrenoceptor, as well as exerting agonist actions of its own through a secondary β_1-adrenoceptor site at higher concentrations (Pak *et al.*, 1996). To examine both the antagonist and agonist properties of CGP 12177, concentration-response curves of CGP 12177 in the absence and presence of 100 nM cimaterol were obtained in the [^{3}H]cAMP accumulation assay. 100 nM is the cimaterol EC_{80} concentration in CHO-β_1-CS cells (Chapter 3), and allows a robust enough assay window to detect inhibition by CGP 12177 in CHO-β_1-CS cells. Functional responses were measured in CHO-β_1-CS and CHO-β_1YFP_N cells to examine whether the responses mediated by the YFP_N-tagged β_1AR were comparable to those of the untagged receptor. In both cell lines, β_1-adrenoceptor homodimers were transient (i.e. not constrained), and the CGP 12177 pharmacology was similar in these two cell lines (Figure 7.15). CGP 12177 (10^{-11} – 10^{-8} M) inhibited 100 nM cimaterol-stimulated [^{3}H]cAMP accumulation in CHO-β_1-CS and CHO-β_1YFP_N cells with pIC_{50} values of 8.56 ± 0.05 (n=3) and 8.47 ± 0.09 (n=3), respectively. At higher concentrations CGP 12177 caused a [^{3}H]cAMP accumulation that was partial compared to the response of 100 nM cimaterol alone, in both cell lines (Table 7.2; Figure 7.15). Furthermore, the CGP 12177 EC_{50} values were similar in the presence or absence of 100 nM cimaterol (Table 7.2; Figure 7.14) in CHO-β_1-CS ($P > 0.05$, unpaired t-test) and CHO-β_1YFP_N cells ($P > 0.05$, unpaired t-test). Although these data are preliminary and the affinity of CGP 12177 at the catecholamine site was not further

investigated, these data suggest that the YFP_N-tag did not affect the CGP 12177 pharmacology at the β_1-adrenoceptor.

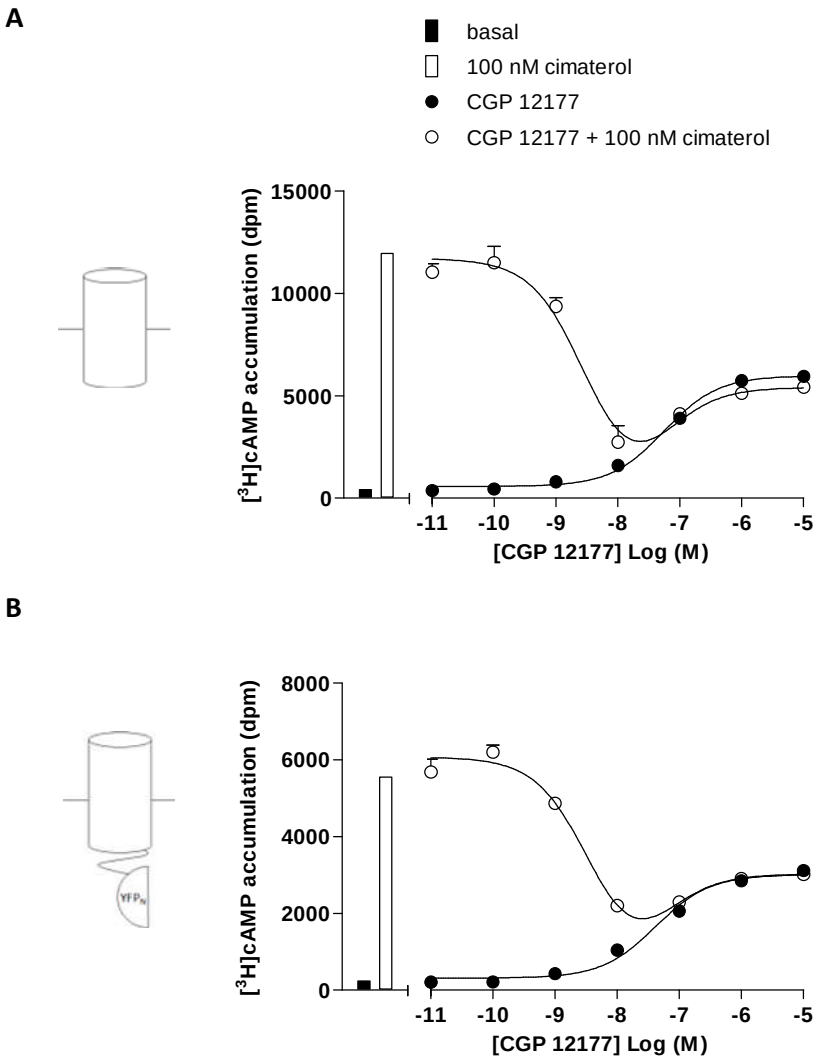

Figure 7.15 CGP 12177 concentration-response curves in the absence and presence of 100 nM cimaterol on **A**, CHO-β_1-CS and **B**, CHO-β_1YFP_N cells determined in a total [^{3}H]cAMP accumulation assay. Bar graphs show basal level of total [^{3}H]cAMP accumulation in unstimulated cells and [^{3}H]cAMP accumulation following stimulation with 100 nM cimaterol. Bar graph and 0.01 nM (10^{-11}M) CGP 12177 data are mean ± range of error of duplicate determinations, whereas all other data are mean ± s.e.m. of triplicate determinations from one single experiment which is representative of a total of three separate experiments.

Table 7.2 CGP 12177 stimulatory and inhibitory parameters determined in CHO-β_1-CS and CHO-β_1YFP$_N$ clonal cell lines in the total [^{3}H]cAMP accumulation assay in the absence and presence of 100 nM cimaterol. The pIC_{50} values represent the inhibition of 100 nM cimaterol by 10 nM CGP 12177.

	CHO-β_1-CS	CHO-β_1YFP$_N$	n
absence of 100 nM cimaterol			
pEC_{50}	7.27 ± 0.12	7.31 ± 0.08	3
E_{MAX} (% of 100 nM cimaterol)	55.5 ± 10.7	60.7 ± 11.0	3
presence of 100 nM cimaterol			
pEC_{50}	7.24 ± 0.04	7.42 ± 0.07	3
E_{MAX} (% of 100 nM cimaterol)	55.9 ± 10.6	61.0 ± 11.1	3
pIC_{50}	8.56 ± 0.05	8.47 ± 0.09	3

Following this, we obtained preliminary data in the [^{3}H]cAMP accumulation assay using CHO-β_1YFP$_N$-β_1YFP$_C$ and CHO-β_1YFP$_N$-β_{1D138A}YFP$_C$ cells, in which β_1-adrenoceptors that formed homodimers were constrained through irreversible reconstitution of the full length YFP from the two YFP fragments (YFP$_N$ and YFP$_C$) fused to the C-terminus of β_1-adrenoceptors. Both cell lines were generated from the same clonal CHO-β_1YFP$_N$ cell line, suggesting similar expression levels of the YFP$_N$-tagged β_1-adrenoceptor in these cell lines. However, we did not investigate the expression levels of YFP$_C$-tagged β_1AR and β_{1D138A}AR. In the [^{3}H]cAMP accumulation assay, the antagonist and agonist properties of CGP 12177 were retained in both cell lines. The obtained data revealed a reduced E_{MAX} in CHO-β_1YFP$_N$-β_{1D138A}YFP$_C$ cells compared to CHO-β_1YFP$_N$-β_1YFP$_C$ cells, whilst the CGP 12177 EC_{50} and IC_{50} values derived from the CGP 12177 concentration-response curves in the absence and presence of 100 nM cimaterol, respectively, were comparable between the two cell lines (Figure 7.16, Table 7.3). An increased agonist response may be due to increased receptor expression which can lead to a partial agonist response becoming a full(er) agonist response without affecting the EC_{50} of that agonist response. To investigate potential differences in levels of receptor expression in these two cell lines, cimaterol concentration-response curves were obtained in CHO-β_1YFP$_N$-β_1YFP$_C$ and CHO-β_1YFP$_N$-β_{1D138A}YFP$_C$ cells and compared to the cimaterol response obtained in CHO-β_1-CS and CHO-β_1YFP$_N$ cells (Figure 7.17). The concentration-response curve of a full agonist will be left-shifted in a system with a greater receptor reserve (i.e. greater receptor expression) which is reflected in a lower EC_{50} value. However, the

EC_{50} values derived for cimaterol were similar in all four cell lines ($P > 0.05$, one-way ANOVA analysis followed by Tukey's post hoc test). This may suggest similar levels of β_1-adrenoceptor expression in all cell lines, but it is noteworthy that we do not know what percentage of receptors dimerised in the different cell lines and what potential effect these dimers may have had on the functional responses measured. Interestingly, upon closer inspection of the CGP 12177 data obtained in CHO-β_1YFP_N-β_1YFP_C and CHO-β_1YFP_N-$\beta_{1D138A}YFP_C$ cells, the response to 10 µM CGP 12177 (E_{MAX}) was greater than that to 100 nM cimaterol in the first experiment, but smaller in subsequent experiments (Table 7.3). These data were obtained in cells of increasing passages (P2-4) and may suggest that the expression of β_1YFP_C and $\beta_{1D138A}YFP_C$ was lost over time in their respective cell lines. Both cell lines were generated from the same β_1YFP_N cell line, thus a loss of β_1YFP_C and $\beta_{1D138A}YFP_C$ expression over time may be one explanation for the similar cimaterol EC_{50} values determined in CHO-β_1YFP_N, CHO-β_1YFP_N-β_1YFP_C (P5) and CHO-β_1YFP_N-$\beta_{1D138A}YFP_C$ (P5) cell lines.

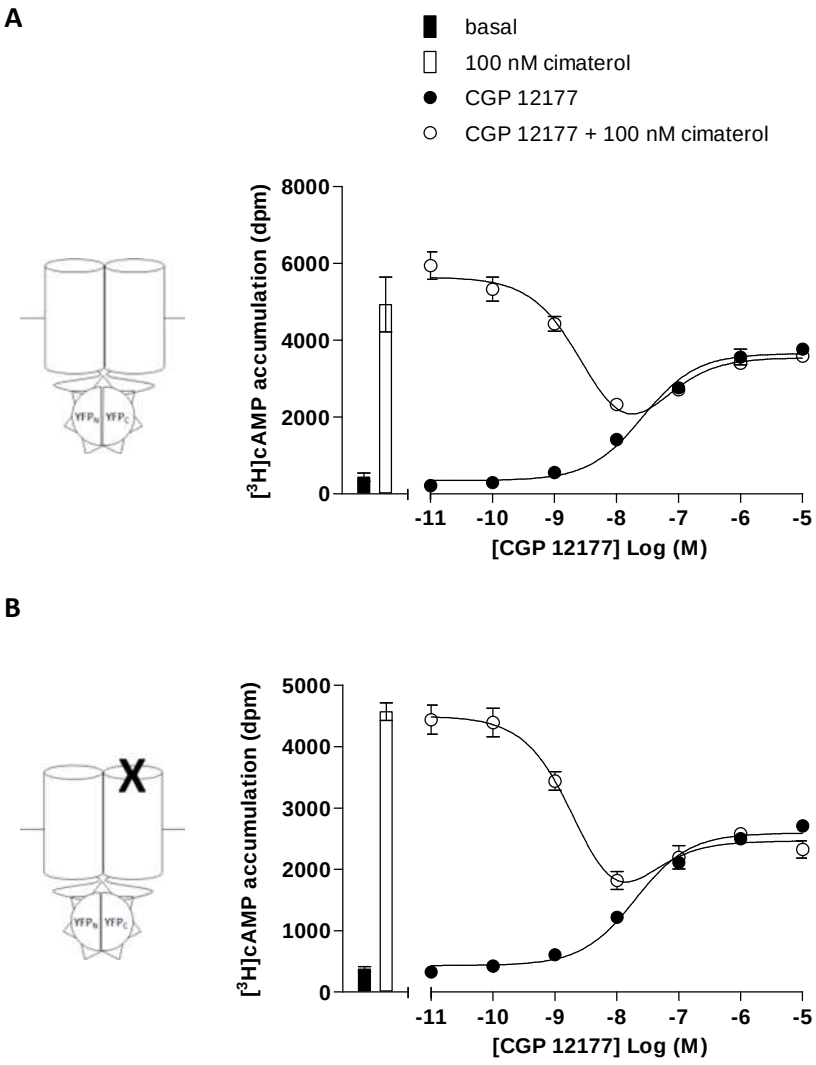

Figure 7.16 CGP 12177 concentration-response curves in the absence and presence of 100 nM cimaterol on **A**, CHO-β_1YFP_N-β_1YFP_C (P4) and **B**, CHO-β_1YFP_N-$\beta_{1D138A}YFP_C$ (P4) cells determined in a total [^{3}H]cAMP accumulation assay. Bar graphs show basal level of total [^{3}H]cAMP accumulation in unstimulated cells and [^{3}H]cAMP accumulation following stimulation with 100 nM cimaterol. Bar graph and 0.01 nM (log M -11) CGP 12177 data are mean ± range of error of duplicate determinations, whereas all other data are mean ± s.e.m. of triplicate determinations from one single experiment which is representative of a total of three separate experiments.

Table 7.3 Summary of CGP 12177 antagonist and agonist properties determined in stable CHO-β_1YFP_N-β_1YFP_C and CHO-β_1YFP_N-$\beta_{1D138A}YFP_C$ cell lines (at passages 2, 3 and 4).

	pIC_{50}	pEC_{50}	E_{MAX} (% of 100 nM cimaterol)	n
CHO-β_1YFP_N-β_1YFP_C	8.14; 8.51; 8.44	7.46; 7.75; 7.58	224.7; 83.6; 72.2	3
CHO-β_1YFP_N-$\beta_{1D138A}YFP_C$	7.98; 8.77; 8.52	7.49; 7.75; 7.70	205.4; 62.4; 52.2	3

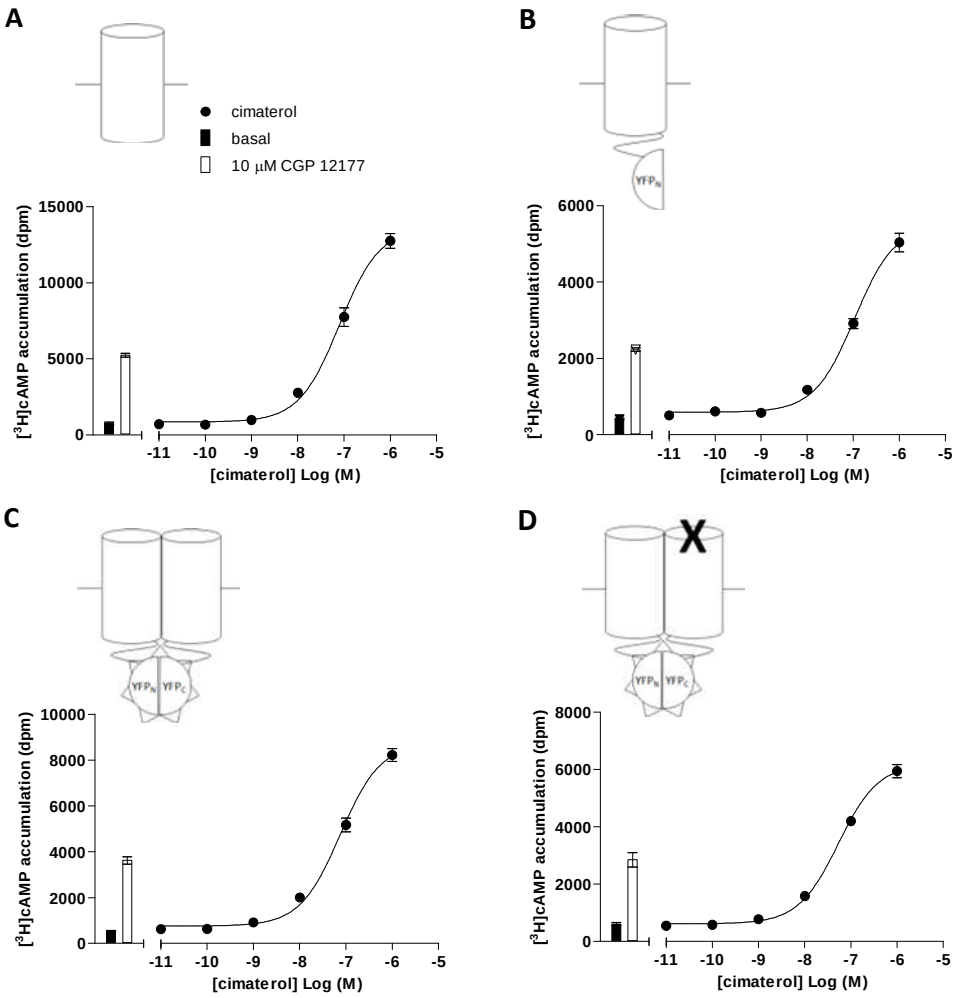

Figure 7.17 Cimaterol concentration-response curves on **A**, CHO-β_1-CS, **B**, CHO-β_1YFP_N, **C**, CHO-β_1YFP_N-β_1YFP_C (P5) and **D**, CHO-β_1YFP_N-$\beta_{1D138A}YFP_C$ (P5) cells determined in a total [^{3}H]cAMP accumulation assay. Bar graphs show basal level of total [^{3}H]cAMP accumulation of unstimulated cells and total [^{3}H]cAMP accumulation level following stimulation with 10 μM CGP 12177. Data are mean ± s.e.m. of triplicate determinations from a single experiment which is representative of two additional separate experiments.

To further investigate the expression of β_1-adrenoceptors in the CHO-β_1YFP_N, CHO-β_1YFP_N-β_1YFP_C (P5) and CHO-β_1YFP_N-$\beta_{1D138A}YFP_C$ cells (P5), the fluorescence of reconstituted YFP and of 20 nM BY-CGP binding to cell surface β_1-adrenoceptors was determined using confocal microscopy (Figure 7.18). As expected, no YFP fluorescence was detected in CHO-β_1YFP_N cells. Interestingly, we also saw no YFP fluorescence in CHO- β_1YFP_N-β_1YFP_C cells and only one cell of the CHO-β_1YFP_N-$\beta_{1D138A}YFP_C$ cell line was found to exhibit YFP fluorescence on the cell membrane to indicate that β_1YFP_N-$\beta_{1D138A}YFP_C$ homodimerisation and YFP reconstitution had taken place. In contrast, good membrane labelling of 20 nM BY-CGP was seen in all three cell lines (Figure 7.18). This suggests that the numbers expressed of β_1YFP_C and $\beta_{1D138A}YFP_C$ were insufficient to form β_1AR homodimers (yellow pixels in merged image in Figure 7.18), and that the binding of 20 nM BY-CGP occurred predominantly to β_1YFP_N monomers. The binding of BY-CGP to CHO-β_1YFP_N cells also highlighted the heterogeneity of β_1YFP_N expression in this cell line as some cells appeared to express β_1YFP_N not at all or at levels too low to detect BY-CGP binding, and thus may also be too low to detect any BiFC YFP fluorescence. It is unlikely that the lack of YFP fluorescence is due to impaired YFP reconstitution upon β_1AR homodimerisation based on the data we have already shown in this chapter, although previous binding and imaging data were collected in transient cells and not stable cell lines. Unfortunately, earlier passages (P2) of the stable cell lines were not imaged to demonstrate initial YFP fluorescence as a result of YFP reconstitution upon β_1AR homodimerisation in these cells.

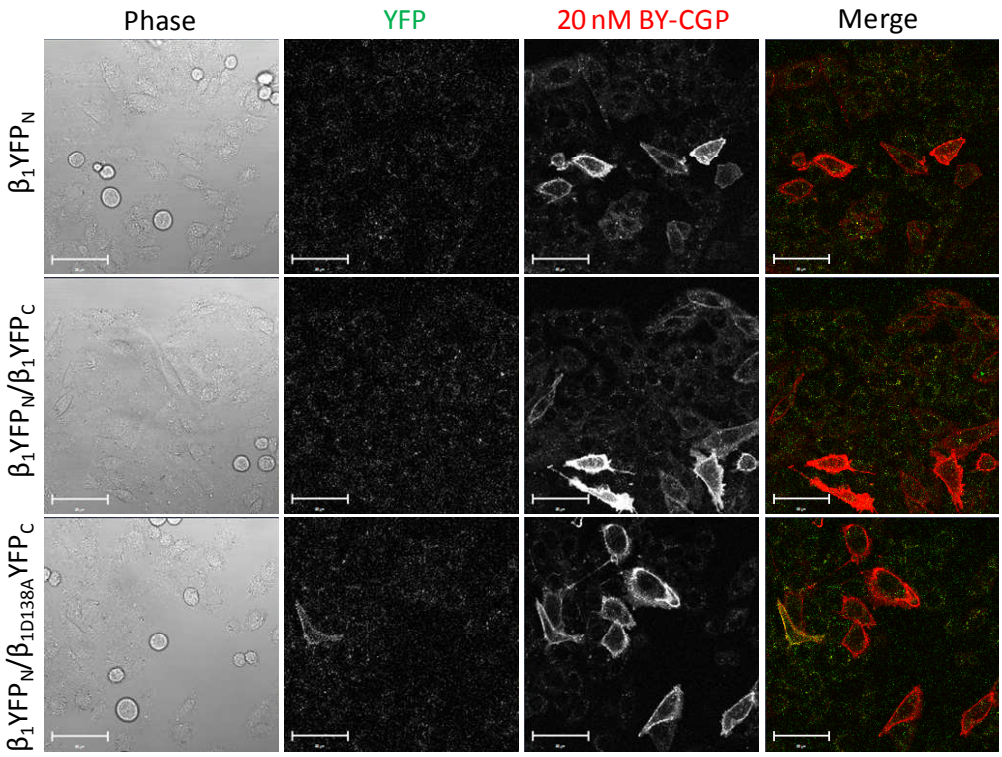

Figure 7.18 Phase and fluorescent confocal images of CHO-β_1YFP$_N$, CHO-β_1YFP$_N$-β_1YFP$_C$ (P5) and CHO-β_1YFP$_N$-β_{1D138A}YFP$_C$ (P5) cells. The fluorescence of reconstituted YFP was measured using 488 nm excitation and the fluorescence of 20 nM BY-CGP binding to the cells was measured using 543 nm excitation. The merged images show 20 nM BY-CGP binding to reconstituted YFP (i.e. constrained β_1AR homodimers) in yellow pixels and to β_1AR monomers (β_1YFP$_N$ or β_1YFP$_C$) or unconstrained β_1AR homodimers (β_1YFP$_N$/β_1YFP$_N$ or β_1YFP$_C$/β_1YFP$_C$) in red pixels. Scale bar = 50 µm.

Previous imaging data shown in this chapter suggested good efficiency of transient transfection of YFP fragment-tagged β_1-adrenoceptor in CHO cells. Thus, we transiently transfected the YFP_C-tagged β_1AR and β_{1D138A}AR constructs into the clonal CHO-β_1YFP_N cell line. We were not able to determine receptor expression levels, but we aimed to ensure comparable levels of β_1YFP_N by using the CHO-β_1YFP_N cell line to transfect into. We then examined the cimaterol response in these cells in the total [^{3}H]cAMP accumulation assay (Figure 7.19). The pEC_{50} of cimaterol was 7.66 ± 0.21 (n=3) in cells expressing two wild-type β_1-adrenoceptor constructs ($\beta_1YFP_N/\beta_1YFP_C$), which was not significantly different to the value derived in cells expressing one native and one non-ligand binding receptor mutant ($\beta_1YFP_N/\beta_{1D138A}YFP_C$; pEC_{50} 7.28 ± 0.06, n=3) and untransfected CHO-β_1YFP_N cells ($P < 0.05$, one-way ANOVA followed by Bonferroni's post hoc test). The maximum CGP 12177 response (E_{MAX}) was determined in CHO-β_1YFP_N cells transfected with wild-type β_1YFP_C and mutant $\beta_{1D138A}YFP_C$ receptor constructs by measuring the [^{3}H]cAMP accumulation in response to 10 µM CGP 12177 and comparing it to the response measured to 10 µM cimaterol in the same cells (Table 7.4). The derived E_{MAX} values for CGP 12177 were similar in CHO-β_1YFP_N cells transfected with β_1YFP_C and $\beta_{1D138A}YFP_C$ ($P > 0.05$, one-way ANOVA followed by Bonferroni's post hoc test). These preliminary data may suggest that the maximum response elicited by CGP 12177 is unaffected by the presence of a non-ligand binding protomer in β_1AR homodimers. However, CGP 12177 concentration response curves would have to be obtained to determine potential effects on its potency, and more importantly the receptor

expression levels would have to be monitored in conjunction with these functional studies. Using fluorescently labelled tags, for example, would allow the detection of each receptor promoter. In conjunction with this, the receptor population that form dimers may be measured by BiFC homodimerisation to provide an insight into the percentage of dimers of the overall receptor population in a given cell system. Only then could any observed functional changes (or lack of it) be attributed to β_1-adrenoceptor homodimerisation.

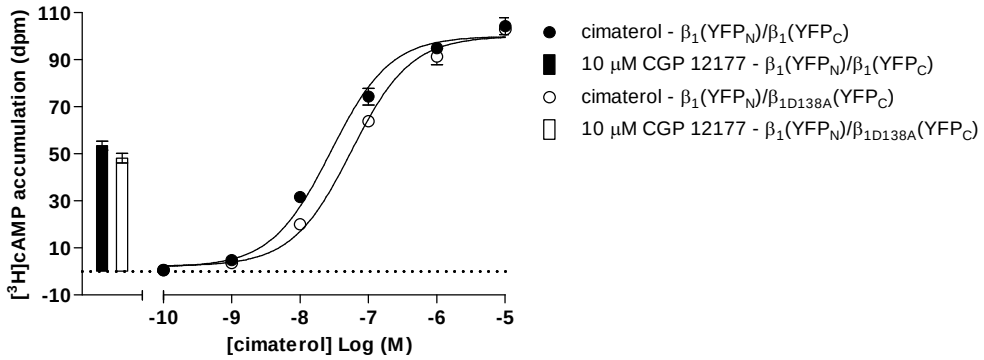

Figure 7.19 Normalised cimaterol concentration-response curves on CHO-K1 cells transiently expressing β_1YFP_N, $\beta_1YFP_N/\beta_1YFP_C$ and $\beta_1YFP_N/\beta_{1D138A}YFP_C$ constructs. Data are mean ± s.e.m. of three separate experiments in which each data point was determined in triplicates.

Table 7.4 The functional responses of cimaterol and CGP 12177 on the untagged native β_1-adrenoceptor stably expressed in CHO-CS cells (β_1) and the YFP_N-tagged native β_1AR in the absence (β_1YFP_N) and presence of YFP_C-tagged native ($\beta_1YFP_N/\beta_1YFP_C$) and mutant β_{1D138A}AR ($\beta_1YFP_N/\beta_{1D138A}YFP_C$) stably expressed in CHO-K1 cells were tested in the [^{3}H]cAMP accumulation assay. *statistical significance ($P < 0.05$) from value determined for stably expressed β_1YFP_N as determined by one-way ANOVA followed by Bonferroni's post hoc test

	cimaterol		10 µM CGP 12177	
	pEC_{50}	*n*	*E_{MAX} (% 10 µM cimaterol)*	*n*
stable expression				
β_1	7.24 ± 0.16	3	35.7 ± 2.8	3
β_1YFP_N	7.16 ± 0.14	3	34.0 ± 0.3	3
$\beta_1YFP_N/\beta_1YFP_C$	7.25 ± 0.10	3	36.3 ± 1.3	3
$\beta_1YFP_N/\beta_{1D138A}YFP_C$	7.33 ± 0.06	3	38.7 ± 0.7	3
transient expression				
$\beta_1YFP_N/\beta_1YFP_C$	7.66 ± 0.21	3	46.4 ± 3.2	3
$\beta_1YFP_N/\beta_{1D138A}YFP_C$	7.28 ± 0.05	3	47.5 ± 3.5*	3

7.4 Discussion

In this chapter, we aimed to investigate the role β_1AR homodimerisation may play in characteristic ligand binding interactions defined for the β_1-adrenoceptor. Homodimers of β_1-adrenoceptors have been reported to be transient (Calebiro *et al.*, 2013; Dorsch *et al.*, 2009) with dimeric interactions reported to last circa four seconds (Calebiro *et al.*, 2013). The short-lived nature of β_1AR homodimer interactions poses a major challenge in the investigation of a potential role of β_1-adrenoceptor homodimerisation in receptor co-operativity and function. Any pharmacological effect of β_1AR homodimerisation will be equally short-lived and thus difficult to detect. However, bimolecular fluorescence complementation (BiFC) traps dimers that have formed without affecting the rate of dimer formation (Hu *et al.*, 2003a). BiFC allows the detection of dimeric and/or higher order oligomeric receptor complexes (Vidi *et al.*, 2010) by measuring the reconstitution of two halves of a fluorescent protein that were each attached to one receptor protomer (Rose *et al.*, 2010). The reconstitution of the fluorescent protein upon receptor dimerisation is an irreversible reaction, thus 'trapping' (or constraining) formed dimers, but making it impossible to study the dynamics of receptor oligomerisation using this technique. Here, we used the irreversibility of BiFC to our advantage, locking β_1-adrenoceptors into stable dimeric complexes to allow us to investigate ligand-receptor interactions at the dimeric complex. Throughout this thesis, we have used CHO-CS cells expressing wild-type human β_1-adrenoceptors that form transient

homodimers according to Dorsch *et al.* (2009) and Calebiro *et al.* (2013). If β_1AR homodimers play a role in the ligand-binding interactions defined in this cell line, we envisioned to highlight this role in a system where β_1AR homodimers are constrained (i.e. stable) after they have spontaneously formed. This BiFC-mediated prevention of dimer dissociation will therefore increase the percentage of β_1AR homodimers of the overall receptor population, thus increasing any dimer-mediated effects on the β_1AR pharmacology. Indeed, the dissociation rate of BODIPY-TMR-CGP was enhanced 12-fold in the presence of 1 µM CGP 12177 and 1 µM propranolol compared to the dissociation rate of the fluorescent ligand in the absence of an unlabelled ligand in CHO-K1 cells that were transiently expressed with β_1YFP_N and β_1YFP_C (i.e. stable constrained homodimers). In contrast, only a 3-fold difference in dissociation rate was observed in CHO-β_1-CS cells (i.e. unconstrained dimers). Thus, a greater enhancement of the BODIPY-TMR-CGP dissociation rate was observed in cells expressing constrained dimers compared to unconstrained dimers, suggesting that the allosteric effect of unlabelled ligands on the dissociation rate of BODIPY-TMR-CGP is mediated across a β_1AR homodimer interface. However, this enhanced difference in the BY-CGP dissociation rate was mainly due to the change in the BY-CGP dissociation rate in the absence of unlabelled ligand as it was significantly slowed in cells expressing $\beta_1YFP_N/\beta_1YFP_C$ homodimers compared to transient dimers in CHO-β_1-CS cells. This suggests that the formation of β_1-adrenoceptor dimers results in a conformational change that affects the dissociation kinetics of BY-CGP at the catecholamine site to which 3 nM BY-

CGP predominantly binds. This therefore indicates distinct BY-CGP dissociation kinetics at β_1-adrenoceptor dimers and monomers. Unfortunately, we were not able to accurately determine the BY-CGP association rate, and the BY-CGP affinity, to constrained $\beta_1YFP_N/\beta_1YFP_C$ homodimers. It is important to note that we could not establish the percentage of dimers of the overall receptor population. Furthermore, the kinetic parameters determined were always a combination of constrained receptor dimers ($\beta_1YFP_N/\beta_1YFP_C$), transient receptor dimers ($\beta_1YFP_N/\beta_1YFP_N$ and $\beta_1YFP_C/\beta_1YFP_C$) and receptor monomers (β_1YFP_N and β_1YFP_C). Even though we used BiFC to specifically detect constrained receptor dimers and only analysed cells that showed clear membrane YFP fluorescence intensity, the fluorescent ligand will still have bound to transient dimers and monomers also expressed on the surface of the cells analysed. An analysis of membrane BY-CGP fluorescence intensities following a co-localisation analysis (of YFP and BY-CGP fluorescence) may have reduced influences by non-BiFC receptor populations.

Interestingly, the dissociation rates of BY-CGP in the presence of unlabelled ligands determined in cells expressing $\beta_1YFP_N/\beta_1YFP_C$ homodimers and CHO-β_1-CS cells (i.e. transient dimers) were comparable. We have already shown that the BODIPY-TMR-CGP dissociation rate in the presence of CGP 12177 and propranolol appeared to reach a "plateau" beyond which the dissociation rate could not be enhanced any further (Chapter 4). Thus, the concentration of 1 µM CGP 12177 and 1 µM propranolol may represent too high concentrations at both transient dimers and constrained wild-type dimers ($\beta_1YFP_N/\beta_1YFP_C$) to

detect a difference between the two dimeric complexes. To investigate this further, a range of CGP 12177 and propranolol concentrations would have to be tested at the constrained homodimer complexes. The concentration at the midpoint of the resulting concentration-response curve represents the K_B/α, where α is a measure of co-operativity between the two binding sites. Differences in α may point to potential effects of constraining β_1-adrenoceptors into stable homodimers.

To further test whether the effects of unlabelled ligands are mediated across a β_1-adrenoceptor homodimer interface, we performed the same kinetic perfusion experiments in cells expressing constrained β_1-adrenoceptor homodimers where one protomer contained a point mutation that abolished binding of β-adrenoceptor ligands to both, the high (site 1) and low (site 2) affinity β_1-adrenoceptor binding sites ($\beta_{1D138A}YFP_C$). Indeed, the effect seen in constrained wild-type β_1AR homodimers was reduced in wild-type/mutant β_1AR homodimers ($\beta_1YFP_N/\beta_{1D138A}YFP_C$) and reflected more closely the pharmacology observed in CHO-β_1-CS cells. Interestingly, the BY-CGP dissociation rate determined in cells expressing $\beta_1YFP_N/\beta_{1D138A}YFP_C$ homodimers was slower than that measured in CHO-β_1-CS cells, but faster than that obtained in cells expressing wild-type $\beta_1YFP_N/\beta_1YFP_C$ homodimers. This may point to an effect of the introduced mutation on the conformation of the β_1AR dimeric complex that resulted in a different BY-CGP dissociation rate. Alternatively, this intermediate dissociation rate may reflect that of a different percentage of dimers of the overall receptor population. As

described above, constraining dimers using BiFC is expected to increase the percentage of β_1AR dimers by preventing dissociation of normally transient β_1AR dimers. However, the YFP fragment-tagged β_1AR constructs were transiently transfected into CHO-K1 cells prior to each experiment and the transfection efficiency of the different constructs may not be comparable, thus resulting in different percentages of trapped $\beta_1YFP_N/\beta_1YFP_C$ and $\beta_1YFP_N/\beta_{1D138A}YFP_C$ dimers. Therefore, a less reduced BY-CGP dissociation rate in cells expressing $\beta_1YFP_N/\beta_{1D138A}YFP_C$ homodimers may be due to a lower percentage of these dimers compared to wild-type $\beta_1YFP_N/\beta_1YFP_C$ dimers expressed in CHO-K1 cells. Because 3 nM BY-CGP predominantly binds to the catecholamine site (site 1) of the β_1-adrenoceptor, the introduced mutation abolishing ligand binding to the second β_1AR site (i.e. second protomer) would not be expected to affect its dissociation rate, whereas a different percentage of dimers would do precisely that, if the dissociation kinetics of BY-CGP at β_1AR homodimers and monomers were markedly different. To further investigate this hypothesis, it would be interesting to perform the same kinetic experiments on cells expressing wild-type β_1-adrenoceptors that cannot dimerise, for example, if key residues that formed part of the structural dimer interface were mutated. Computational modelling and mutagenesis studies performed on a variety of GPCRs provide new structural insights into dimeric interfaces (Hu *et al.*, 2012; Johnston *et al.*, 2011; Wang *et al.*, 2009), and most recently the crystal structure of β_1-adrenoceptor dimers has been reported (Huang *et al.*, 2013).

It is worth noting that there are limitations to comparing the association and dissociation kinetics of 3 nM BY-CGP determined in CHO-K1 cells transiently transfected with YFP_N/YFP_C-tagged β_1-adrenoceptor constructs to stable CHO-β_1-CS cells. Apart from the transient transfection, the cells expressing the BiFC constructs undergo a 24 hour 30 °C incubation to allow the correct folding and maturation of the reconstituted fluorescent protein. The stable CHO-β_1-CS cells were not treated the same way. Furthermore, the C-terminal fluorescent protein tags used to achieve BiFC may affect β_1-adrenoceptor conformations in such a way that they affect allosteric interactions. Therefore, future experiments investigating the differences of BY-CGP kinetics at transient and constrained dimers should use transiently transfected YFP-tagged β_1-adrenoceptors as a control.

The presence of unlabelled ligands also had a reduced effect on the dissociation of 3 nM BY-CGP in cells expressing β_1YFP_N/$\beta_{1D138A}YFP_C$ homodimers compared to cells expressing β_1YFP_N/β_1YFP_C homodimers. Again, a lower percentage of constrained dimers may have resulted in a reduced effect on the BY-CGP dissociation rate. Unfortunately, we do not know the percentage of dimers expressed in CHO-K1 cells, and since different percentages of dimers may influence the results as described above, it is difficult to conclusively attribute changes in BY-CGP dissociation rates to a mutation introduced into one β_1-adrenoceptor protomer. However, upon close inspection of the BY-CGP dissociation rates in the presence of unlabelled ligands in all three cell systems (CHO-β_1-CS cells, CHO-K1 cells expressing

$\beta_1YFP_N/\beta_1YFP_C$ and $\beta_1YFP_N/\beta_{1D138A}YFP_C$ dimers), it becomes evident that the BY-CGP dissociation rates in the presence of unlabelled ligands in cells expressing the wild-type/mutant β_1AR homodimers were even slower than in CHO-β_1-CS cells, i.e. in cells where dimers were not constrained, but were transient. One explanation of this may be that the $\beta_1YFP_N/\beta_{1D138A}YFP_C$ dimers detected by BiFC do not contribute to the enhanced BY-CGP dissociation rate, as the unlabelled ligand cannot bind to the secondary site ($\beta_{1D138A}YFP_C$ protomer) to cause an enhanced off rate of BY-CGP. Instead, the enhanced off rate is facilitated by transient dimers ($\beta_1YFP_N/\beta_1YFP_N$). As mentioned above, the trace of BY-CGP fluorescence was analysed for cells that showed clear YFP fluorescence (i.e. BiFC), but these cells will also have expressed transient ligand binding dimers ($\beta_1YFP_N/\beta_1YFP_N$) and monomers ($\beta_1YFP_N$). The transient non-ligand binding dimers ($\beta_{1D138A}YFP_C/\beta_{1D138A}YFP_C$) and monomers ($\beta_{1D138A}YFP_C$) will not have been picked up by the fluorescent ligand either. If the BY-CGP dissociation rate seen in cells expressing $\beta_1YFP_N/\beta_{1D138A}YFP_C$ homodimers was due to transient $\beta_1YFP_N/\beta_1YFP_N$ homodimers, one might expect comparable off rates to those seen in CHO-β_1-CS cells. However, the percentage of β_1YFP_N monomers available to form transient dimers in cells expressing $\beta_1YFP_N/\beta_{1D138A}YFP_C$ dimers will be reduced compared to β_1AR monomers available in CHO-β_1-CS cells (unconstrained dimers). Since BiFC traps transient dimers into stable dimers, thereby increasing the percentage of dimers of the overall receptor population, it also effectively depletes ligand binding β_1YFP_N monomers, thus reducing the percentage of monomers available to form transient dimers, which results in a reduced effect of

unlabelled ligands on the BY-CGP dissociation rate. This explanation suggests that an increased proportion of $\beta_{1D138A}YFP_C$ to β_1YFP_N co-transfected into CHO-K1 would further reduce the effects of unlabelled ligands on the dissociation rate of BY-CGP as increasing amounts of non-ligand binding $\beta_{1D138A}YFP_C$ would increasingly trap more and more β_1YFP_N into stable homodimers to which unlabelled ligands cannot bind to enhance the BY-CGP off rate, and leaving fewer and fewer β_1YFP_N monomers available to form transient dimers to cause any effects on the BY-CGP dissociation rate. A similar observation of reduced effects of unlabelled ligands on the dissociation rate of a fluorescent ligand in the presence of increasing amounts of a non-ligand binding receptor was made for A_3 homodimers (May *et al.*, 2011). It is also noteworthy that 1 μM CGP 12177 enhanced the BY-CGP dissociation rate to a greater extent than 1 μM propranolol in cells expressing $\beta_1YFP_N/\beta_{1D138A}YFP_C$ dimers. This is in line with previous data from this thesis that determined a higher K_B/α (affinity of a ligand for the secondary site with a ligand bound to the first site) for CGP 12177 than for propranolol (Chapter 6, Table 6.4).

The hypothesis suggesting that the secondary β_1-adrenoceptor site is facilitated by a second β_1AR in a homodimer formation is also consistent with the conclusion drawn by Baker *et al.* (2008) following a mutagenesis study to identify key residues of site 1 and site 2 of the β_1-adrenoceptor. The results of that study suggested that the two β_1-adrenoceptor sites must be overlapping as introduced single point mutations affected ligand binding to both sites

equally (Baker *et al.*, 2008). In the dimerisation model, the two sites do not overlap, but instead they are the "same" binding site with the second orthosteric site becoming the allosteric site in a β_1AR homodimer formation. Furthermore, the kinetic data shown in this chapter do not suggest two separate binding sites in a β_1-adrenoceptor monomer. If this was the case, the same effect of unlabelled ligands on the dissociation rate of the fluorescent ligand would have been expected to be observed in dimers with a ligand binding and non-ligand binding second β_1-adrenoceptor protomer. However, we observed a clear difference in the effect of unlabelled ligands on the BODIPY-TMR-CGP dissociation rate, suggesting that the dimerisation of β_1-adrenoceptors plays an important role in the ligand-receptor interactions.

The binding studies strongly suggest a role of β_1AR homodimers in the ligand-binding interactions of β-adrenoceptor ligands at this receptor. To further investigate whether homodimerisation of the β_1-adrenoceptor also plays a role in the functional responses observed for β-adrenoceptor ligands, we performed [^{3}H]cAMP accumulation experiments in cells expressing β_1YFP_N/ β_1YFP_C constructs and β_1YFP_N/$\beta_{1D138A}YFP_C$ constructs. The co-expression of YFP_N- and YFP_C-tagged β_1AR constructs allowed reconstitution of full length YFP when the two halves of the YFP were brought into close proximity of one another through β_1AR homodimerisation. The kinetic binding studies highlighted that trapping dimers in stable conformations using BiFC caused a detectable change in dissociation rate of the fluorescent analogue of CGP 12177. Thus, we examined whether effects on the functional response of the

parent compound could be detected using the same approach (BiFC) in conjunction with the [^{3}H]cAMP accumulation assay.

First, we established that the YFP_N-tag did not appear to affect the CGP 12177 pharmacology at the β_1-adrenoceptor, as experiments carried out in CHO-β_1-CS and CHO-β_1YFP_N (stable clonal cell lines; unconstrained dimers) revealed similar CGP 12177 agonist and antagonist effects. In both cell lines CGP 12177 was a partial agonist compared to cimaterol, consistent with previous CGP 12177 data reported throughout this thesis and reports in the literature (Baker *et al.*, 2003a; Joseph *et al.*, 2004; Konkar *et al.*, 2000; Pak *et al.*, 1996).

We then generated stable cell lines expressing $\beta_1YFP_N/\beta_1YFP_C$ and $\beta_1YFP_N/\beta_{1D138A}YFP_C$ receptors. We did not investigate the level of β_1YFP_N in the clonal stable CHO-β_1YFP_N cell line, but using the same cell line to transfect the YFP_C-tagged β_1AR construct into, we attempted to ensure that the level of β_1YFP_N was comparable in all three cell lines (parent CHO-β_1YFP_N cell line and CHO-β_1YFP_N-β_1YFP_C and CHO-β_1YFP_N-$\beta_{1D138A}YFP_C$ cell lines). CGP 12177 agonist and antagonist data obtained in the absence and presence of 100 nM cimaterol revealed a reduced maximal response of CGP 12177 in CHO-β_1YFP_N-β_1YFP_C cells compared to CHO-β_1YFP_N-$\beta_{1D138A}YFP_C$ cells. This may be explained by different levels of receptor expression as submaximal responses are caused by partial agonists that occupy all available receptors to elicit their functional response. Thus, an increased receptor expression will result in an increased response to that agonist. However, the first CGP 12177 set of data obtained in CHO-β_1YFP_N-β_1YFP_C and CHO-β_1YFP_N-$\beta_{1D138A}YFP_C$ cells revealed

CGP 12177 responses greater than those caused by 100 nM cimaterol, which was different to the response seen in CHO-β_1YFP_N cells alone. A full concentration-response curve of cimaterol was not obtained at the same time as the initial CGP 12177 functional data, which made it impossible to accurately define a maximal system response and to clearly describe the CGP 12177 response observed here. A greater receptor expression level could explain the increased response in CHO-β_1YFP_N-β_1YFP_C cells, however, the same cannot be done for CHO-β_1YFP_N-$\beta_{1D138A}YFP_C$ cells, as the introduced $\beta_{1D138A}YFP_C$ receptor is non-ligand binding. Baker *et al.* (2008) observed no specific binding of [^{3}H]CGP 12177 cells expressing the D138A β_1AR and also reported no functional response to full agonists isoprenaline and cimaterol (Baker *et al.*, 2008). Whether this is due to impaired binding of these ligands to the receptor or impaired functionality of the receptor, is unclear. If the D138A β_1-adrenoceptor retained functionality, this may affect the pharmacology and functionality of the β_1AR dimer. The minimal functional GPCR unit has been described as one receptor/one G protein (Whorton *et al.*, 2007; Whorton *et al.*, 2008). Even for GPCR dimers the 2:1 stoichiometry of two receptors to one G protein is generally accepted (Damian *et al.*, 2006; Hlavackova *et al.*, 2005) although a 2:2 stoichiometry of GPCR protomers to G proteins has been described for the neuropeptide Y2 receptor (Parker *et al.*, 2008), thus making possible an amplification of the signalling response. Another explanation for the increased CGP 12177 response seen at both wild-type/wild-type and wild-type/mutant β_1AR homodimers may be higher-order oligomers.

Repeat experiments of the above described data did not confirm the initial findings, with CGP 12177 being a partial agonist compared to cimaterol in subsequent experiments. In fact, the CGP 12177 pharmacology was similar to that observed in CHO-β_1-CS and CHO-β_1YFP_N cells, suggesting that the expression of the wild-type and mutant β_1YFP_C receptor was lost over time as cells were passaged between each experiment. Cimaterol concentration-response curves that were obtained in the same cell lines in subsequent experiments to address the question of receptor expression levels revealed similar EC_{50} values, supporting the notion of unstable and reduced expression of wild-type and mutant β_1YFP_C receptor. Furthermore, imaging experiments showed that little or no YFP fluorescence, but BY-CGP binding could be detected in CHO-β_1YFP_N-β_1YFP_C and CHO-β_1YFP_N-$\beta_{1D138A}YFP_C$ cells, supporting the hypothesis that the expression of YFP_C-tagged β_1AR was very low.

The use of transiently transfected cells worked well in the kinetic binding studies, so we aimed to use a similar approach for the functional studies. Using CHO-β_1YFP_N cells that were transiently transfected with the β_1YFP_C and the $\beta_{1D138A}YFP_C$ construct. This appeared to work, as a small (but statistically insignificant) difference in cimaterol EC_{50} values was observed in CHO-β_1YFP_N cells transfected with β_1YFP_C construct, reflecting an increased receptor expression following the introduction of additional β_1-adrenoceptors. In contrast, cimaterol EC_{50} values obtained in $\beta_{1D138A}YFP_C$ transfected and untransfected CHO-β_1YFP_N cells were similar. Whether the lack of a change in the cimaterol EC_{50} between these two cell populations was due to cell surface

non-ligand binding receptors or unsuccessful transfection and/or expression of the receptor construct in these cells, is unclear. It will be difficult to determine accurate expression levels, using for example a traditional radioligand binding approach as the expressed non-ligand binding $\beta_{1D138A}YFP_C$ receptor will not be picked up using this technique. However, the YFP fragment-tagged β_1-adrenoceptors could be fused to an additional fluorescent tag at the N-terminus (e.g. SNAP-tag) that would allow the expression of each receptor protomer to be measured, in addition to monitoring their dimerisation using BiFC. This approach, in conjunction with [^{3}H]cAMP accumulation experiments should be used to examine a potential role of dimerisation in the functional β_1-adrenoceptor responses, and would have been the main focus of further studies if time had allowed. Furthermore, ligand-binding interaction of the fluorescently labelled CGP 12177 ligand with SNAP-tagged β_1-adrenoceptors could be investigated at the single molecule level using fluorescence correlation spectroscopy (FCS). FCS allows the distinction of free and bound receptor complexes based on their diffusion speed, i.e. a small low molecular weight molecule passes quicker through the 0.25 fL FCS detection volume than a membrane bound receptor (Briddon *et al.*, 2007). Using FCS in conjunction with photon counting histogram (PCH) analysis, monomeric and dimeric complexes of fluorescently labelled receptor can also be distinguished based on the detected molecular brightness per receptor species (Herrick-Davis *et al.*, 2012; Patel *et al.*, 2002). Furthermore, two-colour fluorescence cross-correlation spectroscopy (FCCS) allows the investigation of the binding of a fluorescent ligand to a receptor species that

is labelled with a different wavelength-separated fluorophore (Neugart *et al.*, 2009; Weidemann *et al.*, 2011). Thus, BODIPY-TMR-CGP binding to constrained β_1-adrenoceptor BiFC dimers could be examined at the single molecule level. The advantage of using this technique is that high expression of the receptor is not needed due to the inverse relationship between the particle (e.g. receptor) number and the detected FCS signal (Briddon *et al.*, 2007), making it feasible to use a stable (or inducible) mixed population cell line. Alternatively, the dissociation kinetic experiments performed here on constrained dimers could also be done on β_1-adrenoceptors that cannot dimerise, in order to investigate CGP 12177 ligand-binding and functional characteristics at the β_1-adrenoceptor monomer.

7.5 Conclusion

Bimolecular fluorescence complementation was successfully used to detect and constrain β_1AR homodimers that contained a wild-type or non-ligand binding D138A mutant β_1-adrenoceptor second protomer. Kinetic binding experiments revealed that unlabelled ligands enhanced the BODIPY-TMR-CGP dissociation rate in cells expressing wild-type β_1AR homodimers compared to cells expressing unconstrained (i.e. transient) dimers. Furthermore, these effects were reduced in cells expressing wild-type/mutant β_1AR homodimers, thus highlighting a role of β_1AR dimers in the ligand-binding interactions of β-adrenoceptor ligands to the β_1-adrenoceptor.

We were unable to obtain reproducible functional data in stable cell lines expressing β_1AR homodimers, but preliminary data obtained in cells transiently expressing β_1AR homodimers revealed differences in EC_{50} values of full agonist cimaterol. Future experiments will need to investigate whether this is due to differences in receptor expression levels, or in fact the introduced mutation, and thus to establish a potential role of the β_1AR homodimer in the β_1AR-mediated cellular responses and also to potentially identify the β_1AR second protomer as the second site of the β_1-adrenoceptor.

Chapter 8

General discussion and conclusion

8.1 General discussion

The endogenous β-adrenoceptor agonists adrenaline and noradrenaline bind to the endogenous (orthosteric) binding site of the β_1-adrenoceptor to cause cardiostimulation (Mutlu *et al.*, 2008). Blocking these stimulatory effects with β-blockers is a vital line of treatment in a variety of heart diseases such as hypertension and myocardial infarction (Baker *et al.*, 2011b; Poirier *et al.*, 2012; Sanz-Rosa *et al.*, 2012). β-blockers such as propranolol are antagonists that bind to the same site as the endogenous agonists, thereby preventing receptor activation. Antagonists are described to have no efficacy of their own (i.e. do not activate the receptor). However, at the β_2-adrenoceptor some β-blockers were found to exhibit small agonist actions (Baker *et al.*, 2003b). Interestingly, propranolol was found to decrease basal cAMP levels but increase SPAP levels in the CRE-mediated SPAP gene reporter assay, highlighting biased agonism of propranolol at this receptor (Baker *et al.*, 2003b). Similarly, CGP 12177 was initially described as an antagonist, but was also found to exert partial agonist effects. Interestingly, these agonist effects were elicited at much higher concentrations than those needed to inhibited catecholamine-induced receptor activation (Kaumann *et al.*, 1983; Staehelin *et al.*, 1983). Kaumann *et al.* (1983) examined the affinities of a variety of β-adrenoceptor partial agonists from their inhibitory and stimulatory effects measured in isolated feline heart tissues. The affinity values determined using the two different approaches compared well for conventional agonists (e.g. practolol), whereas a defined difference in affinity values was observed for

non-conventional agonists, such as CGP 12177 (Kaumann *et al.*, 1980; Kaumann *et al.*, 1983). A radiolabelled version of CGP 12177 was used to further investigate its pharmacology. Initial studies used isolated tissues, which express mainly β_1-adrenoceptors, but also β_2- and β_3-adrenoceptors (Kaumann *et al.*, 2008). The observed pharmacology of non-conventional agonists could not be attributed conclusively to either receptor, which led to the proposal of the existence of a fourth β-adrenoceptor (Kaumann, 1997). However, studies performed in CHO cells expressing recombinant β_1-adrenoceptors clearly showed the β_1AR alone was responsible for the pharmacology of CGP 12177 (Pak *et al.*, 1996). The high and low affinity binding sites or receptor conformations were defined, although the nature of the secondary site is still unknown. A site-directed mutagenesis study by Baker *et al.* (2008) aimed to identify key residues of each of the two β_1-adrenoceptor sites, but instead found that the mutations tested affected both sites to similar extents (Baker *et al.*, 2008). Here we used a fluorescently labelled version of CGP 12177 and fluorescence confocal microscopy in a kinetic binding approach to investigate ligand-receptor interactions at the human β_1-adrenoceptor in single living cells. Using this approach, an allosteric mode of action of CGP 12177 was revealed at this receptor.

First, we confirmed the CGP 12177 pharmacology using CHO cells expressing the human β_1-adrenoceptor and the CRE-SPAP reporter gene construct (Chapter 3). In the SPAP transcription assay, we determined that CGP 12177 inhibited cimaterol-induced responses with high affinity (circa 0.2 nM) at the

catecholamine β_1-adrenoceptor site (site 1), and exhibited partial agonist effects through a secondary β_1-adrenoceptor site (site 2) with much lower affinity (circa 26 nM). This difference in affinity values is circa 100-fold, which is consistent with reports in the literature (Baker *et al.*, 2003a; Konkar *et al.*, 2000; Pak *et al.*, 1996). A similar pharmacology was observed for the fluorescent analogue of CGP 12177, BODIPY-TMR-CGP 12177 (BY-CGP), which inhibited cimaterol-induced responses with high affinity (circa 0.6 nM) and exerted partial agonist effects with low affinity (circa 87 nM), thus also displaying a circa 100-fold difference in affinity for the two proposed β_1-adrenoceptor sites (Chapter 4).

The same trend was observed for β-adrenoceptor antagonists propranolol and CGP 20712A, as high affinity values of antagonists were determined for the catecholamine β_1-adrenoceptor site from parallel rightward shifted cimaterol concentration-response curves, and lower affinity values were derived from parallel rightward shifted CGP 12177 concentration-response curves. The low antagonist affinity values for the secondary site have caused the CGP 12177 agonist effect to be deemed “resistant” to β-blocker action, which holds true only for the concentrations of β-blockers used to inhibit agonist effects through the catecholamine site. Interestingly, the cimaterol concentration-response curves were shifted in manner consistent with competitive mechanism of action of the antagonists used, and no co-operative interactions between two binding sites were detected. This may be due to the concentrations of antagonists used to shift the cimaterol

concentration-response curves, which were all lower than the affinity of these ligands for the secondary β_1-adrenoceptor site. Higher antagonist concentrations (K_{Dsite2} concentrations and higher) may have revealed allosteric mechanisms of actions of the ligands used, by not shifting the cimaterol concentration-response curve any further right. Alternatively, a different agonist could be used to induce a response through the catecholamine site, as allosteric effects of ligands are probe-dependent, i.e. they act as an allosteric modulator for one ligand, but not another, or to a different extent (Christopoulos *et al.*, 2002). Interestingly, 10 and 30 nM CGP 12177 were not able to shift the concentration-response curve to the β-adrenoceptor agonist isoprenaline any further than 3 nM CGP 12177, but increased the basal response in a concentration-dependent manner consistent with these CGP 12177 concentrations eliciting an agonist response through the secondary β_1-adrenoceptor site (Baker *et al.*, 2002). This "bunching up" of the concentration-response curve was not seen when using cimaterol in this thesis, suggesting a probe-dependency of the CGP 12177 allosteric effects at the human β_1-adrenoceptor.

The affinity of the fluorescently labelled CGP 12177 (BY-CGP) was circa 3-fold lower at both sites compared to the affinities determined for the parent compound. With an affinity of circa 0.6 nM, BY-CGP was used in fluorescence microscopy studies to further investigate ligand-receptor interaction at the secondary β_1-adrenoceptor site. We demonstrated in confocal microscopy studies that BY-CGP allowed visualisation of β_1-adrenoceptors expressed in

CHO cells. The specific binding of BY-CGP to β_1-adrenoceptors was highlighted by co-localising BY-CGP fluorescence with fluorescently labelled SNAP-tagged β_1AR expressed in CHO cells. In addition, BY-CGP binding to native β_1-adrenoceptors was concentration-dependent, and could be displaced in a concentration-dependent manner by CGP 20712A (Chapter 4). Interestingly, the CGP 20712A displacement binding curve was shallower when displacing 20 nM BY-CGP compared to displacing 2 nM BY-CGP. Using the IX Ultra confocal plate reader in an automated higher throughput live cell fluorescence-based ligand binding assay, we further investigated this, and revealed two-phase antagonist displacement binding curves in the presence of 10, 20 and 100 nM BY-CGP in CHO-β_1-CS cells, yielding high and low IC_{50} values (Chapter 5). In addition, the proportion of the secondary phase of the displacement binding curves increased with increasing BY-CGP concentrations, which was consistent with BY-CGP binding to the secondary low affinity β_1-adrenoceptor site. Crucially, two-phase displacement binding curves were not obtained in CHO-β_2-CS cells, as only one binding site has been described for the β_2-adrenoceptor (Rasmussen *et al.*, 2007). The displacement binding curves were shifted rightwards with increasing BY-CGP concentrations, and when log IC_{50} values determined for each of the two β_1-adrenoceptor sites were plotted against the log of the BY-CGP concentrations used, the obtained slopes were shallow (i.e. not slopes of 1.0), which has been described as a characteristic of allosteric modulators (Christopoulos *et al.*, 2002; Hulme *et al.*, 2010). However, shallow slopes were also seen when correlating antagonist IC_{50} values obtained in CHO-β_2-CS cells with BY-CGP concentrations. This was

likely due to non-equilibrium conditions in the competition binding assay. BY-CGP has been described as a long acting partial agonist at the human β_2-adrenoceptor (Baker *et al.*, 2003d), and subsequent BY-CGP kinetic experiments performed in CHO-β_1-CS cells revealed a slow dissociation rate of BY-CGP at the human β_1-adrenoceptor (Chapter 6), indicating that equilibrium conditions could not have been achieved within a 1 hour incubation time for BY-CGP.

To further investigate the ligand-receptor interactions at the human β_1-adrenoceptor, we performed kinetic binding experiments using BY-CGP and CHO-β_1-CS cells. The confocal perfusion system allowed visualisation of BY-CGP binding to CHO-β_1-CS cells in real time, and uniquely, allowed the determination of BY-CGP dissociation rates under infinite dilution conditions (May *et al.*, 2010a). This allowed the comparison of BY-CGP dissociation rates in the absence and presence of unlabelled ligands. The dissociation rate of 3 nM BY-CGP was enhanced in the presence of increasing concentrations of unlabelled CGP 12177 and propranolol, and these effects of CGP 12177 and propranolol on the BY-CGP dissociation rate were saturable, suggesting an allosteric mechanism of action at the β_1-adrenoceptor. Using a kinetic binding approach is a very sensitive way to detect allosteric modulators, as allosteric effects may not be apparent in equilibrium binding assays (Christopoulos *et al.*, 2002). The BY-CGP dissociation rates in the presence of increasing concentrations of CGP 12177 and propranolol were plotted against the CGP 12177 and propranolol concentrations used, and the fitted curve revealed the

KB/α at the midpoint of these curves. The KB/α represents the affinity of the unlabelled ligand for the allosteric site (site 2) with a ligand bound to the orthosteric site (site 1), and this value determined for CGP 12177 and propranolol compared well to the affinity value of both ligands determined in the SPAP transcription assay. This is not altogether unexpected, as ligand-receptor interactions at the secondary site were always determined with a ligand bound to site 1, due to the ligands displaying higher affinity for the orthosteric site than the allosteric site. This suggests that the affinity for the secondary site may be quite different in the absence of a ligand bound to site 1. The co-operativity factor describing the co-operative interaction between the two receptor sites cannot be determined without knowing the affinity for the secondary site at the unoccupied receptor. The effects of unlabelled ligands on the BY-CGP dissociation rates clearly demonstrated allosteric interactions; however, these may not necessarily lead to altered affinities of ligands at equilibrium. This is the case if the affinity of unlabelled ligands for the occupied receptor is the same as for the unoccupied receptor, thus resulting in a co-operativity factor of 1 (Christopoulos *et al.*, 2002).

Our preliminary data indicated that the allosteric interactions were mediated across a β_1-adrenoceptor homodimer interface (Chapter 7), where the secondary binding site is facilitated by a second β_1-adrenoceptor orthosteric site that becomes the allosteric site upon dimerisation. Thus, the secondary site "becomes" a low affinity site either as a result of conformational changes that occur during dimerisation, or as a result of a ligand binding to one β_1-

adrenoceptor site in the dimer (i.e. through allosteric interactions). In order to better understand the interactions between the protomers of the dimer and ligands binding to the β_1-adrenoceptor, we would need to determine affinity values of ligands for the monomeric β_1-adrenoceptor as well as the dimer. The β_1-adrenoceptor is reported to form transient homodimers (Calebiro *et al.*, 2013; Dorsch *et al.*, 2009), which means that affinity values of ligands determined in this thesis reflect a combination of the affinity to the dimeric and the monomeric β_1-adrenoceptor. That the affinities are likely different for these two receptor conformations was suggested by the BY-CGP dissociation rate obtained in cells in which β_1-adrenoceptor dimers that spontaneously formed were trapped in stable dimers by bimolecular fluorescence complementation (BiFC). In these cells the BY-CGP dissociation rate was significantly slower compared to off rate determined in CHO-β_1-CS cells (were receptors form transient dimers). This also highlights that the formation of homodimers induces conformational changes within the receptor complex that affect the BY-CGP affinity at the receptor.

The reciprocal nature of allosteric interactions between two ligands means that kinetic binding experiments using a fluorescently labelled propranolol ligand to measure dissociation rates in the absence and presence of unlabelled CGP 12177 should confirm the data presented here. We have in fact tested a fluorescent propranolol derivative in this thesis, but were unable to use it in kinetic binding experiments due to high non-specific binding levels (Chapter 6). As such, using a different fluorescent propranolol derivative

would be an important next experiment to validate the allosteric interactions reported in this thesis. Furthermore, the next experiments should address the concentration-dependency of the effect observed when cotransfecting wild-type and mutant non-ligand binding β_1-adrenoceptor constructs. Increasing concentrations of the non-ligand binding protomer would be expected to increasingly displace wild-type β_1-adrenoceptors as the second protomer in β_1-adrenoceptor homodimers, as was observed for the adenosine A_3 receptor (May *et al.*, 2011). This would demonstrate a clear role of β_1-adrenoceptor homodimers in the receptor-ligand interactions, where homodimerisation affects the dissociation rate of the ligand bound to the high affinity catecholamine site of the β_1-adrenoceptor. We observed that β_1-adrenoceptor homodimerisation slowed the dissociation of fluorescently labeled CGP 12177, thus increasing its duration of action at the receptor. It would be interesting to see whether the same was true for the endogenous β-adrenoceptor ligands in recombinant cell systems as well as primary cardiomyocytes, as this might highlight that β_1-adrenoceptor homodimerisation contributes to prolonged receptor-ligand interactions, and thus a more sustained cellular response. The transient nature of β_1-adrenoceptor homodimers may therefore represent a means of fine-tuning cardiomyocyte contraction responses upon agonist stimulation. Agonist treatment alone was reported not to affect the oligomerisation state of the β_1-adrenoceptor, although this was so far only investigated for isoprenaline and using a recombinant cell line (Calebiro *et al.*, 2013). Nevertheless, the potential of increasing the β_1-adrenoceptor homodimerisation state in

cardiomyocytes may present an interesting future therapeutic target in the treatment of cardiac conditions in which the cardiac output is too low, such as bradycardia or hypotension.

8.2 General conclusion

The investigation of dissociation rates of a labelled ligand under infinite dilution in the absence of excess concentrations of an unlabelled competitor ligand is a very powerful and sensitive tool to detect allosteric modulators that affect the dissociation rate of the labelled ligand. Using this approach in conjunction with a fluorescently labelled CGP 12177 and confocal microscopy, we have shown for the first time an allosteric mechanism of action for CGP 12177 at the human β_1-adrenoceptor. This clearly distinguishes two separate β_1-adrenoceptor binding sites, which preliminary data suggest are facilitated by two orthosteric β_1-adrenoceptor sites in a β_1-adrenoceptor homodimer. We have also shown that the dissociation rate of the fluorescent CGP 12177 analogue was slower when measured in a receptor population that contains a higher percentage of β_1-adrenoceptor homodimers, suggesting a role of β_1-adrenoceptor homodimers in the ligand-binding interactions at this receptor. The co-operativity between the two receptor sites in cellular responses will now have to be investigated, which may reveal the nature of the agonist effect observed for non-conventional β-adrenoceptor agonists at the human β_1-adrenoceptor.

Chapter 9

Appendices and references

Appendix I – supplementary data

S1 Comparison of signal DNA sequence to 5-HT3A DNA sequence

The query sequence was used in the NCBI BLAST program with the settings such to find a match against any nucleotide sequence. The best match was found against the 5-HT3A sequence.

Query sequence	signal DNA sequence from above (S2) sequence
Subject sequence	5-HT3A DNA sequence (accession number AY605711)

```
gb|AY605711.1| Mus musculus serotonin-gated ion channel subunit
A short splice
variant (Htr3a) mRNA, complete cds, alternatively spliced
Length=1452

GENE ID: 15561 Htr3a | 5-hydroxytryptamine (serotonin) receptor
3A
[Mus musculus]

Score =  139 bits (75),  Expect = 2e-30
Identities = 75/75 (100%), Gaps = 0/75 (0%)
Strand=Plus/Plus

Query  1   ATGCGGCTCTGCATCCCGCAGGTGCTGTTGGCCTTGTTCCTTTCCATGCTGACAGGGCCG  60
           ||||||||||||||||||||||||||||||||||||||||||||||||||||||||||||
Sbjct  1   ATGCGGCTCTGCATCCCGCAGGTGCTGTTGGCCTTGTTCCTTTCCATGCTGACAGGGCCG  60

Query  61  GGAGAAGGCAGCCGG  75
           |||||||||||||||
Sbjct  61  GGAGAAGGCAGCCGG  75
```

S2 DNA and protein sequence of the complete SNAP-tagged β_1AR fusion protein

	start and end position of DNA sequence (bases)	DNA sequence length (bases)	Protein sequence length (residues)
signal sequence	22 – 105	84	28
SNAP-tag sequence	106 – 654	549	183
β_1AR sequence	655 – 2085	1431	477
fusion protein sequence	22 – 2085	2064	688

SNAP-tagged β_1-adrenoceptor fusion protein DNA sequence

```
1       CTTAAGCTTGGTACCGCCACCATGCGGCTCTGCATCCCGCAGGTGCTGTTGGCCTTGTTC
61      CTTTCCATGCTGACAGGGCCGGGAGAAGGCAGCCGGAAGCTTACCCTGGACAAAGACTGC
121     GAAATGAAGCGCACCACCCTGGATAGCCCTCTGGGCAAGCTGGAACTGTCTGGGTGCGAA
181     CAGGGCCTGCACGAGATCAAGCTGCTGGGCAAAGGAACATCTGCCGCCGACGCCGTGGAA
241     GTGCCTGCCCCAGCCGCCGTGCTGGGCGGACCAGAGCCACTGATGCAGGCCACCGCCTGG
301     CTCAACGCCTACTTTCACCAGCCTGAGGCCATCGAGGAGTTCCCTGTGCCAGCCCTGCAC
361     CACCCAGTGTTCCAGCAGGAGAGCTTTACCCGCCAGGTGCTGTGGAAACTGCTGAAAGTG
421     GTGAAGTTCGGAGAGGTCATCAGCTACCAGCAGCTGGCCGCCCTGGCCGGCAATCCCGCC
481     GCCACCGCCGCCGTGAAAACCGCCCTGAGCGGAAATCCCGTGCCCATTCTGATCCCCTGC
541     CACCGGGTGGTGTCTAGCTCTGGCGCCGTGGGGGGCTACGAGGGCGGGCTCGCCGTGAAA
601     GAGTGGCTGCTGGCCCACGAGGGCCACAGACTGGGCAAGCCTGGGCTGGGATCCCTGGGC
661     GCGGGGGTGCTCGTCCTGGGCGCCTCCGAGCCCGGTAACCTGTCGTCGGCCGCACCGCTC
721     CCCGACGGCGCGGCCACCGCGGCGCGGCTGCTGGTGCCCGCGTCGCCGCCCGCCTCGTTG
781     CTGCCTCCCGCCAGCGAAAGCCCCGAGCCGCTGTCTCAGCAGTGGACAGCGGGCATGGGT
841     CTGCTGATGGCGCTCATCGTGCTGCTCATCGTGGCGGGCAATGTGCTGGTGATCGTGGCC
901     ATCGCCAAGACGCCGCGGCTGCAGACGCTCACCAACCTCTTCATCATGTCCCTGGCCAGC
961     GCCGACCTGGTCATGGGGCTGCTGGTGGTGCCGTTCGGGGCCACCATCGTGGTGTGGGGC
1021    CGCTGGGAGTACGGCTCCTTCTTCTGCGAGCTGTGGACCTCAGTGGACGTGCTGTGCGTG
1081    ACGGCCAGCATCGAGACCCTGTGTGTCATTGCCCTGGACCGCTACCTCGCCATCACCTCG
1141    CCCTTCCGCTACCAGAGCCTGCTGACGCGCGCGCGGGCGCGGGGCCTCGTGTGCACCGTG
1201    TGGGCCATCTCGGCCCTGGTGTCCTTCCTGCCCATCCTCATGCACTGGTGGCGGGCGGAG
1261    AGCGACGAGGCGCGCCGCTGCTACAACGACCCCAAGTGCTGCGACTTCGTCACCAACCGG
1321    GCCTACGCCATCGCCTCGTCCGTAGTCTCCTTCTACGTGCCCCTGTGCATCATGGCCTTC
1381    GTGTACCTGCGGGTGTTCCGCGAGGCCCAGAAGCAGGTGAAGAAGATCGACAGCTGCGAG
1441    CGCCGTTTCCTCGGCGGCCCAGCGCGGCCGCCCTCGCCCTCGCCCTCGCCCGTCCCCGCG
1501    CCCGCGCCGCCGCCCGGACCCCCGCGCCCCGCCGCCGCCGCCGCCACCGCCCCGCTGGCC
1561    AACGGGCGTGCGGGTAAGCGGCGGCCCTCGCGCCTCGTGGCCCTGCGCGAGCAGAAGGCG
1621    CTCAAGACGCTGGGCATCATCATGGGCGTCTTCACGCTCTGCTGGCTGCCCTTCTTCCTG
1681    GCCAACGTGGTGAAGGCCTTCCACCGCGAGCTGGTGCCCGACCGCCTCTTCGTCTTCTTC
1741    AACTGGCTGGGCTACGCCAACTCGGCCTTCAACCCCATCATCTACTGCCGCAGCCCCGAC
1801    TTCCGCAAGGCCTTCCAGGGACTGCTCTGCTGCGCGCGCAGGGCTGCCCGCCGGCGCCAC
1861    GCGACCCACGGAGACCGGCCGCGCGCCTCGGGCTGTCTGGCCCGGCCCGGACCCCCGCCA
1921    TCGCCCGGGGCCGCCTCGGACGACGACGACGACGATGTCGTCGGGGCCACGCCGCCCGCG
1981    CGCCTGCTGGAGCCCTGGGCCGGCTGCAACGGCGGGGCGGCGGCGGACAGCGACTCGAGC
2041    CTGGACGAGCCGTGCCGCCCCGGCTTCGCCTCGGAATCCAAGGTGTAGGAATTCTGCAGA
```

The start codons of the three separate components of the fusion protein are highlighted in grey, including the mutated start codons (ATG → CTG) which allow continuous transcription of the fusion protein. The stop codon is also highlighted in grey and marks the end of the fusion protein. Underlined sequences are restriction enzyme sites recognised by *Kpn*I (GGTACC), *BamH*I (GGATCC)and *EcoR*I (GAATTC).

The sequence before (<22bp) and after (>2088bp) is the sequence of the pcDNA3.1(Neo+) plasmid vector.

SNAP-tagged β_1-adrenoceptor fusion protein amino acid sequence

LKLGTATMRLCIPQVLLALFLSMLTGPGEGSRKLTLDKDCEMKRTTLDSPLGKLELS
GCEQGLHEIKLLGKGTSAADAVEVPAPAAVLGGPEPLMQATAWLNAYFHQPEAIE
EFPVPALHHPVFQQESFTRQVLWKLLKVVKFGEVISYQQLAALAGNPAATAAVKT
ALSGNPVPILIPCHRVVSSSGAVGGYEGGLAVKEWLLAHEGHRLGKPGLGSLGAG
VLVLGASEPGNLSSAAPLPDGAATAARLLVPASPPASLLPPASESPEPLSQQWTAG
MGLLMALIVLLIVAGNVLVIVAIAKTPRLQTLTNLFIMSLASADLVMGLLVVPFGAT
IVVWGRWEYGSFFCELWTSVDVLCVTASIETLCVIALDRYLAITSPFRYQSLLTRAR
ARGLVCTVWAISALVSFLPILMHWWRAESDEARRCYNDPKCCDFVTNRAYAIASS
VVSFYVPLCIMAFVYLRVFREAQKQVKKIDSCERRFLGGPARPPSPSPSPVPAPAP
PPGPPRPAAAAATAPLANGRAGKRRPSRLVALREQKALKTLGIIMGVFTLCWLPFF
LANVVKAFHRELVPDRLFVFFNWLGYANSAFNPIIYCRSPDFRKAFQGLLCCARRA
ARRRHATHGDRPRASGCLARPGPPPSPGAASDDDDDDVVGATPPARLLEPWAGC
NGGAAADSDSSLDEPCRPGFASESKVStopEFCR

The start codons of the three separate components of the fusion protein are highlighted in grey as well as the stop codon of the fusion protein.

S3 CHO-ssβ_1-CS clonal cell lines that show no expression of SNAP-tagged β_1-adrenoceptors following BG-488 labelling Transmitted light and confocal images of CHO-ssβ_1-CS clones are shown. Fluorescence of BG-488 (1 µM) labelled SNAP-tagged β_1-adrenoceptors was measured using 488 nm excitation and a 505 nm long-pass emission filter using the Zeiss LSM710 confocal microscope. Scale bars = 50 µm.

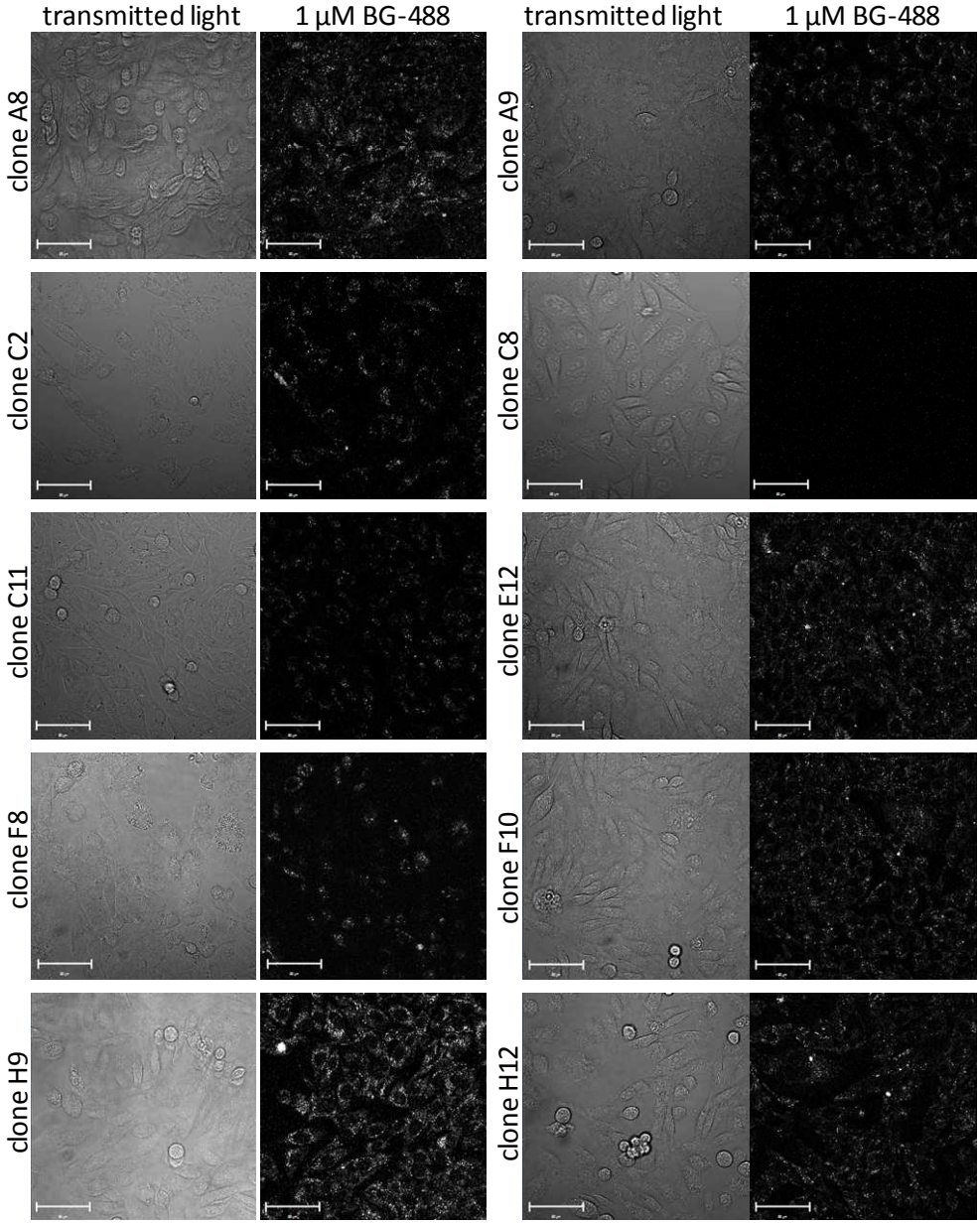

S4 Expression of SNAP-tagged β_1-adrenoceptors in CHO-ssβ_1-CS clonal cell lines following BG-488 labelling Transmitted light and confocal images of CHO-ssβ_1-CS clones are shown. Fluorescence of BG-488 (1 µM) labelled SNAP-tagged β_1-adrenoceptors was measured using 488 nm excitation and a 505 nm long-pass emission filter using the Zeiss LSM710 confocal microscope. Scale bars = 50 µm.

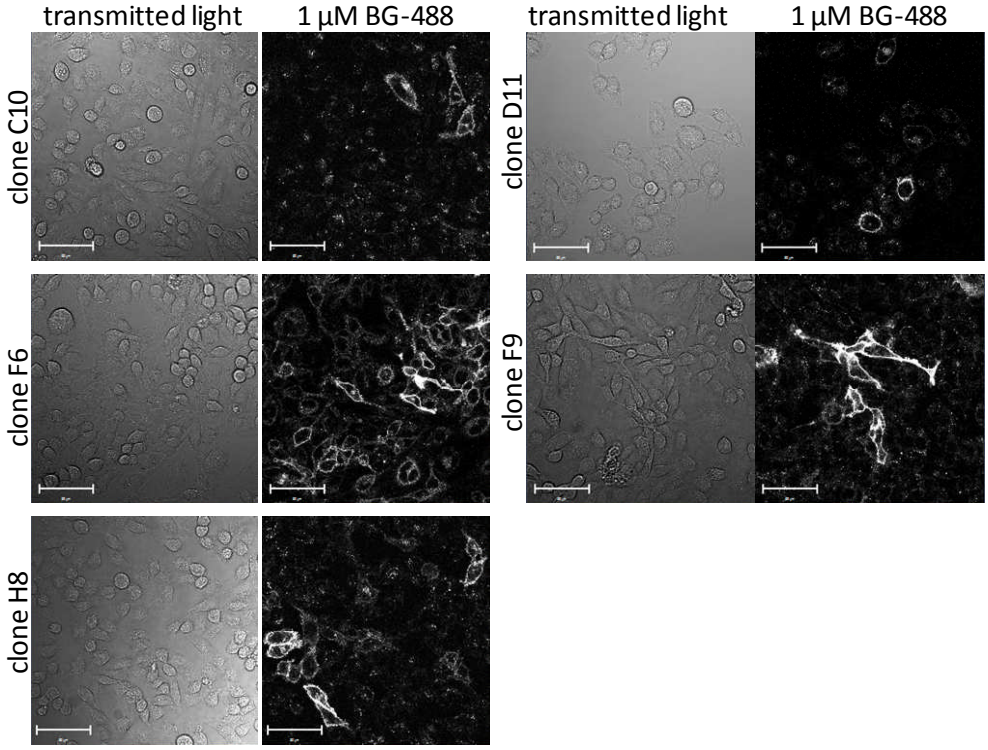

S5 Comparison of SNAP-tag amino acid sequence to human methylated-DNA-protein-cysteine methyltransferase (MGMT) amino acid sequence

The NCBI BLAST program was used for this alignment.

Query sequence	SNAP-tag amino acid sequence from above (S2) sequence
Subject sequence	MGMT amino acid sequence (accession number NP_002403)

```
Score =   340 bits (873), Expect = 8e-124, Method:
Compositional matrix adjust.
Identities = 167/179 (93%), Positives = 169/179 (94%), Gaps =
0/179 (0%)

Query  1    LDKDCEMKRTTLDSPLGKLELSGCEQGLHEIKLLGKGTSAADAVEVPAPAAVLGGPEPLM  60
            +DKDCEMKRTTLDSPLGKLELSGCEQGLHEIKLLGKGTSAADAVEVPAPAAVLGGPEPLM
Sbjct  32   MDKDCEMKRTTLDSPLGKLELSGCEQGLHEIKLLGKGTSAADAVEVPAPAAVLGGPEPLM  91

Query  61   QATAWLNAYFHQPEAIEEFPVPALHHPVFQQESFTRQVLWKLLKVVKFGEVISYQQLAAL  120
            Q TAWLNAYFHQPEAIEEFPVPALHHPVFQQESFTRQVLWKLLKVVKFGEVISYQQLAAL
Sbjct  92   QCTAWLNAYFHQPEAIEEFPVPALHHPVFQQESFTRQVLWKLLKVVKFGEVISYQQLAAL  151

Query  121  AGNPAATAAVKTALSGNPVPILIPCHRVVSSSGAVGGYEGGLAVKEWLLAHEGHRLGKP  179
            AGNP A  AV  A+ GNPVPILIPCHRVV SSGAVG Y GGLAVKEWLLAHEGHRLGKP
Sbjct  152  AGNPKAARAVGGAMRGNPVPILIPCHRVVCSSGAVGNYSGGLAVKEWLLAHEGHRLGKP  210
```

The active site of the human alkylguanine alkyltransferase (hAGT) is highlighted in grey (Pegg, 2011) and is unaltered in the SNAP-tag. The hAGT protein was truncated to reduce the size of the engineered SNAP-tag. The mutations were introduced to increase enzyme activity compare to wild-type hAGT and to decrease affinity towards double-stranded DNA (Juillerat *et al.*, 2003, 2005), thus enhancing specificity of protein labelling.

S6 Affinity of BODIPY-TMR-CGP 12177 (BY-CGP) at the SNAP-tagged β_1-adrenceptor

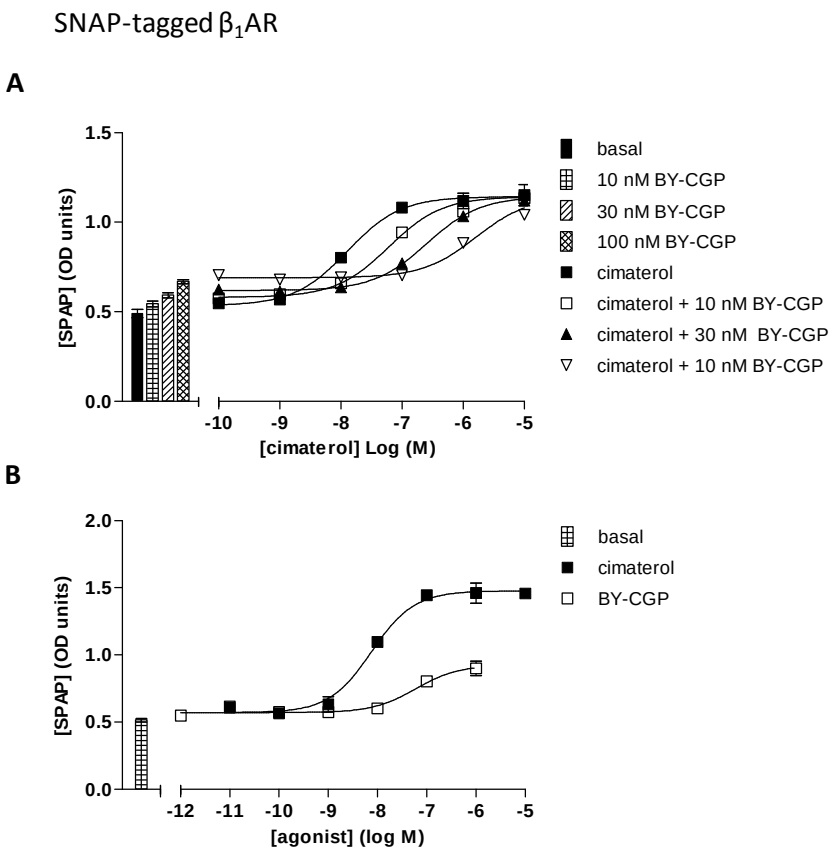

A, SPAP secretion of cimaterol in the absence and presence of increasing concentrations of BY-CGP. Bars show basal SPAP secretion from unstimulated cells and that in response to 10, 30 and 100 nM BY-CGP. **B**, SPAP secretion of increasing concentrations of cimaterol and BY-CGP alone. Bar shows basal SPAP secretion from unstimulated cells. Data points are mean ± s.e.m. of triplicate determinations from a single experiments and are representative of a total of A, five and B, five separate experiments. From these data the log affinity values of BY-CGP were determined to be 8.99 ± 0.08 (n=5) at site 1 and 7.11 ± 0.09 (n=5) at site 2 of the SNAP-tagged β_1-adrenoceptor.

S7 Affinity of BODIPY630/650-S-PEG8-propranolol (BY-PROP) at the SNAP-tagged β_1-adrenceptor

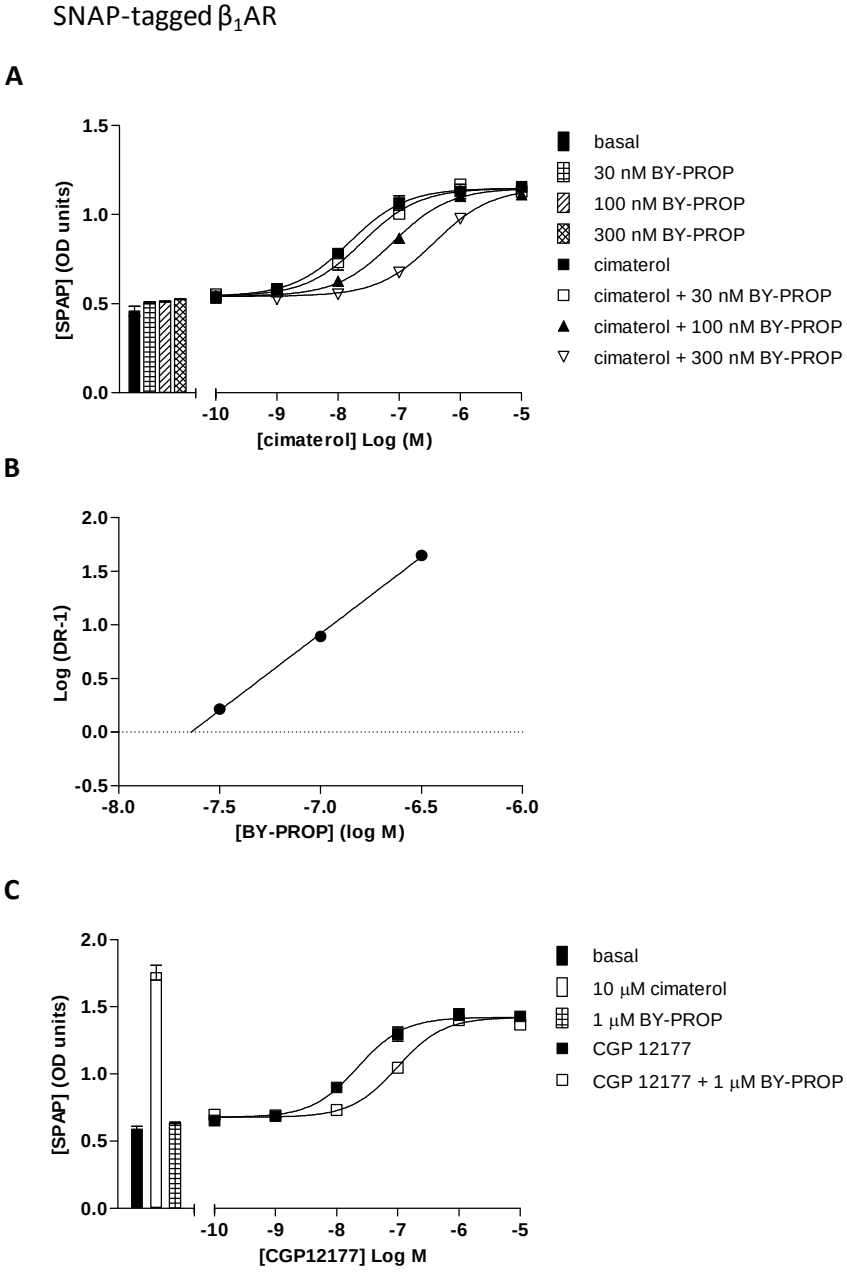

SPAP secretion of **A**, cimaterol and **C**, CGP 12177 in the absence and presence of increasing concentrations of BY-PROP. Bars show basal SPAP secretion from unstimulated cells and that in response to **A**, 30, 100 and 300 nM and **C**, 1 μM BY-PROP. Data points are mean ± s.e.m. of triplicate determinations from a single experiments and are representative of a total of A, six and C, four separate experiments. **B**, Schild plot of data shown in A (slope 1.43, R^2 1.00). From these data the log affinity values of BY-PROP were determined to be 7.45 ± 0.06 (n=6) with a Schild slope of 1.43 ± 0.05 (n=6), and 6.44 ± 0.10 (n=4) at site 2 of the SNAP-tagged β_1-adrenoceptor.

S8 Comparison of perfusion data obtained using the Zeiss LSM710 and the Zeiss LSM510 confocal microscope

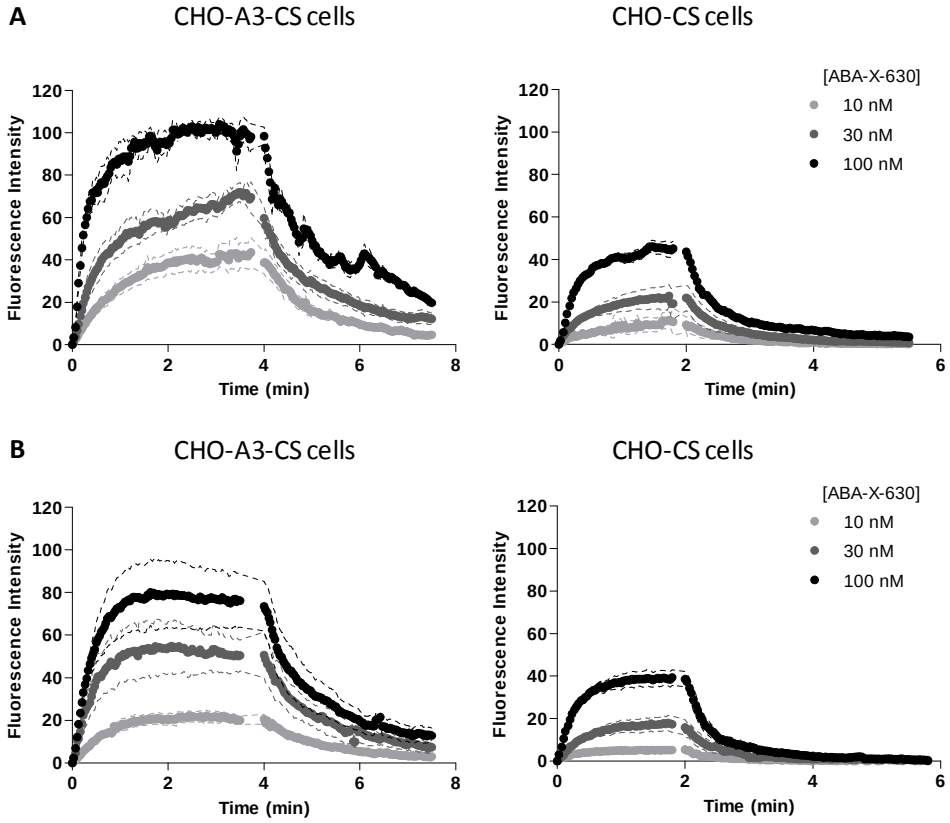

Data shows association and dissociation of 10, 30 and 100 nM ABA-X-630 at CHO-A3-CS and CHO-CS cells using the Zeiss **A**, LSM710 and **B**, LSM510 confocal perfusion system. Regions of interest were drawn around the membranes of ten cells for each perfusion slide and the ABA-X-630 fluorescence intensities plotted against time. Data are mean ± s.e.m of 4-6 separate perfusion slides obtained on three separate experimental days. The kinetic parameters of ABA-X-630 binding to these cells are summarised and compared in the table below.

ABA-X-BY630	k_{onobs}	$k_{off(fast)}$	$k_{off(slow)}$	k_{on}	pK_D	n
	min^{-1}	min^{-1}	min^{-1}	$x10^7 M^{-1} min^{-1}$	M^{-1}	
LSM710 system						
CHO-CS						
10 nM	N/A	N/A				
30 nM	2.20 ± 0.39	2.20 ± 0.28				4
100 nM	3.16 ± 0.42	2.18 ± 0.19				6
CHO-A3-CS						
10 nM	1.14 ± 0.20	2.19	0.65 ± 0.05	4.92 ± 1.61	7.81 ± 0.09	5
30 nM	1.45 ± 0.25	2.19	0.38 ± 0.06	3.58 ± 0.94	7.96 ± 0.17	6
100 nM	2.53 ± 0.33	2.19	0.34 ± 0.06	2.19 ± 0.29	7.82 ± 0.06	4
LSM510 system						
CHO-CS						
10 nM	N/A	N/A				
30 nM	2.66 ± 0.49	2.34 ± 0.32				4
100 nM	3.63 ± 0.57	2.25 ± 0.22				4
CHO-A3-CS						
10 nM	1.53 ± 0.16	2.30	0.53 ± 0.06	10.04 ± 1.74	8.27 ± 0.10	4
30 nM	2.25 ± 0.33	2.30	0.54 ± 0.06	5.71 ± 0.95	8.01 ± 0.07	4
100 nM	2.51 ± 0.34	2.30	0.38 ± 0.04	2.14 ± 0.36	7.74 ± 0.10	4
May *et al*. (2010)						
CHO-K1						
10 nM	-	-				
30 nM	3.84	3.68				
100 nM	4.65	3.95				
CHO-A3						
10 nM	0.89	-	0.51	3.79	7.83	
30 nM	1.82	3.81	0.40	4.74	7.94	
100 nM	2.53	3.81	0.43	2.10	7.73	

Summary of association and dissociation data obtained in CHO cells either expressing the A3 receptor and in untransfected CHO cells. Data are mean ± s.e.m of (n) number of separate perfusion slide preparations and are compared to data in the literature (May *et al.*, 2010).

S9 DNA and protein sequence of the complete YFP-tagged native β_1AR fusion protein

	start and end position of DNA sequence (bases)	DNA sequence length (bases)	Protein sequence length (residues)
β_1AR sequence	1-1431	1431	477
linker sequence	1432-1458	27	9
eYFP sequence	1459-2175	717	239
fusion protein sequence	1-2175	2175	725

YFP-tagged β_1-adrenoceptor fusion protein DNA sequence

```
1       ATGGGCGCGGGGGTGCTCGTCCTGGGCGCCTCCGAGCCCGGTAACCTGTCGTCGGCCGCA
61      CCGCTCCCCGACGGCGCGGCCACCGCGGCGCGGCTGCTGGTGCCCGCGTCGCCGCCCGCC
121     TCGTTGCTGCCTCCCGCCAGCGAAAGCCCCGAGCCGCTGTCTCAGCAGTGGACAGCGGGC
181     ATGGGTCTGCTGATGGCGCTCATCGTGCTGCTCATCGTGGCGGGCAATGTGCTGGTGATC
241     GTGGCCATCGCCAAGACGCCGCGGCTGCAGACGCTCACCAACCTCTTCATCATGTCCCTG
301     GCCAGCGCCGACCTGGTCATGGGGCTGCTGGTGGTGCCGTTCGGGGCCACCATCGTGGTG
361     TGGGGCCGCTGGGAGTACGGCTCCTTCTTCTGCGAGCTGTGGACCTCAGTGGACGTGCTG
421     TGCGTGACGGCCAGCATCGAGACCCTGTGTGTCATTGCCCTGGACCGCTACCTCGCCATC
481     ACCTCGCCCTTCCGCTACCAGAGCCTGCTGACGCGCGCGCGGGCGCGGGGCCTCGTGTGC
541     ACCGTGTGGGCCATCTCGGCCCTGGTGTCCTTCCTGCCCATCCTCATGCACTGGTGGCGG
601     GCGGAGAGCGACGAGGCGCGCCGCTGCTACAACGACCCCAAGTGCTGCGACTTCGTCACC
661     AACCGGGCCTACGCCATCGCCTCGTCCGTAGTCTCCTTCTACGTGCCCCTGTGCATCATG
721     GCCTTCGTGTACCTGCGGGTGTTCCGCGAGGCCCAGAAGCAGGTGAAGAAGATCGACAGC
781     TGCGAGCGCCGTTTCCTCGGCGGCCCAGCGCGGCCGCCCTCGCCCTCGCCCTCGCCCGTC
841     CCCGCGCCCGCGCCGCCGCCCGGACCCCCGCGCCCCGCCGCCGCCGCCGCCACCGCCCCG
901     CTGGCCAACGGGCGTGCGGGTAAGCGGCGGCCCTCGCGCCTCGTGGCCCTGCGCGAGCAG
961     AAGGCGCTCAAGACGCTGGGCATCATCATGGGCGTCTTCACGCTCTGCTGGCTGCCCTTC
1021    TTCCTGGCCAACGTGGTGAAGGCCTTCCACCGCGAGCTGGTGCCCGACCGCCTCTTCGTC
1081    TTCTTCAACTGGCTGGGCTACGCCAACTCGGCCTTCAACCCCATCATCTACTGCCGCAGC
1141    CCCGACTTCCGCAAGGCCTTCCAGGGACTGCTCTGCTGCGCGCGCAGGGCTGCCCGCCGG
1201    CGCCACGCGACCCACGGAGACCGGCCGCGCGCCTCGGGCTGTCTGGCCCGGCCCGGACCC
1261    CCGCCATCGCCCGGGGCCGCCTCGGACGACGACGACGACGATGTCGTCGGGGCCACGCCG
1321    CCCGCGCGCCTGCTGGAGCCCTGGGCCGGCTGCAACGGCGGGGCGGCGGCGGACAGCGAC
1381    TCCAGCCTGGACGAGCCGTGCCGCCCCGGCTTCGCCTCGGAATCCAAGGTGGGCTCGAGG
1441    GATCCACCGGTCGCCACCCTGGTGAGCAAGGGCGAGGAGCTGTTCACCGGGGTGGTGCCC
1501    ATCCTGGTCGAGCTGGACGGCGACGTAAACGGCCACAAGTTCAGCGTGTCCGGCGAGGGC
1561    GAGGGCGATGCCACCTACGGCAAGCTGACCCTGAAGTTCATCTGCACCACCGGCAAGCTG
1621    CCCGTGCCCTGGCCCACCCTCGTGACCACCTTCGGCTACGGCCTGCAGTGCTTCGCCCGC
1681    TACCCCGACCACATGAAGCAGCACGACTTCTTCAAGTCCGCCATGCCCGAAGGCTACGTC
1741    CAGGAGCGCACCATCTTCTTCAAGGACGACGGCAACTACAAGACCCGCGCCGAGGTGAAG
1801    TTCGAGGGCGACACCCTGGTGAACCGCATCGAGCTGAAGGGCATCGACTTCAAGGAGGAC
1861    GGCAACATCCTGGGGCACAAGCTGGAGTACAACTACAACAGCCACAACGTCTATATCATG
1921    GCCGACAAGCAGAAGAACGGCATCAAGGTGAACTTCAAGATCCGCCACAACATCGAGGAC
1981    GGCAGCGTGCAGCTCGCCGACCACTACCAGCAGAACACCCCCATCGGCGACGGCCCCGTG
2041    CTGCTGCCCGACAACCACTACCTGAGCTACCAGTCCGCCCTGAGCAAAGACCCCAACGAG
2101    AAGCGCGATCACATGGTCCTGCTGGAGTTCGTGACCGCCGCCGGGATCACTCTCGGCATG
2161    GACGAGCTGTACAAGTAA
```

The start codons of the two separate components of the fusion protein are highlighted in grey, including the mutated YFP start codon (ATG → CTG), which allows continuous transcription of the fusion protein. The stop codon (TAA) is also highlighted in grey and marks the end of the fusion protein. The β_1AR sequence is the

same as the β_1AR sequence used in previous experiments, apart from a change of the base 1383 (guanine to cytosine) which was silent and did not cause an amino acid change (TCG -> TCC, encoding the amino acid serine at position 461). The linker sequence is double underlined.

YFP-tagged β_1-adrenoceptor fusion protein amino acid sequence

M G A G V L V L G A S E P G N L S S A A P L P D G A A T A A R L L V P A S P P A S L L P P A S E S P E P L S Q Q
W T A G M G L L M A L I V L L I V A G N V L V I V A I A K T P R L Q T L T N L F I M S L A S A D L V M G L L V V
P F G A T I V V W G R W E Y G S F F C E L W T S V D V L C V T A S I E T L C V I A L D R Y L A I T S P F R Y Q S L
L T R A R A R G L V C T V W A I S A L V S F L P I L M H W W R A E S D E A R R C Y N D P K C C D F V T N R A Y
A I A S S V V S F Y V P L C I M A F V Y L R V F R E A Q K Q V K K I D S C E R R F L G G P A R P P S P S P S P V P
A P A P P P G P P R P A A A A A T A P L A N G R A G K R R P S R L V A L R E Q K A L K T L G I I M G V F T L C
W L P F F L A N V V K A F H R E L V P D R L F V F F N W L G Y A N S A F N P I I Y C R S P D F R K A F Q G L L C
C A R R A A R R R H A T H G D R P R A S G C L A R P G P P P S P G A A S D D D D D D D V V G A T P P A R L L E
P W A G C N G G A A A D S D S S L D E P C R P G F A S E S K V G S R D P P V A T L V S K G E E L F T G V V P I
L V E L D G D V N G H K F S V S G E G E G D A T Y G K L T L K F I C T T G K L P V P W P T L V T T F G Y G L Q C
F A R Y P D H M K Q H D F F K S A M P E G Y V Q E R T I F F K D D G N Y K T R A E V K F E G D T L V N R I E L
K G I D F K E D G N I L G H K L E Y N Y N S H N V Y I M A D K Q K N G I K V N F K I R H N I E D G S V Q L A D
H Y Q Q N T P I G D G P V L L P D N H Y L S Y Q S A L S K D P N E K R D H M V L L E F V T A A G I T L G M D E
L Y K Stop

The start codons of the two separate components of the fusion protein are highlighted in grey as well as the stop codon of the fusion protein. The linker sequence is double underlined.

S10 DNA and protein sequence of the complete YFP_N-tagged native β_1AR fusion protein

	start and end position of DNA sequence (bases)	DNA sequence length (bases)	Protein sequence length (residues)
β_1AR sequence	1-1431	1431	477
linker sequence	1432-1458	27	9
$eYFP_N$ sequence	1459-1923	465	155
fusion protein sequence	1-1923	1923	641

YFP_N-tagged β_1-adrenoceptor fusion protein DNA sequence

```
1       ATGGGCGCGGGGGTGCTCGTCCTGGGCGCCTCCGAGCCCGGTAACCTGTCGTCGGCCGCA
61      CCGCTCCCCGACGGCGCGGCCACCGCGGCGCGGCTGCTGGTGCCCGCGTCGCCGCCCGCC
121     TCGTTGCTGCCTCCCGCCAGCGAAAGCCCCGAGCCGCTGTCTCAGCAGTGGACAGCGGGC
181     ATGGGTCTGCTGATGGCGCTCATCGTGCTGCTCATCGTGGCGGGCAATGTGCTGGTGATC
241     GTGGCCATCGCCAAGACGCCGCGGCTGCAGACGCTCACCAACCTCTTCATCATGTCCCTG
301     GCCAGCGCCGACCTGGTCATGGGGCTGCTGGTGGTGCCGTTCGGGGCCACCATCGTGGTG
361     TGGGGCCGCTGGGAGTACGGCTCCTTCTTCTGCGAGCTGTGGACCTCAGTGGACGTGCTG
421     TGCGTGACGGCCAGCATCGAGACCCTGTGTGTCATTGCCCTGGACCGCTACCTCGCCATC
481     ACCTCGCCCTTCCGCTACCAGAGCCTGCTGACGCGCGCGCGGGCGCGGGGCCTCGTGTGC
541     ACCGTGTGGGCCATCTCGGCCCTGGTGTCCTTCCTGCCCATCCTCATGCACTGGTGGCGG
601     GCGGAGAGCGACGAGGCGCGCCGCTGCTACAACGACCCCAAGTGCTGCGACTTCGTCACC
661     AACCGGGCCTACGCCATCGCCTCGTCCGTAGTCTCCTTCTACGTGCCCCTGTGCATCATG
721     GCCTTCGTGTACCTGCGGGTGTTCCGCGAGGCCCAGAAGCAGGTGAAGAAGATCGACAGC
781     TGCGAGCGCCGTTTCCTCGGCGGCCCAGCGCGGCCGCCCTCGCCCTCGCCCTCGCCCGTC
841     CCCGCGCCCGCGCCGCCGCCCGGACCCCCGCGCCCCGCCGCCGCCGCCGCCACCGCCCCG
901     CTGGCCAACGGGCGTGCGGGTAAGCGGCGGCCCTCGCGCCTCGTGGCCCTGCGCGAGCAG
961     AAGGCGCTCAAGACGCTGGGCATCATCATGGGCGTCTTCACGCTCTGCTGGCTGCCCTTC
1021    TTCCTGGCCAACGTGGTGAAGGCCTTCCACCGCGAGCTGGTGCCCGACCGCCTCTTCGTC
1081    TTCTTCAACTGGCTGGGCTACGCCAACTCGGCCTTCAACCCCATCATCTACTGCCGCAGC
1141    CCCGACTTCCGCAAGGCCTTCCAGGGACTGCTCTGCTGCGCGCGCAGGGCTGCCCGCCGG
1201    CGCCACGCGACCCACGGAGACCGGCCGCGCGCCTCGGGCTGTCTGGCCCGGCCCGGACCC
1261    CCGCCATCGCCCGGGGCCGCCTCGGACGACGACGACGACGATGTCGTCGGGGCCACGCCG
1321    CCCGCGCGCCTGCTGGAGCCCTGGGCCGGCTGCAACGGCGGGGCGGCGGCGGACAGCGAC
1381    TCCAGCCTGGACGAGCCGTGCCGCCCCGGCTTCGCCTCGGAATCCAAGGTGGGCTCGAGG
1441    GATCCACCGGTCGCCACCCTGGTGAGCAAGGGCGAGGAGCTGTTCACCGGGGTGGTGCCC
1501    ATCCTGGTCGAGCTGGACGGCGACGTAAACGGCCACAAGTTCAGCGTGTCCGGCGAGGGC
1561    GAGGGCGATGCCACCTACGGCAAGCTGACCCTGAAGTTCATCTGCACCACCGGCAAGCTG
1621    CCCGTGCCCTGGCCCACCCTCGTGACCACCTTCGGCTACGGCCTGCAGTGCTTCGCCCGC
1681    TACCCCGACCACATGAAGCAGCACGACTTCTTCAAGTCCGCCATGCCCGAAGGCTACGTC
1741    CAGGAGCGCACCATCTTCTTCAAGGACGACGGCAACTACAAGACCCGCGCCGAGGTGAAG
1801    TTCGAGGGCGACACCCTGGTGAACCGCATCGAGCTGAAGGGCATCGACTTCAAGGAGGAC
1861    GGCAACATCCTGGGGCACAAGCTGGAGTACAACTACAACAGCCACAACGTCTATATCATG
1921    GTCTAGAGGGCCCGTTTAAACCCGCTG
```

The start codons of the two separate components of the fusion protein are highlighted in grey, including the mutated start YFP codon (ATG → CTG) which allows continuous transcription of the fusion protein. The stop codon (TAG) is also highlighted in grey and marks the end of the fusion protein. The β_1AR sequence matches that of the β_1YFP sequence (i.e. includes the silent mutation at position 1383). The linker sequence is double underlined. The YFP_N sequence matches the first part (base 1459-1923) of the YFP sequence used in the β_1YFP construct (YFP

amino acids 1-155), apart from a change of base 1922, where the cytosine was mutated to a thymine and caused an amino acid residue change from alanine to valine (GCC -> GTC) at position 641 of the fusion protein (position 155 of the YFP_N fragment). This introduced the *Xba*I restriction enzyme site (underlined sequence) at the end of the fusing protein sequence. The sequence after (>1926 bases) is the sequence of the pcDNA3.1(Neo+) plasmid vector.

YFP_N-tagged β_1-adrenoceptor fusion protein amino acid sequence

M G A G V L V L G A S E P G N L S S A A P L P D G A A T A A R L L V P A S P P A S L L P P A S E S P E P L S Q Q
W T A G M G L L M A L I V L L I V A G N V L V I V A I A K T P R L Q T L T N L F I M S L A S A D L V M G L L V V
P F G A T I V V W G R W E Y G S F F C E L W T S V D V L C V T A S I E T L C V I A L D R Y L A I T S P F R Y Q S L
L T R A R A R G L V C T V W A I S A L V S F L P I L M H W W R A E S D E A R R C Y N D P K C C D F V T N R A Y
A I A S S V V S F Y V P L C I M A F V Y L R V F R E A Q K Q V K K I D S C E R R F L G G P A R P P S P S P S P V P
A P A P P P G P P R P A A A A A T A P L A N G R A G K R R P S R L V A L R E Q K A L K T L G I I M G V F T L C
W L P F F L A N V V K A F H R E L V P D R L F V F F N W L G Y A N S A F N P I I Y C R S P D F R K A F Q G L L C
C A R R A A R R R H A T H G D R P R A S G C L A R P G P P P S P G A A S D D D D D D D V V G A T P P A R L L E
P W A G C N G G A A A D S D S S L D E P C R P G F A S E S K V G S R D P P V A T L V S K G E E L F T G V V P I
L V E L D G D V N G H K F S V S G E G E G D A T Y G K L T L K F I C T T G K L P V P W P T L V T T F G Y G L Q C
F A R Y P D H M K Q H D F F K S A M P E G Y V Q E R T I F F K D D G N Y K T R A E V K F E G D T L V N R I E L
K G I D F K E D G N I L G H K L E Y N Y N S H N V Y I M V Stop R A R L N P L

The start codons of the two separate components of the fusion protein are highlighted in grey as well as the stop codon of the fusion protein. The linker sequence is double underlined. The sequence after the stop codon is the sequence of the pcDNA3.1(Neo+) plasmid vector.

S11 DNA and protein sequence of the complete YFP_C-tagged native β_1AR fusion protein

	start and end position of DNA sequence (bases)	DNA sequence length (bases)	Protein sequence length (residues)
β_1AR sequence	1-1431	1431	477
linker sequence	1432-1455	24	8
$eYFP_C$ sequence	1456-1713	258	86
fusion protein sequence	1-1713	1713	571

YFP_C-tagged β_1-adrenoceptor fusion protein DNA sequence

```
1       ATGGGCGCGGGGGTGCTCGTCCTGGGCGCCTCCGAGCCCGGTAACCTGTCGTCGGCCGCA
61      CCGCTCCCCGACGGCGCGGCCACCGCGGCGCGGCTGCTGGTGCCCGCGTCGCCGCCCGCC
121     TCGTTGCTGCCTCCCGCCAGCGAAAGCCCCGAGCCGCTGTCTCAGCAGTGGACAGCGGGC
181     ATGGGTCTGCTGATGGCGCTCATCGTGCTGCTCATCGTGGCGGGCAATGTGCTGGTGATC
241     GTGGCCATCGCCAAGACGCCGCGGCTGCAGACGCTCACCAACCTCTTCATCATGTCCCTG
301     GCCAGCGCCGACCTGGTCATGGGGCTGCTGGTGGTGCCGTTCGGGGCCACCATCGTGGTG
361     TGGGGCCGCTGGGAGTACGGCTCCTTCTTCTGCGAGCTGTGGACCTCAGTGGACGTGCTG
421     TGCGTGACGGCCAGCATCGAGACCCTGTGTGTCATTGCCCTGGACCGCTACCTCGCCATC
481     ACCTCGCCCTTCCGCTACCAGAGCCTGCTGACGCGCGCGCGGGCGCGGGGCCTCGTGTGC
541     ACCGTGTGGGCCATCTCGGCCCTGGTGTCCTTCCTGCCCATCCTCATGCACTGGTGGCGG
601     GCGGAGAGCGACGAGGCGCGCCGCTGCTACAACGACCCCAAGTGCTGCGACTTCGTCACC
661     AACCGGGCCTACGCCATCGCCTCGTCCGTAGTCTCCTTCTACGTGCCCCTGTGCATCATG
721     GCCTTCGTGTACCTGCGGGTGTTCCGCGAGGCCCAGAAGCAGGTGAAGAAGATCGACAGC
781     TGCGAGCGCCGTTTCCTCGGCGGCCCAGCGCGGCCGCCCTCGCCCTCGCCCTCGCCCGTC
841     CCCGCGCCCGCGCCGCCGCCCGGACCCCCGCGCCCCGCCGCCGCCGCCGCCACCGCCCCG
901     CTGGCCAACGGGCGTGCGGGTAAGCGGCGGCCCTCGCGCCTCGTGGCCCTGCGCGAGCAG
961     AAGGCGCTCAAGACGCTGGGCATCATCATGGGCGTCTTCACGCTCTGCTGGCTGCCCTTC
1021    TTCCTGGCCAACGTGGTGAAGGCCTTCCACCGCGAGCTGGTGCCCGACCGCCTCTTCGTC
1081    TTCTTCAACTGGCTGGGCTACGCCAACTCGGCCTTCAACCCCATCATCTACTGCCGCAGC
1141    CCCGACTTCCGCAAGGCCTTCCAGGGACTGCTCTGCTGCGCGCGCAGGGCTGCCCGCCGG
1201    CGCCACGCGACCCACGGAGACCGGCCGCGCGCCTCGGGCTGTCTGGCCCGGCCCGGACCC
1261    CCGCCATCGCCCGGGGCCGCCTCGGACGACGACGACGACGATGTCGTCGGGGCCACGCCG
1321    CCCGCGCGCCTGCTGGAGCCCTGGGCCGGCTGCAACGGCGGGGCGGCGGCGGACAGCGAC
1381    TCCAGCCTGGACGAGCCGTGCCGCCCCGGCTTCGCCTCGGAATCCAAGGTGGGCTCGAGC
1441    CACAACGTCTATATCCTGGCCGACAAGCAGAAGAACGGCATCAAGGTGAACTTCAAGATC
1501    CGCCACAACATCGAGGACGGCAGCGTGCAGCTCGCCGACCACTACCAGCAGAACACCCCC
1561    ATCGGCGACGGCCCCGTGCTGCTGCCCGACAACCACTACCTGAGCTACCAGTCCGCCCTG
1621    AGCAAAGACCCCAACGAGAAGCGCGATCACATGGTCCTGCTGGAGTTCGTGACCGCCGCC
1681    GGGATCACTCTCGGCATGGACGAGCTGTACAAGTAA
```

The start codons of the two separate components of the fusion protein are highlighted in grey, including the mutated start YFP codon (ATG → CTG), which allows continuous transcription of the fusion protein. The stop codon (TAA) is also highlighted in grey and marks the end of the fusion protein. The β_1AR sequence matches that of the β_1YFP sequence (i.e. includes the silent mutation at position 1383). The linker sequence is double underlined. The last 18 bases (6 amino acids) of the linker sequence match those from base 1900–1917 of the β_1YFP sequence and the β_1YFP_N sequence (YFP_N amino acids 148-153), thus creating a sequence overlap of the two separate YFP fragments. The YFP_C sequence matches the last part (bases 1918-2178) of the YFP sequence used in the β_1YFP construct (YFP amino acids 154-

239), apart from the change of base 1456 from adenine to cytosine (ATG → CTG, start codon methionine to leucine).

YFP$_C$-tagged β_1-adrenoceptor fusion protein amino acid sequence

M G A G V L V L G A S E P G N L S S A A P L P D G A A T A A R L L V P A S P P A S L L P P A S E S P E P L S Q Q
W T A G M G L L M A L I V L L I V A G N V L V I V A I A K T P R L Q T L T N L F I M S L A S A D L V M G L L V V
P F G A T I V V W G R W E Y G S F F C E L W T S V D V L C V T A S I E T L C V I A L D R Y L A I T S P F R Y Q S L
L T R A R A R G L V C T V W A I S A L V S F L P I L M H W W R A E S D E A R R C Y N D P K C C D F V T N R A Y
A I A S S V V S F Y V P L C I M A F V Y L R V F R E A Q K Q V K K I D S C E R R F L G G P A R P P S P S P S P V P
A P A P P P G P P R P A A A A A T A P L A N G R A G K R R P S R L V A L R E Q K A L K T L G I I M G V F T L C
W L P F F L A N V V K A F H R E L V P D R L F V F F N W L G Y A N S A F N P I I Y C R S P D F R K A F Q G L L C
C A R R A A R R R H A T H G D R P R A S G C L A R P G P P P S P G A A S D D D D D D D V V G A T P P A R L L E
P W A G C N G G A A A D S D S S L D E P C R P G F A S E S K V G S S H N V Y I L A D K Q K N G I K V N F K I R
H N I E D G S V Q L A D H Y Q Q N T P I G D G P V L L P D N H Y L S Y Q S A L S K D P N E K R D H M V L L E F
V T A A G I T L G M D E L Y K Stop

The start codons of the two separate components of the fusion protein are highlighted in grey as well as the stop codon of the fusion protein. The linker sequence is double underlined.

S12 DNA and protein sequence of the complete SNAP-tagged β_{1D138A}AR fusion protein

	start and end position of DNA sequence (bases)	DNA sequence length (bases)	protein sequence length (residues)
signal sequence	22 – 105	84	28
SNAP-tag sequence	106 – 654	549	183
β_{1D138A}AR sequence	655 – 2085	1431	477
fusion protein sequence	22 – 2085	2064	688

SNAP-tagged β_1-adrenoceptor fusion protein DNA sequence

```
1       CTTAAGCTTGGTACCGCCACCATGCGGCTCTGCATCCCGCAGGTGCTGTTGGCCTTGTTC
61      CTTTCCATGCTGACAGGGCCGGGAGAAGGCAGCCGGAAGCTTACCCTGGACAAAGACTGC
121     GAAATGAAGCGCACCACCCTGGATAGCCCTCTGGGCAAGCTGGAACTGTCTGGGTGCGAA
181     CAGGGCCTGCACGAGATCAAGCTGCTGGGCAAAGGAACATCTGCCGCCGACGCCGTGGAA
241     GTGCCTGCCCCAGCCGCCGTGCTGGGCGGACCAGAGCCACTGATGCAGGCCACCGCCTGG
301     CTCAACGCCTACTTTCACCAGCCTGAGGCCATCGAGGAGTTCCCTGTGCCAGCCCTGCAC
361     CACCCAGTGTTCCAGCAGGAGAGCTTTACCCGCCAGGTGCTGTGGAAACTGCTGAAAGTG
421     GTGAAGTTCGGAGAGGTCATCAGCTACCAGCAGCTGGCCGCCCTGGCCGGCAATCCCGCC
481     GCCACCGCCGCCGTGAAAACCGCCCTGAGCGGAAATCCCGTGCCCATTCTGATCCCCTGC
541     CACCGGGTGGTGTCTAGCTCTGGCGCCGTGGGGGGCTACGAGGGCGGGCTCGCCGTGAAA
601     GAGTGGCTGCTGGCCCACGAGGGCCACAGACTGGGCAAGCCTGGGCTGGGATCCCTGGGC
661     GCGGGGGTGCTCGTCCTGGGCGCCTCCGAGCCCGGTAACCTGTCGTCGGCCGCACCGCTC
721     CCCGACGGCGCGGCCACCGCGGCGCGGCTGCTGGTGCCCGCGTCGCCGCCCGCCTCGTTG
781     CTGCCTCCCGCCAGCGAAAGCCCCGAGCCGCTGTCTCAGCAGTGGACAGCGGGCATGGGT
841     CTGCTGATGGCGCTCATCGTGCTGCTCATCGTGGCGGGCAATGTGCTGGTGATCGTGGCC
901     ATCGCCAAGACGCCGCGGCTGCAGACGCTCACCAACCTCTTCATCATGTCCCTGGCCAGC
961     GCCGACCTGGTCATGGGGCTGCTGGTGGTGCCGTTCGGGGCCACCATCGTGGTGTGGGGC
1021    CGCTGGGAGTACGGCTCCTTCTTCTGCGAGCTGTGGACCTCAGTGGCCGTGCTGTGCGTG
1081    ACGGCCAGCATCGAGACCCTGTGTGTCATTGCCCTGGACCGCTACCTCGCCATCACCTCG
1141    CCCTTCCGCTACCAGAGCCTGCTGACGCGCGCGCGGGCGCGGGGCCTCGTGTGCACCGTG
1201    TGGGCCATCTCGGCCCTGGTGTCCTTCCTGCCCATCCTCATGCACTGGTGGCGGGCGGAG
1261    AGCGACGAGGCGCGCCGCTGCTACAACGACCCCAAGTGCTGCGACTTCGTCACCAACCGG
1321    GCCTACGCCATCGCCTCGTCCGTAGTCTCCTTCTACGTGCCCCTGTGCATCATGGCCTTC
1381    GTGTACCTGCGGGTGTTCCGCGAGGCCCAGAAGCAGGTGAAGAAGATCGACAGCTGCGAG
1441    CGCCGTTTCCTCGGCGGCCCAGCGCGGCCGCCCTCGCCCTCGCCCTCGCCCGTCCCCGCG
1501    CCCGCGCCGCCGCCCGGACCCCCGCGCCCCGCCGCCGCCGCCGCCACCGCCCCGCTGGCC
1561    AACGGGCGTGCGGGTAAGCGGCGGCCCTCGCGCCTCGTGGCCCTGCGCGAGCAGAAGGCG
1621    CTCAAGACGCTGGGCATCATCATGGGCGTCTTCACGCTCTGCTGGCTGCCCTTCTTCCTG
1681    GCCAACGTGGTGAAGGCCTTCCACCGCGAGCTGGTGCCCGACCGCCTCTTCGTCTTCTTC
1741    AACTGGCTGGGCTACGCCAACTCGGCCTTCAACCCCATCATCTACTGCCGCAGCCCCGAC
1801    TTCCGCAAGGCCTTCCAGGGACTGCTCTGCTGCGCGCGCAGGGCTGCCCGCCGGCGCCAC
1861    GCGACCCACGGAGACCGGCCGCGCGCCTCGGGCTGTCTGGCCCGGCCCGGACCCCCGCCA
1921    TCGCCCGGGGCCGCCTCGGACGACGACGACGACGATGTCGTCGGGGCCACGCCGCCCGCG
1981    CGCCTGCTGGAGCCCTGGGCCGGCTGCAACGGCGGGGCGGCGGCGGACAGCGACTCGAGC
2041    CTGGACGAGCCGTGCCGCCCCGGCTTCGCCTCGGAATCCAAGGTGTAGGAATTCTGCAGA
```

The start codons of the three separate components of the fusion protein are highlighted in grey, including the mutated start codons (ATG → CTG) that allow continuous transcription of the fusion protein. The stop codon is also highlighted in grey and marks the end of the fusion protein. The entire ssβ_{1D138A}AR sequence matches that of the ssβ_1AR sequence described earlier, apart from the change of

base 413 (boxed in; base 1067 in the fusion protein sequence) from adenine to cytosine that caused the desired amino acid change at position 138 of the β_1AR from an aspartic acid (D) to an alanine (A) residue. The sequence before (<22bp) and after (>2088bp) the fusion protein DNA sequence is the sequence of the pcDNA3.1(Neo+) plasmid vector.

SNAP-tagged β_{1D138A}-adrenoceptor fusion protein amino acid sequence

L K L G T A T M R L C I P Q V L L A L F L S M L T G P G E G S R K L T L D K D C E M K R T T L D S P L G K L E L S
G C E Q G L H E I K L L G K G T S A A D A V E V P A P A A V L G G P E P L M Q A T A W L N A Y F H Q P E A I E
E F P V P A L H H P V F Q Q E S F T R Q V L W K L L K V V K F G E V I S Y Q Q L A A L A G N P A A T A A V K T
A L S G N P V P I L I P C H R V V S S S G A V G G Y E G G L A V K E W L L A H E G H R L G K P G L G S L G A G
V L V L G A S E P G N L S S A A P L P D G A A T A A R L L V P A S P P A S L L P P A S E S P E P L S Q Q W T A G
M G L L M A L I V L L I V A G N V L V I V A I A K T P R L Q T L T N L F I M S L A S A D L V M G L L V V P F G A T
I V V W G R W E Y G S F F C E L W T S V A V L C V T A S I E T L C V I A L D R Y L A I T S P F R Y Q S L L T R A R
A R G L V C T V W A I S A L V S F L P I L M H W W R A E S D E A R R C Y N D P K C C D F V T N R A Y A I A S S
V V S F Y V P L C I M A F V Y L R V F R E A Q K Q V K K I D S C E R R F L G G P A R P P S P S P S P V P A P A P
P P G P P R P A A A A A T A P L A N G R A G K R R P S R L V A L R E Q K A L K T L G I I M G V F T L C W L P F F
L A N V V K A F H R E L V P D R L F V F F N W L G Y A N S A F N P I I Y C R S P D F R K A F Q G L L C C A R R A
A R R R H A T H G D R P R A S G C L A R P G P P P S P G A A S D D D D D D D V V G A T P P A R L L E P W A G C
N G G A A A D S D S S L D E P C R P G F A S E S K V Stop E F C R

The start codons of the three separate components of the fusion protein are highlighted in grey as well as the stop codon of the fusion protein. The boxed in amino acid residue is the desired D138A mutation in the β_1AR sequence.

S13 DNA and protein sequence of the complete YFP_C-tagged β_{1D138A}AR fusion protein

	start and end position of DNA sequence (bases)	DNA sequence length (bases)	Protein sequence length (residues)
β_{1D138A}AR sequence	1-1431	1431	477
linker sequence	1432-1455	24	8
$eYFP_C$ sequence	1456-1713	258	86
fusion protein sequence	1-1713	1713	571

YFP_C-tagged β_{1D138A}-adrenoceptor fusion protein DNA sequence

```
1       ATGGGCGCGGGGGTGCTCGTCCTGGGCGCCTCCGAGCCCGGTAACCTGTCGTCGGCCGCA
61      CCGCTCCCCGACGGCGCGGCCACCGCGGCGCGGCTGCTGGTGCCCGCGTCGCCGCCCGCC
121     TCGTTGCTGCCTCCCGCCAGCGAAAGCCCCGAGCCGCTGTCTCAGCAGTGGACAGCGGGC
181     ATGGGTCTGCTGATGGCGCTCATCGTGCTGCTCATCGTGGCGGGCAATGTGCTGGTGATC
241     GTGGCCATCGCCAAGACGCCGCGGCTGCAGACGCTCACCAACCTCTTCATCATGTCCCTG
301     GCCAGCGCCGACCTGGTCATGGGGCTGCTGGTGGTGCCGTTCGGGGCCACCATCGTGGTG
361     TGGGGCCGCTGGGAGTACGGCTCCTTCTTCTGCGAGCTGTGGACCTCAGTGGCCGTGCTG
421     TGCGTGACGGCCAGCATCGAGACCCTGTGTGTCATTGCCCTGGACCGCTACCTCGCCATC
481     ACCTCGCCCTTCCGCTACCAGAGCCTGCTGACGCGCGCGCGGGCGCGGGGCCTCGTGTGC
541     ACCGTGTGGGCCATCTCGGCCCTGGTGTCCTTCCTGCCCATCCTCATGCACTGGTGGCGG
601     GCGGAGAGCGACGAGGCGCGCCGCTGCTACAACGACCCCAAGTGCTGCGACTTCGTCACC
661     AACCGGGCCTACGCCATCGCCTCGTCCGTAGTCTCCTTCTACGTGCCCCTGTGCATCATG
721     GCCTTCGTGTACCTGCGGGTGTTCCGCGAGGCCCAGAAGCAGGTGAAGAAGATCGACAGC
781     TGCGAGCGCCGTTTCCTCGGCGGCCCAGCGCGGCCGCCCTCGCCCTCGCCCTCGCCCGTC
841     CCCGCGCCCGCGCCGCCGCCCGGACCCCCGCGCCCCGCCGCCGCCGCCGCCACCGCCCCG
901     CTGGCCAACGGGCGTGCGGGTAAGCGGCGGCCCTCGCGCCTCGTGGCCCTGCGCGAGCAG
961     AAGGCGCTCAAGACGCTGGGCATCATCATGGGCGTCTTCACGCTCTGCTGGCTGCCCTTC
1021    TTCCTGGCCAACGTGGTGAAGGCCTTCCACCGCGAGCTGGTGCCCGACCGCCTCTTCGTC
1081    TTCTTCAACTGGCTGGGCTACGCCAACTCGGCCTTCAACCCCATCATCTACTGCCGCAGC
1141    CCCGACTTCCGCAAGGCCTTCCAGGGACTGCTCTGCTGCGCGCGCAGGGCTGCCCGCCGG
1201    CGCCACGCGACCCACGGAGACCGGCCGCGCGCCTCGGGCTGTCTGGCCCGGCCCGGACCC
1261    CCGCCATCGCCCGGGGCCGCCTCGGACGACGACGACGACGATGTCGTCGGGGCCACGCCG
1321    CCCGCGCGCCTGCTGGAGCCCTGGGCCGGCTGCAACGGCGGGGCGGCGGCGGACAGCGAC
1381    TCCAGCCTGGACGAGCCGTGCCGCCCCGGCTTCGCCTCGGAATCCAAGGTGGGCTCGAGC
1441    CACAACGTCTATATCCTGGCCGACAAGCAGAAGAACGGCATCAAGGTGAACTTCAAGATC
1501    CGCCACAACATCGAGGACGGCAGCGTGCAGCTCGCCGACCACTACCAGCAGAACACCCCC
1561    ATCGGCGACGGCCCCGTGCTGCTGCCCGACAACCACTACCTGAGCTACCAGTCCGCCCTG
1621    AGCAAAGACCCCAACGAGAAGCGCGATCACATGGTCCTGCTGGAGTTCGTGACCGCCGCC
1681    GGGATCACTCTCGGCATGGACGAGCTGTACAAGTAA
```

The start codons of the two separate components of the fusion protein are highlighted in grey, including the mutated start YFP codon (ATG → CTG) which allows continuous transcription of the fusion protein. The stop codon (TAA) is also highlighted in grey and marks the end of the fusion protein. The entire $\beta_{1D138A}YFP_C$ sequence matches that of the β_1YFP_C sequence, apart from the change of base 413 (boxed in) from adenine to cytosine that caused the desired amino acid change at position 138 from an aspartic acid (D) to an alanine (A) residue. The linker sequence is double underlined.

YFP$_C$-tagged β_{1D138A}-adrenoceptor fusion protein amino acid sequence

M G A G V L V L G A S E P G N L S S A A P L P D G A A T A A R L L V P A S P P A S L L P P A S E S P E P L S Q Q
W T A G M G L L M A L I V L L I V A G N V L V I V A I A K T P R L Q T L T N L F I M S L A S A D L V M G L L V V
P F G A T I V V W G R W E Y G S F F C E L W T S V A V L C V T A S I E T L C V I A L D R Y L A I T S P F R Y Q S L
L T R A R A R G L V C T V W A I S A L V S F L P I L M H W W R A E S D E A R R C Y N D P K C C D F V T N R A Y
A I A S S V V S F Y V P L C I M A F V Y L R V F R E A Q K Q V K K I D S C E R R F L G G P A R P P S P S P S P V P
A P A P P P G P P R P A A A A A T A P L A N G R A G K R R P S R L V A L R E Q K A L K T L G I I M G V F T L C
W L P F F L A N V V K A F H R E L V P D R L F V F F N W L G Y A N S A F N P I I Y C R S P D F R K A F Q G L L C
C A R R A A R R R H A T H G D R P R A S G C L A R P G P P P S P G A A S D D D D D D V V G A T P P A R L L E
P W A G C N G G A A A D S D S S L D E P C R P G F A S E S K V G S S H N V Y I L A D K Q K N G I K V N F K I R
H N I E D G S V Q L A D H Y Q Q N T P I G D G P V L L P D N H Y L S Y Q S A L S K D P N E K R D H M V L L E F
V T A A G I T L G M D E L Y K Stop

The start codons of the two separate components of the fusion protein are highlighted in grey as well as the stop codon of the fusion protein. The linker sequence is double underlined. The boxed in amino acid residue is the desired D138A mutation.

Appendix II – buffer compositions

DEA buffer

used to measure SPAP activity

100 mM (100 mL) Diethanolamine

280 mM (16.36 g) NaCl

0.5 mM (0.102 g) $MgCl_2.6H_2O$

made up to 1 litre with double distilled water

used HCl to achieve pH 9.85

autoclaved to sterilise

stored at 4 °C

PNPP was dissolved in DEA buffer at a concentration of 100 mM. 500 µL PNPP added to 10 mL DEA buffer was used to assess the SPAP content of one 96-well plate.

TBE buffer

Used in gel electrophoresis experiments

90 mM (10.9 g) Tris-Base

90 mM (5.56 g) Boric acid

2 mM (0.58 g) EDTA

made up to 1 litre in double distilled water

autoclaved to sterilise

stored at room temperature

HBSS – HEPES buffered saline solution

used in all confocal imaging experiments

10 mM (2.38 g) HEPES

147 mM (8.46 g) NaCl

24 mM (0.37 g) KCl

1 mM (0.24 g) $MgSO_4.7H_20$

2 mM (0.22 g) Sodium Pyruvate

1.3 mM (0.19 g) $CaCl_2$

1.43 mM (0.12 g) $NaHCO_3$

made up to 1 litre in double distilled water

used NaOH to achieve pH 7.45

autoclaved to sterilise

stored at 4 °C

References

Alvarez-Curto E, Ward RJ, Pediani JD, Milligan G (2010). Ligand regulation of the quaternary organization of cell surface M3 muscarinic acetylcholine receptors analyzed by fluorescence resonance energy transfer (FRET) imaging and homogeneous time-resolved FRET. *The Journal of biological chemistry* 285(30): 23318-23330.

Angel TE, Chance MR, Palczewski K (2009). Conserved waters mediate structural and functional activation of family A (rhodopsin-like) G protein-coupled receptors. *Proceedings of the National Academy of Sciences of the United States of America* 106(21): 8555-8560.

Arunlakshana O, Schild HO (1959). Some quantitative uses of drug antagonists. *British journal of pharmacology and chemotherapy* 14(1): 48-58.

Audet M, Bouvier M (2012). Restructuring G-protein- coupled receptor activation. *Cell* 151(1): 14-23.

Audet M, Lagace M, Silversides DW, Bouvier M (2010). Protein-protein interactions monitored in cells from transgenic mice using bioluminescence resonance energy transfer. *FASEB journal : official publication of the Federation of American Societies for Experimental Biology* 24(8): 2829-2838.

Avissar S, Amitai G, Sokolovsky M (1983). Oligomeric structure of muscarinic receptors is shown by photoaffinity labeling: subunit assembly may explain high- and low-affinity agonist states. *Proceedings of the National Academy of Sciences of the United States of America* 80(1): 156-159.

Bachman ES, Dhillon H, Zhang CY, Cinti S, Bianco AC, Kobilka BK*, et al.* (2002). betaAR signaling required for diet-induced thermogenesis and obesity resistance. *Science (New York, N.Y.)* 297(5582): 843-845.

Baker JG (2005). The selectivity of beta-adrenoceptor antagonists at the human beta1, beta2 and beta3 adrenoceptors. *British journal of pharmacology* 144(3): 317-322.

Baker JG, Adams LA, Salchow K, Mistry SN, Middleton RJ, Hill SJ*, et al.* (2011a). Synthesis and characterization of high-affinity 4,4-difluoro-4-bora-3a,4a-diaza-s-indacene-labeled fluorescent ligands for human beta-adrenoceptors. *Journal of medicinal chemistry* 54(19): 6874-6887.

Baker JG, Hall IP, Hill SJ (2003a). Agonist actions of "beta-blockers" provide evidence for two agonist activation sites or conformations of the human beta1-adrenoceptor. *Molecular pharmacology* 63(6): 1312-1321.

Baker JG, Hall IP, Hill SJ (2003b). Agonist and inverse agonist actions of beta-blockers at the human beta 2-adrenoceptor provide evidence for agonist-directed signaling. *Molecular pharmacology* 64(6): 1357-1369.

Baker JG, Hall IP, Hill SJ (2003c). Influence of agonist efficacy and receptor phosphorylation on antagonist affinity measurements: differences between second messenger and reporter gene responses. *Molecular pharmacology* 64(3): 679-688.

Baker JG, Hall IP, Hill SJ (2002). Pharmacological characterization of CGP 12177 at the human beta(2)-adrenoceptor. *British journal of pharmacology* 137(3): 400-408.

Baker JG, Hall IP, Hill SJ (2003d). Pharmacology and direct visualisation of BODIPY-TMR-CGP: a long-acting fluorescent beta2-adrenoceptor agonist. *British journal of pharmacology* 139(2): 232-242.

Baker JG, Hall IP, Hill SJ (2004). Temporal characteristics of cAMP response element-mediated gene transcription: requirement for sustained cAMP production. *Molecular pharmacology* 65(4): 986-998.

Baker JG, Hill SJ, Summers RJ (2011b). Evolution of beta-blockers: from anti-anginal drugs to ligand-directed signalling. *Trends in pharmacological sciences* 32(4): 227-234.

Baker JG, Middleton R, Adams L, May LT, Briddon SJ, Kellam B*, et al.* (2010). Influence of fluorophore and linker composition on the pharmacology of fluorescent adenosine A1 receptor ligands. *British journal of pharmacology* 159(4): 772-786.

Baker JG, Proudman RG, Hawley NC, Fischer PM, Hill SJ (2008). Role of key transmembrane residues in agonist and antagonist actions at the two conformations of the human beta1-adrenoceptor. *Molecular pharmacology* 74(5): 1246-1260.

Ballesteros J, Palczewski K (2001). G protein-coupled receptor drug discovery: implications from the crystal structure of rhodopsin. *Current opinion in drug discovery & development* 4(5): 561-574.

Barwell J, Gingell JJ, Watkins HA, Archbold JK, Poyner DR, Hay DL (2012). Calcitonin and calcitonin receptor-like receptors: common themes with family B GPCRs? *British journal of pharmacology* 166(1): 51-65.

Bayburt TH, Leitz AJ, Xie G, Oprian DD, Sligar SG (2007). Transducin activation by nanoscale lipid bilayers containing one and two rhodopsins. *The Journal of biological chemistry* 282(20): 14875-14881.

Becker A, Hessenius C, Licha K, Ebert B, Sukowski U, Semmler W*, et al.* (2001). Receptor-targeted optical imaging of tumors with near-infrared fluorescent ligands. *Nature biotechnology* 19(4): 327-331.

Birdsall NJ, Lazareno S (2005). Allosterism at muscarinic receptors: ligands and mechanisms. *Mini reviews in medicinal chemistry* 5(6): 523-543.

Black JW, Duncan WA, Durant CJ, Ganellin CR, Parsons EM (1972). Definition and antagonism of histamine H 2 -receptors. *Nature* 236(5347): 385-390.

Bockaert J, Pin JP (1999). Molecular tinkering of G protein-coupled receptors: an evolutionary success. *The EMBO journal* 18(7): 1723-1729.

Bohme I, Beck-Sickinger AG (2009). Illuminating the life of GPCRs. *Cell communication and signaling : CCS* 7: 16.

Boorsma M, Nieba L, Koller D, Bachmann MF, Bailey JE, Renner WA (2000). A temperature-regulated replicon-based DNA expression system. *Nature biotechnology* 18(4): 429-432.

Borjesson M, Magnusson Y, Hjalmarson A, Andersson B (2000). A novel polymorphism in the gene coding for the beta(1)-adrenergic receptor associated with survival in patients with heart failure. *European heart journal* 21(22): 1853-1858.

Bouvier M (2001). Oligomerization of G-protein-coupled transmitter receptors. *Nature reviews. Neuroscience* 2(4): 274-286.

Brauner-Osborne H, Wellendorph P, Jensen AA (2007). Structure, pharmacology and therapeutic prospects of family C G-protein coupled receptors. *Current drug targets* 8(1): 169-184.

Brayton CF (1986). Dimethyl sulfoxide (DMSO): a review. *The Cornell veterinarian* 76(1): 61-90.

Breitwieser GE (2004). G protein-coupled receptor oligomerization: implications for G protein activation and cell signaling. *Circulation research* 94(1): 17-27.

Briddon SJ, Gandia J, Amaral OB, Ferre S, Lluis C, Franco R*, et al.* (2008). Plasma membrane diffusion of G protein-coupled receptor oligomers. *Biochimica et biophysica acta* 1783(12): 2262-2268.

Briddon SJ, Hill SJ (2007). Pharmacology under the microscope: the use of fluorescence correlation spectroscopy to determine the properties of ligand-receptor complexes. *Trends in pharmacological sciences* 28(12): 637-645.

Briones AM, Daly CJ, Jimenez-Altayo F, Martinez-Revelles S, Gonzalez JM, McGrath JC*, et al.* (2005). Direct demonstration of beta1- and evidence against beta2- and beta3-adrenoceptors, in smooth muscle cells of rat small mesenteric arteries. *British journal of pharmacology* 146(5): 679-691.

Brodde OE (2008). Beta-1 and beta-2 adrenoceptor polymorphisms: functional importance, impact on cardiovascular diseases and drug responses. *Pharmacology & therapeutics* 117(1): 1-29.

Brodde OE, Bruck H, Leineweber K (2006). Cardiac adrenoceptors: physiological and pathophysiological relevance. *Journal of pharmacological sciences* 100(5): 323-337.

Brodde OE, Michel MC (1999). Adrenergic and muscarinic receptors in the human heart. *Pharmacological reviews* 51(4): 651-690.

Bulenger S, Marullo S, Bouvier M (2005). Emerging role of homo- and heterodimerization in G-protein-coupled receptor biosynthesis and maturation. *Trends in pharmacological sciences* 26(3): 131-137.

Burstein ES, Spalding TA, Brann MR (1998). The second intracellular loop of the m5 muscarinic receptor is the switch which enables G-protein coupling. *The Journal of biological chemistry* 273(38): 24322-24327.

Bylund DB, Toews ML (1993). Radioligand binding methods: practical guide and tips. *The American journal of physiology* 265(5 Pt 1): L421-429.

Calebiro D, Nikolaev VO, Gagliani MC, de Filippis T, Dees C, Tacchetti C*, et al.* (2009). Persistent cAMP-signals triggered by internalized G-protein-coupled receptors. *PLoS biology* 7(8): e1000172.

Calebiro D, Rieken F, Wagner J, Sungkaworn T, Zabel U, Borzi A*, et al.* (2013). Single-molecule analysis of fluorescently labeled G-protein-coupled receptors reveals complexes with distinct dynamics and organization. *Proceedings of the National Academy of Sciences of the United States of America* 110(2): 743-748.

Campos C, Kamiya M, Banala S, Johnsson K, Gonzalez-Gaitan M (2011). Labelling cell structures and tracking cell lineage in zebrafish using SNAP-tag. *Developmental dynamics : an official publication of the American Association of Anatomists* 240(4): 820-827.

Canals M, Burgueno J, Marcellino D, Cabello N, Canela EI, Mallol J*, et al.* (2004). Homodimerization of adenosine A2A receptors: qualitative and quantitative assessment by fluorescence and bioluminescence energy transfer. *Journal of neurochemistry* 88(3): 726-734.

Cao TT, Brelot A, von Zastrow M (2005). The composition of the beta-2 adrenergic receptor oligomer affects its membrane trafficking after ligand-induced endocytosis. *Molecular pharmacology* 67(1): 288-297.

Casadesus J, Low D (2006). Epigenetic gene regulation in the bacterial world. *Microbiology and molecular biology reviews : MMBR* 70(3): 830-856.

Cazzola M, Page CP, Calzetta L, Matera MG (2012). Pharmacology and therapeutics of bronchodilators. *Pharmacological reviews* 64(3): 450-504.

Cerra MC, Imbrogno S (2012). Phospholamban and cardiac function: a comparative perspective in vertebrates. *Acta physiologica (Oxford, England)* 205(1): 9-25.

Chabre M, le Maire M (2005). Monomeric G-protein-coupled receptor as a functional unit. *Biochemistry* 44(27): 9395-9403.

Chapple CR, Amarenco G, Lopez Aramburu MA, Everaert K, Liehne J, Lucas M*, et al.* (2013). A proof-of-concept study: Mirabegron, a new therapy for overactive bladder. *Neurourology and urodynamics*.

Chelikani P, Reeves PJ, Rajbhandary UL, Khorana HG (2006). The synthesis and high-level expression of a beta2-adrenergic receptor gene in a tetracycline-inducible stable mammalian cell line. *Protein science : a publication of the Protein Society* 15(6): 1433-1440.

Cheng HC (2001). The power issue: determination of KB or Ki from IC50. A closer look at the Cheng-Prusoff equation, the Schild plot and related power equations. *Journal of pharmacological and toxicological methods* 46(2): 61-71.

Christian F, Szaszak M, Friedl S, Drewianka S, Lorenz D, Goncalves A*, et al.* (2011). Small molecule AKAP-protein kinase A (PKA) interaction disruptors that activate PKA interfere with compartmentalized cAMP signaling in cardiac myocytes. *The Journal of biological chemistry* 286(11): 9079-9096.

Christopoulos A, Kenakin T (2002). G protein-coupled receptor allosterism and complexing. *Pharmacological reviews* 54(2): 323-374.

Christopoulos A, Lanzafame A, Ziegler A, Mitchelson F (1997). Kinetic studies of co-operativity at atrial muscarinic M2 receptors with an "infinite dilution" procedure. *Biochemical pharmacology* 53(6): 795-800.

Ciruela F, Vilardaga JP, Fernandez-Duenas V (2010). Lighting up multiprotein complexes: lessons from GPCR oligomerization. *Trends in biotechnology* 28(8): 407-415.

Collins S, Cao W, Robidoux J (2004). Learning new tricks from old dogs: beta-adrenergic receptors teach new lessons on firing up adipose tissue metabolism. *Molecular endocrinology (Baltimore, Md.)* 18(9): 2123-2131.

Congreve M, Marshall F (2010). The impact of GPCR structures on pharmacology and structure-based drug design. *British journal of pharmacology* 159(5): 986-996.

Cordeaux Y, Briddon SJ, Alexander SP, Kellam B, Hill SJ (2008). Agonist-occupied A3 adenosine receptors exist within heterogeneous complexes in membrane microdomains of individual living cells. *FASEB journal : official publication of the Federation of American Societies for Experimental Biology* 22(3): 850-860.

Cvejic S, Devi LA (1997). Dimerization of the delta opioid receptor: implication for a role in receptor internalization. *The Journal of biological chemistry* 272(43): 26959-26964.

Dalrymple MB, Pfleger KD, Eidne KA (2008). G protein-coupled receptor dimers: functional consequences, disease states and drug targets. *Pharmacology & therapeutics* 118(3): 359-371.

Daly CJ, McGrath JC (2003). Fluorescent ligands, antibodies, and proteins for the study of receptors. *Pharmacology & therapeutics* 100(2): 101-118.

Daly CJ, Ross RA, Whyte J, Henstridge CM, Irving AJ, McGrath JC (2010). Fluorescent ligand binding reveals heterogeneous distribution of adrenoceptors and 'cannabinoid-like' receptors in small arteries. *British journal of pharmacology* 159(4): 787-796.

Damian M, Martin A, Mesnier D, Pin JP, Baneres JL (2006). Asymmetric conformational changes in a GPCR dimer controlled by G-proteins. *The EMBO journal* 25(24): 5693-5702.

Day RN, Davidson MW (2009). The fluorescent protein palette: tools for cellular imaging. *Chemical Society reviews* 38(10): 2887-2921.

Deckert CM, Heiker JT, Beck-Sickinger AG (2006). Localization of novel adiponectin receptor constructs. *Journal of receptor and signal transduction research* 26(5-6): 647-657.

Delos Santos NM, Gardner LA, White SW, Bahouth SW (2006). Characterization of the residues in helix 8 of the human beta1-adrenergic receptor that are involved in coupling the receptor to G proteins. *The Journal of biological chemistry* 281(18): 12896-12907.

Deupi X, Kobilka B (2007). Activation of G protein-coupled receptors. *Advances in protein chemistry* 74: 137-166.

DeWire SM, Ahn S, Lefkowitz RJ, Shenoy SK (2007). Beta-arrestins and cell signaling. *Annual review of physiology* 69: 483-510.

Donaldson J, Brown AM, Hill SJ (1988). Influence of rolipram on the cyclic 3',5'-adenosine monophosphate response to histamine and adenosine in slices of guinea-pig cerebral cortex. *Biochemical pharmacology* 37(4): 715-723.

Dorsch S, Klotz KN, Engelhardt S, Lohse MJ, Bunemann M (2009). Analysis of receptor oligomerization by FRAP microscopy. *Nature methods* 6(3): 225-230.

Dowling MR, Charlton SJ (2006). Quantifying the association and dissociation rates of unlabelled antagonists at the muscarinic M3 receptor. *British journal of pharmacology* 148(7): 927-937.

Drake MT, Shenoy SK, Lefkowitz RJ (2006). Trafficking of G protein-coupled receptors. *Circulation research* 99(6): 570-582.

Drazner MH, Peppel KC, Dyer S, Grant AO, Koch WJ, Lefkowitz RJ (1997). Potentiation of beta-adrenergic signaling by adenoviral-mediated gene transfer in adult rabbit ventricular myocytes. *The Journal of clinical investigation* 99(2): 288-296.

Dubois EA, Somsen GA, van den Bos JC, Janssen AG, Boer GJ, Batink HD*, et al.* (1996). Pharmacologic characterization in vitro and in vivo of iodine 123-labeled derivatives of the beta-adrenoceptor antagonist CGP12177, designed for the imaging of cardiac beta-receptors. *Journal of nuclear cardiology : official publication of the American Society of Nuclear Cardiology* 3(3): 242-252.

Emorine LJ, Feve B, Pairault J, Briend-Sutren MM, Nahmias C, Marullo S*, et al.* (1992). The human beta 3-adrenergic receptor: relationship with atypical receptors. *The American journal of clinical nutrition* 55(1 Suppl): 215S-218S.

Endoh M (2008). Cardiac Ca2+ signaling and Ca2+ sensitizers. *Circulation journal : official journal of the Japanese Circulation Society* 72(12): 1915-1925.

Estrada R, Wang L, Jala VR, Lee JF, Lin CY, Gray RD*, et al.* (2009). Ligand-induced nuclear translocation of S1P(1) receptors mediates Cyr61 and CTGF transcription in endothelial cells. *Histochemistry and cell biology* 131(2): 239-249.

Falk MM, Lauf U (2001). High resolution, fluorescence deconvolution microscopy and tagging with the autofluorescent tracers CFP, GFP, and YFP to study the structural composition of gap junctions in living cells. *Microscopy research and technique* 52(3): 251-262.

Fan X, Petitt M, Gamboa M, Huang M, Dhal S, Druzin ML*, et al.* (2012). Transient, inducible, placenta-specific gene expression in mice. *Endocrinology* 153(11): 5637-5644.

Fernandez-Duenas V, Llorente J, Gandia J, Borroto-Escuela DO, Agnati LF, Tasca CI*, et al.* (2012). Fluorescence resonance energy transfer-based technologies in the study of protein-protein interactions at the cell surface. *Methods (San Diego, Calif.)* 57(4): 467-472.

Ferrandon S, Feinstein TN, Castro M, Wang B, Bouley R, Potts JT*, et al.* (2009). Sustained cyclic AMP production by parathyroid hormone receptor endocytosis. *Nature chemical biology* 5(10): 734-742.

Franco R, Casado V, Cortes A, Ferrada C, Mallol J, Woods A*, et al.* (2007). Basic concepts in G-protein-coupled receptor homo- and heterodimerization. *TheScientificWorldJournal* 7: 48-57.

Franco R, Casado V, Mallol J, Ferrada C, Ferre S, Fuxe K*, et al.* (2006). The two-state dimer receptor model: a general model for receptor dimers. *Molecular pharmacology* 69(6): 1905-1912.

Fredriksson R, Lagerstrom MC, Lundin LG, Schioth HB (2003). The G-protein-coupled receptors in the human genome form five main families. Phylogenetic analysis, paralogon groups, and fingerprints. *Molecular pharmacology* 63(6): 1256-1272.

Fredriksson R, Schioth HB (2005). The repertoire of G-protein-coupled receptors in fully sequenced genomes. *Molecular pharmacology* 67(5): 1414-1425.

Freedman NJ, Liggett SB, Drachman DE, Pei G, Caron MG, Lefkowitz RJ (1995). Phosphorylation and desensitization of the human beta 1-adrenergic receptor. Involvement of G protein-coupled receptor kinases and cAMP-dependent protein kinase. *The Journal of biological chemistry* 270(30): 17953-17961.

Freemantle N, Cleland J, Young P, Mason J, Harrison J (1999). beta Blockade after myocardial infarction: systematic review and meta regression analysis. *BMJ (Clinical research ed.)* 318(7200): 1730-1737.

Frielle T, Collins S, Daniel KW, Caron MG, Lefkowitz RJ, Kobilka BK (1987). Cloning of the cDNA for the human beta 1-adrenergic receptor. *Proceedings of the National Academy of Sciences of the United States of America* 84(22): 7920-7924.

Frielle T, Kobilka B, Lefkowitz RJ, Caron MG (1988). Human beta 1- and beta 2-adrenergic receptors: structurally and functionally related receptors derived from distinct genes. *Trends in neurosciences* 11(7): 321-324.

Fu C, Wang H, Wang S, Shi Y, Zhou X, Sun K*, et al.* (2008). Association of beta 1-adrenergic receptor gene polymorphisms with left ventricular hypertrophy in human essential hypertension. *Clinical biochemistry* 41(10-11): 773-778.

Fung JJ, Deupi X, Pardo L, Yao XJ, Velez-Ruiz GA, Devree BT*, et al.* (2009). Ligand-regulated oligomerization of beta(2)-adrenoceptors in a model lipid bilayer. *The EMBO journal* 28(21): 3315-3328.

Gaborik Z, Hunyady L (2004). Intracellular trafficking of hormone receptors. *Trends in endocrinology and metabolism: TEM* 15(6): 286-293.

Galandrin S, Oligny-Longpre G, Bonin H, Ogawa K, Gales C, Bouvier M (2008). Conformational rearrangements and signaling cascades involved in ligand-biased mitogen-activated protein kinase signaling through the beta1-adrenergic receptor. *Molecular pharmacology* 74(1): 162-172.

Galcera-Tomas J, Castillo-Soria FJ, Villegas-Garcia MM, Florenciano-Sanchez R, Sanchez-Villanueva JG, de La Rosa JA*, et al.* (2001). Effects of early use of atenolol or captopril on infarct size and ventricular volume: A double-blind comparison in patients with anterior acute myocardial infarction. *Circulation* 103(6): 813-819.

Gales C, Rebois RV, Hogue M, Trieu P, Breit A, Hebert TE*, et al.* (2005). Real-time monitoring of receptor and G-protein interactions in living cells. *Nature methods* 2(3): 177-184.

Gao ZG, Van Muijlwijk-Koezen JE, Chen A, Muller CE, Ijzerman AP, Jacobson KA (2001). Allosteric modulation of A(3) adenosine receptors by a series of 3-(2-pyridinyl)isoquinoline derivatives. *Molecular pharmacology* 60(5): 1057-1063.

Gautier A, Juillerat A, Heinis C, Correa IR, Jr., Kindermann M, Beaufils F*, et al.* (2008). An engineered protein tag for multiprotein labeling in living cells. *Chemistry & biology* 15(2): 128-136.

Gautier A, Nakata E, Lukinavicius G, Tan KT, Johnsson K (2009). Selective cross-linking of interacting proteins using self-labeling tags. *Journal of the American Chemical Society* 131(49): 17954-17962.

Gentles AJ, Karlin S (1999). Why are human G-protein-coupled receptors predominantly intronless? *Trends in genetics : TIG* 15(2): 47-49.

Gerits N, Kostenko S, Shiryaev A, Johannessen M, Moens U (2008). Relations between the mitogen-activated protein kinase and the cAMP-dependent protein kinase pathways: comradeship and hostility. *Cellular signalling* 20(9): 1592-1607.

Gong H, Kovar JL, Baker B, Zhang A, Cheung L, Draney DR*, et al.* (2012). Near-infrared fluorescence imaging of mammalian cells and xenograft tumors with SNAP-tag. *PloS one* 7(3): e34003.

Goupil E, Tassy D, Bourguet C, Quiniou C, Wisehart V, Petrin D*, et al.* (2010). A novel biased allosteric compound inhibitor of parturition selectively impedes the prostaglandin F2alpha-mediated Rho/ROCK signaling pathway. *The Journal of biological chemistry* 285(33): 25624-25636.

Granier S, Kim S, Shafer AM, Ratnala VR, Fung JJ, Zare RN*, et al.* (2007). Structure and conformational changes in the C-terminal domain of the beta2-adrenoceptor: insights from fluorescence resonance energy transfer studies. *The Journal of biological chemistry* 282(18): 13895-13905.

Green SA, Liggett SB (1994). A proline-rich region of the third intracellular loop imparts phenotypic beta 1-versus beta 2-adrenergic receptor coupling and sequestration. *The Journal of biological chemistry* 269(42): 26215-26219.

Green SA, Spasoff AP, Coleman RA, Johnson M, Liggett SB (1996). Sustained activation of a G protein-coupled receptor via "anchored" agonist binding. Molecular localization of the salmeterol exosite within the 2-adrenergic receptor. *The Journal of biological chemistry* 271(39): 24029-24035.

Gregory KJ, Sexton PM, Christopoulos A (2010). Overview of receptor allosterism. *Current protocols in pharmacology / editorial board, S.J. Enna (editor-in-chief) ... [et al.]* Chapter 1: Unit 1 21.

Guimaraes S, Moura D (2001). Vascular adrenoceptors: an update. *Pharmacological reviews* 53(2): 319-356.

Gurevich VV, Gurevich EV (2008). How and why do GPCRs dimerize? *Trends in pharmacological sciences* 29(5): 234-240.

Gutkind JS, Offermanns S (2009). A new G(q)-initiated MAPK signaling pathway in the heart. *Developmental cell* 16(2): 163-164.

Haase H, Karczewski P, Beckert R, Krause EG (1993). Phosphorylation of the L-type calcium channel beta subunit is involved in beta-adrenergic signal transduction in canine myocardium. *FEBS letters* 335(2): 217-222.

Haddad C, Wilkinson M, Roeder LM, Tildon JT, Armour JA (1987). Binding of the hydrophilic beta-adrenergic antagonist [3H]CGP-12177 to cardiac tissue slices: characterization and ontogenetic studies in dogs. *Canadian journal of physiology and pharmacology* 65(9): 1928-1933.

Haidekker MA, L'Heureux N, Frangos JA (2000). Fluid shear stress increases membrane fluidity in endothelial cells: a study with DCVJ fluorescence. *American journal of physiology. Heart and circulatory physiology* 278(4): H1401-1406.

Hakalahti AE, Tapanainen JM, Junttila JM, Kaikkonen KS, Huikuri HV, Petaja-Repo UE (2010a). Association of the beta-1 adrenergic receptor carboxyl terminal variants with left ventricular hypertrophy among diabetic and non-diabetic survivors of acute myocardial infarction. *Cardiovascular diabetology* 9: 42.

Hakalahti AE, Vierimaa MM, Lilja MK, Kumpula EP, Tuusa JT, Petaja-Repo UE (2010b). Human beta1-adrenergic receptor is subject to constitutive and regulated N-terminal cleavage. *The Journal of biological chemistry* 285(37): 28850-28861.

Hall RA (2004). Beta-adrenergic receptors and their interacting proteins. *Seminars in cell & developmental biology* 15(3): 281-288.

Hamm HE (1998). The many faces of G protein signaling. *The Journal of biological chemistry* 273(2): 669-672.

Han Y, Moreira IS, Urizar E, Weinstein H, Javitch JA (2009). Allosteric communication between protomers of dopamine class A GPCR dimers modulates activation. *Nature chemical biology* 5(9): 688-695.

Hanoune J, Defer N (2001). Regulation and role of adenylyl cyclase isoforms. *Annual review of pharmacology and toxicology* 41: 145-174.

Hara T, Hirasawa A, Sun Q, Koshimizu TA, Itsubo C, Sadakane K*, et al.* (2009). Flow cytometry-based binding assay for GPR40 (FFAR1; free fatty acid receptor 1). *Molecular pharmacology* 75(1): 85-91.

Hargreaves AC, Lummis SC, Taylor CW (1994). Ca2+ permeability of cloned and native 5-hydroxytryptamine type 3 receptors. *Molecular pharmacology* 46(6): 1120-1128.

He J, Xu J, Castleberry AM, Lau AG, Hall RA (2002). Glycosylation of beta(1)-adrenergic receptors regulates receptor surface expression and dimerization. *Biochemical and biophysical research communications* 297(3): 565-572.

Hebert TE, Moffett S, Morello JP, Loisel TP, Bichet DG, Barret C*, et al.* (1996). A peptide derived from a beta2-adrenergic receptor transmembrane domain inhibits both receptor dimerization and activation. *The Journal of biological chemistry* 271(27): 16384-16392.

Heim R, Cubitt AB, Tsien RY (1995). Improved green fluorescence. *Nature* 373(6516): 663-664.

Henderson R, Unwin PN (1975). Three-dimensional model of purple membrane obtained by electron microscopy. *Nature* 257(5521): 28-32.

Hern JA, Baig AH, Mashanov GI, Birdsall B, Corrie JE, Lazareno S*, et al.* (2010). Formation and dissociation of M1 muscarinic receptor dimers seen by total internal reflection fluorescence imaging of single molecules. *Proceedings of the National Academy of Sciences of the United States of America* 107(6): 2693-2698.

Herrick-Davis K, Grinde E, Lindsley T, Cowan A, Mazurkiewicz JE (2012). Oligomer size of the serotonin 5-hydroxytryptamine 2C (5-HT2C) receptor revealed by fluorescence correlation spectroscopy with photon counting histogram analysis: evidence for homodimers without monomers or tetramers. *The Journal of biological chemistry* 287(28): 23604-23614.

Herrick-Davis K, Weaver BA, Grinde E, Mazurkiewicz JE (2006). Serotonin 5-HT2C receptor homodimer biogenesis in the endoplasmic reticulum: real-time visualization with confocal fluorescence resonance energy transfer. *The Journal of biological chemistry* 281(37): 27109-27116.

Hill SJ, Baker JG, Rees S (2001). Reporter-gene systems for the study of G-protein-coupled receptors. *Current opinion in pharmacology* 1(5): 526-532.

Hlavackova V, Goudet C, Kniazeff J, Zikova A, Maurel D, Vol C*, et al.* (2005). Evidence for a single heptahelical domain being turned on upon activation of a dimeric GPCR. *The EMBO journal* 24(3): 499-509.

Hogg JC (1984). The pathology of asthma. *Clinics in chest medicine* 5(4): 567-571.

Hu CD, Kerppola TK (2003a). Simultaneous visualization of multiple protein interactions in living cells using multicolor fluorescence complementation analysis. *Nature biotechnology* 21(5): 539-545.

Hu J, Thor D, Zhou Y, Liu T, Wang Y, McMillin SM*, et al.* (2012). Structural aspects of M(3) muscarinic acetylcholine receptor dimer formation and activation. *FASEB journal : official publication of the Federation of American Societies for Experimental Biology* 26(2): 604-616.

Hu LA, Chen W, Martin NP, Whalen EJ, Premont RT, Lefkowitz RJ (2003b). GIPC interacts with the beta1-adrenergic receptor and regulates beta1-

adrenergic receptor-mediated ERK activation. *The Journal of biological chemistry* 278(28): 26295-26301.

Hu LA, Tang Y, Miller WE, Cong M, Lau AG, Lefkowitz RJ*, et al.* (2000). beta 1-adrenergic receptor association with PSD-95. Inhibition of receptor internalization and facilitation of beta 1-adrenergic receptor interaction with N-methyl-D-aspartate receptors. *The Journal of biological chemistry* 275(49): 38659-38666.

Huang J, Chen S, Zhang JJ, Huang XY (2013). Crystal structure of oligomeric beta1-adrenergic G protein-coupled receptors in ligand-free basal state. *Nature structural & molecular biology* 20(4): 419-425.

Hulme EC, Trevethick MA (2010). Ligand binding assays at equilibrium: validation and interpretation. *British journal of pharmacology* 161(6): 1219-1237.

Iqbal A, Arslan S, Okumus B, Wilson TJ, Giraud G, Norman DG*, et al.* (2008). Orientation dependence in fluorescent energy transfer between Cy3 and Cy5 terminally attached to double-stranded nucleic acids. *Proceedings of the National Academy of Sciences of the United States of America* 105(32): 11176-11181.

Iriki M, Simon E (2012). Differential control of efferent sympathetic activity revisited. *The journal of physiological sciences : JPS* 62(4): 275-298.

Jean-Alphonse F, Hanyaloglu AC (2011). Regulation of GPCR signal networks via membrane trafficking. *Molecular and cellular endocrinology* 331(2): 205-214.

Johnston JM, Aburi M, Provasi D, Bortolato A, Urizar E, Lambert NA*, et al.* (2011). Making structural sense of dimerization interfaces of delta opioid receptor homodimers. *Biochemistry* 50(10): 1682-1690.

Jones KA, Borowsky B, Tamm JA, Craig DA, Durkin MM, Dai M*, et al.* (1998). GABA(B) receptors function as a heteromeric assembly of the subunits GABA(B)R1 and GABA(B)R2. *Nature* 396(6712): 674-679.

Jordan BA, Devi LA (1999). G-protein-coupled receptor heterodimerization modulates receptor function. *Nature* 399(6737): 697-700.

Joseph SS, Lynham JA, Colledge WH, Kaumann AJ (2004). Binding of (-)-[3H]-CGP12177 at two sites in recombinant human beta 1-adrenoceptors and interaction with beta-blockers. *Naunyn-Schmiedeberg's archives of pharmacology* 369(5): 525-532.

Joseph SS, Lynham JA, Molenaar P, Grace AA, Colledge WH, Kaumann AJ (2003). Intrinsic sympathomimetic activity of (-)-pindolol mediated through a (-)-propranolol-resistant site of the beta1-adrenoceptor in human atrium and recombinant receptors. *Naunyn-Schmiedeberg's archives of pharmacology* 368(6): 496-503.

Juillerat A, Gronemeyer T, Keppler A, Gendreizig S, Pick H, Vogel H*, et al.* (2003). Directed evolution of O6-alkylguanine-DNA alkyltransferase for efficient labeling of fusion proteins with small molecules in vivo. *Chemistry & biology* 10(4): 313-317.

Juillerat A, Heinis C, Sielaff I, Barnikow J, Jaccard H, Kunz B*, et al.* (2005). Engineering substrate specificity of O6-alkylguanine-DNA alkyltransferase for specific protein labeling in living cells. *Chembiochem : a European journal of chemical biology* 6(7): 1263-1269.

Kampmeier F, Niesen J, Koers A, Ribbert M, Brecht A, Fischer R*, et al.* (2010). Rapid optical imaging of EGF receptor expression with a single-chain antibody SNAP-tag fusion protein. *European journal of nuclear medicine and molecular imaging* 37(10): 1926-1934.

Kasai RS, Suzuki KG, Prossnitz ER, Koyama-Honda I, Nakada C, Fujiwara TK*, et al.* (2011). Full characterization of GPCR monomer-dimer dynamic equilibrium by single molecule imaging. *The Journal of cell biology* 192(3): 463-480.

Kaumann A, Semmler AB, Molenaar P (2007). The effects of both noradrenaline and CGP12177, mediated through human beta1 -adrenoceptors, are reduced by PDE3 in human atrium but PDE4 in CHO cells. *Naunyn-Schmiedeberg's archives of pharmacology* 375(2): 123-131.

Kaumann AJ (1997). Four beta-adrenoceptor subtypes in the mammalian heart. *Trends in pharmacological sciences* 18(3): 70-76.

Kaumann AJ (1989). Is there a third heart beta-adrenoceptor? *Trends in pharmacological sciences* 10(8): 316-320.

Kaumann AJ, Blinks JR (1980). Stimulant and depressant effects of beta-adrenoceptor blocking agents on isolated heart muscle. A positive inotropic effect not mediated through andrenoceptors. *Naunyn-Schmiedeberg's archives of pharmacology* 311(3): 205-218.

Kaumann AJ, Engelhardt S, Hein L, Molenaar P, Lohse M (2001). Abolition of (-)-CGP 12177-evoked cardiostimulation in double beta1/beta2-adrenoceptor knockout mice. Obligatory role of beta1-adrenoceptors for putative beta4-adrenoceptor pharmacology. *Naunyn-Schmiedeberg's archives of pharmacology* 363(1): 87-93.

Kaumann AJ, Lynham JA (1997). Stimulation of cyclic AMP-dependent protein kinase in rat atria by (-)-CGP 12177 through an atypical beta-adrenoceptor. *British journal of pharmacology* 120(7): 1187-1189.

Kaumann AJ, Molenaar P (2008). The low-affinity site of the beta1-adrenoceptor and its relevance to cardiovascular pharmacology. *Pharmacology & therapeutics* 118(3): 303-336.

Kaumann AJ, Morris TH, Bojar H (1983). Heart beta-receptors: on the functional role of heterogeneous binding sites. *Journal of receptor research* 3(1-2): 61-70.

Kaupmann K, Malitschek B, Schuler V, Heid J, Froestl W, Beck P*, et al.* (1998). GABA(B)-receptor subtypes assemble into functional heteromeric complexes. *Nature* 396(6712): 683-687.

Kenakin T (1997). Agonist-specific receptor conformations. *Trends in pharmacological sciences* 18(11): 416-417.

Kenakin T (1990). Drugs and receptors. An overview of the current state of knowledge. *Drugs* 40(5): 666-687.

Kenakin T (2005). New concepts in drug discovery: collateral efficacy and permissive antagonism. *Nature reviews. Drug discovery* 4(11): 919-927.

Kenakin T (2008). Overview of receptor interactions of agonists and antagonists. *Current protocols in pharmacology / editorial board, S.J. Enna (editor-in-chief) ... [et al.]* Chapter 4: Unit 4 1.

Kenakin T, Miller LJ (2010). Seven transmembrane receptors as shapeshifting proteins: the impact of allosteric modulation and functional selectivity on new drug discovery. *Pharmacological reviews* 62(2): 265-304.

Kenakin TP, Beek D (1984). The measurement of the relative efficacy of agonists by selective potentiation of tissue responses: studies with isoprenaline and prenalterol in cardiac tissue. *Journal of autonomic pharmacology* 4(3): 153-159.

Keppler A, Gendreizig S, Gronemeyer T, Pick H, Vogel H, Johnsson K (2003). A general method for the covalent labeling of fusion proteins with small molecules in vivo. *Nature biotechnology* 21(1): 86-89.

Kerppola TK (2008). Bimolecular fluorescence complementation (BiFC) analysis as a probe of protein interactions in living cells. *Annual review of biophysics* 37: 465-487.

Kilpatrick LE, Briddon SJ, Hill SJ, Holliday ND (2010). Quantitative analysis of neuropeptide Y receptor association with beta-arrestin2 measured by bimolecular fluorescence complementation. *British journal of pharmacology* 160(4): 892-906.

Kilpatrick LE, Holliday ND (2012). Dissecting the pharmacology of G protein-coupled receptor signaling complexes using bimolecular fluorescence complementation. *Methods in molecular biology (Clifton, N.J.)* 897: 109-138.

Kiss AL, Botos E (2009). Endocytosis via caveolae: alternative pathway with distinct cellular compartments to avoid lysosomal degradation? *Journal of cellular and molecular medicine* 13(7): 1228-1237.

Klebe G, Bohm HJ (1997). Energetic and entropic factors determining binding affinity in protein-ligand complexes. *Journal of receptor and signal transduction research* 17(1-3): 459-473.

Kniazeff J, Prezeau L, Rondard P, Pin JP, Goudet C (2011). Dimers and beyond: The functional puzzles of class C GPCRs. *Pharmacology & therapeutics* 130(1): 9-25.

Knoflach F, Mutel V, Jolidon S, Kew JN, Malherbe P, Vieira E*, et al.* (2001). Positive allosteric modulators of metabotropic glutamate 1 receptor:

characterization, mechanism of action, and binding site. *Proceedings of the National Academy of Sciences of the United States of America* 98(23): 13402-13407.

Kolakowski LF, Jr. (1994). GCRDb: a G-protein-coupled receptor database. *Receptors & channels* 2(1): 1-7.

Kompa AR, Summers RJ (1999). Desensitization and resensitization of beta 1- and putative beta 4-adrenoceptor mediated responses occur in parallel in a rat model of cardiac failure. *British journal of pharmacology* 128(7): 1399-1406.

Konkar AA, Zhu Z, Granneman JG (2000). Aryloxypropanolamine and catecholamine ligand interactions with the beta(1)-adrenergic receptor: evidence for interaction with distinct conformations of beta(1)-adrenergic receptors. *The Journal of pharmacology and experimental therapeutics* 294(3): 923-932.

Langmead CJ, Christopoulos A (2006). Allosteric agonists of 7TM receptors: expanding the pharmacological toolbox. *Trends in pharmacological sciences* 27(9): 475-481.

Lazareno S, Popham A, Birdsall NJ (2000). Allosteric interactions of staurosporine and other indolocarbazoles with N-[methyl-(3)H]scopolamine and acetylcholine at muscarinic receptor subtypes: identification of a second allosteric site. *Molecular pharmacology* 58(1): 194-207.

Lazareno S, Popham A, Birdsall NJ (2002). Analogs of WIN 62,577 define a second allosteric site on muscarinic receptors. *Molecular pharmacology* 62(6): 1492-1505.

Lee PH, Hanson BJ (2010). Development of a GPR23 cell-based beta-lactamase reporter assay. *Methods in enzymology* 485: 349-368.

Leff P (1995a). Inverse agonism: theory and practice. *Trends in pharmacological sciences* 16(8): 256.

Leff P (1995b). The two-state model of receptor activation. *Trends in pharmacological sciences* 16(3): 89-97.

Leff P, Dougall IG, Harper D (1993). Estimation of partial agonist affinity by interaction with a full agonist: a direct operational model-fitting approach. *British journal of pharmacology* 110(1): 239-244.

Leff P, Martin GR, Morse JM (1985). Application of the operational model of agonism to establish conditions when functional antagonism may be used to estimate agonist dissociation constants. *British journal of pharmacology* 85(3): 655-663.

Leff P, Scaramellini C, Law C, McKechnie K (1997). A three-state receptor model of agonist action. *Trends in pharmacological sciences* 18(10): 355-362.

Levin MC, Marullo S, Muntaner O, Andersson B, Magnusson Y (2002). The myocardium-protective Gly-49 variant of the beta 1-adrenergic receptor exhibits constitutive activity and increased desensitization and down-regulation. *The Journal of biological chemistry* 277(34): 30429-30435.

Leyris JP, Roux T, Trinquet E, Verdie P, Fehrentz JA, Oueslati N*, et al.* (2011). Homogeneous time-resolved fluorescence-based assay to screen for ligands targeting the growth hormone secretagogue receptor type 1a. *Analytical biochemistry* 408(2): 253-262.

Liang Q, Molkentin JD (2003). Redefining the roles of p38 and JNK signaling in cardiac hypertrophy: dichotomy between cultured myocytes and animal models. *Journal of molecular and cellular cardiology* 35(12): 1385-1394.

Liang W, Fishman PH (2004). Resistance of the human beta1-adrenergic receptor to agonist-induced ubiquitination: a mechanism for impaired receptor degradation. *The Journal of biological chemistry* 279(45): 46882-46889.

Loison S, Cottet M, Orcel H, Adihou H, Rahmeh R, Lamarque L*, et al.* (2012). Selective fluorescent nonpeptidic antagonists for vasopressin V(2) GPCR: application to ligand screening and oligomerization assays. *Journal of medicinal chemistry* 55(20): 8588-8602.

Los GV, Encell LP, McDougall MG, Hartzell DD, Karassina N, Zimprich C*, et al.* (2008). HaloTag: a novel protein labeling technology for cell imaging and protein analysis. *ACS chemical biology* 3(6): 373-382.

Lowe MD, Grace AA, Kaumann AJ (1999). Blockade of putative beta4- and beta1-adrenoceptors by carvedilol in ferret myocardium. *Naunyn-Schmiedeberg's archives of pharmacology* 359(5): 400-403.

Lundstrom K, Wagner R, Reinhart C, Desmyter A, Cherouati N, Magnin T*, et al.* (2006). Structural genomics on membrane proteins: comparison of more than 100 GPCRs in 3 expression systems. *Journal of structural and functional genomics* 7(2): 77-91.

Luttrell LM, Kenakin TP (2011). Refining efficacy: allosterism and bias in G protein-coupled receptor signaling. *Methods in molecular biology (Clifton, N.J.)* 756: 3-35.

Luttrell LM, Lefkowitz RJ (2002). The role of beta-arrestins in the termination and transduction of G-protein-coupled receptor signals. *Journal of cell science* 115(Pt 3): 455-465.

Ma YC, Huang J, Ali S, Lowry W, Huang XY (2000). Src tyrosine kinase is a novel direct effector of G proteins. *Cell* 102(5): 635-646.

Malbon CC (2004). Frizzleds: new members of the superfamily of G-protein-coupled receptors. *Frontiers in bioscience : a journal and virtual library* 9: 1048-1058.

Mantyh PW, Rogers SD, Allen CJ, Catton MD, Ghilardi JR, Levin LA*, et al.* (1995). Beta 2-adrenergic receptors are expressed by glia in vivo in the normal and injured central nervous system in the rat, rabbit, and human. *The Journal of neuroscience : the official journal of the Society for Neuroscience* 15(1 Pt 1): 152-164.

Maqbool A, Hall AS, Ball SG, Balmforth AJ (1999). Common polymorphisms of beta1-adrenoceptor: identification and rapid screening assay. *Lancet* 353(9156): 897.

Marchese A, Paing MM, Temple BR, Trejo J (2008). G protein-coupled receptor sorting to endosomes and lysosomes. *Annual review of pharmacology and toxicology* 48: 601-629.

Marchese A, Trejo J (2013). Ubiquitin-dependent regulation of G protein-coupled receptor trafficking and signaling. *Cellular signalling* 25(3): 707-716.

Marullo S, Bouvier M (2007). Resonance energy transfer approaches in molecular pharmacology and beyond. *Trends in pharmacological sciences* 28(8): 362-365.

Mason DA, Moore JD, Green SA, Liggett SB (1999). A gain-of-function polymorphism in a G-protein coupling domain of the human beta1-adrenergic receptor. *The Journal of biological chemistry* 274(18): 12670-12674.

Maurel D, Comps-Agrar L, Brock C, Rives ML, Bourrier E, Ayoub MA*, et al.* (2008). Cell-surface protein-protein interaction analysis with time-resolved FRET and snap-tag technologies: application to GPCR oligomerization. *Nature methods* 5(6): 561-567.

May LT, Avlani VA, Langmead CJ, Herdon HJ, Wood MD, Sexton PM*, et al.* (2007). Structure-function studies of allosteric agonism at M2 muscarinic acetylcholine receptors. *Molecular pharmacology* 72(2): 463-476.

May LT, Briddon SJ, Hill SJ (2010a). Antagonist selective modulation of adenosine A1 and A3 receptor pharmacology by the food dye Brilliant Black BN: evidence for allosteric interactions. *Molecular pharmacology* 77(4): 678-686.

May LT, Bridge LJ, Stoddart LA, Briddon SJ, Hill SJ (2011). Allosteric interactions across native adenosine-A3 receptor homodimers: quantification using single-cell ligand-binding kinetics. *FASEB journal : official publication of the Federation of American Societies for Experimental Biology* 25(10): 3465-3476.

May LT, Self TJ, Briddon SJ, Hill SJ (2010b). The effect of allosteric modulators on the kinetics of agonist-G protein-coupled receptor interactions in single living cells. *Molecular pharmacology* 78(3): 511-523.

McDonnell J, Latif ML, Rees ES, Bevan NJ, Hill SJ (1998). Influence of receptor number on the stimulation by salmeterol of gene transcription in CHO-K1 cells transfected with the human beta2-adrenoceptor. *British journal of pharmacology* 125(4): 717-726.

McGrath JC, Arribas S, Daly CJ (1996). Fluorescent ligands for the study of receptors. *Trends in pharmacological sciences* 17(11): 393-399.

McLean AJ, Milligan G (2000). Ligand regulation of green fluorescent protein-tagged forms of the human beta(1)- and beta(2)-adrenoceptors; comparisons with the unmodified receptors. *British journal of pharmacology* 130(8): 1825-1832.

Mercier JF, Salahpour A, Angers S, Breit A, Bouvier M (2002). Quantitative assessment of beta 1- and beta 2-adrenergic receptor homo- and heterodimerization by bioluminescence resonance energy transfer. *The Journal of biological chemistry* 277(47): 44925-44931.

Middleton RJ, Briddon SJ, Cordeaux Y, Yates AS, Dale CL, George MW*, et al.* (2007). New fluorescent adenosine A1-receptor agonists that allow quantification of ligand-receptor interactions in microdomains of single living cells. *Journal of medicinal chemistry* 50(4): 782-793.

Middleton RJ, Kellam B (2005). Fluorophore-tagged GPCR ligands. *Current opinion in chemical biology* 9(5): 517-525.

Mie M, Naoki T, Uchida K, Kobatake E (2012). Development of a split SNAP-tag protein complementation assay for visualization of protein-protein interactions in living cells. *The Analyst* 137(20): 4760-4765.

Milligan G (2004). Applications of bioluminescence- and fluorescence resonance energy transfer to drug discovery at G protein-coupled receptors. *European journal of pharmaceutical sciences : official journal of the European Federation for Pharmaceutical Sciences* 21(4): 397-405.

Milligan G (2009). G protein-coupled receptor hetero-dimerization: contribution to pharmacology and function. *British journal of pharmacology* 158(1): 5-14.

Milligan G, Smith NJ (2007). Allosteric modulation of heterodimeric G-protein-coupled receptors. *Trends in pharmacological sciences* 28(12): 615-620.

Misra S, Wu Y, Venkataraman G, Sopory SK, Tuteja N (2007). Heterotrimeric G-protein complex and G-protein-coupled receptor from a legume (Pisum sativum): role in salinity and heat stress and cross-talk with phospholipase C. *The Plant journal : for cell and molecular biology* 51(4): 656-669.

Motulsky HJ, Mahan LC (1984). The kinetics of competitive radioligand binding predicted by the law of mass action. *Molecular pharmacology* 25(1): 1-9.

Mutlu GM, Factor P (2008). Alveolar epithelial beta2-adrenergic receptors. *American journal of respiratory cell and molecular biology* 38(2): 127-134.

Nakata H, Suzuki T, Namba K, Oyanagi K (2010). Dimerization of G protein-coupled purinergic receptors: increasing the diversity of purinergic receptor signal responses and receptor functions. *Journal of receptor and signal transduction research* 30(5): 337-346.

Neil-Dwyer G, Bartlett J, McAinsh J, Cruickshank JM (1981). Beta-adrenoceptor blockers and the blood-brian barrier. *British journal of clinical pharmacology* 11(6): 549-553.

Neugart F, Zappe A, Buk DM, Ziegler I, Steinert S, Schumacher M*, et al.* (2009). Detection of ligand-induced CNTF receptor dimers in living cells by fluorescence cross correlation spectroscopy. *Biochimica et biophysica acta* 1788(9): 1890-1900.

New DC, Wong YH (2007). Molecular mechanisms mediating the G protein-coupled receptor regulation of cell cycle progression. *Journal of molecular signaling* 2: 2.

Nikolaev VO, Bunemann M, Schmitteckert E, Lohse MJ, Engelhardt S (2006). Cyclic AMP imaging in adult cardiac myocytes reveals far-reaching beta1-adrenergic but locally confined beta2-adrenergic receptor-mediated signaling. *Circulation research* 99(10): 1084-1091.

Nobles KN, Xiao K, Ahn S, Shukla AK, Lam CM, Rajagopal S*, et al.* (2011). Distinct phosphorylation sites on the beta(2)-adrenergic receptor establish a barcode that encodes differential functions of beta-arrestin. *Science signaling* 4(185): ra51.

Noel F, Mendonca-Silva DL, Quintas LE (2001). Radioligand binding assays in the drug discovery process: potential pitfalls of high throughput screenings. *Arzneimittel-Forschung* 51(2): 169-173.

Noma T, Lemaire A, Naga Prasad SV, Barki-Harrington L, Tilley DG, Chen J*, et al.* (2007). Beta-arrestin-mediated beta1-adrenergic receptor transactivation

of the EGFR confers cardioprotection. *The Journal of clinical investigation* 117(9): 2445-2458.

Nomura W, Tanabe Y, Tsutsumi H, Tanaka T, Ohba K, Yamamoto N*, et al.* (2008). Fluorophore labeling enables imaging and evaluation of specific CXCR4-ligand interaction at the cell membrane for fluorescence-based screening. *Bioconjugate chemistry* 19(9): 1917-1920.

Noor N, Patel CB, Rockman HA (2011). Beta-arrestin: a signaling molecule and potential therapeutic target for heart failure. *Journal of molecular and cellular cardiology* 51(4): 534-541.

Ormo M, Cubitt AB, Kallio K, Gross LA, Tsien RY, Remington SJ (1996). Crystal structure of the Aequorea victoria green fluorescent protein. *Science (New York, N.Y.)* 273(5280): 1392-1395.

Ostrom RS, Bogard AS, Gros R, Feldman RD (2012). Choreographing the adenylyl cyclase signalosome: sorting out the partners and the steps. *Naunyn-Schmiedeberg's archives of pharmacology* 385(1): 5-12.

Ostrom RS, Gregorian C, Drenan RM, Xiang Y, Regan JW, Insel PA (2001). Receptor number and caveolar co-localization determine receptor coupling efficiency to adenylyl cyclase. *The Journal of biological chemistry* 276(45): 42063-42069.

Ostrom RS, Naugle JE, Hase M, Gregorian C, Swaney JS, Insel PA*, et al.* (2003). Angiotensin II enhances adenylyl cyclase signaling via Ca2+/calmodulin. Gq-Gs cross-talk regulates collagen production in cardiac fibroblasts. *The Journal of biological chemistry* 278(27): 24461-24468.

Overton MC, Blumer KJ (2002). Use of fluorescence resonance energy transfer to analyze oligomerization of G-protein-coupled receptors expressed in yeast. *Methods (San Diego, Calif.)* 27(4): 324-332.

Pak MD, Fishman PH (1996). Anomalous behavior of CGP 12177A on beta 1-adrenergic receptors. *Journal of receptor and signal transduction research* 16(1-2): 1-23.

Pak Y, Pham N, Rotin D (2002). Direct binding of the beta1 adrenergic receptor to the cyclic AMP-dependent guanine nucleotide exchange factor

CNrasGEF leads to Ras activation. *Molecular and cellular biology* 22(22): 7942-7952.

Palczewski K, Kumasaka T, Hori T, Behnke CA, Motoshima H, Fox BA*, et al.* (2000). Crystal structure of rhodopsin: A G protein-coupled receptor. *Science (New York, N.Y.)* 289(5480): 739-745.

Palm D, Munch G, Dees C, Hekman M (1989). Mapping of beta-adrenoceptor coupling domains to Gs-protein by site-specific synthetic peptides. *FEBS letters* 254(1-2): 89-93.

Palmer TD, Rosman GJ, Osborne WR, Miller AD (1991). Genetically modified skin fibroblasts persist long after transplantation but gradually inactivate introduced genes. *Proceedings of the National Academy of Sciences of the United States of America* 88(4): 1330-1334.

Panetta R, Greenwood MT (2008). Physiological relevance of GPCR oligomerization and its impact on drug discovery. *Drug discovery today* 13(23-24): 1059-1066.

Parker MS, Sah R, Balasubramaniam A, Sallee FR, Sweatman T, Park EA*, et al.* (2008). Dimers of the neuropeptide Y (NPY) Y2 receptor show asymmetry in agonist affinity and association with G proteins. *Journal of receptor and signal transduction research* 28(5): 437-451.

Patel PA, Tilley DG, Rockman HA (2008). Beta-arrestin-mediated signaling in the heart. *Circulation journal : official journal of the Japanese Circulation Society* 72(11): 1725-1729.

Patel RC, Kumar U, Lamb DC, Eid JS, Rocheville M, Grant M*, et al.* (2002). Ligand binding to somatostatin receptors induces receptor-specific oligomer formation in live cells. *Proceedings of the National Academy of Sciences of the United States of America* 99(5): 3294-3299.

Pegg AE (2011). Multifaceted roles of alkyltransferase and related proteins in DNA repair, DNA damage, resistance to chemotherapy, and research tools. *Chemical research in toxicology* 24(5): 618-639.

Pellissier LP, Barthet G, Gaven F, Cassier E, Trinquet E, Pin JP*, et al.* (2011). G protein activation by serotonin type 4 receptor dimers: evidence that

turning on two protomers is more efficient. *The Journal of biological chemistry* 286(12): 9985-9997.

Perlman RL, Chalfie M (1977). Catecholamine release from the adrenal medulla. *Clinics in endocrinology and metabolism* 6(3): 551-576.

Pierce KL, Premont RT, Lefkowitz RJ (2002). Seven-transmembrane receptors. *Nature reviews. Molecular cell biology* 3(9): 639-650.

Pierre S, Eschenhagen T, Geisslinger G, Scholich K (2009). Capturing adenylyl cyclases as potential drug targets. *Nature reviews. Drug discovery* 8(4): 321-335.

Pisterzi LF, Jansma DB, Georgiou J, Woodside MJ, Chou JT, Angers S*, et al.* (2010). Oligomeric size of the m2 muscarinic receptor in live cells as determined by quantitative fluorescence resonance energy transfer. *The Journal of biological chemistry* 285(22): 16723-16738.

Poirier L, Lacourciere Y (2012). The evolving role of beta-adrenergic receptor blockers in managing hypertension. *The Canadian journal of cardiology* 28(3): 334-340.

Polakova E, Zahradnikova A, Jr., Pavelkova J, Zahradnik I, Zahradnikova A (2008). Local calcium release activation by DHPR calcium channel openings in rat cardiac myocytes. *The Journal of physiology* 586(16): 3839-3854.

Prasher DC, Eckenrode VK, Ward WW, Prendergast FG, Cormier MJ (1992). Primary structure of the Aequorea victoria green-fluorescent protein. *Gene* 111(2): 229-233.

Prenner L, Sieben A, Zeller K, Weiser D, Haberlein H (2007). Reduction of high-affinity beta2-adrenergic receptor binding by hyperforin and hyperoside on rat C6 glioblastoma cells measured by fluorescence correlation spectroscopy. *Biochemistry* 46(17): 5106-5113.

Pucadyil TJ, Chattopadhyay A (2007). Cholesterol depletion induces dynamic confinement of the G-protein coupled serotonin(1A) receptor in the plasma membrane of living cells. *Biochimica et biophysica acta* 1768(3): 655-668.

Puck TT, Cieciura SJ, Robinson A (1958). Genetics of somatic mammalian cells. III. Long-term cultivation of euploid cells from human and animal subjects. *The Journal of experimental medicine* 108(6): 945-956.

Rajagopal S, Ahn S, Rominger DH, Gowen-MacDonald W, Lam CM, Dewire SM*, et al.* (2011). Quantifying ligand bias at seven-transmembrane receptors. *Molecular pharmacology* 80(3): 367-377.

Rapacciuolo A, Suvarna S, Barki-Harrington L, Luttrell LM, Cong M, Lefkowitz RJ*, et al.* (2003). Protein kinase A and G protein-coupled receptor kinase phosphorylation mediates beta-1 adrenergic receptor endocytosis through different pathways. *The Journal of biological chemistry* 278(37): 35403-35411.

Rashid AJ, So CH, Kong MM, Furtak T, El-Ghundi M, Cheng R*, et al.* (2007). D1-D2 dopamine receptor heterooligomers with unique pharmacology are coupled to rapid activation of Gq/11 in the striatum. *Proceedings of the National Academy of Sciences of the United States of America* 104(2): 654-659.

Rasmussen SG, Choi HJ, Rosenbaum DM, Kobilka TS, Thian FS, Edwards PC*, et al.* (2007). Crystal structure of the human beta2 adrenergic G-protein-coupled receptor. *Nature* 450(7168): 383-387.

Rathz DA, Brown KM, Kramer LA, Liggett SB (2002). Amino acid 49 polymorphisms of the human beta1-adrenergic receptor affect agonist-promoted trafficking. *Journal of cardiovascular pharmacology* 39(2): 155-160.

Rayo J, Amara N, Krief P, Meijler MM (2011). Live cell labeling of native intracellular bacterial receptors using aniline-catalyzed oxime ligation. *Journal of the American Chemical Society* 133(19): 7469-7475.

Reymond L, Lukinavicius G, Umezawa K, Maurel D, Brun MA, Masharina A*, et al.* (2011). Visualizing biochemical activities in living cells through chemistry. *Chimia* 65(11): 868-871.

Romano C, Yang WL, O'Malley KL (1996). Metabotropic glutamate receptor 5 is a disulfide-linked dimer. *The Journal of biological chemistry* 271(45): 28612-28616.

Rose RH, Briddon SJ, Hill SJ (2012). A novel fluorescent histamine H(1) receptor antagonist demonstrates the advantage of using fluorescence correlation spectroscopy to study the binding of lipophilic ligands. *British journal of pharmacology* 165(6): 1789-1800.

Rose RH, Briddon SJ, Holliday ND (2010). Bimolecular fluorescence complementation: lighting up seven transmembrane domain receptor signalling networks. *British journal of pharmacology* 159(4): 738-750.

Salahpour A, Espinoza S, Masri B, Lam V, Barak LS, Gainetdinov RR (2012). BRET biosensors to study GPCR biology, pharmacology, and signal transduction. *Frontiers in endocrinology* 3: 105.

Salomon Y, Londos C, Rodbell M (1974). A highly sensitive adenylate cyclase assay. *Analytical biochemistry* 58(2): 541-548.

Sample V, Newman RH, Zhang J (2009). The structure and function of fluorescent proteins. *Chemical Society reviews* 38(10): 2852-2864.

Sanz-Rosa D, Garcia-Prieto J, Ibanez B (2012). The future: therapy of myocardial protection. *Annals of the New York Academy of Sciences* 1254: 90-98.

Sarsero D, Molenaar P, Kaumann AJ (1998). Validity of (-)-[3H]-CGP 12177A as a radioligand for the 'putative beta4-adrenoceptor' in rat atrium. *British journal of pharmacology* 123(3): 371-380.

Sarsero D, Russell FD, Lynham JA, Rabnott G, Yang I, Fong KM*, et al.* (2003). (-)-CGP 12177 increases contractile force and hastens relaxation of human myocardial preparations through a propranolol-resistant state of the beta 1-adrenoceptor. *Naunyn-Schmiedeberg's archives of pharmacology* 367(1): 10-21.

Sawa M, Harada H (2006). Recent developments in the design of orally bioavailable beta3-adrenergic receptor agonists. *Current medicinal chemistry* 13(1): 25-37.

Scherrer G, Tryoen-Toth P, Filliol D, Matifas A, Laustriat D, Cao YQ*, et al.* (2006). Knockin mice expressing fluorescent delta-opioid receptors uncover G protein-coupled receptor dynamics in vivo. *Proceedings of the National Academy of Sciences of the United States of America* 103(25): 9691-9696.

Schneider E, Keller M, Brennauer A, Hoefelschweiger BK, Gross D, Wolfbeis OS*, et al.* (2007). Synthesis and characterization of the first fluorescent nonpeptide NPY Y1 receptor antagonist. *Chembiochem : a European journal of chemical biology* 8(16): 1981-1988.

Sen S, Jaakola VP, Heimo H, Engstrom M, Larjomaa P, Scheinin M*, et al.* (2003). Functional expression and direct visualization of the human alpha 2B -adrenergic receptor and alpha 2B -AR-green fluorescent fusion protein in mammalian cell using Semliki Forest virus vectors. *Protein expression and purification* 32(2): 265-275.

Serge A, de Keijzer S, Van Hemert F, Hickman MR, Hereld D, Spaink HP*, et al.* (2011). Quantification of GPCR internalization by single-molecule microscopy in living cells. *Integrative biology : quantitative biosciences from nano to macro* 3(6): 675-683.

Shan J, Weinstein H, Mehler EL (2010). Probing the structural determinants for the function of intracellular loop 2 in structurally cognate G-protein-coupled receptors. *Biochemistry* 49(50): 10691-10701.

Shaywitz AJ, Greenberg ME (1999). CREB: a stimulus-induced transcription factor activated by a diverse array of extracellular signals. *Annual review of biochemistry* 68: 821-861.

Shi CS, Sinnarajah S, Cho H, Kozasa T, Kehrl JH (2000). G13alpha-mediated PYK2 activation. PYK2 is a mediator of G13alpha -induced serum response element-dependent transcription. *The Journal of biological chemistry* 275(32): 24470-24476.

Shimomura O, Johnson FH, Saiga Y (1962). Extraction, purification and properties of aequorin, a bioluminescent protein from the luminous hydromedusan, Aequorea. *Journal of cellular and comparative physiology* 59: 223-239.

Sillence MN, Hooper J, Zhou GH, Liu Q, Munn KJ (2005). Characterization of porcine beta1- and beta2-adrenergic receptors in heart, skeletal muscle, and adipose tissue, and the identification of an atypical beta-adrenergic binding site. *Journal of animal science* 83(10): 2339-2348.

Simonds WF (1999). G protein regulation of adenylate cyclase. *Trends in pharmacological sciences* 20(2): 66-73.

Smith NJ, Milligan G (2010). Allostery at G protein-coupled receptor homo- and heteromers: uncharted pharmacological landscapes. *Pharmacological reviews* 62(4): 701-725.

Staehelin M, Hertel C (1983). [3H]CGP-12177, a beta-adrenergic ligand suitable for measuring cell surface receptors. *Journal of receptor research* 3(1-2): 35-43.

Stangherlin A, Zaccolo M (2011). Local termination of 3'-5'-cyclic adenosine monophosphate signals: the role of A kinase anchoring protein-tethered phosphodiesterases. *Journal of cardiovascular pharmacology* 58(4): 345-353.

Stangherlin A, Zaccolo M (2012). Phosphodiesterases and subcellular compartmentalized cAMP signaling in the cardiovascular system. *American journal of physiology. Heart and circulatory physiology* 302(2): H379-390.

Stephenson RP (1956). A modification of receptor theory. *British journal of pharmacology and chemotherapy* 11(4): 379-393.

Stieger K, Belbellaa B, Le Guiner C, Moullier P, Rolling F (2009). In vivo gene regulation using tetracycline-regulatable systems. *Advanced drug delivery reviews* 61(7-8): 527-541.

Stoddart LA, Vernall AJ, Denman JL, Briddon SJ, Kellam B, Hill SJ (2012). Fragment screening at adenosine-A(3) receptors in living cells using a fluorescence-based binding assay. *Chemistry & biology* 19(9): 1105-1115.

Strotmann R, Schrock K, Boselt I, Staubert C, Russ A, Schoneberg T (2011). Evolution of GPCR: change and continuity. *Molecular and cellular endocrinology* 331(2): 170-178.

Styer KL, Singh V, Macosko E, Steele SE, Bargmann CI, Aballay A (2008). Innate immunity in Caenorhabditis elegans is regulated by neurons expressing NPR-1/GPCR. *Science (New York, N.Y.)* 322(5900): 460-464.

Sueyoshi K, Hashiba K, Kawai T, Kitagawa F, Otsuka K (2011). Hydrophobic labeling of amino acids: transient trapping-capillary/microchip electrophoresis. *Electrophoresis* 32(10): 1233-1240.

Sun Y, McGarrigle D, Huang XY (2007). When a G protein-coupled receptor does not couple to a G protein. *Molecular bioSystems* 3(12): 849-854.

Sunahara RK, Taussig R (2002). Isoforms of mammalian adenylyl cyclase: multiplicities of signaling. *Molecular interventions* 2(3): 168-184.

Svalo J, Nordling J, Bouchelouche K, Andersson KE, Korstanje C, Bouchelouche P (2013). The novel beta(3)-adrenoceptor agonist mirabegron reduces carbachol-induced contractile activity in detrusor tissue from patients with bladder outflow obstruction with or without detrusor overactivity. *European journal of pharmacology* 699(1-3): 101-105.

Tang Y, Hu LA, Miller WE, Ringstad N, Hall RA, Pitcher JA*, et al.* (1999). Identification of the endophilins (SH3p4/p8/p13) as novel binding partners for the beta1-adrenergic receptor. *Proceedings of the National Academy of Sciences of the United States of America* 96(22): 12559-12564.

Taylor SS, Ilouz R, Zhang P, Kornev AP (2012). Assembly of allosteric macromolecular switches: lessons from PKA. *Nature reviews. Molecular cell biology* 13(10): 646-658.

Teichmann A, Schmidt A, Wiesner B, Oksche A, Schulein R (2012). Live cell imaging of G protein-coupled receptors. *Methods in molecular biology (Clifton, N.J.)* 897: 139-169.

Tesmer JJ (2010). The quest to understand heterotrimeric G protein signaling. *Nature structural & molecular biology* 17(6): 650-652.

Tesmer JJ, Sunahara RK, Gilman AG, Sprang SR (1997). Crystal structure of the catalytic domains of adenylyl cyclase in a complex with Gsalpha.GTPgammaS. *Science (New York, N.Y.)* 278(5345): 1907-1916.

Tesmer JJ, Sunahara RK, Johnson RA, Gosselin G, Gilman AG, Sprang SR (1999). Two-metal-Ion catalysis in adenylyl cyclase. *Science (New York, N.Y.)* 285(5428): 756-760.

Tilley DG (2011). G protein-dependent and G protein-independent signaling pathways and their impact on cardiac function. *Circulation research* 109(2): 217-230.

Tilley DG, Kim IM, Patel PA, Violin JD, Rockman HA (2009). beta-Arrestin mediates beta1-adrenergic receptor-epidermal growth factor receptor interaction and downstream signaling. *The Journal of biological chemistry* 284(30): 20375-20386.

Tirat A, Freuler F, Stettler T, Mayr LM, Leder L (2006). Evaluation of two novel tag-based labelling technologies for site-specific modification of proteins. *International journal of biological macromolecules* 39(1-3): 66-76.

Tuteja N (2009). Signaling through G protein coupled receptors. *Plant signaling & behavior* 4(10): 942-947.

Vaidehi N, Floriano WB, Trabanino R, Hall SE, Freddolino P, Choi EJ*, et al.* (2002). Prediction of structure and function of G protein-coupled receptors. *Proceedings of the National Academy of Sciences of the United States of America* 99(20): 12622-12627.

Van Petegem F (2012). Ryanodine receptors: structure and function. *The Journal of biological chemistry* 287(38): 31624-31632.

Vauquelin G, Packeu A (2009). Ligands, their receptors and ... plasma membranes. *Molecular and cellular endocrinology* 311(1-2): 1-10.

Vernall AJ, Stoddart LA, Briddon SJ, Hill SJ, Kellam B (2012). Highly potent and selective fluorescent antagonists of the human adenosine A(3) receptor based on the 1,2,4-triazolo[4,3-a]quinoxalin-1-one scaffold. *Journal of medicinal chemistry* 55(4): 1771-1782.

Veyrat-Durebex C, Pomerleau L, Langlois D, Gaudreau P (2005). Internalization and trafficking of the human and rat growth hormone-releasing hormone receptor. *Journal of cellular physiology* 203(2): 335-344.

Vidi PA, Przybyla JA, Hu CD, Watts VJ (2010). Visualization of G protein-coupled receptor (GPCR) interactions in living cells using bimolecular fluorescence complementation (BiFC). *Current protocols in neuroscience / editorial board, Jacqueline N. Crawley ... [et al.]* Chapter 5: Unit 5 29.

Vigh L, Nakamoto H, Landry J, Gomez-Munoz A, Harwood JL, Horvath I (2007). Membrane regulation of the stress response from prokaryotic models to mammalian cells. *Annals of the New York Academy of Sciences* 1113: 40-51.

Vogel SS, Thaler C, Koushik SV (2006). Fanciful FRET. *Science's STKE : signal transduction knowledge environment* 2006(331): re2.

Wagener BM, Marjon NA, Revankar CM, Prossnitz ER (2009). Adaptor protein-2 interaction with arrestin regulates GPCR recycling and apoptosis. *Traffic (Copenhagen, Denmark)* 10(9): 1286-1300.

Waldeck B (1996). Some pharmacodynamic aspects on long-acting beta-adrenoceptor agonists. *General pharmacology* 27(4): 575-580.

Wang HX, Konopka JB (2009). Identification of amino acids at two dimer interface regions of the alpha-factor receptor (Ste2). *Biochemistry* 48(30): 7132-7139.

Warne T, Edwards PC, Leslie AG, Tate CG (2012). Crystal structures of a stabilized beta1-adrenoceptor bound to the biased agonists bucindolol and carvedilol. *Structure (London, England : 1993)* 20(5): 841-849.

Warne T, Moukhametzianov R, Baker JG, Nehme R, Edwards PC, Leslie AG*, et al.* (2011). The structural basis for agonist and partial agonist action on a beta(1)-adrenergic receptor. *Nature* 469(7329): 241-244.

Warne T, Serrano-Vega MJ, Baker JG, Moukhametzianov R, Edwards PC, Henderson R*, et al.* (2008). Structure of a beta1-adrenergic G-protein-coupled receptor. *Nature* 454(7203): 486-491.

Watts AO, van Lipzig MM, Jaeger WC, Seeber RM, van Zwam M, Vinet J*, et al.* (2012). Identification and profiling of CXCR3-CXCR4 chemokine receptor heteromer complexes. *British journal of pharmacology*.

Weidemann T, Worch R, Kurgonaite K, Hintersteiner M, Bokel C, Schwille P (2011). Single cell analysis of ligand binding and complex formation of interleukin-4 receptor subunits. *Biophysical journal* 101(10): 2360-2369.

Weiss JM, Morgan PH, Lutz MW, Kenakin TP (1996). The cubic ternary complex receptor-occupancy model. III. resurrecting efficacy. *Journal of theoretical biology* 181(4): 381-397.

White JH, Wise A, Main MJ, Green A, Fraser NJ, Disney GH*, et al.* (1998). Heterodimerization is required for the formation of a functional GABA(B) receptor. *Nature* 396(6712): 679-682.

Whorton MR, Bokoch MP, Rasmussen SG, Huang B, Zare RN, Kobilka B*, et al.* (2007). A monomeric G protein-coupled receptor isolated in a high-density lipoprotein particle efficiently activates its G protein. *Proceedings of the National Academy of Sciences of the United States of America* 104(18): 7682-7687.

Whorton MR, Jastrzebska B, Park PS, Fotiadis D, Engel A, Palczewski K*, et al.* (2008). Efficient coupling of transducin to monomeric rhodopsin in a phospholipid bilayer. *The Journal of biological chemistry* 283(7): 4387-4394.

Williams C, Hill SJ (2009). GPCR signaling: understanding the pathway to successful drug discovery. *Methods in molecular biology (Clifton, N.J.)* 552: 39-50.

Wisler JW, DeWire SM, Whalen EJ, Violin JD, Drake MT, Ahn S*, et al.* (2007). A unique mechanism of beta-blocker action: carvedilol stimulates beta-arrestin signaling. *Proceedings of the National Academy of Sciences of the United States of America* 104(42): 16657-16662.

Wolfe BL, Marchese A, Trejo J (2007a). Ubiquitination differentially regulates clathrin-dependent internalization of protease-activated receptor-1. *The Journal of cell biology* 177(5): 905-916.

Wolfe BL, Trejo J (2007b). Clathrin-dependent mechanisms of G protein-coupled receptor endocytosis. *Traffic (Copenhagen, Denmark)* 8(5): 462-470.

Wong SK, Parker EM, Ross EM (1990). Chimeric muscarinic cholinergic: beta-adrenergic receptors that activate Gs in response to muscarinic agonists. *The Journal of biological chemistry* 265(11): 6219-6224.

Xiang YK (2011). Compartmentalization of beta-adrenergic signals in cardiomyocytes. *Circulation research* 109(2): 231-244.

Xue C, Hsueh YP, Heitman J (2008). Magnificent seven: roles of G protein-coupled receptors in extracellular sensing in fungi. *FEMS microbiology reviews* 32(6): 1010-1032.

Yan X, Gao S, Tang M, Xi J, Gao L, Zhu M*, et al.* (2011). Adenylyl cyclase/cAMP-PKA-mediated phosphorylation of basal L-type Ca(2+) channels in mouse embryonic ventricular myocytes. *Cell calcium* 50(5): 433-443.

Yang F, Moss LG, Phillips GN, Jr. (1996). The molecular structure of green fluorescent protein. *Nature biotechnology* 14(10): 1246-1251.

Yang Y, Mou Y, Hu SJ, Fu M (2009). Beneficial effect of rosuvastatin on cardiac dysfunction is associated with alterations in calcium-regulatory proteins. *European journal of heart failure* 11(1): 6-13.

Ying LQ, Branchaud BP (2011). Selective labeling and monitoring pH changes of lysosomes in living cells with fluorogenic pH sensors. *Bioorganic & medicinal chemistry letters* 21(12): 3546-3549.

Yoshiura S, Ohta N, Matsuzaki F (2012). Tre1 GPCR signaling orients stem cell divisions in the Drosophila central nervous system. *Developmental cell* 22(1): 79-91.

Zhang G, Liu Y, Ruoho AE, Hurley JH (1997). Structure of the adenylyl cyclase catalytic core. *Nature* 386(6622): 247-253.

Zhong J, Dessauer CW, Keef KD, Hume JR (1999). Regulation of L-type Ca2+ channels in rabbit portal vein by G protein alphas and betagamma subunits. *The Journal of physiology* 517 (Pt 1): 109-120.

Zinchuk V, Zinchuk O, Okada T (2007). Quantitative colocalization analysis of multicolor confocal immunofluorescence microscopy images: pushing pixels to explore biological phenomena. *Acta histochemica et cytochemica* 40(4): 101-111.